Modulation of the effects of TRAIL by the extracellular matrix in cancer and development of new Tenascin-C-targeting peptides

William Erne

UNIVERSITÉ DE STRASBOURG

ÉCOLE DOCTORALE des Sciences de la Vie et de la Santé

UMR_S INSERM 1109

Immuno-Rhumathologie Moléculaire

THÈSE présentée par :

William ERNE

soutenue le : **18 décembre 2020**

pour obtenir le grade de : **Docteur de l'université de Strasbourg**

Discipline : Sciences de la Vie et de la Santé

Spécialité : Aspects moléculaires et cellulaires de la Biologie

Modulation des effets de TRAIL par la matrice extracellulaire dans le cancer et développement de nouveaux peptides ciblant la Ténascine-C

THÈSE dirigée par :

Dr. Gertraud OREND	Université de Strasbourg

RAPPORTEURS :

Prof. Véronique ORIAN-ROUSSEAU	Université de Karlsruhe, Allemagne
Prof. Stéphane DEDIEU	Université de Reims, France

AUTRES MEMBRES DU JURY :

Dr. Frédéric GROS	Université de Strasbourg

Acknowledgements

First of all, I would like to sincerely thank my thesis director, Gertraud OREND, who gave me the opportunity to perform my PhD (and master thesis) in her group. In total this represents five important years of my life that I will never forget. More than just supervising a student, she allowed me to try out my ideas (that sometimes were more than original) and to work in the best conditions we could have. Most of all, she gave the opportunity to me, a small student from the middle of France barely speaking English, to join my professional and personal lives in Strasbourg, and to grow up.

I would like to express my gratitude to the people who heavily participated to sharp my technical skills and my scientific spirit. I am speaking about the Old Guard from the MN3T, who taught me a lot during my master and the first year of my PhD. Many thanks to Patricia, Tristan, Sun, Constance, Annick, Christiane, Olivier and Mika.

I also especially want to thank Selven, alias Maître Murdamoothoo, who supervised me during my master thesis (and knowing myself, that was not always easy for him) and who, like me, lived the transition from the Old Guard to the Young Guard. I hope the Padawan has lived up to the Master's teachings.

Then comes the Young Guard! I spent most of my PhD with them and we shared a lot of good moments together as well as some tuff times that I believe made us closer and stronger. I would like to extend my sincere thanks to Alev (my young Padawan-in-law), Chérine, Rolando, Thomas, Aurore, Nathalie, Li and Gilles who supported me during every moments of my PhD. The nights we spent looking for TNC eluting, drop after drop, are unforgettable. I wish good luck to Marine who also comes from my region and will begin her PhD; take flight, young one.

I also want to thank Fanny and Isabelle, who provide us technical and administrative support every day. They are a pillar for the team and we could not work in good conditions without them.

Since I have worked in two institutes, I really want to thank all the persons from Hautepierre who welcomed me during the first part of my PhD, and all the members of the INSERM UMR_s 1109, who nicely welcomed us in the Institut d'hématologie-Immunologie and provided me good advices during my PhD.

I had the opportunity to give courses at the Faculté de Pharmacie and I would like to thank Marie-Claude KILHOFFER, Maria ZENIOU, Maxime LEHMANN and Emmanuel BOUTANT for the great experience it was to teach students.

I thank the Ministère français de l'Enseignement supérieur, de la Recherche et de l'Innovation, the Ligue contre le cancer, the Fondation ARC pour la recherche sur le cancer, the Agence nationale de la recherche and the INSERM for financing my salary, the equipment and the consumable I used during my PhD. I also want to thank the Université de Strasbourg and the École doctorale des Sciences de la Vie et de la Santé, in particular Catherine SCHUSTER, Pascal DARBON, Géraldine SCHVERER and Mélanie MUSER for providing their support each time I had administrative questions related to the university.

This thesis is also the result of many years of support from my family and friends. I would like to sincerely thank my parents, Christian and Corinne, for everything they did for me during the last 30 years. I am pride to say that they provided me a good education and that they fully supported me during my scholar life, so that today I can present my PhD work. I also want to thank my brothers Peter and Steven (yes, my mother likes English names) for supporting me in any condition.

I also want to thank my outer Rhin family, Karin, Klaus, Mitu, Konrad, Leonora, Cristoph and young Janor for their nice welcome, support and patience, in particular since I am still uncappable to align correctly three words in German.

I would like to thank my friends from Tours, Delphine, Maxime, Hélène and Yann with whom I passed my bachelor and master's degree, and who demonstrate that friendship is not a question of distance.

Last but not least, I cannot thank enough my girlfriend Ramona for sharing with me these last years, enjoying the good days and enduring the bad days with me. I could not have finished my PhD without here support, in particular during this lovely year 2020.

I will conclude with special thanks to my cat Cyka, who makes sure every day that I do not miss a good day of work, waking up before 6:00 a.m. (every day!). Then I have a special thought for a mathematics teacher, who told me once, while he was desperate to give me really bad marks again: *"Be ambitious! Even monkeys managed to walk on the Moon, so why not you?"*

Thanks

Table of content

1. Summary (in French)

Introduction

Les tumeurs sont des écosystèmes complexes possédant un microenvironnement tumoral (MET) dont les fonctions sont encore mal comprises. Le stroma, très proche morphologiquement des cellules cancéreuses, comprend les cellules stromales, leurs facteurs solubles et les molécules de la matrice extracellulaire (MEC). En plus de fournir un échafaudage physique et architectural pour le tissu, la MEC participe activement à la progression tumorale en interagissant avec les cellules du MET. Ces interactions médiées par des récepteurs modulent des processus cellulaires tels que la survie, de la prolifération et l'invasion (Butcher et al., 2009; Frantz et al., 2010).

La Ténascine-C (TNC), protéine de la MEC, est majoritairement absente des tissus sains ; mais est exprimée en abondance dans le cancer. Son expression élevée est corrélée avec des survies sans métastases et globales réduites chez les patients atteints de cancer du sein (Orend et al., 2014; Oskarsson, 2013; Sun et al., 2019). La TNC est connue pour sa capacité à lier de nombreuses molécules du stroma, dont la fibronectine (FN), entrainant la formation d'alignements de matrice denses et parallèles, nommés TMT (Tumor Matrix Tracks, (Midwood et al., 2016)). Ces fibres de TNC et FN sont souvent retrouvées lors de phénomène d'inflammation, de fibrose et dans le cancer (van Obberghen-Schilling et al., 2011). Les deux protéines matricielles possèdent des sites d'interaction avec des récepteurs cellulaires et des facteurs solubles, permettant des échanges entre les divers acteurs cellulaires et moléculaires du stroma (Chiquet-Ehrismann et al., 1988 ; Huang et al., 2001 ; Orend et al., 2003). Il a été décrit que les domaines fibronectine de type III, plateformes d'interactions moléculaires, sont présents dans la TNC et la FN, permettant l'intéraction des deux protéines matricielles entres elles et avec le stroma (Bloom et al., 1999; Huang et al., 2001; Orend et al., 2003).

Les cancers sont souvent caractérisés par un état inflammatoire précoce, suivi d'une réponse immunitaire faiblement immunogène favorisant la progression tumorale (Zitvogel et al., 2006). L'impact du MET, plus particulièrement de sa MEC, sur l'immunité antitumorale reste à l'heure actuelle mal connu. La possibilité que la TNC joue un rôle dans l'immunité antitumorale est étayée par son rôle en tant que DAMP (Damage Associated Molecular Pattern), phénomène décrit dans d'autres états pathologiques tels que l'inflammation (Piccinini and Midwood, 2012). De plus, nos résultats récents suggèrent des propriétés régulatrices multiples de la TNC sur

l'immunité tumorale, notamment en interagissant avec des molécules immuno-modulatrices comme les chimiokines CCL21 (Spenlé et al., 2020), CXCL12 (Murdamoothoo et al., en révision) et la cytokine TRAIL (Erne et al., en préparation).

TRAIL ('tumor-necrosis-factor related apoptosis inducing ligand') est une cytokine de la famille du TNF (Facteur de Nécrose Tumorale) exprimée par les cellules du système immunitaire dans le but d'éliminer les cellules tumorales (Pitti et al., 1996; Wiley et al., 1995). La signalisation via TRAIL est initiée par la liaison d'un trimer de TRAIL à un trimer de récepteur TRAIL-R1/R2, induisant la mort cellulaire par apoptose ou par nécroptose (Jouan-Lanhouet et al., 2012). Suite à sa découverte, TRAIL a fait l'objet de nombreuses études liées à une caractéristique spécifique : être capable d'induire l'apoptose de cellules infectées ou cancéreuses, sans entrainer la mort des cellules saines (Ashkenazi et al., 1999; Lemke et al., 2014; Walczak et al., 1999). Depuis, de nombreux essais cliniques utilisant TRAIL ont été entrepris pour exploiter sa capacité antitumorale mais aucun effet significatif n'a été constaté (Micheau et al., 2013; Stuckey and Shah, 2013). Des facteurs tels qu'une courte demi-vie de TRAIL, un dosage sous-optimal, le développement de résistances, ou encore l'activation d'une signalisation alternative par TRAIL perturbent le développement d'une thérapie efficace utilisant TRAIL (von Karstedt et al., 2017). En plus d'avoir des effets pro-tumoraux sur certaines cellules cancéreuses (von Karstedt et al., 2015), il a aussi été montré que TRAIL et ses récepteurs jouent de nombreux rôles dans la régulation de l'immunité antitumorale (Sag et al., 2019). Enfin, nos travaux récents ont montré que la TNC pouvaient entrainer le développement tumoral via l'activation de voies de résistance à l'apoptose et des processus de transition épithélio-mésenchymateuse (TEM, (Sun et al., 2019)), ce qui pourrait grandement impacter la sensibilité des cellules tumorales à TRAIL.

Etant donné les nombreux effets de la TNC dans des processus pathologiques tels que le cancer, il apparait clair qu'un ciblage spécifique de cette molécule pourrait améliorer la compréhension des mécanismes activés par la TNC tout en apportant de nouvelles opportunités thérapeutiques. Notre hypothèse est que la TNC participe au développement tumoral et métastatique en dérégulant la réponse immunitaire antitumorale, notamment en interférant avec les chimiokines et cytokines telles que TRAIL. Les objectifs de cette thèse seront donc de mieux comprendre les effets de TRAIL dans le cancer du sein, tout en décrivant le rôle que la TNC joue dans ces processus ; puis de développer des peptides spécifiques visant à cibler et inhiber les effets pathologiques de la TNC.

Objectifs et résultats :

Objectif 1 : Identifier les interactions entre la TNC et TRAIL dans le modèle NT193 et en décrire les effets sur le développement du cancer du sein.

Pour comprendre les rôles de TRAIL et de la TNC dans le cancer du sein, nous avons utilisé notre modèle murin de greffe orthotopique syngénique basé sur la lignée cellulaire cancéreuse NT193 (Arpel et al., 2014) susceptible d'induire des tumeurs mammaires et des métastases pulmonaires (Sun et al., 2019). L'utilisation de cellules NT193 génétiquement modifiées pour sous-exprimer la TNC (via 'small hairpin RNA') et leur greffe dans des souris exprimant ou non la TNC (respectivement ''Wild Type'' WT ou ''Knockout'' KO) nous a permis de mieux comprendre l'impact de la TNC dans ce type de cancer. Nous avons d'abord constaté une diminution de l'expression de TRAIL lorsque la TNC était fortement exprimée dans les modèles MMTV-NeuNT et NT193, supposant une régulation de TRAIL par la TNC dans la tumeur. Nous avons de plus montré que les cellules cancéreuses NT193 exprimaient TRAIL sans subir d'apoptose. Cette propriété a déjà été observé dans d'autres lignées cancéreuses (Huber et al., 2005; Inoue et al., 2002; von Karstedt et al., 2015). En travaillant avec des lignées NT193 épithéliales (NT193E) ou mésenchymateuses (NT193M), nous avons observé que les cellules NT193E n'entraient en apoptose qu'après traitement avec MD5-1 (agoniste du récepteur de TRAIL DR5) et TRAIL recombinant. Ces observations illustrent les problèmes liés au développement de thérapies à base de TRAIL, à savoir la formation d'un complexe TRAIL-DR5 stable et l'apparition de résistance liée à la TEM (Graves et al., 2014; Lu et al., 2014).

Nous avons ensuite montré que la TNC entrainait une diminution de l'apoptose induite par la combinaison TRAIL+MD5-1 sur les cellules NT193E, suite à l'activation d'une voie de résistance dépendante de TGFβR1 ('transforming growth factor beta receptor 1') que nous avions précédemment décrite (Sun et al., 2019). De plus, nous avons mis en évidence une interaction physique entre TRAIL et la TNC, ce qui pourrait affecter la signalisation de TRAIL. Pour mieux comprendre la régulation de TRAIL par la TNC, nous avons développé des modèles de coculture en sphéroïdes des lignées NT193E et M, dans le but de se rapprocher du contexte tumoral. Nous avons pu obtenir des sphéroïdes épithéliaux enveloppés de cellules mésenchymateuses produisant de la TNC, rappelant l'organisation du MET. En utilisant des cellules NT193M sous-exprimant la TNC dans les cocultures en sphéroïdes, nous avons constaté que le traitement TRAIL+MD5-1 induisait plus d'apoptose que dans un

contexte de sphéroïde contenant de la TNC, indiquant une nouvelle fois que la TNC peut entrainer une résistance aux thérapies utilisant TRAIL.

De plus en plus d'études rapportent des effets immuno-régulateurs TRAIL dans le cancer (Sag et al., 2019). Nous avons donc voulu connaitre le rôle de TRAIL produit par les cellules NT193 dans la tumeur étant donné que la cytokine seule n'induit pas de mort cellulaire en culture. Après avoir greffé des cellules NT193, génétiquement modifiées pour sous-exprimer TRAIL, dans des souris hôtes WT ou KO pour la TNC, nous avons observé que les tumeurs sous-exprimant TRAIL étaient plus grosses et généraient plus de métastases pulmonaires. Par analyse en cytométrie en flux, nous avons relevé une diminution du nombre de cellules dendritiques (CD) et de macrophages (MP) présents dans les tumeurs sous-exprimant TRAIL chez les souris WT, indiquant une régulation de ces cellules immunitaires par TRAIL en présence de TNC. De plus, nous avons mis en évidence la présence de nombreux vides architecturaux dans les tumeurs, contenant des MP dépendamment de l'expression de TRAIL et de la TNC. Ces résultats suggèrent une régulation de la phagocytose antitumorale par TRAIL et la TNC. Par des analyses transcriptomiques et protéomiques, nous avons identifié CXCR4 ('chemokine (C-X-C motif) receptor 4'), récepteur membranaire et régulateur de l'activation et de la migration de CD et MP, comme un candidat potentiel dont l'expression serait modulée par TRAIL. En effet, nous avons pu démontrer en culture que l'expression de TRAIL par les cellules NT193 entrainait une augmentation de la migration de CD et de MP, dépendant de CXCR4, vers les cellules tumorales dans des modèles d'invasion de matrigel et d'infiltration de sphéroïdes.

Enfin, nous avons constaté que la TNC pouvait entrainer la diminution d'expression de TRAIL par les cellules NT193 en interagissant avec les intégrines α4β1 ou α9β1. L'analyse de données publiques de patients atteints du cancer du sein montre une meilleure survie globale au cancer lorsque les expressions de TRAIL et CXCR4 sont élevées. Ainsi, une inhibition de ce système par la TNC entrainerait une diminution de la survie des patients. Cette étude décrit une régulation complexe de TRAIL par la TNC et illustre l'importance de la prise en compte du MET dans la mise en place de thérapies anticancéreuses utilisant TRAIL.

Objectif 2 : Moduler les fonctions de la TNC en ciblant un nouveau motif de régulation de la matrice à l'aide de peptides 'MAREMO'

Afin de cibler la TNC et de bloquer ses effets pro-tumoraux et fibrotiques, nous avons développé de peptides à visée thérapeutique mimant spécifiquement le site d'interaction de la TNC sur la FN. Nous avons d'abord constaté par ELISA et résonance plasmonique de surface (RPS) une forte affinité des domaines FN5 et FN13 pour un substrat de TNC, laissant supposer des sites de liaison dans ces domaines. Sachant que des séquences protéiques possédant des fonctions importantes sont généralement conservées entre les espèces, nous avons comparé les domaines FN5 et FN13 de divers vertébrés et avons observé une forte conservation des acides aminés formant deux boucles (boucle I et boucle II) dans les structures modélisées de ces domaines. Du fait de l'organisation de ces boucles et de leur localisation spatiale, nous avons suggéré qu'elles permettraient l'interaction avec la TNC et avons nommé ces séquences MAREMO (pour MAtrix REgulating MOtif). Nous avons alors généré les peptides P5 et P13 en liant les séquences correspondant aux boucles I et II de FN5 et FN13. Pour chaque expérience, des peptides aux séquences mixées (S5 et S13) ont été utilisés comme contrôles.

Suite à nos récentes découvertes concernant l'interaction de la TNC avec CCL21, CXCL12 et TRAIL (Spenlé et al., 2020 ; Murdamoothoo et al., en révision ; Erne et al., en préparation), nous avons voulu tester le potentiel bloquant des P5 et P13 sur la liaison de ces molécules avec la TNC. Nous avons d'abord mis en évidence par microscopie électronique une forte liaison de CCL21, CXCL12 et de TRAIL au niveau du cinquième domaine fibronectine de type III de la TNC (TN5). Après avoir constaté une importante liaison des peptides P5 et P13 au domaine TN5, nous avons démontré que l'ajout de P5 et P13 diminuait grandement l'interaction de la TNC avec CCL21, CXCL12 et TRAIL, à l'inverse des contrôles S5 et S13. Cette expérience montre que la TNC est capable de jouer le rôle de réservoir de facteurs solubles, modulant la concentration locale et la présentation de ces molécules. En utilisant P5 et P13, nous pourrions donc bloquer cet effet.

Sachant qu'un substrat de TNC peut immobiliser des CD via CCL21 (Spenlé et al., 2020), nous avons voulu inhiber l'effet de chimio rétention de la TNC. En mesurant la quantité de CD retenues dans des inserts de migration contenant de la TNC et CCL21 ou CXCL12, nous avons constaté que l'ajout de P5 et P13 diminuait le nombre de cellules maintenues par la TNC. L'utilisation des peptides S5 et S13, ainsi que de substrats de collagène I ou de FN n'a entrainé aucune différence dans la chimio rétention, indiquant bien que les peptides P5 et

P13 interagissent spécifiquement avec la TNC, ce qui bloque sa liaison avec CCL21 et CXCL12, et inhibe son effet immobilisateur sur des cellules immunitaires.

La TNC joue un rôle important dans l'assemblage de la MEC en condition pathologique telle que la fibrose rénale, notamment en activant les fibroblastes et la surproduction de MEC (Fu et al., 2017). Des techniques de RPS et de microscopie électronique nous ont d'abord permis de montrer que des fragments de FNIII4-6 et FNIII12-14 lient la TNC au niveau de TN5, et que cette liaison physique pouvait être bloquée par l'addition des P5 et P13. Nous avons ensuite montré que les peptides P5 et P13 pré-incubés avec de la TNC sur la FN restaurent l'adhésion de cellules cancéreuses, ce qui avait précédemment été observé avec le domaine FN13 (Orend et al., 2003). De plus, l'observation des points focaux d'ancrage formés par les cellules sur le substrat démontre que les peptides P5 et P13 inhibent l'effet antiadhésif de la TNC en permettant à nouveau aux cellules de former ces points d'adhésion avec la FN. En utilisant des cellules mésangiales (MES), nous avons montré que l'induction de l'expression de protéines matricielles comme la FN et le collagène I par la TNC était inhibé par les peptides. Ces résultats montrent que la TNC peut interagir avec les récepteurs cellulaires et les protéines de la MEC, telle que la FN. En utilisant les peptides, nous pourrions ainsi bloquer ces interactions et inhiber l'effet de la TNC dans les pathologies impliquant un fort remaniement de la matrice, comme la fibrose et le cancer.

En utilisant les cellules NT193M qui produisent fortement la TNC et résistent à l'apoptose induite par TRAIL, nous avons voulu voir si les peptides pouvaient inhiber la liaison de TRAIL à la TNC, ce qui pourrait rétablir l'activation de la mort cellulaire par TRAIL. Nous avons ainsi montré que les peptides pré-incubés avec la TNC induisaient une meilleure sensibilité des cellules à l'apoptose médiée par TRAIL. Sur des NT193M sous-exprimant la TNC, nous avons observé que les peptides n'affectent plus la sensibilité des cellules à TRAIL. Cette expérience montre que les peptides pourraient avoir un intérêt thérapeutique dans les traitements anticancéreux utilisant TRAIL en bloquant l'immobilisation de TRAIL par la TNC.

Enfin, en analysant par spectrométrie de masse les protéines liées à la TNC lors de la purification de TNC murine, nous avons identifié de nombreux facteurs solubles et matriciels susceptibles d'interagir directement avec la TNC. Certaines de ces protéines possédant des domaines de type FNIII, nous avons pu mettre en évidence des séquences ressemblant au MAREMO. Sachant que les domaines FNIII sont connus pour être des sites d'interaction protéique, nous formulons l'hypothèse que la TNC pourrait interagir avec ces protéines en fonction de la présence et du degré de conservation de la séquence MAREMO. Une analyse

plus poussée de l'ensemble des protéines contenant des domaines FNIII permettrait d'identifier des candidats dont l'interaction avec la TNC pourrait être vérifiée à l'aide de peptides MAREMO.

Conclusion :

La TNC joue un rôle important dans les pathologies impliquant un remodelage matriciel comme le cancer et la fibrose. Durant cette thèse, j'ai d'abord mis en évidence le fonctionnement complexe de la cytokine TRAIL, qui malgré un intérêt thérapeutique évident, demande encore des études approfondies sur sa régulation. La TNC, de par sa forte expression dans les cancers, peut notamment interférer avec TRAIL et les thérapies dérivées, en créant des phénomènes de résistance qui pourraient être délétères pour les patients. Ensuite, nous avons généré des peptides ciblant spécifiquement la TNC à partir de séquences MAREMO dans le but de bloquer les fonctionnalités de la TNC dans le microenvironnement. Nous avons ainsi décrit des effets inhibiteurs des peptides sur les mécanismes liés à la rétention de chimiokines, à l'interaction cellulaire et matricielle, et à la résistance à TRAIL par la TNC. Le développement des peptides MAREMO pourrait apporter une solution thérapeutique visant à contrecarrer les effets pathologiques de la TNC, comme notamment l'inhibition de la réponse immunitaire et la réorganisation pathologique de la MEC dans le cancer et la fibrose.

2. Contribution to manuscripts

This thesis as provided results for two major publications (Manuscript I & II) ready for submission. Moreover, I participated to the publication of several articles (listed in Appendix) where I provided results, animals for experimentations, technical support during experiments, and help during the reviewing.

Manuscript I: Tenascin-C counteracts TRAIL control over tumor immunity, growth and progression

William Erne, Devadarssen Murdamoothoo, Zhen Sun, Matthias Mörgelin, Gérard Cremel, Nicodème Paul, Raphael Carapito, Aurélie Hirschler, Christine Carapito, Thomas Loustau, Gertraud Orend **Ready to submit**

Manuscript II: Modulating tenascin-C functions by targeting the MAtrix REgulating MOtif, "MAREMO"

William Erne*, Pia Abel zur Wiesch*, Thomas Imhof+, Thomas Loustau+, Chérine Abou-Faycal+, Chengbei Li, Ayoub Ksouri, Marija Marko, Gerard Crémel, Balkiss Bouhaouala, Matthias Mörgelin+, Manuel Koch, Gertraud Orend **Ready to submit**

***** equal contribution

\+ equal contribution

Appendix I: Tenascin-C increases lung metastasis by impacting blood vessel invasions

Zhen Sun, Inés Velazquez-Quesada, Devadarssen Murdamoothoo, Constance Ahowesso, Alev Yilmaz, Caroline Spenlé, Gerlinde Averous, **William Erne**, Felicitas Oberndorfer, Andre Oszwald, Renate Kain, Catherine Bourdon, Pierre Mangin, Claire Deligne, Kim Midwood, Chérine Abou-Faycal, Olivier Lefebvre, Annick Klein, Michael van der Heyden, Marie-Pierre Chenard, Gerhard Christofori, Carole Mathelin, Thomas Loustau, Thomas Hussenet and Gertraud Orend Matrix Biol. 83, 26–47.

Appendix II: Matrix-Targeting Immunotherapy Controls Tumor Growth and Spread by Switching Macrophage Phenotype

Claire Deligne, Devadarssen Murdamoothoo, Anís N. Gammage, Martha Gschwandtner, **William Erne**, Thomas Loustau, Anna M. Marzeda, Raphael Carapito, Nicodème Paul, Inès Velazquez-Quesada, Imogen Mazzier, Zhen Sun, Gertraud Orend, and Kim S. Midwood
Cancer Immunol. Res. 8, 368–382.

Appendix III: Tenascin-C orchestrates an immune suppressive tumor microenvironment in oral squamous cell carcinoma

Caroline Spenlé*, Thomas Loustau*, Devadarssen Murdamoothoo, **William Erne**, Stephanie Beghelli-de la Forest Divonne, Romain Veber, Luciana Petti, Pierre Bourdely, Matthias Mörgelin, Eva-Maria Brauchle, Gérard Cremel, Vony Randrianarisoa, Abdouramane Camara, Samah Rekima, Sebastian Schaub, Kelly Nouhen, Thomas Imhof, Uwe Hansen, Nicodème Paul, Raphael Carapito, Nicolas Pythoud, Aurélie Hirschler, Christine Carapito, Hélène Dumortier, Christopher G. Mueller, Manuel Koch, Katja Schenke-Layland, Shigeyuki Kon, Anne Sudaka, Fabienne Anjuère, Ellen Van Obberghen-Schilling, Gertraud Orend
Cancer Immunol Res 2020;8:1122–38.
***** equal contribution

Appendix IV: Generation and characterization of dromedary Tenascin-C and Tenascin-W specific antibodies

Sayda Dhaouadi, Devadarssen Murdamoothoo, Asma Tounsi, **William Erne**, Rahma Benabderrazek, Zakaria Benlasfar, Lotfi Hendaoui, Ruth Chiquet-Ehrismann, Samir Boubaker, Gertraud Orend, Ismaïl Hendaoui, Balkiss Bouhaouala-Zahara
Biochemical and Biophysical Research Communications 2020:530:471-478

Tenascin-C immobilizes infiltrating cytotoxic T lymphocytes through CXCL12 enhancing lung metastasis in breast cancer

Devadarssen Murdamoothoo*, Zhen Sun*, Alev Yilmaz, Claire Deligne, Ines Velazquez-Quesada, **William Erne**, Matthias Mörgelin, Gérard Cremel, Nicodème Paul, Raphael Carapito, Chérine Abou-Faycal, Romain Veber, Hélène Dumortier, Jingping Yuan, Kim S. Midwood, Thomas Loustau and Gertraud Orend **Ready to submit**
***** equal contribution

3. Abbreviations

%	Percent
3D	3 Dimensions
4NQO	4-Nitroquinoline 1-oxide
aa	amino acid
ADCC	Antibody-Dependent Cellular Cytotoxicity
AICD	Activation-Induced Cell Death
AKT	Protein kinase B
AO/EB	Acridin Orange / Ethidium Bromide
AP-1	Activator Protein 1
APAF1	Apoptotic Protease Activating Factor 1
ATAC	Arimidex, Tamoxifen, Alone or in Combination
Atg	Autophagy related
ATP	Adenosine Triphosphate
B-cell	B Lymphocyte
BCL-2	B-Cell Lymphoma 2
BID	BH3-Interacting Domain
BRCA1/2	Breast cancer type 1/2
CAF	Cancer Associated Fibroblast
Casp	Caspase
CCL	Chemokine (C-C motif) Ligand
CCR	Chemokine (C-C motif) Receptor
CD	Cluster of Differentiation
CDC	Complement-Dependent cellular Cytotoxicity
CEBP	CCAAT/Enhancer-Binding Protein
CendR	C-end Rule
cFLIP	cellular FLICE-Like Inhibitory Protein
cIAP	cellular-IAP
CK8/18	Cytokeratines-8 /-18
CNTN	Contactin
Col	Collagen
COX-2	Cyclooxygenase-2
CSF-1	Colony-Stimulating Factor 1
CTLA-4	Cytotoxic T-Lymphocyte-Associated protein 4
CXCL	Chemokine (C-X-C motif) Ligand
CXCR	Chemokine (C-X-C motif) Receptor
DAMP	Danger Associated Molecular Pattern
DC	Dendritic Cell
DD	Death Domain
DISC	Death-Inducing Signaling Complex
DNA	Deoxyribonucleic Acid
DR5	Death Receptor 5

EBCTCG	Early Breast Cancer Trialists' Collaborative Group
E-Cad	E-Cadherin
ECM	Extracellular Matrix
EDTA	Ethylenediaminetetraacetic acid
EGF	Epidermal Growth Factor
EGFL	EGF-Ligand
EGFR	EGF-Receptor
ELISA	Enzyme-Linked Immunosorbent Assay
EM	Electronic Microscopy
EMT	Epithelial-to-Mesenchymal Transition
EndMT	Endothelial-to-Mesenchymal Transition
eNOS	endothelial Nitric Oxide Synthase
ER	Estrogen Receptor
ERK	Extracellular signal-Regulated Kinase
ETA	Evolutionary Trace Annotation
FADD	Fas-Associated Death Domain
FAK	Focal Adhesion Kinase
FAP	Fibroblast Activation Protein
FasL	Fas Ligand
FBG	Fibrinogen Globe
FBS	Fetal Bovine Serum
Fmoc	9-fluorenylmethyloxycarbonyl
FN	Fibronectin
FNIII	Fibronectin type-III
FSP-1	Fibroblast Specific Protein 1
GAS	Interferon-γ-Activated Sequence
GH	Growth Hormone
GHR	Growth Hormone Receptor
GKLF	Gut-enriched Krüppel-Like Factor
GMEM	Glioma-Mesenchymal Extracellular Matrix
GTP	Guanosine Triphosphate
HBS	Heparin Binding Site
HER-2	Human Epidermal growth factor Receptor 2
HIV	Human Immunodeficiency Virus
HR	Hormone Receptor
ICAM-1	Intercellular Adhesion Molecule 1
IF	Immunofluorescence
IFN	Interferon
IgG1	Immunoglobulin G 1
IHC	Immunohistochemistry
IL	Interleukin
ILC	Innate Lymphoid Cell
ILZ-TRAIL	Isoleucine Zipped-TRAIL

JNK	JUN N-terminal Kinase
KD	Knockdown
kDa	kilo Dalton
KO	Knockout
LDL	Low Density Lipoprotein
LEC	Lymphatic Endothelial Cell
LM	Laminin
LPS	Lipopolysaccharide
LUBAC	Linear Ubiquitin chain Assembly Complex
LZ-TRAIL	Leucine Zipped-TRAIL
MAREMO	MAtrix REgulating MOtif
MCL1	Induced myeloid leukemia cell differentiation protein
MDP	Membrane Proximal Domain
miR	micro RNA
MMP	Matrix Metalloproteinase
MMTV	Mouse Mammary Tumor Virus
MP	Macrophage
mRNA	messenger RNA
NEMO	Nuclear NFkB Essential Modifier
NFAT	Nuclear Factor of Activated T-cells
NFkB	Nuclear Factor kappa-light-chain-enhancer of activated B cells
NK	Natural Killer
NRP1	Neuropilin-1 Receptor
NSCLC	Non-Small Cell Lung Cancer
OPG	Osteoprotegerin
OSCC	Oral Squamous Cell Carcinoma
PBS	Phosphate-Buffered Saline
PD1	Programmed cell death protein 1
PDB	Protein Data Bank
PDGF	Platelet-Derived Growth Factor
PD-L1	Programmed cell death protein 1 Ligand
PgR	Progesterone Receptor
pH	potential of Hydrogen
PI3K	Phosphoinositide 3-kinases
PTPR	receptor-type tyrosine-protein phosphatase
qRTPCR	quantitative Reverse Transcription Polymerase Chain Reaction
rhTRAIL	recombinant human TRAIL
RIPK1	Receptor-Interacting serine/threonine Protein Kinase 1
RNA	Ribonucleic acid
scFv	single-chain variable Fragment
SDF-1	Stromal cell-Derived Factor 1
shRNA	small hairpin RNA
siRNA	small interfering RNA

SMAC	Second Mitochondria-derived Activators of Caspase
SMART	Simultaneously Multiple Aptamers and RGD Targeting
SOX4	Sex determining region Y-box 4
SRP	Surface Resonance Spectrometry
STAT3	Signal Transducer and Activator of Transcription 3
TACS	Tumor-Associated-Collagen-Signatures
TAM	Tumor Associated Macrophage
TBS	Tris-Buffered Saline
T-cell	T Lymphocyte
TCR	T-Cell Receptor
TGFβ	Transforming Growth Factor beta
Th1/2/17	Helper T cell 1/2/17
TLR	Toll-Like Receptor
TME	Tumor Microenvironment
TMT	Tumor Matrix Track
TNC	Tenascin-C
TNF	Tumor Necrosis Factor
TNFRSF	TNF Receptor Super Family
TNFSF	TNF Super Family
TNN	Tenascin-W
TNR	Tenascin-R
TNX	Tenascin-X
TRA	TRAIL-R Agonist
TRAF2	TNF Receptor-Associated Factor 2
TRAIL	TNF-Related Apoptosis-Inducing Ligand
TRAIL-R	TRAIL Receptor
Treg	Regulatory T cell
TSLP	Thymic Stromal Lymphopoietin
VEGF	Vascular Endothelial Growth Factor
VEGFR	Vascular Endothelial Growth Factor Receptor
Vim	Vimentin
VLDL	Very Low-Density Lipoprotein
WT	Wildtype
X3CL1	C-X3-C motif chemokine 1 / Fractalkine
XIAP	X-linked Inhibitors of Apoptosis
YAP	Yes-Associated Protein 1
α-SMA	alpha Smooth Muscle Actin

4. Introduction

Cancer is a common term designating a large group of diseases characterized by abnormal cell proliferation and spreading of tumor cells to other organs. In 2018, the most common cancers were lung (2.09 million cases), breast (2.09 million cases), colorectal (1.80 million cases), prostate (1.28 million cases), skin (non-melanoma) (1.04 million cases) and stomach (1.03 million cases) cancer. The most common cancers leading to death were located in the lung (1.76 million deaths), colorectum (862 000 deaths), stomach (783 000 deaths), liver (782 000 deaths) and breast (627 000 deaths). In total, this pathology was responsible for 9.6 million deaths worldwide (World Health Organization, 2020).

Tumors are classed in two groups. On one side, benign tumors are composed of a mass of cells lacking the capability to invade other tissues. They can generally be treated and/or removed without representing a high risk for the patients. On the other side, malign tumors are aggressive due to their capacity to invade the adjacent tissue and to generate metastasis in other organs. Because of their heterogeneity, malign tumors are difficult to treat and represent a real threat for the patient. The process of tumor generation from pre-cancerous lesions to malignant tumors is the consequence of predisposing genetic factors and external carcinogens including physical, chemical and biological agents. The World Heath Organization estimated that 30 to 50% of cancers may be prevented if risk factors (like tobacco, alcohol, unhealthy diet, urban air pollution, …) were avoided in combination with prevention strategies and early diagnosis.

Cancer also represents an economic challenge for countries. In Europe, the total cost of cancer was estimated at 199 billion euros in 2018 (Hofmarcher et al., 2020). The increase of cancer cases each year gradually weight more on country's health care systems as the pathology leads to expenditures comprising cancer drugs, informational care and productivity loss.

The stakes in the fight against cancer are therefore enormous, since the discovery of effective treatments will provide answers to human, social and economic problems.

5.1. Breast Cancer

Breast cancer is one of the deadliest cancer in the world. In 2018, in France, breast cancer was the most common cancer in women with 58,459 new cases and 12,146 deaths. Median ages at diagnosis and death are 63 and 74, respectively (Defossez et al., 2019). Early detection and identification of breast cancer is a key point to treat this disease as the 5-year relative survival rate is around 88% for early breast cancers (Cowppli-Bony et al., 2017). Yet, the survival drops to 20% with the apparition of metastasis (most frequent: bone, lung, pleura, liver, brain (Wang et al., 2019)).

5.1.1. Classical staging of breast cancer

Breast cancer is a complex disease due to its location in a glandular environment regulated by hormones and its propensity to spread into other organs to form metastasis. As a consequence, this pathology has been stratified in different subtypes, depending on the stage of the tumor and of genetic markers, in order to provide the best possible treatment to the patients. One of the most used classification system was introduced by Pierre Denoix in the 1940's (Denoix, 1953) and aims to stratify cancers according to the tumor extent (T), the regional invasion of lymph nodes (N) and the absence or presence of metastasis (M). The TNM system has been improved over years by the International Classification of Diseases for Oncology (ICD-O), thus determining a cancer stage depending on the TNM status ((Bonneterre, 2008),Table 1).

		T status	N status	M status	Stage
T-Tumor		Tis	N0	M0	**0**
T1	Tumor size < 2 cm	T1	N0	M0	**I**
T2	Tumor size > 2cm and < 5 cm	T0	N1	M0	
T3	Tumor size > 5 cm	T1	N1	M0	**IIA**
T4	Tumor growing in the nearby chest or skin tissue	T2	N0	M0	
N-Lymph node		T2	N1	M0	**IIB**
N0	No regional node metastasis	T3	N0	M0	
N1	Movable node metastasis	T0	N2	M0	**IIIA**
N2	Non-movable node metastasis	T1	N2	M0	
N3	Cancer developed in the internal mammary lymph nodes	T2	N2	M0	
M-Metastasis		T3	N1/N2	M0	
M0	No metastasis in distant organs	T4	N0-3	M0	**IIIB**
M1	Metastasis in distant organs	T0-4 T0-4	N3 N0-3	M0 M1	**IIIC** **IV**

Table 1: Staging of breast cancer according to the ICD-10 TNM classification. Note that primary tumor can be absent (T0) or remain as in-situ carcinomas (Tis).

With the development of immunohistochemistry (IHC) and genetic profiling of tumor, breast cancer can also by divided into at least four categories depending of the molecular subtypes: luminal A, luminal B, HER2-positive and basal-like (Perou et al., 2000; Sørlie et al., 2001). IHC and multigene assays are now used to determined steroid hormone receptor (HR) status (estrogen receptor (ER), progesterone receptor (PgR) and human epidermal growth factor receptor 2 (HER2). Cancer cells expressing these receptors can be stimulated by the corresponding hormones, generally leading to tumor growth. In return, HR's are potential target for anticancer therapies (reviewed in (Harbeck et al., 2010)). In addition to the hormone receptor status, tumor proliferation is evaluated by measuring the expression of the antigen Ki67 which is expressed during the cell cycle (Polley et al., 2013). Depending on the subtypes, the HR status and the proliferation index, breast tumors can be categorized as follows: luminal A-like subtype (ER+ or/and PgR+, HER2-, low proliferation); luminal B-like subtype (ER+ or/and PgR+, HER2-, high proliferation); HER2 subtype, non-luminal (HER2+, ER+ and PgR-) or luminal (HER2+ and ER+ or/and PgR+); basal-like subtype (HER2-, ER- and PgR- = triple-negative breast cancer). Depending on the stage of the tumor and the

subtype, different therapeutic approaches are chosen according to the oncologist prognosis and the patient's wishes.

5.1.2. Local and systemic therapies used against breast cancer

Treatment depends on the type of cancer, the location and the health condition of the patient. Over the last decades, comprehension of breast cancer allowed the development of diverse therapeutic approaches involving surgery, radiotherapy, chemotherapy, hormone therapy and targeted cancer drug therapy (reviewed in (Harbeck and Gnant, 2017)).

5.1.2.1. Breast surgery

Until the 80's, total or partial mastectomy was an efficient, but radical, way to remove breast tumors via removing a large piece of breast tissue (Halsted, 1898). Despite the achievement of removing the tumor, the physical and psychological lesions caused to the patients by the operation were important and raised the question of a more conservative surgery (Keynes, 1937). It had been reported that mastectomies lead to several types of deleterious breast deformities for the patients (Berrino et al., 1987). Oncoplastic breast conserving surgery consist of removing as many tumoral tissue as possible together with preserving healthy tissue and allowing breast plastic reconstruction (Gabka et al., 1997). With time, it had been demonstrated that radical mastectomy and conservative surgery accompanied with radiotherapy and / neoadjuvant systemic therapies lead to the same survival rate, confirming the interest of the second method (Clarke et al., 2005; Fisher et al., 2002; Veronesi et al., 2002). Dissection of the axillary lymph nodes is also possible but the benefit of this approach is still controversial and certainly needs more time and studies (Giuliano et al., 2011; Jagsi et al., 2014).

5.1.2.2. Radiotherapy

Radiotherapy is commonly used after breast and lymph node surgery in order to kill remaining cancer cells, thus allowing the application of less aggressive conservative surgery (Fisher et al., 1977). During irradiation, high energy electromagnetic radiation like X-rays, gamma rays and particulate radiation will produce ions in the cells of the irradiated tissues, leading to breakage of chemical bonds and formation of highly reactive free radicals that will

damage molecules, such as DNA. The two mainly used approaches are external beam radiation therapy and brachytherapy (Chand-Fouché et al., 2016; Teymournia et al., 2009). The first technique consists of an external machine focusing radiations on the areas containing cancer cells. The second technique was developed later and is also known as internal radiation. During brachytherapy, a radioactive device is placed in the tumor bed for a short time. Over this period, rays will be generated and will impact the surrounding area. Even though radiotherapy is efficient to kill cancer cells, the risk of side effects and toxicity cannot be neglected as the radiation also impacts healthy cells and tissues (Brown et al., 2015; Darby et al., 2005).

5.1.2.3. Chemotherapy

Chemotherapy relies on the use of chemical agents to cure cancer. Importantly, chemotherapy (as hormone and targeted therapies) constitutes systemic therapies as the anticancer drugs are directly injected into the blood and will circulate in the whole body, potentially impacting many tissues. This way of delivery presents a major advantage as it will affect invasive tumors and distant metastasis that cannot be targeted with surgery and radiotherapy. In 1968, Fisher and colleagues reported the first use of chemotherapy, as an adjuvant alkylating agent (thiotepa) given after radical mastectomy significantly decreased recurrence rate (Fisher et al., 1968). More beneficial effects of chemotherapies combined with surgery on primary tumors and axillary lymph nodes were described over the next ten years, opening the age of combined chemotherapy regimens (Albain et al., 2009; Bonadonna et al., 1976; Mansour et al., 1989). Chemotherapies regimens are divided as first, second and third-generation corresponding to three levels of benefit reached by a regimen (reviewed in (Anampa et al., 2015)). First generation regimens integrate treatments leading to a 35% decrease of mortality compared to no treatment. In the second generation, combinations inducing a decrease of 20% mortality compared to the first generation are included. Finally, third generation chemotherapies are composed of combinations reducing the mortality of 20% compared to the second generation. Most of the combined chemotherapies use molecules from the anthracycline and taxane families. Anthracyclines are derived from the antibiotic rhodomycin B produced by Streptomyces (Hortobágyi, 1997). The two most common anthracyclines are doxorubicin and epirubicin, used to block the DNA replication by inhibiting the enzyme topoisomerase II (Binaschi et al., 1998). While doxorubicin is the most efficient drug against metastatic breast cancer, it also presents a higher toxicity compared to

epirubicin (Torti et al., 1986). Paclitaxel and docetaxel are derived from the taxane molecules that block the cell cycle by inhibiting microtubule depolymerization ((Wani et al., 1971). Like the anthracyclines, taxanes are also efficient against breast cancer metastasis but present a high toxicity (Jones et al., 2005; Sledge et al., 2003). Among the other used anticancer drugs, 5-fluorouracyl must be cited as it is frequently combined with other chemotherapeutic agents in the three generations of regimens. The 5-fluorouracyl is an antimetabolite integrating into the DNA instead of thymidine, thus blocking DNA replication (Cameron et al., 1994). Despite the high efficacy of killing breast tumor cells and metastasis, chemotherapeutic agents are commonly used as adjuvants of therapies presenting a better specificity to the cancer cells.

5.1.2.4. Hormone therapy

Luminal and HER2 breast cancer subtypes may express ER's and PgR's, meaning that estrogen and progesterone can promote cancer progression as the two hormones are naturally produced by premenopausal patients (Tanos et al., 2012). Around two-third of the human breast cancer cell lines express ER's in association with PgR's (Herynk and Fuqua, 2004; Kohler et al., 2015). Hormone therapy (or endocrine therapy) is commonly used as adjuvant during anticancer treatments since breast cancer cells frequently express HR's. Tamoxifen (competitive inhibitor of estrogen) is widely used against ER-positive breast cancers. Several studies demonstrated a reduction of mortality and recurrence after 5 and 10 years of tamoxifen treatment (Davies et al., 2013; Early Breast Cancer Trialists' Collaborative Group (EBCTCG), 2011). However, it had been noted that 10 years of treatments with tamoxifen may cause endometrial cancers and pulmonary embolus. In combination with tamoxifen, aromatase inhibitors can be used as they block the production of estrogen (Arimidex, Tamoxifen, Alone or in Combination (ATAC) Trialists' Group et al., 2008; Early Breast Cancer Trialists' Collaborative Group (EBCTCG), 2011). Yet, this combined therapy can be reinforced by ovarian function suppressors, but it only showed overall survival increase for postmenopausal patients (Gnant et al., 2015). As ovarian function suppression may not be total, chirurgical ablation of ovaries can be performed depending on the patient's wish. Moreover, it had been described that ovaries ablation decreases the risk of breast cancer in patients presenting mutation of the genes *BRCA1* and *BRCA2* (Metcalfe et al., 2015).

5.1.2.5. Targeted therapy

Chemotherapy and hormone therapy have the disadvantage to be unspecific for cancer cells. The objective of targeted therapy is to find and target a marker specific for the tumoral cells in order to decrease as much as possible adverse effects on healthy cells. The best example of targeted therapy is certainly the monoclonal antibody Herceptin® (chemical name: trastuzumab) developed in 1990 and now widely used against HER2+ tumors (Carter et al., 1992). Trastuzumab will inhibit the receptor functions, thus preventing the stimulation of the pro-tumoral PI3K/AKT signaling pathway by epidermal growth factor binding (EGF). In the meantime, trastuzumab can trigger antibody-dependent cellular cytotoxicity (ADCC, (Klapper et al., 2000)). In combination with adjuvant chemotherapies, trastuzumab significantly increase patient survival to HER2+ primary and metastatic breast cancers (Piccart-Gebhart et al., 2005; Romond et al., 2005; Slamon et al., 2001). Some targeted therapies do not aim directly at the tumor cells. Avastin® (chemical name: bevacizumab) is a monoclonal antibody directed against the vascular endothelial growth factor (VEGF) produced by cancer cells and inducing angiogenesis (Banerjee et al., 2007; Hicklin and Ellis, 2005). Since bevacizumab inhibits the formation of new vessels that are vital for the development of the tumors (by providing oxygen and nutrients), this therapy demonstrated promising survival effects for triple-negative and metastatic breast cancers (Miles et al., 2013; Sikov et al., 2015). In recent years, targeting the immune system raised interest since many studies demonstrated a role of the immune response in breast cancer long-term survival (Emens, 2018). Two main targets investigated in the new immune checkpoint therapies are the cytotoxic T-lymphocyte-associated protein 4 (CTLA-4) and the programmed death ligand-1 (PD-L1)(Rotte, 2019). By targeting CTLA-4 with tremelimumab and Ipilimumab, the treatments aim at boosting activation of T-cells during the priming phase of the immune response (McArthur et al., 2016; Vonderheide et al., 2010). Therapeutic approaches against PD-1 signaling aim to counteract T-cell activation during the effector phase of the immune response by inhibiting PD-L1, with avelumab (Dirix et al., 2018) and atezolizumab (Herbst et al., 2014), or the receptor PD-1 with pembrolizumab (Nanda et al., 2016).

The therapeutic arsenal against breast cancer has been in constant evolution over the last decades. Up to date, early breast cancer is generally well responssive. However, survival drastically drops with the apparition of metastasis. As the new targeted therapies demonstrated good effects by aiming at non-tumoral cells, it appears important to investigate

more in details the role of the tumor microenvironment (TME) in breast cancer and anti-cancer therapies.

5.2. Tumor Microenvironment

Tumors can not only be reduced to a mass of cancer cells anarchically proliferating. Malignant cells also interact with the surrounding environment forming an ecosystem with its own properties (Balkwill et al., 2012). This abnormal 'organ' is composed of cancer cells, stromal cells (including fibroblasts, endothelial cells, immune cells, etc.), soluble factors like hormones or immune cytokines and an extracellular matrix (ECM) that provides more than a simple scaffold (Figure 1). Understanding the role of the TME in tumor growth and metastasis formation is crucial to develop new therapies. In breast cancer, it is described that primary tumor location impacts patient's survival, supporting an important role of the environment where cancer cells are growing (Kroman et al., 2003; Sohn et al., 2008). Moreover, it is now well admitted that the local microenvironment can determine the development of metastasis as it was hypothesized by Paget in 1889 with the notion of ''Seed and Soil'' (Paget, 1989). In his theory, S. Paget postulated that the cancer cells, ''the seeds'' can grow only in organs presenting a favorable microenvironment, ''the soil'', as he observed a nonrandom distribution of breast cancer metastasis. Concerning *BRCA1/2*-related carcinomas, it has been demonstrated that the mutations in the tumor cells was associated with a specific genomic instability in the stromal cells, supporting a crosstalk between cancer and stromal cells (Weber et al., 2006). Finally, the impact of the microenvironment on cancer progression has also been described through the role of blood vessels and matrix remodeling (Oskarsson, 2013; Ribatti, 2008). Altogether, this information demonstrates that it is necessary to understand the roles of each component of the TME in order to get a better therapeutical approach for eradicating the tumor.

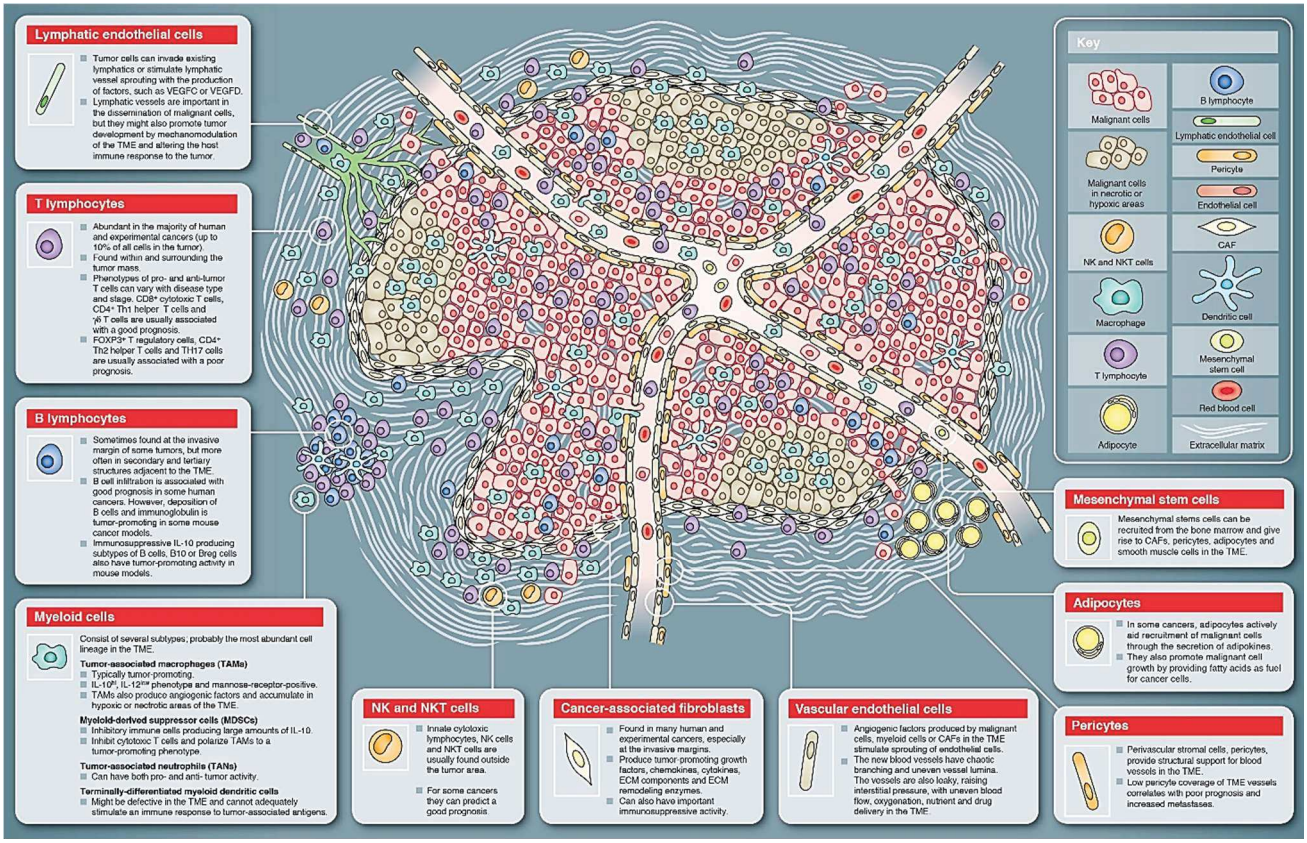

Figure 1: Composition of the tumor microenvironment (adapted from Balkwill et al., 2012).

Tumor cells are proliferating in the tissue, accompanied by infiltrating fibroblasts and immune cells. Other stromal cells like endothelial cells and adipocytes are also impacted and contribute to tissue remodeling by forming new blood vessels and supplying cancer cells. The ECM is completely reorganized due to matrix degradation and production of new matrix proteins.

5.2.1. Cancer cells

The main protagonists in a tumor are the cancer cells. Malignant cells are originally normal cells that have escaped genetic control and are now outside the cell development cycle of their tissue of origin. The alteration of tumor suppressor genes and oncogene expression lead to the acquisition of pro-tumoral properties originally described as the first of the six hallmarks of cancer (Figure 2, (Hanahan and Weinberg, 2000)). A decade later, the understanding of cancer cells development lead to modify the hallmarks by adding new parameters. The new essential hallmarks of cancer were then evading growth suppressors, avoiding immune destruction, enabling replicative immortally, tumor promotion inflammation, activating invasion and metastasis, inducing angiogenesis, genome instability and mutation, resisting cell death, deregulating cellular energetics, sustaining proliferative signaling (Figure 2, (Hanahan and Weinberg, 2011)). More recently, the role of the TME has been well

recognized as an additional overarching hallmark of cancer supporting cancer cell development (Fouad and Aanei, 2017; Hanahan and Weinberg, 2017).

Breast cancer cells are characterized by a genetic background containing specific molecular alterations (Geyer et al., 2009). Interestingly, some of these alterations are now used as biomarkers in order to classify the different types of breast cancer (review in (Rakha et al., 2010)). Among these biomarkers, the most used are certainly the HR to estrogen and progesterone, and HER2. For research, many breast cancer cell lines have been established over time from the different subtypes of cancer. If the cell lines are commonly used as breast cancer models, some studies recently raised controversial questions about the correspondence between cellular models and the pathology (Dai et al., 2017; Neve et al., 2006).

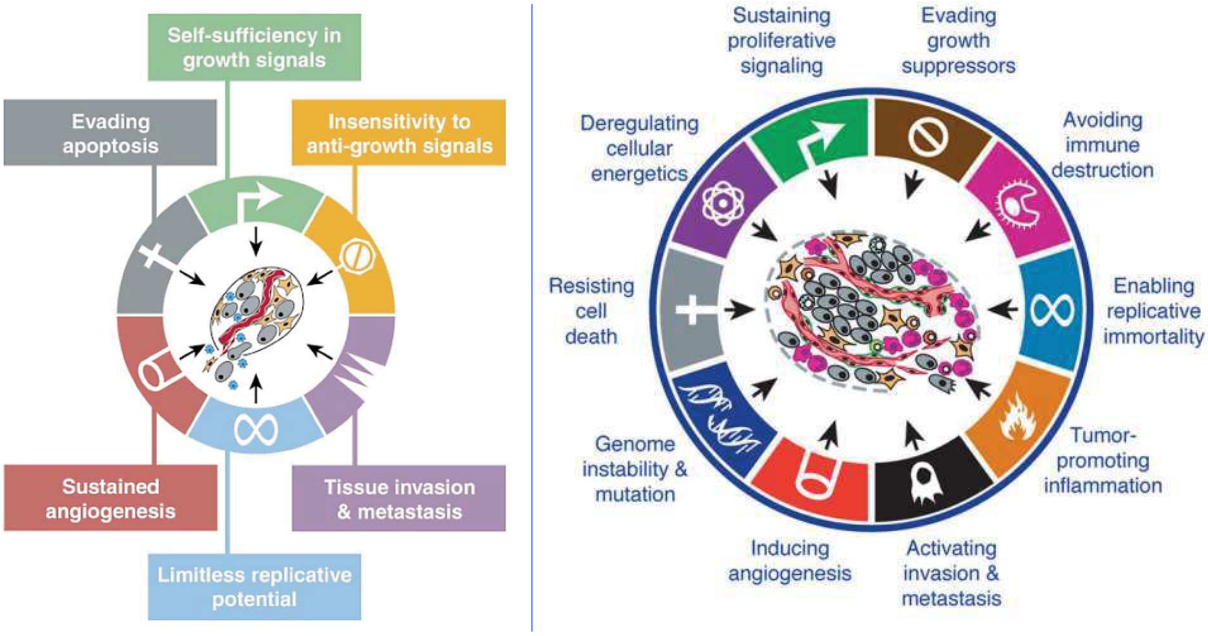

Figure 2: The Hallmarks of cancer: old and next generation (adapted from Hanahan and Weinberg, 2000 and 2011).

Left panel: the original hallmarks of cancer described as the functional capabilities acquired by most of the cancer cells during their development. Right panel: the new hallmarks of cancer integrate more specific internal characteristic and interaction with the TME via the immune cells.

5.2.2. Stromal cells

By the term tumor stroma, cells matrix and soluble factors are described. The stromal cells populations are mainly fibroblasts, endothelial cells (forming blood and lymphatic vessels) and immune cells (Mueller and Fusenig, 2004). As it is now clear that the stroma plays a key role in breast cancer progression, it is important to describe the major stromal cells types.

5.2.2.1. Cancer associated fibroblasts

Fibroblasts are the most represented cell type in the connective tissue and are responsible for the architecture of the tissue by secreting and remodeling ECM molecules (Gabbiani et al., 1971). Fibroblasts are activated during wound healing and fibrosis, two processes that resemble to the stages of early cancer development in term of matrix modeling. Since activated fibroblasts share similarities during wound healing and cancer, the second cell category is designated as cancer associated fibroblast (CAF) in order to differentiate these fibroblasts from normal activated fibroblasts (Dvorak, 2015). The origin of the CAFs is not clear and several hypotheses remain. CAFs may be activated resident fibroblasts (Kojima et al., 2010; Moskovits et al., 2006), bone-marrow-derived mesenchymal stem cells (Spaeth et al., 2009) or cancer cells that have undergone epithelial-to-mesenchymal transition (EMT) (Kalluri and Zeisberg, 2006). Moreover, other sources of CAFs have been described, like endothelial cells undergoing endothelial-to-mesenchymal transition (EndMT) (Zeisberg et al., 2007). In breast cancer, high expression of alpha smooth muscle actin (α-SMA), fibroblast specific protein-1 (FSP-1) or fibroblast activation protein (FAP) is generally used as a marker of CAF (Loeffler et al., 2006; Shiga et al., 2015). However, CAFs can also be heterogenous depending on the cancer subtype (Tafani et al., 2010). Accumulating studies show pro-tumoral roles of CAFs in breast cancer progression. Firstly, high infiltration of tumors with CAFs is associated with bad prognosis and metastasis formation in invasive ductal carcinoma (Hasebe et al., 2001). CAFs can also promote cancer cell growth and angiogenesis through the secretion of stromal cell-derived factor 1 (SDF-1,=CXCL12) (Orimo et al., 2005). An other study demonstrated that transient interaction between cancer cells and CAFs induced the production of the transforming growth factor beta (TGFβ), thus increasing tumoricity *in vivo* (Stuelten et al., 2010). The interaction between breast cancer cells and CAFs has also been observed through a crosstalk mediated by the chemokine ligand 2 (CCL2) as fibroblasts are

recruited and activated by CCL2 secreted by the tumor cells, that produce in return more CCL2 leading to metastasis formation ((Tsuyada et al., 2012). Finally, CAFs facilitate invasion of cancer cells via ECM remodeling through increasing matrix metalloproteinase MMP14 expression and MMP9 activity (Hu et al., 2008). The roles of the ECM secreted by the CAFs will be discussed in section 5.2.4.

5.2.2.2. Vascular cells

Cancer cells, as most of the normal cells, need nutrients and oxygen to survive. During epithelial tumor development, the need of nutrients will grow will increasing tumor size. Moreover, as the size increases, the center of the tumor is more and more distant from the original blood vessel, generating the phenomenon of hypoxia (Petrova et al., 2018). Angiogenesis is then required for tumors bigger than 1-2 mm in diameter (Ribatti, 2008). Angiogenesis has been quickly identified as a promoter of cancer progression and is listed as a hallmark of cancer (Hanahan and Weinberg, 2000). The formation of new blood vessels requires in particular the recruitment of endothelial cells and pericytes, under the control of soluble pro-angiogenic factors as vascular endothelial growth factors (VEGFs) (Claesson-Welsh and Welsh, 2013). In fact, VEGF receptors (VEGF-R2 and VEGF-R3) have been localized, and observed as upregulated, on tumor blood vessels, supporting the pro-tumoral role of angiogenesis in tumor growth (Smith et al., 2010). In breast cancer, several targeted therapies using antibodies (like bevacizumab, ramucirumab or olaratumab) have been developed in order to target angiogenesis, and demonstrated positive effects on patient survival (reviewed in (Kong et al., 2017)). The targeting of blood vessels in cancer is difficult as on one hand, the disruption of nutrient and oxygen supplies will affect tumor growth, on the other hand, it can also affect the delivery of anticancer therapeutics (Stylianopoulos and Jain, 2013). Tumors also contain lymphatic vessels, formed by lymphatic endothelial cells (LECs), that play a role in tumor progression. Lymphatic vessels can expand through VEGFD/E signaling and impact cancer progression and survival prognosis. In the TME, LECs can promote immune tolerance leading to cancer progression (Lund et al., 2012). Moreover, lymphatic vessels are open doors to cancer cell dissemination and metastasis formation (Ma et al., 2018). In breast cancer, a crosstalk has been described between cancer cells and LECs through the pro-lymphangiogenic factor COX-2 and β1-integrin receptors, promoting lymphangiogenesis and metastasis (Black et al., 2016; Elder et al., 2018). In a near future,

specific targeting of the lymphatic vessels may give new therapeutic opportunities (Yamakawa et al., 2018).

5.2.2.3. Immune cells

The immune response in cancer is widely studied since it is known that the activity of the immune cells is important during the initiation and tumor progression (Dunn et al., 2002). The interaction between cancer cells and the immune system has been divided into three phases referred as the “three Es” of cancer immunoediting (Elimination, Equilibrium and Escape, (Dunn et al., 2004)). In the first step of cancer development, the abnormal cells will be detected and destroyed by the innate immune system, and in particular by natural killer (NK) cells. This initial phase of elimination, that occurs due to the immunosurveillance, normally leads to the eradication of cancer cells before they become a threat, but NK cells can also be involved in the development of a tumor due to the selection pressure imposed on the cancer cells by the immune response (Tu et al., 2017). As some cancer cells survive while others die, the immune response entered into the equilibrium phase. Finally, as the selection pressure is high, more cancer cells will develop resistance that will help to escape the immune system and make the immune response ineffective.

In terms of immune cells infiltrating the breast cancer TME, the immune response is composed of NK cells, innate lymphoid cells (ILCs) and myeloid cells comprising granulocytes, macrophages (MPs), and dendritic cells (DCs) forming the innate response; while B and T-cells are forming the adaptive immune response (Edechi et al., 2019). In spontaneous breast cancer mouse models, it was described that ILCs play an important role in the immunosurveillance as mice lacking these cells developed rapidly aggressive tumors (Dadi et al., 2016). It has also been demonstrated that breast tissue is more infiltrated by myeloid cells in presence of mammary tumors (Toor et al., 2017). However, these infiltrating myeloid cells can exhibit immune suppressive properties and produce pro-tumoral factors, like the cytokine thymic stromal lymphopoietin (TSLP), that increases tumor progression (Bronte et al., 2016; Kuan and Ziegler, 2018). Moreover, soluble factors secreted by tumor cells can affect MPs. This population of myeloid cells called tumor associated MPs (TAMs) is classically divided into antitumoral M1 and pro-tumoral M2 MPs depending of their activation in the tumor (Mantovani et al., 2006). For example, M1 MPs can secrete interleukin 12 (IL-12) and tumor necrosis factor alpha (TNFα) that induce inflammation and tumor rejection. On

the opposite, M2 MPs usually secrete IL-10 and TGFβ that have an immunosuppressive effect and promote tumor progression (Allavena et al., 2008). Following the activation of the innate system, cells from the adaptive system also play an important role in tumor control. T-lymphocytes are a major part of immune infiltrating cells. Briefly, T-cells are divides into two groups (according to the expression of the T-cell receptors (TCRs)) composed of CD8+ cytotoxic T-cells and CD4+ helper T-cells (which are further subdivided into Th1, Th2, Th17 and Treg cells). It had been demonstrated that both groups can have pro- and antitumoral effects (DeNardo et al., 2009; Grivennikov et al., 2010; Kuan and Ziegler, 2018). Finally, B cells have mostly a role as immune response regulators in breast cancer (Shen et al., 2018). The role of B cells still remains controversial as they have been associated with a better disease-free survival and with factors of poor prognosis (such as HRs negative tumors) and with lymph node metastasis (Guan et al., 2016; Mao et al., 2016).

5.2.2.4. Other cell types

Normal breast tissue is mainly composed of adipocytes that play an important role in energy balance. Furthermore, breast tissue also contains nerves, and therefore neurons. Since these two cell types can be in contact with tumor cells during breast cancer development, one can consider that they play a role during tumor progression. For instance, adipocytes can impact tumor progression via the release of hormones, cytokines and their metabolic substrates (Chu et al., 2019). For example, it has been demonstrated that adipocytes can promote breast cancer proliferation, metastasis formation and angiogenesis through the secretion of very low density lipoproteins (VLDL) and LDL (Lu et al., 2017). Moreover, adipocytes can secrete cytokines such as IL-6, IL-8, IFN_{γ}-inducible protein 10, CCL2, and CCL5 that can increase early tumor development and metastasis (Picon-Ruiz et al., 2016). Concerning neurons, the conformation of the nerves affects breast tumors, as the thickness of nerve fibers can be used as prognostic factor in patients (Huang et al., 2014). One study also revealed a crosstalk between nerves and cancer cells via the exchange of neuromodulator molecules responsible of neuroplasticity, new nerve formation and neuropathic pain sensation in pancreatic cancers (Demir et al., 2012).

Given the normal roles of stromal cells in tissue homeostasis, it is not surprising to find multiple interactions between breast cancer and stromal cells. From matrix remodeling fibroblasts to immune cells, it is now well admitted that cancer cells can corrupt/redirect the

function of other cell types present in the TME. Despite a direct interaction mediated by receptors, the communication between cells is frequently done via secreted molecules highly abundant in the TME.

5.2.3. Soluble factors

Each cell type has its own signaling arsenal and secreted factors. From cell growth to killing, the TME is composed of a large quantity of soluble molecules regulating, or deregulating, the tissue. Among these factors, some families are particularly important during tumor development, like hormones, cytokines and secreted enzymes. As previously described, hormones play a significant role in breast cancer. Beyond estrogen, progesterone and EGF, other hormones can impact the proliferation of cancer cells. In breast cancer, growth hormone (GH) plays a role in tumor development as silencing the growth hormone receptor (GHR) inhibits chemoresistance and metastasis formation in ER- cancer (Arumugam et al., 2019). In addition, high levels of stress hormones cortisol and corticosterone, accompanied with overexpression of glucocorticoid receptors (GRs) have been associated with cancer aggressiveness and low survival (Obradović et al., 2019). Finally, the potential role of insulin on cancer development is still under debate and represents a major topic as a significant part of the population is subject to diabetes (Yee et al., 2020). Cytokine families represent a major part of the soluble factors disseminated in the TME. These molecules are mostly expressed by immune cells but can be also produced by other stromal cells and even cancer cells (Chow and Luster, 2014; Nicolini et al., 2006). Immune cytokines and chemokines can regulate immune cell activation and chemotaxis, or even trigger cell death and inflammation. For instance, numerous chemokines and their corresponding receptors have been associated with breast cancer progression, like CCL21/CCR7, or CXCL12/CXCR4 (Karagiannis et al., 2020; Rizeq and Malki, 2020). Moreover, immune cells naturally produce antitumoral cytokines belonging to the tumor necrosis factor (TNF) superfamily in order to clean the tissues from abnormal cells like cancer cells or microbe-infected cells (Aggarwal, 2003). Among these molecules, TNF-related apoptosis-inducing ligand (TRAIL) represents an opportunity to target breast cancer and will be presented in more details in section 5.4. The last important class of soluble factors includes enzymes, and in particular matrix remodeling enzymes such as cathepsins and MMPs. Cathepsins have several described roles in breast cancer development including the regulation of tissue remodeling, angiogenesis and cell proliferation, as well as cancer

progression and metastasis (Gocheva and Joyce, 2007). It has been shown that altered expression of cathepsins D and B was associated with poor prognosis (Sun et al., 2016). Furthermore, MMPs, that are known to degrade proteins of the ECM, play a major role in cancer cell dissemination, spreading and metastasis (Duffy et al., 2000).

5.2.4. Extracellular Matrix

Decades ago, the ECM was reduced to only macromolecular fibrous proteins. However, the ‘’matrisome’’ also includes non-fibrous proteoglycans and ECM-regulating enzymes that shape every tissue (Hynes and Naba, 2012). The network of matrix proteins is specific to the tissue and is evolving under the control cells producing the matrix and soluble factors degrading fibrous proteins, such as MMPs. The ECM is present in the thin layers forming basement membranes and in more relaxed fibrous structures constituting the interstitial matrix (Theocharis et al., 2016). Despite its basic description as a scaffold structuring the cellular organization, the ECM interaction with cells activates intracellular signaling modulating cell behavior (Bissell et al., 1982; Ghajar and Bissell, 2008). The main fibrous ECM proteins are collagens, elastins, fibronectin (FN) and laminins (LMs) (Frantz et al., 2010). Collagens alone have effects on cell adhesion, chemotaxis, migration and tissue development due to their wide expression in the body (up to 30% of proteins mass, (Rozario and DeSimone, 2010)). It is now well described that the interactions between ECM proteins and cells are mediated by receptors from the integrin family, allowing the activation of intracellular signaling pathways and cytoskeleton reorganization (Harburger and Calderwood, 2009).

Cancer can be seen as a wound that never heals by generating a constant reorganization of the matrix fibers of the TME. Tissue remodeling modifies the physical forces applied to the cells, thus impacting cell behavior and promoting carcinogenesis (Butcher et al., 2009). Furthermore, ECM molecules can also act as reservoirs for soluble factors like VEGF and TGFβ that are known for their pro-tumoral properties (Griggs et al., 2017; Wijelath et al., 2006). Overexpression of collagen during early development of a tumor induces dense fibrotic tissue in the mammary gland that can be detect by mammography imaging, therefore reveling the presence of breast cancer (Ursin et al., 2005). Moreover, recent studies demonstrated the effects of FN expression and fibril formation on the interaction of tumor cells with fibroblasts, promoting breast cancer development (Berger et al., 2020; Libring et

al., 2020). In addition, different isoforms of LM also regulate tumor progression (Carpenter et al., 2018; Chia et al., 2007; Pal et al., 2014). Last but not least, growing evidence show that the matricellular protein tenascin-C (TNC) is an important factor of poor prognosis in breast cancer (Oskarsson et al., 2011).

5.3. Tenascin-C

The hexameric extracellular glycoprotein TNC (also known as cytotactin) has been discovered in the 1990's (Bourdon et al., 1983; Chiquet and Fambrough, 1984; Erickson and Inglesias, 1984; Grumet et al., 1985). TNC was initially observed in human gliomas surrounding the vasculature and thus defined as a glioma-mesenchymal extracellular matrix (GMEM) antigen (Bourdon et al., 1983), and as myotendinous antigen (Chiquet and Fambrough, 1984) altogether reflecting expression at different sites.

5.3.1. Structure and expression

TNC belongs to the tenascin family that includes tenascin-R, -W and -X (Chiquet-Ehrismann and Tucker, 2011). Monomers of TNC are composed of several domains including an N-terminal assembly domain, an epidermal growth factor-like (EGF-L) domain containing 14.5 EGF-L repeats, which are adjacent to an assembly of 17 fibronectin type-III (FNIII) domains (8 constant and up to 9 spliced in domains). Finally, the C-terminal fibrinogen-like globe (FBG) completes a monomer (Figure 3). Alternative FNIII-like domains can be spliced in and added between the fifth and sixth FNIII-like domain, allowing the generation of TNC isoforms with different molecular weight (Guttery et al., 2010). TNC isoforms are tissue specific (Lowy and Oskarsson, 2015). For example, TNC isoforms containing the FNIII A1, C and D repeat are frequently found in tumor tissue (Brack et al., 2006; Frantz et al., 2010). The molecular weight of TNC can range between 190 and 330 kDa, depending on the alternative splicing and glycosylation (Taylor et al., 1989).

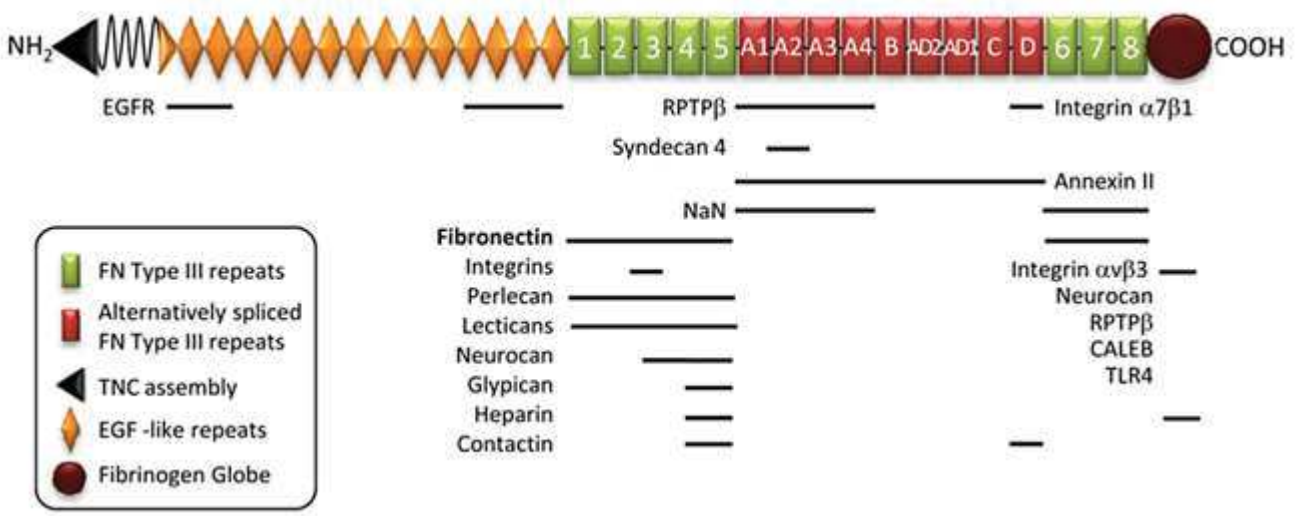

Figure 3: Tenascin-C structure and interacting molecules (adapted from Obberghen-Schilling et al., 2011).

TNC is composed of four types of domains: the NH_2-assembly domain, several EGF-L domains, followed by FNIII-like domains and the C-terminal FBG. Locations of binding sites within TNC and interacting molecules are shown.

Six monomers of TNC can assemble into a hexamer, called hexabrachion, due to the sequential assembly of trimers through the N-terminal domains (Kammerer et al., 1998). Using pulse chase labeling of glioma cells, it had been described that newly synthetized TNC is quickly assembled into hexamers, even before the transport through the Golgi (Redick and Schwarzbauer, 1995). Then after secretion, the multimerization of TNC responsible of the formation of extracellular fibrillar tracks is permitted by cysteines, notably the residues 64, 111 and 113 (Chung and Erickson, 1997; Chung et al., 1995). Finally, TNC can be cleaved by MMPs, notably by the MMPs-1, 2, 3 and 7 (Giblin and Midwood, 2014; Vyavahare et al., 2000) and degraded by the proteasome during autophagy (Li et al., 2020).

TNC expression can be stimulated by many signaling pathways and is executed by several transcription factors. For instance, signaling by TLR4/NFkB, TGFβ/Smad3/4, PDGF/Ets, c-Jun/NFkB, Sox4 and Notch, can upregulate TNC transcription (Goh et al., 2010; Jinnin et al., 2004; Mettouchi et al., 1997; Scharer et al., 2009; Sivasankaran et al., 2009). In the opposite, only a few signaling pathways are described to downregulate TNC. It has been reported that the transcription factor GATA6 and corticoids are able to inhibit TNC expression and its associated downstream signaling (Chiquet-Ehrismann and Chiquet, 2003; Ghatnekar and Trojanowska, 2008).

5.3.2. Physiological roles of Tenascin-C

TNC is mostly expressed during embryogenesis and embryonic organ development whereases after birth, ECM containing TNC remains confined to specific areas (Chiquet-Ehrismann et al., 2014). Brain, thymus, breast and lung are the organs presenting the higher expression of TNC during embryogenesis (Saga et al., 1992). TNC seems to play a major role in the nervous system development and organization as mice lacking TNC presented abnormal response to stress and injuries (Nakao et al., 1998). For instance, TNC is expressed around neurons and glial cells (Faissner, 1997). In addition, mice with a TNC knockout (KO) showed hyperlocomotion and poor swimming ability that may be explained by a lack in myelinization and in oligodendrocytes maturation (Fukamauchi et al., 1996; Kiernan et al., 1999). Moreover, lack of TNC leads to an abnormal development of the hippocampus (Gurevicius et al., 2009; Rigato et al., 2002). TNC expression has also been reported around epithelia in growing kidneys, teeth and hair follicles, suggesting a role in epithelial organ morphogenesis (Chiquet, 1992).

In adult tissues, TNC is rare and its expression is mostly reduced to tissues submitted to high tension like tendons, ligaments and smooth muscles (Fluck et al., 2000). New expression of TNC has also been reported in epithelia, such as in the kidney medullary stroma and in stem cells niches (Aufderheide et al., 1987; Chiquet-Ehrismann et al., 2014; Talts et al., 1997).

TNC plays an important role during several phases of tissue repair following injuries like incision wounds, skin photo-damage or tendon rupture (Betz et al., 1993; Filsell et al., 1999; Riley et al., 1996). TNC mRNA and proteins are quickly detected after tissue damages (Latijnhouwers et al., 1996; Seité et al., 2000). Interestingly, it had been reported that TNC molecules can be concentrated close to sites of high immune cell infiltration during acute inflammation (Seyger et al., 1997). A potential role of TNC on the immune response during wound healing has been suggested since it stimulated lymphocyte migration via promoting adhesion and rolling of the cells (Clark et al., 1997). Moreover, immune infiltration was reduced during tissue repair when TNC was not expressed in mice During tissue repairing, keratinocytes produced TNC that in return stimulated cell proliferation and migration (Ishii et al., 2008; Latijnhouwers et al., 1996). As the tissue was rebuilding, TNC accumulated at wound edges of the dermis and in granulation tissue (Betz et al., 1993; Mackie et al., 1988). In kidney experimental injury, immature granulation tissue was observed in case of low levels

of TNC, indicating that TNC was required for complete tissue repair after injury (Nakao et al., 1998).

5.3.3. Pathological roles of Tenascin-C in cancer

Despite an expression relatively low and localized, TNC is normally not a major component of the ECM in adult tissues. However, under pathological conditions inducing inflammation and wound healing-like processes, TNC is highly re-expressed and can play major roles in the development of the disease. As a matter of fact, it had been well described that TNC orchestrates many mechanisms occurring during cancers development, and in particular in breast cancer (reviewed in (Orend et al., 2014)). For instance, it had been described that TNC is overexpressed in breast cancer tissue compared to normal mammary tissue (Figure 4A, (Degen et al., 2007)). Moreover, the isoforms containing the FNIII domains B, D and AD1 seem to be more frequent is this cancer type (Adams et al., 2002; Derr et al., 1997). In term of tumor development, TNC is quickly expressed in the tumor stroma surrounding the tumors, in particular in the invasion fronts (Figure 4B, (Jahkolal et al., 1998; Oskarsson et al., 2011)). TNC has also been associated with lung tumor aggressiveness causing lung metastasis (Figure 4C, (Oskarsson et al., 2011; Sun et al., 2019)). Even if the roles of TNC are not yet well understood in every types of tumor, it is now clear that TNC is a factor of poor prognosis in many cancers, including breast cancer (Ioachim et al., 2002; Ishihara et al., 1995; Ming et al., 2019). As TNC can impact several processes during breast cancer development, I will describe in more details the roles of TNC in some of the major mechanisms driving mammary carcinoma lung metastasis formation.

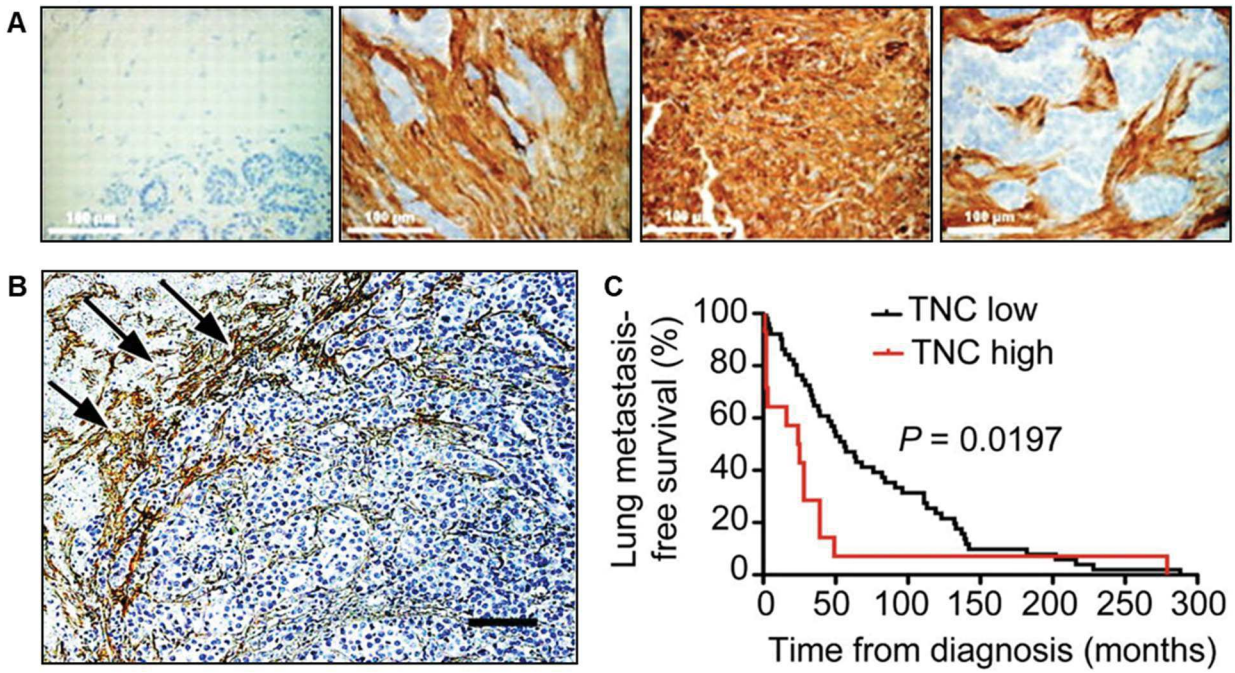

Figure 4: Tenascin-C is a factor of poor prognosis in breast cancer (adapted from (A) Degen et al., 2007; (B, C) Oskarsson et al., 2011).

(A) IHC images showing the expression of TNC in human mammary tissue. Left image shows healthy tissue whereas the three next pictures are from breast cancer tissue. Scale bar 100µm. (B) IHC image pointing at TNC expression at the invasive front of human lung metastasis. Scale bar 50µm. (C) Kaplan-Meier curses representing lung metastasis-free survival after breast cancer diagnosis in patients expressing high or low levels of TNC.

5.3.3.1. Adhesion

In the TME, TNC participates in the formation of composite matrix fibers called tumor matrix tracks (TMT). It is well described that the composition of these TMT will influence processes like migration and invasion, depending on the cells adhesion on the matrix proteins composing the TMT (Walker et al., 2018). The role of TNC in adhesion has been intensively studied in context with FN. In fact, TNC and FN are frequently coexpressed in cancer, including breast cancer (Obberghen-Schilling et al., 2011). Interestingly, TNC and FN have opposite effects on cell adhesion. Firstly, it has been described that FN coating promotes cell adhesion (Chiquet-Ehrismann et al., 1988). Moreover, focal adhesions and actin filament stabilization are induced by FN, notably through its interaction with integrin α5β1 (Murphy-Ullrich et al., 1991; Spring et al., 1989). In these three examples, it has been demonstrated that TNC can block the described effects of FN. The impact of TNC on cell spreading and focal adhesion has been observed on breast cancer cell lines like MDA-MB-435 or MCF-7 (Chiquet-Ehrismann et al., 1989; Tôkés et al., 2000). The study of TNC and FN properties in

cell adhesion revealed an important binding site between TNC and FN. By using heparin and syndecan-4, two molecules binding the FNIII13 repeat of FN, it has been demonstrated that the anti-adhesive properties of TNC toward FN were removed (Huang et al., 2001; Ingham et al., 2004). Moreover, the role of FNIII13 as a binding site for TNC was supported via restoring cellular adhesion on a coating of FN/TNC with specific peptides mimicking the cationic cradle of FNIII13 (Bloom et al., 1999; Huang et al., 2001). As TNC modulates cell adhesion on TMT, several signaling pathways are differentially regulated, such as Wnt signaling promoting tumor growth (Ruiz et al., 2004; Saupe et al., 2013).

5.3.3.2. Migration / Invasion

TNC is known to stimulate cell migration and invasion of many cell types including fibroblasts (Tamaoki et al., 2005; Wenk et al., 2000), endothelial cells (Langlois et al., 2014; Rupp et al., 2016) and cancer cells (Orend and Chiquet-Ehrismann, 2006; Saupe et al., 2013; Tavazoie et al., 2008). Concerning breast cancer, TNC stimulated cancer cell (T47D, MCF-7, MDA-MB-231, MDA-MB-468 and GI-101) migration and invasion involving MMP-13 that was increased and could lead to ECM degradation (Hancox et al., 2009). Increased cancer cell invasion was also observed after MMP-9 and MMP-12 overexpression by TNC (Ilunga et al., 2004; Sarkar et al., 2006). TNC pro-migratory and pro-invasion signaling has been studied in osteosarcoma *in vitro* and *in vivo* models. Involving integrin α9β1, TNC can interfere with YAP/TAZ transcriptional regulator signaling and promote amoeboid cell migration, promoting lung metastasis formation (Sun et al., 2018).

Moreover, TNC induced EMT as evidenced by high vimentin (Vim) and β-catenin, and low E-cadherin (E-Cad) levels promoting breast cancer progression (Dandachi et al., 2001; Nagaharu et al., 2011). TNC-induced EMT is not clearly defined but it is important to understand since this phenomenon is one of the major mechanism potentially leading to metastasis development (Dongre and Weinberg, 2019). It has been described that TNC induces an EMT-like phenotype in MCF-7 cells (Nagaharu et al., 2011). In addition, it was observed that the FBG domain of tenascin-X, that is homologous to the C-terminal domain of TNC, can trigger EMT-like changes in normal epithelial mammary cells (NMuMG) via TGFβ signaling activation (Alcaraz et al., 2014). Indeed, in the MMTV-NeuNT breast cancer model (Muller et al., 1988), our previous work demonstrated that TNC promotes breast cancer micro

metastasis invasions in the blood circulation leading to lung metastasis via activating EMT-induced TGFβ signaling (see Appendix I, (Sun et al., 2019)).

5.3.3.3. Proliferation / Survival

It is not a coincidence that four out of the six initial hallmarks of cancer were related to cell proliferation and survival (Figure 1). Cancer cells are by definition capable to overtake the natural regulation of these two processes. The role of TNC inducing breast cancer cell proliferation was quickly described after the discovery of TNC (Chiquet-Ehrismann et al., 1986). It was described later that adhesion of tumor cells on a FN/TNC substratum blocking syndecan-4 / integrin α5β1 mediated signaling promoted cell proliferation (Huang et al., 2001). However, the opposite effect was observed in anchorage dependent fibroblasts (MRC-5, REF52 and NIH3T3) where a FN/TNC substratum inhibited cell cycle progression (Crossin, 1991; Orend et al., 2003). Interestingly, reconstituted basement membranes containing TNC triggered proliferation of non-cancerous MCF-10A mammary cells in 3D (Taraseviciute et al., 2010). In this study, cell expansion signaling was triggered by c-met signaling, altogether supporting a pro-tumoral role of TNC through an impact on cell proliferation.

It was described in melanoma, mammary and neuroblastoma cell culture models that TNC promotes the growth of oncospheres preferentially via stimulating cancer cell survival instead of proliferation (Fukunaga-Kalabis et al., 2010; Oskarsson et al., 2011; Pezzolo et al., 2011). Indeed, in a 4T1 model of lung metastasis, it has been demonstrated that TNC producing a metastatic niche by stromal cells promotes cancer cell survival and resistance to apoptosis (O'Connell et al., 2011; Oskarsson, 2013). Moreover, TNC can stimulate the ERK/NFkB signaling pathway that is known to protect cells against apoptosis (Shi et al., 2015). As TNC stimulates an EMT-like plasticity, it has been described that both canonical and non-canonical TGFβ pathways were activated by TNC and lead to cell death resistance (Sun et al., 2019), altogether suggesting several mechanisms by which TNC could support tumor cell survival.

5.3.3.4. Angiogenesis

During tumor growth, the supply of nutrients and oxygen becomes vital for survival of the cancer cells located deep inside the tumor mass. For instance, the impact of TNC on angiogenesis has not been intensively studied in breast cancer. In non-pathological

conditions, TNC is generally not expressed in blood vessels and angiogenic tissues (Kimura et al., 2014; Martina et al., 2010; Mustafa et al., 2012). However, TNC can be locally expressed around blood vessels in the TME of glioblastoma and non-small cell lung cancer (NSCLC) (Ishiwata et al., 2005; Martina et al., 2010). Importantly, TNC exerts multiples effects on endothelial cell adhesion, proliferation, migration and tube formation. For instance, TNC can interact with integrins α2β1 and αvβ3 on endothelial cells and induce a sprouting phenotype activating angiogenesis (Canfield and Schor, 1995). Moreover, it has been described that TNC promotes the formation of new leaky blood vessels in a pancreatic cancer model (Saupe et al., 2013). In fact, by deregulating Wnt signaling, TNC induced the generation of new blood vessels presenting morphological anomalies like break points and contractions. In addition, TNC promoted angiogenesis by increasing pro-angiogenic factors expression like Ephrin-B2 and VEGF (Rupp et al., 2016; Tanaka et al., 2004). Interestingly, whereas Ephrin-B2 stimulated endothelial cells survival and proliferation leading to tubulogenesis ; the direct contact of endothelial cells with TNC induced apoptosis and the formation of holes in the new vessel tubes (Rupp et al., 2016). The combination of these two effects triggered the growth of new leaky vessels associated with glioblastoma development.

5.3.3.5. Immunomodulation

Even if ECM shapes every tissue constituting our body, the study of the interactions between matrix proteins and the immune response is not old. Recently, attention has grown on the regulation of inflammation by the ECM (Sorokin, 2010). Since it is now described that matrix proteins and MMPs play major roles in cytokines regulation and immune cells migration (Cauwe et al., 2007; Morrison et al., 2009; Vestweber, 2007), potential immunomodulatory roles of the ECM are also investigated during cancer development. Concerning TNC, it has been demonstrated that inflammation processes triggers its expression. For instance, in rheumatoid arthritis, TNC expression rises where TNC enhances the effects of chronic inflammation by interacting with toll-like receptor 4 (TLR4), via the FBG, on MPs (Midwood et al., 2009; Piccinini and Midwood, 2012). In response, the activated MPs produce cytokines such as IL-6, IL-8 and TNFα that increase the destruction of the joints. Since TNC presented the same effects via involving integrin α9β1 (Asano et al., 2014), it was postulated that TNC may by recognized by the immune cells as a danger associated molecular pattern (DAMP) molecule (Goh et al., 2010; Midwood et al., 2009).

In a prostate cancer model, TNC inhibited the early interaction between cancer cells and T-cells (Jachetti et al., 2015). Interestingly, it was observed that the TNC produced by cancer cells also decreased the proliferation of the T-cells by inhibiting the actin polymerization through integrin α5β1 interaction. In the MMTV-NeuNT breast cancer model, it was recently shown that TNC promoted tumor development by priming TAMs toward a M2 phenotype (see Appendix II, (Deligne et al., 2020)). Once again, MPs were activated via a TLR4-FBG interaction. In this study, the prominent role of TNC was demonstrated by using an anti-FBG antibody that exerted a better therapeutic effect than anti-PD-L1 antibody on tumor growth and lung metastasis. As the M2 phenotype was inhibited by the anti-FBG antibody, more cytotoxic T-cells were infiltrating the tumors, indicating that blocking TNC immunomodulatory effects could reactivate immunosurveillance. In a second study using MMTV-NeuNT mice and the novel NT193 breast cancer cell line derived from a MMTV-NeuNT mammary tumor (Arpel et al., 2014), TNC promoted tumor growth through disrupting CXCL12/CXCR4 signaling and preventing cytotoxic T-cell infiltration into the tumor nests (Murdamoothoo et al., in revision). We observed that CD8+ lymphocytes are immobilized by TNC in the TMT, where NT193 cells secreted CXCL12.

Finally, we also described an impact of TNC on DCs activation and functions in a murine 4NQO-induced oral squamous cell carcinoma (OSCC) model (see Appendix III, (Spenlé et al., 2020)). We demonstrated that TNC triggered the formation of an immune suppressive lymphoid stroma via CCL21/CCR7 signaling supporting the development of tongue tumors and lymph node metastasis. In fact, dendritic cells were immobilized in the TMT. In contrast to DCs, Treg cells infiltrated more the tumor nest in tumors expressing TNC than lacking TNC. As DCs express CCR7, we investigated the role on TNC in CCL21/CCR7 interaction and we observed that TNC binds CCL21, leading to DCs immobilization. In addition, TNC also induced the secretion of immune suppressive cytokines like IL-10 that promote tumor development (Spenlé et al., 2020).

TNC seems to play an important role in the immune response due to its interactions with immune cytokines. While TNC can act as a DAMP, promoting inflammation, and as a cytokine reservoir, immobilizing immune cells in the stroma ; it has also been demonstrated that TNC can protect stem cells / mesenchymal cells against death-inducer cytokines such as FasL (Rodrigues et al., 2013). Moreover, TNC can be expressed in response to TNFα, leading to cancer cells migration and lower survival in hepatocellular carcinomas (Nong et al., 2015).

Altogether, the recent studies support immune modulatory properties of TNC, in particular concerning cytokines as it can regulate their expression, spatial localization and functions.

5.4. Cure cancer by targeting Tenascin-C?

Over the last decades, the new targeting therapies largely contributed to the overall survival of patients. Concerning breast cancer, the addition of targeted therapies to the more classical surgery, radiotherapy and chemotherapy now allows a 5-year relative survival rate of 80-90% for early breast cancers (Cowppli-Bony et al., 2017). However, one in five patients does not respond to therapy, and this value increases significantly after metastasis formation. It is now clear that TNC plays important roles in tumor development, and in particular by promoting metastasis. Knowing the therapeutic opportunities that targeting TNC may offer, several systems have been developed in order to specifically inhibit the pro-tumoral actions of TNC. Among these approaches, nucleic acids, antibodies and peptides have been tested (reviewed in (Orend et al., 2014; Spenlé et al., 2015)).

5.4.1. Nucleic acids

Therapeutic nucleic acids are composed of DNA, RNA or closely related chemical products involving antisense oligonucleotides, ribozymes, small interfering RNAs (siRNA) and aptamers aiming to specifically regulated expression of cancer-relevant genes (Burnett and Rossi, 2012; Sridharan and Gogtay, 2016). In cancer, several therapeutic nucleic acids have been developed to recognize or decrease TNC expression in the tumor. Firstly, some aptamers have been generated with the idea to target TNC. Aptamers are short single-stranded DNA or RNA molecules that can bind to a specific target like proteins or peptides due to spatial conformation (Keefe et al., 2010). For example, the TTA1 aptamer was designed to specifically bind to the FBG domain of recombinant TNC or TNC expressed by U251 glioblastoma cells (Hicke et al., 2001). Aptamers are interesting because they are small and stable molecules that can be used to deliver a desired compound to a location in contact with TNC. In this regard, the TTA1 has been radio-labeled with technetium-99m (^{99}mTc-TTA1), giving the opportunity to localize tumors in glioma xenograft (Schmidt et al., 2004), as well as in breast, colon, and lung xenograft (Hicke et al., 2006). Aptamers have also been combined with nanoparticles for targeting tumor areas expressing TNC. For example, the Simultaneously Multiple Aptamers and RGD Targeting (SMART) was designed with three

aptamers directed against TNC, nucleolin (AS1411) and integrin αvβ3 (RGD) in cancer (Ko et al., 2011). As nucleolin and integrin αvβ3 targeting allowed to detect cancer cells (Ko et al., 2009), the addition of TTA1 gave the opportunity to specifically target cancer cells expressing TNC like C6, DU145 or A549 cells (Ko et al., 2011). This approach was however only tested *in vitro*.

Secondly, therapeutic nucleic acids can be used to decrease TNC expression levels that are very high in tumors. For instance, the ATN-RNA (siRNA) has been generated to silence TNC mRNAs and upon injection into the resected tumor areas of glioblastoma caused a reduction of tumor growth *in vivo* (Rolle et al., 2010; Zukiel and Nowak, 2006). The inhibitory effects of ATN-RNA have also been recently confirmed in cultured MDA-MB-231 cells in culture, demonstrating a blocking in cell adhesion, proliferation and migration (Wawrzyniak et al., 2020). However, as the authors use siRNAs, the silencing of TNC cannot be maintained over time.

5.4.2. Antibodies

Antibodies are widely used in targeted therapy as they can bind to specific targets, exert antagonism and generate ADCC with their Fc domains. As TNC has been studied during the last thirty years, many antibodies have been developed against TNC for research and clinical use. One of the first antibodies directed against mouse TNC (MTn-12 clone) was produced in rat and is used to detect TNC during intestinal development (Aufderheide and Ekblom, 1988). Later, the TN11 clone, targeting human TNC, enabled the detection TNC in glioblastoma (Carnemolla et al., 1999). Based on the same phage display technology that Carnemolla et al. (1999) used the anti-human TNC G11 presented the ability to target TNC in glioma xenografts and to specifically emit radioactivity in the tumor when labeled with ^{18}F-fluorodeoxyglucose (Silacci et al., 2006). In clinical studies, the F16 anti-TNC antibody has been the most used in phase I and II trials in patients with glioma (Paganelli et al., 1994, 2001; Riva et al., 1999), breast cancer (Catania et al., 2015; De Braud et al., 2011) and Hodgkin's lymphoma (Aloj et al., 2014). The F16 antibody was principally coupled with IL-2 (Teleukin®) in order to deliver the pro-inflammatory cytokine to activate an immune response against the tumor (Catania et al., 2015; Kovacs et al., 1996). F16 was also labeled with ^{131}Iodine (Tenarad®) to eliminate tumor cells in contact with TNC by radiotherapy (Aloj et al., 2014). The use of the F16 antibody in clinic is promising since the treatments were generally

well tolerated by the patients and tumor growth was at least reduced (Spenlé et al., 2015). Since 2013, a phase II clinical trial using Teleukin® is in progress on melanomas (EudraCT 2012-004018-33).

In parallel to antibodies, nanobodies have been recently developed to target TNC. Nanobodies are produced in camelids and present advantages in terms of size, stability, solubility and specificity (Jovčevska and Muyldermans, 2020; Van Audenhove and Gettemans, 2016). For instance, Hynes and collaborators have recently generated several nanobodies targeting TNC (NJTs, United States Patent Application 20190225693). Interestingly, the authors demonstrated that coupled ^{64}Cu-NJTs offered the opportunity to detect micro metastasis in mice, thus opening the possibility to deliver therapeutic compounds specifically to tumors cells that are surrounded by TNC. Moreover, in collaboration with B. Bouhaouala and colleagues (Tunis University), our team recently worked on the development and characterization of specific nanobodies directed against human TNC and Tenascin-W (TNN). Importantly, these new nanobodies were able to detect human TNC in tumor tissue and block some of its activities (see Appendix IV, (Dhaouadi et al., 2020), Dhaouadi et al,. 2020, in preparation). In the coming years, we may have a new possibility to target human TNC *in vivo*, making use of the advantages that nanobodies have over antibodies.

5.4.3. Peptides

Peptides constitute another therapeutic approach used to target cancer cells. Since peptides are small molecules, they can have several advantages compared to antibodies (Fosgerau and Hoffmann, 2015; Trier et al., 2019). For instance, their synthesis (frequently by 9-fluorenylmethyloxycarbonyl (Fmoc) solid-phase peptide synthesis) is generally shorter and cheaper than producing antibodies. Moreover, peptides are poorly immunogenic and their capacity to reach a target is better because of their small size. However, small size can be problematic as it can lead to self-aggregation and easier degradation (Zapadka et al., 2017). Only a few TNC targeting peptides have been developed. At the advent of phage display technology this methodology was used to isolate anti-TNC peptides (Parmley and Smith, 1988; Scott and Smith, 1990). The FH peptide (FHKHKSPALSPV) was obtained by comparing full length TNC produced in tumors to a recombinant TNC (containing the FNIII-like repeats A1, A2, A3, A4, B, C and D) produced in bacteria (Kim et al., 2012). Among 35

sequences generated by phage display, the authors got two close consensus sequences leading to the creation of the FH peptide. It has been described that this peptide can specifically recognize TNC by immunostaining in cancer cells, xenografts and tissue samples from adenocarcinoma and squamous cell carcinoma. Moreover, the authors demonstrated the efficiency of the FH peptide to inhibit TNC anti-adhesive and pro-migratory properties *in vitro* (Kim et al., 2012). Unfortunately, in vivo results in immune competent models with stochastic tumors have not yet been generated.

Lingasamy et al. recently developed two peptides against TNC (Lingasamy et al., 2019, 2020). By using phage display library selection against the isoform C of TNC (TNC-C) and oncofetal fibronectin (FN-EDB), the authors were able to generate the PL1 peptide (PPRRGLIKLKTS) recognizing both TNC-C and FN-EDB (Lingasamy et al., 2019) and the PL3 peptide (AGRGRLVR) specifically detecting TNC-C (Lingasamy et al., 2020). In the first study, the authors developed PL1 in order to target cancer tissue knowing that TNC-C and FN-EDB are overexpressed in cancer. Indeed, it was observed that PL1 coupled with iron oxide particles accumulated in orthotopically engrafted glioblastoma and pancreatic tumors. Interestingly, PL1 was also functionalized with a proapoptotic peptide $_{D}$[KLAKLAK]$_{2}$ and induced a slight increased survival in tumor bearing mice. In the second study, the authors designed the anti-TNC PL3 peptide to also recognize the receptor of neuropilin-1 (NRP1) via its C-end Rule (CendR) motif, as this receptor is frequently overexpressed in cancer cells (Teesalu et al., 2009). With the same idea as for PL1, the authors demonstrated that PL3 particles can reach engrafted glioblastoma tumors and to induce apoptosis. As the authors suggested, PL1 and PL3 are interesting since they allow the targeting of the tumor and the delivery of anti-cancer compounds through exploiting the fact that TNC is overexpressed in tumors. However, up to now the two peptides only detect a specific isoform of TNC that is not present in all cancers. Moreover, the functions of TNC have also not been targeted with these peptides. As TNC is a good target for delivery of agents into cancer tissue, one could imagine that a combination with “finding TNC” and targeting pro-tumoral effects of TNC such as its immune suppressive and pro-angiogenic actions bear potential for anti-cancer therapy.

5.5. TRAIL

Among the large family of cytokines, the tumor necrosis factor (TNF) superfamily regroups important proteins playing active roles during the anti-tumoral immune response. The TNF

family is composed of 19 ligands and 29 dedicated receptors capable to promote either apoptosis, proliferation, survival or differentiation processes participating to major mechanisms in the body like hematopoiesis, inflammation, protection from infections and immunosurveillance (Aggarwal et al., 2012). However, as TNF members are involved in the modulation of immunity, their deregulation can lead to severe diseases like autoimmune diseases, rheumatoid arthritis, septic shock and cancer (Aggarwal, 2003). One example illustrating the complexity of the TNF superfamily cytokines is the TNF-related apoptosis-induced ligand (TRAIL) that was initially described as a specific cancer cell death inducer, but that was meanwhile shown to exhibit many anti- and pro-tumoral functions.

5.5.1. Structure and expression

TRAIL (also called Apo2-L) was discovered simultaneously by two teams due to its similarity with TNF-α and FasL (Pitti et al., 1996; Wiley et al., 1995). TRAIL is a type II transmembrane protein encoded by the gene *Tnfsf10* (Wang et al., 2000). Monomers of TRAIL are composed of a short intracellular N-terminal domain, a transmembrane domain and a long C-terminal domain containing the receptor-binding region (Figure 5A). Like most of the TNF family cytokines, TRAIL is more active as a trimer and binds a trimer of receptors (Figure 5B-C, (Cha et al., 1999; Seol and Billiar, 2000)). It has been described that the cysteine 230 (Cys-230) triggers the stabilization of TRAIL as a dimer due to disulfide bonds formation, resulting in a decreased killing activity (Bodmer et al., 2000; Seol and Billiar, 2000). Interestingly, in presence of zinc ions, the conformation of the loop containing the Cys-230 changed, leading to mixed disulfide-bond formation allowing the trimerization of TRAIL and a higher killing activity (Figure 5B, (Bodmer et al., 2000; Cha et al., 1999; Hymowitz et al., 2000)). The molecular weight of one monomer is predicted as 32.5 kDa, but TRAIL can reach 41 kDa when the protein is matured and glycosylated. The extracellular receptor-binding region can be cleaved (on the amino acid 114) and released as soluble active form of TRAIL (Mariani and Krammer, 1998). A basal plasmatic concentration of 100 pg/mL of soluble TRAIL has been measured, yet this concentration is too low to induce apoptosis (Gibellini et al., 2007). Finally, it has been demonstrated that both transmembrane and soluble forms of TRAIL can activate TRAIL receptor signaling (Ehrlich et al., 2003; Wajant, 2019).

The gene *Tnfsf10* is highly regulated, potentially due to the apoptotic activity of TRAIL. It has been described in human that the *Tnfsf10* promoter has binding sites for several

transcription factors such as interferon-γ-activated sequence (GAS), NFAT, NHF3, GKLF, AP-1, CEBP or GATA (Wang et al., 2000). For instance, IFN-γ treatment triggers immediate expression of TRAIL by mononuclear phagocytes, followed by induction of apoptosis in cancer cells (ovarian, lung, colon, melanoma and prostate, (Griffith et al., 1999a)). Moreover, TRAIL expression is induced during T-cell activation by calcineurin-mediated dephosphorylation that increases NFAT activity (Wang et al., 2000, 2011). Finally, as for FasL, NFkB is also capable to stimulate *de novo* expression of TRAIL by primary T lymphocytes (Baetu et al., 2001).

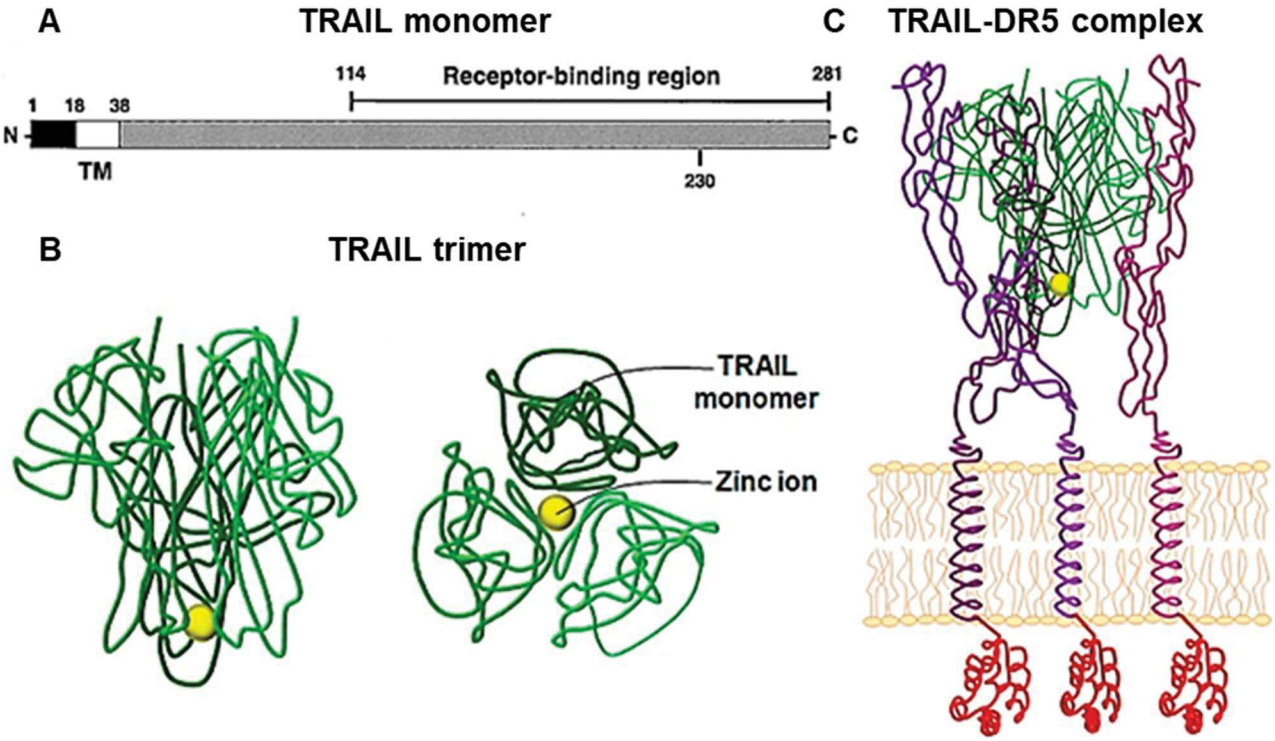

Figure 5: Structures of TRAIL monomers, trimers and TRAIL-DR5 complex (adapted from (A) Seol and Billiar, 2000; (B, C) Naval et al., 2019).

(A) TRAIL monomer is composed of an intracellular N-terminal domain (amino acids 1-18) followed by the transmembrane domain (TM, amino acids 18-38) and the extracellular domain (amino acids 38-281). The receptor-binding region (amino acids 114-281) is located in the C-terminal domain of TRAIL. Note the presence of Cys-230 in the receptor-binding domain. (B) Modelized structures of TRAIL trimer (green) visualized from the side (left panel) or from the top (right panel). Note that the Zinc ion (yellow) is located between the three monomers. (C) Modelized structure of TRAIL-DR5 complex formed by the fitting of a TRAIL trimer into the central space formed by a trimer of DR5 (purple). Intracellular death domains are represented in red.

5.5.2. TRAIL apoptotic signaling

In human and mouse, several receptors are specifically binding to TRAIL (Figure 6A-B). The TRAIL-R1 and TRAIL-R2 in human, plus TRAIL-R in mouse (also called DR5) contain intracellular death domains (DD) that can activate apoptotic signaling (Pan et al., 1997; Walczak et al., 1997; Wu et al., 1999). DR5 shares 40-50% homology with TRAIL-R1 and -R2. In contrast to TRAIL-R1/R2, decoy receptors TRAIL-R3 and TRAIL-R4 in human, as well as mDcTRAIL-R1 and mDcTRAIL-R2 in mouse can bind TRAIL without inducing death signaling since these receptors have no functional DD or no DD at all (MacFarlane et al., 1997; Schneider et al., 1997, 2003). Finally, TRAIL can also bind a soluble receptor, the osteoprotegerin (OPG), that is present in human and mouse but does not induce apoptosis (Emery et al., 1998). Interestingly, human TRAIL weakly binds to DR5 whereas mouse TRAIL highly activates human TRAIL-Rs, supporting that human and mouse TRAIL signaling present numerous similarities (Bossen et al., 2006). In normal conditions, the binding of TRAIL to its death receptors activates intracellular signaling ultimately causing apoptosis (Pitti et al., 1996; Wiley et al., 1995). Following the formation of the death-inducing signaling complex (DISC), pro-apoptotic signals can activate cell death through the extrinsic and intrinsic apoptotic pathways (Figure 6C, reviewed in (Almasan and Ashkenazi, 2003; von Karstedt et al., 2017)). TRAIL has also been reported to trigger caspase independent cell death, called necroptosis, that allows programmed cell death to occur even if the caspases are inhibited (Jouan-Lanhouet et al., 2012; Linkermann and Green, 2014).

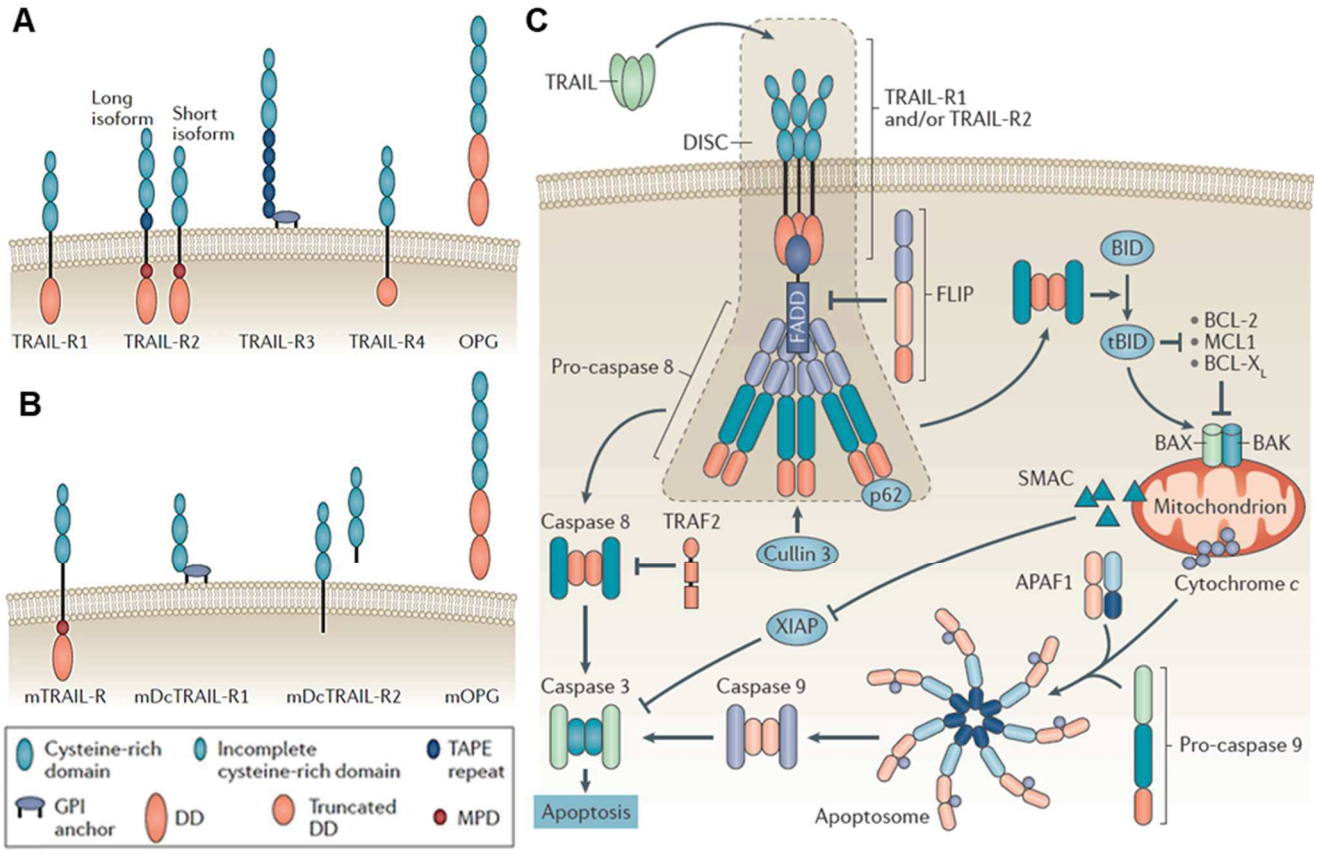

Figure 6: Human and mouse TRAIL-receptors regulating TRAIL-apoptotic pathway (adapted from von Karstedt et al., 2017).

(A) In human TRAIL-R1 and TRAIL-R2 can activate apoptosis signaling through their intracellular death domain (DD). TRAIL-R3 and TRAIL-R4 do not transmit apoptotic signals because they lack the DD or have a truncated one, respectively. Osteoprotegerin (OPG) is soluble and cannot initiate TRAIL-signaling. Note that two isoforms of TRAIL-R2 exist depending of the presence of the TAPE repeat (amino acids: Thr, Ala, Pro, Gln). (B) In mouse, only mTRAIL-R (DR5) activates TRAIL-intracellular pathways whereas decoy receptor mDcTRAIL-R1 and mDcTRAIL-R2 lack the DDs. mOPG presents similar characteristics to hOPG. MDP: membrane-proximal domain.

(C) TRAIL-induced apoptosis is initiated when a trimer of TRAIL binds to a trimer of TRAIL-R (R1, R2 or DR5), recruiting Fas-associated death domains (FADD) and pro-caspases 8, leading to the formation of the death-inducing signaling complex (DISC). The active cleaved form of caspase 8 can either directly activate caspases 3 or indirectly through mitochondria. When BH3-interacting domain death agonist (BID) is truncated (tBID), it can translocate to the mitochondria via BAX/BAK, leading to mitochondrial outer membrane permeabilization, and release of cytochrome C and second mitochondria-derived activators of caspase (SMAC). Cytochrome C can aggregate with apoptotic protease activating factor 1 (APAF1) to form apoptosomes that can cleave pro-caspases 9 into active caspases 9, leading to caspase 3 activation. SMAC can inhibit the X-linked inhibitors of apoptosis (XIAP) that block the activation of caspase 3. Inhibitory checkpoints control apoptosis, as cellular FLICE-like inhibitory proteins (cFLIP) can block FADD by competitive binding, or BCL-2, MCL1, BCL-X_L can inhibit the translocation of tBID, or TNF receptor-associated factor 2 (TRAF2) can direct caspase 8 to proteasomal degradation. In fine, activation of the caspase

3 triggers the cleavage of several pro-apoptotic proteins leading to apoptosis program execution.

5.5.3. TRAIL-sensitivity in cancer

The major interest of studying TRAIL was that TRAIL can initiate the apoptotic program of abnormal cells, like cancer cells, without killing normal cells (Ashkenazi et al., 1999; Walczak et al., 1999). TRAIL is mostly expressed by immune cells. In innate immune cells such as monocytes, MP, DC and NK cells, TRAIL can be induced by lipopolysaccharide (LPS) or pro-inflammatory cytokines (Fanger et al., 1999; Griffith et al., 1999a; Halaas et al., 2000; Takeda et al., 2001). For instance, MPs and DC were able to express TRAIL after being stimulated with IFN-γ or LPS, and to induce apoptosis in co-cultured OVCAR3 (ovarian carcinoma cell line) and WM793 cells (a melanoma cell line). However, normal lung fibroblasts, microvascular endothelial cells or skeletal muscle cells, and the WM 164 melanoma cell line were resistant to TRAIL-induced apoptosis (Fanger et al., 1999; Griffith et al., 1999a). TRAIL is also largely expressed by adaptive immune cells as it can be a component of T-cells cytotoxicity. For example, INF-α and IFN-β can stimulate the production of TRAIL by CD4+ and CD8+ peripheral blood T-cells, leading to the killing of renal carcinoma cell lines (Kayagaki et al., 1999). Furthermore, WM 793 cancer cells are also sensitive to TRAIL apoptosis generated by B-cells (Kemp et al., 2004). Since most of the immune cells can produce TRAIL, on a basal level or upon stimulation, cure cancer with TRAIL-induced apoptosis quickly became a whim for many researchers.

Concerning breast cancer, TRAIL-sensitivity is not clear and illustrates the complexity of TRAIL signaling. The first human breast cancer cell line characterized as TRAIL-sensitive was the MDA-MB-231 (Ashkenazi et al., 1999). However, it was described that some breast cancer cell are not killed by TRAIL, depending on their genotype (Chinnaiyan et al., 2000; Neve et al., 2006; Rahman et al., 2009a). In conclusion of these studies, it was shown that triple-negative cell lines exhibited high sensitivity to TRAIL-induced apoptosis, while HER2+ cells were modestly sensitive and ER+ cells were TRAIL resistant.

Several studies have been performed to explain the differences of sensitivity between the cancer cells. The most obvious possibility relies on the expression of the receptors. It was proposed that a loss of TRAIL-R1 and -R2 may explain a decrease in TRAIL apoptosis, as it was observed in neuroblastoma (Yang et al., 2003). However, several studies in breast cancer demonstrated that expression levels of the death receptors cannot be associated with

TRAIL sensitivity (Buchsbaum et al., 2003; Keane et al., 1999). Other studies investigated the roles of the decoy receptors and the OPG, as an over-expression of these receptors potentially leads to sequestrating TRAIL without activating TRAIL-R1/R2 downstream signaling. However, high levels of TRAIL-R3, -R4 and OPG cannot explain a lower sensitivity to TRAIL in melanoma and breast cancer cells (Griffith et al., 1999b; Rahman et al., 2009b).

TRAIL resistance may also occur due to deregulation of intracellular apoptotic signaling, since this death program is tightly regulated (Lemke et al., 2014). For example, the formation of the DISC complex during apoptosis is controlled by three spliced variants of cellular-FLIP ($cFLIP_L$, $cFLIP_S$ and $cFLIP_R$) that can compete with the pro-caspase 8 in the DISC, thus inhibiting the cleavage of the caspase 8 (Golks et al., 2005; Krueger et al., 2001). In HER2+ tumors, high expression of $cFLIP_L$ was associated with poor prognosis and promoted TRAIL resistance in SKBR3 HER2+ cancer cells (Zang et al., 2014). Moreover, the Bcl-2 family comprises pro-survival factors such as BCL-2, MCL1, BCL-X_L that regulate the mitochondrial intrinsic apoptosis pathway (Shamas-Din et al., 2013). It has been reported that BCL-2 overexpression induces TRAIL resistance in neuroblastoma, glioblastoma or breast carcinoma cell lines (Fulda et al., 2002). On the opposite, a decrease of MCL1 in MDA-MB-231 sensitized the cells to TRAIL killing (De Blasio et al., 2019). Finally, XIAPs can inhibit apoptosis via blocking caspase 3 activation (Deveraux et al., 1997) and has also been described as potential activator of TRAIL resistance in breast cancer cells (Allensworth et al., 2012; Lee et al., 2006).

Evading apoptosis is one of the major mechanisms occurring during cancer progression (Hanahan and Weinberg, 2000). It is known that EMT induces numerous phenotypic changes in epithelial cells that modify properties such as proliferation, invasion or survival (Ribatti et al., 2020). Regarding TRAIL, the impact of EMT in breast cancer is controversial. It was first observed that breast cancer cells expressing mesenchymal markers were more susceptible to undergo apoptosis after TRAIL treatment (Charafe-Jauffret et al., 2006; Neve et al., 2006; Rahman et al., 2009b). However, these studies focused on triple-negative and basal-like cells, and showed that cells expressing markers like vimentin were TRAIL-sensitive whereas cell lines from the same subtypes expressing epithelial markers were TRAIL resistant. An other study supported these observations by demonstrating that treating MDA-MB-231 triple-negative cells with TRAIL triggered cell death and decreased bone metastasis in mice (Thai et al., 2006). As mesenchymal markers seem to be associated with TRAIL sensitivity in triple-negative / basal-like breast cancer cells, more recent studies support a protective role of EMT

against TRAIL-induced apoptosis. For example, it was demonstrated that mesenchymal phenotypes induced by treatment trigger TRAIL resistance (Lu et al., 2014). Interestingly, the authors observed that E-cadherin promotes death receptor clustering and formation of death complexes through interactions with the actin cytoskeleton. This hypothesis is supported by other authors who induced TRAIL apoptosis in resistant MDA-MB-468 cells via pre-treating with the antibody MS-275. The treatment with MS-275 triggered a “cadherin switch” and reversed EMT, leading to cell death and tumor regression after TRAIL treatment (Srivastava et al., 2010). Since E-cadherin is important for cell-cell junctions, the disruption of the junctions during EMT may trigger TRAIL resistance (Gallegos and Brugge, 2014). As the aggregation of TRAIL-Rs appears to be a key in the initiation of TRAIL signaling, several studies demonstrated the importance of TRAIL-Rs clustering (Naval et al., 2019). For instance, inhibiting the aggregation of death receptors in signaling platforms like lipid rafts induces TRAIL resistance (Ouyang et al., 2013; Song et al., 2007). These last observations also support a desensitizing effect of EMT as lipid raft destabilization to be associated with the mesenchymal phenotype (Wu et al., 2020).

5.5.4. TRAIL therapies and clinical trials

Knowing the therapeutic opportunities that TRAIL may bring to the anticancer arsenal, several approaches have been tested to overcome TRAIL resistance and to induce cancer cell death. Typically, TRAIL therapies relay on TRAIL-Rs agonists (TRAs) that are mostly divided into recombinant forms of TRAIL and agonistic antibodies stabilizing TRAIL-Rs/ligand complexes (Lemke et al., 2014; de Miguel et al., 2016).

5.5.4.1. Recombinant TRAIL

As soon as TRAIL was characterized as a TNF specific killer of cancer cells, recombinant forms of TRAIL have been developed to study the anticancer potential of TRAIL in the clinic (Dubuisson and Micheau, 2017). The first recombinant human TRAIL (rhTRAIL) developed for clinical application was produced in bacteria as a non-tagged protein containing the amino acid 114–281 of TRAIL (Lawrence et al., 2001). This rhTRAIL (also called dulanermin) did not show sufficient therapeutic activity due to its weak stability and the establishment of TRAIL resistance pathways by the tumors (Micheau et al., 2013; Ouyang et al., 2018). Whereas dulanermin did not induce hepatotoxicity (Jo et al., 2000), the half-life of the

compound was short (around 1 hour) and did not cause significant tumor regression, in particular in lung cancer (Blackhall et al., 2010; Herbst et al., 2010a; Soria et al., 2011). Numerous rhTRAILs have been generated after the advent of dularnermin in order to solve to problem of stability and half-life. For example, rhTRAILs have been coupled to leucine and isoleucine zippers (LZ-, ILZ-TRAIL (Walczak et al., 1999)), to immunoglobulin Fc domains (Fc-TRAIL, (Wang et al., 2014)) or to poly-histidine tags (6xHis-TRAIL, (Kim et al., 2004)) in order to facilitate the formation of active rhTRAIL trimers. Interestingly, TNC has been used for stabilizing TRAIL trimers (Berg et al., 2007). In this study, the authors used the chicken C-terminal TNC-FBG to generate stable TRAIL trimers that induced apoptosis in cancer cells whereas conventional rhTRAILs were not efficient. In order to specifically deliver rhTRAILs to cancer cells, trimers of rhTRAIL have been attached to molecules targeting cancer markers like single-chain variable fragment (scFv, (Ahmad et al., 2012)). For example, regarding breast cancer, scFv-TRAILs have been developed against EGFR and ErbB2 to specifically induce apoptosis in cancer cells expressing these markers (Bremer et al., 2005; Schneider et al., 2010).

5.5.4.2. Antibodies against TRAIL-Rs

Antibodies directed against TRAIL-Rs have two major advantages compared to rhTRAILs: the half-life after injection is much higher than rhTRAILs and the presence of Fc domains enables the activation of ADCC and complement-dependent cellular cytotoxicity (CDC). Antibodies have been developed against TRAIL-R1 and TRAIL-R2 (Dubuisson and Micheau, 2017; Lemke et al., 2014). Nowadays, TRAIL-R1 has only been targeted in clinical trials by mapatumumab (Pukac et al., 2005). Despite its pro-apoptotic activity *in vitro* and *in vivo*, combined to low toxicity in clinical phases I and II studies, mapatumumab did not demonstrate a significant effect on solid cancers such as hepatic or lung cancers (Ciuleanu et al., 2016; von Pawel et al., 2014; Tolcher et al., 2007). More antibodies have been tested in clinical trials against TRAIL-R2. For instance, conatumumab (AMG 655), drozitumab, lexatumumab, LBY135, tigatuzumab were tested in phases I and II studies and gave the same unsatisfying results as mapatumumab (Forero-Torres et al., 2013; Herbst et al., 2010b; Kang et al., 2011; Sharma et al., 2014; Shimada et al., 2007). While trials were discontinued for these antibodies, one last TRAIL-R2 agonist, DS-8273a, is still tested in phase I trials against unresectable stage III or stage IV melanomas (NCT02983006).

The first generation of TRAIL-Rs antibodies, like rhTRAILs, aimed at directly activating the receptors in order to induce apoptosis. However, clinical trials demonstrated that this approach is not sufficient to induce tumor regression. TRAIL multiple resistance pathways and mechanisms may counteract cell death in cancer cells, as introduced in 5.4.3. Yet, new antibodies are developed and tested in pre-clinical tests and allow to target TRAIL-Rs at different angles. Recent studies described the importance of TNF-receptor clustering (TRAIL-Rs included) for optimal activation (Pan et al., 2019; Vanamee and Faustman, 2018). It has been demonstrated in human by using AMG 655 in combination with rhTRAIL that the co-treatment was able to induce more apoptosis due to a better clustering of the rhTRAIL/TRAIL-R/AMG 655 complex compared to rhTRAIL and AMG 655 alone (Graves et al., 2014; Tuthill et al., 2015). Indeed, other antibodies only used in pre-clinical studies, like the KMTR2, can promote TRAIL-R2 superoligomerization, thus inducing apoptosis in glioma *in vitro* and *in vivo* models (Nagane et al., 2010; Tamada et al., 2015). Similar results were observed in mouse with DR5 agonist MD5-1, yet hepatotoxicity was detected due to DR5 overactivation (Finnberg et al., 2016). Meanwhile, even if TRAIL-Rs crosslinking is important to induce a strong activation of apoptosis ; it is also known that the same TRAIL-Rs may lead to the activation of pro-survival pathways (Shlyakhtina et al., 2017). Thus, understanding the non-canonical pathways of TRAIL is necessary to develop efficient TRAIL therapies.

5.5.5. Non-canonical effects of TRAIL

Although TRAIL is mostly known for acting as an immune cytokine killing abnormal cells, it has also modulatory effects on angiogenesis, in cancer and on immunity through apoptotic and non-apoptotic pathways. Among them, NFkB, JUN N-terminal kinase (JNK), p38, ERK or PI3K/AKT signaling have been described to promote pro-tumorigenic cellular processes such as proliferation, migration and invasion, after activation by TRAIL (Figure 7, reviewed in (Azijli et al., 2013; von Karstedt et al., 2017)).

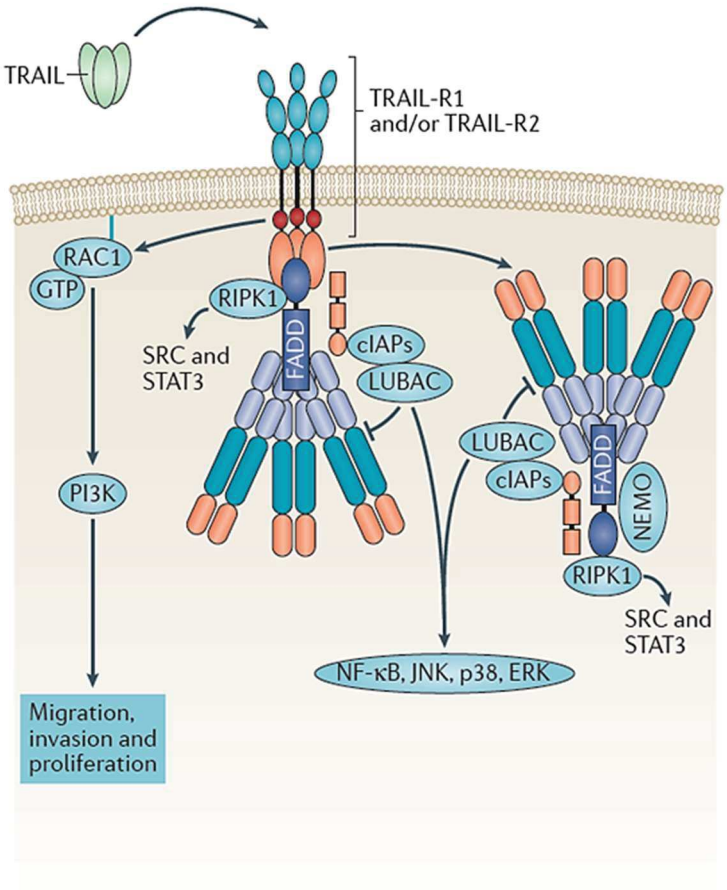

Figure 7: TRAIL non-apoptotic pathways (adapted from von Karstedt et al., 2017).

After the formation of the DISC, a secondary complex composed of FADD, pro-caspase 8 and TRAF2 can associate with the receptor-interacting serine/threonine protein kinase 1 (RIPK1), cellular-IAPs (cIAPs), the linear ubiquitin chain assembly complex (LUBAC) and the nuclear NFkB essential modifier (NEMO), potentially leading to NFkB, JNK, p38 and ERK pathway activation. When pro-caspase 8 is inhibited, non-receptor tyrosine kinase Src and (signal transducer and activator of transcription 3 (STAT3) can also be activated, promoting migration.TRAIL-R2 may also activate Rac1 GTPase, leading to PI3K/AKT dependent migration, invasion and proliferation (von Karstedt et al., 2015).

5.5.5.1. Angiogenesis

By studying TRAIL effects on cancer development and vascular diseases, several studies described complex regulatory properties of TRAIL on angiogenesis. For instance, it was described that TRAIL can cause cell death in around 30% of cultured human umbilical vein endothelial cells (HUVECs) (Li et al., 2003). However, the remaining cells were resistant and presented an activation of cellular adhesion via NFkB, E-selectin, ICAM-1 and IL-8. Another study demonstrated that TRAIL resistance in HUVECs requires the activation of the pro-survival pathway PI3K/AKT (Alladina et al., 2005). Moreover, TRAIL was described as a promoter of endothelial cell proliferation (Di Bartolo et al., 2015). On the other hand, TRAIL blocks activation of VEGF-induced angiogenic signaling in HUVECs by inhibiting ERK, Src, FAK, paxillin, AKT, and eNOS (Na et al., 2014).

The roles of TRAIL on angiogenesis has also been studied in cancer. In glioma, TRAIL inhibited new vessel formation induced by human glioblastoma cells secreting VEGF (Cantarella et al., 2006). Interestingly, the authors observed that TRAIL impacted angiogenesis through non-apoptotic effects since caspase 8 was activated without induction of apoptosis. A decrease of VEGF expression by TRAIL, leading to less angiogenesis, was

also observed in NSCLC (Chen et al., 2019). In addition, it has been described that TRAIL can induce apoptosis of endothelial cells expressing DR5 especially within the pancreatic TME, but not in context of normal tissue (Wilson et al., 2012). However, in diver human sarcomas, TRAIL was associated with higher angiogenesis (Secchiero et al., 2004). Altogether, the current results suggest a modulatory role of TRAIL in angiogenesis that involve apoptotic and non-apoptotic signaling that appear to be context dependent.

5.5.5.2. Cancer promotion

Even if the major role of TRAIL is to induce apoptosis in cancer cells, several resistance mechanisms can occur and lead to a loss of TRAIL sensitivity. However, losing the proapoptotic effects does not mean that TRAIL-Rs are incapable to transduce intracellular signals ; in particular in cancer cells, non-canonical signaling was described (Azijli et al., 2013; von Karstedt et al., 2017). The initialization of the non-canonical TRAIL signaling is complex and begins with the assembly of a secondary protein complex following the formation of the DISC (Figure 7). From this moment, it has been described that several pathways can be activated and promote cancer progression. Among these pathways, the TRAIL pro-survival part of NFkB signaling was described in HEK293 cells (Schneider et al., 1997). Melanoma cells lines treated with a low concentration of TRAIL, in order to obtain TRAIL resistance, exhibited a higher expression of NFkB, protecting in return the cells against apoptosis (Franco et al., 2001). Moreover, NFkB can induce cell migration and invasion in TRAIL apoptosis-resistant cholangiocarcinoma cells (Ishimura et al., 2006). A kinome analysis performed on TRAIL resistant cancer cell lines treated with TRAIL also revealed that several kinases involved in Src, STAT3, FAK, ERK and AKT pathways were promoting survival accompanied with migration and invasion (Azijli et al., 2012).

Interestingly, some genetic markers were associated with TRAIL non-canonical activity in cancer cells. For example, it has been described that *KRAS*-mutated colorectal cancer cell lines, NSCLC and pancreatic ductal adenocarcinoma allow the activation of non-canonical pathways by TRAIL, leading to tumor progression and faster metastasis development (Hoogwater et al., 2010; von Karstedt et al., 2015). In these two studies, the authors demonstrated that TRAIL treatment caused activation of the small GTPases Raf-1 and Rac1 in *KRAS*-mutated cells (frequent in human cancers (Bos, 1989)) upon stimulation of TRAIL-R2, subsequently promoting migration, invasion and metastasis.

Importantly, von Karstedt et al. (2015) proved that cancer cells can express TRAIL themselves, thus activating their own pro-tumoral pathways through TRAIL non-apoptotic signaling. Moreover, it has been observed that adenocarcinoma HT-29 cells can express functional TRAIL on their surface and induce apoptosis in Jurkat cells (Inoue et al., 2002). These results were confirmed later by Huber et al. (2005), who demonstrated that SW403 and 1869 col human colorectal cancer lines, as well as CRC28462 short-term lines generated from liver metastases, can induce T-cells apoptosis by secreting killing vesicles bearing FasL and TRAIL *in vitro* and *in vivo*. Considering the immunomodulatory potential of TRAIL (see 5.4.5.3.), a better understanding of cancer cells propensity to produce TRAIL and impact tumor immunity and tumor growth is important.

5.5.5.3. Immunomodulation

Our immune system depends on a highly regulated homeostasis of lymphocyte progenitors. A fine-tuned equilibrium between cell proliferation and cell death enables the expansion of immune cells expressing functional antigen receptors, without keeping the cells presenting self-reactive specificity. During this selection process, an efficient programmed cell death is mandatory for the maturation of our immunity (Opferman, 2008). If the initial studies demonstrated that TRAIL produced by immune cells plays a major role in immunosurveillance, it become increasingly clear that this cytokine also modulates immune responses directly (Bossi et al., 2015; Sag et al., 2019).

Lymphoid cells are the prime target of TRAIL in cancer as they use TRAIL as an anti-cancer cytokine. Firstly, NK cells and ILCs generally express killing cytokines like TRAIL to induce cancer cell death (Martinez-Lostao et al., 2015; Paul and Lal, 2017). However, it has also been described that these cells can regulate the adaptive immune response via TRAIL (Schuster et al., 2016). For example, activated CD4+ and CD8+ T-cells can be killed by TRAIL produced by NK cells and ILCs (Peppa et al., 2013; Schuster et al., 2014). Interestingly, the two studies demonstrated that T-cell selection by TRAIL was important for the response to chronic virus infections, notably by limiting the collateral damage generated by active T-cells (Schuster et al., 2014).

Considering T-cells, it is interesting to note that only the activated cells express TRAIL and TRAIL-Rs (Dorothée et al., 2002; Mirandola et al., 2004; Wendling et al., 2000). Thus, immature T-cells are not sensitive to TRAIL. As mature T-cells are regulated by TRAIL

produced by NK cells during viral infection, a similar regulation was observed during HIV infection with TRAIL produced by plasmacytoid DCs (Stary et al., 2009). Moreover, TRAIL is also a modulator of the balance between Th1 and Th2 T-cells. For instance, it has been demonstrated that Th2 cells can express TRAIL without being sensitive to TRAIL apoptosis, whereas Th1 cells do not express TRAIL but can be killed by TRAIL (Zhang et al., 2003). Experiments in mice revealed that TRAIL deficient animals developed a severe thymocyte apoptosis deficiency, leading to splenomegaly and lymphadenopathy due to a pathological accumulation of CD4+ / CD8+ T-cells and B-cells (Sedger et al., 2010). The regulatory effects of TRAIL on lymphocyte activation was also supported by showing that TRAIL participates in the regulation of peripheral blood cell populations via promoting activation-induced cell death (AICD) in these cells (Martínez-Lorenzo et al., 1998). In the meantime, it is also known that TRAIL can induce proliferation of Tregs that are known to maintain immune tolerance, and increase the probability of autoimmune diseases in case of deficiency (Ikeda et al., 2010; Sakaguchi et al., 2012). Like T-cells, the B-cells also became sensitive to TRAIL after activation (Staniek et al., 2019). Interestingly, it was reported that TRAIL could impact the production of antibodies by activated B-cells as neutralizing TRAIL triggered an increase of IgG1 antibodies in the serum of mice (Kayagaki et al., 2002).

TRAIL also impacts the functions of myeloid cells. Following the previous immune cell types, neutrophils express TRAIL upon activation, notably during inflammation (Kemp et al., 2005). It has been reported that neutrophils express more decoy receptors than TRAIL-Rs, correlating with a low sensitivity to TRAIL apoptosis (Kamohara et al., 2004; Lum et al., 2005). However, neutrophils become sensitive to TRAIL after activation or aging (Lum et al., 2005). It has been demonstrated that TRAIL participates in the elimination of activated, stressed and aged neutrophils (McGrath et al., 2011). In this study, the authors observed that TRAIL deficient mice presented more inflammation in LPS-mediated acute lung injury and zymosan-induced peritonitis, because of a lack to regulating the abundance of neutrophils. Conversely, injection of soluble TRAIL or DR5 agonists in mice decreased the quantity of neutrophils and of inflammation during bacterial infection (Hoffmann et al., 2007).

To complete this overview, TRAIL can also regulate DCs and MPs. Leverkus et al. (2000), introduced for the first time the fact that TRAIL may be a potent immunomodulator. The authors observed that mature DCs were TRAIL and FasL resistant whereas immature DCs underwent apoptosis by TRAIL. Interestingly, the authors demonstrated that TRAIL resistant pathways, implicating cFLIP and caspase 8 inhibition, were responsible for the expansion of

DCs (Leverkus et al., 2000). It was then suggested that TRAIL and FasL were necessary to physiologically regulate DCs proliferation. The higher sensitivity to TRAIL of immature DCs was confirmed later (Cho et al., 2010; Hayakawa et al., 2004). Only few studies described non-apoptotic effects of TRAIL on DCs. In DCs activated with LPS, it has been observed that TRAIL can trigger the expression of activation markers such as CD80, CD86 and IL-12 (Cho et al., 2010). However, TRAIL produced by NK cells could decrease the antigen-presenting potential on DCs in a mouse model, thus leading to lowering the population of CD4+ and CD8+ lymphocytes (Iyori et al., 2011).

Finally, peripheral MPs express both TRAIL-R1 and TRAIL-R2 whereas tissue resident MPs have reduced expression of TRAIL-R2 (Liguori et al., 2016). It is interesting to note that the M1 or M2 status of the MPs affect the expression of TRAIL-Rs, M2 cells express more TRAIL-Rs compared to M1 cells (Germano et al., 2013; Liguori et al., 2016). However, another study demonstrated the opposite in rheumatoid arthritis (Li et al., 2013). In comparison to human, murine monocytes and MPs both express DR5 (Liguori et al., 2016). It has been reported that M2 MPs are more sensitive to TRAIL apoptosis than M1 cells, due to their higher expression of TRAIL-R2, accompanied by a better crosslinking of the receptor (Huang and Hsu, 2017; Liguori et al., 2016). In that case, TRAIL apoptosis may help to decrease the proportion of pro-tumoral M2 MPs during tumor progression, as trabectedin sensitized M2 cells toward TRAIL apoptosis (D'Incalci, 2013; Germano et al., 2013). On the other hand, TRAIL also has non-apoptotic effects on MPs. For example, TRAIL triggers the maturation of myeloid precursors into monocytes (Secchiero et al., 2002). Furthermore, TRAIL induces the migration of monocytes via TRAIL-R1 activation followed by PI3K and Rho GTPase as downstream effectors (Wei et al., 2010). Interestingly, TRAIL non-apoptotic signaling plays different roles during cancer progression. For instance, TRAIL can induce the secretion of proinflammatory cytokines (IL-1β, IL-6, TNFα) by MPs, leading to a reorienting of TAMs toward a M1 phenotype promoting tumor regression (Gao et al., 2015). However, TRAIL was also described as an anti-inflammatory cytokine promoting a M2 phenotype in colon cancer (Kim et al., 2018). In addition, TRAIL could promote a tumor-supportive immune microenvironment by activating non-apoptotic signals in cancer cells, leading to the secretion of pro-M2 factors (Hartwig et al., 2017). Interestingly, Hartwig et al. (2017), demonstrated a complex interaction between cancer cells and MPs, where TRAIL-induced secretome containing chemokines such as CCL2 could trigger the infiltration of M2 MPs supporting the development of lung xenografts.

Altogether, the presented studies illustrate the complexity of TRAIL signaling. Indeed, TRAIL cannot be simply considered as a pro-apoptotic factor. In future studies and clinical trials, TRAIL non-canonical processes must be well taken into account if we want to efficiently cure cancer with TRAIL therapies.

6. Hypothesis and Aims

It is now clear that the matrix protein TNC promotes several pro-tumoral mechanisms (Midwood et al., 2016; Orend et al., 2014). Over the last decade, the roles of TNC in breast cancer development have been clarified. As high expression of TNC in the tumors have been correlated with faster lung metastasis formation and poor overall survival for breast cancer patients (Oskarsson, 2013), our team and collaborators have recently demonstrated that TNC promotes lung metastasis by regulating blood vessels invasions (Sun et al., 2019). Moreover, we described several effects of TNC affecting anti-tumoral immune response via deregulating MPs (Deligne et al., 2020), T-cells (Murdamoothoo et al., in revision) and dendritic cells in an head and neck tumor model (Spenlé et al., 2020). Furthermore, we learned that this immunomodulating effect of TNC depends on direct interactions between TNC and immune cytokines.

My thesis project is based on the observations made by Devadarssen Murdamoothoo and Zhen Sun on the MMTV-NeuNT breast cancer model (Muller et al., 1988) and the NT193 syngeneic orthotopic grafting model (Sun et al., 2019). In the two models, my predecessors described pro-tumoral effects of TNC in breast cancer. In fact, preliminary results indicated that TNC promotes breast cancer progression and lung metastasis formation by decreasing tumor cells apoptosis. By looking for candidates, we identified TRAIL, a pro-apoptotic factor, as an immune cytokine potentially dysregulated by TNC, thus leading to cancer cells survival. Knowing that TNC binds to soluble factors and cytokines, the aims of my work were as following:

Aim 1: Identify the interactions between TNC and TRAIL signaling in the NT193 model and describe the effects on breast cancer development.

Aim 2: Develop specific peptides targeting and inhibiting TNC functions based on our newly described MAtrix REgulating MOtif, “MAREMO”.

7. Manuscript I: Tenascin-C counteracts TRAIL control over tumor immunity, growth and progression

William Erne[1,2], Devadarssen Murdamoothoo[1], Zhen Sun[1], Matthias Mörgelin[3], Gérard Cremel[1], Nicodème Paul[4], Raphael Carapito[4], Aurélie Hirschler[5], Christine Carapito[5], Thomas Loustau[1,2], Gertraud Orend[1,2,+]

[1] University Strasbourg, INSERM U1109, MN3T (The Microenvironmental Niche in Tumorigenesis and Targeted Therapy), 3 avenue Molière, Strasbourg, Hautepierre, France

[2] University Strasbourg, INSERM U1109, The Tumor Microenvironment Laboratory, Hopital Civil, Institut d'Hématologie et d'Immunologie, Fédération de Médecine Translationnelle de Strasbourg (FMTS), 1Place de l'Hôpital, 67091 Strasbourg, France

[3] Colzyx AB, Scheelevägen 2, 223 81 Lund, Sweden

[4] INSERM U1109, GENOMAX, 67091 Strasbourg

[5] IPHC, Cronenbourg

+ Correspondence:

Gertraud Orend, INSERM U1109, The Tumor Microenvironment Laboratory, 67091 Strasbourg, France, gertraud.orend@inserm.fr, https://orend-tme-group.com

7.1. Abstract

Applying the death ligand TRAIL promised to eradicate cancer, however clinical trials were not yet supportive. In MMTV-NeuNT and syngeneic tumor grafts derived thereof we describe a novel function of the extracellular matrix molecule tenascin-C (TNC) in immune-suppression of cancer by counteracting TRAIL. Although cultured tumor cells expressed TRAIL and its receptor DR5, and were sensitive to killing by recombinant TRAIL *in vivo,* cells expanded and were metastatic. To understand TRAIL actions, we grafted tumor cells with a knockdown of TRAIL and observed bigger tumors and more lung metastasis which correlated with reduced infiltration of myeloid cells as determined by flow cytometry. No difference in tumor growth was seen upon grafting of cells with lowered DR5, supporting that TRAIL regulates anti-tumor immunity, rather than tumor cell killing via TRAIL/DR5. By using conditioned medium from tumor cells with lowered TRAIL we observed reduced myeloid cell invasion into tumor spheroids. RNA seq and proteomic analysis of tumor cells and inhibitor studies revealed CXCR4 as relevant downstream target in myeloid cells, promoting macrophages to destroy tumor tissue. This was reduced in tumors with lowered TRAIL. TRAIL immunity control may be counteracted by TNC through downregulating TRAIL expression via integrin $\alpha4\beta1/\alpha9\beta1$, and physically confining TRAIL in the stroma as shown by surface plasmon resonance spectroscopy and negative electron microscopy. Moreover, through epithelial-to-mesenchymal transition, TNC conferred resistance by lowering DR5 expression. Relevance for human breast cancer was detected by Kaplan Meier analysis, demonstrating combined low TNC with high TRAIL to correlate with longer patient survival. Altogether our study demonstrated an important function of matrix in counteracting TRAIL which harbors therapeutic potential. Finally, our study predicts that tumors may be responsive to TRAIL-induced cytotoxicity the lower TNC levels are.

7.2. Introduction

Tumor necrosis factor (TNF)-related apoptosis-induced ligand TRAIL (or Apo2-L) was shown to regulate tumor cell survival and tumor immunity (Pitti et al., 1996; Wiley et al., 1995). TRAIL is a type II transmembrane protein that can be released as trimeric molecule by proteolytic cleavage. TRAIL is inducing signaling through binding to its receptors TRAIL-R1/R2, or DR5 in mouse, causing cell death by apoptosis or necroptosis, respectively (Jouan-Lanhouet et al., 2012; Wu et al., 1999). As exogenous TRAIL was shown to kill tumor cells without an apparent negative effect on normal cells, TRAIL and TRAIL-R agonists were considered to be promising anticancer therapeutics (Ashkenazi et al., 1999; Walczak et al., 1999). Yet clinical trials were not successful where TRAIL stability and other technical issues, as well as alternative functions of TRAIL promoting tumorigenesis could be responsible (Lemke et al., 2014; Stuckey and Shah, 2013; von Karstedt et al., 2015). In particular, TRAIL signaling can generate an immune-suppressive tumor microenvironment (TME) by promoting a tumor supportive M2-like myeloid phenotype (Falschlehner et al., 2009; Hartwig et al., 2017; Sag et al., 2019). Tenascin-C (TNC), an extracellular matrix molecule promoting cancer by multiple mechanisms, may be relevant as TNC itself promoted an immune-suppressive TME and in particular an M2 macrophage (MP) phenotype (Midwood et al., 2016; Oskarsson, 2013; Spenlé et al., 2020). Moreover, targeting the TNC specific effects reduced tumor growth and metastasis demonstrating that targeting matrix can enhance immune checkpoint therapy and restore anti-tumor immunity (Deligne et al., 2020; Spenlé et al., 2020).

Our study was instigated by the observation that TRAIL levels inversely correlated with TNC levels in tumors, suggesting a potential TNC-TRAIL interdependence that we addressed and confirmed here. Although tumor cells expressed TRAIL, and its receptor DR5, and were sensitive to apoptosis in culture using a TRAIL targeting approach, cells expanded and formed lung metastasis *in vivo*. By using grafting of tumor cells or tumor spheroid cultures with a knockdown (KD) of TRAIL (or DR5) we demonstrated that TRAIL induced CXCR4 signaling in dendritic cells (DC) and MP, causing attraction into the tumor. Here, we discovered three mechanisms by which TNC counteracted TRAIL-induced killing, which is probably relevant given the high abundance of TNC in cancer tissue and correlation with malignancy and shorter patient survival. TNC downregulated TRAIL expression through

integrin α4β1/α9β1, bound and inactivated TRAIL, and rendered cells refractory to TRAIL killing, potentially through TGFβ pro-survival signaling and epithelial-to-mesenchymal transition (EMT). We propose that blockade of TRAIL repression by TNC may be an opportunity to restore TRAIL-based anti-tumor immunity. Altogether our observations have therapeutic and diagnostic potential as breast cancer patients with high TRAIL and high CXCR4 expressing tumors had a longer overall and relapse-free survival. Since TNC counteracted TRAIL, our results predict that tumors with low TNC may be more responsive to TRAIL therapy.

7.3. Results

TRAIL levels were higher in tumors with low TNC and were associated with tumor plasticity

We investigated TRAIL levels in MMTV-NeuNT and NT193 tumors and observed higher *Tnfsf10* (for easier reading "TRAIL") levels in tumors with lower or no TNC suggesting that TNC may have an impact on TRAIL function in these tumors (**Fig. 1A, B**).

E-cadherin has previously been identified to promote TRAIL-mediated killing (Lu et al., 2014). As we noticed that NT193 cells are highly plastic *in vitro* and *in vivo* (Sun et al., 2019), we asked whether epithelial (E) and mesenchymal (M) cells have potentially different TRAIL expression levels since cancer cells can express TRAIL (von Karstedt et al., 2015). Therefore, we established E and M cells from the NT193 pool of cells by subcloning, and confirmed E and M properties by RNA seq, immunofluorescence (IF) and western blot analysis (**Fig. 1C-E, S1A**). Moreover, E cells expressed higher TRAIL and DR5 levels compared to M cells (**Fig. 1F**). Expression of TRAIL and DR5 (*Tnfrsf10b*) and other TRAIL-Rs members was also different in the RNA seq and qRTPCR analysis with TRAIL, DR5, DcTRAIL-R1 (*Tnfrsf23)* and DcTRAIL-R2 *(Tnfrsf22)* being lower and higher in M than E cells, respectively (**Fig. S1B-E**). Moreover, M cells expressed abundantly TNC whereas no TNC expression was detectable in E cells (**Fig. 1G, S1F**). We also observed that M cells proliferated and migrated more than E cells in a MTS and wound closure assay, respectively (**Fig. 1H, I**).

TRAIL induced cell death in NT193E but not NT193M cells

To address whether TRAIL killed tumor cells, we determined caspase 3 and 7 (Casp 3/7) activity and quantified cell death by Acridin Orange/Ethidium Bromide (AO/EB) incorporation. We observed that recombinant TRAIL alone was not inducing cell death but required the MD5-1 antibody, that previously had been utilized to stabilize the TRAIL-DR5 signaling complex (Finnberg et al., 2016; Naval et al., 2019), to raise Casp 3/7 activity and to induce cell death in E cells. In contrast, M cells were not killed by TRAIL/MD5-1 (**Fig. 2A-D, S2A-D**). We also investigated cell death in another cell line that previously was reported to be sensitive

to TRAIL-induced killing (Martin et al., 2011) and observed that in EO771 cells, again TRAIL (or MD5-1) alone did not activate Casp 3/7 nor induced cell death, whereas combined treatment triggered cell death (**Fig. S2E-J**).

TNC binds TRAIL and reduces TRAIL tumor cell cytotoxicity via TGFβ-signaling

As TNC can bind soluble factors such as CCL21, CXCL12 and others (De Laporte et al., 2013; Spenlé et al., 2020; Murdamoothoo et al., in revision) we investigated whether TNC may bind TRAIL. Indeed, by surface plasmon resonance spectrometry (SRP) we observed that TRAIL binds strongly to TNC with a Kd of 2,8 x 10-9 M which is a magnitude higher than the interaction with CCL21 (**Fig. 3A**, (Spenlé et al., 2020)). The SRP profile indicated that TRAIL is poorly dissociating from TNC. Binding of TRAIL to TNC was also seen by negative electron microscopy and occurred in the same domain as binding of TGFβ, CCL21 and CXCL12 (**Fig. 3B, C,** (Spenlé et al., 2020; Murdamoothoo et al., in revision)). Moreover, the underlying mechanism offers opportunities for targeting cancer (Erne et al., in preparation).

Next, we asked whether TNC impacted tumor cell killing by TRAIL and observed reduced Casp 3/7 activity and lower cell death when TNC was added (**Fig. 3D, E**). To address how TNC reduces TRAIL-induced killing we blocked TGFβR1 with GW788388 and observed that cell death was reverted to levels without TNC, suggesting that TNC protects cells from TRAIL killing through TGFβ signaling. We previously had shown that TNC enhances pro-survival signaling and induces EMT in NT193 cells through TGFβ signaling (Sun et al., 2019). As M cells expressed little DR5 and were resistant towards TRAIL-induced killing (**Fig. 1, 2**) TNC may protect from TRAIL killing through EMT-associated plasticity.

NT193M cells protected NT193E cells from TRAIL-induced cytotoxicity

To mimic the 3D context of tumors we established homotypic spheroids from E and M cells, and noticed that M cells grew slower than E cells giving rise to smaller spheroids (**Fig. S4A, B**). As M cells expressed TNC we wondered whether we could recapitulate the organization of a tumor when we mixed both cells. Therefore, we generated heterotypic spheroids and observed sorting of E cells into nests that were surrounded by M cells. As in tumors, E cell

nests were separated from each other by TNC (**Fig. 4A**). Moreover, E cell spheroids were sensitive to TRAIL as Casp 3/7 activity and AO/EB levels increased with TRAIL/MD5-1, which was not the case in M cell spheroids that were unresponsive despite existing sensitivity to apoptosis by staurosporine (**Fig. 4D, S4C-E**). To determine a potential role of TNC we reduced TNC levels by knockdown (KD) in M cells, that we confirmed by IF and immunoblot (**Fig. 4A-C**). Next, we determined Casp 3/7 activity and AO/EB in mixed spheroids (**Fig. 4 E-H**). We saw cell death to be reduced when M cells were added (**Fig. 4E, G**) unless TNC levels were reduced causing enhanced cell death (**Fig. 4F, H**). Thus, M cells protected E cells from TRAIL-induced cytotoxicity which was regulated by TNC. This mechanism could be relevant in highly plastic tumors.

Impact of DR5 and TRAIL on tumor growth and immune cell infiltration

To determine how NT193E-produced TRAIL signaling impacts tumor growth and progression, we generated E cells with a shTRAIL KD for engraftment. We confirmed reduced TRAIL expression at mRNA and protein level (**Fig. 5A, B**). Upon engraftment, shTRAIL cells generated tumors. Similar to the cultured cells, TRAIL mRNA levels were lowered and TRAIL protein was not detectable by IF in the tumors. This was in contrast to control tumors that ubiquitously expressed TRAIL (**Fig. 5C, D**). Control tumors had similar TRAIL levels in a TNCKO as in a WT host suggesting that tumor cells were the major source of TRAIL which was confirmed by tissue staining of TRAIL and cancer cell markers cytokeratines-8 / -18 (CK8/18, **Fig. 5C, D**). We observed that shTRAIL tumors were bigger than control tumors both in a WT and TNCKO host (**Fig. 5E-G**). In a WT host shTRAIL tumors were bigger than in a TNCKO host, suggesting a role of host-derived TNC on survival (**Fig. 5G**). Independent of TRAIL, host TNC only slightly increased the tumor volume presumably reflecting the integration of opposing functions of TNC in cancer (**Fig. 5H,** (Deligne et al., 2020; Midwood et al., 2016; Spenlé et al., 2020)). Next, we stained for Cl. Casp3 and Ki67, and observed that apoptosis was reduced whereas proliferation was increased in shTRAIL tumors which may contribute to the bigger tumor volume (**Fig. 5I, J, S5A**). This effect was not seen when shTRAIL cells were engrafted into a TNCKO host (**Fig. 5I, J**). In NT193 grafted tumor mice, tumor cells formed lung metastasis (Sun et al., 2019). Here, we investigated lung metastasis by qRTPCR for *ErbB2* and noticed more *ErbB2* expression in lungs from shTRAIL than control tumor mice **(Fig. 5K)**. No difference was seen in lungs from a TNCKO tumor mouse,

altogether, suggesting that TRAIL reduces metastasis presumably as consequence of lowering the tumor volume (**Fig. 5E, K**).

We also generated cells with a KD for DR5 and proved reduced *DR5* by qRTPCR and immunoblot (**Fig. S5B, C**). Cultured cells were also resistant to TRAIL/MD5-1 induced apoptosis revealing efficient DR5 reduction (**Fig. S5D**). Upon engraftment, no or little difference in tumor volume was seen between shDR5 and control cells when grafted in a WT or TNCKO host, respectively (**Fig. S5E-G**). Altogether, these results suggest that tumor growth was regulated by TRAIL mostly impacting other functions than TRAIL/DR5-induced tumor cell cytotoxicity.

TRAIL impacted infiltration of myeloid cells

As TNC regulated the phenotype of myeloid cells, in particular DC and MP (Deligne et al., 2020; Spenlé et al., 2020), we determined the abundance of activated DCs (CD11c+/CD80+/CD86+) and MPs (F4/80+) by flow cytometry. In TRAIL KD tumors, we observed less CD11c+/CD80+/CD86+ and F4/80+ cells (**Fig. 6A, B, S6A-C)**. No difference was seen when shTRAIL cells were grafted in a TNCKO host (**Fig. 6A, B**), suggesting that TNC is also important for regulating DC and MP infiltration. In tumors from both hosts we observed less B cells upon TRAIL KD which may reflect changes in the humoral anti-tumor response (**Fig. S6D**).

By investigating the phenotype of the infiltrating MP by flow cytometry, we noticed that despite less MP in TRAIL KD tumors, the remaining MP had mostly an M1 phenotype, indicating that TRAIL may trigger the infiltration of M2 MPs (**Fig. 6C**). We determined the spatial localization of CD68+ (MP) and CD11c+ cells by IF, and confirmed high numbers of MP in the TNC-rich stroma and an ubiquitous distribution of DC in control tumors (**Fig. 6D, S6A, B**; (Deligne et al., 2020). No difference in the spatial distribution of DCs was noticed in shTRAIL tumors (**Fig. S6A, B**).

Through investigation of mosaic images of the tumors, we noticed that shTRAIL tumors had a very different overall appearance than control tumors. Tumors with TRAIL KD were a dense mass of tumor cells and TME in contrast to a fuzzy, disintegrated, swiss cheese like appearance of control tumors (**Fig. 6D**). Moreover, shTRAIL tumors appeared to have less holes than control tumors which indeed was the case as confirmed by quantification (**Fig. 6E**). Moreover, we also noticed many CD68+ cells outside the tumor nest, inside the tumor matrix tracks (TMT) and most importantly inside the holes of control tumors, likely representing phagocytosis by MP that was reduced in shTRAIL tumors as the number of holes was lower (**Fig. 6E**). Whereas the number of CD68+ holes was equal between the different tumors, the number of CD68+ MP inside the holes was reduced in shTRAIL tumors, which may contribute to smaller holes (**Fig. 6G, S6C, E**). Taken into account that MP were more numerous and mostly of an M2 phenotype in WT tumors (**Fig. 6B,C**), MP may also reduce the tumor volume via phagocytosis (Zhou et al., 2020), as we saw smaller shC tumors (**Fig. 5E, F**). Despite less B cells, it remains to be seen whether less active and numerous MP also triggered a weaker adaptive immune response in shTRAIL tumors. Interestingly, we observed TNC in the stroma of tumors from cells engrafted into a TNCKO host indicating that epithelial tumor cells have gained mesenchymal characteristics, as E cells did not express TNC in culture, altogether suggesting that M cell-associated TRAIL resistance may indeed be relevant *in vivo* (**Fig. S6C**).

We also investigated DC and MP infiltration of DR5 KD tumors by flow cytometry and noticed that DC numbers were reduced whereas MP and B cell numbers remained unchanged compared to the control tumors (**Fig. S6F-I**). Interestingly, in KO/shDR5 tumors MP numbers were reduced, and had mostly a CD206 negative M1-like phenotype suggesting that not only tumor cell derived but also host derived TNC promotes an M2 phenotype (**Fig. S6I,** (Deligne et al., 2020)).

Altogether, TRAIL acted primarily on the immune system and not by killing the tumor cells through TRAIL/DR5 signaling, although NT193 cells were sensitive to TRAIL-induced killing *in vitro*. Many possibilities could explain this phenotype including cell intrinsic properties that have to be investigated in the future. However, we revealed a role of matrix in impairing TRAIL. In particular, TNC confining TRAIL in the stroma thereby impairing DC and MP may

contribute to corrupted anti-tumor immunity. Moreover, TRAIL increasing abundance of DC and MP was regulated by host-derived TNC that impacted tumor cell plasticity, suggesting a complex interconnection.

TRAIL promoted myeloid cell invasion into tumor spheroids through CXCR4

We performed an RNA seq analysis of tumors with low and high TRAIL to determine how TRAIL regulated myeloid cell abundance and functions. We noticed that genes regulating MP-associated cytokine release and phagosome formation were impacted by the TRAIL KD (**Fig. 7A, S7A**). Moreover, *Cxcr4* was reduced in shTRAIL tumors (independent of host TNC) which we confirmed by qRTPCR (**Fig. 7B, S7A**). Also, *Mapk1* and *Mapk3,* encoding for ERK1 and 2, downstream molecules of CXCR4, were downregulated in shTRAIL tumors suggesting a profound effect of TRAIL on CXCR4 signaling (**Fig. 7A, C, D**).

As we had previously observed that NT193 cells express CXCL12, the ligand of CXCR4 (Murdamoothoo et al., in revision), and that *Cxcr4* was higher in WT shC than shTRAIL tumors (**Fig. 7A, B**), we determined whether E cells grown on the lower bottom of a Boyden chamber device influenced matrigel invasion of DC2.4 dendritic cells and RAW267 macrophages. Indeed, we noticed that cells invaded the matrigel and passed through to the lower side of the filter where cells were counted **(Fig. 7E)**. The number of DC2.4 and RAW267 cells was reduced when shTRAIL tumor cells were plated at the bottom, suggesting that TRAIL regulates DC2.4 and RAW267 attraction via the NT193E cell secretome (**Fig. 7F, G**). We also used our tumor cell spheroid model to determine DC and MP invasion (**Fig. 7H**). Fluorescently tagged DC and MP invaded the spheroids, yet less when the tumor cells expressed little TRAIL **(Fig. 7I, J)**. Next, we determined whether CXCR4 signaling was involved. Indeed, invasion of myeloid cells through matrigel or into tumor cell spheroids was significantly reduced upon CXCR4 inhibition (by AMD3100), reaching levels as with shTRAIL cells (**Fig. 7E-J**). By analyzing the secretome of the NT193E shC and NT193E shTRAIL cells via mass spectrometry, we noticed that TRAIL impacted the secretion of 52 molecules related to immune response as revealed by the comparison of the proteome of the conditioned medium from shC and shTRAIL cells (**Fig. 7K, S7B, Table S1**). This proteome included TGFβ2, TGFβ3, X3CL1 and CSF1 to be more secreted by shC cells which could play a role in upregulating CXCR4 by TRAIL as previously shown (Ferretti et al., 2011; Korbecki et al.,

2020; Lee et al., 1999; Mylonas et al., 2019; Stephenson et al., 2019). Future studies have to identify by which mechanism TRAIL upregulates CXCR4 expression in DC and MP.

TNC represses TRAIL through integrin α4β1/α9β1 and, combined low expression of TRAIL and CXCR4 correlated with poor patient survival

As TRAIL levels were higher in tumors with no or lowered TNC (**Fig. 1A, B**) and tumor cells were a major source of TRAIL **(Fig. 5A-D**), we asked how TNC affected TRAIL expression in the tumor cells. Therefore, we treated E cells with TNC and determined TRAIL expression by qRTPCR. Indeed, TRAIL levels were significantly lower with TNC (**Fig. 8A**). Next, we wanted to know how TNC downregulated TRAIL and used inhibitors. We observed that BOP, an inhibitor of α4β1 and α9β1 integrins relieved repression by TNC. In contrast inhibition of TLR4 (Cli95), TGFβR1 (GW788388) or receptor tyrosine kinases (Sunitinib) did not affect TRAIL repression by TNC (**Fig. 8A**). With specific inhibitors for α4 and α9 integrins, respectively, it may be possible to identify through which integrin TNC regulates TRAIL expression (**Fig. 8B**).

Our results suggest that TRAIL activates innate immunity through CXCR4 (and downstream signaling partners) in DC and MP that are attracted by CXCL12, highly expressed by the tumor cells via TNC activating TLR4 (Murdamoothoo et al., in revision). By downregulating TRAIL, TNC may impair the immune functions of TRAIL. We used Kaplan Meier analysis to determine whether *TNFSF10* levels in combination with *CXCR4* and *ITGAX* (CD11c) have predictive value in breast cancer. Indeed, high *TNFSF10* in combination with high *CXCR4* and high *ITGAX* correlated with longer overall and relapse-free survival in breast cancer patient cohorts GSE42568 and GSE1456_133A (**Fig. 8C, D, S8A, B**). Moreover, by stratifying the patients of cohort GSE42568 according to low or high *TNC*, we observed that high *TNC* abrogates overall survival benefit of high *TNFSF10*, suggesting relevance of our results from the murine cancer model for human breast cancer (**Fig. 8E, F**). Altogether, this analysis suggests that high levels of TNC in breast tumors decrease the antitumoral effects of TRAIL.

7.4. Discussion

The death ligand TRAIL is a promising target for anti-cancer therapy, yet our knowledge is limited how TRAIL acts in context of a complex TME. Here, by using our novel syngeneic NT193 tumor grafting model where we grafted cells with downregulated TRAIL and DR5, respectively into a WT or TNCKO host, we were able to discriminate between tumor cell and host specific responses and their regulation by TNC. Ablation of TRAIL signaling in the tumor cells (by DR5 KD) did not affect tumorigenesis whereas TRAIL KD significantly increased tumor growth and lung metastasis revealing a major role of TRAIL shaping anti-tumor immunity. Thus, our model with engineered TRAIL and DR5 levels may be useful to independently target the immunity and tumor cell killing functions of TRAIL by drugs.

We have recently shown that TRAIL enhances myeloid cell attraction by the tumor cells expressing CXCL12 (Murdamoothoo et al., in revision). TRAIL was previously shown to induce an M2-like MP phenotype through CCL2 (Hartwig et al., 2017). Since CCL2 has been identified as a possible inducer of CXCR4 in human monocytes (Campbell et al., 2007), the interaction between TRAIL, CCL2 and CXCR4 has to be investigated in the future.

Here, we have shown that TNC impairs TRAIL by three mechanisms. TNC repressed the TRAIL immune function by downregulating TRAIL expression through integrins α4β1/α9β1. We have previously described that TNC impairs YAP signaling through integrin α9β1 (Sun et al., 2018). Whether TNC impairs TRAIL expression through YAP has to be addressed in the future.

By binding TRAIL, TNC potentially impairs TRAIL penetration of tumor cell spheroids and tumor cell killing. Moreover, cancer cell plasticity and enhanced survival signaling by TNC, seen in NT193 tumors (Sun et al., 2019), may contribute to impaired TRAIL killing, which could be explained by poor DR5 expression upon EMT. Altogether, we identified a novel immune-suppressive action of TNC through impairing TRAIL sensitivity.

The TNC sequence is highly conserved within the mammalian kingdom and has no gross deletions or other large changes in its sequence arguing for important not yet well understood roles of TNC in normal tissues. As TNC expression is very restricted in adult tissues, it may be meaningful that TNC is expressed in lymphoid organs where it is believed that TNC may fulfill a role in immune cell education (Drumea-Mirancea et al., 2006; Midwood et al., 2009; Spenlé et al., 2015). Upon tissue damage TNC is immediately upregulated where it acts as DAMP by recruiting immune cells for defense and repair (Midwood et al., 2009, 2016). It is possible that this function is preserved in tumors where we have noted that TNC may upregulate an antigen processing and presenting signature (Deligne et al., 2020; Spenlé et al., 2020). This defense function is presumably overcome when TNC is forming TMT, resembling reticular fibers in lymphoid organs (Midwood et al., 2009; Spenlé et al., 2015), that we have shown to serve as niches to corrupt anti-tumor immunity (Spenlé et al., 2020; Murdamoothoo et al., in revision). To maintain tissue homeostasis TNC functions need to be balanced via potent molecular executers. In this light it is not surprising that TNC regulates the death inducer TRAIL. At first glance downregulation of TRAIL functions by TNC appears counter-intuitive but may reflect a response within a network of pro- and anti-immunity regulatory mechanisms to prevent uncontrolled immunity. Here, the observed impact of TNC on TRAIL recruitment of macrophages into tumor holes, presumably reflecting phagocytosis is remarkable and may allow a glance into the ancient heritage of TNC as potential defender against microbes such as bacteria and HIV (Fouda et al., 2013; Meijer et al., 2020; Yuan et al., 2018). That TNC may regulate MP associated phagocytosis was already implied but a link to TRAIL was unknown (Ma et al., 2019).

Here, we identified mechanisms how to sharpen TRAIL as knife to eradicate cancer. Targeting plasticity, release of TRAIL from TNC (e.g. by a 19 amino acid MAREMO peptide (Erne et al., in preparation)) and blocking α4β1/α9β1 integrins to increase TRAIL expression could be considered to restore TRAIL immune function in particular in combination with MD5-1 to strengthen the TRAIL/TRAIL-R complex and subsequent signaling (Finnberg et al., 2016). Moreover, the immune-suppressive actions of TNC impairing TRAIL could be used for patient stratification. As high TRAIL correlated with longer breast cancer patient survival, we predict that TRAIL killing is better the lower the TNC levels are.

7.5. Material and methods

Mice

Experiments involving mice were done according to the guidelines of INSERM and the ethical committee of Alsace, France (CREMEAS). Directive 2010/63/EU concerning the protection of animals used for scientific purposes was applied.

Murine cancer model

MMTV-NeuNT mice were generated on a FVB background expressing a mutated form of *neu* constitutively activating Erbb2 (NeuNT) specifically in the mammary glands under the control of the mouse mammary tumor virus (MMTV) promoter (Muller et al., 1988). TNC +/+ and -/- mice were generated on a FVB background via TNC +/- breeding as previously described (Sun et al., 2019). Female mice were used at 2-3 months of age. For orthotopic grafting, 5 x 10^6 NT193 cells were injected in a sterile 50µL Phosphate Buffered Saline solution (PBS, Dutscher X0515-500) into the left fourth mammary gland after surgical opening. Tumor growth was measured with a caliper twice a week during 7 weeks and tumor volume was calculated according to the formula V = ½ (length x width²). Mice were sacrificed at indicated time points, and breast tumors and lungs were collected. Tissues were frozen in liquid nitrogen for mRNA preservation or embedded in tissue freezing medium (Leica 14020108926) in order to perform genes expression analyses and immunostainings.

Tissue Immunofluorescence staining (IF)

Tissue sections (7 µm thick) were incubated for 1 hour with a blocking solution (5% normal goat serum in PBS, Southern Biotech 0060-01) at room temperature before overnight incubation with primary antibodies at 4°C. After washing, the slides were incubated with corresponding secondary antibodies for 1 hour at room temperature. The slides were then washed, stained with DAPI (Sigma D9542) for 10 minutes at room temperature and finally sealed with Fluoromount-G™ (Thermo Fischer 00-4958-02). Fluorescence pictures were acquired with a Zeiss Axio Imager Z2 microscope and analyzed with Zen Lite 2012 edition software. The image acquisition setting (microscope, magnification, light intensity, exposure time) was kept constant per experiment conditions. Antibodies are listed in **Table S2**.

Cells Immunofluorescence staining

Cells cultured in Nunc™ Lab-Tek™ II Chamber Slides™ (Thermo Fisher 154534) were fixed with 4% paraformaldehyde (PFA, Santa Cruz SC-281692) in PBS for 10 minutes, then permeabilized with 0.25% Triton (EUROMEDEX 2000-A) in PBS for 15 minutes. After washing, blocking solution was applied for 30 minutes before primary antibody incubation for 1 hour at room temperature. Corresponding secondary antibodies and rhodamine coupled phalloidin (Thermo Fisher P1951) were incubated 45 minutes after washing. DAPI staining, slide sealing and image acquisition was similar to tissue IF.

Cell culture

The NT193 murine breast cancer cell line has been established in our laboratory from a primary MMTV-NeuNT breast tumor (Arpel et al., 2014). NT193 cells were cultured in Dulbecco's modified Eagle's medium (DMEM Dutscher L0104-500) containing 4.5 g/L glucose, L-glutamine, sodium pyruvate supplemented with 10% of inactivated fetal bovine serum (FBS, Dutscher S1510-500), penicillin (10 000 U/mL), streptomycin (10 mg/mL) (Dutscher P06-07100). EO771 murine breast cancer cells (Casey et al., 1951) were cultured in DMEM containing 4.5 g/L glucose, L-glutamine, sodium pyruvate, with HEPES (20mM, Merck PHG0001) supplemented with 10% of inactivated FBS, penicillin (10 000 U/mL), streptomycin (10 mg/mL). RAW 264.7 murine macrophage cells (Raschke et al., 1978) were maintained in DMEM containing 4.5 g/L glucose, L-glutamine, sodium pyruvate, supplemented with 10% of inactivated FBS, penicillin (10 000 U/mL), streptomycin (10 mg/mL). DC2.4 murine dendritic cells (Shen et al., 1997) were cultured in Roswell Park Memorial Institute 1640 (RPMI-1640, Dutscher L0500-500) medium containing 4.5 g/L glucose, L-glutamine, sodium pyruvate, with HEPES (20mM) supplemented with 10% of inactivated FBS. New vials of cells were thawed each 10-15 trypsinizations (Trypsin-EDTA Ca^{2+}, Mg^{2+} free, Dutscher P10-022100 + P10-15100) and cell culture was realized at 37°C in a humidified atmosphere of 5% CO_2. Recombinant his-tagged human TNC was purified in house prior to cell culture and binding experiments, as previously described (Giblin et al., 2018; Huang et al., 2001). Before TNC incubation, cells were pretreated with inhibitors for TGFβRI (GW788388, 10 µM, 45 minutes, Selleckchem S2750) in TRAIL killing experiments and with inhibitors for TLR4 (Cli95, 1µg/mL, 6 hours, InvivoGen tlrl-cli95), receptor tyrosine

kinases (SU6668, 30 µM, 60 minutes, Tocris bioscience 3335), and α9β1/α4β1 integrins (BOP, 1 µM, 45 minutes, Tocris bioscience 6047) in *Tnfsf10* expression measurements.

Transduction of cells and subcloning

NT193 cells have been previously engineered to express normal or lower amount of TNC by transduction with a lentivirus expressing shRNA against TNC (shTNC: TRCN0000312138, 5'-CCGGGCATCAACACAACCAGTCTAACTCGAGTTAGACTGGTTGTGTTGATGCTTTTTG-3') or control shRNA (shC: SHC202V, Sigma-Aldrich) (Sun et al., 2019). For stable inhibition of *Tnfsf10* and *Tnfrsf10b* expression, shRNA expressing lentiviruses were generated as previously described (Hyenne et al., 2015). Sequences for shRNA *Tnfsf10*.f: 5′-CCGGCCGGGATCTACCTGGTATCAGTTTGCTCGAGCAAACTGATACCAGGTAGATCTTTTTTGG-3′ and *Tnfrsf10b*.f: 5'-CCGCAGGGTTTCGGATGAGCTGACACCATGGAGCCTCCAGGACCCAGCACGCCCACA-3' were inserted into the BamHI to EcoRI sites of the pLKO.1 vector. Transduced cells were subcloned in 96-wells plates (Falcon 353072) and selected with normal medium containing 10 µg/mL of puromycin (Thermo Fisher A11138-03) in order to dissociate epithelial (NT193E) and mesenchymal cells (NT193M), and generate the following cell lines: NT193E shC, NT193M shC, NT193E shTNC, NT193M shTNC, NT193E shTRAIL and NT193E shDR5. Selection pressure was maintained over time.

Cell expansion measurement

After trypsinization and cell counting, 1000 NT193E or NT193M cells were seeded into 96-well plates in normal medium, at 37°C in a humidified atmosphere of 5% CO_2. Cell growth was assessed by using CellTiter 96® AQueous Non-Radioactive Cell Proliferation Assay (Promega G5421) according to the manufacturer's instructions. In brief, cell expansion was measured after 4, 24, 48 and 72 hours by incubating CellTiter 96® reagent for 2 hours at 37°C. The optical density (OD: 490 nm) was measured with a Varioskan LUX Multimode Microplate Reader (Thermo Fischer).

Wound healing assay

NT193E and NT193M cells were grown to confluency in 24-well plates (Falcon 353047) in normal medium prior to 6 hours of starving in medium containing no FBS. Then cell proliferation was inhibited by treating with mitomycin C (Sigma M4287) at 2 µg/mL for 2 hours. The wound was done by scratching the cell monolayer using a 200 µL tip. Cell debris was removed by washing with PBS before incubating the cells in medium containing no FBS. Two pictures of each wound were acquired directly after the scratch and after 16 hours of incubation at 37°C in a humidified atmosphere of 5% CO_2. The relative wound healing was calculated by measuring and subtracting the cell-free surface before and after the incubation.

Gene expression analysis by qRTPCR

Total RNA was prepared from cultured cells or frozen tissues using TriReagent (Life Technologies AM9738) with a cell scraper or with a tissue homogenizer according to the manufacturer's instructions. RNA was treated with DNAse I (Roche 04716728001) and reverse transcribed (MultiScribe reverse transcriptase, Applied Biosystems 10117254) before determination of the concentration and the purity with a NanoDrop 2000 (Thermo Fisher). qPCR was done on cDNA (diluted 1:5 in water) with a QuantStudio™ 5 Real-Time PCR System (Applied Biosystems) using TaqMan™ Fast Advanced Master Mix (Applied Diosystems 4444557). *Gapdh* was used as housekeeping gene for the comparative cycle threshold method (2-ddCt). Primers are listed in **Table S3**.

Gene expression analysis by RNA-Sequencing

Total RNA was prepared as for RTq-PCR. RNA integrity was assessed with an Agilent total RNA Pico Kit on a 2100 Bioanalyser instrument (Agilent Technologies 5065-4401) (RINs at 10), and ribosomal RNA was depleted with the Low Input RiboMinusTM Eukaryote System v2 kit (Thermo Fisher A15026). To prepare the sequencing library, the Ion Total RNA-sep kit v2 (Thermo Fisher 4475936) was used following the manufacturer's instructions. The libraries were loaded at a concentration of 20 pM on an Ion PI™ Chip Kit v3 (Thermo Fisher A26770) using the Ion Chef Instrument (Thermo Fisher). Sequencing was performed on an Ion Proton sequencer (Thermo Fisher) with the Ion PI™ Hi-Q™ Sequencing 200 Kit (Thermo Fisher A26433). Transcriptomic data was processed using the RNASeqAnalysis plugin from the

Torrent Suite Software 5.06, and the reads were mapped using STAR and Bowtie2 (Dobin et al., 2013; Langmead and Salzberg, 2012). The total read maps are available in BAM (Binary Alignment Map) format for raw reads counts extraction. Read counts were found with the htseq-count tool of the Python package HTSeq (Anders et al., 2015). Differential analyses were performed using the DESEQ2 package from the Bioconductor framework (Love et al., 2014). Upregulated and downregulated genes were selected based on the adjusted p-value cutoff 10% and heatmapping was done using online heatmapper (http://www.heatmapper.ca, (Babicki et al., 2016)).

Western blotting (WB)

Cell lysates were prepared using Radioimmunoprecipitation assay (RIPA) buffer (150mM Tris-HCl pH8, 150mM NaCl, 1% NP-40, 1% sodium deoxycholate, 0.1% SDS) supplemented with protease and phosphatase inhibitors (Pierce EDTA-Free mini tablets, Thermo Fischer A32961) and protein concentration was assessed with Bradford assay (BioRad 500-0006). Proteins (20µg/well) were loaded with Laemmli buffer (BioRad 161-0747) containing 10% β-mercaptoethanol (Merck 1.120006) into precasted 4-20% gradient gels (BioRad 4561094). Electrophoresis and protein transfer on nitrocellulose membranes were realized with BioRad equipment and consumables (Mini-PROTEAN Tetra electrophoresis and Trans-Blot Turbo™ systems). The blots were soaked in blocking solution (5% non-fat milk diluted in 0.01% Tween-20 PBS) during 1 hour at room temperature before incubation with primary antibodies overnight at 4°C. Secondary antibodies were incubated 1.5 hour at room temperature. Amersham ECL Western Blotting detection reagent (GE Healthcare RPN2106) or SuperSignal™ West Femto Maximum Sensitivity Substrate (ThermoFisher 34095) were used to detect protein bands in a ChemiDoc™ Imager (BioRad). Antibodies are listed in **Table S2**.

Quantitative proteomics

Sample preparation. Protein precipitation of NT193 culture supernatant was performed according to the protocol as previously described (Chevallet et al., 2007). Briefly, after adding Sodium Lauroyl Sarcosinate (NLS) to a final concentration of 0.1% and TCA trichloroacetic acid to a final concentration of 7.5 %, proteins were precipitated on ice for 2 hours and were pelleted by centrifugation for 30 minutes at 10 000g at 4°C. Supernatant was removed and

the pellet was re-suspended in cold tetrahydrofuran to wash the protein pellet. This step was repeated 2 times for 10 min at 10 000 g at 4°C. Finally, the protein pellet was resuspended in Laemmli type buffer (10 mM Tris pH 6.8, 1mM EDTA, 5% SDS, 10 glycerol). Samples were vortexed and sonicated 2 times during 5 minutes in an ice-cold bath. Concentration of all samples was determined using the DC™ Protein Assay (Bio-Rad 5000111). After addition of dithiothreitol (50 mM final concentration), 15 µg of each protein extract were heated at 95°C for 5 minutes and stacked in an in-house prepared 5% acrylamide SDS-PAGE stacking gel. Gel bands were cut, destained, reduced with 10 mM dithiothreitol, alkylated using 55 mM iodoacetamide prior to overnight digestion at 37°C using Sequencing Grade Modified Trypsin (Promega V5111).

NanoLC-MS/MS analysis. Extracted tryptic peptides (800 ng) were analysed by nanoLC-MS/MS on a nanoUPLC system (nanoAcquityUPLC, Waters, USA) coupled to a quadrupole-Orbitrap hybrid mass spectrometer (Q-Exactive plus, Thermo Fisher). Chromatographic separation was conducted over a 79 minutes linear gradient from 1 to 35% of solvent B (0.1 % formic acid in acetonitrile) at a flow rate of 400 nL/min. A Top 10 method was used with automatic switching between MS and MS/MS modes to acquire high resolution MS/MS spectra. All samples were injected using a randomized injection sequence. To minimize carry-over, a solvent blank injection was performed after each sample. NanoLC-MS/MS data was interpreted to do label-free extracted ion chromatogram-based differential analysis using MaxQuant software (version 1.6.14, (Tyanova et al., 2016)). Peaks were assigned with the Andromeda search engine against a concatenated database containing all mouse and bovine entries extracted from UniProtKB-SwissProt (release 19-10-2020; 23 073 sequences, Taxonomy ID 10090 and 9913). No “match between runs” were done between the samples. Carbamidomethylation of cysteines was set as fixed modification whereas oxidation of methionines and protein N-terminal acetylation were defined as variable modifications. The maximum false discovery rate was 1% at peptide and protein levels with the use of a decoy strategy. Only unique mouse peptides were kept and their intensities were summed for a given protein. Non-normalized protein intensity values were exported and used for differential analysis using Prostar software (version 1.18.6, (Wieczorek et al., 2017)). To be considered, proteins must be identified in a minimum of 4 out of 5 replicates in at least one condition. The “det quantile” imputation mode was applied for the missing values. A Limma moderated t-test was applied on the dataset to perform differential analysis. The adaptive Benjamini-Hochberg procedure was applied to adjust the p-values and FDR values under 1%.

TRAIL killing activity in 2D cell culture

Mouse recombinant SUPERKILLERTRAIL® (Enzo Lifesciences ALX-201-130-C020) was used alone or in combination with MD5-1 antibody (Functional grade, eBioscience™ 16-5883-82) to induce cell death. Briefly, NT193 and EO771 cells were seeded in their corresponding media in 96-well plates, at 10 000 cells/well, for 24 hours before treatment. TRAIL, MD5-1 or TRAIL+MD5-1 treatments were applied for 16 hours in the respective cell media (final volume 100 µL). Caspases 3 and 7 activity were assessed using Caspase-Glo® 3/7 Assay according to the manufacturer's instructions (Promega G811A). Cells were incubated with the Caspase-Glo® 3/7 reagent for 1.5 hour before luciferase luminescence measurement with a Varioskan™ LUX (Thermo Fischer). Cell death and viability was assessed by acridine orange / ethidium bromide (AO/EB) incorporation measurement. Briefly, cells were seeded and treated with TRAIL as previously explained. AO/EB solution (5 µL/well, stock solution at 100 µg/mL in PBS) was mixed to the cells 5 minutes before plate centrifugation (300 x g, 5 minutes). Fluorescence pictures of the centers of each well were acquired using a Motic™ AE31E trinocular microscope and cell counting was done with Zen Lite 2012 edition software. For 2D culture, MD5-1 concentration was maintained at 50 ng/mL.

TRAIL killing activity in spheroids

NT193 spheroids were generated according to the hanging drop method (Berens et al., 2015). In details, the bottom of 10 cm dishes (Corning 430167) was filled with 10 mL of sterile PBS prior cell seeding. After trypsinization and cell counting, 5000 NT193E or NT193M cells were suspended in 30 µL droplets (normal medium), on the inner face of the lid of a cell culture dish to form mono-cultured spheroids. Then the dishes were closed, inverted and incubated at 37°C in a humidified atmosphere of 5% CO_2. Medium was changed every 48 hours. Co-cultured spheroids were obtained similarly by mixing 2500 NT193E cells with 2500 NT193M shC or NT193M shTNC, respectively by droplets. After 4 days, spheroids were recovered in 4% PFA/PBS for 10 minutes prior to embedding in tissue freezing medium in order to perform immunostainings. TRAIL + MD5-1 treatment was applied in normal medium after 48 hours of spheroid growth. After an additional 48 hours, spheroids were collected in 96-wells plates for caspases 3/7 activity and AO/EB incorporation measurement. The same protocol as in 2D cell culture was applied, with the difference that reagents volumes were adapted to a final volume of 50 µL (25 µL coming from the spheroids droplets and 25 µL from

fresh medium). Apoptosis sensibility was verified using staurosporine (1 µg/mL, Sigma S4400).

TNC-TRAIL binding assessment by surface plasmon resonance

Recombinant TNC was immobilized at high surface density (around 7000 resonance units) on an activated CM5 chip (GE Healthcare BR-1000-12), at 25°C, using amine-coupling procedure according to the manufacturer's instruction. Recombinant TRAIL (75 nM and 300 nM) has been deposited on the CM5 chip in binding solution (10mM HEPES, 150 mM sodium chloride, 0.005% (v/v) surfactant P20, pH 7.4) at a flow rate of 10 µL/minute. Background correction was made with a blank CM5 chip prior to the binding experiment. The CM5 chip was regenerated between each measurement via injecting 100 µL of a regenerating buffer (10 mM glycine, pH 2.0), in one minute. The dissociation constant (Kd) was calculated using the 1:1 Langmuir association model as described by Biacore Inc. The Surface plasmon resonance (SPR) binding experiment was performed with a Biacore 2000 instrument (Biacore Inc).

TNC-TRAIL binding assessment by transmission electron microscopy

Physical interaction between TNC and TRAIL was assessed by negative electron microscopy imaging as previously described (Bober et al., 2010). In brief, recombinant TRAIL (3 molar excess) was conjugated to 5 nm colloidal gold (Baschong and Wrigley, 1990) prior to incubation with TNC (20 nM) in tris buffered saline solution (TBS), pH 7.4, at 37°C for 1 hour. Heparin (10 molar excess, Merck 1304016) was preincubated with TNC for the inhibition experiments at 37°C for 1 hour. Samples were visualized with a Philips/FEI CM 100 TWIN transmission electron microscope operated at 60 kV accelerating voltage. Pictures were taken with a side-mounted Olympus Veleta camera with a resolution of 2048 x 2048 pixels and the ITEM acquisitions software. Binding of TRAIL to TNC was determined by counting the number of gold particles linked to TNC monomers (500 images). EGF (shown not to bind to TNC (De Laporte et al., 2013)) and Bovine Serum Albumine (BSA, EUROMEDEX 04-100-812-E) were used as controls.

FACS analysis

Small slices of mammary tumors were digested in RPMI containing Collagenase D (1 mg/mL, Roche 11088866001), DNase I (0.2 mg/mL, Invitrogen 18047-019) and 2% of FBS for 2 hours at 37°C. After inhibiting the digestion by adding EDTA (final concentration 5 mM), the digested tissue was passed through 70 µm and 40 µm cell strainers with flow cytometry buffer (PBS, 2% FBS, 1 mM EDTA) in order to singularize cells. Cells were then stained with Dead viability dye-efluor 450 (Thermo Fisher 65-0863-18) and saturated in 2% Fc Block solution (CD16/CD32, Thermo Fisher 14-0161-85) at 4°C for 15 minutes prior to incubating the surface antibody solutions at 4°C for 30 minutes. Solution 1: anti-CD45-FITC, anti-CD11c-PE, anti-B220-APC, anti-MHCII-APC EF780, anti-CD80-Percp Cy7 and anti-CD86-AF700; solution 2: anti-CD45-FITC, anti-CD3e-PE, anti-CD4-APC EF780; solution 3: anti-CD45-FITC, anti-F4/80-APC EF780 and anti-CD206-Percp Cy7. Data were acquired with a Beckman Coulter Gallios flow cytometer and analyzed with FlowJo software. Antibodies are listed in **Table S2**.

Boyden chamber invasion with DC2.4 and RAW 264.7 cells

Boyden chamber invasion assays on DC2.4 and RAW 264.7 were performed in 8 µm-pore sized polycarbonate membrane transwells (Greiner 662638). NT193E shC or shTRAIL cells were seeded at 25 000 cells/well in normal medium in 24-well plates, for 24 hours. Medium was then changed for 1% FBS medium containing no puromycin, for 24 hours. Matrigel (4 mg/mL, Corning 356234) was polymerized in the insert in DMEM for 30 minutes, at 37°C. After 6 hours starving followed by trypsinization and counting, DC2.4 and RAW 264.7 were seeded in the insert at 50 000 cells/insert medium containing no FBS. After 48 hours, cells in the inserts were fixed in iced cold methanol and stained with DAPI. Matrigel and cells in the upper chamber were removed with a cotton dub. Three pictures per well were taken and analyzed by the ImageJ software. For CXCR4 inhibition, AMD3100 (Sigma 239820) was added at 5 µg/mL to the medium during the DC2.4 and RAW 264.7 seeding.

Spheroid infiltration with DC2.4 and RAW 264.7

NT193E shC and NT193 shTRAIL cells were grown for 4 days in full medium, followed by growth in 1% FBS containing medium without puromycin, for 24 hours. After 6 hours starving,

DC2.4 and RAW 264.7 were stained using CellTracker™ Green CMFDA labeling according to the manufacturer's instructions (Invitrogen C7025). Following trypsinization and counting, cells were seeded at 5000 cells/spheroid in 30 µL droplets of medium containing 1% FBS. After 24 hours, infiltrated spheroids were collected into 96-well plates, then fixed in 4% PFA /PBS for 15 minutes and permeabilized with 0.25% Triton/PBS for 20 minutes. DAPI staining, slide sealing and image acquisition was similar to tissue IF. For CXCR4 inhibition, AMD3100 was added at 5 µg/mL to the medium during the DC2.4 and RAW 264.7 seeding.

Patient survival analysis

Human breast cancer overall survival and relapse-free survival were obtained and analyzed with Kaplan-Meier representation via PROGgeneV2 (Goswami and Nakshatri, 2014). The cohorts were stratified according to *Tnc* high or low expression (mean as the median could not be reached). For stratification of TRAIL, CXCR4 and ITGAX the median of expression was used.

Statistical analysis

Gaussian distribution was tested by the d'Agostino-Pearson normality test. Unpaired t-test (with Welch's correction in case of unequal variance) or ANOVA two-way test were applied when data followed a normal distribution. Otherwise, Mann Whitney test or a non-parametric ANOVA followed by Dunns post-test were used. RNA-Seq and proteomic data were analyzed using a Limma moderated t-test. Analysis and graphical representation were done using GraphPad Prism (version 6). P values <0.05 were considered statistically significant. Data are representative of at least two individual experiments, expressed as the mean ± SEM. (*p<0.05; **p<0.01; ***p<0.001; ****p<0.0001).

7.6. Figures

Figure 1

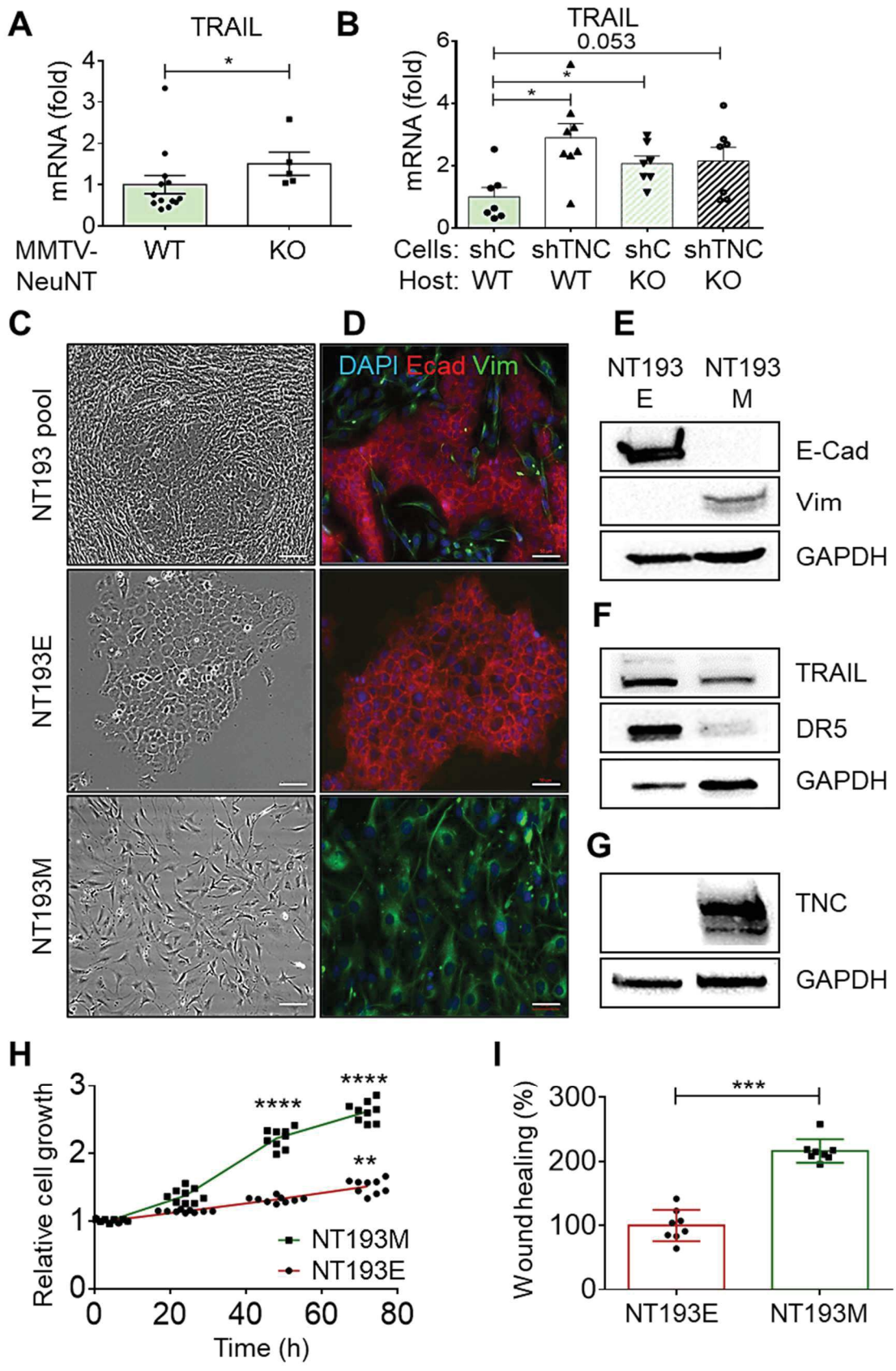
A
TRAIL
mRNA (fold)
MMTV-NeuNT
WT
KO
B
TRAIL
0.053
mRNA (fold)
Cells: shC shTNC shC shTNC
Host: WT WT KO KO
C
NT193 pool
NT193E
NT193M
D
DAPI Ecad Vim
E
NT193 E
NT193 M
E-Cad
Vim
GAPDH
F
TRAIL
DR5
GAPDH
G
TNC
GAPDH
H
Relative cell growth
Time (h)
NT193M
NT193E
I
Wound healing (%)
NT193E
NT193M

Figure 1: TRAIL levels are higher in tumors with low TNC and are associated with tumor plasticity

TRAIL mRNA levels in MMTV-NeuNT **(A)** and NT193 tumors **(B)**. WT, N = 13, KO, N = 5 **(A)**, WT/shc, N = 7, WT/shTNC, N = 8, KO/shC, N = 7, KO/shTNC, N = 7 **(B)**. **(A)** Mann-Whitney test, mean ± SEM (*p < 0.05). **(B)** Kruskal-Wallis test, mean ± SEM (*p < 0.05). Representative images of NT193 pool, NT193E and NT193M cells, phase contrast **(C)** and IF **(D)**, N = 3, scale bar 50 µm. **(E - G)** Immunoblots for the indicated molecules, N = 2. **(H)** Cell proliferation in full medium, N = 3 experiments, n = 3 replicates. Kruskal-Wallis test, mean ± SEM (**p < 0.01; ****p < 0.0001). **(I)** Wound closure, N = 4 experiments, n = 2 replicates. Mann-Whitney test, mean ± SEM (***p < 0.001).

Figure 2

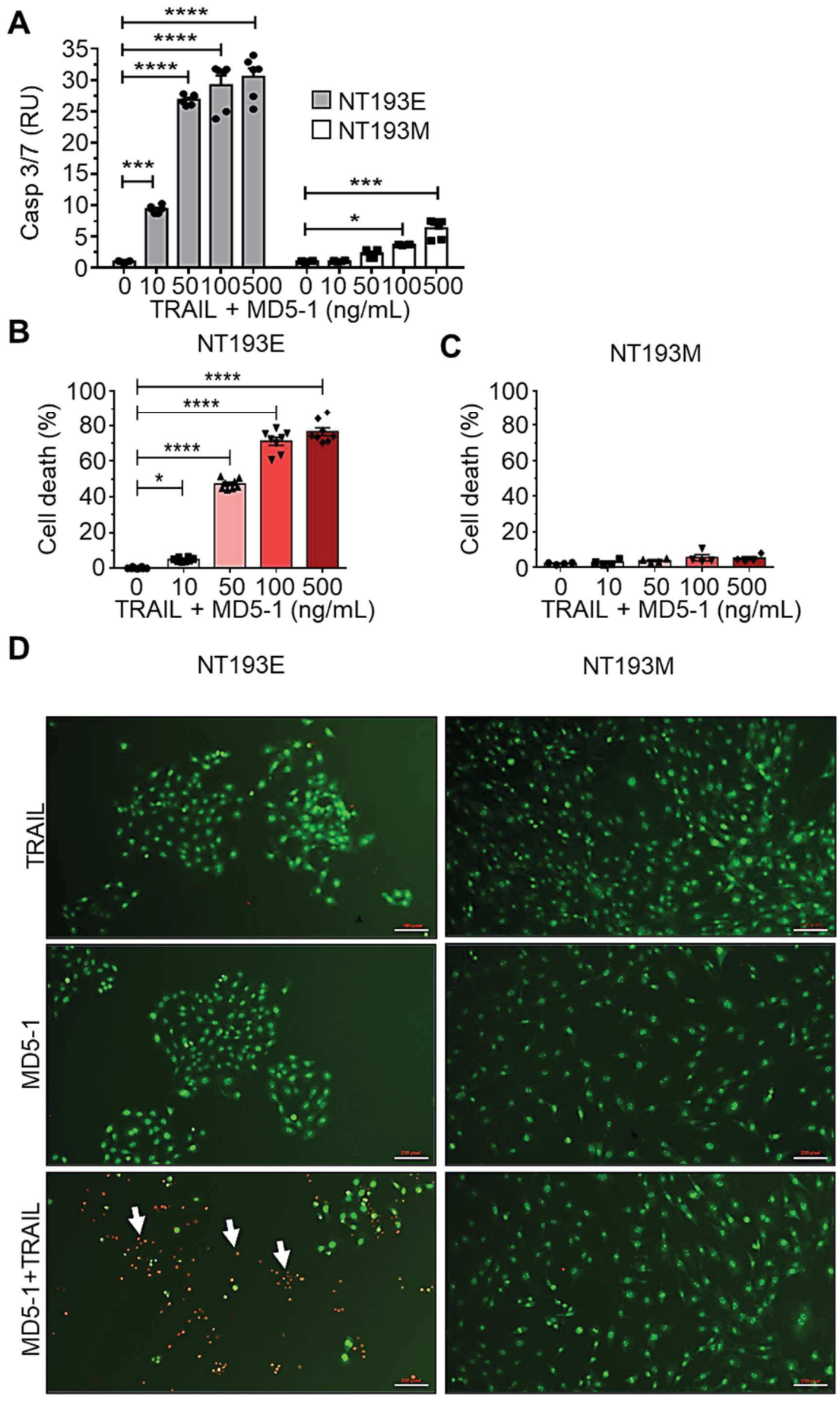
A
Casp 3/7 (RU)
NT193E
NT193M
TRAIL + MD5-1 (ng/mL)
B
NT193E
Cell death (%)
TRAIL + MD5-1 (ng/mL)
C
NT193M
Cell death (%)
TRAIL + MD5-1 (ng/mL)
D
NT193E
NT193M
TRAIL
MD5-1
MD5-1+TRAIL

Figure 2: NT193E cells are killed by combined TRAIL+MD5-1 treatment in contrast to resistant NT193M cells

(A) Casp 3/7 activity in NT193E and NT193M cells after incubation with TRAIL+MD5-1, N = 3 experiments, n = 2 replicates**.** Kruskal-Wallis test, mean ± SEM (*p < 0.05; ****p < 0.0001). **(B, C)** Percentage of dead cells in NT193E **(B)** and NT193M **(C)** cells upon incubation with TRAIL+MD5-1. **(D)** Representative IF images of NT193E and NT193M cells upon staining with AO/EB after treatment with MD5-1 (50 ng/mL) or TRAIL (100 ng/mL) + MD5-1 (50 ng/mL), scale bar 100 µm. Arrows point at dead cells. **(B, C, D)** NT193E, N = 4 experiments, n = 2 replicates; NT193M, N = 2 experiments, n = 2 replicates. **(B)** ANOVA one-way test, mean ± SEM (*p < 0.05; ****p < 0.0001). **(C)** Kruskal-Wallis test, mean ± SEM, no differences.

Figure 3

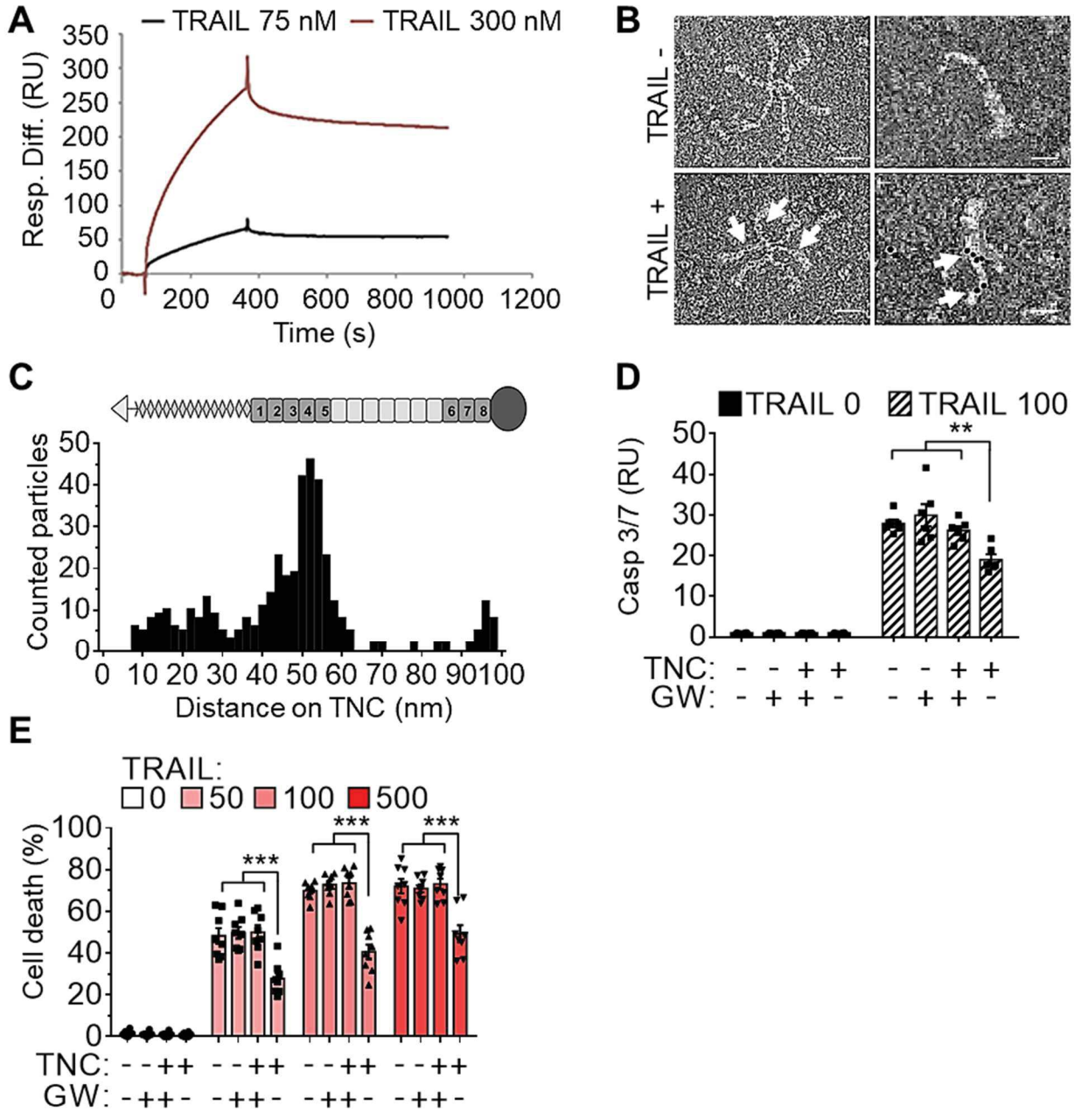
A
TRAIL 75 nM
TRAIL 300 nM
Resp. Diff. (RU)
Time (s)
B
TRAIL -
TRAIL +
C
Counted particles
Distance on TNC (nm)
D
TRAIL 0
TRAIL 100
Casp 3/7 (RU)
TNC:
GW:
E
TRAIL:
0
50
100
500
Cell death (%)
TNC:
GW:

Figure 3: TNC binds TRAIL and protects NT193E cells from TRAIL-induced cytotoxicity through TGFβ signaling

(A) Binding of TRAIL to TNC as measured by surface plasmon resonance spectrometry. **(B, C)** Negative electron microscopic images of TRAIL (adsorbed to gold beads) binding to TNC. **(B)** Representative micrographs of TNC hexamers (left panels) and monomers (right panels) binding to TRAIL, scale bars 100 nm (left), 50 nm (right). **(C)** Quantification of bound TRAIL particles along the length of TNC monomers. N = 2 experiments, n = 500 images. **(D, E)** Casp 3/7 activity (**D**) and cell death (AO/EB) labelling (**E**) in NT193E cells upon pretreatment with TNC (10 µg/mL) and GW788388 (10 µM), followed by incubation with TRAIL and MD5-1 (50 ng/mL). **(D)** N = 3 experiments, n = 2 replicates, Kruskal-Wallis test, mean ± SEM (**p < 0.01). **(E)** N = 4 experiments, n = 2 replicates. Kruskal-Wallis test, mean ± SEM (***p < 0.001).

Figure 4

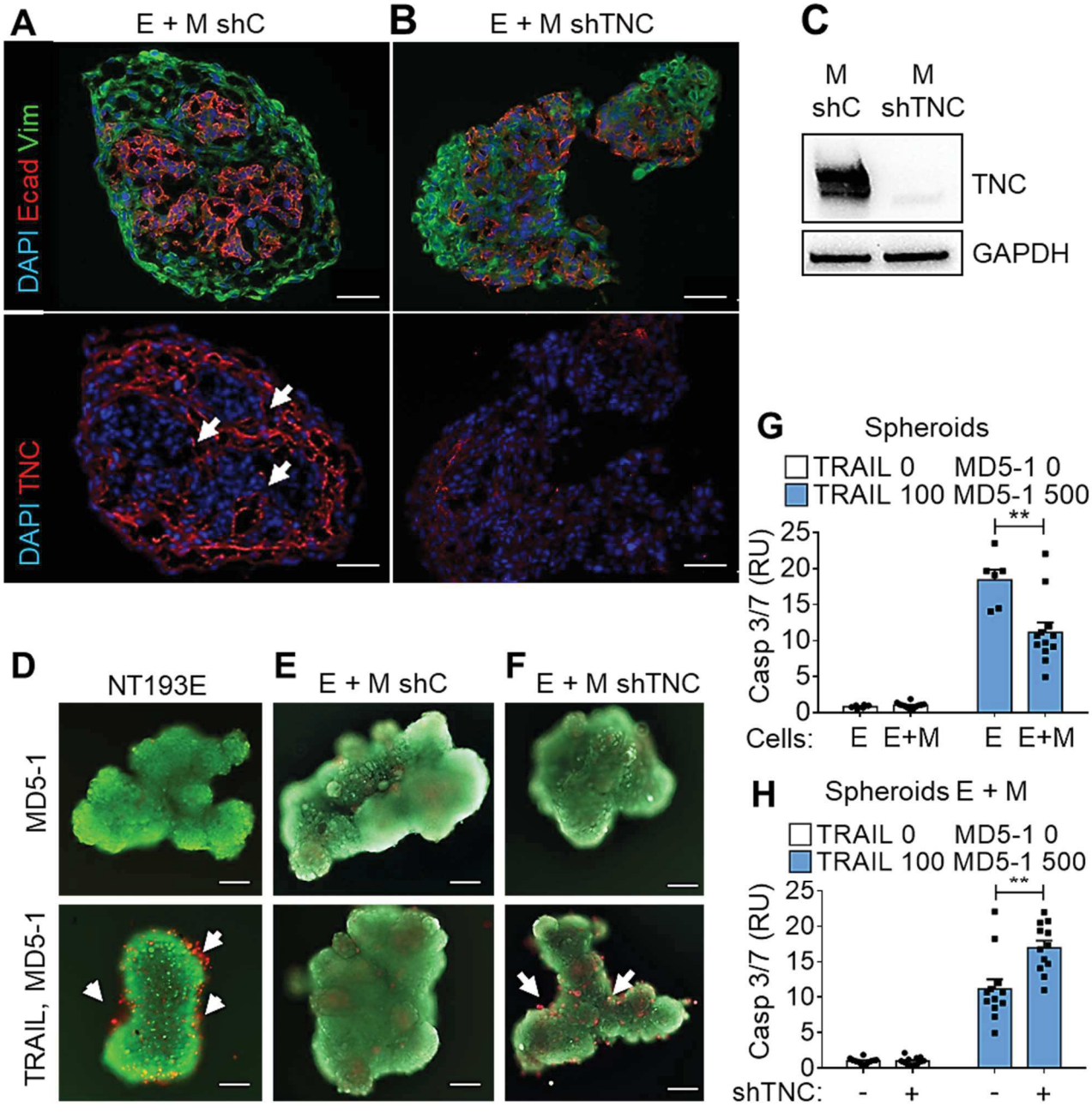
A
E + M shC
B
E + M shTNC
DAPI Ecad Vim
DAPI TNC
C
M shC
M shTNC
TNC
GAPDH
D
NT193E
E
E + M shC
F
E + M shTNC
MD5-1
TRAIL, MD5-1
G
Spheroids
TRAIL 0
MD5-1 0
TRAIL 100
MD5-1 500
Casp 3/7 (RU)
Cells:
E
E+M
H
Spheroids E + M
shTNC:

Figure 4: Assessment of TRAIL-induced cell death in heterotypic spheroid co-cultures in dependence of TNC

(A, B) Representative IF images of homotypic and heterotypic spheroids of E and M cells (shC or shTNC), N = 2 experiments. Scale bars 50 µm. **(C)** Immunoblots for the indicated molecules, N = 2 experiments. **(D-F)** AO/EB images of NT193E **(D)** or E and M cells (shC or shTNC, **(E, F)**) spheroids upon incubation with MD5-1 (500 ng/mL) or TRAIL (ng/mL) and MD5-1 (ng/mL), N = 4 experiments. **(G, H)** Casp 3/7 activity in homotypic and heterotypic spheroids of E and M cells **(G)** or E and M cells (shC or shTNC) **(H)**, upon incubation with no TRAIL and no MD5-1 or TRAIL (100 ng/mL) and MD5-1 (500 ng/mL), N = 4 experiments, n = 3 replicates. Mann-Whitney test, mean ± SEM (**p < 0.01).

Figure 5

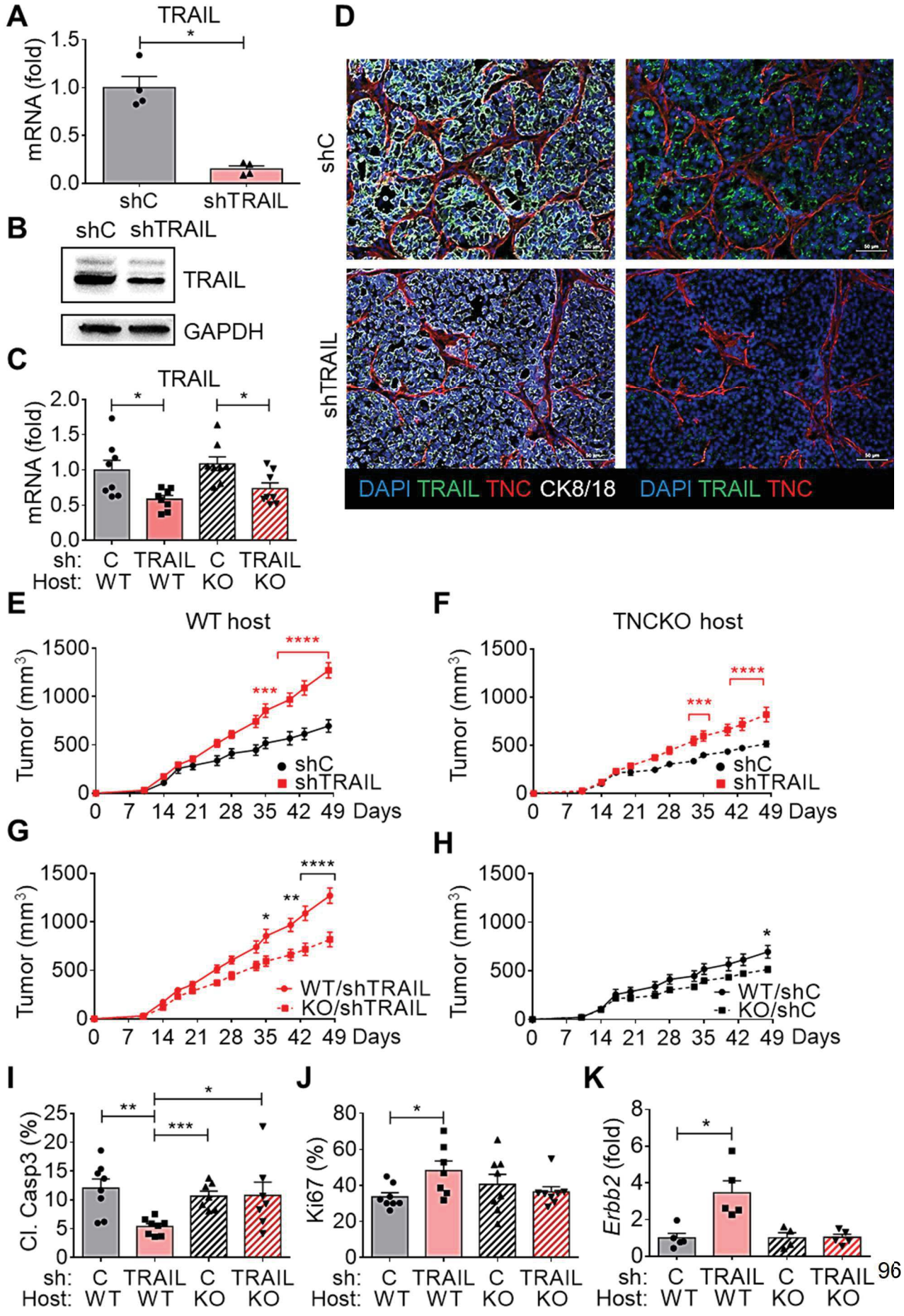
A
TRAIL
mRNA (fold)
shC
shTRAIL
B
shC shTRAIL
TRAIL
GAPDH
C
TRAIL
mRNA (fold)
sh: C TRAIL C TRAIL
Host: WT WT KO KO
D
shC
shTRAIL
DAPI TRAIL TNC CK8/18 DAPI TRAIL TNC
E
WT host
Tumor (mm3)
shC
shTRAIL
Days
F
TNCKO host
Tumor (mm3)
shC
shTRAIL
Days
G
Tumor (mm3)
WT/shTRAIL
KO/shTRAIL
Days
H
Tumor (mm3)
WT/shC
KO/shC
Days
I
Cl. Casp3 (%)
sh: C TRAIL C TRAIL
Host: WT WT KO KO
J
Ki67 (%)
sh: C TRAIL C TRAIL
Host: WT WT KO KO
K
Erbb2 (fold)
sh: C TRAIL C TRAIL
Host: WT WT KO KO

Figure 5: TRAIL and TNC impact tumor growth and lung metastasis

(A-D) TRAIL levels in cultured cells and tumors. **(A)** TRAIL mRNA levels (qRTPCR) in E cells (shC or shTRAIL), N = 4. Mann-Whitney test, mean ± SEM (*p < 0.05). **(B)** Representative immunoblot, N = 2. **(C)** TRAIL mRNA levels (qRTPCR) in tumors, N = 8. Mann-Whitney tests, mean ± SEM (*p < 0.05). **(D)** Representative IF images of shC and shTRAIL tumors grown in WT mice. Scale bars 50 µm, N = 5. **(E-H)** Tumor volume. WT/shC, N = 12, WT/shTRAIL, N = 13, KO/shC, N = 10, KO/shTRAIL, N = 11. ANOVA two-way test, mean ± SEM (*p < 0.05, **p < 0.01, ***p < 0.001, ****p < 0.0001). **(I, J)** Quantification of Cl. Casp 3+ **(I)** and Ki67+ **(J)** cells in relation to DAPI+ cells in tumors. N = 8 tumors per group (4 random images per tumor). Kruskal-Wallis test, mean ± SEM (*p < 0.05, **p < 0.01, ***p < 0.001). **(K)** *ErbB2* expression (qRTPCR) in 50% of lung tissue from tumor bearing mice, N = 4 - 5 mice. Kruskal-Wallis test, mean ± SEM (*p < 0.05).

Figure 6

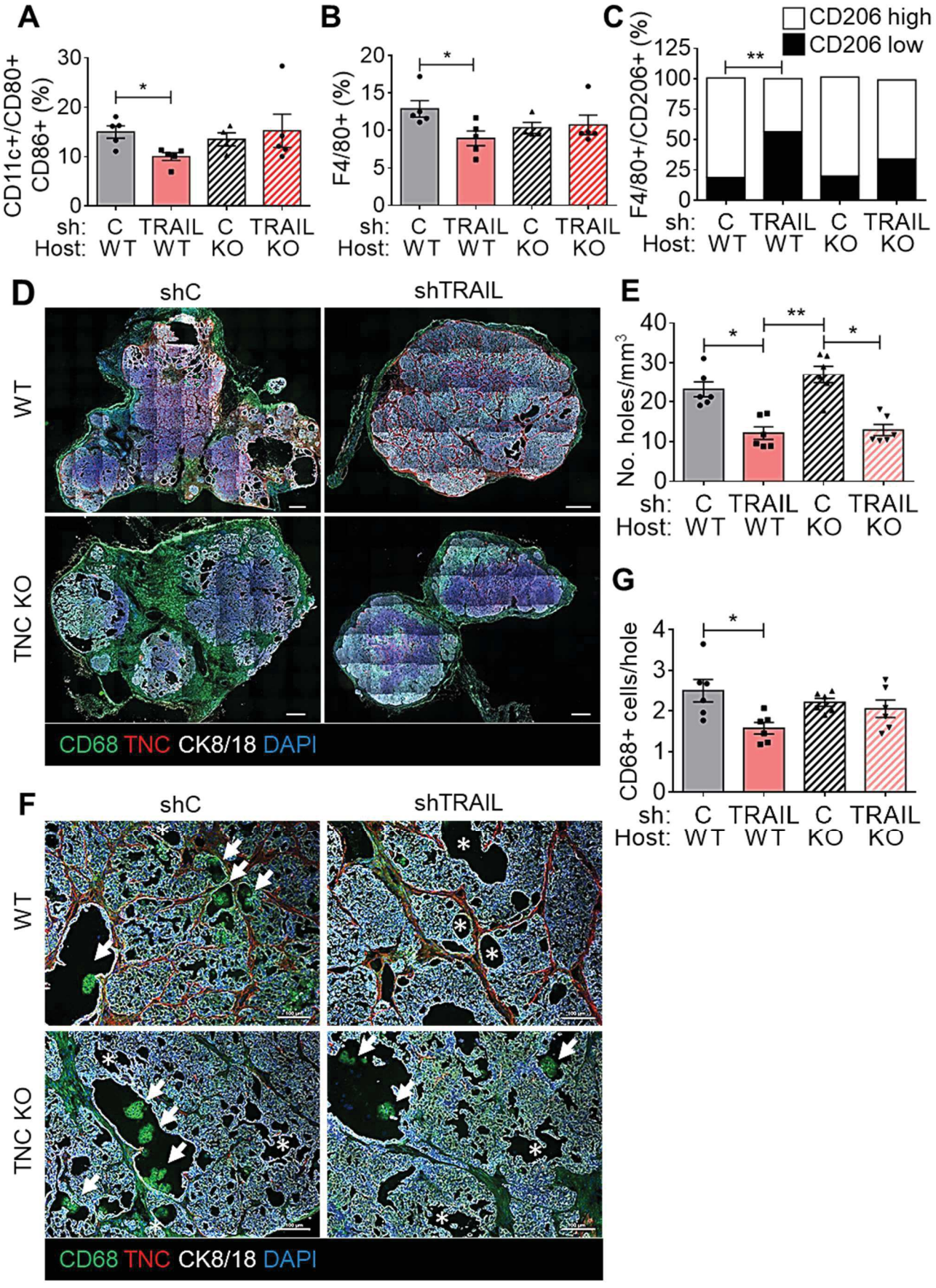
A
CD11c+/CD80+ CD86+ (%)
30
20
10
0
*
sh: C TRAIL C TRAIL
Host: WT WT KO KO
B
F4/80+ (%)
20
15
10
5
0
*
sh: C TRAIL C TRAIL
Host: WT WT KO KO
C
CD206 high
CD206 low
F4/80+/CD206+ (%)
125
100
75
50
25
0
**
sh: C TRAIL C TRAIL
Host: WT WT KO KO
D
shC
shTRAIL
WT
TNC KO
CD68 TNC CK8/18 DAPI
E
No. holes/mm3
40
30
20
10
0
*
**
*
sh: C TRAIL C TRAIL
Host: WT WT KO KO
G
CD68+ cells/hole
4
3
2
1
0
*
sh: C TRAIL C TRAIL
Host: WT WT KO KO
F
shC
shTRAIL
WT
TNC KO
CD68 TNC CK8/18 DAPI

Figure 6: TRAIL impacts immune cell infiltration

(A-C) Abundance of immune cell subtypes (flow cytometry) as percentage of CD45+ cells in the indicated tumors. N = 4-5 mice. Mann-Whitney test, mean ± SEM (*p < 0.05, **p < 0.01). **(D)** Representative IF images of CD68+ cells in mosaic images revealing the overall tumor organization and presence of CD68+ cells in cell-free holes. Scale bars 1 mm. **(E)** Quantification of total number of holes bigger than 25 μm in diameter in mosaic pictures. N = 6 tumors, Kruskal-Wallis test, mean ± SEM (*p < 0.05, **p < 0.01). **(F)** Representative IF images of CD68+ cells in tumor holes. Arrows point at CD68+ clusters in the holes. Asterisks point at holes without CD68+ cells. N = 6. Scale bar 100 μm. **(G)** Quantification of CD68+ cell per hole. N = 6 tumors, n = 4 images, Kruskal-Wallis test, mean ± SEM (*p < 0.05).

Figure 7

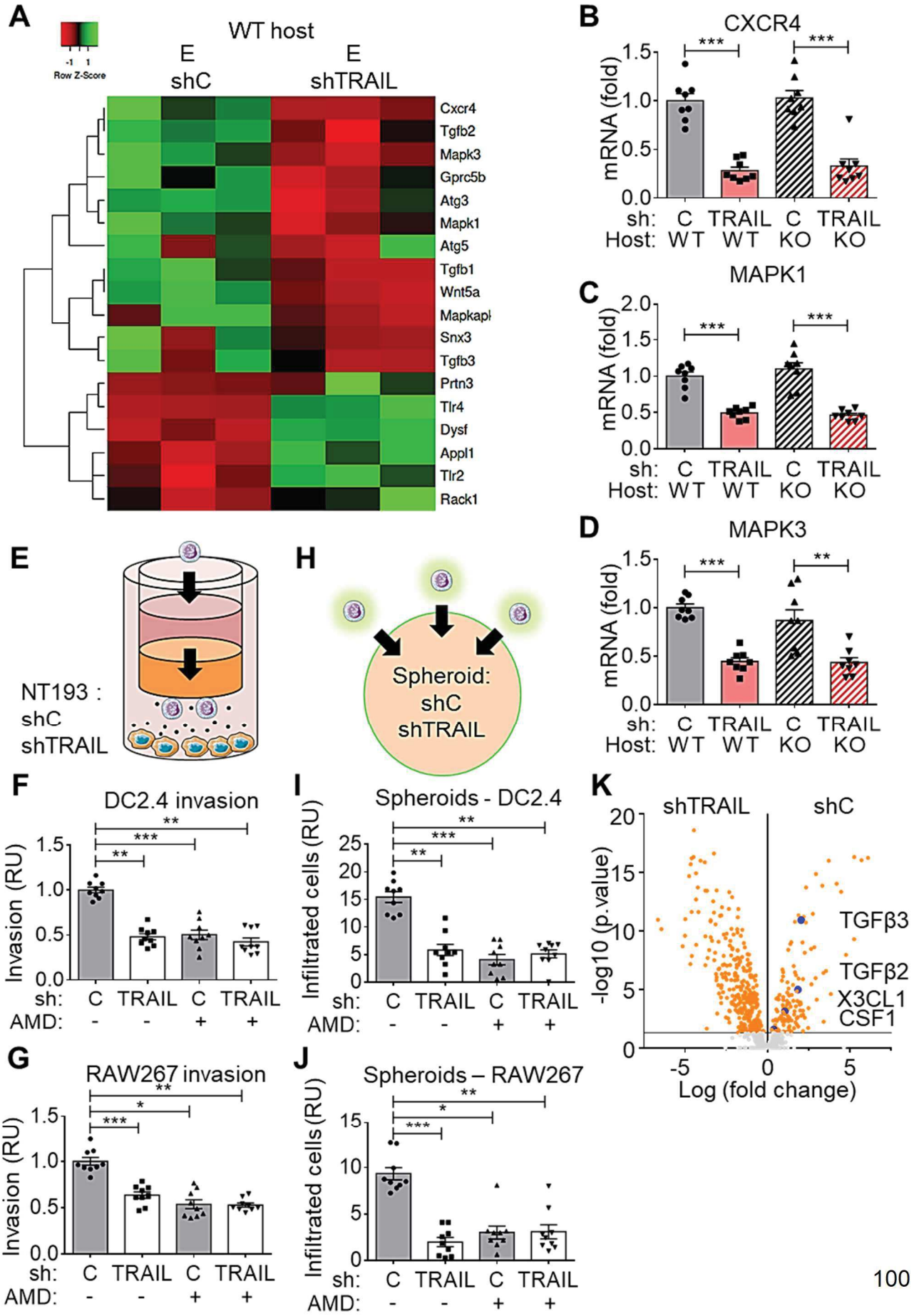
A
WT host
E shC
E shTRAIL
Row Z-Score
Cxcr4
Tgfb2
Mapk3
Gprc5b
Atg3
Mapk1
Atg5
Tgfb1
Wnt5a
Mapkapl
Snx3
Tgfb3
Prtn3
Tlr4
Dysf
Appl1
Tlr2
Rack1
B
CXCR4
mRNA (fold)
sh: C TRAIL C TRAIL
Host: WT WT KO KO
C
MAPK1
D
MAPK3
E
NT193 :
shC
shTRAIL
H
Spheroid:
shC
shTRAIL
F
DC2.4 invasion
Invasion (RU)
AMD: - - + +
I
Spheroids - DC2.4
Infiltrated cells (RU)
K
shTRAIL
shC
-log10 (p.value)
TGFβ3
TGFβ2
X3CL1
CSF1
Log (fold change)
G
RAW267 invasion
J
Spheroids – RAW267

Figure 7: Impact of TRAIL on CXCR4 expression and CXCR4 dependent immune cell infiltration

(A) Expression of macrophages regulating genes in shC and shTRAIL tumors of WT hosts, determined by RNA seq analysis represented as heatmap, N = 3, $p < 0.05$. **(B-D)** Expression of the indicated molecules in tumors (qRTPCR). N = 8 tumors. Mann-Whitney tests, mean ± SEM (**$p < 0.01$, ***$p < 0.001$). **(E-J)** DC2.4 **(F, I)** and RAW267 cell **(G, J)** invasion of matrigel coated Boyden chamber devices **(E-G)** towards CM secreted by NT193E shC or NT193E shTRAIL cells, with or without ADM3100 (5 µg/mL). N = 3 experiments, n = 3 replicates. **(H-J)** Invasion of labeled DC2.4 and RAW267 into E shC or E shTRAIL spheroids. Quantification of the green label, in the presence or absence of AMD3100 (5 µg/mL). N = 3 experiments, n = 3 replicates. Kruskal-Wallis test, mean ± SEM (*$p < 0.05$, **$p < 0.01$, ***$p < 0.001$). **(K)** Volcano plot representing proteins secreted by NT193E shC and NT193E shTRAIL cells, determined by mass spectrometry analysis, N = 5, Limma moderated t-test, $p < 0.05$.

Figure 8

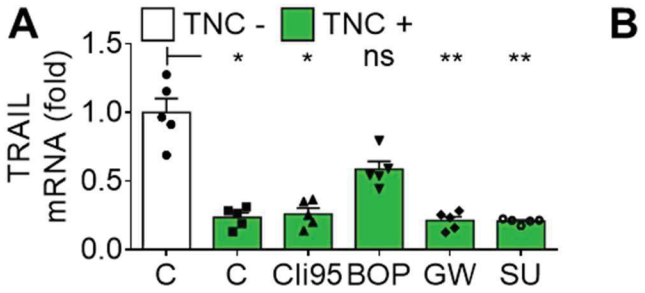

B

TRAIL expression upon treatment with TNC and anti-α9β1 and anti-α4β1.

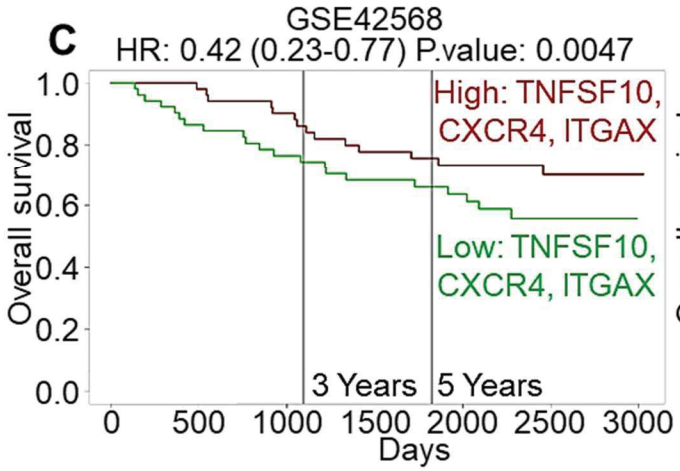

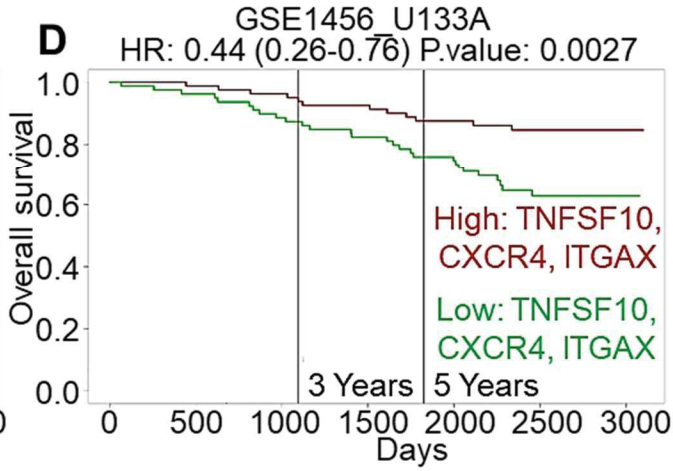

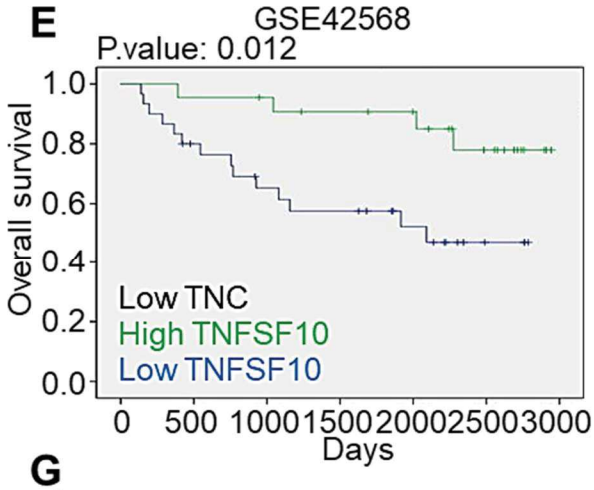

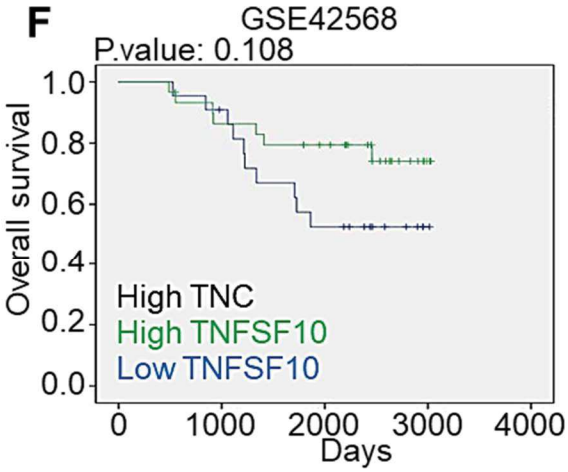

G

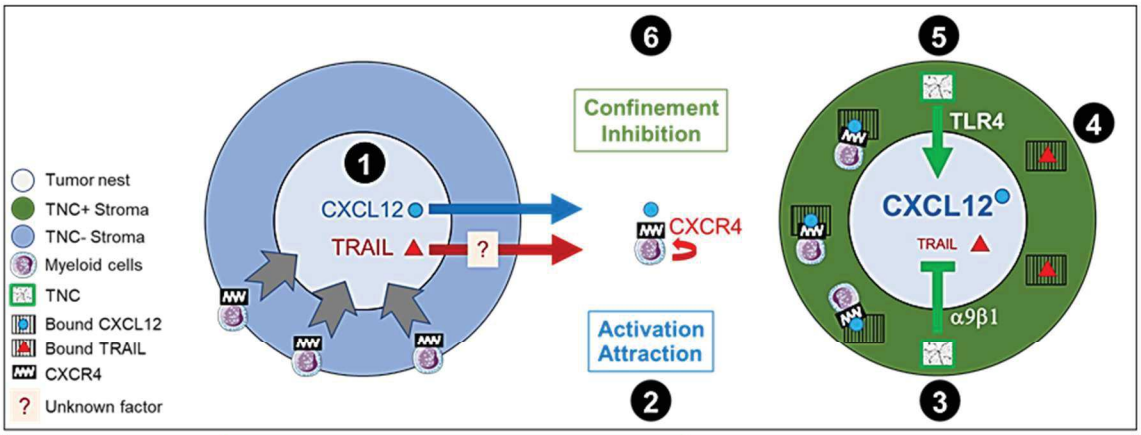

	TRAIL	Tenascin-C
TNC counteracts TRAIL control over anti-tumor immunity	• Myeloid cell infiltration through CXCR4 • Holes containing macrophages • Tumor cell proliferation low, apoptosis high • Tumor growth and lung invasion low	• TRAIL repression through α9β1 integrin • TRAIL trapping through binding • TRAIL inhibition • TRAIL killing resistance through TGFβ

Figure 8: Impact of TNC on TRAIL expression and prognostic value of TRAIL expression in human breast cancer and schematic on TNC functions in counteracting TRAIL

(A) Quantification of TRAIL expression by qRTPCR in dependence of soluble TNC (10 µg/mL) added to NT193E shC cells, together with Cli95 (1 µg/mL), BOP (1 µM), GW788388 (10 µM) and SU6668 (30 µM) pre-treatment, N = 5. Kruskal-Wallis test, mean ± SEM (*p < 0.05, ns = not significant). **(C, D)** Kaplan Meier analysis of breast cancer patient overall survival in relation to combined high or low expression of the indicated molecules. **(C)** GSE42568, n = 54. HR: 0.42 (0.23 – 0.77). **(D)** GSE1456_U133A, n = 80. HR: 0.44 (0.26 – 0.76). **(E)** Schematic depicting the different modes of TRAIL action and how TNC counteracts TRAIL. An interconnection of TNC and TRAIL regulating anti-tumor immunity and tumor growth was discovered. **1.-** In the NeuNT/NT193 model, tumor cell nests are surrounded by matrix-rich stroma where tumor cells express TRAIL and CXCL12 (Sun et al., 2019, Murdamoothoo, in revision). **2.-** Tumor cells secrete soluble factors inducing CXCR4 altogether attracting myeloid cells into the tumor. Higher B cell numbers may increase an anti-tumor antibody response which altogether could explain less tumor cell apoptosis and less phagocytic holes and, more tumor growth and more metastasis upon TRAIL ablation. **3.-** We showed that TNC counteracts anti-tumor immunity by TRAIL through integrin $\alpha4\beta1/\alpha9\beta1$-mediated repression of TRAIL thus lowering TRAIL and CXCR4 levels in myeloid cells. **4.-** Through direct interaction, TNC impairs TRAIL activating myeloid cells. **5.-** Despite induction of CXCL12 by TNC (through TLR4, Murdamoothoo et al., in revision), (**6.**) myeloid cells are impaired in infiltrating the tumor nests due to confinement in the TMT by a TNC/CXCL12 complex (Murdamoothoo et al., in revision). Moreover, induction of EMT by TNC (through TGFβ signaling (Sun et al., 2019)) renders tumor cells resistant to TRAIL-induced killing. Thus, TNC may increase tumor growth and progression into lung metastasis by several actions where TNC impairment of myeloid cell activation by TRAIL is an important novel mechanism.

7.7. Supplemental figures

Table S1: Soluble proteins detected in conditioned medium produced by NT193E shC and NT193E shTRAIL

Table S2: Antibody list

Table S3: Primer list

Figure S1: Gene expression analysis of NT193E and NT193M cells

Figure S2: TRAIL plus MD5-1 induces cell death in NT193E and EO771 but not in NT193M cells

Figure S4: In contrast to M spheroids E cell spheroids are sensitive to TRAIL-induced apoptosis

Figure S5 Impact of TRAIL and DR5 knockdown on tumor growth

Figure S6: Impact of TRAIL and DR5 knockdown on immune cells infiltration

Figure S7: Impact of TRAIL knock down on tumor genes expression and NT193 secreted proteins

Figure S8: Prognostic value of TRAIL expression in human breast cancer

Table S1: Soluble proteins detected in conditioned medium produced by NT193E shC and NT193E shTRAIL cells

Mass spectrometry data, p-value < 0.05, N = 5, only the significantly expressed proteins are represented.

Protein name	Log2 fold change	p-value
ATS4	6,675	4,58827E-22
GCNT3	-4,473	2,65977E-19
SPB11	-3,256	2,47705E-17
PCOC1	5,250	5,01727E-17
TEST2	-4,490	5,09566E-17
GPC4	6,089	5,90669E-17
PDLI5	-4,613	6,44762E-17
PADI2	5,695	9,1523E-17
HA18	-4,066	1,02646E-16
TOR3A	3,712	1,02735E-16
B4GA1	-3,814	1,39585E-16
FLNA	-4,672	2,08504E-16
KLK8	-4,342	1,22122E-15
TINAL	2,936	1,41149E-15
IBP3	-4,764	2,15661E-15
MOXD1	4,183	9,74771E-15
TRFE	3,322	1,44059E-14
VEGFC	-4,232	1,96304E-14
SIA8A	2,336	1,98587E-14
MYDGF	-3,095	3,57359E-14
ZYX	-3,773	3,72494E-14
CAP1	-3,676	3,87355E-14
CBPM	4,463	4,66112E-14
DIP2B	-2,325	5,00667E-14
LAMA3	-2,152	1,35096E-13
CTL2	-4,342	2,13753E-13
GPC6	-3,300	2,99607E-13
SIA7B	-2,768	9,79269E-13
XPP1	-2,348	1,36013E-12
HBEGF	-1,775	1,39938E-12
ITA6	-4,614	2,44779E-12
EGFR	-4,196	2,48957E-12
LFNG	-3,255	2,78543E-12
SEM4D	-3,297	2,95311E-12
IGSF3	2,742	3,5876E-12

LGMN	-2,811	4,71774E-12
ANT3	1,875	4,73272E-12
CD166	-2,883	5,32818E-12
COIA1	2,195	6,28898E-12
TSP1	-1,806	6,97901E-12
PEDF	2,119	9,43647E-12
SLIT2	-4,991	9,95527E-12
COCA1	-6,657	1,16109E-11
TGFB3	2,035	1,23973E-11
TLN1	-3,456	1,25629E-11
MMP10	-3,458	1,55583E-11
PPN	1,656	1,69498E-11
LRP6	2,316	1,97828E-11
CDON	-3,164	2,83028E-11
TXD16	-2,193	6,87867E-11
CO3	-6,444	7,25114E-11
LAMB2	-1,844	7,5557E-11
SO2A1	-1,532	8,24753E-11
HTRA1	-1,826	1,46E-10
GSH1	-2,486	1,76505E-10
PDIA3	-2,065	2,10041E-10
VINC	-2,663	2,10249E-10
DSG3	-1,627	2,66185E-10
ATS7	-5,011	2,67502E-10
SEM3E	-3,775	2,99506E-10
ATL4	-3,454	3,50109E-10
DCBD2	-2,549	4,29713E-10
LMAN1	5,246	5,27376E-10
PCP	-3,368	7,14619E-10
CO4A2	-2,263	7,29366E-10
SRBS2	-2,977	8,55676E-10
A1AG2	1,432	9,47594E-10
HS3S1	2,118	1,00396E-09
LAMB3	-1,444	1,15331E-09
GDN	1,377	1,34302E-09
PR2C3	-4,338	1,58369E-09
EHD1	-2,295	1,85076E-09
QSOX1	-5,149	2,07342E-09
NPNT	2,836	2,52673E-09
HSP13	-1,383	2,6003E-09
ITAV	-2,141	3,0415E-09
AGRG6	2,636	3,53043E-09

ZO1	-2,131	3,84981E-09
BSSP4	1,253	4,23309E-09
SPTN1	-3,544	4,43607E-09
NECT2	-1,827	4,52443E-09
NPTN	-1,813	4,79846E-09
CHID1	2,249	7,48126E-09
FINC	-3,188	7,51963E-09
LAMC2	-1,215	9,89193E-09
CATC	-1,134	1,07733E-08
CAH2	4,754	1,14822E-08
CLN5	-2,211	1,27328E-08
PARVA	-2,669	1,40715E-08
SEM3C	-4,601	1,42223E-08
CCBE1	-1,541	1,75264E-08
TRFL	-1,843	2,07828E-08
WDR1	-1,774	2,10262E-08
BGLR	-3,631	2,1343E-08
MANBA	-2,038	2,82598E-08
CBPQ	-1,956	2,94799E-08
UROK	-1,206	2,96607E-08
DLG1	-3,232	3,31376E-08
TXND5	-1,670	3,62023E-08
GGTA1	-1,691	5,1053E-08
LAMA5	-1,053	6,27303E-08
SAPL1	-1,148	6,53966E-08
CP089	-4,689	6,97975E-08
ITA8	-2,625	7,43371E-08
ACTN1	-1,878	8,16045E-08
SORL	-1,769	8,21297E-08
ES8L2	-2,272	8,49951E-08
KLK14	-2,719	8,59495E-08
TLR8	-3,780	8,71924E-08
ITB1	-1,197	8,74093E-08
PDIA4	-2,472	9,69748E-08
ADA17	1,588	1,02536E-07
CDC37	-1,875	1,44282E-07
ITA3	-1,466	1,45352E-07
NIBA2	-2,923	1,65395E-07
FLRT3	-1,057	1,71932E-07
ERAP1	-2,975	1,87607E-07
GCNT1	0,898	2,04491E-07
G6PI	-1,423	2,51919E-07

UXS1	-1,101	2,53038E-07
MEG10	3,540	2,71369E-07
MMP3	-1,278	2,7443E-07
H6ST1	0,944	3,40509E-07
C1QT1	1,660	3,49218E-07
ROA3	3,382	3,98285E-07
KLRA1	-2,572	3,99415E-07
AP1G1	-1,956	4,05153E-07
ATF6B	-1,966	4,81408E-07
SYRC	-2,348	4,92831E-07
PLD3	-3,131	4,93915E-07
SEM5A	-2,784	5,03462E-07
CSF3	1,717	6,04442E-07
PDC6I	-1,057	6,30782E-07
CATB	-0,971	6,38343E-07
DSC2	-0,714	6,57337E-07
GALT4	-1,974	7,31897E-07
LMAN2	0,933	7,80571E-07
IDUA	-1,836	7,91829E-07
ANM1	-2,556	8,71061E-07
PSA	-3,082	9,26285E-07
ST14	-0,864	9,31393E-07
CATL1	-1,024	9,33919E-07
MVP	-2,693	9,53007E-07
MAMC2	-0,858	9,559E-07
SEM4C	2,908	1,0841E-06
S39AA	1,877	1,22709E-06
IMPA1	2,144	1,31545E-06
MYH9	-1,828	1,52134E-06
ERFE	-2,485	1,54062E-06
DIAC	-2,214	1,63501E-06
PURB	-3,109	1,69297E-06
HYAL1	-0,747	1,75968E-06
SYCC	-1,981	1,78002E-06
CH3L1	0,871	1,78897E-06
COR1C	-1,449	1,8336E-06
GRAE	-1,569	2,48845E-06
B3GT5	1,204	2,53585E-06
PPGB	-1,244	2,68787E-06
ADAM9	2,658	3,6973E-06
PLGF	1,540	4,28656E-06
MA1A1	-2,990	4,3778E-06

LSR	-1,156	4,44497E-06
OX2G	-2,793	4,48853E-06
HA13	-0,665	4,6917E-06
PEPD	-1,505	4,73719E-06
LTBP4	-1,865	6,16021E-06
IQGA1	-1,689	6,39867E-06
B4GN3	-1,667	6,80447E-06
FGFR1	-0,864	7,3162E-06
EPHA1	1,814	7,33623E-06
DNPEP	-2,810	7,74591E-06
L2GL2	-1,266	7,76124E-06
CHADL	1,264	8,66241E-06
DAF1	-1,600	8,91104E-06
CO4A1	-2,065	9,88413E-06
TGFB2	1,841	1,06082E-05
DJC10	-2,305	1,06319E-05
MSLN	-1,619	1,12733E-05
ECM1	-1,112	1,14666E-05
EF1D	1,785	1,42873E-05
FUCO	-1,386	1,66758E-05
SIAE	-2,699	1,74883E-05
COR1B	-1,021	1,84902E-05
ACTN4	-1,346	1,87709E-05
RAI3	-0,807	1,94459E-05
HNRPC	1,193	1,94517E-05
HA1D	-2,949	2,25059E-05
GOLI4	-1,033	2,49165E-05
NHLC3	-1,004	2,54618E-05
ECT2	3,840	2,56121E-05
BMP1	-0,649	2,69303E-05
CATW	-1,776	2,81887E-05
PLEC	-1,127	2,91864E-05
FUCO2	0,729	3,00377E-05
AK1A1	1,455	3,00618E-05
ITB5	-0,844	3,14798E-05
CATO	-1,389	3,23843E-05
SERC	1,302	3,37536E-05
ASM	-1,495	3,43789E-05
BROX	-1,864	3,47622E-05
PRS27	-2,124	3,57831E-05
CDCP1	-0,952	3,60642E-05
MPRI	-1,374	3,63794E-05

TIMP2	-1,921	3,97151E-05
PNPH	-1,398	4,00389E-05
HA1L	-0,717	4,03724E-05
HGFA	0,952	4,7132E-05
MBTP1	-1,193	4,91915E-05
THSD4	-2,824	4,94561E-05
SPIT1	0,612	5,34915E-05
EXTL2	-1,722	5,35913E-05
PRDX4	-1,221	5,36781E-05
IDS	-2,465	5,40184E-05
IL6RB	-1,090	5,57415E-05
RRAS2	-1,760	5,60014E-05
BGAL	-0,904	5,6341E-05
GT251	-1,470	5,98468E-05
CERU	0,536	6,35605E-05
GXLT1	-0,773	6,66795E-05
PTK7	-0,631	7,05365E-05
T132A	0,669	7,41692E-05
BACH	-2,007	7,65331E-05
PIPNA	-1,263	7,66505E-05
SODC	2,974	7,76536E-05
SPTB2	-2,026	7,84041E-05
KPYM	-0,894	7,91954E-05
NUCL	0,952	8,23166E-05
SPB6	-1,153	8,7442E-05
B3GN2	-0,845	8,8326E-05
AREG	-0,937	8,88154E-05
LDHA	1,176	9,59699E-05
PLET1	1,561	9,77068E-05
PCD12	1,801	9,95622E-05
ADA15	-1,632	0,000103206
SNX18	-0,980	0,000106985
ATPB	1,924	0,000125852
CADH2	-2,181	0,000126633
NOMO1	-0,744	0,000128817
TPP1	-1,259	0,000130374
SDC4	-0,851	0,000131627
sept-09	-0,976	0,000131789
WFDC2	-1,096	0,000133474
OSTP	2,002	0,000134711
EZRI	-0,985	0,000134804
TFR1	-1,668	0,000136307

INHBA	-2,820	0,00015066
MGT4B	-0,654	0,000154315
PPCE	-1,437	0,000155921
B3GA3	1,313	0,000157106
TSK	-2,165	0,000168505
sept-02	-2,079	0,00018057
PTPRG	-1,044	0,000180779
CO5A1	2,010	0,000181226
PCOC2	1,195	0,000181959
IMA4	-1,769	0,000188151
LRIG1	-0,598	0,000196999
CAHD1	1,939	0,000202968
EPCAM	-0,654	0,000219512
PRS33	0,916	0,000219831
GNAI2	-1,986	0,000225857
DNJC3	-0,644	0,000274038
PSMD1	-1,921	0,00027495
GPD1L	1,707	0,00028344
AQP5	1,397	0,000301692
FARP1	-1,396	0,000314265
PPA5	0,968	0,000345539
SEM3B	1,118	0,00034637
GELS	-0,887	0,000349056
NUDC	-1,414	0,000357919
LAMC1	-0,703	0,000357995
UBP8	-0,952	0,000375827
PFKAP	2,475	0,000405615
HEXB	-1,618	0,000415063
CATH	-1,368	0,000439247
LYAG	0,961	0,000469276
B4GN1	0,536	0,000530651
EHD4	-1,693	0,000533995
TSN9	-0,958	0,000544481
GGH	1,223	0,000545372
CD276	-0,922	0,000563006
SERA	-1,949	0,000590704
BTBDG	1,979	0,000646147
U119B	-2,327	0,000663654
ITM2B	2,145	0,000669711
TM1L1	-1,151	0,000695073
ESTD	-1,711	0,000699644
SPB5	-1,528	0,000706903

PSB6	1,638	0,000734493
GNS	-2,292	0,000763595
LRP5	0,591	0,000780231
X3CL1	1,040	0,000808834
PLOD3	0,947	0,000809731
FPRP	-1,269	0,00084179
ARRD1	-0,487	0,000852848
DEST	-1,829	0,000853412
5NTD	-0,978	0,000874728
GARS	-0,973	0,000986497
CRIM1	-1,769	0,00100724
TCPE	-1,560	0,001065705
MYH14	-3,059	0,001163322
RGMB	1,017	0,001207315
CHSTE	-1,145	0,00126083
CO9A1	1,607	0,001445846
HARS1	-1,331	0,001476734
GSHR	-1,115	0,001480684
ROA0	2,162	0,00148479
PINLY	-0,573	0,001679428
NDKB	2,035	0,001752801
TCO2	1,210	0,001811593
FURIN	-1,043	0,001851621
BIP	0,822	0,001912977
PGBM	-1,062	0,002007766
PUR2	-1,369	0,002344949
NBEA	1,826	0,002446871
FAAA	-1,404	0,002523114
TPM4	-2,524	0,002526049
NRP1	-1,131	0,0026055
PSB5	2,253	0,002618399
PLOD2	1,327	0,002678539
SYSC	-1,718	0,002806686
CSN2	-1,170	0,002826598
PAFA	-0,631	0,002957899
GLOD4	0,719	0,003015564
IMA1	-1,361	0,003037411
CD81	1,759	0,003038432
TXNL1	-0,620	0,003106379
BLMH	-2,385	0,003133448
PAG15	-1,450	0,003154458
CO6A1	0,996	0,003372916

TPP2	-1,135	0,003406701
WNT5B	0,499	0,003676066
GANAB	0,491	0,003742686
FABP5	1,209	0,003764745
GLCM	0,473	0,003781643
PDIA6	0,890	0,003786918
ITB4	0,475	0,003982037
VP37C	-0,801	0,004465159
FCL	-1,101	0,004538702
CALX	-0,738	0,004607916
TRFM	1,451	0,004639888
NGAL	1,009	0,004709158
DSG2	0,337	0,004723557
NOTC2	-0,534	0,004732257
KIF23	0,953	0,004881437
XYLK	0,568	0,004970709
CAZA2	-0,509	0,004999708
CLIC1	-1,150	0,005030252
EDIL3	0,896	0,00507413
VLDLR	1,050	0,005195356
HS90A	-0,484	0,005270921
APLP1	1,271	0,005312539
MAOX	-0,840	0,005354004
SAP3	-0,757	0,005372227
PUR9	-0,727	0,005566755
ALBU	3,400	0,005834453
HNRPL	1,691	0,00684336
NUCB1	-2,318	0,006847924
AGAL	-1,611	0,007367375
SAP	-0,456	0,007480324
PP1A	-0,817	0,007578545
IMB1	-0,997	0,00813272
MGAT2	-0,722	0,009091146
PA2G4	-0,586	0,009177796
MPZL2	-0,999	0,009196573
DAG1	-0,524	0,009215916
SYDC	-1,425	0,009371816
XPO1	-0,961	0,00982991
CADM1	-1,375	0,01048172
CD82	-1,547	0,010516712
OTUB1	1,784	0,010857538
TCPQ	-0,505	0,011077995

CCN2	0,968	0,011170797
GALC	0,446	0,011342034
FLNB	-0,837	0,011638863
EHD2	-0,800	0,012080766
PAI1	-0,692	0,012331353
IL1AP	-0,373	0,012729568
MA2B2	-1,585	0,01281342
UNC5B	-1,085	0,013202242
EFNA1	-0,840	0,01347001
CATD	-0,899	0,013777804
CYTB	1,326	0,013812357
NCKP1	-0,627	0,013827179
VASN	-0,854	0,014822933
CASP3	1,860	0,015206083
PURA	-0,861	0,016008013
LKHA4	-0,969	0,016024426
CBPE	0,465	0,016128601
PPIB	-0,620	0,016145816
ANXA6	-1,714	0,016584463
GDIB	-1,769	0,017044498
RISC	-1,433	0,017233762
CLUS	-0,883	0,017529763
HNRPQ	-1,497	0,017768617
EPHA2	-0,500	0,018667516
DLDH	1,284	0,018676787
PLOD1	-0,809	0,019524933
S10A6	2,460	0,02004816
CNDP2	-1,331	0,020688281
IF5	-0,974	0,020849313
B4GT1	1,602	0,020976253
LAMB1	-0,902	0,021616165
JAG1	-3,691	0,022849483
SET	-1,067	0,023430883
GNPTG	0,573	0,023558651
VMA5A	-0,771	0,024739021
DDX6	-0,684	0,0249467
CSF1	0,369	0,027068267
PTPRK	0,255	0,028337136
MAP2	-0,734	0,028459609
FUMH	-0,969	0,028613772
THIO	1,316	0,028674776
PROS	-0,702	0,029737551

NAGAB	-1,389	0,030208389
PURA2	-1,661	0,031352745
LAD1	-0,506	0,031427942
RENR	0,682	0,03168497
ARSB	-1,346	0,032075257
METRL	-0,667	0,033022195
PRDX2	0,524	0,034244012
VP26B	-1,563	0,034245396
ALDOA	0,488	0,035654977
SIA8F	-0,284	0,035837287
FRRS1	-0,622	0,036728973
EFNA5	-1,364	0,037003435
XRP2	-0,245	0,037108
ANXA5	2,141	0,037145672
FAS	-0,759	0,038264767
G6PD1	0,958	0,038821792
6PGL	1,251	0,040536648
MA2B1	-0,821	0,040633429
TCPZ	-0,466	0,040645746
PTGDS	0,344	0,040693513
EMAL2	-1,169	0,040695533
F10A1	-1,017	0,040973513
ENPL	1,453	0,042039638
LG3BP	0,578	0,042632056
ADA10	-0,491	0,042996122
AGRIN	1,121	0,044467657
ELAV1	1,126	0,047185324
CTND1	-0,371	0,047476231
PRP19	-0,797	0,047862851
VAT1	0,331	0,047907651
TRI23	0,487	0,048438833
EPHB6	-1,790	0,04865325

Table S2: Antibody list

Target	Antibody type / Application	Reference
GAPDH	Primary / WB	Cell Signalling 2118S
E-Cadherin	Primary / WB, IF	Cell Signalling 3195S
Vimentin	Primary / WB, IF	Cell Signalling 5741S
Trail	Primary / WB, IF	Abcam ab2435
DR5	Primary / WB	R&D MAB1121
TNC	Primary / WB, IF	G. OREND
Cl. Cas 3	Primary / IF	Cell Signalling 9661S
CK8/18	Primary / IF	Progen GP11
CD68	Primary / IF	Abcam ab1252212
F4/80	Primary / IF	Abcam ab6640
CD11c	Primary / IF	DB Pharmingen 550283
Ki67	Primary / IF	Thermo Fisher Sp6
Col IV	Primary / IF	P. SIMON-ASSMAN
CD45	FACS	Thermo Fisher 11-0451-82
MHCII	FACS	Thermo Fisher 47-5321-80
CD11c	FACS	Thermo Fisher 12-0114-81
CD80	FACS	Thermo Fisher 16-10A1
CD86	FACS	Thermo Fisher 25-0862-80
F4/80	FACS	Thermo Fisher BM8
B220	FACS	Thermo Fisher 17-0452-81
CD206	FACS	Thermo Fisher MR6F3
Anti-rabbit	Secondary WB	Cell Signalling 7074S
Anti-rat	Secondary WB	Cell Signalling 7077S
Anti-mouse	Secondary WB	Cell Signalling 7076S
Anti-rabbit	Secondary IF	Jackson Lab 111-165-003
Anti-rat	Secondary IF	Jackson Lab A11006
Anti-mouse	Secondary IF	Jackson Lab 115-165-003
Anti-guinea pig	Secondary IF	Jackson Lab 706-165-148
Anti-armenian hamster	Secondary IF	Jackson Lab 127-005-160

Table S3: Primer list

Gene symbol	Primer references
Gapdh	Taqman probe: Mm99999915_g1 Thermo Fisher
Cxcl12	Taqman probe: Mm00445553_m1 Thermo Fisher
Tnfsf10	Taqman probe: Mm01283606_m1 Thermo Fisher
Tnfrsf10b	Taqman probe: Mm00445831_m1 Thermo Fisher
Tnfrsf23	Taqman probe: Mm00656375_m1 Thermo Fisher
Tnfrsf22	Taqman probe: Mm00445831_m1 Thermo Fisher
Cxcr4	Taqman probe: Mm01996749_s1 Thermo Fisher
Mapk1	Taqman probe: Mm00442479_m1 Thermo Fisher
Mapk3	Taqman probe: Mm01278702_gH Thermo Fisher

Figure S1

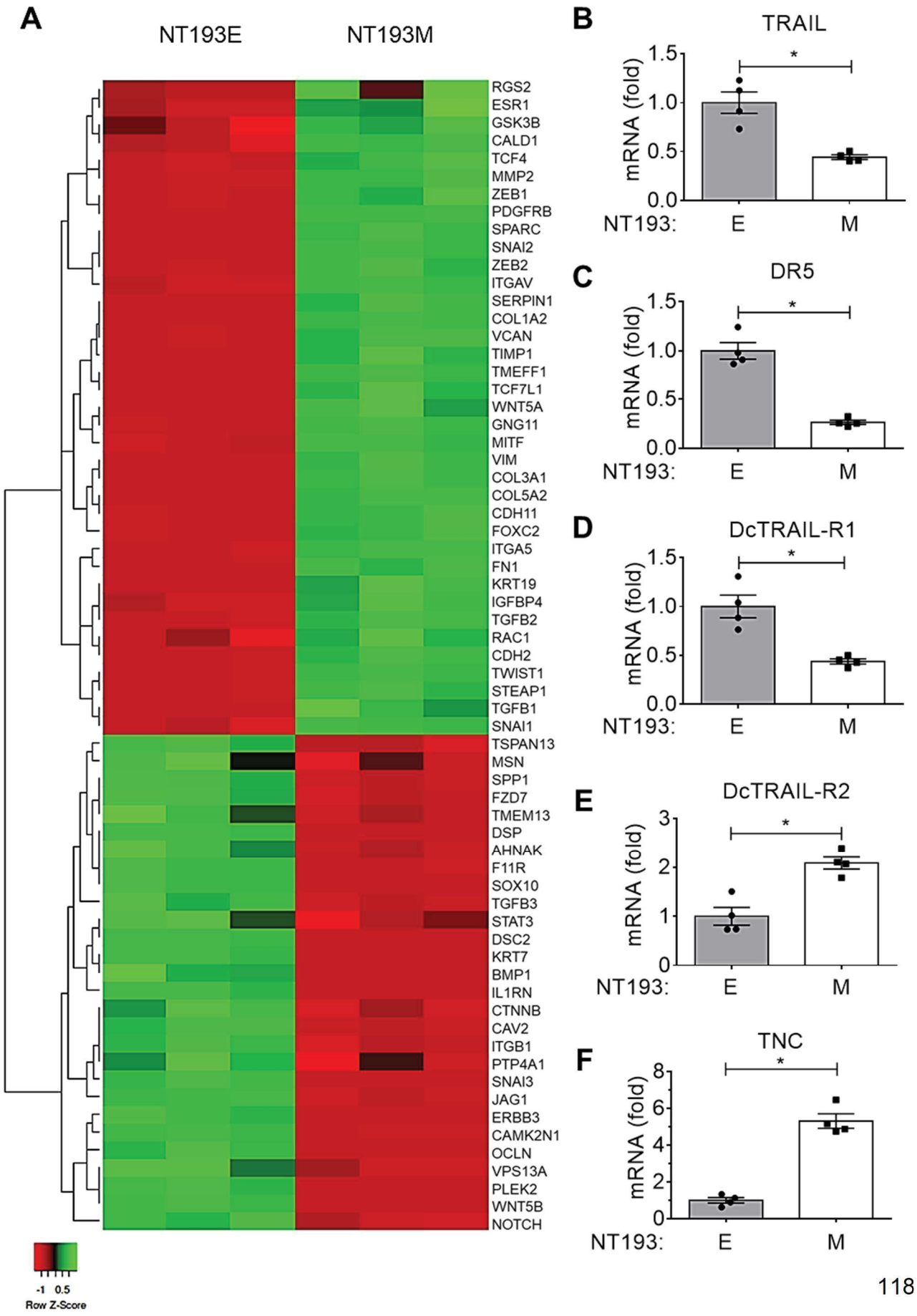
A
NT193E
NT193M
RGS2
ESR1
GSK3B
CALD1
TCF4
MMP2
ZEB1
PDGFRB
SPARC
SNAI2
ZEB2
ITGAV
SERPIN1
COL1A2
VCAN
TIMP1
TMEFF1
TCF7L1
WNT5A
GNG11
MITF
VIM
COL3A1
COL5A2
CDH11
FOXC2
ITGA5
FN1
KRT19
IGFBP4
TGFB2
RAC1
CDH2
TWIST1
STEAP1
TGFB1
SNAI1
TSPAN13
MSN
SPP1
FZD7
TMEM13
DSP
AHNAK
F11R
SOX10
TGFB3
STAT3
DSC2
KRT7
BMP1
IL1RN
CTNNB
CAV2
ITGB1
PTP4A1
SNAI3
JAG1
ERBB3
CAMK2N1
OCLN
VPS13A
PLEK2
WNT5B
NOTCH
-1 0.5
Row Z-Score
B
TRAIL
mRNA (fold)
NT193:
E
M
C
DR5
D
DcTRAIL-R1
E
DcTRAIL-R2
F
TNC

Figure S1: Gene expression analysis of NT193E and NT193M cells

(A) Expression of EMT-related genes in NT193E and NT193M cells (N = 3) determined by RNA seq analysis represented as heatmap, Limma moderated t-test, $p < 0.05$. **(B-F)** Expression of the indicated genes as determined by qRTPCR in NT193E and NT193M cells, N = 4 experiments. Mann-Whitney test, mean ± SEM (*$p < 0.05$).

Figure S2

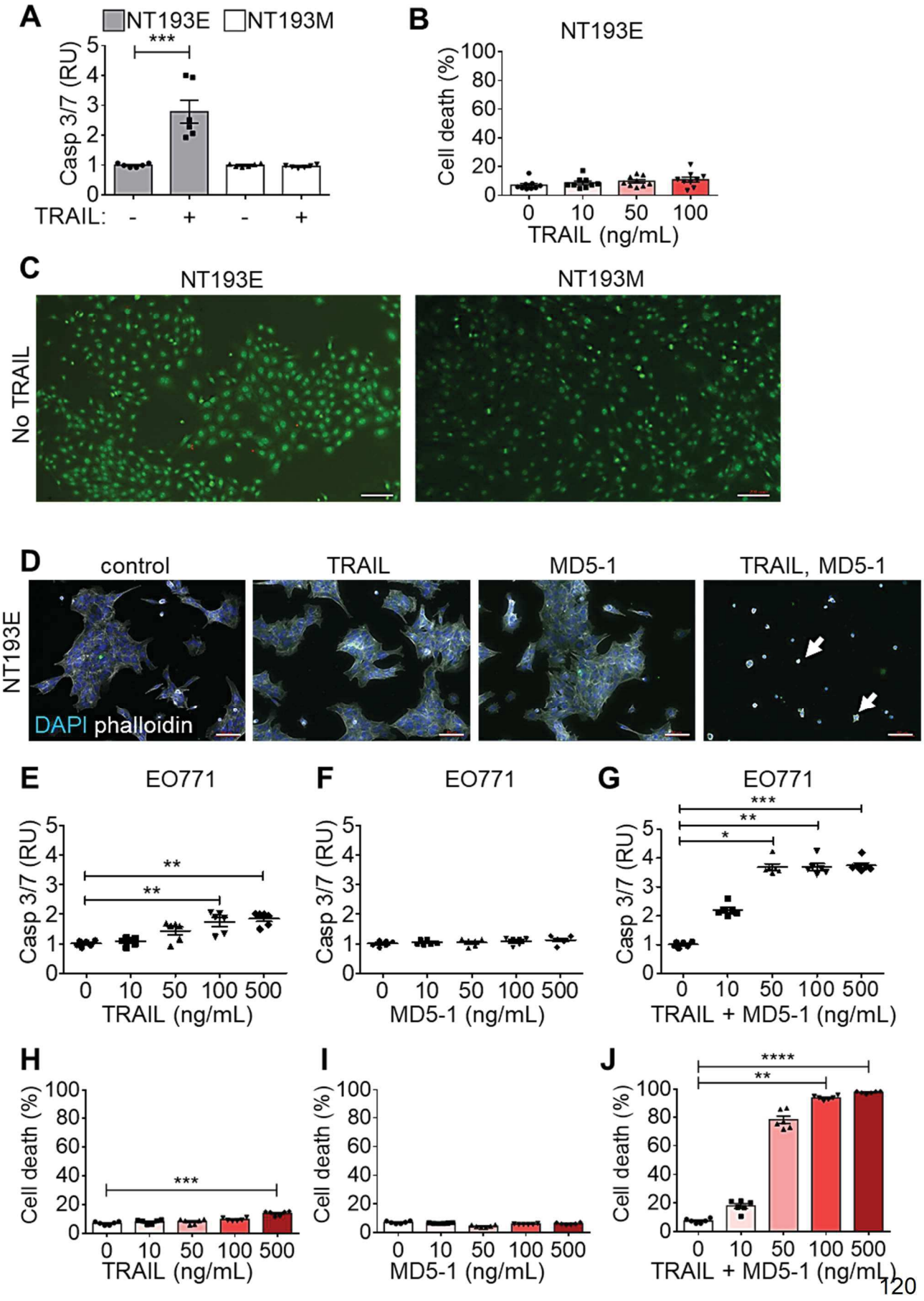
A
NT193E
NT193M
***
Casp 3/7 (RU)
TRAIL: - + - +
B
NT193E
Cell death (%)
TRAIL (ng/mL)
C
NT193E
NT193M
No TRAIL
D
control
TRAIL
MD5-1
TRAIL, MD5-1
NT193E
DAPI phalloidin
E
EO771
Casp 3/7 (RU)
TRAIL (ng/mL)
F
EO771
MD5-1 (ng/mL)
G
EO771
TRAIL + MD5-1 (ng/mL)
H
Cell death (%)
TRAIL (ng/mL)
I
Cell death (%)
MD5-1 (ng/mL)
J
Cell death (%)
TRAIL + MD5-1 (ng/mL)

Figure S2: TRAIL plus MD5-1 induces cell death in NT193E and EO771 but not in NT193M cells

(A) Casp 3/7 activity in NT193E and NT193M cells after incubation with TRAIL (100 ng/mL), N = 3 experiments, n = 2 replicates**.** Mann-Whitney test, mean ± SEM (***p < 0.001). **(B)** Number of dead NT193E cells after TRAIL treatment, N = 4, n = 2 replicates **(C, D)** Representative IF images (N = 4) of NT193E and NT193M cells stained with AO/EB (100 ng/mL), N = 2 experiments, n = 2 replicates, scale bar 100 µm. **(D)** Kruskal-Wallis test, mean ± SEM, no differences. **(E, F, G)** Casp 3/7 activity in EO771 cells, N = 3 experiments, n = 2 replicates**.** Kruskal-Wallis test, mean ± SEM (*p < 0.05; **p < 0.01; ***p < 0.001). **(H, I, J)** Percentage of dead EO771 cells, N = 3 experiments, n = 2 replicates. Kruskal-Wallis test, mean ± SEM (**p < 0.01; ***p < 0.001; ****p < 0.0001).

Figure S4

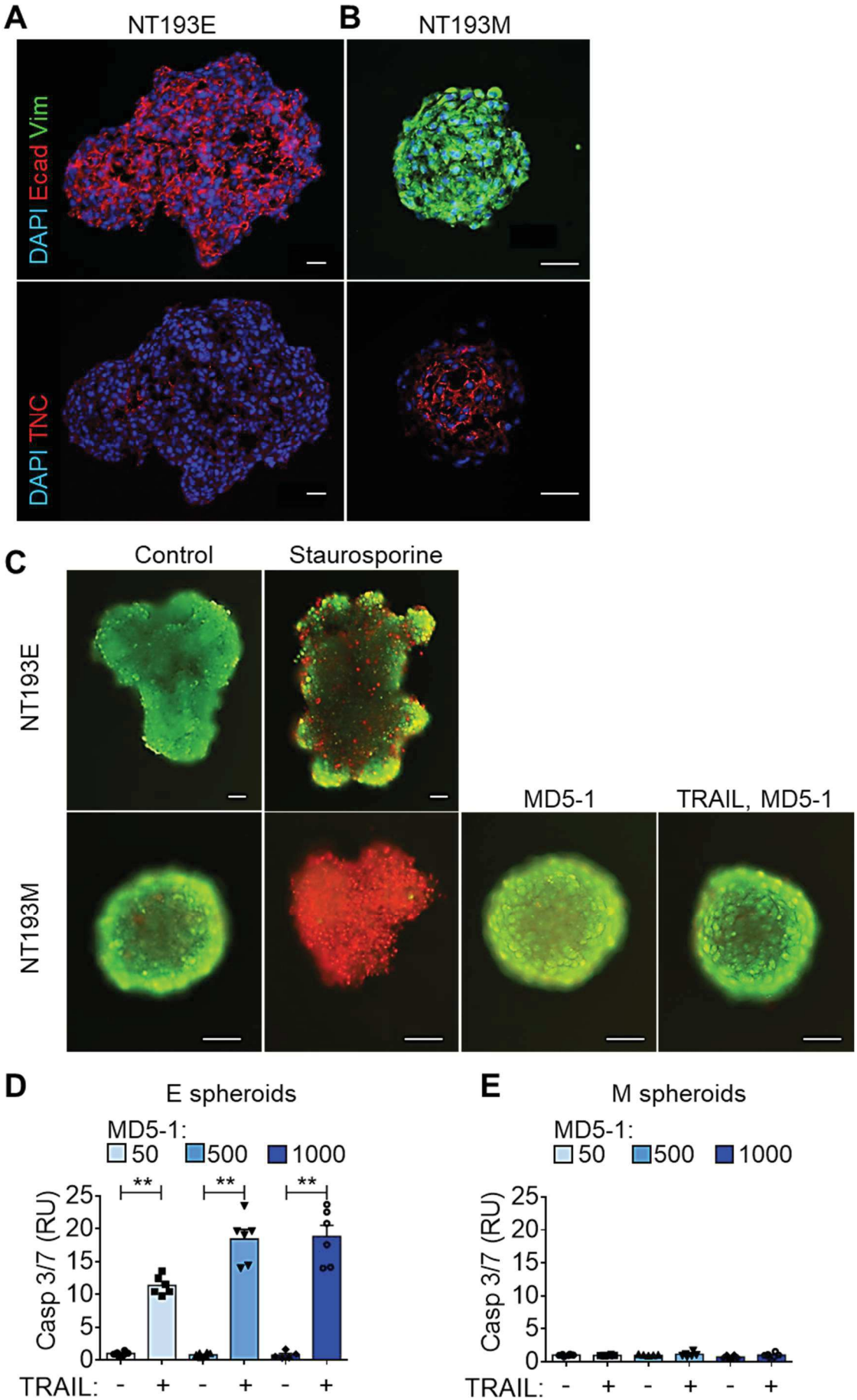
A
NT193E
B
NT193M
DAPI Ecad Vim
DAPI TNC
C
Control
Staurosporine
NT193E
NT193M
MD5-1
TRAIL, MD5-1
D
E spheroids
MD5-1:
50
500
1000
Casp 3/7 (RU)
25
20
15
10
5
0
**
**
**
TRAIL: - + - + - +
E
M spheroids
MD5-1:
50
500
1000
Casp 3/7 (RU)
25
20
15
10
5
0
TRAIL: - + - + - +

Figure S4: In contrast to M spheroids E cell spheroids are sensitive to TRAIL-induced apoptosis

(A, B) Representative IF images of NT193E **(A)** or NT193M **(B)** spheroids and TNC expression, scale bars 50 µm, N = 2. **(C)** Representative images of NT193E and NT193M spheroids stained with AO/EB after treatments with staurosporine (1 µg/mL), MD5-1 (500 ng/mL) or TRAIL (100 ng/mL) and MD5-1 (500 ng/mL). Scale bars 50 µm. N = 3. **(D, E)** Casp 3/7 activity in NT193E **(D)** and NT193M **(E)** spheroids upon incubation with increasing concentrations of MD5-1 (ng/mL) and TRAIL (100 ng/mL). **(D)** N = 3 (total 6 spheroids). Mann-Whitney test, mean ± SEM (**p < 0.01). **(E)** N = 3 experiments, n = 2 replicates. Mann-Whitney test, mean ± SEM, no differences.

Figure S5

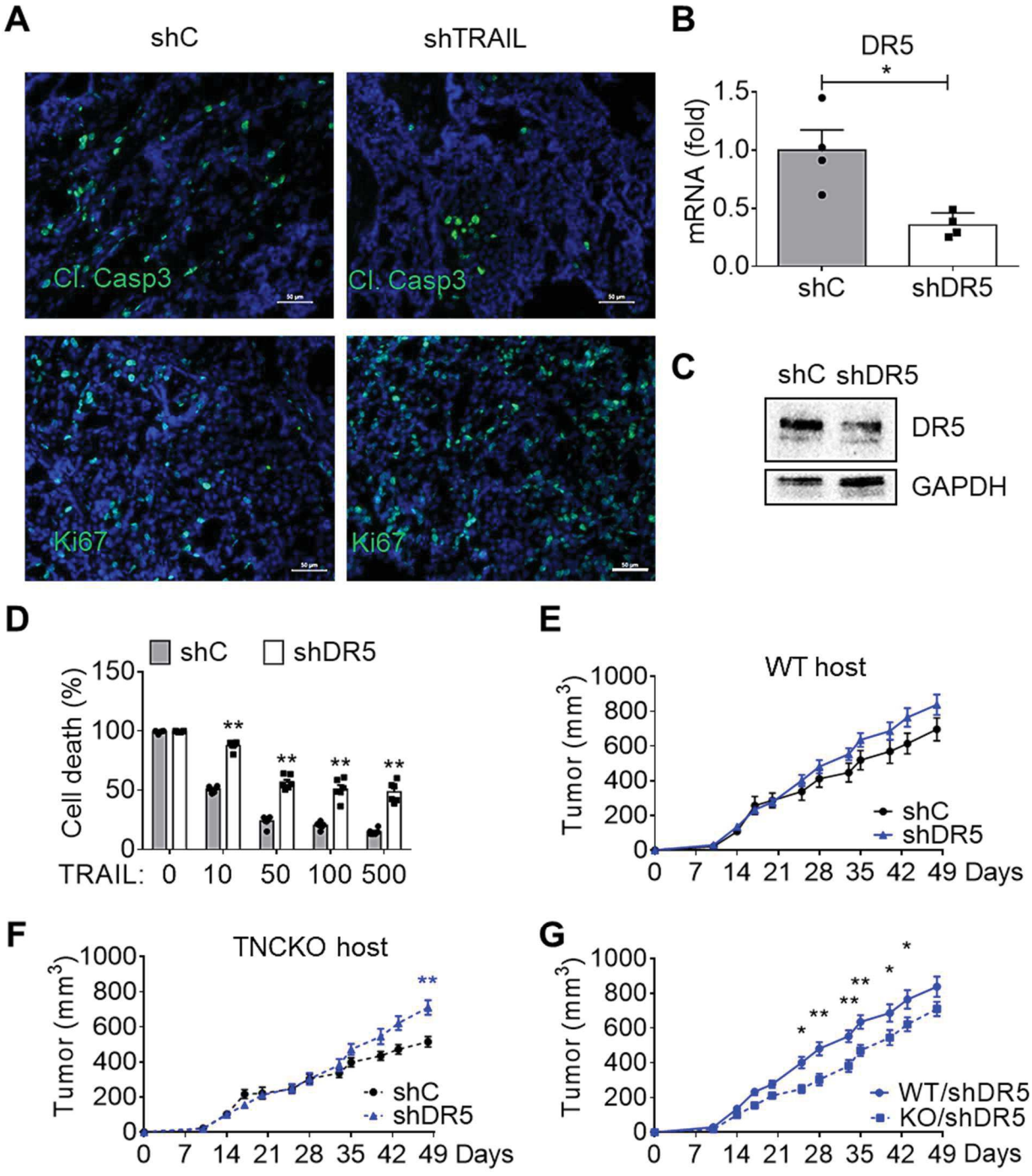
A
shC
shTRAIL
Cl. Casp3
Cl. Casp3
Ki67
Ki67
B
DR5
*
mRNA (fold)
1.5
1.0
0.5
0.0
shC
shDR5
C
shC shDR5
DR5
GAPDH
D
shC
shDR5
Cell death (%)
150
100
50
0
**
**
**
**
TRAIL: 0 10 50 100 500
E
WT host
Tumor (mm3)
1000
800
600
400
200
0
shC
shDR5
0 7 14 21 28 35 42 49 Days
F
TNCKO host
Tumor (mm3)
**
shC
shDR5
0 7 14 21 28 35 42 49 Days
G
Tumor (mm3)
*
**
**
**
*
*
WT/shDR5
KO/shDR5
0 7 14 21 28 35 42 49 Days

Figure S5 Impact of TRAIL and DR5 knockdown on tumor growth

(A) IF images of shTRAIL and control tumors to assess apoptosis (Cl. Casp3) and proliferation (Ki67). Scale bar 50 µm. **(B)** DR5 mRNA levels (qRTPCR) in E cells (shC or shDR5), N = 4. Mann-Whitney test, mean ± SEM (*p < 0.05). **(C)** Immunoblots for the indicated molecules, N = 2. **(D)** Impact of DR5 KD on TRAIL (ng/mL) + MD5-1 (50 ng/mL) on apoptosis, N = 3 experiments, n = 2 replicates. Mann-Whitney test, mean ± SEM (**p < 0.01). **(E-G)** Tumor volume. WT/shC, N = 12, WT/DR5, N = 12, KO/shC, N = 10, KO/shTRAIL, N = 9. ANOVA two-way tests, mean ± SEM (*p < 0.05, **p < 0.01).

Figure S6

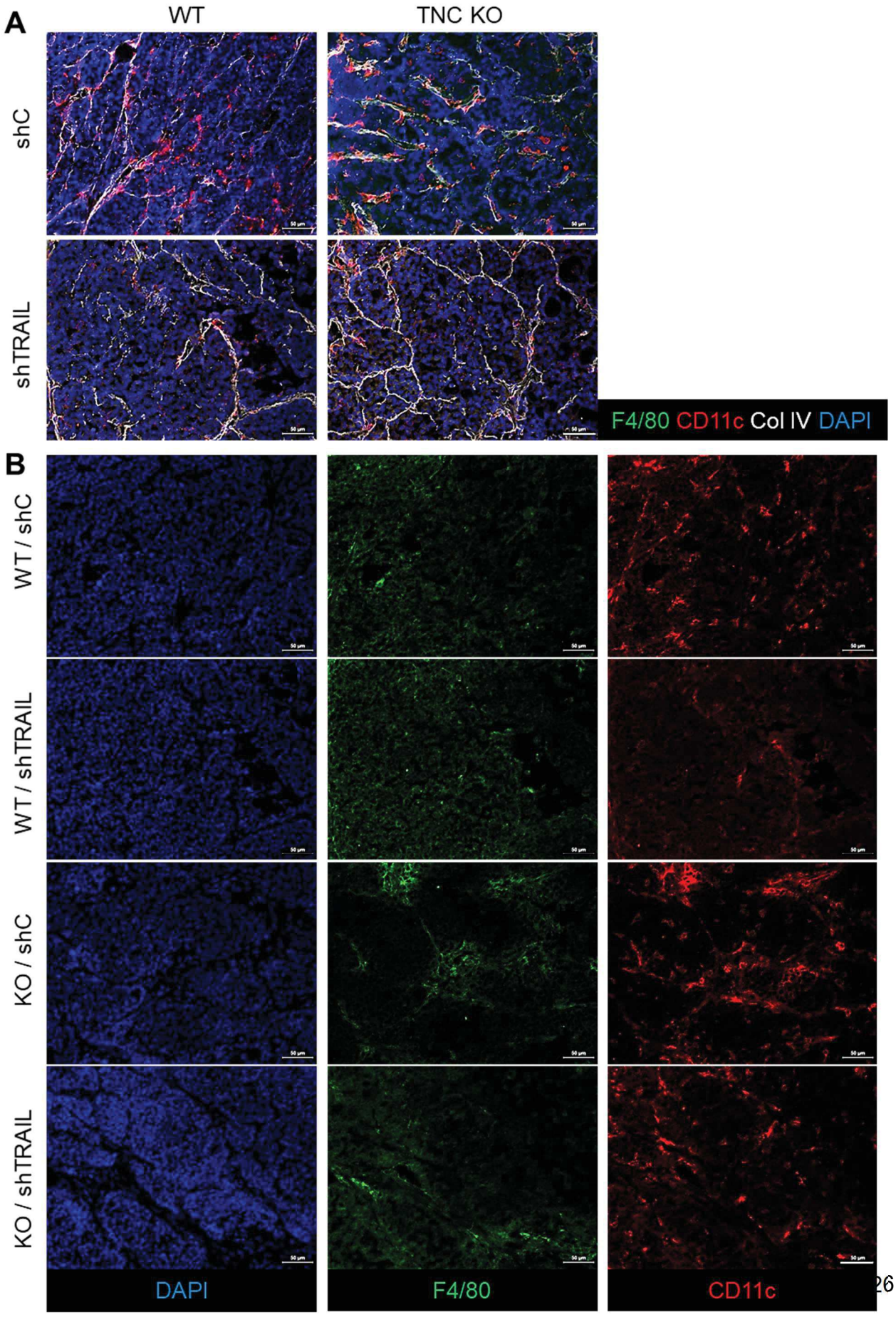
A
WT
TNC KO
shC
shTRAIL
F4/80 CD11c Col IV DAPI
B
WT / shC
WT / shTRAIL
KO / shC
KO / shTRAIL
DAPI
F4/80
CD11c

Figure S6

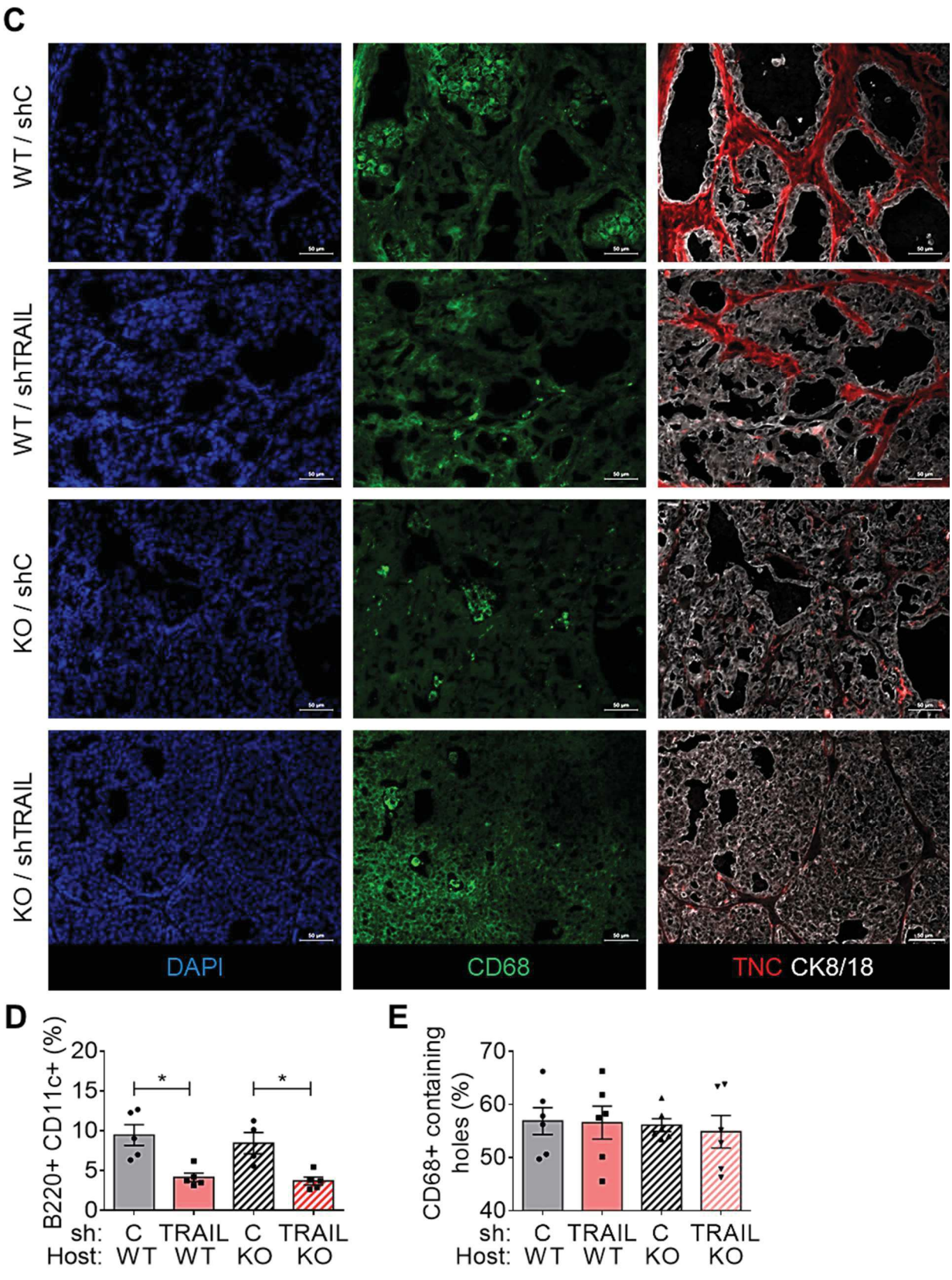
C
WT / shC
WT / shTRAIL
KO / shC
KO / shTRAIL
DAPI
CD68
TNC CK8/18
D
B220+ CD11c+ (%)
20
15
10
5
0
*
*
sh: C TRAIL C TRAIL
Host: WT WT KO KO
E
CD68+ containing holes (%)
70
60
50
40
sh: C TRAIL C TRAIL
Host: WT WT KO KO

Figure S6

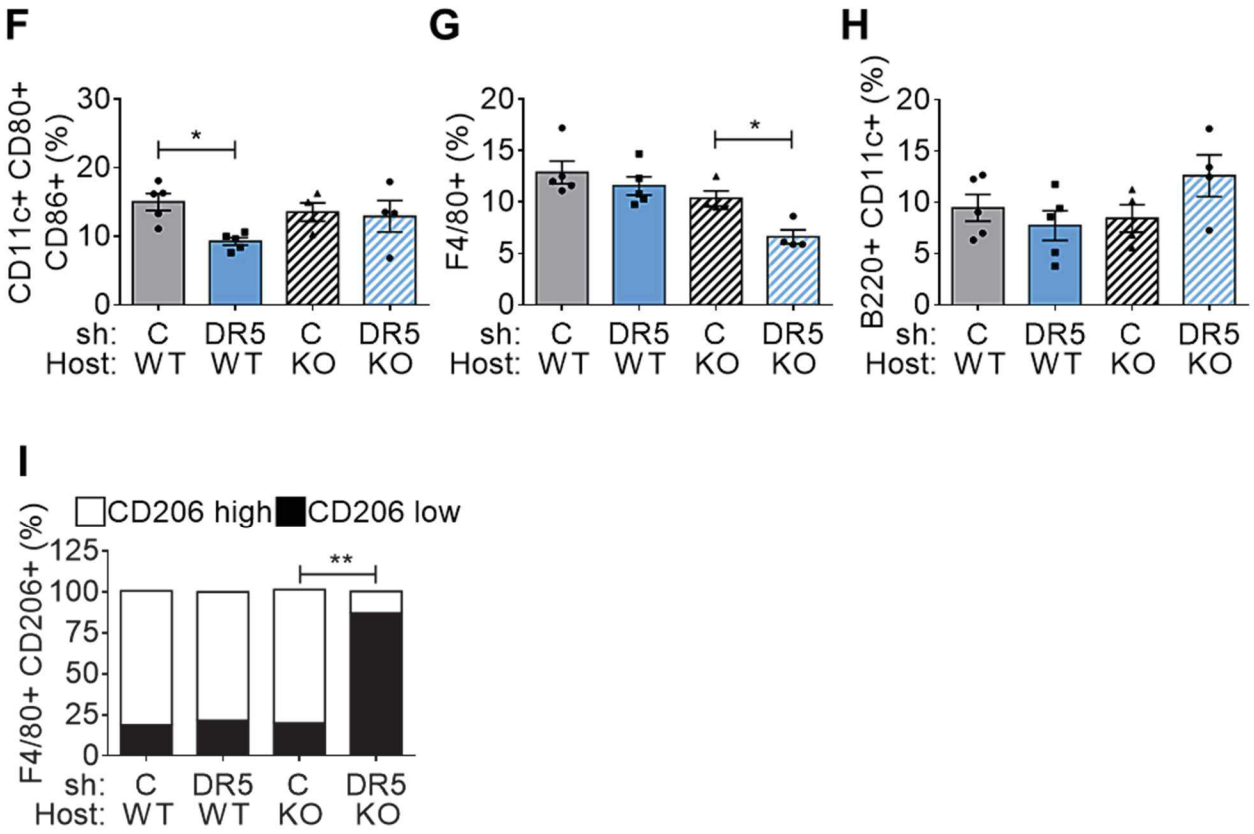
F
CD11c+ CD80+ CD86+ (%)
30
20
10
0
*
sh: C DR5 C DR5
Host: WT WT KO KO
G
F4/80+ (%)
20
15
10
5
0
*
sh: C DR5 C DR5
Host: WT WT KO KO
H
B220+ CD11c+ (%)
20
15
10
5
0
sh: C DR5 C DR5
Host: WT WT KO KO
I
CD206 high
CD206 low
F4/80+ CD206+ (%)
125
100
75
50
25
0
**
sh: C DR5 C DR5
Host: WT WT KO KO

Figure S6: Impact of TRAIL and DR5 knockdown on immune cells infiltration

(A-C) Representative IF images of CD11c+ cells **(A)** and separated channels of shTRAIL tumors for the indicated molecules **(B, C)**. N = 5. Scale bars 50 µm. **(D)** Abundance of immune cell subtypes (flow cytometry) as percentage of CD45+ cells in the indicated tumors, N = 4-5 mice. Mann-Whitney test, mean ± SEM (*p < 0.05). **(E)** Percentage of holes containing CD68+ cells in tumors. N = 6. Kruskal-Wallis test, mean ± SEM, no difference. **(F-I)** Abundance of immune cell subtypes (flow cytometry) as percentage of CD45+ cells in the indicated tumors. N = 4-5 mice. Mann-Whitney test, mean ± SEM (*p < 0.05, **p < 0.01).

Figure S7

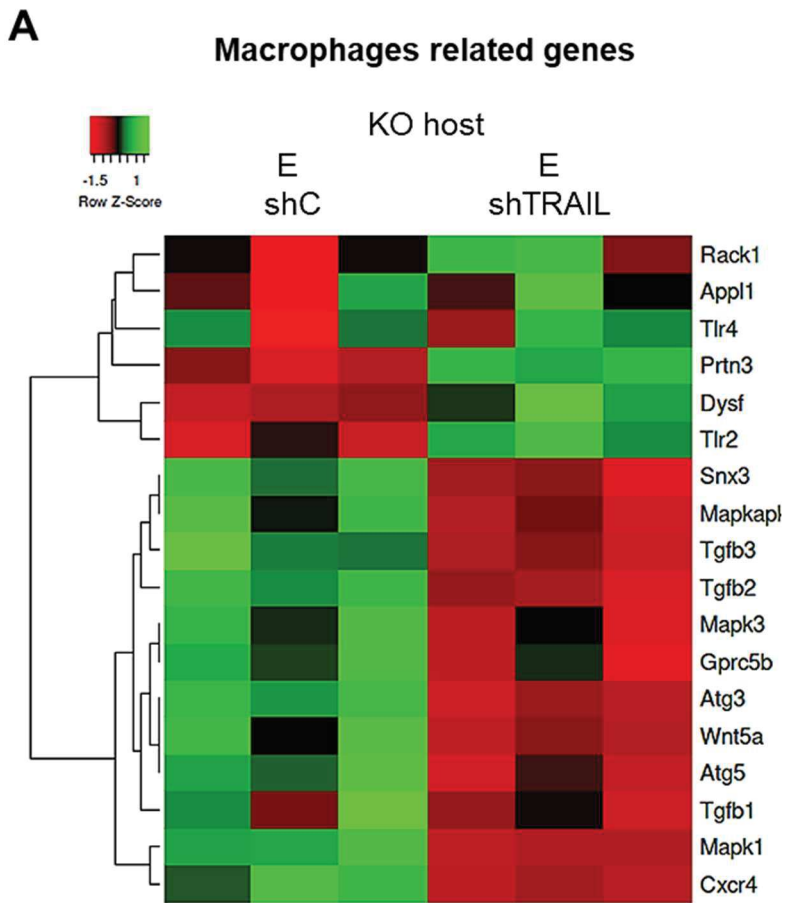
A
Macrophages related genes
KO host
E
shC
E
shTRAIL
-1.5
1
Row Z-Score
Rack1
Appl1
Tlr4
Prtn3
Dysf
Tlr2
Snx3
Mapkapl
Tgfb3
Tgfb2
Mapk3
Gprc5b
Atg3
Wnt5a
Atg5
Tgfb1
Mapk1
Cxcr4

Figure S7

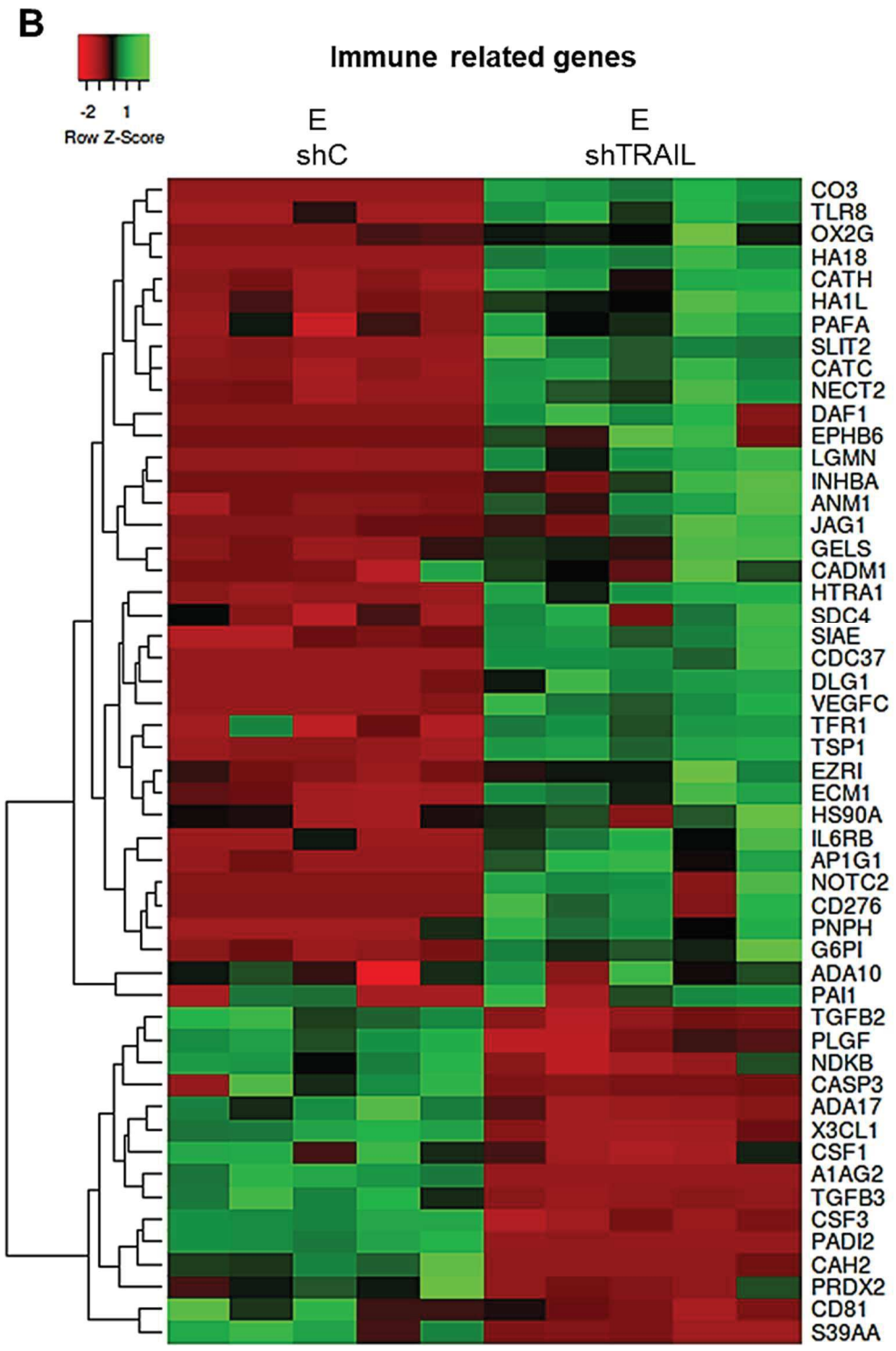
B
Immune related genes
-2
1
Row Z-Score
E
shC
E
shTRAIL
CO3
TLR8
OX2G
HA18
CATH
HA1L
PAFA
SLIT2
CATC
NECT2
DAF1
EPHB6
LGMN
INHBA
ANM1
JAG1
GELS
CADM1
HTRA1
SDC4
SIAE
CDC37
DLG1
VEGFC
TFR1
TSP1
EZRI
ECM1
HS90A
IL6RB
AP1G1
NOTC2
CD276
PNPH
G6PI
ADA10
PAI1
TGFB2
PLGF
NDKB
CASP3
ADA17
X3CL1
CSF1
A1AG2
TGFB3
CSF3
PADI2
CAH2
PRDX2
CD81
S39AA

Figure S7: Impact of TRAIL knock down on tumor gene expression and protein secretion of NT193 cells

(A) Expression of macrophages regulating genes in shC and shTRAIL tumors of KO hosts, determined by RNA seq analysis represented as heatmap, N = 3, $p < 0.05$. **(B)** Expression of immune response regulation associated proteins secreted by NT193E shC and shTRAIL cells, determined by mass spectrometry analysis represented as heatmap, Limma moderated t-test, N = 5, $p < 0.05$.

Figure S8

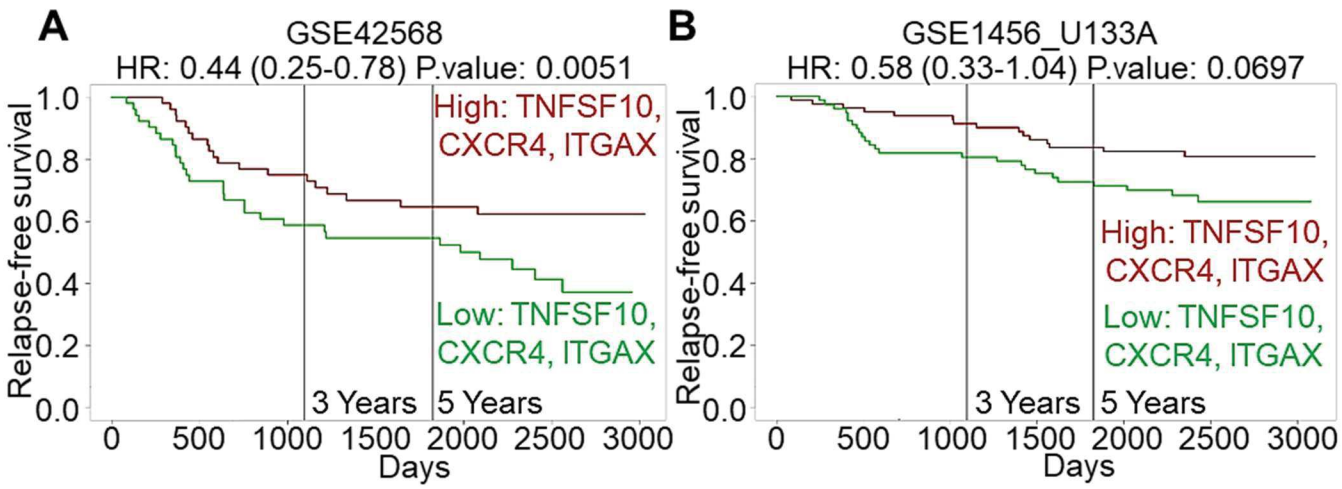

Figure S8: Prognostic value of TRAIL expression in human breast cancer

(A, B) Kaplan Meier analysis of breast cancer patient relapse-free survival in relation to combined high or low expression of the indicated molecules (above or below the median). **(A)** GSE42568, n = 54. HR: 0.44 (0.26 – 0.76). **(B)** GSE1456_U133A, n = 80. HR: 0.56 (0.33 – 1.04).

Acknowledgement

We are grateful for support by the animal facility and the Genomax facility of INSERM U1109, O. Lefebvre for shRNA lentivirus production, L. Aubergeon and A. Yilmaz for support during flow cytometry, F. Steinbach for technical support. We acknowledge support by Worldwide Cancer Research (WCR10-047), Association pour la Recherche sur le cancer (ARC), the Universty Strasbourg and INSERM and, personal fellowships to WE (French ministry of research MRT) and DM (ARC).

7.8. References

Anders, S., Pyl, P.T., and Huber, W. (2015). HTSeq—a Python framework to work with high-throughput sequencing data. Bioinformatics 31, 166–169.

Arpel, A., Sawma, P., Spenlé, C., Fritz, J., Meyer, L., Garnier, N., Velázquez-Quesada, I., Hussenet, T., Aci-Sèche, S., Baumlin, N., et al. (2014). Transmembrane Domain Targeting Peptide Antagonizing ErbB2/Neu Inhibits Breast Tumor Growth and Metastasis. Cell Reports 8, 1714–1721.

Ashkenazi, A., Pai, R.C., Fong, S., Leung, S., Lawrence, D.A., Marsters, S.A., Blackie, C., Chang, L., McMurtrey, A.E., Hebert, A., et al. (1999). Safety and antitumor activity of recombinant soluble Apo2 ligand. Journal of Clinical Investigation 104, 155–162.

Babicki, S., Arndt, D., Marcu, A., Liang, Y., Grant, J.R., Maciejewski, A., and Wishart, D.S. (2016). Heatmapper: web-enabled heat mapping for all. Nucleic Acids Res 44, W147–W153.

Baschong, W., and Wrigley, N.G. (1990). Small colloidal gold conjugated to fab fragments or to immunoglobulin g as high-resolution labels for electron microscopy: A technical overview. J. Elec. Microsc. Tech. 14, 313–323.

Berens, E.B., Holy, J.M., Riegel, A.T., and Wellstein, A. (2015). A Cancer Cell Spheroid Assay to Assess Invasion in a 3D Setting. JoVE (Journal of Visualized Experiments) e53409.

Bober, M., Enochsson, C., Collin, M., and Mörgelin, M. (2010). Collagen VI is a subepithelial adhesive target for human respiratory tract pathogens. J Innate Immun 2, 160–166.

Campbell, G.R., Watkins, J.D., Singh, K.K., Loret, E.P., and Spector, S.A. (2007). Human Immunodeficiency Virus Type 1 Subtype C Tat Fails To Induce Intracellular Calcium Flux and Induces Reduced Tumor Necrosis Factor Production from Monocytes. J Virol 81, 5919–5928.

Chevallet, M., Diemer, H., Van Dorssealer, A., Villiers, C., and Rabilloud, T. (2007). Toward a better analysis of secreted proteins: the example of the myeloid cells secretome. Proteomics 7, 1757–1770.

De Laporte, L., Rice, J.J., Tortelli, F., and Hubbell, J.A. (2013). Tenascin C Promiscuously Binds Growth Factors via Its Fifth Fibronectin Type III-Like Domain. PLoS ONE 8, e62076.

Deligne, C., Murdamoothoo, D., Gammage, A.N., Gschwandtner, M., Erne, W., Loustau, T., Marzeda, A.M., Carapito, R., Paul, N., Velazquez-Quesada, I., et al. (2020). Matrix-Targeting Immunotherapy Controls Tumor Growth and Spread by Switching Macrophage Phenotype. Cancer Immunol Res 8, 368–382.

Dobin, A., Davis, C.A., Schlesinger, F., Drenkow, J., Zaleski, C., Jha, S., Batut, P., Chaisson, M., and Gingeras, T.R. (2013). STAR: ultrafast universal RNA-seq aligner. Bioinformatics 29, 15–21.

Drumea-Mirancea, M., Wessels, J.T., Müller, C.A., Essl, M., Eble, J.A., Tolosa, E., Koch, M., Reinhardt, D.P., Sixt, M., Sorokin, L., et al. (2006). Characterization of a conduit system containing laminin-5 in the human thymus: a potential transport system for small molecules. J Cell Sci 119, 1396–1405.

Falschlehner, C., Schaefer, U., and Walczak, H. (2009). Following TRAIL's path in the immune system. Immunology 127, 145–154.

Ferretti, E., Bertolotto, M., Deaglio, S., Tripodo, C., Ribatti, D., Audrito, V., Blengio, F., Matis, S., Zupo, S., Rossi, D., et al. (2011). A novel role of the CX3CR1/CX3CL1 system in the cross-talk between chronic lymphocytic leukemia cells and tumor microenvironment. Leukemia 25, 1268–1277.

Finnberg, N.K., Gokare, P., Navaraj, A., Lang Kuhs, K.A., Cerniglia, G., Yagita, H., Takeda, K., Motoyama, N., and El-Deiry, W.S. (2016). Agonists of the TRAIL death receptor DR5 sensitize intestinal stem cells to chemotherapy-induced cell death and trigger gastrointestinal toxicity. Cancer Res 76, 700–712.

Fouda, G.G., Jaeger, F.H., Amos, J.D., Ho, C., Kunz, E.L., Anasti, K., Stamper, L.W., Liebl, B.E., Barbas, K.H., Ohashi, T., et al. (2013). Tenascin-C is an innate broad-spectrum, HIV-1–neutralizing protein in breast milk. PNAS 110, 18220–18225.

Giblin, S.P., Murdamoothoo, D., Deligne, C., Schwenzer, A., Orend, G., and Midwood, K.S. (2018). Chapter 21 - How to detect and purify tenascin-C. In Methods in Cell Biology, R.P. Mecham, ed. (Academic Press), pp. 371–400.

Goswami, C.P., and Nakshatri, H. (2014). PROGgeneV2: enhancements on the existing database. BMC Cancer 14.

Hartwig, T., Montinaro, A., von Karstedt, S., Sevko, A., Surinova, S., Chakravarthy, A., Taraborrelli, L., Draber, P., Lafont, E., Arce Vargas, F., et al. (2017). The TRAIL-Induced Cancer Secretome Promotes a Tumor-Supportive Immune Microenvironment via CCR2. Molecular Cell 65, 730-742.e5.

Huang, W., Chiquet-Ehrismann, R., Moyano, J.V., Garcia-Pardo, A., and Orend, G. (2001). Interference of tenascin-C with syndecan-4 binding to fibronectin blocks cell adhesion and stimulates tumor cell proliferation. Cancer Res. 61, 8586–8594.

Hyenne, V., Apaydin, A., Rodriguez, D., Spiegelhalter, C., Hoff-Yoessle, S., Diem, M., Tak, S., Lefebvre, O., Schwab, Y., Goetz, J.G., et al. (2015). RAL-1 controls multivesicular body biogenesis and exosome secretion. J Cell Biol 211, 27–37.

Jouan-Lanhouet, S., Arshad, M.I., Piquet-Pellorce, C., Martin-Chouly, C., Le Moigne-Muller, G., Van Herreweghe, F., Takahashi, N., Sergent, O., Lagadic-Gossmann, D., Vandenabeele, P., et al. (2012). TRAIL induces necroptosis involving RIPK1/RIPK3-dependent PARP-1 activation. Cell Death Differ 19, 2003–2014.

Korbecki, J., Simińska, D., Kojder, K., Grochans, S., Gutowska, I., Chlubek, D., and Baranowska-Bosiacka, I. (2020). Fractalkine/CX3CL1 in Neoplastic Processes. Int J Mol Sci 21.

Langmead, B., and Salzberg, S.L. (2012). Fast gapped-read alignment with Bowtie 2. Nature Methods 9, 357–359.

Lee, B., Sharron, M., Montaner, L.J., Weissman, D., and Doms, R.W. (1999). Quantification of CD4, CCR5, and CXCR4 levels on lymphocyte subsets, dendritic cells, and differentially conditioned monocyte-derived macrophages. PNAS 96, 5215–5220.

Lemke, J., von Karstedt, S., Zinngrebe, J., and Walczak, H. (2014). Getting TRAIL back on track for cancer therapy. Cell Death & Differentiation 21, 1350–1364.

Love, M.I., Huber, W., and Anders, S. (2014). Moderated estimation of fold change and dispersion for RNA-seq data with DESeq2. Genome Biology 15, 550.

Lu, M., Marsters, S., Ye, X., Luis, E., Gonzalez, L., and Ashkenazi, A. (2014). E-Cadherin Couples Death Receptors to the Cytoskeleton to Regulate Apoptosis. Molecular Cell 54, 987–998.

Ma, D., Liu, S., Lal, B., Wei, S., Wang, S., Zhan, D., Zhang, H., Lee, R.S., Gao, P., Lopez-Bertoni, H., et al. (2019). Extracellular Matrix Protein Tenascin C Increases Phagocytosis Mediated by CD47 Loss of Function in Glioblastoma. Cancer Res 79, 2697–2708.

Martin, B.P., Frew, A.J., Bots, M., Fox, S., Long, F., Takeda, K., Yagita, H., Atadja, P., Smyth, M.J., and Johnstone, R.W. (2011). Antitumor activities and on-target toxicities mediated by a TRAIL receptor agonist following cotreatment with panobinostat. International Journal of Cancer 128, 2735–2747.

Meijer, M.T., Uhel, F., Cremer, O.L., Schultz, M.J., van der Poll, T., and Consortium, on behalf of the M. (2020). Tenascin C Plasma Levels in Critically Ill Patients with or Without Sepsis: A Multicenter Observational Study. Shock 54, 62–69.

Midwood, K., Sacre, S., Piccinini, A.M., Inglis, J., Trebaul, A., Chan, E., Drexler, S., Sofat, N., Kashiwagi, M., Orend, G., et al. (2009). Tenascin-C is an endogenous activator of Toll-like receptor 4 that is essential for maintaining inflammation in arthritic joint disease. Nat. Med. 15, 774–780.

Midwood, K.S., Chiquet, M., Tucker, R.P., and Orend, G. (2016). Tenascin-C at a glance. Journal of Cell Science 129, 4321–4327.

Muller, W.J., Sinn, E., Pattengale, P.K., Wallace, R., and Leder, P. (1988). Single-step induction of mammary adenocarcinoma in transgenic mice bearing the activated c-neu oncogene. Cell 54, 105–115.

Mylonas, K.J., Anderson, J., Sheldrake, T.A., Hesketh, E.E., Richards, J.A., Ferenbach, D.A., Kluth, D.C., Savill, J., and Hughes, J. (2019). Granulocyte macrophage-colony stimulating factor: A key modulator of renal mononuclear phagocyte plasticity. Immunobiology 224, 60–74.

Naval, J., de Miguel, D., Gallego-Lleyda, A., Anel, A., and Martinez-Lostao, L. (2019). Importance of TRAIL Molecular Anatomy in Receptor Oligomerization and Signaling. Implications for Cancer Therapy. Cancers 11, 444.

Oskarsson, T. (2013). Extracellular matrix components in breast cancer progression and metastasis. The Breast 22, S66–S72.

Pitti, R.M., Marsters, S.A., Ruppert, S., Donahue, C.J., Moore, A., and Ashkenazi, A. (1996). Induction of Apoptosis by Apo-2 Ligand, a New Member of the Tumor Necrosis Factor Cytokine Family. J. Biol. Chem. 271, 12687–12690.

Sag, D., Ayyildiz, Z.O., Gunalp, S., and Wingender, G. (2019). The Role of TRAIL/DRs in the Modulation of Immune Cells and Responses. Cancers 11, 1469.

Spenlé, C., Gasser, I., Saupe, F., Janssen, K.-P., Arnold, C., Klein, A., van der Heyden, M., Mutterer, J., Neuville-Méchine, A., Chenard, M.-P., et al. (2015). Spatial organization of the tenascin-C microenvironment in experimental and human cancer. Cell Adhesion & Migration 9, 4–13.

Spenlé, C., Loustau, T., Murdamoothoo, D., Erne, W., Beghelli-de la Forest Divonne, S., Veber, R., Petti, L., Bourdely, P., Mörgelin, M., Brauchle, E.-M., et al. (2020). Tenascin-C Orchestrates an Immune-Suppressive Tumor Microenvironment in Oral Squamous Cell Carcinoma. Cancer Immunol Res 8, 1122–1138.

Stephenson, S., Care, M.A., Fan, I., Zougman, A., Westhead, D.R., Doody, G.M., and Tooze, R.M. (2019). Growth Factor–like Gene Regulation Is Separable from Survival and Maturation in Antibody-Secreting Cells. J Immunol 202, 1287–1300.

Stuckey, D.W., and Shah, K. (2013). TRAIL on trial: preclinical advances in cancer therapy. Trends Mol Med 19, 685–694.

Sun, Z., Schwenzer, A., Rupp, T., Murdamoothoo, D., Vegliante, R., Lefebvre, O., Klein, A., Hussenet, T., and Orend, G. (2018). Tenascin-C Promotes Tumor Cell Migration and Metastasis through Integrin α9β1–Mediated YAP Inhibition. Cancer Research 78, 950–961.

Sun, Z., Velázquez-Quesada, I., Murdamoothoo, D., Ahowesso, C., Yilmaz, A., Spenlé, C., Averous, G., Erne, W., Oberndorfer, F., Oszwald, A., et al. (2019). Tenascin-C increases lung metastasis by impacting blood vessel invasions. Matrix Biology 83, 26–47.

Tyanova, S., Temu, T., and Cox, J. (2016). The MaxQuant computational platform for mass spectrometry-based shotgun proteomics. Nature Protocols 11, 2301–2319.

von Karstedt, S., Conti, A., Nobis, M., Montinaro, A., Hartwig, T., Lemke, J., Legler, K., Annewanter, F., Campbell, A.D., Taraborrelli, L., et al. (2015). Cancer Cell-Autonomous TRAIL-R Signaling Promotes KRAS-Driven Cancer Progression, Invasion, and Metastasis. Cancer Cell 27, 561–573.

Walczak, H., Miller, R.E., Ariail, K., Gliniak, B., Griffith, T.S., Kubin, M., Chin, W., Jones, J., Woodward, A., Le, T., et al. (1999). Tumoricidal activity of tumor necrosis factor-related apoptosis-inducing ligand in vivo. Nat. Med. 5, 157–163.

Wieczorek, S., Combes, F., Lazar, C., Giai Gianetto, Q., Gatto, L., Dorffer, A., Hesse, A.-M., Couté, Y., Ferro, M., Bruley, C., et al. (2017). DAPAR & ProStaR: software to perform statistical analyses in quantitative discovery proteomics. Bioinformatics 33, 135–136.

Wiley, S.R., Schooley, K., Smolak, P.J., Din, W.S., Huang, C.-P., Nicholl, J.K., Sutherland, G.R., Smith, T.D., Rauch, C., Smith, C.A., et al. (1995). Identification and characterization of a new member of the TNF family that induces apoptosis. Immunity 3, 673–682.

Wu, G.S., Burns, T.F., Zhan, Y., Alnemri, E.S., and El-Deiry, W.S. (1999). Molecular cloning and functional analysis of the mouse homologue of the KILLER/DR5 tumor necrosis factor-related apoptosis-inducing ligand (TRAIL) death receptor. Cancer Res 59, 2770–2775.

Yuan, W., Zhang, W., Yang, X., Zhou, L., Hanghua, Z., and Xu, K. (2018). Clinical significance and prognosis of serum tenascin-C in patients with sepsis. BMC Anesthesiol 18, 170.

Zhou, J., Tang, Z., Gao, S., Li, C., Feng, Y., and Zhou, X. (2020). Tumor-Associated Macrophages: Recent Insights and Therapies. Front. Oncol. 10.

8. Manuscript II: Modulating tenascin-C functions by targeting the MAtrix REgulating MOtif, "MAREMO"

William Erne[1,2] *, Pia Abel zur Wiesch[3*&], Thomas Imhof[4+], Thomas Loustau[1,2+], Chérine Abou-Faycal[1,2+], Chengbei Li[1,2], Ayoub Ksouri[5], Marija Marko[1], Gerard Crémel[1], Balkiss Bouhaouala[5], Matthias Mörgelin[6+], Manuel Koch[4], Gertraud Orend[1,2,3]

* equal contribution

+ equal contribution

[1] University Strasbourg, INSERM U1109, MN3T (The Microenvironmental Niche in Tumorigenesis and Targeted Therapy), 3 avenue Molière, Strasbourg, Hautepierre, France

[2] University Strasbourg, INSERM U1109, The Tumor Microenvironment Laboratory, Hopital Civil, Institut d'Hématologie et d'Immunologie, Fédération de Médecine Translationnelle de Strasbourg (FMTS), 1Place de l'Hôpital, 67091 Strasbourg, France

[3] University Basel, Tumor Matrix laboratory, Department of Biomedicine, Mattenstrasse 57, Basel, Switzerland

[4] Institute for Dental Research and Oral, Musculoskeletal Research, Center for Biochemistry, University of Cologne, 50931 Cologne, Germany

[5] Laboratoire des Venins et Molécules Thérapeutiques, Institut Pasteur Tunis, 13 Place Pasteur, BP74, 1002, Tunis- Université Tunis El Manar Tunisia, Tunisia

[6] Colzyx AB, Scheelevägen 2, 223 81 Lund, Sweden

+ Correspondence:

Gertraud Orend, INSERM U1109, The Tumor Microenvironment Laboratory, 67091 Strasbourg, France, gertraud.orend@inserm.fr, https://orend-tme-group.com

& current address: Department of Biology, Eberly College of Science, The Pennsylvania State University, University Park, PA, USA, Center for Infectious Disease Dynamics, Huck Institutes of the Life Sciences, The Pennsylvania State University, University Park, PA, USA

8.1. Abstract

The extracellular matrix molecule Tenascin-C (TNC) promotes cancer by multiple mechanisms. Recently, TNC was shown to generate an immune-suppressive tumor microenvironment (TME) through binding soluble chemoattracting factors, thus immobilizing leukocytes in the stroma. TNC also binds to fibronectin (FN), raising the possibility of a potential common TNC binding mechanism. By sequence comparison of two TNC-interacting domains in FN we identified two distant sequences of 4 amino acids (aa) and 8 aa separated by more than 40 aa constituting the MAtrix REgulating MOtif “MAREMO” or M-motif. Amongst vertebrates the M-motif is highly conserved in the fifth (FN5) and thirteenth (FN13) fibronectin type III domains of FN. Moreover, by sequence analysis and structural modeling, we identified an M-motif in TNC itself (TN5) that we confirmed by interaction and competition ELISA and negative electron microscopy. We showed that the M-motif mediates FN interactions with itself as well as with TNC. We generated two peptides P5 and P13 mimicking the M-motif in FN5 and FN13 and showed that these peptides bind to TNC and blocked several functions of TNC, such as binding to FN, cell rounding, matrix fiber assembly, chemokine binding, dendritic cell immobilization and, promoting TRAIL-induced cell death. M-motif like sequences were also found in other matrix molecules, co-purifying together with TNC such as Col12 and Tenascin-W, in TNC receptors such as protein tyrosine receptor phosphatase beta (PTPRB) and contactins, or in the α4 integrin subunit, thus potentially regulating matrix network formation. We propose that MAREMO targeting could be exploited for regulating matrix functions during pathological events such as inflammation, cancer and fibrosis.

8.2. Introduction

The extracellular matrix (ECM) molecule tenascin-C (TNC) plays multiple roles in cancer such as promoting tumor cell survival, proliferation, invasion, angiogenesis and metastasis (Midwood et al., 2016; Sun et al., 2019). TNC can also shape tumor immunity by regulating the behaviour of several subsets of immune cells through distinct mechanisms (Deligne et al., 2020; Hauzenberger et al., 1999; Huang et al., 2001; Jachetti et al., 2015). As recently discovered, TNC is tethering dendritic cells (DC) in the stroma of tongue tumors through binding to CCL21, thereby impairing DC functions (Spenlé et al., 2020). Moreover, through binding to CXCL12, TNC turned into an adhesive substratum for CD8+ T cells causing immobilization inside the stroma, thereby blocking anti-tumor immunity in breast cancer (Murdamoothoo et al., 2020, in revision).

TNC also binds to several matrix molecules amongst them fibronectin (FN), thereby forming parallel aligned dense matrix, so called tumor matrix tracks (TMT) and tumor-associated-collagen-signatures (TACS) (Midwood et al., 2011, 2016; Spenlé et al., 2015; Tomko et al., 2018). TNC and FN are frequently co-expressed in inflamed and tumor tissues suggesting a complicity of these molecules *in vivo* (Van Obberghen-Schilling et al., 2011). This complicity is linked to intricate but poorly understood interactions between FN and TNC which regulates gene expression and cell behaviour (Chiquet-Ehrismann et al., 1988; Huang et al., 2001; Orend et al., 2003; Ruiz et al., 2004). Moreover, both matrix molecules contain recognition sites for transmembrane receptors (e.g. integrins, syndecan-4) through which cells perceive information that shapes their behaviour. Furthermore, similar to FN also TNC binds many soluble factors (e.g. growth factors, chemokines) thereby regulating signalling by these factors (De Laporte et al., 2013; Hynes, 2009; Midwood et al., 2016; Spenlé et al., 2020).

Previously, a detailed analysis revealed that TNC-binding domains in FN are located inside the three heparin binding sites (HBS), in FN-HepI (N-terminal 29 kDa domain), FN-HepII (fibronectin type III repeat (FNIII) 13, FN13) and FN-HepIII (FN4-6) (Huang et al., 2001; Ingham et al., 2004). Moreover, TNC blocked adhesion and spreading of tumor cells and fibroblasts on FN which was not the case in combination with collagen-1 (Col1) or laminin (Huang et al., 2001). The underlying mechanism involved TNC-specific inhibition of

syndecan-4 binding to FN13 (Bloom et al., 1999). In support, overexpression of syndecan-4 (but not of syndecan-1 or syndecan-2) ablated TNC-driven cell rounding and induced cell spreading on a FN/TNC substratum (Huang et al., 2001; Orend et al., 2003). Also, a recombinantly produced FN13 molecule or a small peptide representing the syndecan-4 binding site in FN13 restored cell spreading on the FN/TNC substratum (Orend et al., 2003). What remained unknown was how TNC interacts with the different molecules which we investigated here.

8.3. Results

Conserved sequences in FN5 and FN13 enable homophilic interactions in fibronectin, and mediate binding of fibronectin to tenascin-C

We have previously shown that a sequence derived from FN-HepIII (FNIII 4-6 (FN4-6)) binds TNC but the exact binding site remained unknown (Huang et al., 2001). Now by using purified single, double and triple FNIII domain molecules of FN-HepIII we investigated which FNIII repeat binds to TNC. By ELISA we noticed that FN5 binds similarly well to TNC as FN4/5 and FN4-6 (**Fig. 1A**). By surface plasmon resonance (SPR) measurement we observed rigorous binding of FN4/5 to TNC at pH 8 (**Fig. S1A**). These experiments suggest that in addition to FN13, FN5 is another binding site for TNC.

Sequences with an important function are often conserved amongst species (Lichtarge et al., 1996). We speculated that this may also apply to TNC binding sequences within FN. Therefore, we searched for potential inter-species sequence conservation within the FN5 and FN13 domains, respectively. Indeed, sequence alignments revealed that the sequences of FN5 and FN13 domains are highly conserved amongst vertebrates, in particular in two regions that we called Loop I and Loop II (**Fig. 1B**). Comparing FNIII PDB models in the evolutionary trace annotation server (ETA) revealed that residues with conserved physical and chemical characteristics clustered in FN5 and FN13, in the Loop I and Loop II with the following (human) sequence identity for FN5, TDST (Loop I) and NLQPASEY (Loop II) and for FN13, TETT (Loop I) and GLQPGTDY (Loop II). Loop I in FN5 and FN13 is 4 amino acids (aa) apart from a conserved W. The spacer sequence between Loop I and Loop II is 42 aa in both domains (**Fig. 1B**). Using bioinformatics tools, and the previously determined three-dimensional structures of FN12-14 and FN4-7 (**Table S1**), we investigated the 3D positioning of the two loop sequences. We observed that Loop I and Loop II in FN5 and FN13 are brought into vicinity generating putative niches that resembled each other. We called this sequence Matrix REgulating MOtif “MAREMO” or M-motif (**Fig. 1C-E, S1B**).

As TNC also has several FNIII domains we investigated whether TNC itself potentially has an M-motif. We indeed found a putative M-motif sequence in TN4 with Loop I “TDNS” and Loop II “GLRPGTEY” and in TN5 with Loop I “AETS” and Loop II “GLEPGQEY”. The spacing

in TN4 and TN5 is 44 aa and 41 aa, respectively (**Table S2, Fig. 1F**). This result suggests that either one or both of TN4 and/or TN5 may interact with FN through the M-motif. We compared the 3D organisation of TN5 in comparison to FN13 and observed a strong structural similarity suggesting that TN5 may indeed have an M-motif (**Fig. 1G**).

To determine whether matrix binding functions resided in FN5, FN13 and TN5, we investigated binding of FN4-6 or FN12-14 to TN1-5, full length TNC and to each other. By ELISA we noticed that both FN molecules (FN4-6 and FN12-14) bound to TN1-5 with a similar Kd (44 nM and 52 nM, respectively) (**Fig. 1H**). By negative electron microcopy (EM) imaging we saw that FN4-6 and FN12-14 bound to TNC in the centre of each TNC monomer (TN5), as indicated by the cross shaped structures (**Fig. 1I, J**). We concluded that the central FN5 and FN12 domains interacted with TNC in TN5. By incubating FN4-6 and FN12-14 in a homotypic or heterotypic manner we noticed that each triplet molecule did not bind to each other homotypically. Yet, when mixed, FN4-6 and FN12-14 formed cross-shaped structures, supporting a major interaction domain in FN5 and FN13 which may be involved in FN network formation *in vivo* (**Fig. 1K**).

Peptides mimicking the M-motif in fibronectin bind to tenascin-C

We designed two short peptides of 19 aa by placing Loop I and Loop II of FN5 and FN13, respectively in vicinity to each other. We connected both loop sequences with an artificial linker sequence of 5 aa (SAPAS) instead of the 42 aa that are present in the native FN sequence. The spacer comprised a proline in the middle to bring Loop I and Loop II close to each other in order to mimic the spatial organisation of the M-motif in FN5 and FN13. Of note 3 prolines are present in the native spacer region of FN5 and FN13. To enhance solubility, we added a serine at each end giving rise to peptide P5 (S**TDST**SAPAS**NLQPASEY**S) and peptide P13 (S**TETT**SAPAS**GLQPGTDY**S). We also generated control peptides where we kept the serines at each end of the molecule and conserved the spacing of Loop I and Loop II (SAPAS sequence) but scrambled the sequence within each loop resulting in peptide S5 (STTDSSAPASYESAPGLNS) and peptide S13 (STTETSAPASYDTGPQLGS) (**Fig. 2A**).

Next, we used the known structure of FN4-7 and FN12-14 to model binding of P5 and P13 (**Fig. 2B, Table S1**). This analysis revealed more than 50 putative binding possibilities for P5 and P13 mostly around the M-motif but notably, no binding in the HBS (**Fig. 2B**). Moreover, both peptides were predicted to bind the same sequence in FN13. Modelling the 3D conformation of FN12-14 and TN4-7 in context of P5/P13, revealed that the binding of the peptides in the M-motif may block the interaction between the matrix molecules (**Fig. 2C**).

We next wanted to know whether P5 and P13 bound to TNC. First, we interrogated the interaction probabilities between the amino acids constituting the peptides and FN5. This modelling predicted a major interaction site in Loop II of FN5 and revealed binding of the same amino acids in FN5 to peptides P5 and P13, respectively (**Fig. 2D, Table S3**). Then by negative EM imaging, we observed that both peptides P5 and P13 (yet not S5 nor S13) bound similarly mostly in the middle of the TNC monomer, predominantly in two FNIII domains that potentially represent TN4 and TN5 (**Fig. 2E, F**). As TN5 was previously shown as an interaction site for several molecules including TGFβ (De Laporte et al., 2013), we compared binding of TGFβ to TNC with that of the peptides. This comparison revealed identical binding patterns of TGFβ and P5/P13 to TNC, respectively revealing a major binding site in the middle of the TNC monomer in TN5 (**Fig. S2A-C**). By using heparin, we investigated whether binding of TGFβ to TN5, also in context of the whole TNC molecule, was dependent on glycosaminoglycans (GAG) as previously suggested for the isolated TN5 domain (De Laporte et al., 2013) and indeed saw inhibition of TGFβ binding to TNC by heparin (**Fig. S2A**). This observation confirms that TN5 binding to TGFβ is dependent on its glycosaminoglycans. Moreover, these results suggest that the putative HBS (KX_4KX_2RXR) in TN5 is involved in binding to TGFβ. Which of these amino acids indeed generate the HBS has to be investigated by mutation analysis in the future. In contrast to TGFβ, binding of P5 and P13 to TNC was not competed by heparin suggesting that TGFβ and P5/P13 bind at different sequences within TN5, for instance TGFβ in the HBS and P5/P13 in the M-motif (**Fig. 2F, S2A-C**).

Peptides P5 and P13 inhibit binding of CCL21, CXCL12 and TRAIL to tenascin-C thereby inhibiting tenascin-C chemoretention

We had observed that CCL21, CXCL12 and TRAIL were regulated by TNC in the OSCC, MMTV-NeuNT and NT193 tumors, modulating immune cell responses towards TNC (Spenlé

et al., 2020; Murdamoothoo et al., 2020, in revision; Erne et al., in preparation). We asked whether these molecules potentially bind to TNC and indeed, we have previously shown by SPR measurement that all investigated molecules bind to TNC with different, but high affinities (CCL21 = 5,8 x 10^{-8} M, CXCL12 = 7,9 x 10^{-7} M and TRAIL = 2,8 x 10^{-9} M). This binding has also been confirmed by negative EM imaging and revealed a major binding site in the centre of the TNC molecule, likely TN5 (**Fig. 3A**) (Spenlé et al., 2020; Murdamoothoo et al., 2020, in revision; Erne et al., in preparation). The binding pattern of CCL21, CXCL12 and TRAIL with that of TGFβ in TNC showed an overlap, suggesting that TN5 is a preferential binding site (**Fig. S3A-C**). Similar to TGFβ, heparin reduced binding of all three molecules to TNC suggesting binding in the putative HBS of TN5 (Spenlé et al., 2020, Murdamoothoo et al., 2020, in revision, Erne et al., in preparation). As the soluble factors (CCL21, CXCL12, TRAIL) and P5/P13 bound in the same TNC domain (TN5) we wondered whether P5/P13 affected binding to TNC. We incubated TNC with the soluble factor-adsorbed gold beads in solution in the presence of the peptides before addition of the mixture onto a grid followed by negative EM imaging and quantification. Indeed, addition of P5 or P13 blocked binding of TRAIL, CXCL12 and CCL21 to TNC (whereas the control peptides S5 and S13 did not block binding (**Fig. 3A-D**)).

Next, we wanted to know whether P5/P13 impacted TNC immune functions. As readout we investigated expression of several molecules in dendritic DC2.4 or lymphatic endothelial cells (LEC). Whereas TNC induced *Cxcl12*, *Cd86* and *Ccr7* in DC2.4 cells and *Ccl21* in LEC, only expression of *Ccr7* and *Cd86* was downregulated by P5 and P13 suggesting different mechanisms of gene induction by TNC where the M-motif may be important in the induction of *Ccr7* and *Cd86* by TNC (**Fig. 3E, F, S3D-M**). As binding of CCL21 and CXCL12 by TNC was instrumental in immobilizing dendritic cells and CD8+ T cells respectively (Spenle et al., 2020, Murdamoothoo et al., 2020, in revision), we wondered whether P5/P13 had an impact on chemoretention by TNC. Therefore, we determined immobilization of DC2.4 cells on TNC in context of CCL21 and CXCL12, respectively and observed that both P5 and P13 released cells from the TNC substratum (**Fig. 3G-I**).

Altogether, the TN5 domain represented special properties, in particular an HBS and M-motif on opposite sides of the FNIII domain. Our results suggest that FN5 and FN13 bind to TN5

through the M-motif whereas TGFβ, CCL21, CXCL12 and TRAIL bind to TN5 in the HBS. Moreover, targeting the M-motif in TN5 changed gene expression and relieved chemoretention of DC from a TNC/CCL21 and TNC/CXCL12 substratum, suggesting an allosteric conformational change by which the peptides caused masking of the HBS in TN5.

Peptides P5 and P13 inhibit fibronectin homophilic interactions and tenascin-C actions in cell adhesion, matrix expression and matrix assembly

As FN4-6 interacted with FN12-14, we asked whether this interaction can be inhibited by P5/P13. Indeed, this was the case whereas S5/S13 did not inhibit the binding (**Fig. 4A, S4A, B**). We considered that TNC interacted with FN through the M-motif, thus causing cell rounding on a mixed FN/TNC substratum (Huang et al., 2001). To address this possibility, we performed a cell adhesion assay on a FN/TNC substratum where half of NT193 cells with a mesenchymal phenotype (NT193M) (Erne et al., in preparation) stayed round which was in contrast to cells that spread on FN. We now observed that in the presence of P5 and P13 a large majority of cells spread on the FN/TNC substratum (yet not with S5 or S13) (**Fig. S4C-E**). To determine the quality of spreading we stained NT193M and KRIB cells plated on FN/TNC together with the peptides, with an anti-vinculin antibody to assess focal adhesion formation and phalloidin for detection of actin stress fibres. We observed that P5 and P13 induced focal adhesions and actin stress fibres on FN/TNC without affecting cell adhesion on FN nor TNC alone (**Fig. 4B, S4C-F**). These results suggest that P5 and P13 may compete TNC binding to FN5 and FN13, thus rendering the FN13 site available for ligation by syndecan-4 to cooperate with integrin α5β1 in cell spreading on FN (Bloom et al., 1999).

As the peptides inhibited the anti-adhesive properties of TNC on NT193M or KRIB cells, we wanted to know whether P5 and P13 could impact the intracellular signalling activated by TNC resulting in the expression of other matrix proteins such as FN and Col I, as described for fibrosis (Bhattacharyya et al., 2016). By treating mesangial cells (MES) with TNC and the peptides, we observed that P5 and P13 inhibited the activation of SMAD2 signalling by TNC (indicated by a decrease of SMAD2 phosphorylation) and that P13 also decreased the expression of FN and Col I (**Fig. 4C-F**). By investigating FN and Col matrix assembly by IF we noticed that whereas TNC (in presence of S13) increased matrix assembly, P13 abrogated TNC-induced matrix assembly (**Fig. 4E, F**). Since TNC, FN and collagens are

frequently co-expressed in matrix fibres during pathological conditions such as fibrosis or cancer, the TNC targeting MAREMO peptides could represent a promising therapeutic tool (**Fig. S4G, H**; (Bhattacharyya et al., 2016; Spenlé et al., 2020)).

MAREMO peptides P5 and P13 enhance TRAIL-induced cell death

As TNC counteracts TRAIL cytotoxicity (Erne et al., in preparation) and the MAREMO peptides competed binding of TRAIL to TNC (**Fig. 3B**), we investigated a potential effect on TRAIL functions. We used NT193M cells that express TNC. Whereas these cells were refractory to TRAIL-induced killing (as previously shown, Erne et al., in preparation) we wondered whether TNC produced by NT193M cells could bind to TRAIL, thus lowering sensitivity towards TRAIL-induced cell death. Interestingly, although TRAIL killed only about 5% of NT193M cells, P5 and P13 (but not S5 nor S13) significantly increased caspases 3 and 7 activation, and cell death, which occurred in a TRAIL and MD5-1 concentration dependent manner (**Fig. 5A-C**). Moreover, P5/P13 did not induce cell death in cells with a TNC KD (**Fig. S5A, B**), supporting a role of TNC in inhibiting TRAIL-induced killing through capturing TRAIL that could be relieved with the MAREMO peptides which may have therapeutic potential.

Identification of M-motif sequences in other tenascin-C interacting molecules

Many molecules interact with TNC, yet for most interactions it is unknown how (Brellier and Chiquet-Ehrismann, 2012; Giblin and Midwood, 2014). In addition to interactions with the EGFL repeats (EGFR) and the FBG (e.g. TLR4), interactions with many soluble molecules have been mapped to the FNIII domains with a particular hotspot in TN5 ((De Laporte et al., 2013; Giblin and Midwood, 2014) and EGFR (Iyer et al., 2008). To investigate the question how molecules interact with TNC we first determined those molecules expressed by engineered HEK293:TNC cells that copurified with and adhered to TNC. In particular, during the purification of recombinant TNC we collected all proteins that were bound to TNC and were eluted upon a high salt wash, and determined their identity by mass spectrometry. We found some 600 molecules in the eluate with more than 60 molecules from the matrisome (**Table S4, 5**; (Hynes and Naba, 2012)). Apart from known interactors such as FN, POSTN, aggregan and versican (Midwood and Orend, 2009) we also found tenascin-W/TNN, laminins

(LAM A4, A5, B1, B2, C1), nidogens 1 and 2, several collagens (Col 4A2, 4A6, 5A1, 6A3, 12A1 and 18A1), TGFBI, emilin2, agrin, fibulin1, Cyr61 (CCN1) and matrix remodeling enzymes such as ADAMTS1, LOXL2 and, TIMP1 and TIMP2 (**Table S4**). Moreover, cell surface associated molecules that were previously identified as TNC receptors such as PTPRZ1/PPTPRB and Annexin-2 were present in the eluate (Chiquet-Ehrismann, 1995; Jones and Jones, 2000). In particular, the Annexin family of molecules was represented by several members such as ANX A2, A2P2, A4, A5 and A6.

By sequence comparison we further identified M-motifs in the other tenascin family members (TNN, TNR, TNX), some collagens, contactins, PTPR molecules, integrin α4 and other molecules. In contrast to some molecules known to interact with TNC such as CALEB/CSPG5, syndecan-4, POSTN and Annexin-2 that do not have an M-motif, other molecules listed in **Table S2** have one or several M-motif like sequences. We found FN13-like M-motif consensus sequences in Col12A1-FN1 with sequences for Loop I (DENT) and Loop II (ELVPETEY) and in Col12A1-FN14 with Loop I (STST) and Loop II (NLQPDTSY) that are separated by 43 amino acids (**Table S2, Fig. S6**). In addition, there were at least 4 additional FN5-like M-motif consensus sequences present in Col12A1 with lower sequence homology (**Table S6**). Next, we modelled the 3D conformation of Col12A1-FN1 and observed similarities to the M-motif in FN13 where Loop I and Loop II regions formed a niche resembling the M-motif (**Fig. 6A-E, Table S2**). Future studies have to determine whether TNC and Col12 bind to each other and whether the M-motif plays a role. In support of a potential physical interconnection we have observed an overlap of TNC and Col12 expression in OSCC tumor tissue by IF staining (**Fig. S4G, H**) and found reduced Col12 expression in tumors lacking TNC expression (Spenlé et al., 2020).

Our analysis revealed that whereas all FNIII domains have a similar organization and some sequence similarity, the MAREMO was only present in distinct FNIII domains. We identified a minimal consensus sequence for Loop 1 (FN-type) as “X D/E T/N/S S/T” (where X is any amino acid), 5 aa apart from a conserved W, and observed other Loop I like sequences such as “GSRK” (β4 integrin-type) and “AAHQ” (PTPRC-type) in β4 integrin and PTPRC, respectively. In addition to Loop II “X L X P XX E/D Y” (ED-type found in FN and TNC) we noticed a “X L X P XX K Y” sequence (K-type) in TNX and PTPRC. As in FN and TNC, Loop

I and Loop II are separated by a non-conserved spacer of 40 – 50 aa including more than one proline (**Table S2, Fig. S6**). Since the Loop I and Loop II sequence similarity and spacing is alike to that in FN5 and FN13, it is possible that TNN, TNR, TNX, Col12A1, Col14A1, CNTN1/3, PTPRB/C/D/F and integrin β4 have one or several M-motifs (**Table S6**). This possibility has to be investigated in more detail in the future.

Another interesting candidate was the protein tyrosine phosphatase receptor family (PTPR) as family member beta/zeta (PTPRB) has been shown to bind TNC, now raising the possibility that binding may occur through the M-motif (Adamsky et al., 2001). In PTPRB we found four putative M-motifs (Loop 2 K-type). Moreover, in family members PTPRD and PTPRF one putative M-motif was present. We predict a more distant M-motif in PTPRC (CD45) where the spacing of 40 aa is conserved between Loop I: AAHQ (Loop 1- PTPRC-type) and Loop II: NLKPYTKY (Loop 2 K-type). However, despite some sequence difference, the M-motif of PTPRC shows conformational similarity to that in FN5 and FN13 (**Fig. 6F-H, Table S2**). Thus, a MAREMO may exist in several FNIII containing molecules potentially shaping molecular interactions amongst matrix molecules and binding of cell surface receptors to matrix.

8.4. Discussion

TNC is a highly interactive matrix molecule with an important binding site in TN5 (De Laporte et al., 2013). Here we have investigated the interactions of TNC with other matrix molecules and chemokines in more details. Our study revealed a common sequence in TN5 that is shared by several TNC binding molecules that we coined M-motif, or MAtrix REgulating MOtif (MAREMO). We found the M-motif in FN, TNN, Col12A1 and in TNC itself amongst other molecules. We further showed that the M-motif regulates binding of TNC to FN as peptides mimicking the M-motif prevented binding of TNC to FN and, relieved the anti-adhesive properties of TNC.

Our study revealed two mechanisms by which molecules can interact with TN5, either in the newly identified M-motif or in a HBS that was already inferred inside TN5 by De Laporte et al. (2013). Our results suggest that these interactions are mutually exclusive. Whereas several soluble glycosylated molecules such as TGFβ, CCL21, CXCL12 and TRAIL (that do not have an M-Motif), interacted with TNC in a heparin-dependent manner, presumably in the HBS of TN5, FN may interact with TNC through the M-motif. We developed two peptides, P5 and P13, that mimic the M-motif in FN5 and FN13, respectively. By using negative EM imaging and competition experiments, we could discriminate the different modes of binding. Our results suggest that binding of the peptides P5 and P13 induce an allosteric conformational change in TN5 that masks the HBS, thus blocking binding of the chemokines to TNC (**Fig. 7A-B**).

The M-motif in FN, TNC and other matrix molecules might be an important sequence to regulate molecular interactions. This may in particular apply to syndecan-4. Our results suggest that binding of TNC to FN13 may induce an allosteric conformational change in the HBS thereby denying access to syndecan-4 (**Fig. 7C**). This mechanism could explain how TNC blocks syndecan-4 function (Huang et al., 2001; Orend et al., 2003). The applied peptides P5 and P13 may compete TNC binding to FN13, thus allowing syndecan-4 to bind to FN and, inducing cell spreading on the FN/TNC substratum (**Fig. 7D**).

By using TNC knockout tumor models we had previously shown that TNC is a master regulator of an immune-suppressive TME where TNC binds CCL21, CXCL12 and TRAIL (Spenlé et al., 2020; Murdamoothoo et al., 2020, in revision; Erne et al., in preparation). In the current study, we observed that P5 and P13 inhibited TNC-induced expression of *Ccr7* and *Cd86* in dendritic cells, which could be important in context of inflammatory diseases such as rheumatoid arthritis and fibrosis for future normalization of immunity. P5 and P13 also inhibited chemoretention by TNC/CCL21 and TNC/CXCL12, which raises the possibility that M-motif-comprising peptides may release TNC-bound immune regulatory molecules, thus potentially reducing the immune-suppressive properties of the TME. This possibility has to be addressed by *in vivo* studies. Interestingly, the leukocyte surface molecule CD45/PTPRC has a distant M-motif that is different to that in FN and TNC. Whether this M-motif is utilized as molecular interaction site potentially regulating adhesion of leukocytes to matrix, has to be investigated in the future. In support of this possibility we saw accumulation of CD45+ leukocytes in TNC-rich stroma of several murine tumors such as Rip1Tag2 insulinoma, 4NQO-induced OSCC, NeuNT and NT193 breast tumors as well as in human breast cancer and human tongue tumors (Spenlé et al., 2015, 2020; Murdamoothoo et al., 2020, in revision). In further support, less leukocytes were found in the stroma but more inside the tumor cell nests when the tumors did not express TNC (Spenlé et al., 2020; Murdamoothoo et al., 2020, in revision). In addition to TNC, other matrix molecules with an M-motif potentially may interact with CD45/PTPRC through their M-motif. Thus, the MAREMO may represent a general interaction sequence to modulate leukocyte function by the matrix. As TNC inhibits TRAIL functions in anti-tumor immunity and the MAREMO peptides enhanced cell death, peptides P5 and P13 may have a wide range of applications in diseases where TNC and TRAIL are expressed.

In tumors from TNCKO mice we noticed less dense collagen fibrils. Interestingly, both FN and Col12 formed tight networks with TNC that were lost in the TNCKO tumors (our results, Spenlé et al., 2020). Thus, it is likely that matrix network assembly is altered in the absence of TNC. This possibility is supported by measurements of tissue stiffness through atomic force microscopy (P. Oertle, T. Loustau et al., manuscript in preparation) and relaxation of FN (C. Fonta, V. Vogel, T. Loustau et al., manuscript in preparation), two parameters that were specific for the tumor compared to adjacent normal tissue and changed in the absence of TNC. We hypothesize that TNC is a master regulator of matrix assembly through its

particular “stickiness” provided by binding sites in the EGFL repeats and the fibrinogen globe in addition to the M-motif and HBS in TN5. As TNC can interact with FN through the M-motif we propose that FN and other matrix molecules, such as Col12 and TNN, may use their M-motifs to generate intermolecular interaction networks to form large fibrillar matrix alignments together with TNC and other matrix molecules as seen in the TMT (Spenlé et al., 2015, 2020; Murdamoothoo et al., 2020, in revision), TACS (Tomko et al., 2018) and in other networks found in fibrotic tissues (Bhattacharyya et al., 2016). It will be interesting to see whether blocking the M-motif with the MAREMO peptides P5 and P13 or our novel TN5 specific camelid antibodies and nanobodies ((Dhaouadi et al., 2020), Dhouadi et al., in preparation) impact network formation and immune surveillance in tumors, and immunity in inflamed and fibrotic tissues. Similar to FN and TNC, in many of the matrix molecules with a M-motif, also a putative HBS is present inside the same FNIII domain. It is intriguing to speculate that occupancy of the M-motif alters the structural conformation, thus abrogating the HBS and precluding binding of molecules including soluble factors, syndecan-4 and others to the same FNIII domain. Whether on the contrary, binding of molecules in the HBS impact the accessibility of the M-motif, has to be addressed in the future.

Our study now may also allow to identify novel interactors of TNC due to the presence of an M-motif. This information could be relevant for targeting fibrotic and inflamed tissues with MAREMO peptides like P5 and P13 or other tools such as antibodies, nanobodies, aptamers and other molecules targeting the respective M-motif in order to reduce matrix network formation and binding of chemokines/cytokines/growth factors by TNC. Such targeting may not only reduce the immune-suppressive properties of the TME and the pro-inflammatory conditions of inflamed and fibrotic tissues, but may also reduce tissue stiffness that is recognized as an independent malignancy marker (Arnoldini et al., 2017; Fonta et al., 2020).

Finally, our knowledge may also be useful to generate engineered biomaterials incorporating chemokines or soluble factors that could serve as substratum in wound healing or as anti-inflammatory tools. Single domain molecules of FN5, FN13 or TN5 might be useful due to their HBS that would allow to immobilize the soluble factors. Previously, it was shown that wound healing is improved with soluble wound healing factors due to their capacity to bind to wound specific matrix (including FN and TNC) (Martino et al., 2014). Now we provide an

explanation how binding of these molecules is regulated. Our study proposes that by targeting the M-motif/MAREMO, one would be able to fine tune the binding and release of bound soluble factors.

In summary we identified the MAREMO motif as an important sequence regulating homotypic and heterotypic interactions of matrix with soluble factors and cell surface receptors in a tunable fashion.

8.5. Material and methods

Cell culture

The NT193 murine breast cancer cell line has been established from a primary MMTV-NeuNT breast tumor (Arpel et al., 2014). *Tnc* gene knockdown in NT193M shC and shTNC has been realized using lentiviral particles, as previously described (lentiviral particles: shC-SHC202V; shTNC-TRCN0000312138 from Sigma, (Sun et al., 2019)). NT193M cells were cultured in Dulbecco's modified Eagle's medium (DMEM Dutscher L0104-500) containing 4.5 g/L glucose, L-glutamine, sodium pyruvate supplemented with 10% of inactivated fetal bovine serum (FBS, Dutscher S1510-500), penicillin (10 000 U/mL), streptomycin (10 mg/mL) (Dutscher P06-07100). Selection pressure was maintained over time using puromycin (10 µg/mL, Thermo Fisher A11138-03). KRIB cells (v-Ki-ras transformed human osteosarcoma cells (Berlin et al., 1993)) was maintained in DMEM containing 4.5 g/L glucose, L-glutamine, sodium pyruvate, supplemented with 10% of inactivated FBS, penicillin (10 000 U/mL), streptomycin (10 mg/mL). DC2.4 murine dendritic cells (Shen et al., 1997) were cultured in Roswell Park Memorial Institute 1640 (RPMI-1640, Dutscher L0500-500) medium containing 4.5 g/L glucose, L-glutamine, sodium pyruvate, with HEPES (20mM, Merck PHG0001) supplemented with 10% of inactivated FBS, penicillin (10 000 U/mL), streptomycin (10 mg/mL). Human lymphatic endothelial cells, LECs (ATCC, HDMVECn, PCS-110-010, 2018) were cultured in Endothelial Cell Growth Medium (ECGM Promocell C22110) with penicillin (10 000 U/mL), streptomycin (10 mg/mL) and a supplemental growth factor cocktail according to Promocell. Mesangial cells (MES, (Sarrab et al., 2011)) were cultured in RPMI-1640 containing 4.5 g/L glucose, L-glutamine, sodium pyruvate, supplemented with 10% of inactivated FBS, 1% Insulin-transferrin-selenite (Sigma I1884), penicillin (10 000 U/mL) and streptomycin (10 mg/mL). Cells were kept at 33°C to proliferate in a humidified atmosphere of 5% CO_2. When indicated, cells were kept at 37 °C to differentiate upon degradation of the SV40 T-antigen. New vials of cells were thawed each 10-15 trypsinizations (Trypsin-EDTA Ca^{2+}, Mg^{2+} free, Dutscher P10-022100 + P10-15100) and cell culture was realized at 37°C in a humidified atmosphere of 5% CO_2.

TNC cloning and purification

Recombinant human his-tagged TNC (hTNC) and murine strep-tagged TNC (mTNC) was used. hTNC and mTNC were purified as previously described (Giblin et al., 2018; Huang et al., 2001, Spenlé et al., 2020).

Mass spectrometry analysis

Following mTNC purification, 1 M NaCl eluted proteins (as mentioned above) were subjected to acetone precipitation to reduce the volume and salt concentration. With ice-cold acetone (four times the sample volume) the proteins were precipitated at −20°C overnight, followed by centrifugation at 15,000 g for 10 min at 4°C. After discarding the supernatant, the pellet was air-dried at room temperature for 10 min. Then the protein pellet was resuspended in 8 M urea (Merck 33247), 50 mM triethylammoniumbicarbonate buffer (Merck T7408). The samples were then incubated with DTT (5 mM) (Merck 43819) for 60 min followed by 2-chloroacetamide (40 mM) (Merck 22790) for 30 min in the dark at room temperature for reduction and alkylation of disulfide bonds. Next, the samples were digested by lysyl endopeptidase (Promega V1671) for 4h. The sample urea concentration was then reduced to 2M urea by adding triethylammoniumbicarbonate buffer and trypsin (Promega V5280) digestion was performed overnight. Finally, the digestion was stopped by 1% formic acid and peptides were purified with SDB-RP stage tips as previously described (Rappsilber et al., 2007). Peptides were analyzed using the quadrupole–Orbitrap-based Q Exactive Plus mass spectrometer (Thermo Scientific) at the Cologne Cluster of Excellence proteomics core facility. The relative quantification of the proteins was performed in R program with the artMS plugin (Jimenez-Morales et al., 2020).

Peptides and ECM proteins / fragments

P5 (STDSTSAPASNLQPASEYS), P13 (STETTSAPASGLQPGTDYS), S5 (STTDSSAPASYESAPGLNS) and S13 (STTETSAPASYDTGPQLGS) (Thermo Fisher PEP95UNMOD) were diluted in PBS at a stock concentration of 1 mg/mL and stored at -20°C. Recombinant human FN was expressed and purified as previously described (Huang et al., 2001). FN plasmids encoding FN4-6, FN4-5, FN5 derived from Angeles Garcia-Pardo (Moyano et al., 1997) and, FN13 from Laird Bloom (Bloom et al., 1999) were purified as

described (Huang et al., 2001). The TN1-5, FN4-6 and FN12-14 were cloned into sleeping beauty transposon vectors with a N-terminal double Strep-tag and a BM40 signal peptide. Finally, all molecules were dialyzed against Tris buffered saline (50mM Tris, 150 mM NaCl, pH 7.4) (TBS Fisher Bioreagents BP2472-1).

Binding assay (by ELISA)

Protein biotinylation was performed as previously described (Pankhurst et al., 1998). For the binding assays, non-biotinylated proteins were diluted in TBS, pH 7.4, and 5 µg/well were coated onto 96-well plates (Falcon 353072) at 4° C over night. After washing with TBS, unspecific binding sites were blocked at room temperature with 100 µL Pierce Protein-free blocking solution (Thermo Fisher 37584) for 1 hour. Biotinylated ligands were then serially diluted in protein-free blocking solution to concentrations from 1 µM to 1 nM and 50 µL were used per well. After 90 minutes incubation at room temperature, the ELISA plates were washed 3 times with TBS buffer and a Biotin-HRP antibody 1:10000 (Aviva System Biology OAIA00064) in protein-free blocking solution was applied for 1 hour at room temperature and the plates were washed 3 times. Horseradish peroxidase activity was detected with 50 µL 1-Step Ultra TMB ELISA substrate solution (Thermo Fisher 34028). Then the reaction was stopped with 50 µL 10% H_2SO_4 and the absorbance was measured at 450 nm with a Varioskan™ LUX. The binding curves were plotted and analyzed with GraphPad Prism 5.

Surface Plasmon Resonance analysis

SPR binding experiments were performed with a Biacore 2000 instrument (Biacore) at 25°C. TNC was immobilized at high surface density (around 7000 resonance units) on an activated CM5 ship (GE Healthcare BR-1000-12) using a standard amine-coupling procedure according to the manufacturer's instruction. Soluble molecules were added at a concentration of 10 µg/mL in 10 mM sodium acetate, pH 5.0, at a flow rate of 5 µL/min for 20 minutes before addition of 1 M ethanolamine. CCL21 (R&D Systems 457-6C), CXCL12 (R&D Systems 460-SD-050) and TRAIL (Enzo Lifesciences ALX-201-130-C020) were added to the chip at a flow rate of 10 µL/min in a 10 mM HEPES, 150 mM sodium chloride, 0.005% (v/v) surfactant P20 solution. A blank CM5 chip was used for background correction. The dissociation constant

(Kd) was determined using the 1:1 Langmuir association model as described by the manufacturer.

Negative EM imaging

The interaction of TNC with chemokines and peptides was visualized by negative staining and transmission electron microscopy as described previously (Bober et al., 2010). Briefly, TNC samples (20 nM) were incubated with a 3 molar excess of chemokines or peptides for 1 hour at 37°C in TBS, pH 7.4. For visualization, the proteins were conjugated with 5 nm colloidal gold (Baschong and Wrigley, 1990). For inhibition experiments, TNC samples were pre-incubated with a 10 molar excess of non-labeled peptides, or a 10 molar excess of heparin (10 molar, Merck 1304016), for 1 hour at 37°C. Specimens were examined in a Philips/FEI CM 100 TWIN transmission electron microscope operated at 60 kV accelerating voltage. Images were recorded with a side-mounted Olympus Veleta camera with a resolution of 2048 x 2048 pixels (2k x 2K) and the ITEM acquisitions software.

Binding of molecules to TNC was determined by counting the number of gold particles along the length of the TNC monomer. Numbers from 500 randomly picked distinct TNC molecules were determined as % of all bound molecules. As positive control, TGFβ (R&D Systems 240-B-010) was used that was shown to bind in the TNfnIII5. Previously, negative controls EGF and BSA (shown not to bind to TNC) were used, respectively (De Laporte et al., 2013; Spenlé et al., 2020). For peptide competition, peptides (10 molar excess) were incubated with CXCL12, CCL21 or TRAIL (each 20 nM) for 1 hour in TBS before mixing with TNC for another hour before adsorbing of the mixture on the EM grid, followed by washing steps and standard negative staining procedures.

Sequence and bioinformatic tools

UniProt protein ID sequences are listed in the **Table S7**. Sequence multiple alignments were performed using Clustal Omega (Madeira et al., 2019). The 3D models are obtained from RCSB Protein Data Bank and listed in **Table S1**. The Evolutionary Trace Annotation (ETA) Server has been used to detect the loops I and II in FN 3D models (Matthew Ward et al., 2009). Peptide interacting models with fibronectin type-III domains were predicted using PEP-FOLD 3.5 (Lamiable et al., 2016) and 3D models were visualized with UCSF Chimera

program (Pettersen et al., 2004). Residues interaction contact maps were designed using COCOMAP (bioCOmplexes COntact MAPS, (Vangone et al., 2012)) as previously described (Ksouri et al., 2018).

Cell adhesion assay

In 96-well plates, coating with purified FN and TNC was realized in 0.01% Tween-20 PBS at 1µg/cm² before saturation with heat inactivated BSA as previously described (Huang et al., 2001). The peptides were added to TNC in 0.01% Tween-20 at a concentration of 50 µg/mL 10 minutes before coating (TNC, 1.25 nM, peptides, 25 µM). NT193 cells were then seeded at a concentration of 5 000 cells/well in culture medium without FBS and allowed to adhere at 37°C. Phase contrast pictures were taken after 1 and 3 hours of adhesion and images were analyzed for cell counting with the Zen Lite 2012 edition software.

Immunofluorescence staining

Following the protocol of cell adhesion, NT193M, KRIB and MES cells were fixed with 4% paraformaldehyde (PFA, Santa Cruz SC-281692) in PBS for 10 minutes, then permeabilized with 0.25% Triton (EUROMEDEX 2000-A) in PBS for 15 minutes (except MES with no permeabilization). After washing, blocking solution (5% normal goat serum in PBS, Southern Biotech 0060-01) was applied for 30 minutes before primary antibody anti-vinculin (clone VLN01, Invitrogen) incubation of 1 hour at room temperature. Corresponding secondary antibodies and rhodamine coupled phalloidin (Thermo Fisher P1951) were incubated 45 minutes after washing. The slides were then washed, stained with DAPI (Sigma D9542) for 10 minutes at room temperature and finally sealed with Fluoromount-GTM (Thermo Fisher 00-4958-02). Fluorescence pictures were acquired with a Zeiss Axio Imager Z2 microscope and analyzed with Zen Lite 2012 edition software. Antibodies are listed in **Table S8**.

Tissue Immunofluorescence staining (IF)

Tissue sections (8 µm thick) from murine 4-Nitroquinoline 1-oxide (4NQO) tongue tumors (Spenlé et al., 2020) were incubated for 1 hour with a blocking solution (5% normal goat serum) at room temperature before overnight incubation with primary antibodies at 4°C. After

washing, the slides were incubated with corresponding secondary antibodies for 1 hour at room temperature. Nuclei were stained with DAPI and slides were sealed. Fluorescence pictures were acquired with a Zeiss Axio Imager Z2 microscope and analyzed with Zen Lite 2012 edition software. The image acquisition setting (microscope, magnification, light intensity, exposure time) was kept constant per experiment conditions. Antibodies are listed in **Table S8**.

Chemoretention assay

DC2.4 cells chemoretention assay was performed in 5 µm-pore size transwell chambers (Corning 3421). The lower surface of the transwell inserts was coated with FN, TNC or collagen I (Col1) as described in the cell adhesion assay. The peptides were incubated overnight at 4°C on the coating at a concentration of 50 µg/mL. The insert surfaces were washed before cell plating. In the upper chamber, 20 000 DC2.4 cells were seeded in 1% FBS medium. The same medium containing CCL21 (200 µg/mL) or CXCL12 (100 ng/mL) was used in the lower chamber as a chemoattractant. After 5 hours of migration at 37°C, cells were fixed with ice cold methanol. Cells remaining in the upper chamber were removed with a cotton dub and the cells on the lower side were stained with DAPI. Fluorescence pictures were acquired with a Zeiss Axio Imager Z2 microscope and analyzed for cell counting with Zen Lite 2012 edition software.

Gene expression analysis by qRTPCR

DC2.4 and LEC cells were seeded at 500 000 cells in 6-well plates (Falcon 353046) in corresponding media prior to overnight starving in serum-free medium. Cells were then treated with the peptides at 50 µg/mL, in serum depleted medium, for 24 hours. Cell lysates were prepared after cell scraping for total RNA extraction with TriReagent (Life Technologies AM9738). RNA was treated with DNAse I (Roche 04716728001) and reverse transcribed (MultiScribe reverse transcriptase, Applied Biosystems 10117254) before determination of the concentration and the purity with NanoDrop 2000 (Thermo Fisher). qPCR was done on cDNA (diluted 1:5 in water) with a QuantStudio™ 5 Real-Time PCR System (Applied Biosystems) using TaqMan™ Fast Advanced Master Mix (Applied Diosystems 4444557) or Master Mix PCR Power SYBR™ Green (Applied Biosystems™ 4309155). *Gapdh* was used

as housekeeping gene in the comparative cycle threshold method (2-ddCt). Primers are listed in **Table S9**.

Protein expression assessment by immunoblotting and ELISA

MES, DC2.4 and LEC cells were seeded at 500 000 cells in 6-well plates in corresponding media prior to overnight starvation in serum-free medium. Cells were then treated with the peptides at 50 µg/mL, in serum depleted medium, for 24 hours. Cell lysates were prepared using Radioimmunoprecipitation assay (RIPA) buffer (150mM Tris-HCl pH8, 150mM NaCl, 1% NP-40, 1% sodium deoxycholate, 0.1% SDS) supplemented with protease and phosphatase inhibitors (Pierce EDTA-Free mini tablets, Thermo Fisher A32961) and protein concentration was assessed with a Bradford assay (BioRad 500-0006). For immunoblotting, proteins (20 µg/well) were loaded with Laemmli buffer (BioRad 161-0747) containing 10% β-mercaptoethanol (Merck 1.120006) into precasted 4-20% gradient gels (BioRad 4561094). Electrophoresis and protein transfer on nitrocellulose membranes were realized with BioRad equipment and consumables (Mini-PROTEAN Tetra electrophoresis and Trans-Blot Turbo™ systems). The blots were soaked in blocking solution (5% non-fat milk diluted in 0.01% Tween-20 PBS) during 1 hour at room temperature before incubation with primary antibodies overnight at 4°C. Secondary antibodies were incubated 1.5 hour at room temperature. Amersham ECL Western Blotting detection reagent (GE Healthcare RPN2106) or SuperSignal™ West Femto Maximum Sensitivity Substrate (Thermo Fisher 34095) were used to detect protein bands in a ChemiDoc™ Imager (BioRad). Antibodies are listed in **Table S8**. For ELISA, CCL21 expression was determined by using the 6-Ckine ELISA kit (Thermo Fisher EMCCL21A) according to the manufacturer's instructions. The absorbance of each sample and standard was measured with a plate reader Varioskan™ LUX (Thermo Fisher).

TRAIL killing activity in NT193M cells

Mouse recombinant SUPERKILLERTRAIL® (Enzo Lifesciences ALX-201-130-C020) was used in combination with the MD5-1 antibody (Functional grade, eBioscience™ 16-5883-82) to induce cell death. Briefly, NT193M shC and NT193M shTNC cells were seeded in 96-well plates, at 10 000 cells/well, for 24 hours before treatment. Peptides (50 µg/mL) and killing treatments were applied in the same time for 16 hours (final volume 100 µL). Caspases 3

and 7 activity were assessed using Caspase-Glo® 3/7 Assay according to the manufacturer's instructions (Promega G811A). Cells were incubated with the Caspase-Glo® 3/7 reagent for 1.5 hour before luciferase luminescence measurement with a Varioskan™ LUX. Cell death and viability were assessed by acridine orange/ethidium bromide (AO/EB) incorporation measurement. Briefly, cells were seeded and treated with the peptides and TRAIL+MD5-1 as previously described. AO/EB solution (5 µL/well, stock solution at 100µg/mL in PBS) was added to the cells 5 minutes before centrifugation of the plate (300 x g, 5 minutes). Fluorescence pictures of the centers of each well were acquired using a Motic™ AE31E trinocular microscope and cell counting was done with Zen Lite 2012 edition software.

Statistical analysis

Gaussian distribution was tested by the d'Agostino-Pearson normality test. Unpaired t-test (with Welch's correction in case of unequal variance) or ANOVA two-way test were applied when data followed a normal distribution. Otherwise, Mann Whitney test or a non-parametric ANOVA followed by Dunns post-test were used. Analysis and graphical representation were done using GraphPad Prism (version 6). P values < 0.05 were considered statistically significant. Data are representative of at least two individual experiments, expressed as the mean ± SEM. (*$p<0.05$; **$p<0.01$; ***$p<0.001$; ****$p<0.0001$; ns = not statistically significant).

8.6. Figures

Figure 1

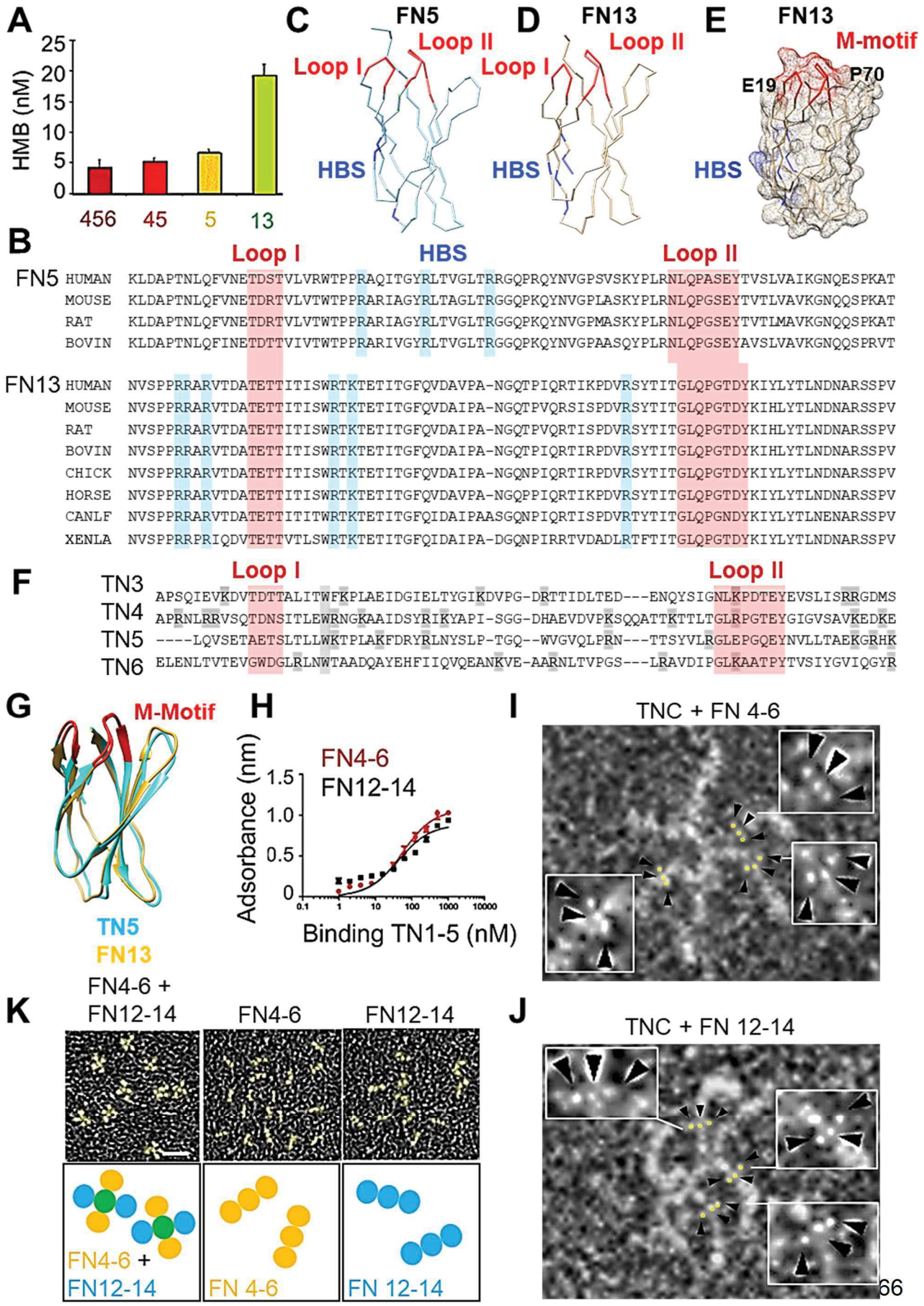
A
HMB (nM)
25
20
15
10
5
0
456
45
5
13
C
FN5
Loop II
Loop I
HBS
D
FN13
Loop II
Loop I
HBS
E
FN13
M-motif
E19
P70
HBS
B
Loop I
HBS
Loop II
FN5 HUMAN KLDAPTNLQFVNETDSTVLVRWTPPRAQITGYRLTVGLTRRGQPRQYNVGPSVSKYPLRNLQPASEYTVSLVAIKGNQESPKAT
MOUSE KLDAPTNLQFVNETDRTVLVTWTPPRARIAGYRLTAGLTRGGQPKQYNVGPLASKYPLRNLQPGSEYTVTLVAVKGNQQSPKAT
RAT KLDAPTNLQFVNETDRTVLVTWTPPRARIAGYRLTVGLTRGGQPKQYNVGPMASKYPLRNLQPGSEYTVTLMAVKGNQQSPKAT
BOVIN KLDAPTNLQFINETDTTVIVTWTPPRARIVGYRLTVGLTRGGQPKQYNVGPAASQYPLRNLQPGSEYAVSLVAVKGNQQSPRVT
FN13 HUMAN NVSPPRRARVTDATETTITISWRTKTETITGFQVDAVPA-NGQTPIQRTIKPDVRSYTITGLQPGTDYKIYLYTLNDNARSSPV
MOUSE NVSPPRRARVTDATETTITISWRTKTETITGFQVDAIPA-NGQTPVQRSISPDVRSYTITGLQPGTDYKIHLYTLNDNARSSPV
RAT NVSPPRRARVTDATETTITISWRTKTETITGFQVDAIPA-NGQTPVQRTISPDVRSYTITGLQPGTDYKIHLYTLNDNARSSPV
BOVIN NVSPPRRARVTDATETTITISWRTKTETITGFQVDAIPA-NGQTPIQRTIRPDVRSYTITGLQPGTDYKIHLYTLNDNARSSPV
CHICK NVSPPRRARVTDATETTITISWRTKTETITGFQVDAIPA-NGQNPIQRTIRPDVRSYTITGLQPGTDYKIYLYTLNDNARSSPV
HORSE NVSPPRRARVTDATETTITISWRTKTETITGFQVDAVPA-NGQPPIQRTIKPDVRSYTITGLQPGTDYKIYLYTLNDNARSSPV
CANLF NVSPPRRARVTDATETTITITWRTKTETITGFQIDAIPAASGQNPIQRTISPDVRTYTITGLQPGNDYKIYLYTLNENARSSPV
XENLA NVSPPRRPRIQDVTETTVTLSWRTKTETITGFQIDAIPA-DGQNPIRRTVDADLRTFTITGLQPGTDYKIYLYTLNDNARSSPV
F
Loop I
Loop II
TN3 APSQIEVKDVTDTTALITWFKPLAEIDGIELTYGIKDVPG-DRTTIDLTED---ENQYSIGNLKPDTEYEVSLISRRGDMS
TN4 APRNLRRVSQTDNSITLEWRNGKAAIDSYRIKYAPI-SGG-DHAEVDVPKSQQATTKTTLTGLRPGTEYGIGVSAVKEDKE
TN5 ----LQVSETAETSLTLLWKTPLAKFDRYRLNYSLP-TGQ--WVGVQLPRN---TTSYVLRGLEPGQEYNVLLTAEKGRHK
TN6 ELENLTVTEVGWDGLRLNWTAADQAYEHFIIQVQEANKVE-AARNLTVPGS---LRAVDIPGLKAATPYTVSIYGVIQGYR
G
M-Motif
TN5
FN13
H
FN4-6
FN12-14
Adsorbance (nm)
1.5
1.0
0.5
0
0.1
1
10
100
1000
10000
Binding TN1-5 (nM)
I
TNC + FN 4-6
K
FN4-6 +
FN12-14
FN4-6
FN12-14
FN4-6 +
FN12-14
FN 4-6
FN 12-14
J
TNC + FN 12-14

Figure 1: Conserved sequences in FN5 and FN13 mediate homophilic interactions in FN, and binding of FN to TNC

(A) ELISA with plastic absorbed TNC upon addition of soluble FN molecules FN4-6 (456), FN4/5 (45), FN5 (5) and FN13 (13) at equimolar amounts. **(B)** Alignment of FN5 and FN13 sequences from different species highlighting the conservation of the amino acids forming the Loop I and Loop II (red) and the HBS (blue). **(C, D)** Structural models of FNIII domains highlighting Loop I, Loop II (red) and HBS in FN5 **(C)** and FN13 **(D)**. **(E)** Glutamate 19 (E19) and proline 70 (P70) are structurally adjacent in the M-Motif (red) of the FN13 model. **(F)** Alignment of TN3, 4, 5, and 6 highlighting the amino acids forming the Loop I and Loop II (red) in TNIII domains. **(G)** Overlay of TN5 and FN13 structural models with M-Motifs in red. **(H)** ELISA with biotinylated FN4-6 and FN12-14 on a TNC coated surface. FN4-6 (Bmax, 1.076, Kd 55.14 nM), FN12-14 (Bmax, 0.887, Kd 42.57 nM). **(I-J)** Negative EM imaging of FN4-6 **(I)** or FN12-14 **(J)** molecules interacting with TNC. Each FNIII domain in FN4-6 and FN12-14 (enlarged in the inlets without marking) are designated with an open circle. N = 2, n = 500 molecules. **(K)** Negative EM imaging of FN4-6 and FN12-14 molecules in homotypic and heterotypic combination. FN4-6 and FN12-14 trimers are colored in yellow. FN4-6 and FN12-14 triplet molecules are schematically depicted in yellow and blue in the bottom panels, respectively. N = 2.

Figure 2

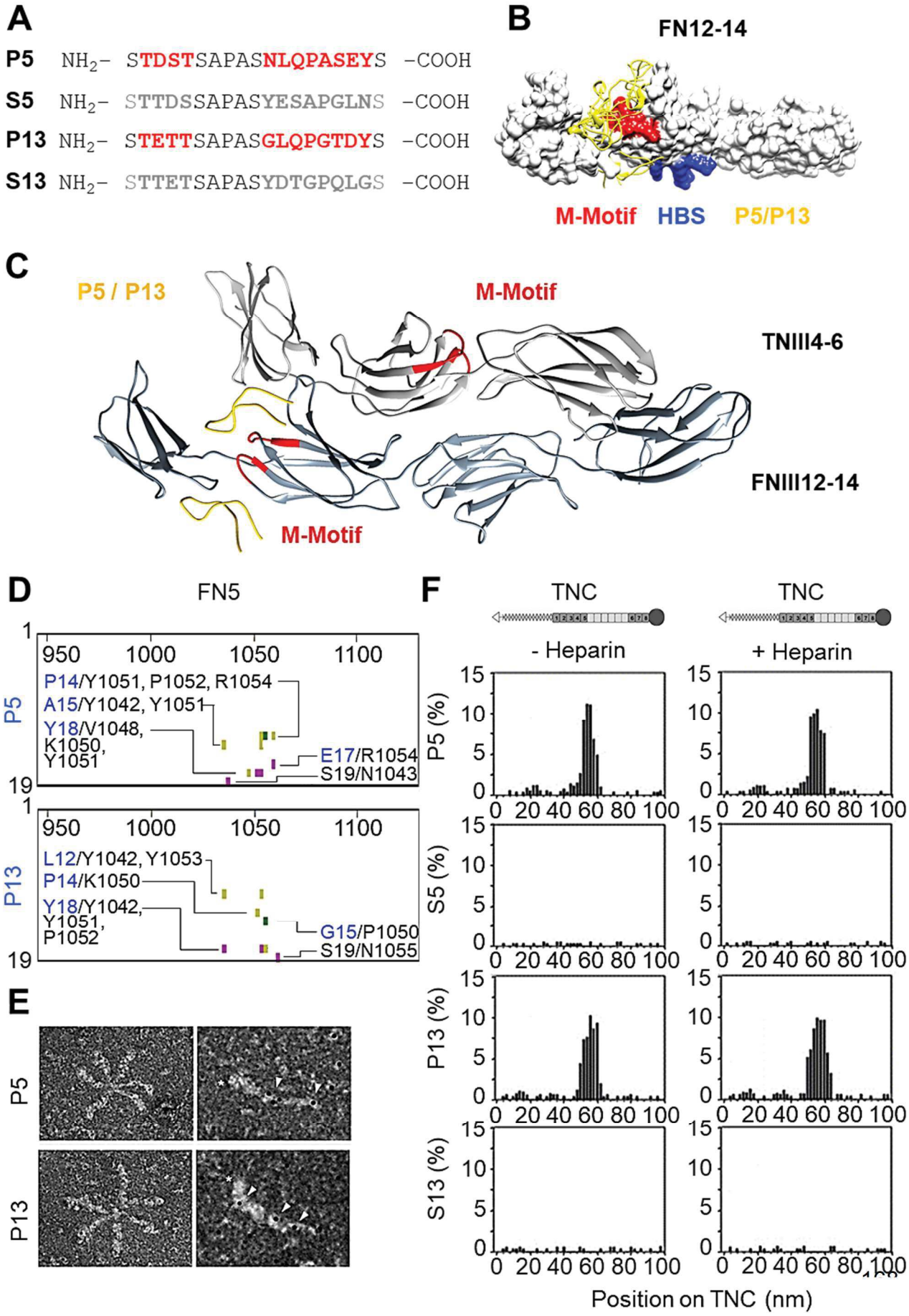
A
P5 NH2– STDSTSAPASNLQPASEYS –COOH
S5 NH2– STTDSSAPASYESAPGLNS –COOH
P13 NH2– STETTSAPASGLQPGTDYS –COOH
S13 NH2– STTETSAPASYDTGPQLGS –COOH
B
FN12-14
M-Motif
HBS
P5/P13
C
P5 / P13
M-Motif
TNIII4-6
FNIII12-14
M-Motif
D
FN5
1
950
1000
1050
1100
19
P5
P14/Y1051, P1052, R1054
A15/Y1042, Y1051
Y18/V1048, K1050, Y1051
E17/R1054
S19/N1043
P13
L12/Y1042, Y1053
P14/K1050
Y18/Y1042, Y1051, P1052
G15/P1050
S19/N1055
E
P5
P13
F
TNC
- Heparin
+ Heparin
P5 (%)
S5 (%)
P13 (%)
S13 (%)
0 20 40 60 80 100
Position on TNC (nm)

Figure 2: Peptides 5 (P5) and 13 (P13) bind to TNC

(A) Sequences of P5, S5, P13 and S13 with amino acids corresponding to the Loop I and Loop II are highlighted in red. **(B)** Prediction of peptide interaction sites close to the M-Motif (red) of FN13 (in a FN12-14 model). HBS in blue. **(C)** Structural model of potential peptide (yellow) inhibition of FN4-7 binding to the M-Motif in TN4-6. **(D)** Contact maps of P5 and P13 in FN5. Violet, green and yellow dots indicate hydrophilic-hydrophilic, hydrophobic-hydrophobic and hydrophilic-hydrophobic contacts, respectively. **(E)** Negative EM imaging of P5 and P13 gold-labeled beads interacting with TNC. Arrows point at beads binding to TNC. Asterisks point at N-terminal domains of the TNC monomer. **(F)** Quantification and localization of bound peptide-coupled beads along a TNC monomer in the absence or presence of heparin, N = 2, n = 500 molecules.

Figure 3

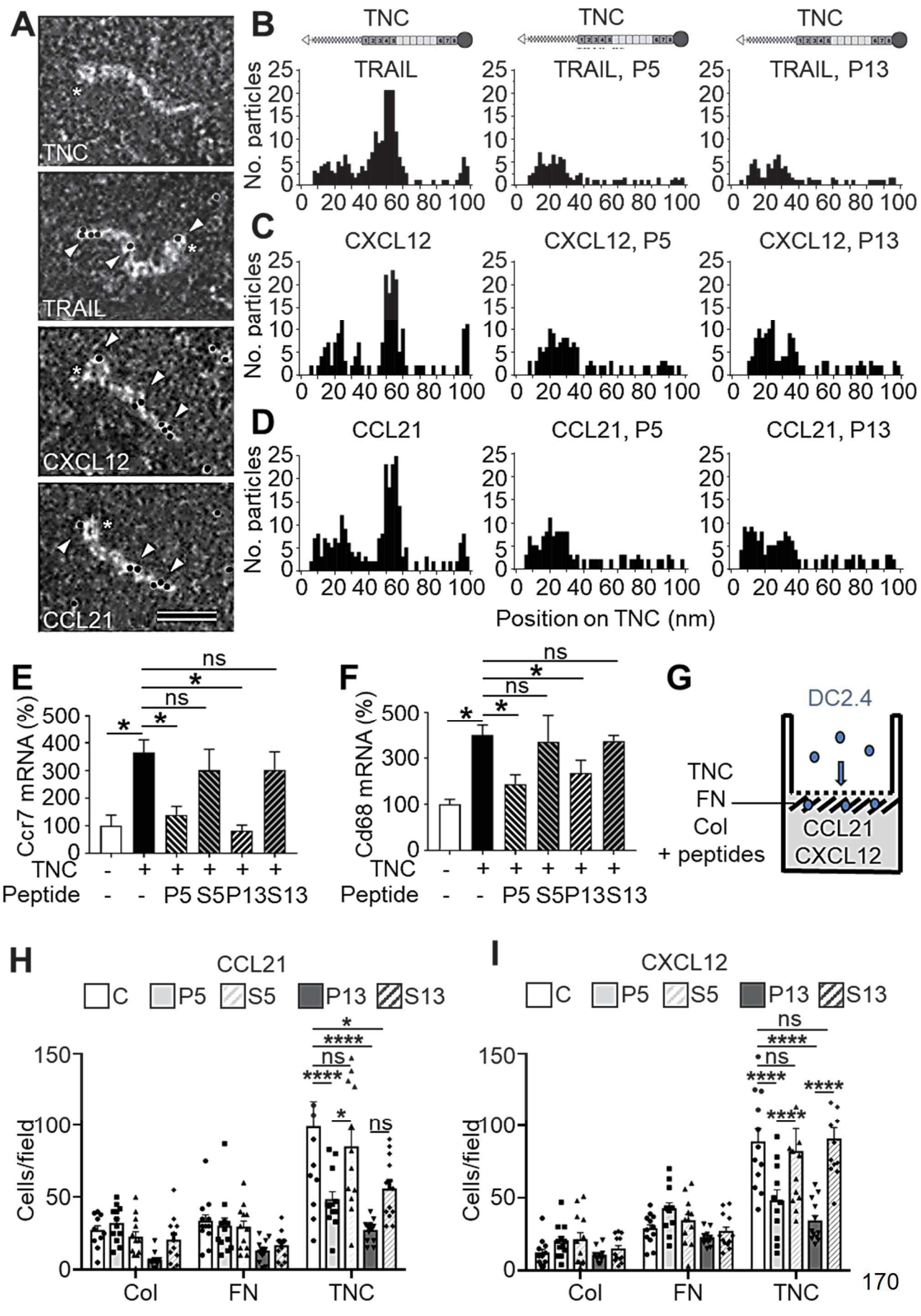
A
TNC
TRAIL
CXCL12
CCL21
B
TNC
TRAIL
TRAIL, P5
TRAIL, P13
No. particles
C
CXCL12
CXCL12, P5
CXCL12, P13
D
CCL21
CCL21, P5
CCL21, P13
Position on TNC (nm)
E
Ccr7 mRNA (%)
TNC
Peptide
P5 S5 P13 S13
F
Cd68 mRNA (%)
G
DC2.4
TNC
FN
Col
+ peptides
CCL21
CXCL12
H
CCL21
C P5 S5 P13 S13
Cells/field
Col FN TNC
I
CXCL12
C P5 S5 P13 S13
Cells/field
Col FN TNC

Figure 3: Inhibitory effects of P5 and P13 on the interaction of TNC with TRAIL, CXCL12 and CCL21

(A) Negative EM imaging of TRAIL, CXCL12 and CCL21 gold-labeled beads interacting with TNC. Arrows point at beads binding to TNC. Asterisks point at N-terminal domain of TNC. **(B-D)** Quantification and localization of TRAIL **(B)**, CXCL12 **(C)**, CCL21 **(D)** - coated beads on TNC in the presence of P5 and P13, N = 2, n = 500 molecules. **(E, F)** Quantification of *Ccr7* **(E)** and *Cd86* **(F)** expression by qRTPCR in dependence of soluble TNC (10 µg/mL) added to DC2.4 cells, and with peptide (50 µg/mL) pre-treatment. N = 4 experiments. Kruskal-Wallis tests, mean ± SEM (*p < 0.05, ns = not significant). Experimental setup **(G)** and results **(H, I)** from chemoretention assay to assess immobilization of DC2.4 cells on TNC, FN and Col-coated inserts (lower side), with or without the peptides, towards CCL21 or CXCL12 in the lower chamber. N = 4 experiments, n = 3 replicates. ANOVA two-way test, mean ± SEM (*p < 0.05; ****p < 0.0001; ns = not significant).

Figure 4

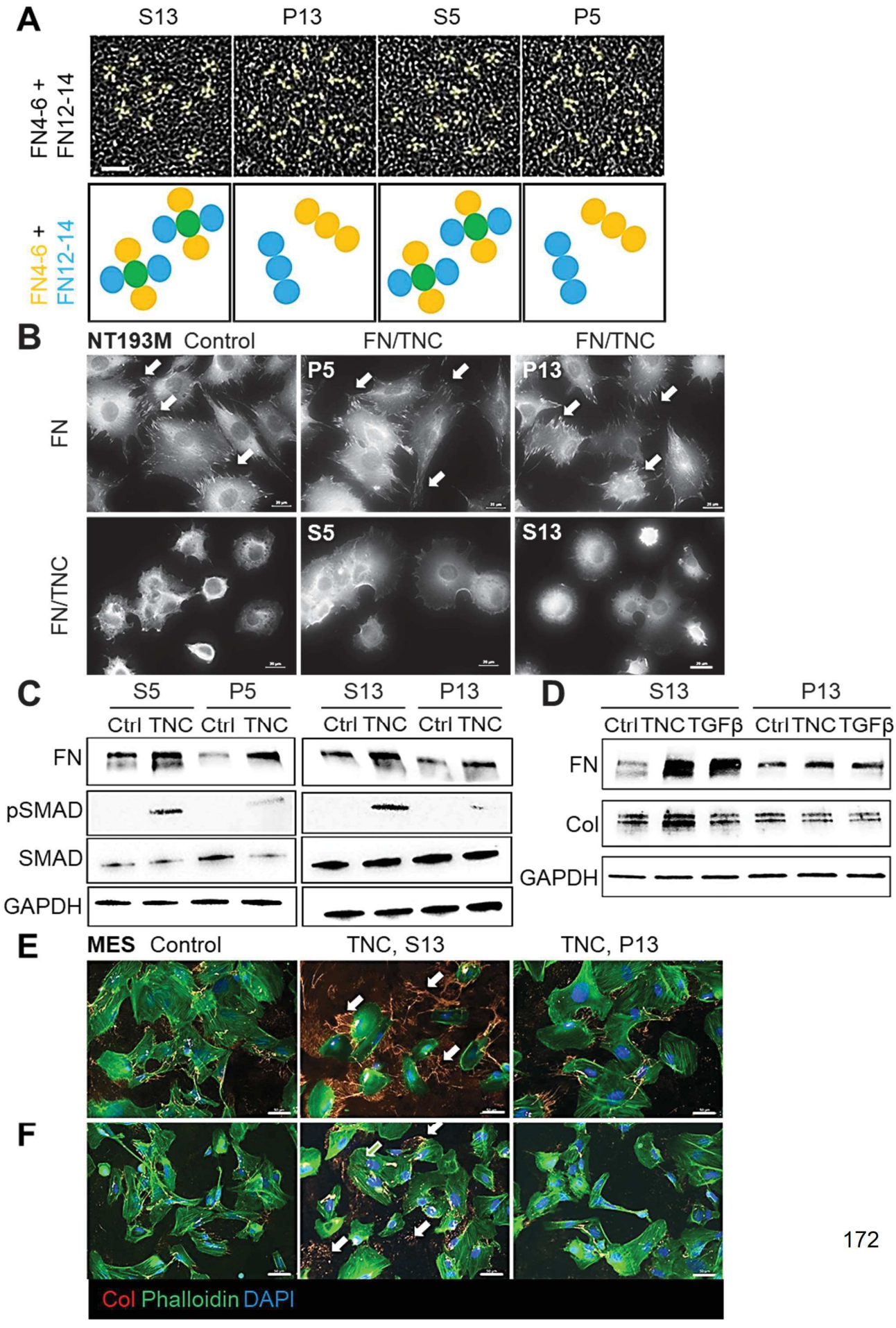
A
S13
P13
S5
P5
FN4-6 + FN12-14
FN4-6 +
FN12-14
B
NT193M Control
FN/TNC
FN/TNC
FN
FN/TNC
P5
P13
S5
S13
C
S5
P5
S13
P13
Ctrl TNC Ctrl TNC
Ctrl TNC Ctrl TNC
FN
pSMAD
SMAD
GAPDH
D
S13
P13
Ctrl TNC TGFβ Ctrl TNC TGFβ
FN
Col
GAPDH
E
MES Control
TNC, S13
TNC, P13
F
Col Phalloidin DAPI

Figure 4: Functional effects of the peptides on the interactions of cells with TNC

(A) Negative EM imaging of FN4-6 and FN12-14 molecules in heterotypic combination in the presence of the peptides. FN4-6 and FN12-14 triplet molecules are schematically depicted in yellow and blue in the bottom panels, respectively. N = 2. Scale bar 10 nm. **(B)** Representative IF images of NT193M cells stained for vinculin upon adhesion on FN or FN/TNC coated surfaces after preincubation with the peptides. Arrows point at focal adhesions, N = 3 experiments. **(C-D)** Representative immunoblot of MES cells treated with TNC or TGFβ and the peptides, N = 3 experiments. **(E)** Representative IF images of FN and Col matrix assembly by MES cells after treatment with TNC and P13 or S13. Arrows point at FN and Col networks, N = 3 experiments.

Figure 5

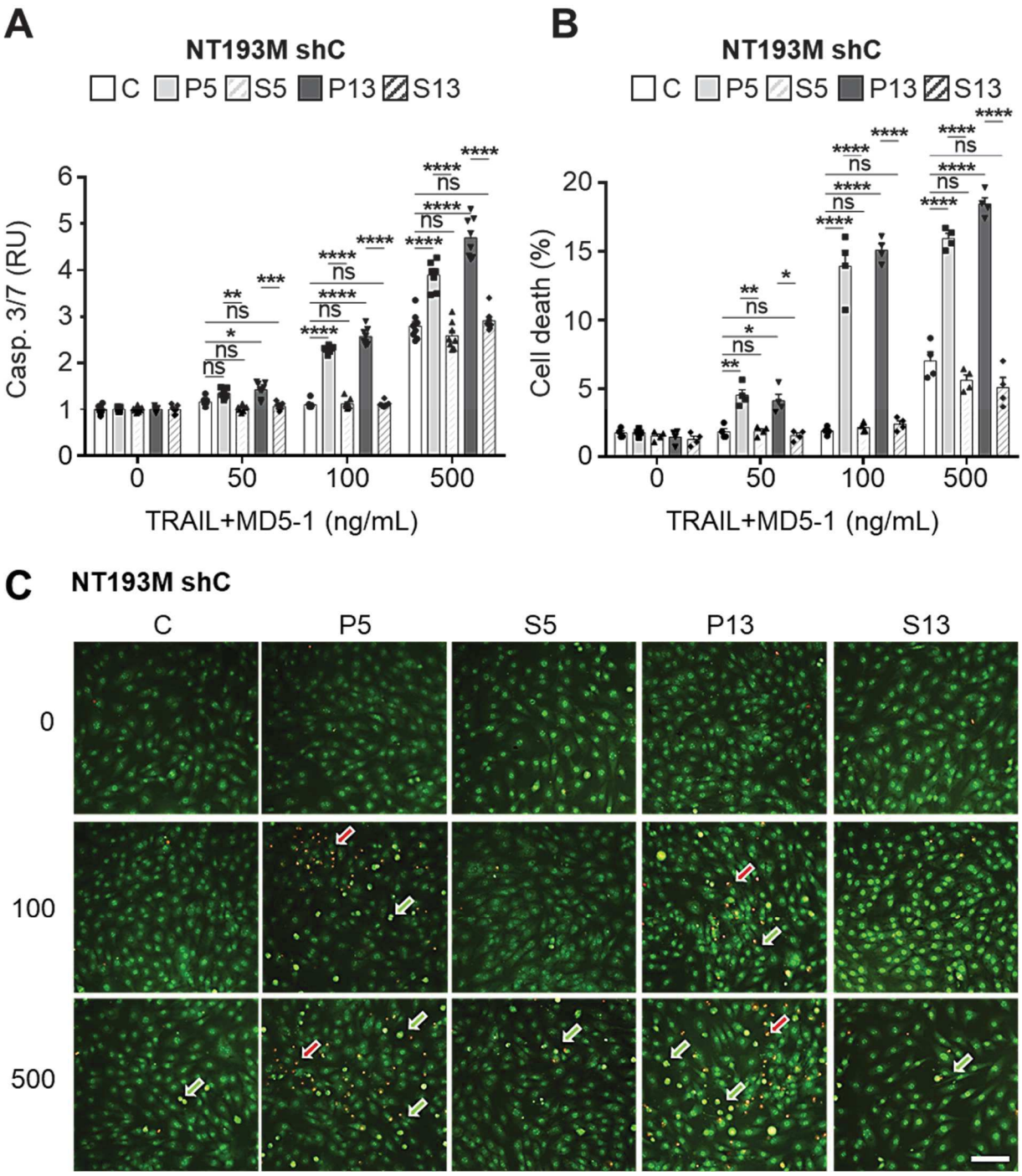
A
NT193M shC
C P5 S5 P13 S13
Casp. 3/7 (RU)
TRAIL+MD5-1 (ng/mL)
B
NT193M shC
C P5 S5 P13 S13
Cell death (%)
TRAIL+MD5-1 (ng/mL)
C
NT193M shC
C P5 S5 P13 S13
0
100
500

Figure 5: Peptides alleviate TNC repression of TRAIL killing function

(A, B) Caspase 3/7 activity **(A)** and cell death (AO/EB) labelling **(B)** in NT193M shC cells upon pretreatment with the peptides (50 µg/mL), followed by incubation with TRAIL (ng/mL) and MD5-1 (50 ng/mL). **(A)** N = 4 experiments, n = duplicates, Kruskal-Wallis test, mean ± SEM (**p < 0.01). **(B)** N = 2 experiments, n = duplicates. Kruskal-Wallis test, mean ± SEM (***p < 0.001). **(C)** Representative IF images of NT193M shC cells upon staining with AO/EB after pretreatment with the peptides (50 µg/mL), followed by incubation with TRAIL (ng/mL) and MD5-1 (50 ng/mL). Scale bar 100 µm, N = 2 experiments. Arrows point at dead cells. Green arrow, dead cell, red arrow, cells in progress of dying.

Figure 6

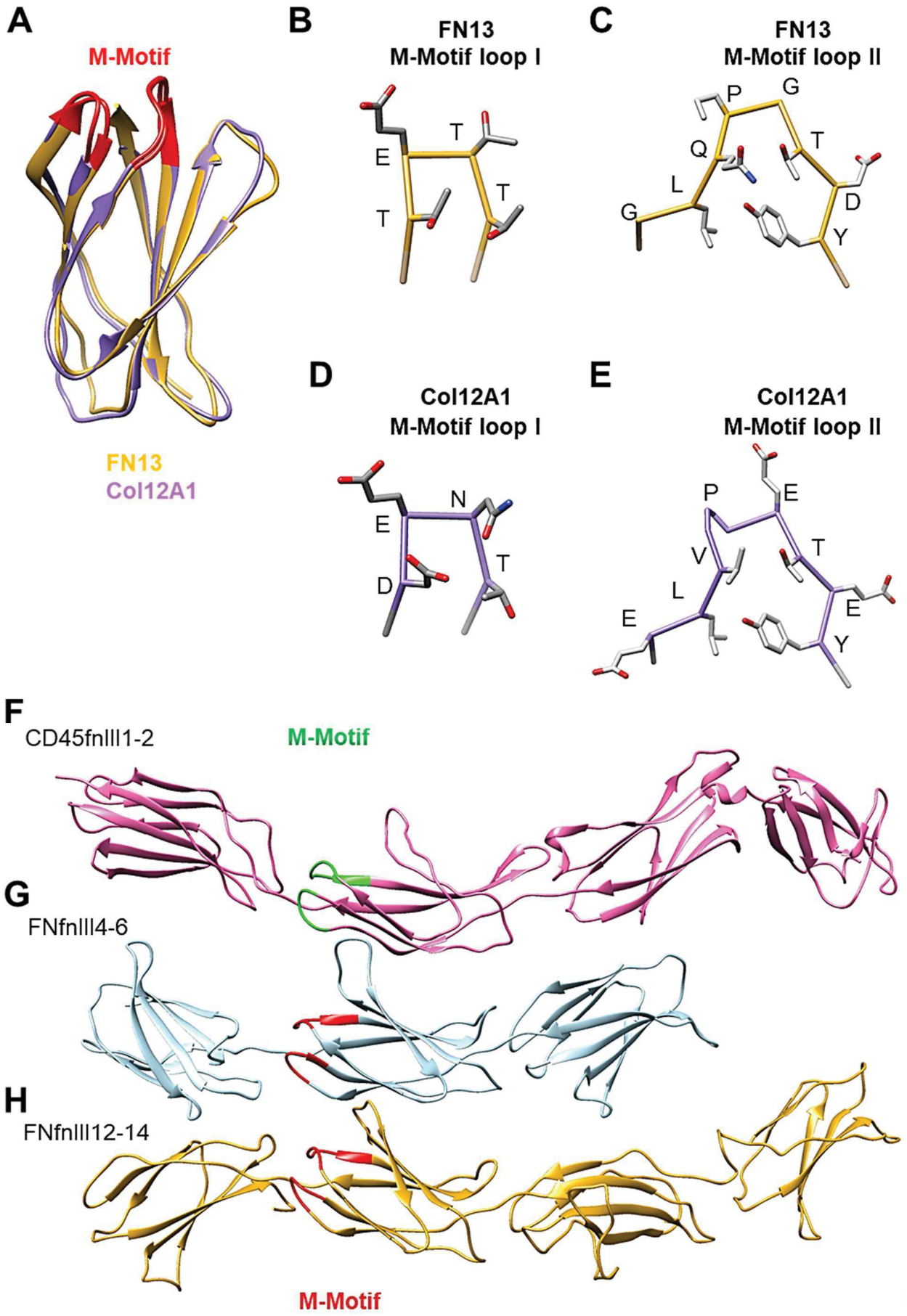
A
M-Motif
FN13
Col12A1
B
FN13
M-Motif loop I
E
T
T
T
C
FN13
M-Motif loop II
P
G
Q
T
L
G
D
Y
D
Col12A1
M-Motif loop I
E
N
D
T
E
Col12A1
M-Motif loop II
P
E
V
T
L
E
E
Y
F
CD45fnIII1-2
M-Motif
G
FNfnIII4-6
H
FNfnIII12-14
M-Motif

Figure 6: Comparison of FNIII domains in Col12, CD45 and FN

(A) Structure modeling of overlayed Col12A1 FNIII and FN5 domains, M-Motif in red. **(B-E)** Structural models of the Loop I and Loop II in FN5 **(B, C)** and the Loop I and Loop II in Col12A1 FNIII **(D, E)**. Structural models of FNIII domains of CD45 **(F)** and FN (FN4-7, **G**; FN12-14, **H**). Loop I and Loop II are marked in red in CD45 fnIII2 and in green in FNIII5.

Figure 7

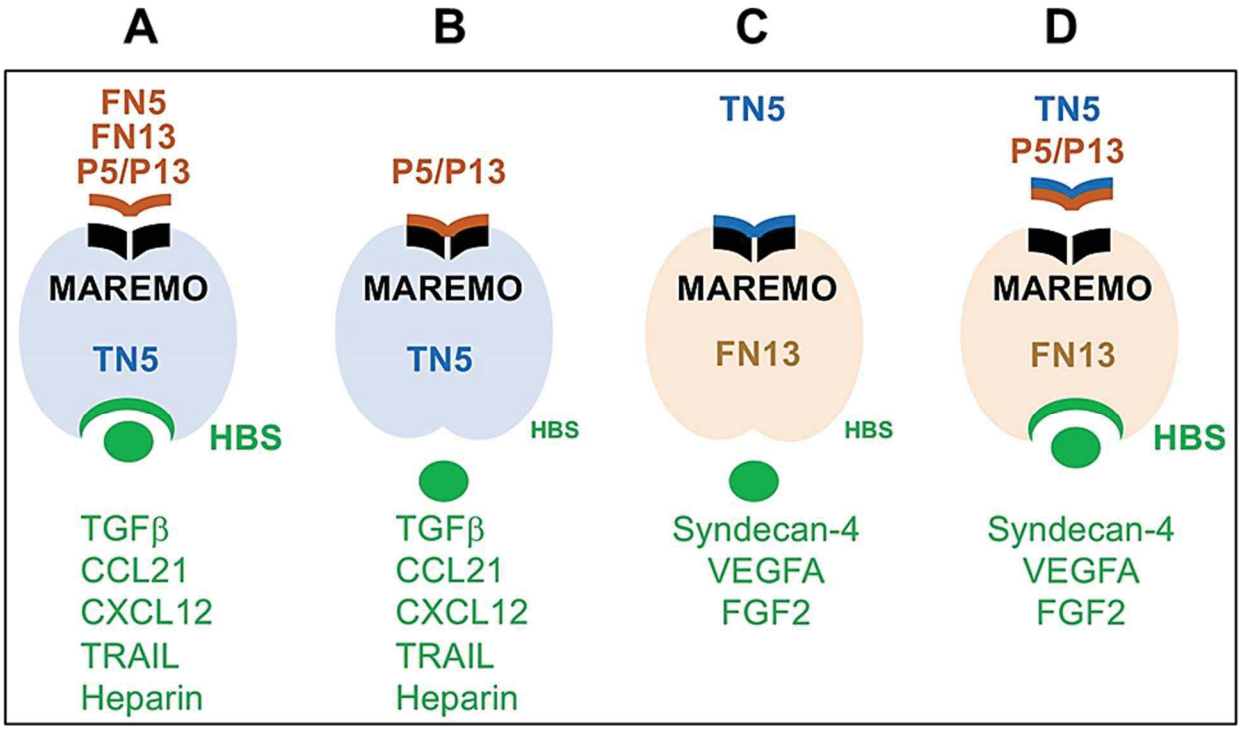
A
B
C
D
FN5
FN13
P5/P13
MAREMO
TN5
HBS
TGFβ
CCL21
CXCL12
TRAIL
Heparin
P5/P13
MAREMO
TN5
HBS
TGFβ
CCL21
CXCL12
TRAIL
Heparin
TN5
MAREMO
FN13
HBS
Syndecan-4
VEGFA
FGF2
TN5
P5/P13
MAREMO
FN13
HBS
Syndecan-4
VEGFA
FGF2

Figure 7: Summary cartoons on the roles of the MAREMO in TNC and FN

(A, B) TGFβ, CCL21, CXCL12 and TRAIL bind in TN5 which is competed by heparin suggesting binding in the heparin binding site (HBS) of TN5. **(A)** P5 and P13, mimicking the M-Motif in FN5 and FN13, also bind to TN5. Binding of P5 and P13 is not competed by heparin suggesting that these peptides do not bind in the HBS but in the M-motif/MAREMO. **(B)** Binding of P5 and P13 to TNC inhibits binding of TGFβ and the chemokines to TNC presumably by an allosteric conformational change thereby ablating the HBS. **(C)** Similarly, TNC binds on the opposite site of the HBS in the M-Motif of FN13. This interaction may cause an allosteric conformational change that abrogates binding of syndecan-4 (and potentially VEGFA, FGF2 and other molecules) to the HBS. **(D)** Identification of binding sites for TNC and syndecan-4 in FN13 at opposite sites within the molecule. As VEGFA and FGF2 also bind to FN13 in a heparin competable manner, it is likely that they share the binding site with syndecan-4 in the HBS.

8.7. Supplemental figures

Table S1: PDB IDs of 3D models used as structural templates

Table S2: Characteristics of molecules with putative M-motif

Table S3: Minimum distances between Fibronectin FN5 Domain and P5 / P13

Table S4: Molecules copurifying with TNC

Table S5: Matrisomal molecules copurifying with TNC

Table S6: Multiple alignments of MAREMO-like sequences in matrix molecules and receptors

Table S7: Uniprot ID sequence numbers

Table S8: Antibody list

Table S9: Primer sequences

Figure S1: Binding of FN4/5 to TNC

Figure S2: Binding of TGFβ, P5 and P13 to TNC

Figure S3: Comparison of the binding sites of the soluble factors on TNC and effects of the peptides on TNC-induced gene expression in DC2.4 and LEC cells

Figure S4: Effects of the peptides on FN4-6 and FN12-14 binding to TNC, and on TNC anti-adhesive properties

Figure S5: effects of the peptides on TRAIL-induced apoptosis

Figure S6: consensus sequences of the loop I and loop II constituting MAREMO in several proteins

Table S1: PDB IDs of 3D models used as structural templates

Model	PDB ID
FNfnIII 4-7	6MFA
FNfnIII 12-14	3R8Q
TNfnIII 4-6	1TDQ
COL12A1fnIII-13	3T1W
CD45fnIII 1-2	5FMV

Table S2: Characteristics of molecules with putative M-motif

Molecule	Loop I	Spacer	W	Putative HBS	P	Loop II	Spacer loop I and II	Number of putative M-motifs
FN FN5 (FN5)	**TDST**	4	+	**R**X$_4$**R**X$_6$**R**X$_4$**R**	3	**NLQPASEY**	42	FN: 2
FN FN13 (FN13)	**TETS**	4	+	**R**X**KR**X$_2$**K**X$_3$**R**	3	**GLQPGTDY**	42	
TNC FN5 (TN5)	A**ETS**	4	+	**K**X$_4$**K**XX**R**X**R**	3	**GL**E**PG**Q**EY**	41	TNC: 2
TNC FN4 (TN4)	**TDNS**	4	+	**R**XX**K-R**X**K**	2	**GL**R**PGTEY**	44	
TNN FN2	**TENS**	4	+	**K**X**R-K**X**R**	4	**GL**H**PGTEY**	45	TNN: 3
TNN FN4	**TENT**	4	+	**K**X$_3$**R-R**X$_5$**K**	1	**GL**R**PG**V**EY**	44	
TNR FN2	**TETT**	4	+	no	3	**GL**K**PG**E**EY**	42	TNR: 2
TNR FN4	**T**A**TS**	4	+	no	2	D**L**V**PGTEY**	45	
Col12A1 FN1	D**ENT**	4	+	**K**X$_8$**R**X$_{12}$**K**	4	E**L**V**P**E**TEY**	43	Col12A1: 2
Col12A1 FN14	**S**T**ST**	4	+	**R**XX**K**	5	**NLQP**D**T**S**Y**	43	
Col14A1 FN3	**TENS**	4	+	**R**X**K-K**XX**K**	2	**GL**L**P**N**TEY**	44	Col14A1: 2
Col14A1 FN5	**T**TD**S**	4	+	no	2	**GL**E**PGTEY**	42	
CNTN1 FN1	RA**TS**	4	+	**K**X$_5$**K-K**XX**K**	3	D**LI****P**WM**EY**	49	CNTN1: 1
CNTN3 FN1	**TDTT**	4	+	**K**XX**K**	1	E**L**N**P**WV**EY**	50	CNTN3: 1
PTPRB FN4	**S**LT**S**	4	+	**K**XXX**K**	3	E**L**V**PG**RL**Y**	41	PTPRB: 4
PTPRB FN12	**S**SY**S**	4	+	**K**XX**K**	1	D**L**T**PG**KK**Y**	42	
PTPRB FN14	**T**TD**S**	4	+	**K**X**K**	2	**GL**V**PG**RK**Y**	41	

PTPRB FN15	AN**TS**	4	+	no	3	**GL**R**PG**RS**Y**	44	
PTPRC FN1	AAHQ	4	+	**K**X_3**K-K**$_{X3}$**K**	2	**NL**K**P**Y**T**K**Y**	40	PTPRC: 1
PTPRD	**TATS**	4	+	**K**X**K**	2	**GL**S**P**Y**SDY**	43	PTPRD: 1
PTPRF	**TATS**	4	+	no	2	**GL**S**P**F**SEY**	43	PTPRF: 1
ITGB4 FN1	GSRK	4	+	**R**X**K**	4	**NL**Y**P**YC**DY**	42	ITGB4: 1
TNX	**T**PD**S**	4	+	no		**GL**E**P**XXK**Y**	40, 41, 42	several

The M-motif was originally identified as a TNC binding site in FN, yet not all TNC binding molecules have a M-motif. This applies e.g. to CALEB/CSPG5, syndecan-4, POSTN and integrin α9β1. A putative M-motif was found in several molecules. In FN5, FN13 and TN5 the FNIII domains have a 4 amino acid (aa) Loop I sequence (**T/A D/E S/T S/T**) positioned 4 aa apart from a conserved W and 41 aa and 42 aa, respectively away from a 8 aa Loop II sequence (**N/G L Q/E P A/G S/T/Q E/D Y**). A minimal consensus sequence for Loop I is "X **D/E T/N/S S/T"** (Loop 1 FN-type), "**GSRK**" (Loop 1 beta4 integrin-type) and "**AAHQ**" (Loop 1 PTPRC-type) and for Loop II "X **L** X **P** XX **E/D Y"** (Loop 2 ED-type) or "X **L** X **P** XX **K Y"** (Loop 2 K-type)**.** Loop I and II are separated by a non-conserved 40 – 50 aa spacers, respectively. Followed by Loop I in the 5th position is always a W followed by a variable number of P (1 – 5). These bulky amino acids may have an impact on the spatial organization of the respective FNIII domain bringing Loop I and Loop II into vicinity in 3D forming a niche that we coined M-motif/MAREMO. We hypothesize that a similar organization generating a niche is also possible for other molecules with a putative M-motif. Between Loop I and II a putative heparin binding site (HBS) is found in some but not all molecules consisting of "R/K X_n R/K" as the simplest motif, e.g. RXK, RXXK, KXR, KXXR and KXXK. According to the structural information for FN13 and FN5 the putative HBS is on the opposite site to the M-motif in 3D. Since the Loop I and Loop II sequence and spacing is alike to that in FN5, FN13 and TN5, it is possible that TNN, TNR, TNX, ColA12, Col14A1, CNTN1/3, PTPRB/C/D/F and integrin β4 have one or several M-motifs.

Table S3: Minimum distances between Fibronectin FN5 Domain and P5 / P13

Peptide P5				FN5 Domain				Interaction	
AA	N° AA	Atom	Chain	AA	N° AA	Atom	Chain	Dist. (Å)	Interaction type
ALA	15	CB	B	TYR	1042	CD2	A	2.76	Phob - Phil
GLU	17	OE1	B	ARG	1054	CD	A	2.88	Phil - Phil
PRO	14	CB	B	PRO	1052	O	A	2.87	Phob - Phob
SER	19	OG	B	ASN	1043	O	A	2.59	Phil - Phil
PRO	14	CG	B	ARG	1054	N	A	2.29	Phob - Phil
TYR	18	OH	B	LYS	1050	O	A	2.67	Phil - Phil
TYR	18	OH	B	VAL	1048	CG2	A	1.86	Phil - Phob
ALA	15	CA	B	TYR	1051	OH	A	2.45	Phob - Phil
TYR	18	CD2	B	TYR	1051	CE1	A	1.99	Phil - Phil
PRO	14	O	B	TYR	1051	OH	A	2.67	Phob - Phil

Peptide P13				FN5 Domain				Interaction	
AA	N° AA	Atom	Chain	AA	N° AA	Atom	Chain	Dist. (Å)	Interaction type
GLY	15	N	B	PRO	1052	CD	A	2.69	Phob - Phob
TYR	18	CE1	B	PRO	1052	O	A	1.47	Phil - Phob
LEU	12	CD1	B	TYR	1042	CD2	A	2.12	Phob - Phil
LEU	12	CB	B	TYR	1051	OH	A	1.81	Phob - Phil
SER	19	CA	B	ASN	1055	ND2	A	2.15	Phil - Phil
TYR	18	CD2	B	TYR	1042	CE2	A	2.83	Phil - Phil
PRO	14	CB	B	LYS	1050	O	A	2.59	Phob - Phil
TYR	18	CE2	B	TYR	1051	CE2	A	2.08	Phil - Phil

Amino acids represented in the contact map. Atoms, interaction distance and interaction type are listed. Distance in ångström and interaction types: Phob = hydrophobic, Phil = hydrophylic.

Table S4: Molecules copurifying with TNC

A2M	DDX17	HIST1H1A	MDC1	PTGES3	RUVBL1	VPS4B
ACAN	DDX18	HIST1H1C	MDH2	PTMA	RUVBL2	VTA1
ACIN1	DDX21	HIST1H1D	MDK	PTPRZ1	S100A13	XRCC5
ACTA1	DDX27	HIST1H1E	MECP2	PURA	SAP18	XRCC6
ACTA2	DDX39B	HIST1H2AG	MFGE8	PXDN	SCAF4	YBX1
ACTB	DDX3X	HIST1H2AH	MGAT5	PYGL	SCAF8	YBX3
ACTC1	DDX3Y	HIST1H2AJ	MIA3	QPCT	SDCBP	YLPM1
ACTG1	DDX5	HIST1H2BH	MIF	RAB11A	SEPSECS	YWHAE
ACTG2	DEK	HIST1H2BJ	MOV10	RAB11B	SERBP1	YWHAG
ADAMTS1	DEK	HIST1H2BK	MRC1	RACGAP1	SET	YWHAQ
ADAR	DHX15	HIST1H2BM	MSH2	RALA	SETSIP	YWHAZ
AGRN	DHX9	HIST1H2BN	MSH6	RALB	SF3B1	ZFR
AHCY	DKC1	HIST1H3A	MSN	RALY	SF3B3	ZNF280B
ALDOA	DNAJA2	HIST1H4A	MTHFD1	RAN	SF3B4	ZNF280C
ANP32E	DYNC1H1	HIST2H2AA3	MYBBP1A	RAP1B	SFPQ	ZNF280D
ANXA2	EBNA1BP2	HIST2H2AB	MYH10	RBBP4	SFRP1	ZNF768
ANXA2P2	EDA	HIST2H2AC	MYH9	RBM39	SLC3A2	ZNF90
ANXA4	EDIL3	HIST2H2BF	MYL6	RBMX	SLC7A1	ZRANB2
ANXA5	EEF1A1	HIST2H3PS2	NACA	RBP4	SLIT2	
ANXA6	EEF1A1P5	HIST3H2BB	NAP1L1	RCN1	SMARCA5	
AP2B1	EEF1B2	HIST3H3	NAP1L4	RHOA	SMC1A	
AP2M1	EEF1E1	HMGA1	NCL	RHOC	SMC3	
AP3B1	EEF1E1-BLOC1S5	HMGA2	NDNF	RNPS1	SMOC1	
APOB	EEF1G	HMGB2	NDRG1	RPA1	SMOC2	
APOBEC3C	EEF2	HMGN1	NID1	RPF2	SNRNP200	
APOC3	EFTUD2	HNRNPA1	NID2	RPL10	SNRNP70	
APRT	EIF2S2	HNRNPA1L2	NME1-NME2	RPL10	SNRPB	
ARF1	EIF2S3	HNRNPA2B1	NME2	RPL10A	SNRPD1	
ARF3	EIF2S3L	HNRNPAB	NME2P1	RPL11	SNRPD2	
ARHGDIA	EIF3A	HNRNPC	NOG	RPL12	SNRPD3	
ATP1A1	EIF3B	HNRNPD	NOLC1	RPL13	SNRPE	
ATP1B3	EIF3C	HNRNPDL	NOP10	RPL13A	SNRPF	
BANF1	EIF3CL	HNRNPH1	NOP2	RPL13a	SNRPG	
BASP1	EIF3D	HNRNPK	NOP56	RPL14	SNRPGP15	
BAZ1B	EIF3E	HNRNPM	NOP58	RPL15	SNRPN	
BAZ2B	EIF3F	HNRNPR	NPM1	RPL17	SPON1	
BRIX1	EIF3H	HNRNPU	NRAS	RPL17-C18orf32	SRFBP1	
BSG	EIF3L	HNRNPUL1	NRF1	RPL18	SRP14	
BTF3	EIF4A1	HNRNPUL2	NTN1	RPL18A	SRP72	
BTF3L4	EIF4A3	HNRNPUL2-BSCL2	NUCKS1	RPL19	SRP9	
C1QBP	EIF4B	HP1BP3	NUTF2	RPL21	SRPK2	
C21orf33	EIF5	HRAS	OLA1	RPL22	SRPX	
CA2	EIF5A	HS6ST2	OLFML2B	RPL23A	SRSF1	
CALM1	EIF5A2	HSP90AA1	PA2G4	RPL24	SRSF2	
CALM2	EIF5AL1	HSP90AB1	PABPC1	RPL26	SRSF3	
CALR	EIF5B	HSP90AB2P	PABPC3	RPL26L1	SRSF5	

CANX	ELAVL1	HSP90B1	PABPN1	RPL27	SRSF6
CBX1	EMILIN2	HSPA1A	PAICS	RPL27A	SRSF7
CBX3	ENO1	HSPA1B	PALMD	RPL28	SRSF9
CBX5	EPB41L2	HSPA5	PARP1	RPL29	SSBP1
CCT2	ERH	HSPA6	PCBP1	RPL3	SSRP1
CCT3	EWSR1	HSPA7	PCBP2	RPL30	STAM
CCT4	EZR	HSPA8	PDCD6IP	RPL31	STAM2
CCT5	F13A1	HSPD1	PFKP	RPL32	STIP1
CCT6A	FASN	HSPE1	PFN1	RPL34	STXBP3
CCT7	FBL	HSPG2	PFN2	RPL35	SUB1
CCT8	FBLN1	HTRA1	PGAM1	RPL35A	SUPT16H
CD81	FEN1	IGF2BP1	PGK1	RPL36	SYNCRIP
CDC42	FHL1	IGJ	PGRMC1	RPL37A	TAF15
CEP290	FKBP4	ILF2	PHGDH	RPL38	TAGAP
CETN2	FN1	ILF3	PKM	RPL4	TCOF1
CETN3	FNDC1	IMPDH2	PLEK	RPL5	TCP1
CFL1	FSTL1	INCENP	PLS3	RPL6	TGFBI
CHD4	FUS	IPO4	PLXDC2	RPL7	THRAP3
CHTOP	G3BP1	JCHAIN	PNN	RPL7A	TIMP1
CIRBP	G3BP2	KATNAL2	POLR2F	RPL8	TIMP3
CKB	GANAB	KCTD12	POLR2H	RPL9	TLN1
CKMT1A	GAPDH	KCTD17	POLR3A	RPLP0	TNC
CKMT1B	GAR1	KCTD2	POLR3B	RPLP0P6	TNN
CKMT2	GART	KCTD5	POP1	RPLP1	TNPO1
CLIC1	GCN1L1	KHDRBS1	POSTN	RPS11	TNPO2
CLTC	GLO1	KIF23	POSTN	RPS12	TOP1
CLU	GNB2	KPNA2	PPHLN1	RPS13	TOP2A
COCH	GNB2L1	KPNB1	PPIA	RPS14	TOP2B
COL12A1	GNL3	KRAS	PPIB	RPS15	TPI1
COL18A1	GPC1	LAMA4	PPP1CC	RPS15A	TRA2A
COL4A2	GPC4	LAMA5	PPP2CA	RPS16	TRA2B
COL4A6	GPI	LAMB1	PPP2CB	RPS18	TRIM28
COL5A1	GSPT1	LAMB2	PPP2R1A	RPS19	TRIP10
COL6A3	GSTP1	LAMC1	PRDX1	RPS2	TROVE2
COPA	GTF2I	LARP1	PRDX2	RPS23	TUBA1B
COPE	H1F0	LARS	PRDX6	RPS24	TUBB
CPE	H1FX	LBR	PRKDC	RPS25	TUBB4B
CPNE3	H2AFJ	LCP1	PRMT5	RPS26	TXN
CPXM1	H2AFV	LDHA	PRPF19	RPS27	U2AF1
CRISPLD1	H2AFY	LDHB	PRPF40A	RPS27A	U2AF2
CS	H2AFY2	LGALS3BP	PRPF4B	RPS3	UBA1
CSE1L	H2AFZ	LOXL2	PRPF8	RPS3A	UBA52
CSNK2A1	H2BFS	LUC7L3	PSIP1	RPS4X	UBB
CSNK2A2	H3F3A	LYAR	PSMC2	RPS6	UBC
CSNK2A3	H3F3A	MARCKS	PSMC3	RPS7	UBTF
CSNK2B	H3F3B	MARCKSL1	PSMC4	RPS8	UCHL1
CSNK2B-LY6G5B-1181	H3F3B	MARS	PSMD11	RPS9	VCAN
CSNK2B-LY6G5B-991	H3F3C	MASP1	PSMD12	RPSA	VCP
CYFIP1	HABP2	MASP2	PSMD13	RRBP1	VIM
CYR61	HDAC2	MATN4	PSMD2	RRP12	VNN1

DARS	HDGF	MATR3	PSMD3	RSL1D1	VPRBP
DDB1	HGS	MCM5	PSME4	RTCB	VPS4A

List of TNC binding molecules as determined by mass spectrometry analysis after the high salt wash during the purification of murine TNC, displayed in alphabetical order.

Table S5: Matrisomal molecules copurifying with TNC

Uniprot ID	Entry name	Protein names
Q61838	A2M	Pregnancy zone protein
Q6GQT1	A2M	Alpha-2-macroglobulin-P
Q61282	ACAN	Aggrecan core protein
P97857	ADAMTS1	A disintegrin and metalloproteinase with thrombospondin motifs 1
P28798	GRN	Progranulin
P07356	ANXA2	Annexin A2
P97429	ANXA4	Annexin A4
P48036	ANXA5	Annexin A5
P14824	ANXA6	Annexin A6
P33622	APOC3	Apolipoprotein C-III
P14211	CALR	Calreticulin
Q06890	CLU	Clusterin
Q62507	COCH	Cochlin
Q60847	COL12A1	Collagen alpha-1
P39061	COL18A1	Collagen alpha-1
P08122	COL4A2	Collagen alpha-2
O88207	COL5A1	Collagen alpha-1
P18406	CYR61	CCN family member 1
O35474	EDIL3	EGF-like repeat and discoidin I-like domain-containing protein 3
Q8K482	EMILIN2	EMILIN-2
Q8BH61	F13A1	Coagulation factor XIII A chain
Q08879	FBLN1	Fibulin-1
P11276	FN1	Fibronectin
Q9QZF2	GPC1	Glypican-1
P51655	GPC4	Glypican-4
P51859	HDGF	Hepatoma-derived growth factor
Q9D0E1	HNRNPM	Heterogeneous nuclear ribonucleoprotein M
P08113	HSP90B1	Endoplasmin
Q05793	HSPG2	Basement membrane-specific heparan sulfate proteoglycan core protein
Q9R118	HTRA1	Serine protease HTRA1
P97927	LAMA4	Laminin subunit alpha-4
Q61001	LAMA5	Laminin subunit alpha-5
P02469	LAMB1	Laminin subunit beta-1
Q61292	LAMB2	Laminin subunit beta-2
P02468	LAMC1	Laminin subunit gamma-1
Q07797	LGALS3BP	Galectin-3-binding protein
P58022	LOXL2	Lysyl oxidase homolog 2
O89029	MATN4	Matrilin-4

P12025	MDK	Midkine
P21956	MFGE8	Lactadherin
Q8C119	NDNF	Protein NDNF
P10493	NID1	Nidogen-1
O88322	NID2	Nidogen-2
O09118	NTN1	Netrin-1
Q3V1G4	OLFML2B	Olfactomedin-like protein 2B
P52480	PKM	Pyruvate kinase PKM
Q62009	POSTN	Periostin
B9EKR1	PTPRZ1	Receptor-type tyrosine-protein phosphatase zeta
Q3UQ28	PXDN	Peroxidasin homolog
P14206	RPSA	40S ribosomal protein SA
Q8C4U3	SFRP1	Secreted frizzled-related protein 1
Q9CW03	SMC3	Structural maintenance of chromosomes protein 3
Q8BLY1	SMOC1	SPARC-related modular calcium-binding protein 1
Q8CD91	SMOC2	SPARC-related modular calcium-binding protein 2
Q8VCC9	SPON1	Spondin-1
Q9R0M3	SRPX	Sushi-repeat-containing protein SRPX
P82198	TGFBI	Transforming growth factor-beta-induced protein ig-h3
P12032	TIMP1	Metalloproteinase inhibitor 1
P39876	TIMP3	Metalloproteinase inhibitor 3
Q80YX1	TNC	Tenascin
Q80Z71	TNN	Tenascin-N
Q62059	VCAN	Versican core protein

Short list of matrisomal molecules that were recovered from the purification of murine TNC in alphabetical order.

Table S6: Multiple alignments of MAREMO-like sequences in matrix molecules and receptors

FN, TNC

Col12A1, TNN

TNX, TNR

Domain Uniprot	Position	Aligned sequences	Loop I	Loop II	Gaps I-II	Spacer
TNX fn III 1	959 - 1051	RPQELGELRVLGRD**ETGR**LRVVWTAQPDTFAYFQLRMRVPEGP GAHEEVLPGDVRQALVP**PPPPGTPY**ELSLHGVPPGGKPSDPIIYQGIMDK	ETGR	PPPPGTPY	9	42
TNX fn III 2	1064 - 1153	-----RLGELTVTDR-**TSDS**LLLRWTVPEGEFDSFVIQYKDRDG----------QPQVVPVEGPQRSAVIT**SLDPGRKY**KFVLYGFVGK-KRHGPLVAEAKILPQSD-------------	TSDS	SLDPGRKY	10	41
TNX fn III 3	1161 - 1249	HLGNLWVTDP TPDSLHLSWTVPEGQFDTFMVQYRDRDG RPQVVPVEGPERSFVVSSLDPDHKYRFTLFGIANK KRYGPLTADGTTAPER	TPDS	SLDPDHKY	10	41
TNX fn III 4	1263 - 1352	-----LLGELTVTGV-TPDSLRLSWTVAQGPFDSFMVQYKDAQG----------QPQAVPVAGDENEVTVPGLDPDRKYKMNLYGLRGR-QRVGPESVVAKTAPQED-------------	TPDS	GLDPDRKY	10	41
TNX fn III 5	1374 - 1460	LLGELTVTGS SPDSLSLFWTVPQGSFDSFTVQYKDRDG RPRAVRVGGKESEVTVGGLEPGHKYKMHLYGLHEG QRVGPVSAVGVTAPQQEETPPA	SPDS	GLEPGHKY	10	41
TNX fn III 6	1476 - 1572	-----RLGELTVTDV-TPNSVGLSWTVPEGQFDSFIVQYKDKDG----------QPQVVPVAADQREVTVYNLEPERKYKMNMYGLHDG-QRMGPLSVVIVTAPLPPAPATEAS--------	TPNS	NLEPERKY	10	41
TNX fn III 7	1574 - 1669	PPLEPRLGELTVTDI-TPDSVGLSWTVPEGEFDSFVVQYKDRDG QPQVVPVAADQREVTIPDLEPSRKYKFLLFGIQDG-KRRSPVSVEAKTVARGDA	TPDS	DLEPSRKY	10	41
TNX fn III 8	1674 - 1764	---PPRLGELWVTDP-TPDSLRLSWTVPEGQFDSFVVQFKDKDG-----------PQVVPVEGHERSVTVTPLDAGRKYRFLLYGLLGK-KRHGPLTADGTTEARSA--------------	TPDS	PLDAGRKY	11	40
TNX fn III 9	1778 - 1860	LGEELQVTTV TQNSVGLSWTVPEGQFDSFVVQYKDRDG QPQVVPVEGSLREVSVPGLDPAHRYKLLLYGLHHG KRVGPISAVAITAGREET	TQNS	GLDPAHRY	10	41
TNX fn III 10	1883 - 1971	-----HLGELTVEEA-TSHTLHLSWMVTEGEFDSFEIQYTDRDG----------QLQMVRTGGDRNDITLSGLESDHRYLVTLYGFSDG-KHVGPVHVEALTVPEE---------------	TSHT	GLESDHRY	10	41
TNX fn III 11	1989 - 2089	-----RLGELTVTDA-TPDSLSLSWTVPEGQFDHFLVQYRNGDG----------QPKAVRVPGHEEGVTISGLEPDHKYKMNLYGFHGG-QRMGPVSVVGVTAAEEE---TPSPTEPSMEA	TPDS	GLEPDHKY	10	41
TNX fn III 12	2097 - 2185	LLGELTVTGS SPDSLSLSWTVPQGRFDSFTVQYKDRDG RPQVVRVGGEESEVTVGGLEPGRKYKMHLYGLHEG RRVGPVSAVGVTAPEE	SPDS	GLEPGRKY	10	41
TNX fn III 13	2196 - 2296	-----RLGQMTVRDT-TSDSLSLSWTVPEGQFDHFLVQFKNGDG----------QPKAVRVPGHEDGVTISGLEPDHKYKMNLYGFHGG-QRVGPVSAVGLTAPGKDEEMAPASTEPP---	TSDS	GLEPDHKY	10	41
TNX fn III 14	2305 - 2390	RLEELTVTDA TPDSLSLSWTVPEGQFDHFLVQYKNGDG QPKATRVPGHEDRVTISGLEPDNKYKMNLYGFHGG QRVGPVSAIGVTAAEEE TPSP	TPDS	GLEPDNKY	10	41
TNX fn III 15	2408 - 2502	PPEEPLLGELTVTGS-SPDSLSLSWTVPQGRFDSFTVQYKDRDG----------RPQVVRVGGEESEVTVGGLEPGRKYKMHLYGLHEG-RRVGPVSTVGVTAPQED--------------	SPDS	GLEPGRKY	10	41
TNX fn III 16	2519 - 2617	PPEEPLLGELTVTGS-SPDSLSLSWTVPQGRFDSFTVQYKDRDG RPQAVRVGGQESKVTVRGLEPGRKYKMHLYGLHEG RRLGPVSAVGVTEDEAETTQA	SPDS	GLEPGRKY	10	41
TNX fn III 17	2625 - 2723	PPIKPRLGELTMTDA-TPDSLSLSWTVPEGQFDHFLVQYRNGDG----------QPKAVRVPGHEDGVTISGLEPDHKYKMNLYGFHGG-QRVGPISVIGVTAAEEE---TPSP--------	TPDS	GLEPDHKY	10	41
TNX fn III 18	2733 - 2840	PPEEPLLGELTVTGS-SPDSLSLSWTIPQGHFDSFTVQYKDRDG----------RPQVMRVRGEESEVTVGGLEPGRKYKMHLYGLHEG-RRVGPVSTVGVTAPEDEAETTQAVPTTTPE-	SPDS	GLEPGRKY	10	41
TNX fn III 19	2841 - 2939	PPNKPRLGELTVTDA-TPDSLSLSWMVPEGQFDHFLVQYRNGDG----------QPKVVRVPGHEDGVTISGLEPDHKYKMNLYGFHGG-QRVGPISVIGVTAAEEE---TPAP--------	TPDS	GLEPDHKY	10	41
TNX fn III 20	2949 - 3042	PPEEPLLGELTVTGS-SPDSLSLSWTIPQGRFDSFTVQYKDRDG----------RPQVVRVRGEESEVTVGGLEPGCKYKMHLYGLHEG-QRVGPVSAVGVTAPKD--------------	SPDS	GLEPGCKY	10	41
TNX fn III 21	3062 - 3153	-----RLGELTVTDA-TPDSLSLSWMVPEGQFDHFLVQYRNGDG----------QPKAVRVPGHEDGVTISGLEPDHKYKMNLYGFHGG-QRVGPVSAIGVTEEETP---SP---------	TPDS	GLEPDHKY	10	41
TNX fn III 22	3168 - 3260	-----LLGELTVTGS-SPDSLSLSWTVPQGRFDSFTVQYKDRDG----------QPQVVRVRGEESEVTVGGLEPGRKYKMHLYGLHEG-QRVGPVSTVGITAPLPTPLP-----------	SPDS	GLEPGRKY	10	41
TNX fn III 23	3264 - 3355	-----RLGELAVAAV-TSDSVGLSWTVAQGPFDSFLVQYRDAQG----------QPQAVPVSGDLRAVAVSGLDPARKYKFLLFGLQNG-KRHGPVPVEARTAPDTKPS-----------	TSDS	GLDPARKY	10	41
TNX fn III 24	3357 - 3446	-----RLGELTVTDA-TPDSVGLSWTVPEGEFDSFVVQYKDKDG----------RLQVVPVAANQREVTVQGLEPSRKYRFLLYGLSGR-KRLGPISADSTTAPLEK-------------	TPDS	GLEPSRKY	10	41
TNX fn III 25	3451 - 3544	-----HLGELTVAEE-TSSSLRLSWTVAQGPFDSFVVQYRDTDG----------QPRAVPVAADQRTVTVEDLEPGKKYKFLLYGLLGG-KRLGPVSALGMTAPEEDTPAP----------	TSSS	DLEPGKKY	10	41
TNX fn III 26	3553 - 3647	PPEEPRLGVLTVTDT-TPDSMRLSWSVAQGPFDSFVVQYEDTNG----------QPQALLVDGDQSKILISGLEPSTPYRFLLYGLHEG-KRLGPLSAEGTTGLAPA-------------	TPDS	GLEPSTPY	10	41
TNX fn III 27	3657 - 3754	-----RLSQLSVTDV-TTSSLRLNWEAPPGAFDSFLLRFGVPSPSTLEPHPRPLLQRELMVPGTRHSAVLRDLRSGTLYSLTLYGLRGP-HKADSIQGTARTLSP---------------	TTSS	DLRSGTLY	0	51
TNX fn III 28	3758 - 3847	-----SPRDLQFSEI-RETSAKVNWMPPPSRADSFKVSYQLADGG----------EPQSVQVDGQARTQKLQGLIPGARYEVTVVSVRGF-EESEPLTGFLTTVPDG--------------	RETS	GLIPGARY	9	42
TNX fn III 29	3848 - 3934	------PTQLRALNL-TEGFAVLHWKPPQNPVDTYDVQVTAPGA----------PPLQAETPGSAVDYPLHDLVLHTNYTATVRGLRGP-NLTSPASITFTTGLE----------------	TEGF	DLVLHTNY	10	41
TNX fn III 30	3935 - 4025	-----APRDLEAKEV-TPRTALLTWTEPPVRPAGYLLSFHTPGG----------QNQEILLPGGITSHQLLGLFPSTSYNARLQAMWGQ-SLLPPVSTSFTTGGLRIP-------------	TPRT	GLFPSTSY	10	41
Consensus TNX fnIII		xxxxxxLGELTVTDxxTPDSLxLSWTVPEGQFDSFVVQYKDrDGxxxxxxxxxxQPQxVrVxGxExEVTVxGLEPxxKYKMNLYGLHqGxKRVGPVSxVGVTAPEeExxxxxxxxxxxxxx	**TPDS**	**GLEPxxKY**		

Domain Uniprot	Position	Aligned sequences	Loop I	Loop II	Gaps I II	Spacer
TNR fn III 1	328 - 420	PPEDLRVAGISDRSIELEWDGPMA-VTEYVISYQPTALGGLQLQQRVP---GDWSGVTITELEPGLTYNISVYAVISNILSLPITAKVATHLSTPQG	SDRS	ELEPGLTY	4	42
TNR fn III 2	421 - 505	----LQFKTI**TETT**VEVQWEPFSFSFDGWEISFIPKNNEGGVTAQV-**P**---SDVTSFNQT**GLKPGEEY**IVNVVALKEQARSPPTSASVSTVID----	**TETT**	**GLKPGEEY**	4	42
TNR fn III 3	506 - 595	GFTQILVRDVSDTVAFVEWIPPRAKVDFILLKYGLVGGEGGRTTFRLQ---PPLSQYSVQALRPGSRYEVSVSAVRGTNESDSATTQFTTEID----	SDTV	ALRPGSRY	3	43
TNR fn III 4	596 - 687	APKNLRVGSR**TATS**LDLEWDNSEAEVQEYKVVYSTLAG-EQYHEVLVPRGIGPTTRATLT**DLVPGTEY**GVGISAVMNSQQSVFATMNARTELD----	**TATS**	**DLVPGTEY**	1	45
TNR fn III 5	688 - 777	SPRDLMVTASSETSISLIWTKASGPIDHYRITFTPS--SGIASEVTVP---KDRTSYTLTDLEPGAEYIISVTAERGRQQSLESTVDAFTGFRPI--	**SETS**	**DLEPGAEY**	5	41
TNR fn III 6	778 - 865	SHLHFSHVTSSSVNITWSDPSPPADRLILNYSPRDEEEEMMEVSLD ATKRHAVLMRLNPATEYEISLNSVRGREESERICTLVHTAMDN	**TSSS**	R**LNPATEY**	3	43
TNR fn III 7	866 - 955	PPKDITISNVTKDSVMVSWSPPVASFDYYRVSYRPTQVGRLDSSVV P NTVTEFTITRLNPATEYEISLNSVRGREESERICTLVHTAMDN	**TKDS**	R**LNPATEY**	4	42
TNR fn III 8	956 - 1042	-PVDLIATNITPTEALLQWKAPVGEVENYVIVLTHFAVAGETILV--D---GVSEEFRLVDLLPSTHYTATMYATNGPLTSGTISTNFSTLLD----	TPTE	DLLPSTHY	5	41
TNR fn III 9	1043 - 1130	PPANLTASEVTRQSALISWQPPRAEIENYVLTYKSTDGSRKELIV--D---AEDTWIRLEGLLENTDYTVLLQAAQDTTWSSITSTAFTTGGR----	TRQS	GLLENTDY	5	41
Consensus TNR fnIII		xPxDLxVSNVTETSVxIEWxxPxAxVDxYVISYxPxxxxGxxLxVxVPxxxxxxTxFTLTxLxPGTEYxVSVSAVRGxxESxxxTTxxSTxLDxxxx	TETS	xLxPGTEY		

Col14A1, PTPRF, PTPRD, ITGB4

Domain Uniprot	Position	Aligned sequences	Loop I	Loop II	Gaps I-II	Spacer
Col14A1 fn III 1	32 - 122	PPTRLRYNVISHDSIQISWKAPRGKFGGYKLLVTPTSGGKT----NQLNLQNTATKAIIQGLMPDQNYTVQIIAYNKDKESKP-AQGQFRIKDLEK	SHDS	GLMPDQNY	4	42
Col14A1 fn III 2	355 - 444	PPTELITSEVTARSFMVNWTHAPGNVEKYRVVYYPTRGGKP----DEVVVDGTVSSTVLKNLMSLTEYQIAVFAIYAHTASEG-LRGTETTLALP-	TARS	NLMSLTEY	4	42
Col14A1 fn III 3	445 - 536	MASDLLLYDV**TENS**MRVKWDAV**P**GA SGYLILYA**P**LTEGLAGD EKEMKICETHTDIELS**GLLPNTEY**TVTVYAMFGEEASDP VTGQETTLALS	**TENS**	**GLLPNTEY**	2	44
Col14A1 fn III 4	537 - 626	PPRNLRISNVGSNSARLTWDPTSRQINGYRIVYNNADGTEI----NEVEVDP-ITTFPLKGLTPLTEYTIAIFSIYDEGQSEP-LTGVFTTEEVPA	GSNS	GLTPLTEY	4	42
Col14A1 fn III 5	627 - 715	-QQYLEIDEV**TTDS**FRVTWHPLSADEGLHKLMWI**P**VYGGKT----EEVVLKEEQDSHVIE**GLEPGTEY**EVSLLAVLDDGSESEVVTAVGTTLDS--	**TTDS**	**GLEPGTEY**	4	42
Col14A1 fn III 6	737 - 829	GIRNLVVGDETTSSLRVKWDISDSDVQQFRVTYMTAQGDPEEEVIGTVMVPGSQNNLLLKPLLPDTEYKVTVTPIYTDGEGVS VSAPGKTLPS	**TTSS**	**PLLPDTEY**	0	46
Col14A1 fn III 7	831 - 921	GPQNLRVSEEWYNRLRITWDPPSSPVKGYRIVYKPVSVPGPT---LETFVGADINTILITNLLSGMDYNVKIFASQASGFSDA-LTGMVKTLFLG-	WYNR	NLLSGMDY	3	43
Col14A1 fn III 8	922 - 1010	-VTNLQAKHVEMTSLCAHWQVHRHA-TAYRVVIESLQDRQK----QESTVGGGTTRHCFYGLQPDSEYKISVYTKLQEIEGPS-VSIMEKTQSLPT	EMTS	GLQPDSEY	5	41
Consensus Col14A1 fnIII		xptNLrVsEVTxNSLRVtWdxxxxxvxqYRIVYxPvxGqKxxxxxxEVxVxxLxTSxVLKGLMPdTEYxVSIFAIyxDgeSExxVTGmxtTLxLxx	TxNS	GLMPdTEY		

Domain Uniprot	Position	Aligned sequences	Loop I	Loop II	Gaps I-II	Spacer
PTPRF fnIII 1	321 - 411	-PPT-DLVVTET**TATS**VTLTWDSGNS----EPVTYYGIQYRAAGTE---------------GPFQEVDGVATTRYSIG**GLSPFSEY**AFRVLAVNSIGRGPPSEAVRARTGEQ-	**TATS**	**GLSPFSEY**	19	43
PTPRF fnIII 2	416 - 510	-PPR-RVQARMLSASTMLVQWEPP--EEPNGLVRGYRVYYTPDSRRPP-------------NAWHKHNTDAGLLTTVGSLLPGITYSLRVLAFTAVGDGPPSPTIQVKTQQG-	SAST	SLLPGITY	15	47
PTPRF fnIII 3	514 - 604	-QPA-DFQAEVESDTRIQLSWLLPPQ----ERIIMYELVYWAAEDE---------------DQQHKVTFDPTSSYTLEDLKPDTLYRFQLAARSDMGVGVFTPTIEARTAQS-	SDTR	DLKPDTLY	19	43
PTPRF fnIII 4	609 - 706	-PPQ-KVMCVSMGSTTVRVSWVPPPADSRNGVITQYSVAYEAVD-GEDRGRHVVDGISREHSSWDL-----------VGLEKWTEYRVWVRAHTDVGPGPESSPVLVRTDED-	GSTT	GLEKWTEY	12	50
PTPRF fnIII 5	711 - 819	-PPR-KVEVEPLNSTAVHVYWKLPVPSKQHGQIRGYQVTYVRLENGEPRGLPIIQDVMLAEAQWRPEE-SEDYETTISGLTPETTYSVTVAAYTTKGDGARSKPKIVTTTGA-	NSTA	GLTPETTY	1	61
PTPRF fnIII 6	820 - 914	VPGRPTMMISTTAMNTALLQWHPP KELPGELLGYRLQYCRADEARP NTIDFGKDDQHFTVTGLHKGTTYIFRLAAKNRAGLGEEFEKE IRTPED	AMNT	GLHKGTTY	17	45
PTPRF fnIII 7	918 - 1010	-PPQ-NLHVTGLTTSTTELAWDPPVLAERNGRIISYTVVFRDINS-----------------QQELQNITTDTRFTLTGLKPDTTYDIKVRAWTSKGSGPLSPSIQSRTMPV-	TTST	GLKPDTTY	19	43
PTPRF fnIII 8	1014 - 1098	-PAK-NFRVAAAMKTSVLLSWEVPDSYKS---AVPFKILYNGQSV----------------------EVDGHSMRKLIA**DLQPNTEY**SFVLMNRGSSAGGLQ-HLVSIRTAPD-	**MKTS**	D**LQPNTEY**	24	38
Consensus PTPRF fnIII		xPPRxnLqVxxlSSTTVxLSWEpPxxxExnGxIixYrIxYxxxDxxxxxxxxxxxxxxxxxxxxwxxexxxxxxxyTIsGLkPdTtYsfRVxAyTSvGxGpxSxxVqVRTxExx	SSTT	GLkPdTtY		

Domain Uniprot	Position	Aligned sequences	Loop I	Loop II	Gaps I-II	Spacer
PTPRD fnIII 1	325 - 415	---PPGTPVVTES**TATS**ITLTWDSGNPEPVS-----YYIIQHKPKNSEEL--YK-----------EIDGVATTRYSVA**GLSPYSDY**EFRVVAVNNIGRGPPSEPVLTQTSEQ--	**TATS**	**GLSPYSDY**	18	43
PTPRD fnIII 2	420 - 516	---APRDVQARMLSSTTILVQWKEP--EEPNGQIQGYRVYYTMDPTQH-VNNWM-----------KHNVADSQITTIGNLVPQKTYSVKVLAFTSIGDGPLSSDIQVITQTGVP	**SSTT**	**NL**VPQK**TY**	14	47
PTPRD fnIII 3	518 - 607	---QPLNFKAEPESETSILLSWTPPR----SDTIANYELVYKDGEHGEEQRI---------------TIEPGTSYRLQGLKPNSLYYFRLAARSPQGLGASTAEISARTMQS--	**SETS**	**GLKPNS**L**Y**	19	42
PTPRD fnIII 4	612 - 709	---PPQDISCTSPSSTSILVSWQPPPVEKQNGIITEYSIKYTAVDGEDDK--PHEILGI---------PSDTTKYLLEQLEKWTEYRITVTAHTDVGPGPESLSVLIRTNED--	SSTS	QLEKWTEY	11	50
PTPRD fnIII 5	714 - 822	---PPRKVEVEAVNSTSVKVSWRSPVPNKQHGQIRGYQVHYVRMENGEPKGQPMLKDVMLADAQWEFDDTTEHDMIISGLQPETSYSLTVTAYTTKGDGARSKPKLVSTTGA--	NST**S**	**GLQPETSY**	1	60
PTPRD fnIII 6	823 - 916	VPGKPR-LVINHTQMNTALIQWHPPVD--TFGPLQGYRLKFGRKDMEPLTTL--------------EF-SEKEDHFTATDIHKGASYVFRLSARNKVGFGEEMVKEISIPEE---	QMNT	DIHKGASY	16	45
PTPRD fnIII 7	921 - 1016	---PPQNLHSEGTTSTSVQLSWQPPVLAERNGIITKYTLLYRDINIPL-L--PMEQLIV---------PADTT-MTLTGLKPDTTYDVKVRAHTSKGPGPYSPSVQFRTLPV--	**TSTS**	**GLKPDTTY**	13	48
PTPRD fnIII 8	1020 - 1106	FAKNFHVKAVMKTSVLLSWEIPENY NSAMPFKILYDDGKMVEEV DGRATQKLIVNLKPEKSYSFVLTNRGNSAGGLQ HRVTAKTAPD	MK**TS**	**NLKPEKSY**	21	40
Consensus PTPRD fnIII		xxxxPRNIxvoxxSSTSILLSWQpPxxxoxNGxIxxYrIlYxxxExxEovxxxxxxxxxxxxxxxoxxxxxtTxytIxgLKPoTSYxfRVtAxTNvGxGpxSxxVlxRTsoxxx	SSTS	gLKPeTSY		

Domain Uniprot	Position	Aligned sequences	Loop I	Loop II	Gaps I-II	Spacer
ITGB4 fnIII 1	1129 - 1218	APQNPNAKAA**GSRK**IHFNWL**PP**S GK**P**MGYRVKYWIQGDSESE AHL LDSKV**P**SVELT**NLYPYCDY**EMKVCAYGAQGEGPYSSLVSCRTHQE	GSRK	**NLY**P**Y**C**DY**	10	42
ITGB4 fnIII 2	1222 - 1321	EPGRLAFNVVSSTVTQLSWAEPAETNGEITAYEVCYGLVNDDNRPIGPMKKVL-VDNPKNRMLLIENLRESQPYRYTVKARNGAGWGPEREAIINLATQPK--	SSTV	NLRESQPY	1	51
ITGB4 fnIII 3	1530 - 1625	TPTRLVFSAL**GPTS**LRVSWQE**P**RCE-R**P**LQGYSVEYQLLNGGEL----HR-LNI**P**-N**P**AQTSVVVE**DLLPNHSY**VFRVRAQSQEGWGRERKGVITIESQVHPQ	GP**TS**	D**LL**P**NHSY**	7	45
ITGB4 fnIII 4	1643 - 1739	APGPLVFTALSPDSLQLSWERPRRPNGDIVGYLVTCEMAQGGGP----ATAFRVDGDSPESRLTVPGLSENVPYKFKVQARTTEGFGPERKGIITIESQDG--	SPDS	GLSENVPY	4	48
Consensus PTPRD fnIII		aPgrLvFSALgptsLQLSWqePrxxnGEImGYxVkYqLvndgexxxxxxkxLxixxDpkqtsVvTeNLxpNxpYKFKVKARSxEGWGPERKgVItTeSQexxx	gpts	NLxpNxpY		

Sequence alignment for the indicated molecules with identification of Loop I and Loop II sequence. High conservation with the MAREMO sequence in FN is marked in bold.

Table S7: Uniprot ID sequence numbers

Protein	UniProt ID
Fibronectin *Homo sapiens (Human)*	P02751
Fibronectin *Mus musculus (Mouse)*	P11276
Fibronectin *Rattus norvegicus (Rat)*	P04937
Fibronectin *Bos taurus (Bovine)*	P07589
Fibronectin *Canis lupus familiaris (Dog)*	Q28275
Fibronectin *Equus caballus (Horse)*	Q28377
Fibronectin *Gallus gallus (Chicken)*	P11722
Fibronectin *Xenopus laevis (African clawed frog)*	Q91740
Tenascin-C *Homo sapiens (Human)*	P24821
Tenascin-X *Homo sapiens (Human)*	P22105
Tenascin-N *Homo sapiens (Human)*	Q9UQP3
Tenascin-R *Homo sapiens (Human)*	Q92752
Collagen XII A1 *Homo sapiens (Human)*	Q99715
Collagen XIV A1 *Homo sapiens (Human)*	Q05707
Receptor-type tyrosine-protein phosphatase F (PTPRF) *Homo sapiens (Human)*	P10586
Receptor-type tyrosine-protein phosphatase D (PTPRD) *Homo sapiens (Human)*	P23468
Integrin beta-4 (ITGB4) *Homo sapiens (Human)*	P16144

Table S8: Antibody list

Target	Antibody type / Application	Reference
GAPDH	Primary / WB	Cell Signalling 2118S
FN	Primary / WB, IF	Sigma F3648
TNC	Primary / WB, IF	G. OREND
Smad 2/3	Primary WB	Cell Signalling 3102S
p-Smad 2	Primary WB	Cell Signalling 3108S
Col I	Primary WB	Abcam Ab34710
Col XII	Primary IF	M. KOCH
Vinculin	Primary IF	Sigma SAB4200729
Anti-rabbit	Secondary WB	Cell Signalling 7074S
Anti-rat	Secondary WB	Cell Signalling 7077S
Anti-mouse	Secondary WB	Cell Signalling 7076S
Anti-rabbit	Secondary IF	Jackson Lab 111-165-003
Anti-rat	Secondary IF	Jackson Lab A11006
Anti-mouse	Secondary IF	Jackson Lab 115-165-003

Table S9: Primer sequences

Gene symbol	Primer name	5'→3' primer sequence/ Ref
Gapdh	Taqman probe: Mm99999915_g1 Thermofisher	
Cxcl12	Taqman probe: Mm00445553_m1 Thermofisher	
Ccl21	mCCL21_F	tccaagggctgcaagaga
	mCCL21_R	tgaagttcgtgggggatct
Ccr7	mCCR7_F	ctccttgtcattttccaggtg
	mCCR7_R	tggtattctcgccgatgtagt
Cd80	mCD80_F	ccatgtccaaggctcattct
	mCD80_R	ggcaaggcagcaatacctta
Cd86	mCD86_F	catgggcttggcaatcctta
	mCD86_R	aaatgggcacgggagatatg

Figure S1

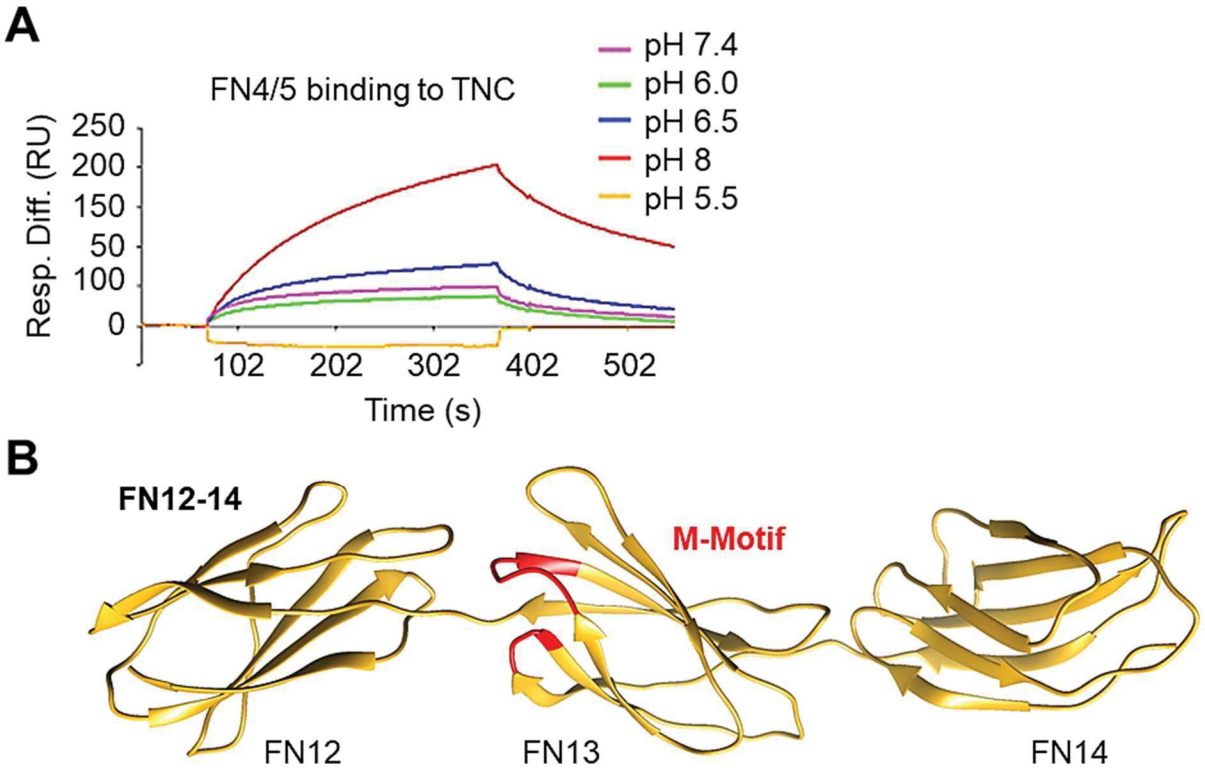
A
FN4/5 binding to TNC
pH 7.4
pH 6.0
pH 6.5
pH 8
pH 5.5
Resp. Diff. (RU)
250
200
150
50
100
0
102
202
302
402
502
Time (s)
B
FN12-14
M-Motif
FN12
FN13
FN14

Figure S1: Binding of FN4/5 to TNC

(A) SPR measurement of soluble FN4/5 molecule to human TNC-coated chip at equimolar concentrations and different pH conditions. **(B)** Structural model of FN12-14 domains with M-Motif highlighted in red.

Figure S2

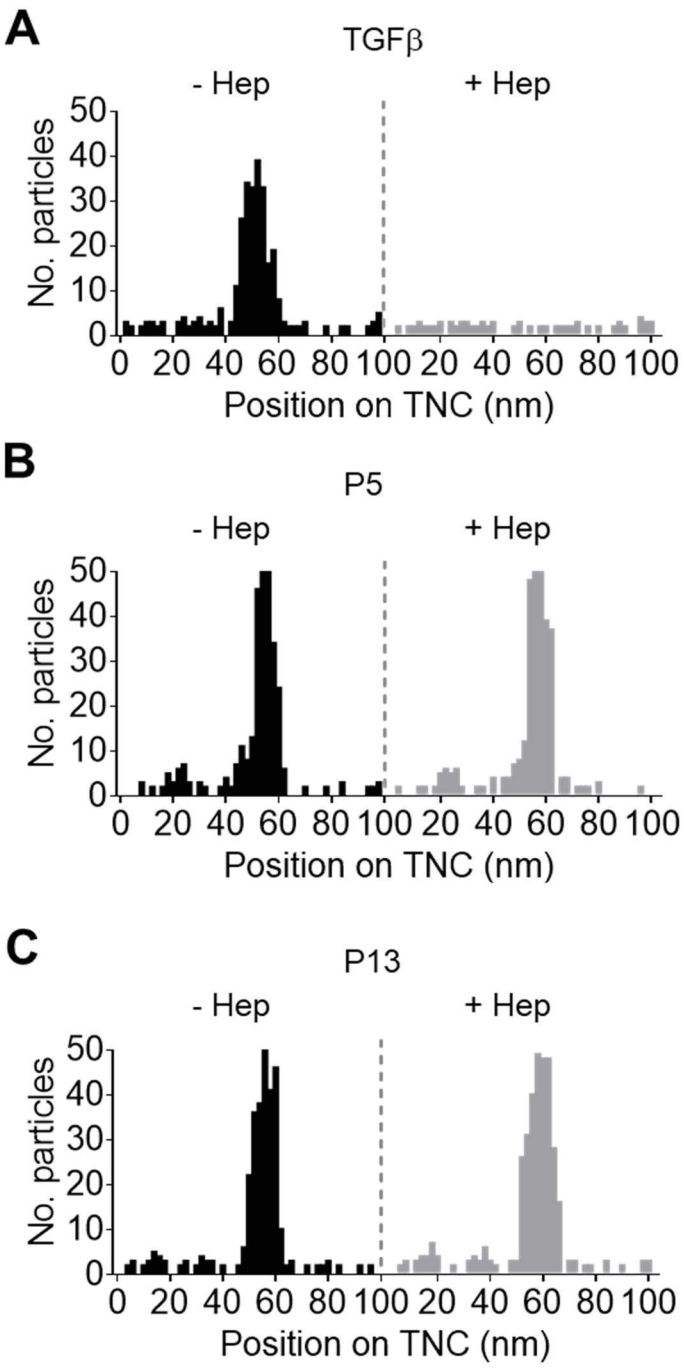
A
TGFβ
- Hep
+ Hep
No. particles
0
10
20
30
40
50
0 20 40 60 80 100 20 40 60 80 100
Position on TNC (nm)
B
P5
- Hep
+ Hep
No. particles
0
10
20
30
40
50
0 20 40 60 80 100 20 40 60 80 100
Position on TNC (nm)
C
P13
- Hep
+ Hep
No. particles
0
10
20
30
40
50
0 20 40 60 80 100 20 40 60 80 100
Position on TNC (nm)

Figure S2: Binding of TGFβ, P5 and P13 to TNC

(A-C) Quantification of beads-coated TGFβ **(A)**, P5 **(B)** and P13 **(C)** along the TNC monomer in the absence (-) or presence (+) of heparin, N = 2 experiments, n = 500 TNC molecules.

Figure S3

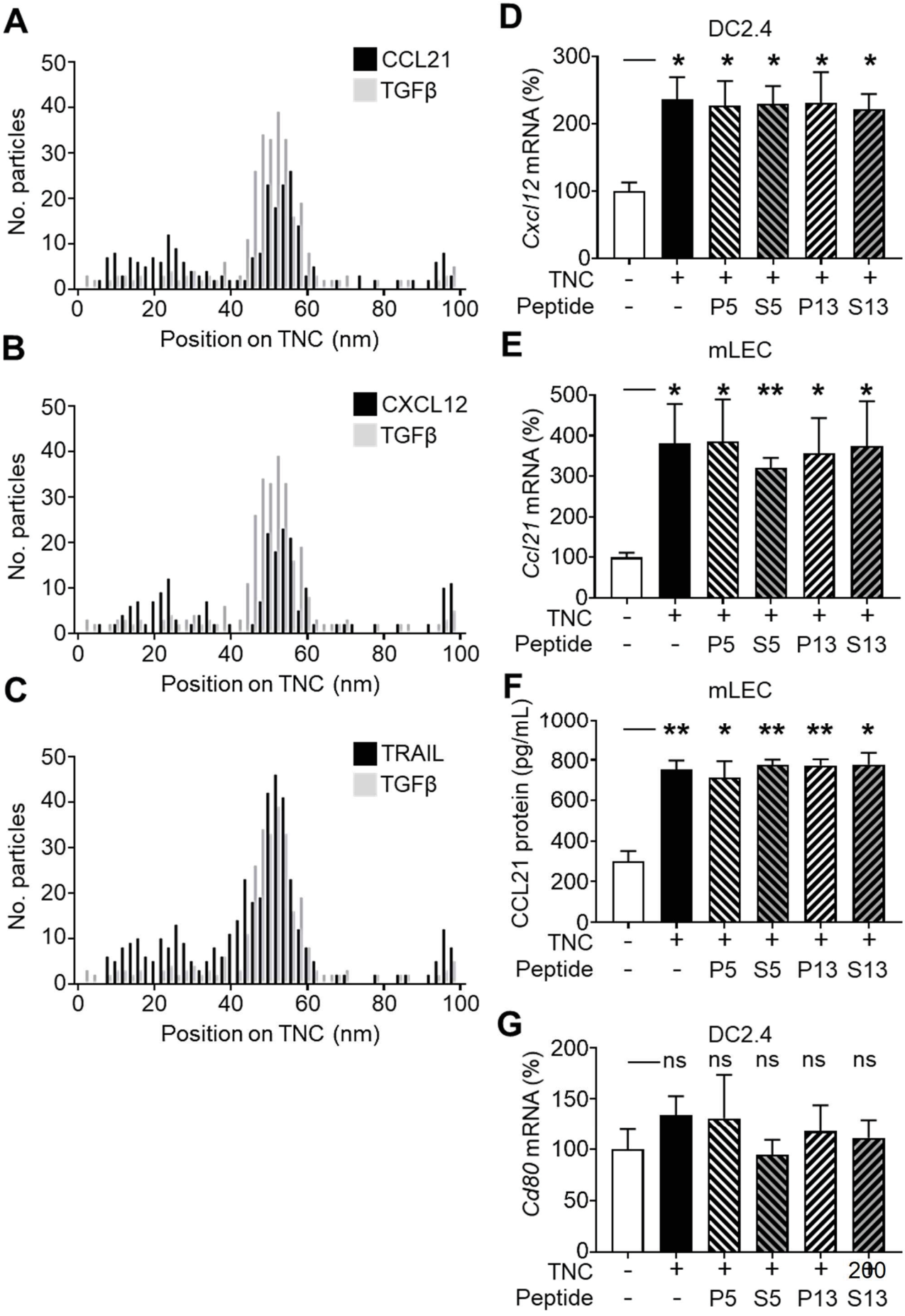
A
CCL21
TGFβ
No. particles
Position on TNC (nm)
B
CXCL12
TGFβ
No. particles
Position on TNC (nm)
C
TRAIL
TGFβ
No. particles
Position on TNC (nm)
D
DC2.4
Cxcl12 mRNA (%)
E
mLEC
Ccl21 mRNA (%)
F
mLEC
CCL21 protein (pg/mL)
G
DC2.4
Cd80 mRNA (%)
TNC
Peptide
P5
S5
P13
S13

Figure S3

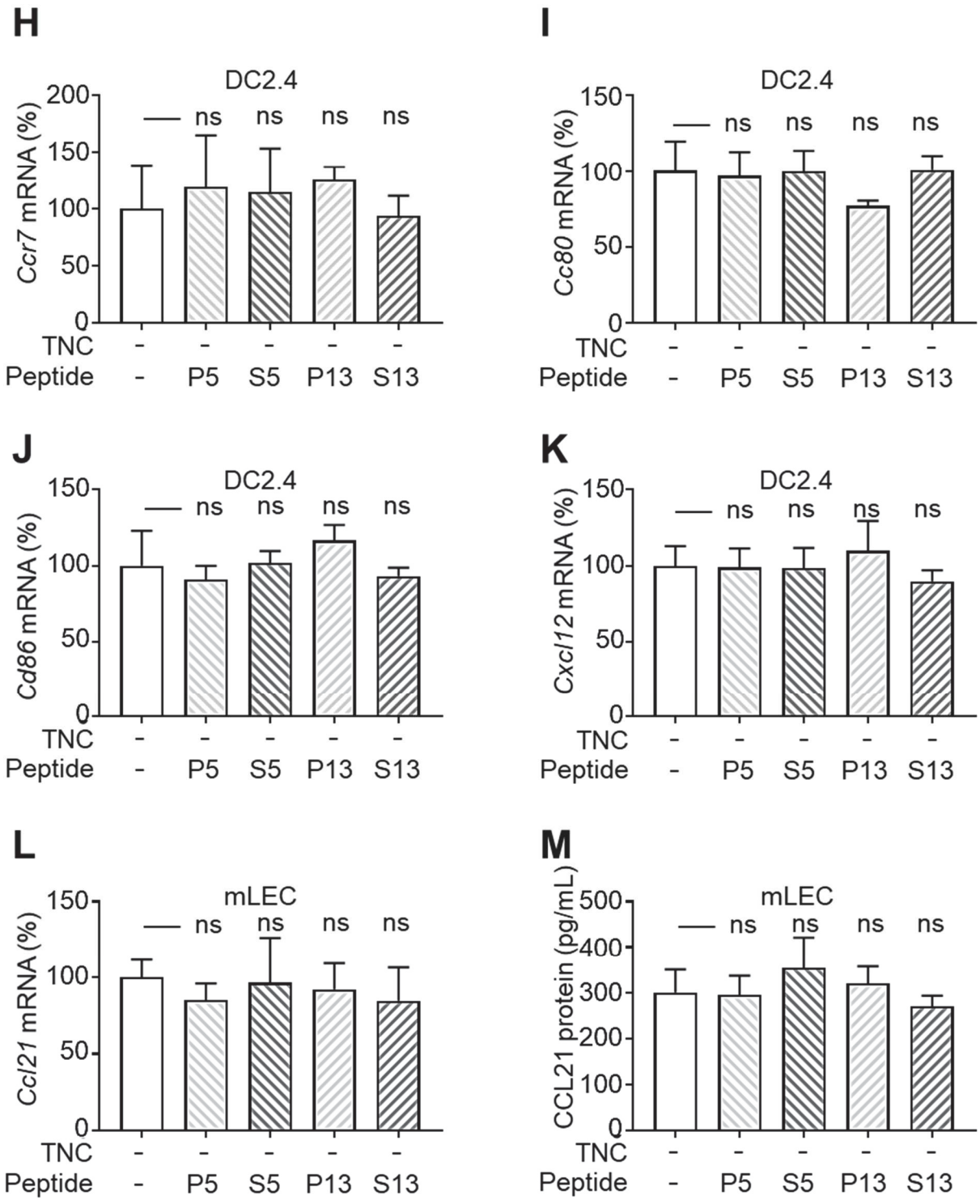
H
DC2.4
Ccr7 mRNA (%)
200
150
100
50
0
ns ns ns ns
TNC - - - - -
Peptide - P5 S5 P13 S13
I
DC2.4
Cc80 mRNA (%)
150
100
50
0
ns ns ns ns
TNC - - - - -
Peptide - P5 S5 P13 S13
J
DC2.4
Cd86 mRNA (%)
150
100
50
0
ns ns ns ns
TNC - - - - -
Peptide - P5 S5 P13 S13
K
DC2.4
Cxcl12 mRNA (%)
150
100
50
0
ns ns ns ns
TNC - - - - -
Peptide - P5 S5 P13 S13
L
mLEC
Ccl21 mRNA (%)
150
100
50
0
ns ns ns ns
TNC - - - - -
Peptide - P5 S5 P13 S13
M
mLEC
CCL21 protein (pg/mL)
500
400
300
200
100
0
ns ns ns ns
TNC - - - - -
Peptide - P5 S5 P13 S13

Figure S3: Comparison of the binding sites of the soluble factors on TNC and effects of the peptides on TNC-induced gene expression in DC2.4 and LEC cells

(A-C) Binding of TGFβ to TNC compared to binding of CCL21 **(A)**, CXCL12 **(B)** and TRAIL **(C)** to TNC. Quantification of beads-adsorbed molecules along the TNC molecules. N = 2, n = 500 TNC molecules. **(D-M)** qRTPCR and ELISA quantification of the indicated genes and protein abundance in DC2.4 **(D, G – K)** and LEC **(E, F, L, M)** cells upon addition of soluble TNC (10 µg/mL) and the peptides (50 µg/mL). N = 4 experiments. Kruskal-Wallis test, mean ± SEM (*p < 0.05; **p < 0.01; ns = not significant).

Figure S4

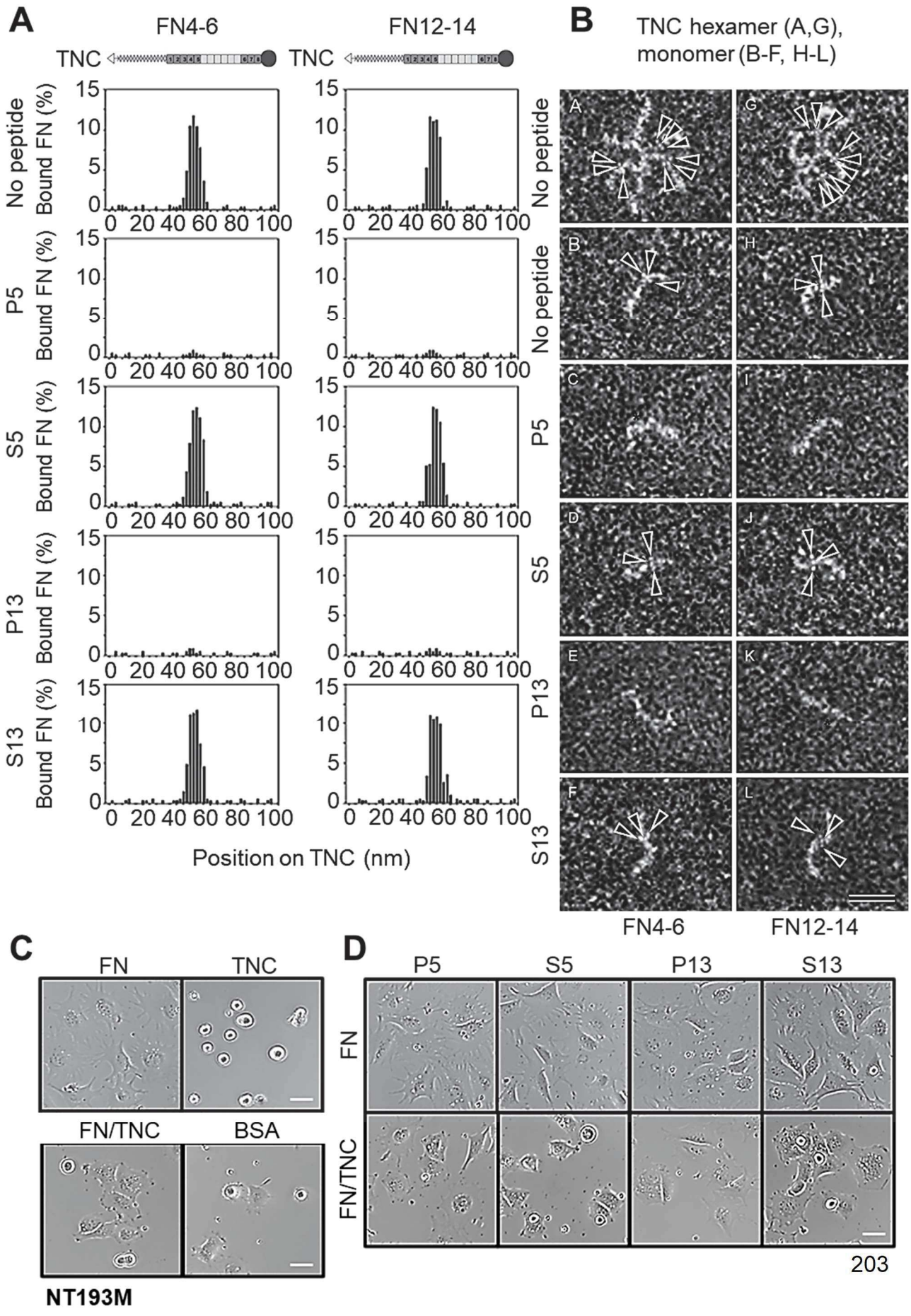
A
FN4-6
FN12-14
TNC
TNC
No peptide
P5
S5
P13
S13
Bound FN (%)
0 20 40 60 80 100
Position on TNC (nm)
B
TNC hexamer (A,G),
monomer (B-F, H-L)
FN4-6
FN12-14
C
FN
TNC
FN/TNC
BSA
NT193M
D
P5
S5
P13
S13
FN
FN/TNC

Figure S4

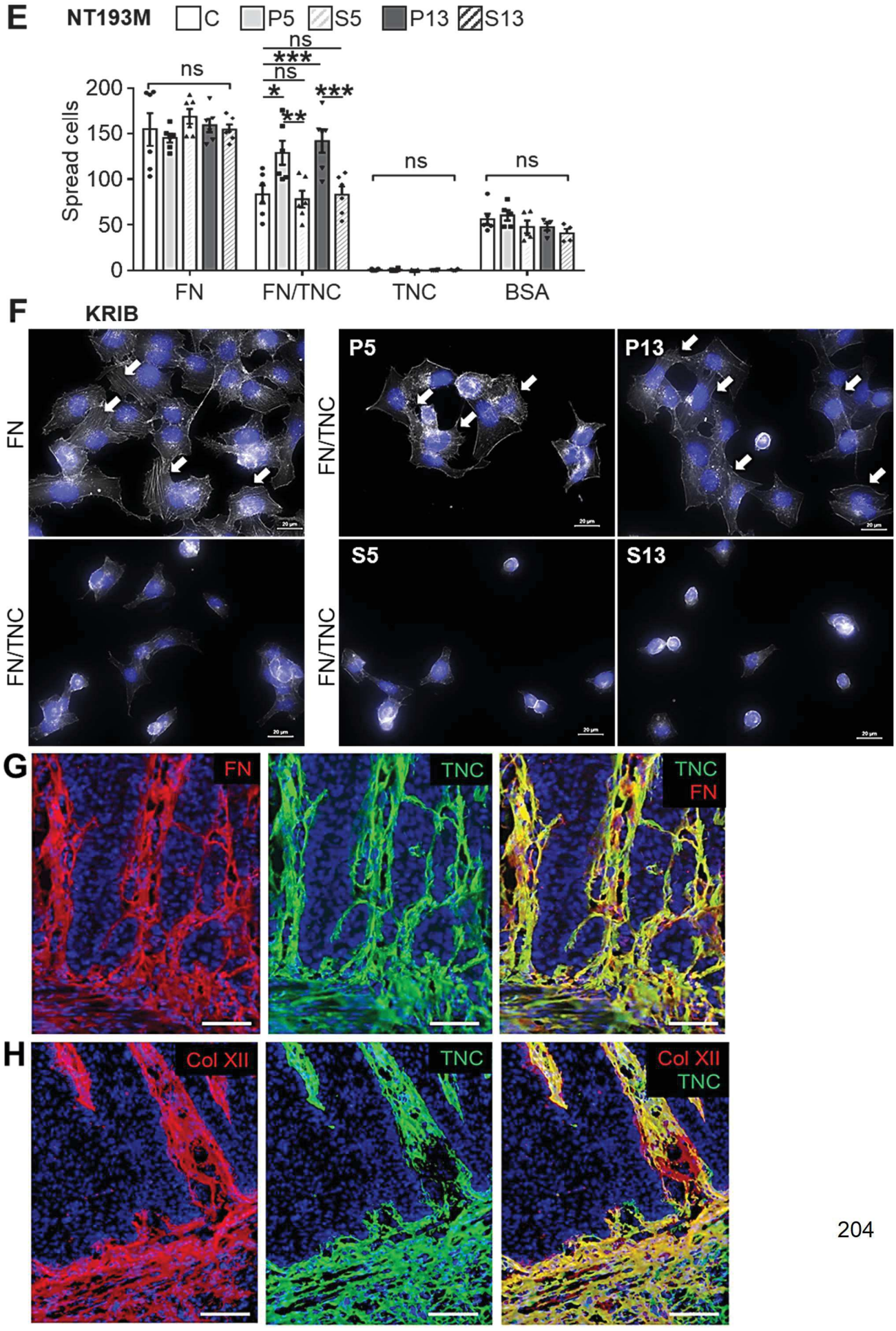
E
NT193M
C
P5
S5
P13
S13
Spread cells
200
150
100
50
0
ns
ns
***
ns
*
**
***
ns
ns
FN
FN/TNC
TNC
BSA
F
KRIB
FN
FN/TNC
P5
P13
FN/TNC
S5
S13
G
FN
TNC
TNC
FN
H
Col XII
TNC
Col XII
TNC

Figure S4: Effects of the peptides on FN4-6 and FN12-14 binding to TNC, and on TNC anti-adhesive properties

(A, B) FN4-6 and FN12-14 binding to TNC in presence of the peptides, **(A)** quantification and **(B)** negative EM images. Scale bar 100 nm, N = 2 experiments, n = 500 TNC molecules. **(C - E)** NT193M cell spreading on FN, TNC, FN/TNC and BSA coated surfaces upon preincubation with the peptides, representative phase contrast images **(A, D)** and quantification of spread cells **(E)**, N = 3 experiments, n = duplicates. Kruskal-Wallis test, mean ± SEM (*p < 0.05; **p < 0.01; ***p < 0.001; ns = not significant). Scale bar 20µm. **(F)** Representative IF images of KRIB cells upon spreading on FN and FN/TNC coated surfaces and preincubation with the peptides. Actin stress fibers are in white. Arrows point at polymerized actin filaments. Scale bar 20 µm, N = 3 experiments. **(G, H)** Representative IF images of TNC matrix tracks in murine OSCC of the tongue upon staining for FN **(G)** and Col12 **(H)**. Scale bar 100 µm.

Figure S5

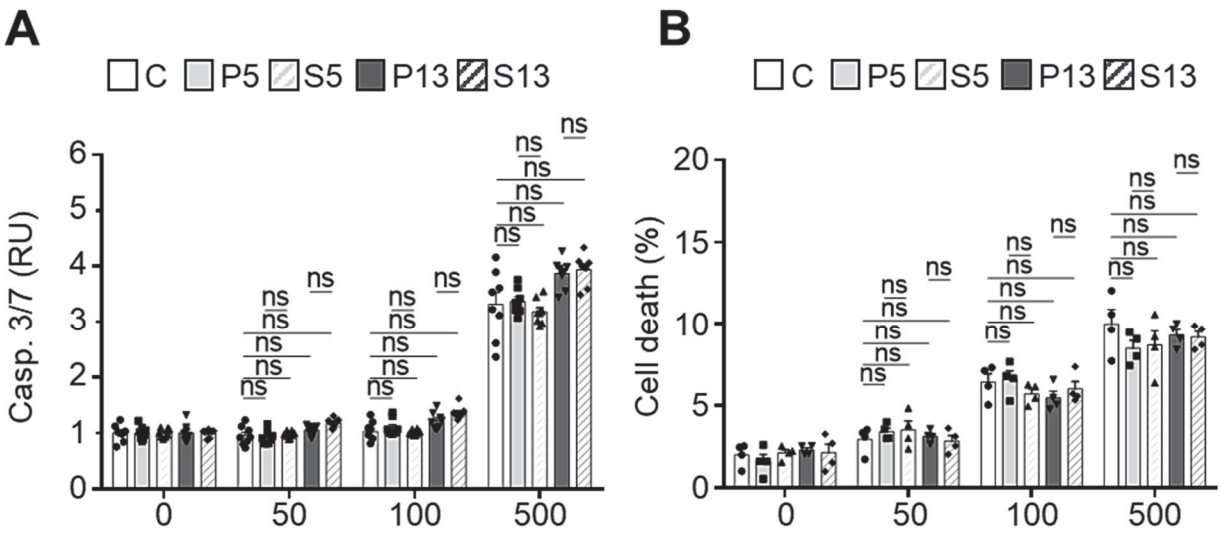
A
C P5 S5 P13 S13
Casp. 3/7 (RU)
0 1 2 3 4 5 6
0 50 100 500
ns
B
C P5 S5 P13 S13
Cell death (%)
0 5 10 15 20
0 50 100 500
ns

Figure S5: effects of the peptides on TRAIL-induced apoptosis

(A, B) Casp 3/7 activity **(A)** and cell death (AO/EB) labelling **(B)** in NT193M sh2 cells upon pretreatment with the peptides (50 µg/mL), followed by incubation with TRAIL (ng/mL) and MD5-1 (50 ng/mL). **(A)** N = 4, n = duplicates, Kruskal-Wallis test, mean ± SEM (**p < 0.01). **(B)** N = 2, n = duplicates. Kruskal-Wallis test, mean ± SEM (***p < 0.001).

Figure S6

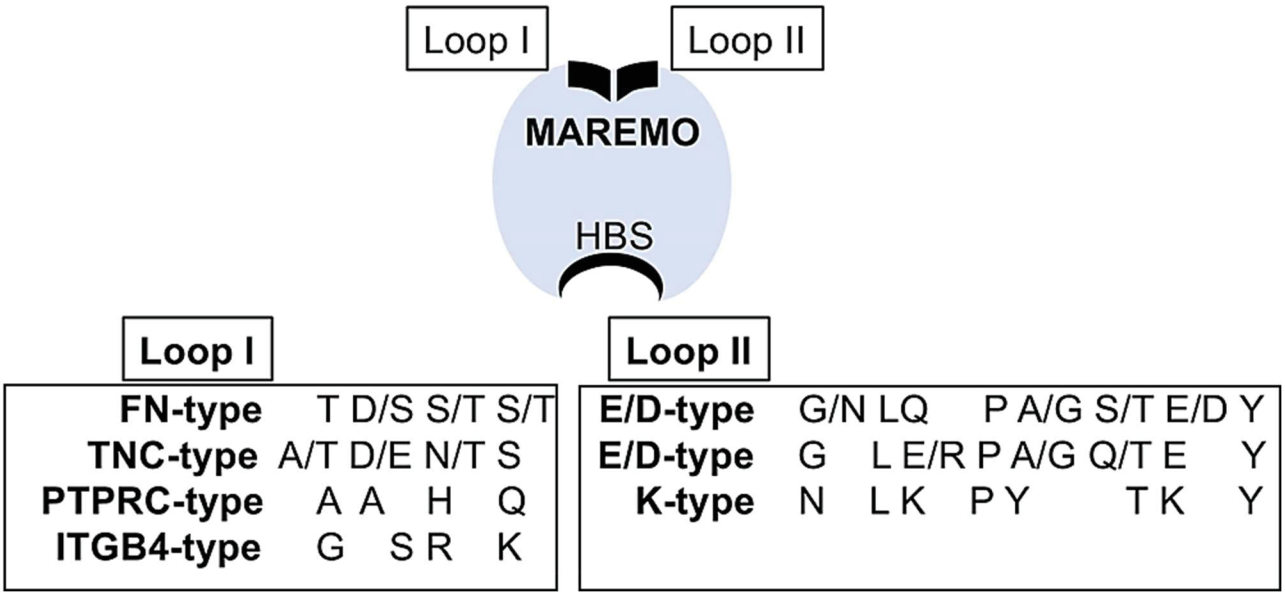
Loop I
Loop II
MAREMO
HBS
Loop I
FN-type T D/S S/T S/T
TNC-type A/T D/E N/T S
PTPRC-type A A H Q
ITGB4-type G S R K
Loop II
E/D-type G/N LQ P A/G S/T E/D Y
E/D-type G L E/R P A/G Q/T E Y
K-type N L K P Y T K Y

Figure S6: consensus sequences of the loop I and loop II constituting MAREMO in several proteins

Schematic of FNIII domains with a M-motif comprising of Loop I (FN, TNC, PTPRC and ITGB4-type) and Loop II (E/D or K-type).

Acknowledgement

We acknowledge F. Steinbach, A. Klein, C. Arnold for their technical support, the Cologne Cluster of Excellence proteomic facility and the EM facility of the Biocenter Basel. This work was funded by ANR-AngioFib, ANR-ACKITEC, INCa/Ligue contre le Cancer-ECMpact, Ligue contre le Cancer CCIRGE, University Strasbourg, INSERM and Swiss National Science Foundation to GO, the Deutsche Forschungsgemeinschaft (FOR2722/ B2) to MK and personal fellowships to WE (French ministry of research, MRT) and to CL (Chinese Scholarship Council, CSC). PAW discovered the M-motif, PAW, WE, TI, TL, CAF, CL, AK, MaMa, GC, MaMö performed experiments, BB, MK and GO supervised the study, and grants to GO and MK financed the work as indicated above.

Disclosure of potential conflict of interest

The discovery of MAREMO has been protected by patent No. 20315253.3 on “Immuno-modulatory compounds for use in the prevention and/or treatment of diseases resulting from Tenascin-C disorders”.

8.8. References

Adamsky, K., Schilling, J., Garwood, J., Faissner, A., and Peles, E. (2001). Glial tumor cell adhesion is mediated by binding of the FNIII domain of receptor protein tyrosine phosphatase β (RPTPβ) to tenascin C. Oncogene *20*, 609–618.

Arnoldini, S., Moscaroli, A., Chabria, M., Hilbert, M., Hertig, S., Schibli, R., Béhé, M., and Vogel, V. (2017). Novel peptide probes to assess the tensional state of fibronectin fibers in cancer. Nature Communications *8*, 1–13.

Arpel, A., Sawma, P., Spenlé, C., Fritz, J., Meyer, L., Garnier, N., Velázquez-Quesada, I., Hussenet, T., Aci-Sèche, S., Baumlin, N., et al. (2014). Transmembrane Domain Targeting Peptide Antagonizing ErbB2/Neu Inhibits Breast Tumor Growth and Metastasis. Cell Reports *8*, 1714–1721.

Baschong, W., and Wrigley, N.G. (1990). Small colloidal gold conjugated to fab fragments or to immunoglobulin g as high-resolution labels for electron microscopy: A technical overview. J. Elec. Microsc. Tech. *14*, 313–323.

Berlin, Ö., Samid, D., Donthineni-Rao, R., Akeson, W., Amiel, D., and Woods, V.L. (1993). Development of a Novel Spontaneous Metastasis Model of Human Osteosarcoma Transplanted Orthotopically into Bone of Athymic Mice. Cancer Res *53*, 4890–4895.

Bhattacharyya, S., Wang, W., Morales-Nebreda, L., Feng, G., Wu, M., Zhou, X., Lafyatis, R., Lee, J., Hinchcliff, M., Feghali-Bostwick, C., et al. (2016). Tenascin-C drives persistence of organ fibrosis. Nature Communications *7*, 11703.

Bloom, L., Ingham, K.C., and Hynes, R.O. (1999). Fibronectin Regulates Assembly of Actin Filaments and Focal Contacts in Cultured Cells via the Heparin-binding Site in Repeat III13. Mol Biol Cell *10*, 1521–1536.

Bober, M., Enochsson, C., Collin, M., and Mörgelin, M. (2010). Collagen VI is a subepithelial adhesive target for human respiratory tract pathogens. J Innate Immun *2*, 160–166.

Brellier, F., and Chiquet-Ehrismann, R. (2012). How do tenascins influence the birth and life of a malignant cell? J Cell Mol Med *16*, 32–40.

Chiquet-Ehrismann, R. (1995). Inhibition of cell adhesion by anti-adhesive molecules. Current Opinion in Cell Biology *7*, 715–719.

Chiquet-Ehrismann, R., Kalla, P., Pearson, C.A., Beck, K., and Chiquet, M. (1988). Tenascin interferes with fibronectin action. Cell *53*, 383–390.

De Laporte, L., Rice, J.J., Tortelli, F., and Hubbell, J.A. (2013). Tenascin C Promiscuously Binds Growth Factors via Its Fifth Fibronectin Type III-Like Domain. PLoS ONE *8*, e62076.

Deligne, C., Murdamoothoo, D., Gammage, A.N., Gschwandtner, M., Erne, W., Loustau, T., Marzeda, A.M., Carapito, R., Paul, N., Velázquez-Quesada, I., et al. (2020). Matrix-targeting immunotherapy controls tumor growth and spread by switching macrophage phenotype. Cancer Immunol Res.

Dhaouadi, S., Murdamoothoo, D., Tounsi, A., Erne, W., Benabderrazek, R., Benlasfar, Z., Hendaoui, L., Chiquet-Ehrismann, R., Boubaker, S., Orend, G., et al. (2020). Generation and characterization of dromedary Tenascin-C and Tenascin-W specific antibodies. Biochemical and Biophysical Research Communications *530*, 471–478.

Fonta, C.M., Arnoldini, S., Jaramillo, D., Moscaroli, A., Oxenius, A., Behe, M., and Vogel, V. (2020). Fibronectin fibers are highly tensed in healthy organs in contrast to tumors and virus-infected lymph nodes. Matrix Biology Plus 100046.

Giblin, S.P., and Midwood, K.S. (2014). Tenascin-C: Form versus function. Cell Adh Migr *9*, 48–82.

Giblin, S.P., Murdamoothoo, D., Deligne, C., Schwenzer, A., Orend, G., and Midwood, K.S. (2018). Chapter 21 - How to detect and purify tenascin-C. In Methods in Cell Biology, R.P. Mecham, ed. (Academic Press), pp. 371–400.

Hauzenberger, D., Olivier, P., Gundersen, D., and Rüegg, C. (1999). Tenascin-C inhibits beta1 integrin-dependent T lymphocyte adhesion to fibronectin through the binding of its fnIII 1-5 repeats to fibronectin. Eur J Immunol *29*, 1435–1447.

Huang, W., Chiquet-Ehrismann, R., Moyano, J.V., Garcia-Pardo, A., and Orend, G. (2001). Interference of tenascin-C with syndecan-4 binding to fibronectin blocks cell adhesion and stimulates tumor cell proliferation. Cancer Res. *61*, 8586–8594.

Hynes, R.O. (2009). The extracellular matrix: not just pretty fibrils. Science *326*, 1216–1219.

Hynes, R.O., and Naba, A. (2012). Overview of the Matrisome—An Inventory of Extracellular Matrix Constituents and Functions. Cold Spring Harb Perspect Biol *4*.

Ingham, K.C., Brew, S.A., and Erickson, H.P. (2004). Localization of a cryptic binding site for tenascin on fibronectin. J. Biol. Chem. *279*, 28132–28135.

Iyer, A.K.V., Tran, K.T., Griffith, L., and Wells, A. (2008). Cell surface restriction of EGFR by a tenascin cytotactin-encoded EGF-like repeat is preferential for motility-related signaling. J Cell Physiol *214*, 504–512.

Jachetti, E., Caputo, S., Mazzoleni, S., Brambillasca, C.S., Parigi, S.M., Grioni, M., Piras, I.S., Restuccia, U., Calcinotto, A., Freschi, M., et al. (2015). Tenascin-C Protects Cancer Stem-like Cells from Immune Surveillance by Arresting T-cell Activation. Cancer Res. *75*, 2095–2108.

Jimenez-Morales, D., Alex, Camposre R., Dollen, J.V., and Swaney, D. (2020). artMS: Analytical R tools for Mass Spectrometry (Bioconductor version: Release (3.11)).

Jones, F.S., and Jones, P.L. (2000). The tenascin family of ECM glycoproteins: Structure, function, and regulation during embryonic development and tissue remodeling. Developmental Dynamics *218*, 235–259.

Ksouri, A., Ghedira, K., Ben Abderrazek, R., Shankar, B.A.G., Benkahla, A., Bishop, O.T., and Bouhaouala-Zahar, B. (2018). Homology modeling and docking of AahII-Nanobody complexes reveal the epitope binding site on AahII scorpion toxin. Biochemical and Biophysical Research Communications *496*, 1025–1032.

Lamiable, A., Thévenet, P., Rey, J., Vavrusa, M., Derreumaux, P., and Tufféry, P. (2016). PEP-FOLD3: faster de novo structure prediction for linear peptides in solution and in complex. Nucleic Acids Res *44*, W449–W454.

Lichtarge, O., Bourne, H.R., and Cohen, F.E. (1996). An evolutionary trace method defines binding surfaces common to protein families. J Mol Biol *257*, 342–358.

Madeira, F., Park, Y. mi, Lee, J., Buso, N., Gur, T., Madhusoodanan, N., Basutkar, P., Tivey, A.R.N., Potter, S.C., Finn, R.D., et al. (2019). The EMBL-EBI search and sequence analysis tools APIs in 2019. Nucleic Acids Res *47*, W636–W641.

Martino, M.M., Briquez, P.S., Güç, E., Tortelli, F., Kilarski, W.W., Metzger, S., Rice, J.J., Kuhn, G.A., Müller, R., Swartz, M.A., et al. (2014). Growth factors engineered for super-affinity to the extracellular matrix enhance tissue healing. Science *343*, 885–888.

Matthew Ward, R., Venner, E., Daines, B., Murray, S., Erdin, S., Kristensen, D.M., and Lichtarge, O. (2009). Evolutionary Trace Annotation Server: automated enzyme function prediction in protein structures using 3D templates. Bioinformatics *25*, 1426–1427.

Midwood, K.S., and Orend, G. (2009). The role of tenascin-C in tissue injury and tumorigenesis. Journal of Cell Communication and Signaling *3*, 287–310.

Midwood, K.S., Hussenet, T., Langlois, B., and Orend, G. (2011). Advances in tenascin-C biology. Cell Mol Life Sci *68*, 3175–3199.

Midwood, K.S., Chiquet, M., Tucker, R.P., and Orend, G. (2016). Tenascin-C at a glance. Journal of Cell Science *129*, 4321–4327.

Moyano, J.V., Carnemolla, B., Domínguez-Jiménez, C., García-Gila, M., Albar, J.P., Sánchez-Aparicio, P., Leprini, A., Querzé, G., Zardi, L., and Garcia-Pardo, A. (1997). Fibronectin Type III5 Repeat Contains a Novel Cell Adhesion Sequence, KLDAPT, Which Binds Activated α4β1 and α4β7 Integrins. J. Biol. Chem. *272*, 24832–24836.

Orend, G., Huang, W., Olayioye, M.A., Hynes, N.E., and Chiquet-Ehrismann, R. (2003). Tenascin-C blocks cell-cycle progression of anchorage-dependent fibroblasts on fibronectin through inhibition of syndecan-4. Oncogene *22*, 3917–3926.

Pettersen, E.F., Goddard, T.D., Huang, C.C., Couch, G.S., Greenblatt, D.M., Meng, E.C., and Ferrin, T.E. (2004). UCSF Chimera—A visualization system for exploratory research and analysis. Journal of Computational Chemistry *25*, 1605–1612.

Rappsilber, J., Mann, M., and Ishihama, Y. (2007). Protocol for micro-purification, enrichment, pre-fractionation and storage of peptides for proteomics using StageTips. Nat Protoc *2*, 1896–1906.

Ruiz, C., Huang, W., Hegi, M.E., Lange, K., Hamou, M.-F., Fluri, E., Oakeley, E.J., Chiquet-Ehrismann, R., and Orend, G. (2004). Differential Gene Expression Analysis Reveals Activation of Growth Promoting Signaling Pathways by Tenascin-C. Cancer Res *64*, 7377–7385.

Sarrab, R.M., Lennon, R., Ni, L., Wherlock, M., Welsh, G., and Saleem, M. (2011). Establishment of conditionally immortalized human glomerular mesangial cells in culture, with unique migratory properties. American Journal of Physiology. Renal Physiology.

Sharma, A., Askari, J.A., Humphries, M.J., Jones, E.Y., and Stuart, D.I. (1999). Crystal structure of a heparin- and integrin-binding segment of human fibronectin. EMBO J. *18*, 1468–1479.

Shen, Z., Reznikoff, G., Dranoff, G., and Rock, K.L. (1997). Cloned dendritic cells can present exogenous antigens on both MHC class I and class II molecules. The Journal of Immunology *158*, 2723–2730.

Spenlé, C., Gasser, I., Saupe, F., Janssen, K.-P., Arnold, C., Klein, A., van der Heyden, M., Mutterer, J., Neuville-Méchine, A., Chenard, M.-P., et al. (2015). Spatial organization of the tenascin-C microenvironment in experimental and human cancer. Cell Adhesion & Migration *9*, 4–13.

Spenlé, C., Loustau, T., Murdamoothoo, D., Erne, W., Beghelli-de la Forest Divonne, S., Veber, R., Petti, L., Bourdely, P., Mörgelin, M., Brauchle, E.-M., et al. (2020). Tenascin-C Orchestrates an Immune-Suppressive Tumor Microenvironment in Oral Squamous Cell Carcinoma. Cancer Immunol Res *8*, 1122–1138.

Sun, Z., Velázquez-Quesada, I., Murdamoothoo, D., Ahowesso, C., Yilmaz, A., Spenlé, C., Averous, G., Erne, W., Oberndorfer, F., Oszwald, A., et al. (2019). Tenascin-C increases lung metastasis by impacting blood vessel invasions. Matrix Biology *83*, 26–47.

Tomko, L.A., Hill, R.C., Barrett, A., Szulczewski, J.M., Conklin, M.W., Eliceiri, K.W., Keely, P.J., Hansen, K.C., and Ponik, S.M. (2018). Targeted matrisome analysis identifies thrombospondin-2 and tenascin-C in aligned collagen stroma from invasive breast carcinoma. Sci Rep *8*, 12941.

Van Obberghen-Schilling, E., Tucker, R.P., Saupe, F., Gasser, I., Cseh, B., and Orend, G. (2011). Fibronectin and tenascin-C: accomplices in vascular morphogenesis during development and tumor growth. Int. J. Dev. Biol. *55*, 511–525.

Vangone, A., Oliva, R., and Cavallo, L. (2012). CONS-COCOMAPS: a novel tool to measure and visualize the conservation of inter-residue contacts in multiple docking solutions. BMC Bioinformatics *13*, S19.

9. Discussion and Perspectives

Cancer cannot be simply reduced to tumor cells. Indeed, tumors are now described as complex “ecosystems” where every actor of the TME plays important roles. The matrix protein TNC is one of the fibrillar molecules constituting the ECM. Whereas TNC is highly expressed during embryogenesis, its expression in adults is decreased and limited to specific tissues such as tendons, ligaments and others. Yet, TNC can be abundantly produced during tissue repair and in inflammatory environments. Thus, in pathological conditions implicating constant tissue remodeling and chronic inflammation like cancer, TNC is highly expressed and has been associated with poor prognosis in several cancers (Midwood et al., 2016; Orend et al., 2014).

There is now good evidence that TNC promotes breast cancer progression by promoting pro-tumoral mechanisms at several levels of tumor development (Oskarsson, 2013). Indeed, our team and others have demonstrated that TNC can promote cancer cell proliferation, migration and invasion in early tumors; as well as cancer cell dissemination and survival in the blood circulation, leading to the formation of lung metastasis and finally poor outcome for the patients (Oskarsson et al., 2011; Sun et al., 2019; Appendix I). We also observed an immune modulatory impact of TNC dysregulating immune cells and cytokines in favor of cancer progression (Deligne et al., 2020; Appendix II)(Murdamoothoo et al., in revision). We also described an immune suppressive effect of TNC in a head and neck tumor model (Spenlé et al., 2020, Appendix III). During my thesis, I worked on two projects with the aim to describe and understand the regulation of the cytokine TRAIL by TNC in our NT193 model (Manuscript I), and to develop new peptides targeting and inhibiting TNC functions (Manuscript II).

In my main project, I developed tools and protocols to study the impact of TNC on TRAIL signaling in breast cancer. According to the current knowledge about TRAIL apoptosis sensitivity in cancer cells where cell plasticity seems to play a role, I have derived epithelial and mesenchymal clones of the NT193 murine cell line. By using these clones, I demonstrated that the NT193E cells express more TRAIL and its death receptor DR5 than the NT193M cells. On the other hand, NT193M cells secrete high amounts of TNC. Interestingly, the TRAIL produced by the NT193 cells is not able to activate apoptosis in these cells whereas combined treatment of TRAIL with the DR5 stabilizing agonist MD5-1 induced apoptosis. In 2D culture and 3D spheroids models, I demonstrated that TNC can potentially inhibit the anti-cancer killing effect of TRAIL combined therapy by activating TGFβ pro-

survival pathways and via sequestrating TRAIL, thus decreasing the activation of DR5. Knowing that TRAIL can initiate non-apoptotic signaling in the TME, I assessed the role of TRAIL produced by the NT193E cells grafted in syngeneic mice. By using NT193E cells knockdown for TRAIL, I observed that TRAIL produced by the cancer cells had a negative impact on tumor growth, potentially by recruiting immune cells such as dendritic cells and macrophages. I confirmed *in vitro* that these myeloid cells were more attracted by NT193E cells expressing TRAIL, presumably via CXCR4 signaling. I also observed that TNC was associated with tumor growth. As we observed that TNC can inhibit the expression of TRAIL in the previously described MMTV-NeuNT and the NT193 grafting models, I confirmed *in vitro* that TNC decreases TRAIL expression in the NT193E cells, potentially through integrins α4β1 and/or α9β1 signaling. Finally, the investigation of publicly available data demonstrated that high expression of TNC coupled to low expression of TRAIL can be associated with poor prognosis in breast cancer patients. Taken together, the results obtained in this first manuscript show that TNC is dysregulating TRAIL. On one hand, TNC may protect cancer cells against TRAIL used as anti-cancer therapy. On the other hand, TNC may prevent the retro-control that TRAIL may have on the tumor by decreasing its expression.

In my second project, I worked on new peptides targeting TNC, with the aim to develop novel tools for anti-cancer therapy. Since TNC is known to interact with other proteins and soluble factors, we first looked for similarities in the amino acid sequences of FN-type III repeats in FN and TNC, as it is known that evolutionary conserved sequences have an important function. Indeed, we detected high homology between TNIII and FNIII, and we demonstrated that FN was prone to interact with TNC through TN5. Thus, by bioinformatic modeling we postulated that two loops were important for the binding of TNC and FN, constituting a MAtrix REgulating MOtif, or “MAREMO”. We designed peptides mimicking the MAREMO sequences of FN5 (P5) and FN13 (P13) and tested their potential to modulate TNC functions. As P5 and P13 were able to specifically bind to TNC, we demonstrated that they can inhibit the binding of TNC to soluble factors such as CXCL12, CCL21, TRAIL, TGFβ and to FN itself. Moreover, P5 and P13 can block TNC functions as we observed that they decrease the chemoretention activity of TNC, its anti-adhesive properties, and its impact on cells matrix proteins production. Furthermore, I highlighted a potential use of the peptides in TRAIL therapy, as they can inhibit the protective effect of TNC against TRAIL sensitivity. Finally, I observed strong similarities between FN-type III repeats constituting many different proteins such as Col12 or CD45. Knowing that TNC, FN and Col12 can tightly colocalize in

tumors, or that TNC can regulate immune cells in cancer (maybe via directly interacting with CD45), the potential use of the peptides in anti-cancer therapies should require more attention in the future.

9.1. The cytokine TRAIL is expressed by NT193 cells

TRAIL has been originally described as a killing cytokine produced by immune cells in order to eliminate abnormal cells, such as cancer cells or infected cells (Almasan and Ashkenazi, 2003). However, more recent publications demonstrated that TRAIL can be produced by other cell types and can activate non-apoptotic pathways in abnormal, as well as in normal cells (von Karstedt et al., 2017). In our study, we observed that the murine breast cancer cell line NT193 expressed the gene *Tnfsf10* and the TRAIL protein. At a first glance, it appears counterintuitive that cancer cells express a cytotoxic molecule that could induce their own death. Yet, we observed no cell death, in particular by AO/EB staining, when culturing the NT193 pool, the NT193M, and notably the NT193E subclone that express the highest TRAIL levels.

One could imagine that NT193E cells possess a basal resistance to TRAIL apoptosis. In fact, we observed that treating the cells with TRAIL alone or with MD5-1 alone did not induce cell death, even if TRAIL could trigger a small increase in caspases 3 and 7 activation. No apoptosis was detected by using high concentration of TRAIL (500 ng/mL) whereas epithelial cancer cells expressing E-cadherin can be killed at lower concentration (50-100 ng/mL) (Lu et al., 2014). However, by combining TRAIL and MD5-1, we were able to induce a strong activation of the caspases and of cell death. These results indicate that the NT193E cells are sensitive to TRAIL apoptosis in case of DR5 crosslinking and addition of stable trimers of TRAIL. It is important to note that we used recombinant trimers of TRAIL stabilized by cysteine bridges since it is known that simple monomers of TRAIL are not efficient to kill cancer cells (Lemke et al., 2014). Our results therefore suggest that in basal conditions, the stability and the oligomerization status of TRAIL and DR5 produced in the NT193E cells is not sufficient to activate apoptosis.

It has been described in several studies that cancer cells can express TRAIL without dying (Huber et al., 2005; Inoue et al., 2002; von Karstedt et al., 2015). Interestingly, von Karstedt et al. (2015) demonstrated that *KRAS*-mutated cancer cells expressed and used both TRAIL and TRAIL-Rs to activate Rac1, promoting tumor growth and metastasis formation. In this

study, the authors focused on pro-tumoral roles of endogenous TRAIL without investigating the sensitivity to exogenous TRAIL. The endogenous TRAIL was not quantified but immunoblots are not in favor of high expression of TRAIL by the cancer cells, meaning that small amounts of endogenous TRAIL could activate non-apoptotic signaling. However, as we observed lower tumor growth when NT193E cells express TRAIL, it is unlikely that endogenous TRAIL promotes pro-tumoral signaling in the NT193 tumor cells. This hypothesis is also defended by the fact that downregulating DR5 in the NT193E cells did not impact tumor growth. The other possibility for endogenous TRAIL is to regulate stromal cells. Indeed, Inoue et al. (2002) observed that endogenous TRAIL produced by HT-29 colon cancer cells can induce cell death in Jurkat cells. Moreover, Huber et al. (2005) demonstrated that human colorectal cancer cells can secrete microvesicles containing TRAIL, as well as FasL, inducing apoptosis in T-lymphocytes. Knowing that TRAIL has many immunomodulatory properties (Sag et al., 2019), it is therefore possible that endogenous TRAIL expressed by NT193E cells impacted immune cells, which indeed is the case in NT193 tumors (see below).

9.2. Endogenous TRAIL induces tumor infiltration of myeloid cells

Studies over the last decade demonstrated that TRAIL is an important regulator of the immune response (Bossi et al., 2015; Sag et al., 2019). As TRAIL appears to regulate selection of mature immune cells via induction of apoptosis, it can also modulate the activation and the functions of immune cell subtypes. In our study, we observed by flow cytometry that downregulating the production of endogenous TRAIL lowered the amount of activated DCs and MPs in the tumors. Moreover, the quantity of these myeloid cells, measured by flow cytometry and IF, was also reduced in conditions of low TRAIL. Since we observed more DCs and MPs when the NT193E shC cells express TRAIL, it is unlikely that the cytokine induces apoptosis in the two immune cell types. However, TRAIL may be responsible for myeloid cell chemoattraction and activation.

Chemotactic cytokines (chemokines) and their receptors play major roles in the immune response, in particular by directing migration of immune cells toward gradients of chemokines leading to tissues requiring the presence of immune cells (Hughes and Nibbs, 2018). This phenomenon is particularly important during inflammation and anti-cancer immune responses. By RNA sequencing analysis of NT193E tumors shC and shTRAIL, we observed a significant decrease of CXCR4, that we confirmed by qRTPCR. Since we already observed

modulations of CXCR4/CXCL12 signaling in the NT193 tumors (Murdamoothoo et al., in revision), we postulated that TRAIL may regulate this signaling. It has been described that TRAIL can modulate CXCR4 expression through miR-146a. Both possibilities have been observed as TRAIL could induce miR-146a in MDA-MB-231 cells resulting in a decrease of CXCR4, and of cancer cells migration (Wang et al., 2013); or TRAIL could reduce miR-146a expression in HTR8/SVneo trophoblastic cells increasing CXCR4 and cell invasion (Xiao et al., 2020). Thus, it is possible that the endogenous TRAIL produced by the NT193 cells induces the expression of CXCR4 in the myeloid cells surrounding the tumor nest, leading to higher tumor infiltration.

On the other hand, TRAIL has also been described as a potential inducer of chemokines, such as CCL2 (Hartwig et al., 2017). In this study, the authors demonstrated that treating TRAIL-resistant cancer cells with TRAIL can activate non-apoptotic pathways leading to CCL2 expression and chemoattraction of MPs. Moreover, the attracted MPs were preferentially M2 MPs. Since the NT193E cells did not die due to the endogenous TRAIL, it is possible that TRAIL cytokine has an autocrine effect on the cancer cells, leading to the secretion of chemokine(s) attracting the myeloid cells. CCL2 is a good candidate to be investigated in the future since it is has been observed that CCL2 could activate CXCR4 signaling (Campbell et al., 2007). Moreover, one can imagine that TRAIL regulates the expression of CXCR4 via an intermediate molecule. Since we also observed a reduced expression of *Mapk1* and *Mapk3*, two downstream genes in CXCR4 signaling in TRAIL knockdown tumors, both possibilities are probable (endogenous TRAIL inducing CXCR4 activation and/or expression). We then decided to use the DC2.4 and RAW267 cells that both express CXCR4 (Figliuolo da Paz et al., 2019; Takiguchi et al., 2014) in 2D matrigel invasion and 3D spheroids infiltration assays to determine the effect of endogenous TRAIL and indeed observed infiltration when the tumor cells expressed TRAIL. By using the CXCR4 antagonist AMD3100, we could show that CXCR4 activity was required for TRAIL to induce myeloid cells attraction. In addition, by analyzing the proteins secreted by the NT193E cells shC and shTRAIL by mass spectrometry, we detected several soluble factors such as TGFβ2, TGFβ3, X3CL1 and CSF-1 to be more abundant in TRAIL expressing cells. These molecules regulate CXCR4 expression and thereby the attraction on the DC2.4 and RAW267 cells (Ferretti et al., 2011; Korbecki et al., 2020; Lee et al., 1999; Mylonas et al., 2019; Stephenson et al., 2019). Notably, no chemokines regulating CXCR4 activation were differently expressed by the NT193E shTRAIL cells in comparison to NT193E shC cells. As we recently demonstrated

that CXCL12 was secreted into the tumor nest (Murdamoothoo et al., in revision), an increase of CXCR4 on the cell surface of the myeloid cells could explain the higher infiltration of DCs and MPs toward the cancer cells when they expressed TRAIL.

9.3. TRAIL regulates macrophages and phagocytosis in tumors

One major role of macrophages is to recognize and phagocytose pathogens in order to present antigens stimulating the immune response (Freeman and Grinstein, 2014). In cancer, it is known that MPs can 'eat' entire cancer cells by phagocytosis (Pathria et al., 2019). For instance, phagocytosis can be modulated by the 'do not eat me' molecule CD47 that is expressed by normal cells, and cancer cells in order to avoid phagocytosis (Liu et al., 2017; Zhao et al., 2016). In our study, we observed a decrease of MPs quantity (in particular with a M2 phenotype) when endogenous TRAIL was lowered. Moreover, by IF imaging, we observed the presence of numerous holes containing CD68+ MPs in the tumors. We therefore hypothesize that the MPs recruited to the tumor may perform phagocytosis, limiting the tumor growth either directly or by activating adaptive immunity.

TRAIL can modulate the activity of immune cells (Bossi et al., 2015; Sag et al., 2019). However, studies are generally focused on the apoptotic properties of TRAIL, even on immune cells, and very little is known about the non-apoptotic regulation of TRAIL in immunity. On MPs, it has been described that TRAIL can trigger a M2 phenotype promoting tumor growth (Hartwig et al., 2017). MPs with a M2 phenotype are generally characterized as pro-tumoral MPs due to their anti-inflammatory properties. Yet, recent studies demonstrated that TAMs with a M2 phenotype can be reprogrammed toward anti-cancer properties, increasing phagocytosis (Gu et al., 2018; Lin et al., 2019). Our RNA sequencing analysis revealed that several genes associated with M2 polarization and phagocytosis (*Atg3, Atg5, Tgfβs*) are upregulated in presence of endogenous TRAIL, indicating a potential relevance of this mechanism. The presence of CD68+ MPs in holes scattered in the tumors is intriguing and gives the impression that these areas have been cleared by the MPs. The holes are delimited by CK8/18+ cancer cells, indicating that these structures are not blood vessels. IF staining for endothelial cells (CD31+) and blood vessels leakage (fibrinogen, von Willebrand factor) have to be made to confirm the presence of non-vascular holes. Deeper analyses have to be done on these holes containing MPs as they may contain other immune cells and potentially be a key point in the anti-tumoral immune response.

9.4. TNC promotes tumor growth and modulates TRAIL function

In breast cancer, TNC is a factor of poor prognosis for patients by promoting several pro-tumoral mechanisms, from early tumor development to metastasis formation (Oskarsson, 2013). In our study, we observed different impacts of TNC on tumor development. We can already see that high TNC expression in the WT hosts promotes bigger tumors. Yet, concerning TNC regulating TRAIL, we observed in general an effect of TRAIL knockdown when TNC is expressed by the host, indicating interactions between the processes mobilized by TNC and TRAIL.

We recently described pro-metastatic impacts of TNC in breast cancer (Sun et al., 2019; Murdamoothoo et al., in revision). In the MMTV-NeuNT and NT193 grafting models, we demonstrated that TNC accelerates the appearance of early breast tumors and the process of blood vessel invasions (BVI) as precursor of lung metastasis. Moreover, we described two opposing roles of TNC during the development on the primary tumor, depending on whether cancer cells or stromal cells express TNC (Murdamoothoo et al., in revision). Our current results support the published results, as we observed bigger tumors in WT hosts than in KO hosts. Yet, it is important to note that we only grafted NT193E cells compared to the past studies that used the NT193 pool containing NT193M cells expressing high amounts of TNC. Therefore, as we could observe that NT193E tumor growth is different depending on TNC after four weeks of development, we could not reproduce the initial tumor rejection induced by TNC coming from the cancer cells. Surprisingly, host TNC does not modify lung invasion measured by qRTPCR. This result could be explained by the incomplete absence of TNC in the KO host. Indeed, we observed by IF staining that TNC is expressed in the KO tumors, by the NT193E cells. As we could already see that these cells express a low amount of TNC in culture and in the spheroids, it appears that NT193E cells can produce TNC in the TME after several weeks of growth. We cannot exclude that the TME stimulates TNC expression by the NT193E cells, thus promoting more EMT and more TNC expression that ablate the previously observed differences between WT and KO conditions. In the next studies, TNC expression must be knock out in the NT193E cells to avoid this issue.

TNC seems to play an active role in TRAIL anti-tumor mechanisms as most of the effects observed in low TRAIL condition appear in presence of host TNC. To summarize, combined high TNC and low TRAIL promote better cell survival and proliferation, and lower myeloid cell infiltration, altogether causing bigger tumors and more lung metastasis. In our recent studies, we have demonstrated that TNC can impact the immune response (Deligne et al., 2020;

Spenlé et al., 2020; Murdamoothoo et al., in revision). In the NT193 grafting model, we and collaborators have found that TNC forms TMT that can corrupt immune cells. For instance, TNC can polarize the MPs toward a pro-tumoral phenotype via TLR4, explaining the bigger tumors in WT hosts (Deligne et al., 2020). Furthermore, it has been described that TNC induces phagocytosis in glioma (Ma et al., 2019). Then, when TRAIL is expressed, additive MP attraction and phagocytosis activation may lead to tumor repression. We also described that TNC can bind to chemokines and cytokines (such as CCL21, CXCL12, TRAIL), thus impairing the recruitment and the activation of DCs and T-cells (Spenlé et al., 2020; Murdamoothoo et al., in revision, Erne et al., in preparation). As TNC promotes the attraction of the DCs and T-cells in the stroma, TRAIL may contribute to release and activate a part of these cells in the tumor nest so they can play their roles against cancer. We mostly investigated in detail the impact of TNC and TRAIL on MPs. However, MPs and DCs are the basis of the immune response. Knowing that all the immune cell types can be sensitive to TRAIL apoptosis and/or non-apoptotic signaling (Sag et al., 2019), it would be important to investigate the status of the other immune cell types, in particular the different T-cell sub populations since we know that they can be affected by TNC in the tumor (Spenlé et al., 2020; Murdamoothoo et al., in revision).

9.5. TNC decreases TRAIL sensitivity of NT193 through TGFβ signaling and EMT plasticity

Since its discovery, TRAIL has been intensively studied for its pro-apoptotic properties. Since the major role of TRAIL is to specifically kill cancer cells and not normal cells, this cytokine could be a magic bullet reinforcing other anti-cancer targeting therapies (Almasan and Ashkenazi, 2003; Lemke et al., 2014). However, one major obstacle faced by the clinical trials using TRAIL is the appearance of apoptosis resistance mechanisms. Indeed, in breast cancer it is already known that not every cell line is sensitive to TRAIL apoptosis (Charafe-Jauffret et al., 2006; Neve et al., 2006; Rahman et al., 2009b). We have generated the NT193E and NT193M cells according to the resistance mechanisms that may occur through EMT. As it is known that the stabilization of DR5 into protein complexes containing E-cadherin is required for TRAIL sensibility (Lu et al., 2014), we could use these two cell lines with a clear epithelial phenotype (E-cadherin expression in NT193E cells) and a mesenchymal

phenotype (vimentin expression in NT193M cells) to address cell responses toward TRAIL in context of cellular plasticity.

In our recent article, we described that TNC can trigger resistance to staurosporin-induced apoptosis via TGFβ-mediated EMT in the NT193 pool (Sun et al., 2019). By repeating the experiment with TRAIL and the NT193E cells, we were able to see that TNC could induce TRAIL-resistance after two hours of treatment. In this short time frame, we did not observe phenotypical changes related to EMT but we suppose that pro-survival pathways such as PI3K/AKT, SMAD or ERK can be already activated and promote cell survival as we had seen their activation upon TNC treatment (Sun et al., 2019). Moreover, as we observed a decrease of DR5 expression by the NT193M cells, the EMT induced by TNC could reduce TRAIL sensitivity in the NT193E cells by lowering DR5 expression. It is possible to generate TRAIL-resistant cancer cells by selecting in culture cells that are surviving to low doses of TRAIL (Wu et al., 2005). It would be interesting to treat the NT193E cells with TNC on a long period in order to describe the EMT and the acquisition of TRAIL-resistance over time. These observations present a strong interest for TRAIL therapies because high expression of TNC has been described in several types of cancer (reviewed in Orend et al., 2014). Since TNC potentially induces TRAIL-resistance, it would be relevant to target TNC during TRAIL therapies in order to reestablish TRAIL specific sensitivity in cancer, as for example as we are currently intending to do with the MAREMO peptides P5 and P13.

9.6. TNC potentially inhibits the control of tumor growth by TRAIL via decreasing its expression through α9β1/α4β1 integrins

As a starting point of this study, we observed a decrease of TRAIL expression when TNC was highly expressed in primary tumors of the MMTV-NeuNT and NT193 grafting models. As high TNC was associated with less apoptosis in the tumors, we postulated that TNC may decrease TRAIL expression leading to a better survival of breast cancer cells. In cell culture, we also observed that NT193E cells treated with TNC have a lower expression of *Tnfsf10*, supporting our hypothesis. Moreover, we measured a lower expression of TRAIL by the NT193M cells that produce high amounts of TNC, in comparison to the NT193E cells. It is known that TNC can interact with several cell surface receptors and induce intracellular signaling (Midwood et al., 2016). For instance, TNC can interact with TLR4 on macrophages and fibroblasts, modulating inflammation (Midwood et al., 2009). Moreover, we recently

described the induction of EMT through TGFβ signaling in the NT193 grafting model, via TGFβR1 (Sun et al., 2019). Furthermore, we recently dissected the molecular mechanism of cell migration activated by TNC via interaction with α9β1 integrins (Sun et al., 2018). In the latter study, it was demonstrated that the interaction of cells with TNC involving α9β1 integrins inhibited the polymerization of actin stress fibers, dysregulating the transcription factors YAP and MKL1, as well as YAP target gene expression, leading to promoting amoeboid-like migration that can occur during metastasis development.

By using inhibitors of known receptors interacting with TNC, we wanted to see if the repression of TRAIL by TNC can be inhibited. Indeed, we observed that antagonizing the integrins α9β1 and α4β1 with the dual integrins inhibitor BOP (Cao et al., 2014) restored the expression of TRAIL by the NT193E cells. Since we only investigated gene expression, it will be important to confirm these results with protein expression analysis, and to determine exactly which integrin is implicated by using more specific antagonists. As an inducer of apoptosis, TRAIL expression is highly regulated by several transcription factors (Allen and El-Deiry, 2012; Wang et al., 2000). Knowing that integrin mediated signaling can lead to the regulation of transcription factors, the regulation of *Tnfsf10* expression by transcription factors regulated by TNC and integrins interaction should be investigated in more details.

By investigating publicly available human breast cancer patient data, we found that TNC high expression in breast cancer can be associated with low expression of TRAIL and poor overall survival in cancer patients. Interestingly, as we described an anti-tumor effect of TRAIL via recruiting myeloid cells to the tumor, the Kaplan Meier analysis also demonstrated that low expression of markers such as TRAIL is associated with poor prognosis. Also, when TNC levels are low, but TRAIL is high, patients survive longer. As a conclusion of this study, we propose that TNC, that can be highly expressed in cancer tissue, exerts an inhibitory effect on TRAIL expression, leading to a decrease of myeloid cells recruitment and progression of the disease. Moreover, the canonical effect of TRAIL should not be forgotten. As immune cells such as NK cells and T-cells express TRAIL in order to kill cancer cells, the interaction between immune cells and TNC (Deligne et al., 2020; Hauzenberger et al., 1999; Jachetti et al., 2015; Spenlé et al., 2020) may also repress TRAIL expression and killing activity, and further contribute to tumor growth (Smyth et al., 2003).

9.7. Peptides mimicking TNC-interaction sites of FN can bind to TN5

The structure and function of a protein is determined by its amino acids sequence. Interestingly, sequences with an important function are often conserved amongst species (Lichtarge et al., 1996), meaning that some properties and functions of a protein can be predicted by recognizing specific patterns of amino acids. Then, in the early 2000's, it has been understood that proteins are an assembly of several patterns, or domains, tuning their properties (Doolittle and Bork, 1993). For example, the matrix protein FN is a chain of three types of domains FNI, FNII and FNIII specializing the protein domains as interaction platforms for soluble factors, cell surface receptors and other matrix proteins (Pankov and Yamada, 2002). The FNIII domain is particularly interesting since this module has been identified in dozens of other proteins, such as TNC and other matrix molecules. Thus, FNIII domains may be important to promote the interaction of proteins with their microenvironment (Campbell and Spitzfaden, 1994; Doolittle and Bork, 1993).

Our first results demonstrated that FN5 and FN13 can bind to TNC. Previous studies support our observation as it was shown that TNC-binding sites in FN are located in FN-HepII (FN13) and FN-HepIII (FN4-6)(Huang et al., 2001). Moreover, interaction between FN and TNC could be inhibited by syndecan-4, that is known to bind to FN13 (Bloom et al., 1999; Huang et al., 2001; Orend et al., 2003). Indeed, we observed by negative EM imaging that recombinant FN4-6 and FN12-14 molecules bind in the middle of TNC, potentially in TN5. Interestingly, the fragments bound to TNC through their middle domain FN5 and FN13, forming crossed structures. As FN is described to assemble as aligned dimers in fibers (Tucker, 2018), the structure of FN binding to TNC is not described. One can imagine that the complete molecules only interact through the MAREMO located on FN-type III domains of FN and TNC, forming bonds with the rest of the molecules 'floating'; or FN and TNC may tightly aligned as in FN fibrils. Negative EM imaging of the full length FN and TNC molecules interacting with each other could bring more information on that subject. We therefore compared FN5, FN13 and TN3-6 domains as it is described that FN interacts with TNC in this region (Obberghen-Schilling et al., 2011). By using bioinformatic tools, we were able to identify the loops I and II in FN5/FN13 with the corresponding sequences TDST/TETT (Loop I) and NLQPASEY/ GLQPGTDY (Loop II), separated by 42 amino acids, but structurally close. We named these sequences Matrix REgulating MOtif "MAREMO" or M-motif as we postulated that they are mediating the interaction of TNC with FN. We generated peptides P5 (STDSTSAPASNLQPASEYS) and P13 (STETTSAPASGLQPGTDYS), with the

corresponding scrambled peptides S5 (STTDSSAPASYESAPGLNS) and S13 (STTETSAPASYDTGPQLGS) in order to mimic the MAREMO present in FN5 and FN13, so to investigate how they affect the interaction of FN and TNC.

Via negative EM imaging of colloidal gold-beads coated with the peptides, we observed and quantified a binding of P5- and P13-coated beads around TN5. Interestingly, the binding was not affected by heparin, indicating that the binding site of the peptides is not located on a HBS. As we saw that P5 and P13 both preferentially bind to TN5, we supposed that this domain of TNC is the most prominent to be targeted by the peptides and may impact binding of TNC to FN. Indeed, by measuring the binding of FN4-6 and FN12-13 fragments on TNC in presence of the peptides, we observed that only P5 and P13, not the scrambled peptides, inhibited the interaction of the FN fragments with TN5. It is important to note that P5 and P13 can also block the homophylic interaction of FN4-6 and FN12-14 fragments, indicating that the peptides may also recognize M-motifs in FN5 and FN13. How can we improve the targeting of TN5? A detailed analysis *in silico* of the docking probabilities of the peptides with each domain of TNC should be realized in order to detect the key amino acids responsible of the binding and the distinct preference to TN5. Then, recombinant fragments of TNC containing directed amino acids mutations of the predicted contact sites could be engineered and incubated with the peptides to clearly identify the amino acids sequence targeted by the peptides. Moreover, it is important to note that FN type-III repeats are also located in other proteins. In order to avoid unspecific targeting, further studies, *in silico* docking and point mutations are required to refine the peptide specificity and to confirm TN5 as the binding domain.

9.8. The peptides inhibit the binding to TNIII HBS

The TN5 domain of TNC is known to be an interaction platform for soluble factors. For instance, TGFβ1, PDGF-BB, NT-3, and FGF-2 binding to TN5 has previously been detected by SRP (De Laporte et al., 2013). In this study, the authors predicted an HBS in TN5 that plays a significant role in molecular interactions with the soluble factors that they have studied. Indeed, HBS are constituted of positively charged amino acids, such as lysine (K) and arginine (R), that can interact with negatively charged heparin, as observed in TN5 (Weber et al., 1995). De Laporte et al. (2013) observed that increasing concentrations of heparin can inhibit the interaction of some of the studied soluble factors to TN5, indicating that the binding properties of TN5 to soluble factors depends on the HBS.

In our study, we demonstrated that heparin cannot inhibit the binding of P5 and P13 to TNC, indicating that the peptides bind to another region of TN5, namely the M-motif. Our recent results describe the binding of the cytokines CXCL12, CCL21 and TRAIL to TNC, likely to the TN5 domain (Spenlé et al., 2020; Murdamoothoo et al., in revision; Erne et al., in preparation). CXCL12, CCL21 and TRAIL do not have FNIII domains, nor a MAREMO sequences. We observed that these soluble factors can bind to TNC through HBS, as heparin inhibited this interaction. Moreover, since binding of CXCL12, CCL12 and TRAIL-coated beads overlaps with that of TGFβ1-coated beads, as observed by negative EM imaging, we propose that these four soluble factors bind in TN5, as it was described for TGFβ1 (De Laporte et al., 2013). When TNC was pre-incubated with P5 and P13, it was interesting to see that the interaction of CXCL12, CCL21 and TRAIL to TN5 was abrogated. If P5 and P13 have a net charge of -2 at pH 7.0 (due to aspartates (D) and glutamates (Q)), they cannot directly block the HBS since they do not bind to this region. In fact, S5 and S13 also have a net charge of -2 at pH 7.0 and do not bind to TNC, confirming that the charge of the peptides is not responsible for the binding to TN5, and the subsequent competition with CXCL12, CCL21 and TRAIL. However, it has been described that binding of heparin to FNIII repeats in FN induces a conformational change of the protein affecting the interaction with soluble factors (Mitsi et al., 2006; Smith et al., 2009). The structural models of FN and TNC that we use show that FNIII repeats can assemble as a chain of domains, with the M-motif close to the intersection between two domains. One can imagine that the binding of the peptides to this region may alter the conformation of the chain (e.g. by modifying the angle between the domains), sterically blocking the interaction with soluble factors. In addition, the conformational changes may affect the global structure of big molecules like TNC and deeply impact the formation of matrix fibers, relevant in cancer and fibrosis. This hypothesis should be verified with in silico modeling and predictions, supported by EM imaging of TNC monomers and hexamers incubated with the peptides.

9.9. MAREMO peptides decrease immunomodulation mediated by TNC

Chemokines play a major role in the immune response as they control leukocytes activation and migration (Griffith et al., 2014). In pathologies like cancer, chemotaxis is crucial for immune surveillance and responses to tumor cell proliferation (Dunn et al., 2004). We recently described pro-tumoral effects of TNC through disrupting the immune response

(Spenlé et al., 2020; Murdamoothoo et al., in revision). In our 4NQO-induced OSCC model, we observed that TNC can generate an immune suppressive microenvironment via CCL21/CCR7 signaling, through inducing immunomodulatory markers, such as CCR7 and CCL21, and sequestrating the DCs by binding to CCL21. In addition, our results in the NT193 grafting model demonstrate that TNC can impact also sequestration of the CD8+ T-cells via binding to CXCL12, inhibiting tumor infiltration by the lymphocytes (Murdamoothoo et al., in revision).

As we found that CXCL12 and CCL21 can bind to TNC, we wanted to know if the peptides can inhibit the immunomodulatory effects of TNC. By quantifying the number of DC2.4 cells retained by a coating of matrix proteins during cell migration in presence of CXCL12 or CCL21, we could observe that TNC kept more DCs in presence of the chemokines than FN and Col I, indicating that CXCL12 or CCL12 were locally concentrated in TNC coating. Then, by preincubating the coating with the peptides, we saw that P5 and P13 decreased the proportion of DCs immobilized on TNC. These results demonstrate that preincubating TNC with the peptides can block the binding with the chemokines and limit the chemoretention of DCs. Up to date, we are the first to demonstrate that TNC can act as a reservoir of chemokines, modulating the immune activity. Previous studies have described interactions between TNC and cells through the presentation of soluble factors. For instance, it has been demonstrated that TNC can bind to soluble Wnt3a and activate the Wnt/β-catenin signaling in stem cell niches of whiskers, as Wnt3a may be locally concentrated to the cell surface by TNC (Hendaoui et al., 2014). This capacity of TNC to sequestrate soluble factors may certainly have an important role during embryogenesis. As it is known that TNC acts as a scaffold for neuronal cells migration (Faissner, 1997; Fukamauchi et al., 1996; Gurevicius et al., 2009), one can imagine that concentrating growth factors and cytokines may play a major role in the orchestration of neurodevelopment.

We also observed that co-treating DCs and LECs with TNC and the peptides leads to repression of *Ccr7* and *Cd86.* TNC stimulated the expression of *Cxcl12*, *Cd86* and *Ccr7* in DC2.4 cells and *Ccl21* in LECs. Spenlé et al., (2020) demonstrated that this activation was mediated by α9β1 integrin that was discussed to bind in TN3, yet proof for a direct complex of TN3 with α9β1 integrin is missing (Yokosaki et al., 1994, 1998). Our negative EM imaging results show that the peptides bind to the TN5 domain, potentially also including nearby FN type-III domains. Moreover, the interaction of the peptides may alter the conformation of TNC

and affect the binding of proteins on the whole TNC molecule, maybe having long distance effects potentially impacting a possible α9β1 integrin / TN3 interaction.

9.10. MAREMO peptides regulate ECM in cancer and fibrosis

One major role of the ECM is to form a scaffold structuring tissues and organs (Frantz et al., 2010). In tissues, matrix fibers are frequently constituted of several matrix proteins. Interestingly, the association of certain ECM molecules can have an important impact in pathological conditions. For instance, co-expression and colocalization of FN and TNC in cancers, such as OSCC and glioma is associated with poor patient outcome (Carnemolla et al., 1999; Sundquist et al., 2017). Moreover, the recent peptide PL1 has been developed to target both TNC and FN based on the tight relation between FN and TNC in cancer, and presented promising results to target brain tumors (Lingasamy et al., 2019). In addition, co-expression of TNC and FN has also been described in fibrotic diseases (Cohen et al., 2016; Estany et al., 2014; Shinohara et al., 2014). As TN1-5 domains contain several binding sites for matrix proteins and integrins, including FN (Obberghen-Schilling et al., 2011), we hypothetize that targeting TN5 with the MAREMO peptides may inhibit the propensity of TNC assembly with FN and other molecules.

It is known that TNC can bind to FN on a matrix coating, inducing cell rounding in culture (Huang et al., 2001). In our study, we used the NT193M and the KRIB cells to confirm that FN/TNC coating triggered cell rounding instead of cell spreading on FN. By incubating TNC with the peptides, we observed restoration of cell spreading, indicating that the anti-adhesive effect of TNC was inhibited by the peptides. IF staining of the cells also revealed that focal adhesions were restored on FN/TNC when the peptides were used, indicating that integrins α5β1 and syndecan-4 responsible for the adhesion of the NT193M and KRIB cells are functional again. These results bring us to see two possibilities for TNC anti-adhesive properties. On one side, the interaction sites between integrins and FN may be covered when TNC is added to FN, thus by incubating TNC with the peptides, we block FN/TNC binding and restore the availability of the syandecan-4 binding site. On a second hand, the peptides could cover interaction sites between TNC and cells that repress cell adhesion, as we previously observed with integrins α9β1/YAP/TAZ signaling (Sun et al., 2018). Importantly, this experiment demonstrates that the peptides may be used to functionally impair the binding

between FN and TNC, thus potentially reverting cancer promoting properties of TNC, such as cell migration and invasion.

Mesangial cells represent an important part on the kidney cell population, constituting the mesangium with the ECM (Scindia et al., 2010). It has been reported that these cells can produce high amounts of matrix molecules under pathological conditions, including FN, TNC and collagens, leading to kidney fibrosis (Campanholle et al., 2013). For instance, TNC has been identified as an inducer of fibrosis in kidney, promoting fibroblasts proliferation and matrix deposition (Fu et al., 2017). By using MES cells, we could show that TNC induced the expression of FN and Col I, supporting the idea that TNC can promote fibrosis in the kidney. Then, by adding TNC together with the peptides to the cells, we observed that FN and Col I secretion was reduced by P5 and P13. Moreover, IF imaging allowed us to see a decreased deposition of FN and Col I upon TNC co-incubation with P13. We need to investigate this process in more detail in order understand whether matrix network formation is impaired because less ECM molecules are secreted or because the peptides also disturb matrix network formation. We also need to understand how the MAREMO peptides reduce signaling and matrix expression. It would also be interesting to know if TNC only acts as an inducer of ECM production in fibrosis or if TNC can also be part of the new scaffold. As TNC, FN and collagens are frequently observed in TMT, and TMT are very poorly established in TNC KO OSCC, which suggested that TNC is a master orchestrator of the TMT (Spenlé et al., 2020), one can imagine that targeting TNC with the MAREMO peptides may affect the complete matrix organization and progression of fibrosis.

9.11. MAREMO peptides may be used as adjuvant in TRAIL therapy

In the first manuscript, we demonstrated that combined treatment of TRAIL and DR5 agonist (MD5-1) induces apoptosis in the NT193E cells. As clinical trials using only TRAIL or TRAIL-Rs agonists failed, the possibility to kill cancer cells by crosslinking the receptors and treating with TRAIL as we did with TRAIL+MD5-1 is considered as a promising therapeutical approach in the current trials (Dubuisson and Micheau, 2017; Lemke et al., 2014).

In our study, we observed that only NT193E cells were sensitive to the combined treatment, whereas no significant effect on the NT193M cells was seen. Importantly, we have shown that the NT193M cells express TNC. As we described physical binding between TNC and TRAIL close to the TN5 domain, we wanted to know if TNC could contribute to TRAIL

resistance by sequestrating the cytokines and decreasing the activation of DR5. Indeed, by adding TRAIL/MD5-1 together with the MAREMO peptides, we observed a significant increase of caspase 3 and 7 activation, followed by cell death. By using NT193M cells with a knockdown of *Tnc*, we could see that apoptosis was not affected by the peptides, indicating that TNC is the major target of the peptides. This experiment suggests that TNC can physically protect cancer cells from apoptosis by sequestrating TRAIL. These results are interesting because in tumors, we frequently see tumor nests, containing cancer cells, surrounded by TMT containing TNC (Sun et al., 2019; Murdamoothoo et al., in revision; Erne et al., in preparation). Moreover, TNC is expressed around blood vessels during several vascular diseases (Imanaka-Yoshida et al., 2014) and during cancer angiogenesis (Langlois et al., 2014; Obberghen-Schilling et al., 2011; Saupe et al., 2013). If we consider the use of TRAIL therapy in cancer, implicating rhTRAILs, the presence of TNC may represent an obstacle to the success of this approach as multiple layers of TNC may decrease the delivery of rhTRAILs to the tumor cells, leading to therapeutic failure. We therefore hypothesize that adding MAREMO peptides during TRAIL therapy may increase the chance of success by lowering the sequestration of TRAIL by TNC.

9.12. FNIII repeats and MAREMO patterns are identified in several proteins: could they bind to TNC and would the peptides be useful against these interactions?

FN-type III repeat is highly preserved amongst species and is found in many proteins. This specific structure mostly plays a role as binding platform for other matrix molecules, cell surface receptors and soluble factors (Doolittle and Bork, 1993). Since we hypothetized that proteins containing MAREMO sequences in FNIII repeats may interact with TNC, we analyzed by mass spectrometry the molecules that stick to TNC during the process of purification of conditioned medium from HEK293:TNC cells overexpressing recombinant murine TNC (Spenlé et al., 2020). We could therefore identify proteins that bound to TNC. Interestingly, more than 600 molecules were identified, including several matrix proteins belonging to the Matrisome (Hynes and Naba, 2012). Moreover, some that proteins co-purified with TNC contain FNIII repeats, such as contactins, collagens and receptor-type tyrosine-protein phosphatases. As we compared by multiple alignments the FNIII domains of several candidates, we could identify common patterns in the regions corresponding to the loops I and II. Even though our list is not exhaustive and under investigation, detecting

proteins that interact with TNC based on the presence of a MAREMO sequence is highly interesting.

As example, we could find that molecules from the receptor-type tyrosine-protein phosphatase (PTPRx) family possess FNIII repeats with loops I and II sharing similarities with a MAREMO sequence. For instance, the loop II in PTPRC, also known as CD45, resemble to FN5 loop II (NLKPYTKY, NLQPASEY respectively). The FNIII repeat of CD45 also contains amino acids positively charged that may act as HBS. By comparing structural models of FN and CD45, we could see the classical conformation of FNIII repeats in both molecules. As CD45 is made of several extracellular FNIII repeats, we postulate that it may be an observation of importance regarding the recent immunomodulatory roles described for TNC (Hauzenberger et al., 1999; Jachetti et al., 2015; Spenlé et al., 2020; Murdamoothoo et al., in revision). If TNC can immobilize immune cells by chemoretention, one can imagine that a secondary interaction between TNC and CD45 may affect different leukocytes, and cancer progression (Hermiston et al., 2003). Moreover, regulation of CD45 by integrins has already been described as modulating the immune response (Freeman et al., 2016; Germena et al., 2015; Roach et al., 1997; Shenoi et al., 1999). It will be interesting to see in the future whether TNC regulates immune cells response through binding to CD45.

10. Summary

During this thesis, I have worked on different pathological aspects of the matrix molecule TNC. Using the NT193 grafting model, I focused on the roles of TNC in breast cancer development where my results describe a complex regulation of the cytokine TRAIL. Indeed, it was demonstrated that TNC can decrease the efficiency of anti-cancer therapies based on TRAIL by inducing pro-survival signaling in the cancer cells and by sequestrating TRAIL, thus preventing apoptosis. Moreover, we show that TNC could impair non-apoptotic anti-tumoral effects of TRAIL through downregulating TRAIL expression. Since TNC is associated with poor cancer prognosis, we worked on the development of TNC-targeting peptides, based on a binding sequence between TNC and FN that we named MAtrix REgulating Motif 'MAREMO'. As we demonstrated that the MAREMO peptides can bind to TNC, we described for the first time functional effects of TNC-targeting peptides on TNC properties. Indeed, we have shown that the MAREMO peptides can abrogate the sequestrating effects that TNC can have on CXCL12, CCL21 and TRAIL. Moreover, we demonstrated that MAREMO peptides can interfere with the production of ECM during pathological conditions like fibrosis. As we identified potential candidates interacting with TNC via MAREMO sequences, the use of MAREMO peptides may help to better understand the functioning of TNC in pathological conditions. Altogether, the results accumulated during my thesis (summarized in figure 8) will participate to enlarge our comprehension of the events triggered by TNC in cancer and to develop therapeutic responses to counteract these mechanisms.

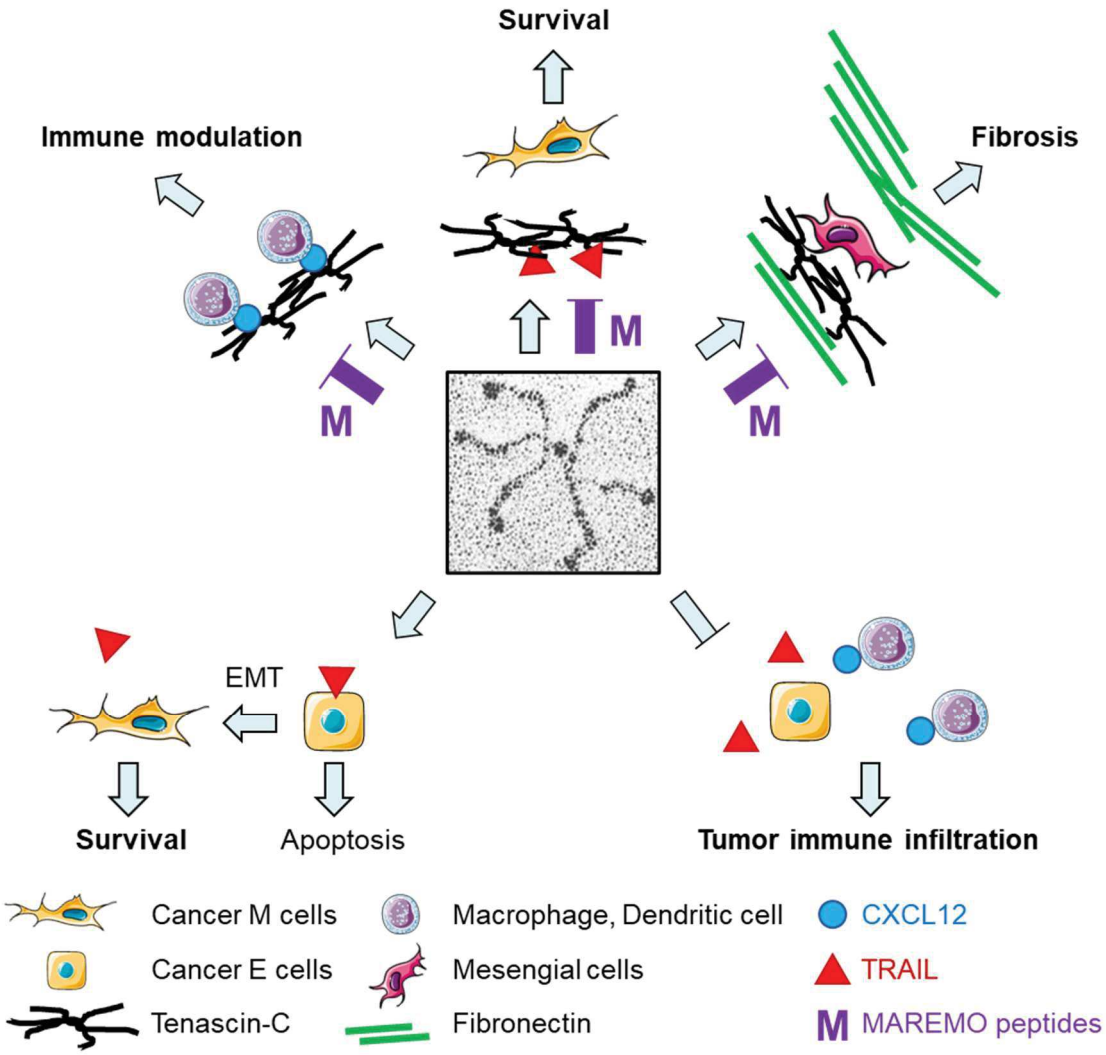

Figure 8: Tenascin-C promotes cancer and fibrosis via mechanisms that can be inhibited by the MAREMO peptides.

In cancer, TNC can bind to soluble factors such as CXCL12, immobilizing immune cells and modulating their activation. TNC can also bind to TRAIL and promote survival by preventing TRAIL from activating apoptosis in cancer cells. In fibrosis, TNC binds to FN and interacts with cells, promoting matrix deposition by mesangial cells in kidney. The new MAREMO peptide can inhibit these mechanisms through binding to TNIII domains and block TNC interaction with cells and soluble factors.

In cancer, TNC can also inhibit TRAIL functions by promoting EMT plasticity leading to resistance against TRAIL therapy, and TNC can inhibit the expression of TRAIL by the cancer cells, decreasing tumor immune infiltration and tumor growth repression.

11. References (introduction and discussion part)

Adams, M., Jones, J.L., Walker, R.A., Pringle, J.H., and Bell, S.C. (2002). Changes in tenascin-C isoform expression in invasive and preinvasive breast disease. Cancer Res. *62*, 3289–3297.

Aggarwal, B.B. (2003). Signalling pathways of the TNF superfamily: a double-edged sword. Nat. Rev. Immunol. *3*, 745–756.

Aggarwal, B.B., Gupta, S.C., and Kim, J.H. (2012). Historical perspectives on tumor necrosis factor and its superfamily: 25 years later, a golden journey. Blood *119*, 651–665.

Ahmad, Z.A., Yeap, S.K., Ali, A.M., Ho, W.Y., Alitheen, N.B.M., and Hamid, M. (2012). scFv antibody: principles and clinical application. Clin. Dev. Immunol. *2012*, 980250.

Albain, K.S., Barlow, W.E., Ravdin, P.M., Farrar, W.B., Burton, G.V., Ketchel, S.J., Cobau, C.D., Levine, E.G., Ingle, J.N., Pritchard, K.I., et al. (2009). Adjuvant chemotherapy and timing of tamoxifen in postmenopausal patients with endocrine-responsive, node-positive breast cancer: a phase 3, open-label, randomised controlled trial. Lancet Lond. Engl. *374*, 2055–2063.

Alcaraz, L.B., Exposito, J.-Y., Chuvin, N., Pommier, R.M., Cluzel, C., Martel, S., Sentis, S., Bartholin, L., Lethias, C., and Valcourt, U. (2014). Tenascin-X promotes epithelial-to-mesenchymal transition by activating latent TGF-β. J. Cell Biol. *205*, 409–428.

Alladina, S.J., Song, J.H., Davidge, S.T., Hao, C., and Easton, A.S. (2005). TRAIL-induced apoptosis in human vascular endothelium is regulated by phosphatidylinositol 3-kinase/Akt through the short form of cellular FLIP and Bcl-2. J. Vasc. Res. *42*, 337–347.

Allavena, P., Sica, A., Garlanda, C., and Mantovani, A. (2008). The Yin-Yang of tumor-associated macrophages in neoplastic progression and immune surveillance. Immunol. Rev. *222*, 155–161.

Allen, J.E., and El-Deiry, W.S. (2012). Regulation of the human TRAIL gene. Cancer Biol. Ther. *13*, 1143–1151.

Allensworth, J.L., Aird, K.M., Aldrich, A.J., Batinic-Haberle, I., and Devi, G.R. (2012). XIAP Inhibition and Generation of Reactive Oxygen Species Enhances TRAIL Sensitivity in Inflammatory Breast Cancer Cells. Mol. Cancer Ther. *11*, 1518–1527.

Almasan, A., and Ashkenazi, A. (2003). Apo2L/TRAIL: apoptosis signaling, biology, and potential for cancer therapy. Cytokine Growth Factor Rev. *14*, 337–348.

Aloj, L., D'Ambrosio, L., Aurilio, M., Morisco, A., Frigeri, F., Caraco', C., Di Gennaro, F., Capobianco, G., Giovannoni, L., Menssen, H.D., et al. (2014). Radioimmunotherapy with Tenarad, a 131I-labelled antibody fragment targeting the extra-domain A1 of tenascin-C, in patients with refractory Hodgkin's lymphoma. Eur. J. Nucl. Med. Mol. Imaging *41*, 867–877.

Anampa, J., Makower, D., and Sparano, J.A. (2015). Progress in adjuvant chemotherapy for breast cancer: an overview. BMC Med. *13*, 195.

Arimidex, Tamoxifen, Alone or in Combination (ATAC) Trialists' Group, Forbes, J.F., Cuzick, J., Buzdar, A., Howell, A., Tobias, J.S., and Baum, M. (2008). Effect of anastrozole and

tamoxifen as adjuvant treatment for early-stage breast cancer: 100-month analysis of the ATAC trial. Lancet Oncol. *9*, 45–53.

Arpel, A., Sawma, P., Spenlé, C., Fritz, J., Meyer, L., Garnier, N., Velázquez-Quesada, I., Hussenet, T., Aci-Sèche, S., Baumlin, N., et al. (2014). Transmembrane Domain Targeting Peptide Antagonizing ErbB2/Neu Inhibits Breast Tumor Growth and Metastasis. Cell Rep. *8*, 1714–1721.

Arumugam, A., Subramani, R., Nandy, S.B., Terreros, D., Dwivedi, A.K., Saltzstein, E., and Lakshmanaswamy, R. (2019). Silencing growth hormone receptor inhibits estrogen receptor negative breast cancer through ATP-binding cassette sub-family G member 2. Exp. Mol. Med. *51*, 1–13.

Asano, T., Iwasaki, N., Kon, S., Kanayama, M., Morimoto, J., Minami, A., and Uede, T. (2014). α9β1 integrin acts as a critical intrinsic regulator of human rheumatoid arthritis. Rheumatology *53*, 415–424.

Ashkenazi, A., Pai, R.C., Fong, S., Leung, S., Lawrence, D.A., Marsters, S.A., Blackie, C., Chang, L., McMurtrey, A.E., Hebert, A., et al. (1999). Safety and antitumor activity of recombinant soluble Apo2 ligand. J. Clin. Invest. *104*, 155–162.

Aufderheide, E., and Ekblom, P. (1988). Tenascin during gut development: appearance in the mesenchyme, shift in molecular forms, and dependence on epithelial-mesenchymal interactions. J. Cell Biol. *107*, 2341–2349.

Aufderheide, E., Chiquet-Ehrismann, R., and Ekblom, P. (1987). Epithelial-mesenchymal interactions in the developing kidney lead to expression of tenascin in the mesenchyme. J. Cell Biol. *105*, 599–608.

Azijli, K., Yuvaraj, S., Peppelenbosch, M.P., Würdinger, T., Dekker, H., Joore, J., Dijk, E. van, Quax, W.J., Peters, G.J., Jong, S. de, et al. (2012). Kinome profiling of non-canonical TRAIL signaling reveals RIP1–Src–STAT3-dependent invasion in resistant non-small cell lung cancer cells. J. Cell Sci. *125*, 4651–4661.

Azijli, K., Weyhenmeyer, B., Peters, G.J., de Jong, S., and Kruyt, F.A.E. (2013). Non-canonical kinase signaling by the death ligand TRAIL in cancer cells: discord in the death receptor family. Cell Death Differ. *20*, 858–868.

Baetu, T.M., Kwon, H., Sharma, S., Grandvaux, N., and Hiscott, J. (2001). Disruption of NF-B Signaling Reveals a Novel Role for NF- B in the Regulation of TNF-Related Apoptosis-Inducing Ligand Expression. J. Immunol. *167*, 3164–3173.

Balkwill, F.R., Capasso, M., and Hagemann, T. (2012). The tumor microenvironment at a glance. J. Cell Sci. *125*, 5591–5596.

Banerjee, S., Dowsett, M., Ashworth, A., and Martin, L.-A. (2007). Mechanisms of Disease: angiogenesis and the management of breast cancer. Nat. Clin. Pract. Oncol. *4*, 536–550.

Berg, D., Lehne, M., Müller, N., Siegmund, D., Münkel, S., Sebald, W., Pfizenmaier, K., and Wajant, H. (2007). Enforced covalent trimerization increases the activity of the TNF ligand family members TRAIL and CD95L. Cell Death Differ. *14*, 2021–2034.

Berger, A.J., Renner, C.M., Hale, I., Yang, X., Ponik, S.M., Weisman, P.S., Masters, K.S., and Kreeger, P.K. (2020). Scaffold stiffness influences breast cancer cell invasion via EGFR-linked Mena upregulation and matrix remodeling. Matrix Biol. J. Int. Soc. Matrix Biol. *85–86*, 80–93.

Berrino, P., Campora, E., and Santi, P. (1987). Postquadrantectomy breast deformities: classification and techniques of surgical correction. Plast. Reconstr. Surg. *79*, 567–572.

Betz, P., Nerlich, A., Tübel, J., Penning, R., and Eisenmenger, W. (1993). Localization of tenascin in human skin wounds--an immunohistochemical study. Int. J. Legal Med. *105*, 325–328.

Binaschi, M., Farinosi, R., Austin, C.A., Fisher, L.M., Zunino, F., and Capranico, G. (1998). Human DNA Topoisomerase IIα-dependent DNA Cleavage and Yeast Cell Killing by Anthracycline Analogues. Cancer Res. *58*, 1886–1892.

Bissell, M.J., Hall, H.G., and Parry, G. (1982). How does the extracellular matrix direct gene expression? J. Theor. Biol. *99*, 31–68.

Black, S.A., Nelson, A.C., Gurule, N.J., Futscher, B.W., and Lyons, T.R. (2016). Semaphorin 7a exerts pleiotropic effects to promote breast tumor progression. Oncogene *35*, 5170–5178.

Blackhall, F.H., Márk, Z., Zatloukal, P., Szima, B., Albert, I., Juhász, E., Yang, X., Smethurst, D., Hei, Y., and Soria, J. (2010). A randomized phase II study of paclitaxel (P) and carboplatin (C) ± bevacizumab (B) ± dulanermin (D) in non-small cell lung cancer (NSCLC). J. Clin. Oncol. *28*, 7534–7534.

Bloom, L., Ingham, K.C., and Hynes, R.O. (1999). Fibronectin Regulates Assembly of Actin Filaments and Focal Contacts in Cultured Cells via the Heparin-binding Site in Repeat III13. Mol. Biol. Cell *10*, 1521–1536.

Bodmer, J.-L., Meier, P., Tschopp, J., and Schneider, P. (2000). Cysteine 230 Is Essential for the Structure and Activity of the Cytotoxic Ligand TRAIL. J. Biol. Chem. *275*, 20632–20637.

Bonadonna, G., Brusamolino, E., Valagussa, P., Rossi, A., Brugnatelli, L., Brambilla, C., De Lena, M., Tancini, G., Bajetta, E., Musumeci, R., et al. (1976). Combination chemotherapy as an adjuvant treatment in operable breast cancer. N. Engl. J. Med. *294*, 405–410.

Bonneterre, D. (2008). Cancéro guide ,le sein.

Bos, J.L. (1989). ras Oncogenes in Human Cancer: A Review. Cancer Res. *49*, 4682–4689.

Bossen, C., Ingold, K., Tardivel, A., Bodmer, J.-L., Gaide, O., Hertig, S., Ambrose, C., Tschopp, J., and Schneider, P. (2006). Interactions of tumor necrosis factor (TNF) and TNF receptor family members in the mouse and human. J. Biol. Chem. *281*, 13964–13971.

Bossi, F., Bernardi, S., Zauli, G., Secchiero, P., and Fabris, B. (2015). TRAIL Modulates the Immune System and Protects against the Development of Diabetes. J. Immunol. Res. *2015*, 1–12.

Bourdon, M.A., Wikstrand, C.J., Furthmayr, H., Matthews, T.J., and Bigner, D.D. (1983). Human Glioma-Mesenchymal Extracellular Matrix Antigen Defined by Monoclonal Antibody. Cancer Res. *43*, 2796–2805.

Brack, S.S., Silacci, M., Birchler, M., and Neri, D. (2006). Tumor-Targeting Properties of Novel Antibodies Specific to the Large Isoform of Tenascin-C. Clin. Cancer Res. *12*, 3200–3208.

Bremer, E., Samplonius, D.F., van Genne, L., Dijkstra, M.H., Kroesen, B.J., de Leij, L.F.M.H., and Helfrich, W. (2005). Simultaneous inhibition of epidermal growth factor receptor (EGFR) signaling and enhanced activation of tumor necrosis factor-related apoptosis-inducing ligand (TRAIL) receptor-mediated apoptosis induction by an scFv:sTRAIL fusion protein with specificity for human EGFR. J. Biol. Chem. *280*, 10025–10033.

Bronte, V., Brandau, S., Chen, S.-H., Colombo, M.P., Frey, A.B., Greten, T.F., Mandruzzato, S., Murray, P.J., Ochoa, A., Ostrand-Rosenberg, S., et al. (2016). Recommendations for myeloid-derived suppressor cell nomenclature and characterization standards. Nat. Commun. *7*.

Brown, L.C., Mutter, R.W., and Halyard, M.Y. (2015). Benefits, risks, and safety of external beam radiation therapy for breast cancer. Int. J. Womens Health *7*, 449–458.

Buchsbaum, D.J., Zhou, T., Grizzle, W.E., Oliver, P.G., Hammond, C.J., Zhang, S., Carpenter, M., and LoBuglio, A.F. (2003). Antitumor efficacy of TRA-8 anti-DR5 monoclonal antibody alone or in combination with chemotherapy and/or radiation therapy in a human breast cancer model. Clin. Cancer Res. Off. J. Am. Assoc. Cancer Res. *9*, 3731–3741.

Burnett, J.C., and Rossi, J.J. (2012). RNA-based therapeutics: current progress and future prospects. Chem. Biol. *19*, 60–71.

Butcher, D.T., Alliston, T., and Weaver, V.M. (2009). A tense situation: forcing tumour progression. Nat. Rev. Cancer *9*, 108–122.

Cameron, D.A., Gabra, H., and Leonard, R.C. (1994). Continuous 5-fluorouracil in the treatment of breast cancer. Br. J. Cancer *70*, 120–124.

Campanholle, G., Ligresti, G., Gharib, S.A., and Duffield, J.S. (2013). Cellular Mechanisms of Tissue Fibrosis. 3. Novel mechanisms of kidney fibrosis. Am. J. Physiol. - Cell Physiol. *304*, C591–C603.

Campbell, I.D., and Spitzfaden, C. (1994). Building proteins with fibronectin type III modules. Structure *2*, 333–337.

Campbell, G.R., Watkins, J.D., Singh, K.K., Loret, E.P., and Spector, S.A. (2007). Human Immunodeficiency Virus Type 1 Subtype C Tat Fails To Induce Intracellular Calcium Flux and Induces Reduced Tumor Necrosis Factor Production from Monocytes. J. Virol. *81*, 5919–5928.

Canfield, A.E., and Schor, A.M. (1995). Evidence that tenascin and thrombospondin-1 modulate sprouting of endothelial cells. J. Cell Sci. *108*, 797–809.

Cantarella, G., Risuglia, N., Dell'eva, R., Lempereur, L., Albini, A., Pennisi, G., Scoto, G.M., Noonan, D.N., and Bernardini, R. (2006). TRAIL inhibits angiogenesis stimulated by VEGF expression in human glioblastoma cells. Br. J. Cancer *94*, 1428–1435.

Cao, B., Hutt, O.E., Zhang, Z., Li, S., Heazlewood, S.Y., Williams, B., Smith, J.A., Haylock, D.N., Savage, G.P., and Nilsson, S.K. (2014). Design, synthesis and binding properties of a fluorescent $\alpha_9\beta_1/\alpha_4\beta_1$ integrin antagonist and its application as an in vivo probe for bone marrow haemopoietic stem cells. Org. Biomol. Chem. *12*, 965–978.

Carnemolla, B., Castellani, P., Ponassi, M., Borsi, L., Urbini, S., Nicolo, G., Dorcaratto, A., Viale, G., Winter, G., Neri, D., et al. (1999). Identification of a Glioblastoma-Associated Tenascin-C Isoform by a High Affinity Recombinant Antibody. Am. J. Pathol. *154*, 1345.

Carpenter, P.M., Ziogas, A., Markham, E.M., Cantillep, A.S., Yan, R., and Anton-Culver, H. (2018). Laminin 332 expression and prognosis in breast cancer. Hum. Pathol. *82*, 289–296.

Carter, P., Presta, L., Gorman, C.M., Ridgway, J.B., Henner, D., Wong, W.L., Rowland, A.M., Kotts, C., Carver, M.E., and Shepard, H.M. (1992). Humanization of an anti-p185HER2 antibody for human cancer therapy. Proc. Natl. Acad. Sci. *89*, 4285–4289.

Catania, C., Maur, M., Berardi, R., Rocca, A., Giacomo, A.M.D., Spitaleri, G., Masini, C., Pierantoni, C., González-Iglesias, R., Zigon, G., et al. (2015). The tumor-targeting immunocytokine F16-IL2 in combination with doxorubicin: dose escalation in patients with advanced solid tumors and expansion into patients with metastatic breast cancer. Cell Adhes. Migr. *9*, 14–21.

Cauwe, B., Van den Steen, P.E., and Opdenakker, G. (2007). The biochemical, biological, and pathological kaleidoscope of cell surface substrates processed by matrix metalloproteinases. Crit. Rev. Biochem. Mol. Biol. *42*, 113–185.

Cha, S.-S., Kim, M.-S., Choi, Y.H., Sung, B.-J., Shin, N.K., Shin, H.-C., Sung, Y.C., and Oh, B.-H. (1999). 2.8 Å Resolution Crystal Structure of Human TRAIL, a Cytokine with Selective Antitumor Activity. Immunity *11*, 253–261.

Chand-Fouché, M.-E., Lam Cham Kee, D., Gautier, M., and Hannoun-Levi, J.-M. (2016). Technique d'irradiation partielle du sein : radiothérapie externe et curiethérapie. Cancer/Radiothérapie *20*, 587–594.

Charafe-Jauffret, E., Ginestier, C., Monville, F., Finetti, P., Adélaïde, J., Cervera, N., Fekairi, S., Xerri, L., Jacquemier, J., Birnbaum, D., et al. (2006). Gene expression profiling of breast cell lines identifies potential new basal markers. Oncogene *25*, 2273–2284.

Chen, Y., Xu, Y., Zhu, K., Cao, Z., and Huang, Z. (2019). Tumor necrosis factor-related apoptosis-inducing ligand modulates angiogenesis and apoptosis to inhibit non-small cell lung carcinoma tumor growth in mice. J. Int. Med. Res. *47*, 3243–3252.

Chia, J., Kusuma, N., Anderson, R., Parker, B., Bidwell, B., Zamurs, L., Nice, E., and Pouliot, N. (2007). Evidence for a Role of Tumor-Derived Laminin-511 in the Metastatic Progression of Breast Cancer. Am. J. Pathol. *170*, 2135–2148.

Chinnaiyan, A.M., Prasad, U., Shankar, S., Hamstra, D.A., Shanaiah, M., Chenevert, T.L., Ross, B.D., and Rehemtulla, A. (2000). Combined effect of tumor necrosis factor-related

apoptosis-inducing ligand and ionizing radiation in breast cancer therapy. Proc. Natl. Acad. Sci. U. S. A. *97*, 1754–1759.

Chiquet, M. (1992). Tenascin: an extracellular matrix protein involved in morphogenesis of epithelial organs. Kidney Int. *41*, 629–631.

Chiquet, M., and Fambrough, D.M. (1984). Chick myotendinous antigen. I. A monoclonal antibody as a marker for tendon and muscle morphogenesis. J. Cell Biol. *98*, 1926–1936.

Chiquet-Ehrismann, R., and Chiquet, M. (2003). Tenascins: regulation and putative functions during pathological stress. J. Pathol. *200*, 488–499.

Chiquet-Ehrismann, R., and Tucker, R.P. (2011). Tenascins and the Importance of Adhesion Modulation. Cold Spring Harb. Perspect. Biol. *3*.

Chiquet-Ehrismann, R., Mackie, E.J., Pearson, C.A., and Sakakura, T. (1986). Tenascin: an extracellular matrix protein involved in tissue interactions during fetal development and oncogenesis. Cell *47*, 131–139.

Chiquet-Ehrismann, R., Kalla, P., Pearson, C.A., Beck, K., and Chiquet, M. (1988). Tenascin interferes with fibronectin action. Cell *53*, 383–390.

Chiquet-Ehrismann, R., Kalla, P., and Pearson, C.A. (1989). Participation of Tenascin and Transforming Growth Factor-β in Reciprocal Epithelial-Mesenchymal Interactions of MCF7 Cells and Fibroblasts. Cancer Res. *49*, 4322–4325.

Chiquet-Ehrismann, R., Orend, G., Chiquet, M., Tucker, R.P., and Midwood, K.S. (2014). Tenascins in stem cell niches. Matrix Biol. *37*, 112–123.

Cho, Y.S., Challa, S., Clancy, L., and Chan, F.K.-M. (2010). Lipopolysaccharide-induced expression of TRAIL promotes dendritic cell differentiation: TRAIL facilitates DC differentiation. Immunology *130*, 504–515.

Chow, M.T., and Luster, A.D. (2014). Chemokines in Cancer. Cancer Immunol. Res. *2*, 1125–1131.

Chu, D.-T., Nguyen Thi Phuong, T., Tien, N.L.B., Tran, D.-K., Nguyen, T.-T., Thanh, V.V., Luu Quang, T., Minh, L.B., Pham, V.H., Ngoc, V.T.N., et al. (2019). The Effects of Adipocytes on the Regulation of Breast Cancer in the Tumor Microenvironment: An Update. Cells *8*.

Chung, C.Y., and Erickson, H.P. (1997). Glycosaminoglycans modulate fibronectin matrix assembly and are essential for matrix incorporation of tenascin-C. J. Cell Sci. *110*, 1413–1419.

Chung, C.Y., Zardi, L., and Erickson, H.P. (1995). Binding of tenascin-C to soluble fibronectin and matrix fibrils. J. Biol. Chem. *270*, 29012–29017.

Ciuleanu, T., Bazin, I., Lungulescu, D., Miron, L., Bondarenko, I., Deptala, A., Rodriguez-Torres, M., Giantonio, B., Fox, N.L., Wissel, P., et al. (2016). A randomized, double-blind, placebo-controlled phase II study to assess the efficacy and safety of mapatumumab with sorafenib in patients with advanced hepatocellular carcinoma. Ann. Oncol. Off. J. Eur. Soc. Med. Oncol. *27*, 680–687.

Claesson-Welsh, L., and Welsh, M. (2013). VEGFA and tumour angiogenesis. J. Intern. Med. *273*, 114–127.

Clark, R.A., Erickson, H.P., and Springer, T.A. (1997). Tenascin supports lymphocyte rolling. J. Cell Biol. *137*, 755–765.

Clarke, M., Collins, R., Darby, S., Davies, C., Elphinstone, P., Evans, V., Godwin, J., Gray, R., Hicks, C., James, S., et al. (2005). Effects of radiotherapy and of differences in the extent of surgery for early breast cancer on local recurrence and 15-year survival: an overview of the randomised trials. Lancet Lond. Engl. *366*, 2087–2106.

Cohen, C., Leal, M.F., Belangero, P.S., Figueiredo, E.A., Smith, M.C., Andreoli, C.V., de Castro Pochini, A., Cohen, M., Ejnisman, B., Faloppa, F., et al. (2016). The roles of Tenascin C and Fibronectin 1 in adhesive capsulitis: a pilot gene expression study. Clinics *71*, 325–331.

Cowppli-Bony, A., Uhry, Z., Remontet, L., Voirin, N., Guizard, A.-V., Trétarre, B., Bouvier, A.-M., Colonna, M., Bossard, N., Woronoff, A.-S., et al. (2017). Survival of solid cancer patients in France, 1989-2013: a population-based study. Eur. J. Cancer Prev. Off. J. Eur. Cancer Prev. Organ. ECP *26*, 461–468.

Crossin, K.L. (1991). Cytotactin binding: inhibition of stimulated proliferation and intracellular alkalinization in fibroblasts. Proc. Natl. Acad. Sci. *88*, 11403–11407.

Dadi, S., Chhangawala, S., Whitlock, B.M., Franklin, R.A., Luo, C.T., Oh, S.A., Toure, A., Pritykin, Y., Huse, M., Leslie, C.S., et al. (2016). Cancer Immunosurveillance by Tissue-resident Innate Lymphoid Cells and Innate-like T Cells. Cell *164*, 365–377.

Dai, X., Cheng, H., Bai, Z., and Li, J. (2017). Breast Cancer Cell Line Classification and Its Relevance with Breast Tumor Subtyping. J. Cancer *8*, 3131–3141.

Dandachi, N., Hauser-Kronberger, C., Moré, E., Wiesener, B., Hacker, G.W., Dietze, O., and Wirl, G. (2001). Co-expression of tenascin-C and vimentin in human breast cancer cells indicates phenotypic transdifferentiation during tumour progression: correlation with histopathological parameters, hormone receptors, and oncoproteins. J. Pathol. *193*, 181–189.

Darby, S.C., McGale, P., Taylor, C.W., and Peto, R. (2005). Long-term mortality from heart disease and lung cancer after radiotherapy for early breast cancer: prospective cohort study of about 300,000 women in US SEER cancer registries. Lancet Oncol. *6*, 557–565.

Davies, C., Pan, H., Godwin, J., Gray, R., Arriagada, R., Raina, V., Abraham, M., Alencar, V.H.M., Badran, A., Bonfill, X., et al. (2013). Long-term effects of continuing adjuvant tamoxifen to 10 years versus stopping at 5 years after diagnosis of oestrogen receptor-positive breast cancer: ATLAS, a randomised trial. Lancet *381*, 805–816.

De Blasio, A., Pratelli, G., Drago-Ferrante, R., Saliba, C., Baldacchino, S., Grech, G., Tesoriere, G., Scerri, C., Vento, R., and Di Fiore, R. (2019). Loss of MCL1 function sensitizes the MDA-MB-231 breast cancer cells to rh-TRAIL by increasing DR4 levels. J. Cell. Physiol. *234*, 18432–18447.

De Braud, F.G., Catania, C., Onofri, A., Pierantoni, C., Cascinu, S., Maur, M., Masini, C., Conte, P.F., Giovannoni, L., Tasciotti, A., et al. (2011). Combination of the immunocytokine F16-IL2 with doxorubicin or paclitaxel in patients with solid tumors: Results from two phase Ib trials. J. Clin. Oncol. *29*, 2595–2595.

De Laporte, L., Rice, J.J., Tortelli, F., and Hubbell, J.A. (2013). Tenascin C Promiscuously Binds Growth Factors via Its Fifth Fibronectin Type III-Like Domain. PLoS ONE *8*, e62076.

Degen, M., Brellier, F., Kain, R., Ruiz, C., Terracciano, L., Orend, G., and Chiquet-Ehrismann, R. (2007). Tenascin-W Is a Novel Marker for Activated Tumor Stroma in Low-grade Human Breast Cancer and Influences Cell Behavior. Cancer Res. *67*, 9169–9179.

Deligne, C., Murdamoothoo, D., Gammage, A.N., Gschwandtner, M., Erne, W., Loustau, T., Marzeda, A.M., Carapito, R., Paul, N., Velazquez-Quesada, I., et al. (2020). Matrix-Targeting Immunotherapy Controls Tumor Growth and Spread by Switching Macrophage Phenotype. Cancer Immunol. Res. *8*, 368–382.

Demir, I.E., Friess, H., and Ceyhan, G.O. (2012). Nerve-Cancer Interactions in the Stromal Biology of Pancreatic Cancer. Front. Physiol. *3*.

DeNardo, D.G., Barreto, J.B., Andreu, P., Vasquez, L., Tawfik, D., Kolhatkar, N., and Coussens, L.M. (2009). CD4(+) T cells regulate pulmonary metastasis of mammary carcinomas by enhancing protumor properties of macrophages. Cancer Cell *16*, 91–102.

Denoix, P.F. (1953). [Nomenclature and classification of cancers based on an atlas]. Acta - Unio Int. Contra Cancrum *9*, 769–771.

Derr, L.B., Chiquet-Ehrismann, R., Gandour-Edwards, R., Spence, J., and Tucker, R.P. (1997). The expression of tenascin-C with the AD1 variable repeat in embryonic tissues, cell lines and tumors in various vertebrate species. Differ. Res. Biol. Divers. *62*, 71–82.

Deveraux, Q.L., Takahashi, R., Salvesen, G.S., and Reed, J.C. (1997). X-linked IAP is a direct inhibitor of cell-death proteases. Nature *388*, 300–304.

Dhaouadi, S., Murdamoothoo, D., Tounsi, A., Erne, W., Benabderrazek, R., Benlasfar, Z., Hendaoui, L., Chiquet-Ehrismann, R., Boubaker, S., Orend, G., et al. (2020). Generation and characterization of dromedary Tenascin-C and Tenascin-W specific antibodies. Biochem. Biophys. Res. Commun. *530*, 471–478.

Di Bartolo, B.A., Cartland, S.P., Prado-Lourenco, L., Griffith, T.S., Gentile, C., Ravindran, J., Azahri, N.S.M., Thai, T., Yeung, A.W.S., Thomas, S.R., et al. (2015). Tumor Necrosis Factor–Related Apoptosis-Inducing Ligand (TRAIL) Promotes Angiogenesis and Ischemia-Induced Neovascularization Via NADPH Oxidase 4 (NOX4) and Nitric Oxide–Dependent Mechanisms. J. Am. Heart Assoc. *4*.

D'Incalci, M. (2013). Trabectedin mechanism of action: what's new? Future Oncol. Lond. Engl. *9*, 5–10.

Dirix, L.Y., Takacs, I., Jerusalem, G., Nikolinakos, P., Arkenau, H.-T., Forero-Torres, A., Boccia, R., Lippman, M.E., Somer, R., Smakal, M., et al. (2018). Avelumab, an anti-PD-L1 antibody, in patients with locally advanced or metastatic breast cancer: a phase 1b JAVELIN Solid Tumor study. Breast Cancer Res. Treat. *167*, 671–686.

Dongre, A., and Weinberg, R.A. (2019). New insights into the mechanisms of epithelial–mesenchymal transition and implications for cancer. Nat. Rev. Mol. Cell Biol. *20*, 69–84.

Doolittle, R.F., and Bork, P. (1993). Evolutionarily Mobile Modules in Proteins. Sci. Am. *269*, 50–56.

Dorothée, G., Vergnon, I., Menez, J., Echchakir, H., Grunenwald, D., Kubin, M., Chouaib, S., and Mami-Chouaib, F. (2002). Tumor-Infiltrating CD4+ T Lymphocytes Express APO2 Ligand (APO2L)/TRAIL upon Specific Stimulation with Autologous Lung Carcinoma Cells: Role of IFN-α on APO2L/TRAIL Expression and -Mediated Cytotoxicity. J. Immunol. *169*, 809–817.

Dubuisson, A., and Micheau, O. (2017). Antibodies and Derivatives Targeting DR4 and DR5 for Cancer Therapy. Antibodies Basel Switz. *6*.

Duffy, M.J., Maguire, T.M., Hill, A., McDermott, E., and O'Higgins, N. (2000). Metalloproteinases: role in breast carcinogenesis, invasion and metastasis. Breast Cancer Res. *2*, 252.

Dunn, G.P., Bruce, A.T., Ikeda, H., Old, L.J., and Schreiber, R.D. (2002). Cancer immunoediting: from immunosurveillance to tumor escape. Nat. Immunol. *3*, 991–998.

Dunn, G.P., Old, L.J., and Schreiber, R.D. (2004). The three Es of cancer immunoediting. Annu. Rev. Immunol. *22*, 329–360.

Dvorak, H.F. (2015). Tumors: Wounds that do not heal--Redux. Cancer Immunol. Res. *3*, 1–11.

Early Breast Cancer Trialists' Collaborative Group (EBCTCG) (2011). Relevance of breast cancer hormone receptors and other factors to the efficacy of adjuvant tamoxifen: patient-level meta-analysis of randomised trials. Lancet *378*, 771–784.

Edechi, C.A., Ikeogu, N., Uzonna, J.E., and Myal, Y. (2019). Regulation of Immunity in Breast Cancer. Cancers *11*.

Ehrlich, S., Infante-Duarte, C., Seeger, B., and Zipp, F. (2003). Regulation of soluble and surface-bound TRAIL in human T cells, B cells, and monocytes. Cytokine *24*, 244–253.

Elder, A.M., Tamburini, B.A.J., Crump, L.S., Black, S.A., Wessells, V.M., Schedin, P.J., Borges, V.F., and Lyons, T.R. (2018). Semaphorin 7A Promotes Macrophage-Mediated Lymphatic Remodeling during Postpartum Mammary Gland Involution and in Breast Cancer. Cancer Res. *78*, 6473–6485.

Emens, L.A. (2018). Breast Cancer Immunotherapy: Facts and Hopes. Clin. Cancer Res. Off. J. Am. Assoc. Cancer Res. *24*, 511–520.

Emery, J.G., McDonnell, P., Burke, M.B., Deen, K.C., Lyn, S., Silverman, C., Dul, E., Appelbaum, E.R., Eichman, C., DiPrinzio, R., et al. (1998). Osteoprotegerin Is a Receptor for the Cytotoxic Ligand TRAIL. J. Biol. Chem. *273*, 14363–14367.

Erickson, H.P., and Inglesias, J.L. (1984). A six-armed oligomer isolated from cell surface fibronectin preparations. Nature *311*, 267–269.

Estany, S., Vicens-Zygmunt, V., Llatjós, R., Montes, A., Penín, R., Escobar, I., Xaubet, A., Santos, S., Manresa, F., Dorca, J., et al. (2014). Lung fibrotic tenascin-C upregulation is associated with other extracellular matrix proteins and induced by TGFβ1. BMC Pulm. Med. *14*, 120.

Faissner, A. (1997). The tenascin gene family in axon growth and guidance. Cell Tissue Res. *290*, 331–341.

Fanger, N.A., Maliszewski, C.R., Schooley, K., and Griffith, T.S. (1999). Human Dendritic Cells Mediate Cellular Apoptosis via Tumor Necrosis Factor–Related Apoptosis-Inducing Ligand (Trail). J. Exp. Med. *190*, 1155–1164.

Ferretti, E., Bertolotto, M., Deaglio, S., Tripodo, C., Ribatti, D., Audrito, V., Blengio, F., Matis, S., Zupo, S., Rossi, D., et al. (2011). A novel role of the CX3CR1/CX3CL1 system in the cross-talk between chronic lymphocytic leukemia cells and tumor microenvironment. Leukemia *25*, 1268–1277.

Figliuolo da Paz, V., Jamwal, D.R., Gurney, M., Midura-Kiela, M., Harrison, C.A., Cox, C., Wilson, J.M., Ghishan, F.K., and Kiela, P.R. (2019). Rapid Downregulation of DAB2 by Toll-Like Receptor Activation Contributes to a Pro-Inflammatory Switch in Activated Dendritic Cells. Front. Immunol. *10*.

Filsell, W., Rudman, S., Jenkins, G., and Green, M.R. (1999). Coordinate upregulation of tenascin C expression with degree of photodamage in human skin. Br. J. Dermatol. *140*, 592–599.

Finnberg, N.K., Gokare, P., Navaraj, A., Lang Kuhs, K.A., Cerniglia, G., Yagita, H., Takeda, K., Motoyama, N., and El-Deiry, W.S. (2016). Agonists of the TRAIL death receptor DR5 sensitize intestinal stem cells to chemotherapy-induced cell death and trigger gastrointestinal toxicity. Cancer Res. *76*, 700–712.

Fisher, B., Ravdin, R.G., Ausman, R.K., Slack, N.H., Moore, G.E., and Noer, R.J. (1968). Surgical adjuvant chemotherapy in cancer of the breast: results of a decade of cooperative investigation. Ann. Surg. *168*, 337–356.

Fisher, B., Montague, E., Redmond, C., Barton, B., Borland, D., Fisher, E.R., Deutsch, M., Schwarz, G., Margolese, R., Donegan, W., et al. (1977). Comparison of radical mastectomy with alternative treatments for primary breast cancer. A first report of results from a prospective randomized clinical trial. Cancer *39*, 2827–2839.

Fisher, B., Anderson, S., Bryant, J., Margolese, R.G., Deutsch, M., Fisher, E.R., Jeong, J.-H., and Wolmark, N. (2002). Twenty-year follow-up of a randomized trial comparing total mastectomy, lumpectomy, and lumpectomy plus irradiation for the treatment of invasive breast cancer. N. Engl. J. Med. *347*, 1233–1241.

Fluck, M., Tunc-Civelek, V., and Chiquet, M. (2000). Rapid and reciprocal regulation of tenascin-C and tenascin-Y expression by loading of skeletal muscle. J. Cell Sci. *113*, 3583–3591.

Forero-Torres, A., Infante, J.R., Waterhouse, D., Wong, L., Vickers, S., Arrowsmith, E., He, A.R., Hart, L., Trent, D., Wade, J., et al. (2013). Phase 2, multicenter, open-label study of tigatuzumab (CS-1008), a humanized monoclonal antibody targeting death receptor 5, in

combination with gemcitabine in chemotherapy-naive patients with unresectable or metastatic pancreatic cancer. Cancer Med. *2*, 925–932.

Fosgerau, K., and Hoffmann, T. (2015). Peptide therapeutics: current status and future directions. Drug Discov. Today *20*, 122–128.

Fouad, Y.A., and Aanei, C. (2017). Revisiting the hallmarks of cancer. Am. J. Cancer Res. *7*, 1016–1036.

Franco, A.V., Zhang, X.D., Berkel, E.V., Sanders, J.E., Zhang, X.Y., Thomas, W.D., Nguyen, T., and Hersey, P. (2001). The Role of NF-κB in TNF-Related Apoptosis-Inducing Ligand (TRAIL)-Induced Apoptosis of Melanoma Cells. J. Immunol. *166*, 5337–5345.

Frantz, C., Stewart, K.M., and Weaver, V.M. (2010). The extracellular matrix at a glance. J. Cell Sci. *123*, 4195–4200.

Freeman, S.A., and Grinstein, S. (2014). Phagocytosis: receptors, signal integration, and the cytoskeleton. Immunol. Rev. *262*, 193–215.

Freeman, S.A., Goyette, J., Furuya, W., Woods, E.C., Bertozzi, C.R., Bergmeier, W., Hinz, B., van der Merwe, P.A., Das, R., and Grinstein, S. (2016). Integrins Form an Expanding Diffusional Barrier that Coordinates Phagocytosis. Cell *164*, 128–140.

Fu, H., Tian, Y., Zhou, L., Zhou, D., Tan, R.J., Stolz, D.B., and Liu, Y. (2017). Tenascin-C Is a Major Component of the Fibrogenic Niche in Kidney Fibrosis. J. Am. Soc. Nephrol. JASN *28*, 785–801.

Fukamauchi, F., Mataga, N., Wang, Y.J., Sato, S., Youshiki, A., and Kusakabe, M. (1996). Abnormal behavior and neurotransmissions of tenascin gene knockout mouse. Biochem. Biophys. Res. Commun. *221*, 151–156.

Fukunaga-Kalabis, M., Martinez, G., Nguyen, T.K., Kim, D., Santiago-Walker, A., Roesch, A., and Herlyn, M. (2010). Tenascin-C promotes melanoma progression by maintaining the ABCB5-positive side population. Oncogene *29*, 6115–6124.

Fulda, S., Meyer, E., and Debatin, K.-M. (2002). Inhibition of TRAIL-induced apoptosis by Bcl-2 overexpression. Oncogene *21*, 2283–2294.

Gabbiani, G., Ryan, G.B., and Majno, G. (1971). Presence of modified fibroblasts in granulation tissue and their possible role in wound contraction. Experientia *27*, 549–550.

Gabka, C.J., Maiwald, G., and Baumeister, R.G. (1997). [Expanding the indications spectrum for breast saving therapy of breast carcinoma by oncoplastic operations]. Langenbecks Arch. Chir. Suppl. Kongressband Dtsch. Ges. Chir. Kongr. *114*, 1224–1227.

Gallegos, L.L., and Brugge, J.S. (2014). Live Free or Die: Cell-Cell Adhesion Regulates Sensitivity to Trail-Induced Apoptosis. Dev. Cell *30*, 3–4.

Gao, J., Wang, D., Liu, D., Liu, M., Ge, Y., Jiang, M., Liu, Y., and Zheng, D. (2015). Tumor necrosis factor–related apoptosis-inducing ligand induces the expression of proinflammatory cytokines in macrophages and re-educates tumor-associated macrophages to an antitumor phenotype. Mol. Biol. Cell *26*, 3178–3189.

Germano, G., Frapolli, R., Belgiovine, C., Anselmo, A., Pesce, S., Liguori, M., Erba, E., Uboldi, S., Zucchetti, M., Pasqualini, F., et al. (2013). Role of Macrophage Targeting in the Antitumor Activity of Trabectedin. Cancer Cell *23*, 249–262.

Germena, G., Volmering, S., Sohlbach, C., and Zarbock, A. (2015). Mutation in the CD45 Inhibitory Wedge Modulates Integrin Activation and Leukocyte Recruitment during Inflammation. J. Immunol. *194*, 728–738.

Geyer, F.C., Lopez-Garcia, M.A., Lambros, M.B., and Reis-Filho, J.S. (2009). Genetic characterization of breast cancer and implications for clinical management. J. Cell. Mol. Med. *13*, 4090–4103.

Ghajar, C.M., and Bissell, M.J. (2008). Extracellular matrix control of mammary gland morphogenesis and tumorigenesis: insights from imaging. Histochem. Cell Biol. *130*, 1105–1118.

Ghatnekar, A., and Trojanowska, M. (2008). GATA-6 is a novel transcriptional repressor of the human Tenascin-C gene expression in fibroblasts. Biochim. Biophys. Acta *1779*, 145–151.

Gibellini, D., Borderi, M., De Crignis, E., Cicola, R., Vescini, F., Caudarella, R., Chiodo, F., and Re, M.C. (2007). RANKL/OPG/TRAIL plasma levels and bone mass loss evaluation in antiretroviral naive HIV-1-positive men. J. Med. Virol. *79*, 1446–1454.

Giblin, S.P., and Midwood, K.S. (2014). Tenascin-C: Form versus function. Cell Adhes. Migr. *9*, 48–82.

Giuliano, A.E., Hunt, K.K., Ballman, K.V., Beitsch, P.D., Whitworth, P.W., Blumencranz, P.W., Leitch, A.M., Saha, S., McCall, L.M., and Morrow, M. (2011). Axillary dissection vs no axillary dissection in women with invasive breast cancer and sentinel node metastasis: a randomized clinical trial. JAMA *305*, 569–575.

Gnant, M., Mlineritsch, B., Stoeger, H., Luschin-Ebengreuth, G., Knauer, M., Moik, M., Jakesz, R., Seifert, M., Taucher, S., Bjelic-Radisic, V., et al. (2015). Zoledronic acid combined with adjuvant endocrine therapy of tamoxifen versus anastrozol plus ovarian function suppression in premenopausal early breast cancer: final analysis of the Austrian Breast and Colorectal Cancer Study Group Trial 12. Ann. Oncol. Off. J. Eur. Soc. Med. Oncol. *26*, 313–320.

Gocheva, V., and Joyce, J.A. (2007). Cysteine cathepsins and the cutting edge of cancer invasion. Cell Cycle Georget. Tex *6*, 60–64.

Goh, F.G., Piccinini, A.M., Krausgruber, T., Udalova, I.A., and Midwood, K.S. (2010). Transcriptional regulation of the endogenous danger signal tenascin-C: a novel autocrine loop in inflammation. J. Immunol. Baltim. Md 1950 *184*, 2655–2662.

Golks, A., Brenner, D., Fritsch, C., Krammer, P.H., and Lavrik, I.N. (2005). c-FLIPR, a new regulator of death receptor-induced apoptosis. J. Biol. Chem. *280*, 14507–14513.

Graves, J.D., Kordich, J.J., Huang, T.-H., Piasecki, J., Bush, T.L., Sullivan, T., Foltz, I.N., Chang, W., Douangpanya, H., Dang, T., et al. (2014). Apo2L/TRAIL and the Death Receptor

5 Agonist Antibody AMG 655 Cooperate to Promote Receptor Clustering and Antitumor Activity. Cancer Cell *26*, 177–189.

Griffith, J.W., Sokol, C.L., and Luster, A.D. (2014). Chemokines and Chemokine Receptors: Positioning Cells for Host Defense and Immunity. Annu. Rev. Immunol. *32*, 659–702.

Griffith, T.S., Wiley, S.R., Kubin, M.Z., Sedger, L.M., Maliszewski, C.R., and Fanger, N.A. (1999a). Monocyte-mediated Tumoricidal Activity via the Tumor Necrosis Factor–related Cytokine, TRAIL. J. Exp. Med. *189*, 1343–1354.

Griffith, T.S., Rauch, C.T., Smolak, P.J., Waugh, J.Y., Boiani, N., Lynch, D.H., Smith, C.A., Goodwin, R.G., and Kubin, M.Z. (1999b). Functional Analysis of TRAIL Receptors Using Monoclonal Antibodies. J. Immunol. *162*, 2597–2605.

Griggs, L.A., Hassan, N.T., Malik, R.S., Griffin, B., Martinez, B.A., Elmore, L.W., and Lemmon, C.A. (2017). Fibronectin Fibrils Regulate TGF-β1-induced Epithelial-Mesenchymal Transition. Matrix Biol. J. Int. Soc. Matrix Biol. *60–61*, 157–175.

Grivennikov, S.I., Greten, F.R., and Karin, M. (2010). Immunity, inflammation, and cancer. Cell *140*, 883–899.

Grumet, M., Hoffman, S., Crossin, K.L., and Edelman, G.M. (1985). Cytotactin, an extracellular matrix protein of neural and non-neural tissues that mediates glia-neuron interaction. Proc. Natl. Acad. Sci. *82*, 8075–8079.

Gu, S., Ni, T., Wang, J., Liu, Y., Fan, Q., Wang, Y., Huang, T., Chu, Y., Sun, X., and Wang, Y. (2018). CD47 Blockade Inhibits Tumor Progression through Promoting Phagocytosis of Tumor Cells by M2 Polarized Macrophages in Endometrial Cancer (Hindawi).

Guan, H., Wan, Y., Lan, J., Wang, Q., Wang, Z., Li, Y., Zheng, J., Zhang, X., Wang, Z., Shen, Y., et al. (2016). PD-L1 is a critical mediator of regulatory B cells and T cells in invasive breast cancer. Sci. Rep. *6*.

Gurevicius, K., Kuang, F., Stoenica, L., Irintchev, A., Gureviciene, I., Dityatev, A., Schachner, M., and Tanila, H. (2009). Genetic ablation of tenascin-C expression leads to abnormal hippocampal CA1 structure and electrical activity in vivo. Hippocampus *19*, 1232–1246.

Guttery, D.S., Shaw, J.A., Lloyd, K., Pringle, J.H., and Walker, R.A. (2010). Expression of tenascin-C and its isoforms in the breast. Cancer Metastasis Rev. *29*, 595–606.

Halaas, Vik, Ashkenazi, and Espevik (2000). Lipopolysaccharide Induces Expression of APO2 Ligand/TRAIL in Human Monocytes and Macrophages. Scand. J. Immunol. *51*, 244–250.

Halsted, W.S. (1898). I. A Clinical and Histological Study of certain Adenocarcinomata of the Breast: and a Brief Consideration of the Supraclavicular Operation and of the Results of Operations for Cancer of the Breast from 1889 to 1898 at the Johns Hopkins Hospital. Ann. Surg. *28*, 557–576.

Hanahan, D., and Weinberg, R.A. (2000). The Hallmarks of Cancer. Cell *100*, 57–70.

Hanahan, D., and Weinberg, R.A. (2011). Hallmarks of Cancer: The Next Generation. Cell *144*, 646–674.

Hanahan, D., and Weinberg, R.A. (2017). Biological Hallmarks of Cancer. In Holland-Frei Cancer Medicine, (American Cancer Society), pp. 1–10.

Hancox, R.A., Allen, M.D., Holliday, D.L., Edwards, D.R., Pennington, C.J., Guttery, D.S., Shaw, J.A., Walker, R.A., Pringle, J.H., and Jones, J.L. (2009). Tumour-associated tenascin-C isoforms promote breast cancer cell invasion and growth by matrix metalloproteinase-dependent and independent mechanisms. Breast Cancer Res. BCR *11*, R24.

Harbeck, N., and Gnant, M. (2017). Breast cancer. The Lancet *389*, 1134–1150.

Harbeck, N., Salem, M., Nitz, U., Gluz, O., and Liedtke, C. (2010). Personalized treatment of early-stage breast cancer: Present concepts and future directions. Cancer Treat. Rev. *36*, 584–594.

Harburger, D.S., and Calderwood, D.A. (2009). Integrin signalling at a glance. J. Cell Sci. *122*, 159–163.

Hartwig, T., Montinaro, A., von Karstedt, S., Sevko, A., Surinova, S., Chakravarthy, A., Taraborrelli, L., Draber, P., Lafont, E., Arce Vargas, F., et al. (2017). The TRAIL-Induced Cancer Secretome Promotes a Tumor-Supportive Immune Microenvironment via CCR2. Mol. Cell *65*, 730-742.e5.

Hasebe, T., Sasaki, S., Imoto, S., and Ochiai, A. (2001). Highly Proliferative Fibroblasts Forming Fibrotic Focus Govern Metastasis of Invasive Ductal Carcinoma of the Breast. Mod. Pathol. *14*, 325–337.

Hauzenberger, D., Olivier, P., Gundersen, D., and Rüegg, C. (1999). Tenascin-C inhibits beta1 integrin-dependent T lymphocyte adhesion to fibronectin through the binding of its fnIII 1-5 repeats to fibronectin. Eur. J. Immunol. *29*, 1435–1447.

Hayakawa, Y., Screpanti, V., Yagita, H., Grandien, A., Ljunggren, H.-G., Smyth, M.J., and Chambers, B.J. (2004). NK Cell TRAIL Eliminates Immature Dendritic Cells In Vivo and Limits Dendritic Cell Vaccination Efficacy. J. Immunol. *172*, 123–129.

Hendaoui, I., Tucker, R.P., Zingg, D., Bichet, S., Schittny, J., and Chiquet-Ehrismann, R. (2014). Tenascin-C is required for normal Wnt/β-catenin signaling in the whisker follicle stem cell niche. Matrix Biol. *40*, 46–53.

Herbst, R.S., Eckhardt, S.G., Kurzrock, R., Ebbinghaus, S., O'Dwyer, P.J., Gordon, M.S., Novotny, W., Goldwasser, M.A., Tohnya, T.M., Lum, B.L., et al. (2010a). Phase I dose-escalation study of recombinant human Apo2L/TRAIL, a dual proapoptotic receptor agonist, in patients with advanced cancer. J. Clin. Oncol. Off. J. Am. Soc. Clin. Oncol. *28*, 2839–2846.

Herbst, R.S., Kurzrock, R., Hong, D.S., Valdivieso, M., Hsu, C.-P., Goyal, L., Juan, G., Hwang, Y.C., Wong, S., Hill, J.S., et al. (2010b). A first-in-human study of conatumumab in adult patients with advanced solid tumors. Clin. Cancer Res. Off. J. Am. Assoc. Cancer Res. *16*, 5883–5891.

Herbst, R.S., Soria, J.-C., Kowanetz, M., Fine, G.D., Hamid, O., Gordon, M.S., Sosman, J.A., McDermott, D.F., Powderly, J.D., Gettinger, S.N., et al. (2014). Predictive correlates of response to the anti-PD-L1 antibody MPDL3280A in cancer patients. Nature *515*, 563–567.

Hermiston, M.L., Xu, Z., and Weiss, A. (2003). CD45: A Critical Regulator of Signaling Thresholds in Immune Cells. Annu. Rev. Immunol. *21*, 107–137.

Herynk, M.H., and Fuqua, S.A.W. (2004). Estrogen receptor mutations in human disease. Endocr. Rev. *25*, 869–898.

Hicke, B.J., Marion, C., Chang, Y.F., Gould, T., Lynott, C.K., Parma, D., Schmidt, P.G., and Warren, S. (2001). Tenascin-C aptamers are generated using tumor cells and purified protein. J. Biol. Chem. *276*, 48644–48654.

Hicke, B.J., Stephens, A.W., Gould, T., Chang, Y.-F., Lynott, C.K., Heil, J., Borkowski, S., Hilger, C.-S., Cook, G., Warren, S., et al. (2006). Tumor Targeting by an Aptamer. J. Nucl. Med. *47*, 668–678.

Hicklin, D.J., and Ellis, L.M. (2005). Role of the Vascular Endothelial Growth Factor Pathway in Tumor Growth and Angiogenesis. J. Clin. Oncol. *23*, 1011–1027.

Hoffmann, O., Priller, J., Prozorovski, T., Schulze-Topphoff, U., Baeva, N., Lunemann, J.D., Aktas, O., Mahrhofer, C., Stricker, S., Zipp, F., et al. (2007). TRAIL limits excessive host immune responses in bacterial meningitis. J. Clin. Invest. *117*, 2004–2013.

Hofmarcher, T., Lindgren, P., Wilking, N., and Jönsson, B. (2020). The cost of cancer in Europe 2018. Eur. J. Cancer *129*, 41–49.

Hoogwater, F.J.H., Nijkamp, M.W., Smakman, N., Steller, E.J.A., Emmink, B.L., Westendorp, B.F., Raats, D.A.E., Sprick, M.R., Schaefer, U., Houdt, W.J.V., et al. (2010). Oncogenic K-Ras Turns Death Receptors Into Metastasis-Promoting Receptors in Human and Mouse Colorectal Cancer Cells. Gastroenterology *138*, 2357–2367.

Hortobágyi, G.N. (1997). Anthracyclines in the treatment of cancer. An overview. Drugs *54 Suppl 4*, 1–7.

Hu, M., Yao, J., Carroll, D.K., Weremowicz, S., Chen, H., Carrasco, D., Richardson, A., Violette, S., Nikolskaya, T., Nikolsky, Y., et al. (2008). Regulation of in situ to invasive breast carcinoma transition. Cancer Cell *13*, 394–406.

Huang, Y.-J., and Hsu, S.-H. (2017). TRAIL-functionalized gold nanoparticles selectively trigger apoptosis in polarized macrophages. Nanotheranostics *1*, 326–337.

Huang, D., Su, S., Cui, X., Shen, X., Zeng, Y., Wu, W., Chen, J., Chen, F., He, C., Liu, J., et al. (2014). Nerve Fibers in Breast Cancer Tissues Indicate Aggressive Tumor Progression. Medicine (Baltimore) *93*.

Huang, W., Chiquet-Ehrismann, R., Moyano, J.V., Garcia-Pardo, A., and Orend, G. (2001). Interference of Tenascin-C with Syndecan-4 Binding to Fibronectin Blocks Cell Adhesion and Stimulates Tumor Cell Proliferation. Cancer Res. *61*, 8586–8594.

Huber, V., Fais, S., Iero, M., Lugini, L., Canese, P., Squarcina, P., Zaccheddu, A., Colone, M., Arancia, G., Gentile, M., et al. (2005). Human Colorectal Cancer Cells Induce T-Cell Death Through Release of Proapoptotic Microvesicles: Role in Immune Escape. Gastroenterology *128*, 1796–1804.

Hughes, C.E., and Nibbs, R.J.B. (2018). A guide to chemokines and their receptors. Febs J. *285*, 2944–2971.

Hymowitz, S.G., O'Connell, M.P., Ultsch, M.H., Hurst, A., Totpal, K., Ashkenazi, A., de Vos, A.M., and Kelley, R.F. (2000). A Unique Zinc-Binding Site Revealed by a High-Resolution X-ray Structure of Homotrimeric Apo2L/TRAIL. Biochemistry *39*, 633–640.

Hynes, R.O., and Naba, A. (2012). Overview of the Matrisome—An Inventory of Extracellular Matrix Constituents and Functions. Cold Spring Harb. Perspect. Biol. *4*.

Ikeda, T., Hirata, S., Fukushima, S., Matsunaga, Y., Ito, T., Uchino, M., Nishimura, Y., and Senju, S. (2010). Dual Effects of TRAIL in Suppression of Autoimmunity: The Inhibition of Th1 Cells and the Promotion of Regulatory T Cells. J. Immunol. *185*, 5259–5267.

Ilunga, K., Nishiura, R., Inada, H., El-Karef, A., Imanaka-Yoshida, K., Sakakura, T., and Yoshida, T. (2004). Co-stimulation of human breast cancer cells with transforming growth factor-β and tenascin-C enhances matrix metalloproteinase-9 expression and cancer cell invasion. Int. J. Exp. Pathol. *85*, 373–379.

Imanaka-Yoshida, K., Yoshida, T., and Miyagawa-Tomita, S. (2014). Tenascin-C in Development and Disease of Blood Vessels. Anat. Rec. *297*, 1747–1757.

Ingham, K.C., Brew, S.A., and Erickson, H.P. (2004). Localization of a Cryptic Binding Site for Tenascin on Fibronectin. J. Biol. Chem. *279*, 28132–28135.

Inoue, H., Shiraki, K., Yamanaka, T., Ohmori, S., Sakai, T., Deguchi, M., Okano, H., Murata, K., Sugimoto, K., and Nakano, T. (2002). Functional Expression of Tumor Necrosis Factor-Related Apoptosis-Inducing Ligand in Human Colonic Adenocarcinoma Cells. Lab. Invest. *82*, 1111–1119.

Ioachim, E., Charchanti, A., Briasoulis, E., Karavasilis, V., Tsanou, H., Arvanitis, D.L., Agnantis, N.J., and Pavlidis, N. (2002). Immunohistochemical expression of extracellular matrix components tenascin, fibronectin, collagen type IV and laminin in breast cancer: their prognostic value and role in tumour invasion and progression. Eur. J. Cancer *38*, 2362–2370.

Ishihara, A., Yoshida, T., Tamaki, H., and Sakakura, T. (1995). Tenascin expression in cancer cells and stroma of human breast cancer and its prognostic significance. Clin. Cancer Res. *1*, 1035–1041.

Ishii, K., Imanaka-Yoshida, K., Yoshida, T., and Sugimura, Y. (2008). Role of stromal tenascin-C in mouse prostatic development and epithelial cell differentiation. Dev. Biol. *324*, 310–319.

Ishimura, N., Isomoto, H., Bronk, S.F., and Gores, G.J. (2006). Trail induces cell migration and invasion in apoptosis-resistant cholangiocarcinoma cells. Am. J. Physiol.-Gastrointest. Liver Physiol. *290*, G129–G136.

Ishiwata, T., Takahashi, K., Shimanuki, Y., Ohashi, R., Cui, R., Takahashi, F., Shimizu, K., Miura, K., and Fukuchi, Y. (2005). Serum tenascin-C as a potential predictive marker of angiogenesis in non-small cell lung cancer. Anticancer Res. *25*, 489–495.

Iyori, M., Zhang, T., Pantel, H., Gagne, B.A., and Sentman, C.L. (2011). TRAIL/DR5 plays a critical role in NK cell-mediated negative regulation of dendritic cell cross-priming of T cells. J. Immunol. Baltim. Md 1950 *187*, 3087–3095.

Jachetti, E., Caputo, S., Mazzoleni, S., Brambillasca, C.S., Parigi, S.M., Grioni, M., Piras, I.S., Restuccia, U., Calcinotto, A., Freschi, M., et al. (2015). Tenascin-C Protects Cancer Stem–like Cells from Immune Surveillance by Arresting T-cell Activation. Cancer Res. *75*, 2095–2108.

Jagsi, R., Chadha, M., Moni, J., Ballman, K., Laurie, F., Buchholz, T.A., Giuliano, A., and Haffty, B.G. (2014). Radiation Field Design in the ACOSOG Z0011 (Alliance) Trial. J. Clin. Oncol. *32*, 3600–3606.

Jahkolal, T., Toivonen, T., Virtanen, I., and Blomqvist, C. (1998). Tenascin-C expression in invasion border of early breast cancer: a predictor of local and distant recurrence. Br. J. Cancer *7*.

Jinnin, M., Ihn, H., Asano, Y., Yamane, K., Trojanowska, M., and Tamaki, K. (2004). Tenascin-C upregulation by transforming growth factor-beta in human dermal fibroblasts involves Smad3, Sp1, and Ets1. Oncogene *23*, 1656–1667.

Jo, M., Kim, T.H., Seol, D.W., Esplen, J.E., Dorko, K., Billiar, T.R., and Strom, S.C. (2000). Apoptosis induced in normal human hepatocytes by tumor necrosis factor-related apoptosis-inducing ligand. Nat. Med. *6*, 564–567.

Jones, S.E., Erban, J., Overmoyer, B., Budd, G.T., Hutchins, L., Lower, E., Laufman, L., Sundaram, S., Urba, W.J., Pritchard, K.I., et al. (2005). Randomized phase III study of docetaxel compared with paclitaxel in metastatic breast cancer. J. Clin. Oncol. Off. J. Am. Soc. Clin. Oncol. *23*, 5542–5551.

Jouan-Lanhouet, S., Arshad, M.I., Piquet-Pellorce, C., Martin-Chouly, C., Le Moigne-Muller, G., Van Herreweghe, F., Takahashi, N., Sergent, O., Lagadic-Gossmann, D., Vandenabeele, P., et al. (2012). TRAIL induces necroptosis involving RIPK1/RIPK3-dependent PARP-1 activation. Cell Death Differ. *19*, 2003–2014.

Jovčevska, I., and Muyldermans, S. (2020). The Therapeutic Potential of Nanobodies. BioDrugs *34*, 11–26.

Kalluri, R., and Zeisberg, M. (2006). Fibroblasts in cancer. Nat. Rev. Cancer *6*, 392–401.

Kammerer, R.A., Schulthess, T., Landwehr, R., Lustig, A., Fischer, D., and Engel, J. (1998). Tenascin-C Hexabrachion Assembly Is a Sequential Two-step Process Initiated by Coiled-coil α-Helices. J. Biol. Chem. *273*, 10602–10608.

Kamohara, H., Matsuyama, W., Shimozato, O., Abe, K., Galligan, C., Hashimoto, S.-I., Matsushima, K., and Yoshimura, T. (2004). Regulation of tumour necrosis factor-related apoptosis-inducing ligand (TRAIL) and TRAIL receptor expression in human neutrophils. Immunology *111*, 186–194.

Kang, Z., Chen, J.-J., Yu, Y., Li, B., Sun, S.-Y., Zhang, B., and Cao, L. (2011). Drozitumab, a human antibody to death receptor 5, has potent antitumor activity against

rhabdomyosarcoma with the expression of caspase-8 predictive of response. Clin. Cancer Res. Off. J. Am. Assoc. Cancer Res. *17*, 3181–3192.

Karagiannis, G.S., Rivera-Sanchez, L., Duran, C.L., Oktay, M.H., and Condeelis, J.S. (2020). Emerging roles of Cxcl12/Cxcr4 signaling axis in breast cancer metastasis. J. Immunol. *204*, 90.4-90.4.

von Karstedt, S., Montinaro, A., and Walczak, H. (2017). Exploring the TRAILs less travelled: TRAIL in cancer biology and therapy. Nat. Rev. Cancer *17*, 352–366.

Kayagaki, N., Yamaguchi, N., Nakayama, M., Eto, H., Okumura, K., and Yagita, H. (1999). Type I Interferons (IFNs) Regulate Tumor Necrosis Factor–related Apoptosis-inducing Ligand (TRAIL) Expression on Human T Cells: A Novel Mechanism for the Antitumor Effects of Type I IFNs. J. Exp. Med. *189*, 1451–1460.

Kayagaki, N., Yamaguchi, N., Abe, M., Hirose, S., Shirai, T., Okumura, K., and Yagita, H. (2002). Suppression of antibody production by TNF-related apoptosis-inducing ligand (TRAIL). Cell. Immunol. *219*, 82–91.

Keane, M.M., Ettenberg, S.A., Nau, M.M., Russell, E.K., and Lipkowitz, S. (1999). Chemotherapy augments TRAIL-induced apoptosis in breast cell lines. Cancer Res. *59*, 734–741.

Keefe, A.D., Pai, S., and Ellington, A. (2010). Aptamers as therapeutics. Nat. Rev. Drug Discov. *9*, 537–550.

Kemp, T.J., Moore, J.M., and Griffith, T.S. (2004). Human B Cells Express Functional TRAIL/Apo-2 Ligand after CpG-Containing Oligodeoxynucleotide Stimulation. J. Immunol. *173*, 892–899.

Kemp, T.J., Ludwig, A.T., Earel, J.K., Moore, J.M., VanOosten, R.L., Moses, B., Leidal, K., Nauseef, W.M., and Griffith, T.S. (2005). Neutrophil stimulation with Mycobacterium bovis bacillus Calmette-Guérin (BCG) results in the release of functional soluble TRAIL/Apo-2L. Blood *106*, 3474–3482.

Keynes, G. (1937). Conservative Treatment of Cancer of the Breast. Br. Med. J. *2*, 643-666.3.

Kiernan, B.W., Garcion, E., Ferguson, J., Frost, E.E., Torres, E.M., Dunnett, S.B., Saga, Y., Aizawa, S., Faissner, A., Kaur, R., et al. (1999). Myelination and behaviour of tenascin-C null transgenic mice. Eur. J. Neurosci. *11*, 3082–3092.

Kim, J.-Y., Kim, Y.-M., Park, J.-M., Han, Y.M., Lee, K.C., Hahm, K.B., and Hong, S. (2018). Cancer preventive effect of recombinant TRAIL by ablation of oncogenic inflammation in colitis-associated cancer rather than anticancer effect. Oncotarget *9*, 1705–1716.

Kim, M.Y., Kim, O.R., Choi, Y.S., Lee, H., Park, K., Lee, C.-T., Kang, K.W., and Jeong, S. (2012). Selection and characterization of tenascin C targeting peptide. Mol. Cells *33*, 71–77.

Kim, S.-H., Kim, K., Kwagh, J.G., Dicker, D.T., Herlyn, M., Rustgi, A.K., Chen, Y., and El-Deiry, W.S. (2004). Death induction by recombinant native TRAIL and its prevention by a caspase 9 inhibitor in primary human esophageal epithelial cells. J. Biol. Chem. *279*, 40044–40052.

Kimura, T., Shiraishi, K., Furusho, A., Ito, S., Hirakata, S., Nishida, N., Yoshimura, K., Imanaka-Yoshida, K., Yoshida, T., Ikeda, Y., et al. (2014). Tenascin C protects aorta from acute dissection in mice. Sci. Rep. *4*, 4051.

Klapper, L.N., Waterman, H., Sela, M., and Yarden, Y. (2000). Tumor-inhibitory Antibodies to HER-2/ErbB-2 May Act by Recruiting c-Cbl and Enhancing Ubiquitination of HER-2. Cancer Res. *60*, 3384–3388.

Ko, H.Y., Choi, K.-J., Lee, C.H., and Kim, S. (2011). A multimodal nanoparticle-based cancer imaging probe simultaneously targeting nucleolin, integrin αvβ3 and tenascin-C proteins. Biomaterials *32*, 1130–1138.

Ko, M.H., Kim, S., Kang, W.J., Lee, J.H., Kang, H., Moon, S.H., Hwang, D.W., Ko, H.Y., and Lee, D.S. (2009). In vitro derby imaging of cancer biomarkers using quantum dots. Small Weinh. Bergstr. Ger. *5*, 1207–1212.

Kohler, B.A., Sherman, R.L., Howlader, N., Jemal, A., Ryerson, A.B., Henry, K.A., Boscoe, F.P., Cronin, K.A., Lake, A., Noone, A.-M., et al. (2015). Annual Report to the Nation on the Status of Cancer, 1975-2011, Featuring Incidence of Breast Cancer Subtypes by Race/Ethnicity, Poverty, and State. JNCI J. Natl. Cancer Inst. *107*.

Kojima, Y., Acar, A., Eaton, E.N., Mellody, K.T., Scheel, C., Ben-Porath, I., Onder, T.T., Wang, Z.C., Richardson, A.L., Weinberg, R.A., et al. (2010). Autocrine TGF-beta and stromal cell-derived factor-1 (SDF-1) signaling drives the evolution of tumor-promoting mammary stromal myofibroblasts. Proc. Natl. Acad. Sci. U. S. A. *107*, 20009–20014.

Kong, D.-H., Kim, M.R., Jang, J.H., Na, H.-J., and Lee, S. (2017). A Review of Anti-Angiogenic Targets for Monoclonal Antibody Cancer Therapy. Int. J. Mol. Sci. *18*.

Korbecki, J., Simińska, D., Kojder, K., Grochans, S., Gutowska, I., Chlubek, D., and Baranowska-Bosiacka, I. (2020). Fractalkine/CX3CL1 in Neoplastic Processes. Int. J. Mol. Sci. *21*.

Kovacs, J.A., Vogel, S., Albert, J.M., Falloon, J., Davey, R.T., Walker, R.E., Polis, M.A., Spooner, K., Metcalf, J.A., Baseler, M., et al. (1996). Controlled trial of interleukin-2 infusions in patients infected with the human immunodeficiency virus. N. Engl. J. Med. *335*, 1350–1356.

Kroman, N., Wohlfahrt, J., Mouridsen, H.T., and Melbye, M. (2003). Influence of tumor location on breast cancer prognosis. Int. J. Cancer *105*, 542–545.

Krueger, A., Schmitz, I., Baumann, S., Krammer, P.H., and Kirchhoff, S. (2001). Cellular FLICE-inhibitory protein splice variants inhibit different steps of caspase-8 activation at the CD95 death-inducing signaling complex. J. Biol. Chem. *276*, 20633–20640.

Kuan, E.L., and Ziegler, S.F. (2018). A tumor-myeloid cell axis, mediated via interleukin 1α and TSLP, promotes breast cancer progression. Nat. Immunol. *19*, 366–374.

Langlois, B., Saupe, F., Rupp, T., Arnold, C., Van der Heyden, M., Orend, G., and Hussenet, T. (2014). AngioMatrix, a signature of the tumor angiogenic switch-specific matrisome, correlates with poor prognosis for glioma and colorectal cancer patients. Oncotarget *5*.

Latijnhouwers, M.A., Bergers, M., Van Bergen, B.H., Spruijt, K.I., Andriessen, M.P., and Schalkwijk, J. (1996). Tenascin expression during wound healing in human skin. J. Pathol. *178*, 30–35.

Lawrence, D., Shahrokh, Z., Marsters, S., Achilles, K., Shih, D., Mounho, B., Hillan, K., Totpal, K., DeForge, L., Schow, P., et al. (2001). Differential hepatocyte toxicity of recombinant Apo2L/TRAIL versions. Nat. Med. *7*, 383–385.

Lee, B., Sharron, M., Montaner, L.J., Weissman, D., and Doms, R.W. (1999). Quantification of CD4, CCR5, and CXCR4 levels on lymphocyte subsets, dendritic cells, and differentially conditioned monocyte-derived macrophages. Proc. Natl. Acad. Sci. *96*, 5215–5220.

Lee, T.-J., Lee, J.T., Park, J.-W., and Kwon, T.K. (2006). Acquired TRAIL resistance in human breast cancer cells are caused by the sustained cFLIPL and XIAP protein levels and ERK activation. Biochem. Biophys. Res. Commun. *351*, 1024–1030.

Lemke, J., von Karstedt, S., Zinngrebe, J., and Walczak, H. (2014). Getting TRAIL back on track for cancer therapy. Cell Death Differ. *21*, 1350–1364.

Leverkus, M., Walczak, H., McLellan, A., Fries, H.W., Terbeck, G., Bröcker, E.B., and Kämpgen, E. (2000). Maturation of dendritic cells leads to up-regulation of cellular FLICE-inhibitory protein and concomitant down-regulation of death ligand-mediated apoptosis. Blood *96*, 2628–2631.

Li, J., Yang, P., Wu, Q., Li, H., Ding, Y., Hsu, H.-C., Spalding, D.M., and Mountz, J.D. (2013). Death receptor 5-targeted depletion of interleukin-23-producing macrophages, Th17, and Th1/17 associated with defective tyrosine phosphatase in mice and patients with rheumatoid arthritis. Arthritis Rheum. *65*, 2594–2605.

Li, J.H., Kirkiles-Smith, N.C., McNiff, J.M., and Pober, J.S. (2003). TRAIL Induces Apoptosis and Inflammatory Gene Expression in Human Endothelial Cells. J. Immunol. *171*, 1526–1533.

Li, Z.-L., Zhang, H.-L., Huang, Y., Huang, J.-H., Sun, P., Zhou, N.-N., Chen, Y.-H., Mai, J., Wang, Y., Yu, Y., et al. (2020). Autophagy deficiency promotes triple-negative breast cancer resistance to T cell-mediated cytotoxicity by blocking tenascin-C degradation. Nat. Commun. *11*, 3806.

Libring, S., Shinde, A., Chanda, M.K., Nuru, M., George, H., Saleh, A.M., Abdullah, A., Kinzer-Ursem, T.L., Calve, S., Wendt, M.K., et al. (2020). The Dynamic Relationship of Breast Cancer Cells and Fibroblasts in Fibronectin Accumulation at Primary and Metastatic Tumor Sites. Cancers *12*.

Lichtarge, O., Bourne, H.R., and Cohen, F.E. (1996). An evolutionary trace method defines binding surfaces common to protein families. J. Mol. Biol. *257*, 342–358.

Liguori, M., Buracchi, C., Pasqualini, F., Bergomas, F., Pesce, S., Sironi, M., Grizzi, F., Mantovani, A., Belgiovine, C., and Allavena, P. (2016). Functional TRAIL receptors in monocytes and tumor-associated macrophages: A possible targeting pathway in the tumor microenvironment. Oncotarget *7*, 41662–41676.

Lin, Y., Xu, J., and Lan, H. (2019). Tumor-associated macrophages in tumor metastasis: biological roles and clinical therapeutic applications. J. Hematol. Oncol.J Hematol Oncol *12*, 76.

Lingasamy, P., Tobi, A., Haugas, M., Hunt, H., Paiste, P., Asser, T., Rätsep, T., Kotamraju, V.R., Bjerkvig, R., and Teesalu, T. (2019). Bi-specific tenascin-C and fibronectin targeted peptide for solid tumor delivery. Biomaterials *219*, 119373.

Lingasamy, P., Tobi, A., Kurm, K., Kopanchuk, S., Sudakov, A., Salumäe, M., Rätsep, T., Asser, T., Bjerkvig, R., and Teesalu, T. (2020). Tumor-penetrating peptide for systemic targeting of Tenascin-C. Sci. Rep. *10*, 5809.

Linkermann, A., and Green, D.R. (2014). Necroptosis. N. Engl. J. Med. *370*, 455–465.

Liu, X., Kwon, H., Li, Z., and Fu, Y. (2017). Is CD47 an innate immune checkpoint for tumor evasion? J. Hematol. Oncol.J Hematol Oncol *10*, 12.

Loeffler, M., Krüger, J.A., Niethammer, A.G., and Reisfeld, R.A. (2006). Targeting tumor-associated fibroblasts improves cancer chemotherapy by increasing intratumoral drug uptake. J. Clin. Invest. *116*, 1955–1962.

Lowy, C.M., and Oskarsson, T. (2015). Tenascin C in metastasis: A view from the invasive front. Cell Adhes. Migr. *9*, 112–124.

Lu, C.-W., Lo, Y.-H., Chen, C.-H., Lin, C.-Y., Tsai, C.-H., Chen, P.-J., Yang, Y.-F., Wang, C.-H., Tan, C.-H., Hou, M.-F., et al. (2017). VLDL and LDL, but not HDL, promote breast cancer cell proliferation, metastasis and angiogenesis. Cancer Lett. *388*, 130–138.

Lu, M., Marsters, S., Ye, X., Luis, E., Gonzalez, L., and Ashkenazi, A. (2014). E-Cadherin Couples Death Receptors to the Cytoskeleton to Regulate Apoptosis. Mol. Cell *54*, 987–998.

Lum, J.J., Bren, G., McClure, R., and Badley, A.D. (2005). Elimination of Senescent Neutrophils by TNF-Related Apoptosis-Inducing Ligand. J. Immunol. *175*, 1232–1238.

Lund, A.W., Duraes, F.V., Hirosue, S., Raghavan, V.R., Nembrini, C., Thomas, S.N., Issa, A., Hugues, S., and Swartz, M.A. (2012). VEGF-C Promotes Immune Tolerance in B16 Melanomas and Cross-Presentation of Tumor Antigen by Lymph Node Lymphatics. Cell Rep. *1*, 191–199.

Ma, D., Liu, S., Lal, B., Wei, S., Wang, S., Zhan, D., Zhang, H., Lee, R.S., Gao, P., Lopez-Bertoni, H., et al. (2019). Extracellular Matrix Protein Tenascin C Increases Phagocytosis Mediated by CD47 Loss of Function in Glioblastoma. Cancer Res. *79*, 2697–2708.

Ma, Q., Dieterich, L.C., Ikenberg, K., Bachmann, S.B., Mangana, J., Proulx, S.T., Amann, V.C., Levesque, M.P., Dummer, R., Baluk, P., et al. (2018). Unexpected contribution of lymphatic vessels to promotion of distant metastatic tumor spread. Sci. Adv. *4*, eaat4758.

MacFarlane, M., Ahmad, M., Srinivasula, S.M., Fernandes-Alnemri, T., Cohen, G.M., and Alnemri, E.S. (1997). Identification and Molecular Cloning of Two Novel Receptors for the Cytotoxic Ligand TRAIL. J. Biol. Chem. *272*, 25417–25420.

Mackie, E.J., Halfter, W., and Liverani, D. (1988). Induction of tenascin in healing wounds. J. Cell Biol. *107*, 2757–2767.

Mansour, E.G., Gray, R., Shatila, A.H., Osborne, C.K., Tormey, D.C., Gilchrist, K.W., Cooper, M.R., and Falkson, G. (1989). Efficacy of adjuvant chemotherapy in high-risk node-negative breast cancer. An intergroup study. N. Engl. J. Med. *320*, 485–490.

Mantovani, A., Schioppa, T., Porta, C., Allavena, P., and Sica, A. (2006). Role of tumor-associated macrophages in tumor progression and invasion. Cancer Metastasis Rev. *25*, 315–322.

Mao, Y., Qu, Q., Chen, X., Huang, O., Wu, J., and Shen, K. (2016). The Prognostic Value of Tumor-Infiltrating Lymphocytes in Breast Cancer: A Systematic Review and Meta-Analysis. PloS One *11*, e0152500.

Mariani, S.M., and Krammer, P.H. (1998). Differential regulation of TRAIL and CD95 ligand in transformed cells of the T and B lymphocyte lineage. Eur. J. Immunol. *28*, 973–982.

Martina, E., Degen, M., Ruegg, C., Merlo, A., Lino, M.M., Chiquet-Ehrismann, R., and Brellier, F. (2010). Tenascin-W is a specific marker of glioma-associated blood vessels and stimulates angiogenesis in vitro. FASEB J. *24*, 778–787.

Martínez-Lorenzo, M.J., Alava, M.A., Gamen, S., Kim, K.J., Chuntharapai, A., Piñeiro, A., Naval, J., and Anel, A. (1998). Involvement of APO2 ligand/TRAIL in activation-induced death of Jurkat and human peripheral blood T cells. Eur. J. Immunol. *28*, 2714–2725.

Martinez-Lostao, L., Miguel, D. de, Al-Wasaby, S., Gallego-Lleyda, A., and Anel, A. (2015). Death ligands and granulysin: mechanisms of tumor cell death induction and therapeutic opportunities. Immunotherapy *7*, 883–882.

McArthur, H.L., Diab, A., Page, D.B., Yuan, J., Solomon, S.B., Sacchini, V., Comstock, C., Durack, J.C., Maybody, M., Sung, J., et al. (2016). A pilot study of preoperative single-dose ipilimumab and/or cryoablation in women with early- stage breast cancer with comprehensive immune profiling. Clin. Cancer Res. Off. J. Am. Assoc. Cancer Res. *22*, 5729.

McGrath, E.E., Marriott, H.M., Lawrie, A., Francis, S.E., Sabroe, I., Renshaw, S.A., Dockrell, D.H., and Whyte, M.K.B. (2011). TNF-related apoptosis-inducing ligand (TRAIL) regulates inflammatory neutrophil apoptosis and enhances resolution of inflammation. J. Leukoc. Biol. *90*, 855–865.

Metcalfe, K., Lynch, H.T., Foulkes, W.D., Tung, N., Kim-Sing, C., Olopade, O.I., Eisen, A., Rosen, B., Snyder, C., Gershman, S., et al. (2015). Effect of Oophorectomy on Survival After Breast Cancer in BRCA1 and BRCA2 Mutation Carriers. JAMA Oncol. *1*, 306–313.

Mettouchi, A., Cabon, F., Montreau, N., Dejong, V., Vernier, P., Gherzi, R., Mercier, G., and Binétruy, B. (1997). The c-Jun-induced transformation process involves complex regulation of tenascin-C expression. Mol. Cell. Biol. *17*, 3202–3209.

Micheau, O., Shirley, S., and Dufour, F. (2013). Death receptors as targets in cancer: TRAIL clinical trials. Br. J. Pharmacol. *169*, 1723–1744.

Midwood, K., Sacre, S., Piccinini, A.M., Inglis, J., Trebaul, A., Chan, E., Drexler, S., Sofat, N., Kashiwagi, M., Orend, G., et al. (2009). Tenascin-C is an endogenous activator of Toll-like receptor 4 that is essential for maintaining inflammation in arthritic joint disease. Nat. Med. *15*, 774–780.

Midwood, K.S., Chiquet, M., Tucker, R.P., and Orend, G. (2016). Tenascin-C at a glance. J. Cell Sci. *129*, 4321–4327.

de Miguel, D., Lemke, J., Anel, A., Walczak, H., and Martinez-Lostao, L. (2016). Onto better TRAILs for cancer treatment. Cell Death Differ. *23*, 733–747.

Miles, D.W., Diéras, V., Cortés, J., Duenne, A.-A., Yi, J., and O'Shaughnessy, J. (2013). First-line bevacizumab in combination with chemotherapy for HER2-negative metastatic breast cancer: pooled and subgroup analyses of data from 2447 patients. Ann. Oncol. Off. J. Eur. Soc. Med. Oncol. *24*, 2773–2780.

Ming, X., Qiu, S., Liu, X., Li, S., Wang, Y., Zhu, M., Li, N., Luo, P., Liang, C., and Tu, J. (2019). Prognostic Role of Tenascin-C for Cancer Outcome: A Meta-Analysis. Technol. Cancer Res. Treat. *18*, 1533033818821106.

Mirandola, P., Ponti, C., Gobbi, G., Sponzilli, I., Vaccarezza, M., Cocco, L., Zauli, G., Secchiero, P., Manzoli, F.A., and Vitale, M. (2004). Activated human NK and CD8+ T cells express both TNF-related apoptosis-inducing ligand (TRAIL) and TRAIL receptors but are resistant to TRAIL-mediated cytotoxicity. Blood *104*, 2418–2424.

Mitsi, M., Hong, Z., Costello, C.E., and Nugent, M.A. (2006). Heparin-mediated conformational changes in fibronectin expose vascular endothelial growth factor binding sites. Biochemistry *45*, 10319–10328.

Morrison, C.J., Butler, G.S., Rodríguez, D., and Overall, C.M. (2009). Matrix metalloproteinase proteomics: substrates, targets, and therapy. Curr. Opin. Cell Biol. *21*, 645–653.

Moskovits, N., Kalinkovich, A., Bar, J., Lapidot, T., and Oren, M. (2006). p53 Attenuates cancer cell migration and invasion through repression of SDF-1/CXCL12 expression in stromal fibroblasts. Cancer Res. *66*, 10671–10676.

Mueller, M.M., and Fusenig, N.E. (2004). Friends or foes — bipolar effects of the tumour stroma in cancer. Nat. Rev. Cancer *4*, 839–849.

Muller, W.J., Sinn, E., Pattengale, P.K., Wallace, R., and Leder, P. (1988). Single-step induction of mammary adenocarcinoma in transgenic mice bearing the activated c-neu oncogene. Cell *54*, 105–115.

Murphy-Ullrich, J.E., Lightner, V.A., Aukhil, I., Yan, Y.Z., Erickson, H.P., and Höök, M. (1991). Focal adhesion integrity is downregulated by the alternatively spliced domain of human tenascin. J. Cell Biol. *115*, 1127–1136.

Mustafa, D.A.M., Dekker, L.J., Stingl, C., Kremer, A., Stoop, M., Smitt, P.A.E.S., Kros, J.M., and Luider, T.M. (2012). A Proteome Comparison Between Physiological Angiogenesis and Angiogenesis in Glioblastoma. Mol. Cell. Proteomics *11*.

Mylonas, K.J., Anderson, J., Sheldrake, T.A., Hesketh, E.E., Richards, J.A., Ferenbach, D.A., Kluth, D.C., Savill, J., and Hughes, J. (2019). Granulocyte macrophage-colony stimulating factor: A key modulator of renal mononuclear phagocyte plasticity. Immunobiology *224*, 60–74.

Na, H.-J., Hwang, J.-Y., Lee, K.-S., Choi, Y.K., Choe, J., Kim, J.-Y., Moon, H.-E., Kim, K.-W., Koh, G.Y., Lee, H., et al. (2014). TRAIL negatively regulates VEGF-induced angiogenesis via caspase-8-mediated enzymatic and non-enzymatic functions. Angiogenesis *17*, 179–194.

Nagaharu, K., Zhang, X., Yoshida, T., Katoh, D., Hanamura, N., Kozuka, Y., Ogawa, T., Shiraishi, T., and Imanaka-Yoshida, K. (2011). Tenascin C induces epithelial-mesenchymal transition-like change accompanied by SRC activation and focal adhesion kinase phosphorylation in human breast cancer cells. Am. J. Pathol. *178*, 754–763.

Nagane, M., Shimizu, S., Mori, E., Kataoka, S., and Shiokawa, Y. (2010). Predominant antitumor effects by fully human anti-TRAIL-receptor 2 (DR5) monoclonal antibodies in human glioma cells in vitro and in vivo. Neuro-Oncol. *12*, 687–700.

Nakao, N., Hiraiwa, N., Yoshiki, A., Ike, F., and Kusakabe, M. (1998). Tenascin-C promotes healing of Habu-snake venom-induced glomerulonephritis: studies in knockout congenic mice and in culture. Am. J. Pathol. *152*, 1237–1245.

Nanda, R., Chow, L.Q.M., Dees, E.C., Berger, R., Gupta, S., Geva, R., Pusztai, L., Pathiraja, K., Aktan, G., Cheng, J.D., et al. (2016). Pembrolizumab in Patients With Advanced Triple-Negative Breast Cancer: Phase Ib KEYNOTE-012 Study. J. Clin. Oncol. *34*, 2460.

Naval, J., de Miguel, D., Gallego-Lleyda, A., Anel, A., and Martinez-Lostao, L. (2019). Importance of TRAIL Molecular Anatomy in Receptor Oligomerization and Signaling. Implications for Cancer Therapy. Cancers *11*, 444.

Neve, R.M., Chin, K., Fridlyand, J., Yeh, J., Baehner, F.L., Fevr, T., Clark, L., Bayani, N., Coppe, J.-P., Tong, F., et al. (2006). A collection of breast cancer cell lines for the study of functionally distinct cancer subtypes. Cancer Cell *10*, 515–527.

Nicolini, A., Carpi, A., and Rossi, G. (2006). Cytokines in breast cancer. Cytokine Growth Factor Rev. *17*, 325–337.

Nong, Y., Wu, D., Lin, Y., Zhang, Y., Bai, L., and Tang, H. (2015). Tenascin-C expression is associated with poor prognosis in hepatocellular carcinoma (HCC) patients and the inflammatory cytokine TNF-α-induced TNC expression promotes migration in HCC cells. Am. J. Cancer Res. *5*, 782–791.

Obberghen-Schilling, E.V., Tucker, R.P., Saupe, F., Gasser, I., Cseh, B., and Orend, G. (2011). Fibronectin and tenascin-C: accomplices in vascular morphogenesis during development and tumor growth. Int. J. Dev. Biol. *55*, 511–525.

Obradović, M.M.S., Hamelin, B., Manevski, N., Couto, J.P., Sethi, A., Coissieux, M.-M., Münst, S., Okamoto, R., Kohler, H., Schmidt, A., et al. (2019). Glucocorticoids promote breast cancer metastasis. Nature *567*, 540–544.

O'Connell, J.T., Sugimoto, H., Cooke, V.G., MacDonald, B.A., Mehta, A.I., LeBleu, V.S., Dewar, R., Rocha, R.M., Brentani, R.R., Resnick, M.B., et al. (2011). VEGF-A and Tenascin-C produced by S100A4+ stromal cells are important for metastatic colonization. Proc. Natl. Acad. Sci. U. S. A. *108*, 16002.

Opferman, J.T. (2008). Apoptosis in the development of the immune system. Cell Death Differ. *15*, 234–242.

Orend, G., and Chiquet-Ehrismann, R. (2006). Tenascin-C induced signaling in cancer. Cancer Lett. *244*, 143–163.

Orend, G., Huang, W., Olayioye, M.A., Hynes, N.E., and Chiquet-Ehrismann, R. (2003). Tenascin-C blocks cell-cycle progression of anchorage-dependent fibroblasts on fibronectin through inhibition of syndecan-4. Oncogene *22*, 3917–3926.

Orend, G., Saupe, F., Schwenzer, A., and Midwood, K. (2014). The extracellular matrix and cancer: regulation of tumor cell biology by tenascin-C (IConcept Press, Limited).

Orimo, A., Gupta, P.B., Sgroi, D.C., Arenzana-Seisdedos, F., Delaunay, T., Naeem, R., Carey, V.J., Richardson, A.L., and Weinberg, R.A. (2005). Stromal Fibroblasts Present in Invasive Human Breast Carcinomas Promote Tumor Growth and Angiogenesis through Elevated SDF-1/CXCL12 Secretion. Cell *121*, 335–348.

Oskarsson, T. (2013). Extracellular matrix components in breast cancer progression and metastasis. The Breast *22*, S66–S72.

Oskarsson, T., Acharyya, S., Zhang, X.H.-F., Vanharanta, S., Tavazoie, S.F., Morris, P.G., Downey, R.J., Manova-Todorova, K., Brogi, E., and Massagué, J. (2011). Breast cancer cells produce tenascin C as a metastatic niche component to colonize the lungs. Nat. Med. *17*, 867–874.

Ouyang, W., Yang, C., Zhang, S., Liu, Y., Yang, B., Zhang, J., Zhou, F., Zhou, Y., and Xie, C. (2013). Absence of death receptor translocation into lipid rafts in acquired TRAIL-resistant NSCLC cells. Int. J. Oncol. *42*, 699–711.

Ouyang, X., Shi, M., Jie, F., Bai, Y., Shen, P., Yu, Z., Wang, X., Huang, C., Tao, M., Wang, Z., et al. (2018). Phase III study of dulanermin (recombinant human tumor necrosis factor-related apoptosis-inducing ligand/Apo2 ligand) combined with vinorelbine and cisplatin in patients with advanced non-small-cell lung cancer. Invest. New Drugs *36*, 315–322.

Paganelli, G., Magnani, P., Zito, F., Lucignani, G., Sudati, F., Truci, G., Motti, E., Terreni, M., Pollo, B., and Giovanelli, M. (1994). Pre-targeted immunodetection in glioma patients: tumour localization and single-photon emission tomography imaging of [99mTc]PnAO-biotin. Eur. J. Nucl. Med. *21*, 314–321.

Paganelli, G., Bartolomei, M., Ferrari, M., Cremonesi, M., Broggi, G., Maira, G., Sturiale, C., Grana, C., Prisco, G., Gatti, M., et al. (2001). Pre-targeted locoregional radioimmunotherapy with 90Y-biotin in glioma patients: phase I study and preliminary therapeutic results. Cancer Biother. Radiopharm. *16*, 227–235.

Paget, S. (1989). The distribution of secondary growths in cancer of the breast. 1889. Cancer Metastasis Rev. *8*, 98–101.

Pal, S., Moulik, S., Dutta, A., and Chatterjee, A. (2014). Extracellular Matrix Protein Laminin Induces Matrix Metalloproteinase-9 in Human Breast Cancer Cell Line MCF-7. Cancer Microenviron. *7*, 71–78.

Pan, G., O&amp, K., apos, Rourke, Chinnaiyan, A.M., Gentz, R., Ebner, R., Ni, Ji., and Dixit, V.M. (1997). The receptor for the cytotoxic ligand TRAIL. Science *276*, 111–114.

Pan, L., Fu, T.-M., Zhao, W., Zhao, L., Chen, W., Qiu, C., Liu, W., Liu, Z., Piai, A., Fu, Q., et al. (2019). Higher-Order Clustering of the Transmembrane Anchor of DR5 Drives Signaling. Cell *176*, 1477-1489.e14.

Pankov, R., and Yamada, K.M. (2002). Fibronectin at a glance. J. Cell Sci. *115*, 3861–3863.

Parmley, S.F., and Smith, G.P. (1988). Antibody-selectable filamentous fd phage vectors: affinity purification of target genes. Gene *73*, 305–318.

Pathria, P., Louis, T.L., and Varner, J.A. (2019). Targeting Tumor-Associated Macrophages in Cancer. Trends Immunol. *40*, 310–327.

Paul, S., and Lal, G. (2017). The Molecular Mechanism of Natural Killer Cells Function and Its Importance in Cancer Immunotherapy. Front. Immunol. *8*.

von Pawel, J., Harvey, J.H., Spigel, D.R., Dediu, M., Reck, M., Cebotaru, C.L., Humphreys, R.C., Gribbin, M.J., Fox, N.L., and Camidge, D.R. (2014). Phase II trial of mapatumumab, a fully human agonist monoclonal antibody to tumor necrosis factor-related apoptosis-inducing ligand receptor 1 (TRAIL-R1), in combination with paclitaxel and carboplatin in patients with advanced non-small-cell lung cancer. Clin. Lung Cancer *15*, 188-196.e2.

Peppa, D., Gill, U.S., Reynolds, G., Easom, N.J.W., Pallett, L.J., Schurich, A., Micco, L., Nebbia, G., Singh, H.D., Adams, D.H., et al. (2013). Up-regulation of a death receptor renders antiviral T cells susceptible to NK cell–mediated deletion. J. Exp. Med. *210*, 99–114.

Perou, C.M., Sørlie, T., Eisen, M.B., van de Rijn, M., Jeffrey, S.S., Rees, C.A., Pollack, J.R., Ross, D.T., Johnsen, H., Akslen, L.A., et al. (2000). Molecular portraits of human breast tumours. Nature *406*, 747–752.

Petrova, V., Annicchiarico-Petruzzelli, M., Melino, G., and Amelio, I. (2018). The hypoxic tumour microenvironment. Oncogenesis *7*, 1–13.

Pezzolo, A., Parodi, F., Marimpietri, D., Raffaghello, L., Cocco, C., Pistorio, A., Mosconi, M., Gambini, C., Cilli, M., Deaglio, S., et al. (2011). Oct-4 + /Tenascin C + neuroblastoma cells serve as progenitors of tumor-derived endothelial cells. Cell Res. *21*, 1470–1486.

Piccart-Gebhart, M.J., Procter, M., Leyland-Jones, B., Goldhirsch, A., Untch, M., Smith, I., Gianni, L., Baselga, J., Bell, R., Jackisch, C., et al. (2005). Trastuzumab after Adjuvant Chemotherapy in HER2-Positive Breast Cancer. N. Engl. J. Med. *353*, 1659–1672.

Piccinini, A.M., and Midwood, K.S. (2012). Endogenous Control of Immunity against Infection: Tenascin-C Regulates TLR4-Mediated Inflammation via MicroRNA-155. Cell Rep. *2*, 914–926.

Picon-Ruiz, M., Pan, C., Drews-Elger, K., Jang, K., Besser, A.H., Zhao, D., Morata-Tarifa, C., Kim, M., Ince, T.A., Azzam, D.J., et al. (2016). Interactions between Adipocytes and Breast Cancer Cells Stimulate Cytokine Production and Drive Src/Sox2/miR-302b–Mediated Malignant Progression. Cancer Res. *76*, 491–504.

Pitti, R.M., Marsters, S.A., Ruppert, S., Donahue, C.J., Moore, A., and Ashkenazi, A. (1996). Induction of Apoptosis by Apo-2 Ligand, a New Member of the Tumor Necrosis Factor Cytokine Family. J. Biol. Chem. *271*, 12687–12690.

Polley, M.-Y.C., Leung, S.C.Y., McShane, L.M., Gao, D., Hugh, J.C., Mastropasqua, M.G., Viale, G., Zabaglo, L.A., Penault-Llorca, F., Bartlett, J.M.S., et al. (2013). An international Ki67 reproducibility study. J. Natl. Cancer Inst. *105*, 1897–1906.

Pukac, L., Kanakaraj, P., Humphreys, R., Alderson, R., Bloom, M., Sung, C., Riccobene, T., Johnson, R., Fiscella, M., Mahoney, A., et al. (2005). HGS-ETR1, a fully human TRAIL-receptor 1 monoclonal antibody, induces cell death in multiple tumour types in vitro and in vivo. Br. J. Cancer *92*, 1430–1441.

Rahman, M., Pumphrey, J.G., and Lipkowitz, S. (2009a). The TRAIL to targeted therapy of breast cancer. Adv. Cancer Res. *103*, 43–73.

Rahman, M., Davis, S.R., Pumphrey, J.G., Bao, J., Nau, M.M., Meltzer, P.S., and Lipkowitz, S. (2009b). TRAIL induces apoptosis in triple-negative breast cancer cells with a mesenchymal phenotype. Breast Cancer Res. Treat. *113*, 217–230.

Rakha, E.A., Reis-Filho, J.S., and Ellis, I.O. (2010). Combinatorial biomarker expression in breast cancer. Breast Cancer Res. Treat. *120*, 293–308.

Redick, S.D., and Schwarzbauer, J.E. (1995). Rapid intracellular assembly of tenascin hexabrachions suggests a novel cotranslational process. J. Cell Sci. *108 (Pt 4)*, 1761–1769.

Ribatti, D. (2008). Judah Folkman, a pioneer in the study of angiogenesis. Angiogenesis *11*, 3–10.

Ribatti, D., Tamma, R., and Annese, T. (2020). Epithelial-Mesenchymal Transition in Cancer: A Historical Overview. Transl. Oncol. *13*.

Rigato, F., Garwood, J., Calco, V., Heck, N., Faivre-Sarrailh, C., and Faissner, A. (2002). Tenascin-C Promotes Neurite Outgrowth of Embryonic Hippocampal Neurons through the Alternatively Spliced Fibronectin Type III BD Domains via Activation of the Cell Adhesion Molecule F3/Contactin. J. Neurosci. *22*, 6596–6609.

Riley, G.P., Harrall, R.L., Cawston, T.E., Hazleman, B.L., and Mackie, E.J. (1996). Tenascin-C and human tendon degeneration. Am. J. Pathol. *149*, 933–943.

Riva, P., Franceschi, G., Frattarelli, M., Riva, N., Guiducci, G., Cremonini, A.M., Giuliani, G., Casi, M., Gentile, R., Jekunen, A.A., et al. (1999). 131I radioconjugated antibodies for the locoregional radioimmunotherapy of high-grade malignant glioma--phase I and II study. Acta Oncol. Stockh. Swed. *38*, 351–359.

Rizeq, B., and Malki, M.I. (2020). The Role of CCL21/CCR7 Chemokine Axis in Breast Cancer Progression. Cancers *12*, 1036.

Roach, T., Slater, S., Koval, M., White, L., McFarland, E.C., Okumura, M., Thomas, M., and Brown, E. (1997). CD45 regulates Src family member kinase activity associated with macrophage integrin-mediated adhesion. Curr. Biol. *7*, 408–417.

Rodrigues, M., Yates, C.C., Nuschke, A., Griffith, L., and Wells, A. (2013). The matrikine tenascin-C protects multipotential stromal cells/mesenchymal stem cells from death cytokines such as FasL. Tissue Eng. Part A *19*, 1972–1983.

Rolle, K., Nowak, S., Wyszko, E., Nowak, M., Zukiel, R., Piestrzeniewicz, R., Gawronska, I., Barciszewska, M.Z., and Barciszewski, J. (2010). Promising human brain tumors therapy with interference RNA intervention (iRNAi). Cancer Biol. Ther. *9*, 396–406.

Romond, E.H., Perez, E.A., Bryant, J., Suman, V.J., Geyer, C.E., Davidson, N.E., Tan-Chiu, E., Martino, S., Paik, S., Kaufman, P.A., et al. (2005). Trastuzumab plus Adjuvant Chemotherapy for Operable HER2-Positive Breast Cancer. N. Engl. J. Med. *353*, 1673–1684.

Rotte, A. (2019). Combination of CTLA-4 and PD-1 blockers for treatment of cancer. J. Exp. Clin. Cancer Res. *38*, 255.

Rozario, T., and DeSimone, D.W. (2010). The extracellular matrix in development and morphogenesis: a dynamic view. Dev. Biol. *341*, 126–140.

Ruiz, C., Huang, W., Hegi, M.E., Lange, K., Hamou, M.-F., Fluri, E., Oakeley, E.J., Chiquet-Ehrismann, R., and Orend, G. (2004). Differential Gene Expression Analysis Reveals Activation of Growth Promoting Signaling Pathways by Tenascin-C. Cancer Res. *64*, 7377–7385.

Rupp, T., Langlois, B., Koczorowska, M.M., Radwanska, A., Sun, Z., Hussenet, T., Lefebvre, O., Murdamoothoo, D., Arnold, C., Klein, A., et al. (2016). Tenascin-C Orchestrates Glioblastoma Angiogenesis by Modulation of Pro- and Anti-angiogenic Signaling. Cell Rep. *17*, 2607–2619.

Sag, D., Ayyildiz, Z.O., Gunalp, S., and Wingender, G. (2019). The Role of TRAIL/DRs in the Modulation of Immune Cells and Responses. Cancers *11*.

Saga, Y., Yagi, T., Ikawa, Y., Sakakura, T., and Aizawa, S. (1992). Mice develop normally without tenascin. Genes Dev. *6*, 1821–1831.

Sakaguchi, S., Powrie, F., and Ransohoff, R.M. (2012). Re-establishing immunological self-tolerance in autoimmune disease. Nat. Med. *18*, 54–58.

Sarkar, S., Nuttall, R.K., Liu, S., Edwards, D.R., and Yong, V.W. (2006). Tenascin-C Stimulates Glioma Cell Invasion through Matrix Metalloproteinase-12. Cancer Res. *66*, 11771–11780.

Saupe, F., Schwenzer, A., Jia, Y., Gasser, I., Spenlé, C., Langlois, B., Kammerer, M., Lefebvre, O., Hlushchuk, R., Rupp, T., et al. (2013). Tenascin-C downregulates wnt inhibitor dickkopf-1, promoting tumorigenesis in a neuroendocrine tumor model. Cell Rep. *5*, 482–492.

Scharer, C.D., McCabe, C.D., Ali-Seyed, M., Berger, M.F., Bulyk, M.L., and Moreno, C.S. (2009). Genome-wide Promoter Analysis of the SOX4 Transcriptional Network in Prostate Cancer Cells. Cancer Res. *69*, 709–717.

Schmidt, K.S., Borkowski, S., Kurreck, J., Stephens, A.W., Bald, R., Hecht, M., Friebe, M., Dinkelborg, L., and Erdmann, V.A. (2004). Application of locked nucleic acids to improve aptamer in vivo stability and targeting function. Nucleic Acids Res. *32*, 5757–5765.

Schneider, B., Münkel, S., Krippner-Heidenreich, A., Grunwald, I., Wels, W.S., Wajant, H., Pfizenmaier, K., and Gerspach, J. (2010). Potent antitumoral activity of TRAIL through generation of tumor-targeted single-chain fusion proteins. Cell Death Dis. *1*, e68.

Schneider, P., Bodmer, J.-L., Thome, M., Hofmann, K., Holler, N., and Tschopp, J. (1997). Characterization of two receptors for TRAIL. FEBS Lett. *416*, 329–334.

Schneider, P., Olson, D., Tardivel, A., Browning, B., Lugovskoy, A., Gong, D., Dobles, M., Hertig, S., Hofmann, K., Van Vlijmen, H., et al. (2003). Identification of a new murine tumor necrosis factor receptor locus that contains two novel murine receptors for tumor necrosis factor-related apoptosis-inducing ligand (TRAIL). J. Biol. Chem. *278*, 5444–5454.

Schuster, I.S., Wikstrom, M.E., Brizard, G., Coudert, J.D., Estcourt, M.J., Manzur, M., O'Reilly, L.A., Smyth, M.J., Trapani, J.A., Hill, G.R., et al. (2014). TRAIL+ NK Cells Control CD4+ T Cell Responses during Chronic Viral Infection to Limit Autoimmunity. Immunity *41*, 646–656.

Schuster, I.S., Coudert, J.D., Andoniou, C.E., and Degli-Esposti, M.A. (2016). "Natural Regulators": NK Cells as Modulators of T Cell Immunity. Front. Immunol. *7*.

Scindia, Y.M., Deshmukh, U.S., and Bagavant, H. (2010). Mesangial pathology in glomerular disease: targets for therapeutic intervention. Adv. Drug Deliv. Rev. *62*, 1337–1343.

Scott, J.K., and Smith, G.P. (1990). Searching for peptide ligands with an epitope library. Science *249*, 386–390.

Secchiero, P., Gonelli, A., Mirandola, P., Melloni, E., Zamai, L., Celeghini, C., Milani, D., and Zauli, G. (2002). Tumor necrosis factor–related apoptosis-inducing ligand induces monocytic maturation of leukemic and normal myeloid precursors through a caspase-dependent pathway. Blood *100*, 2421–2429.

Secchiero, P., Gonelli, A., Carnevale, E., Corallini, F., Rizzardi, C., Zacchigna, S., Melato, M., and Zauli, G. (2004). Evidence for a Proangiogenic Activity of TNF-Related Apoptosis-Inducing Ligand. Neoplasia *6*, 364–373.

Sedger, L.M., Katewa, A., Pettersen, A.K., Osvath, S.R., Farrell, G.C., Stewart, G.J., Bendall, L.J., and Alexander, S.I. (2010). Extreme lymphoproliferative disease and fatal autoimmune thrombocytopenia in FasL and TRAIL double-deficient mice. Blood *115*, 3258–3268.

Seité, S., Colige, A., Piquemal-Vivenot, P., Montastier, C., Fourtanier, A., Lapière, C., and Nusgens, B. (2000). A full-UV spectrum absorbing daily use cream protects human skin against biological changes occurring in photoaging. Photodermatol. Photoimmunol. Photomed. *16*, 147–155.

Seol, D.-W., and Billiar, T.R. (2000). Cysteine 230 Modulates Tumor Necrosis Factor-related Apoptosis-inducing Ligand Activity. Cancer Res. *60*, 3152–3154.

Seyger, M.M., van Pelt, J.P., van den Born, J., Latijnhouwers, M.A., and de Jong, E.M. (1997). Epicutaneous application of leukotriene B4 induces patterns of tenascin and a heparan sulfate proteoglycan epitope that are typical for psoriatic lesions. Arch. Dermatol. Res. *289*, 331–336.

Shamas-Din, A., Kale, J., Leber, B., and Andrews, D.W. (2013). Mechanisms of Action of Bcl-2 Family Proteins. Cold Spring Harb. Perspect. Biol. *5*, a008714–a008714.

Sharma, S., de Vries, E.G., Infante, J.R., Oldenhuis, C.N., Gietema, J.A., Yang, L., Bilic, S., Parker, K., Goldbrunner, M., Scott, J.W., et al. (2014). Safety, pharmacokinetics, and pharmacodynamics of the DR5 antibody LBY135 alone and in combination with capecitabine in patients with advanced solid tumors. Invest. New Drugs *32*, 135–144.

Shen, M., Wang, J., and Ren, X. (2018). New Insights into Tumor-Infiltrating B Lymphocytes in Breast Cancer: Clinical Impacts and Regulatory Mechanisms. Front. Immunol. *9*, 470.

Shenoi, H., Seavitt, J., Zheleznyak, A., Thomas, M.L., and Brown, E.J. (1999). Regulation of Integrin-Mediated T Cell Adhesion by the Transmembrane Protein Tyrosine Phosphatase CD45. J. Immunol. *162*, 7120–7127.

Shi, M., He, X., Wei, W., Wang, J., Zhang, T., and Shen, X. (2015). Tenascin-C induces resistance to apoptosis in pancreatic cancer cell through activation of ERK/NF-κB pathway. Apoptosis *20*, 843–857.

Shiga, K., Hara, M., Nagasaki, T., Sato, T., Takahashi, H., and Takeyama, H. (2015). Cancer-Associated Fibroblasts: Their Characteristics and Their Roles in Tumor Growth. Cancers *7*, 2443–2458.

Shimada, O., Wu, X., Jin, X., Nouh, M.A.A.-M., Fiscella, M., Albert, V., Matsuda, T., and Kakehi, Y. (2007). Human agonistic antibody to tumor necrosis factor-related apoptosis-inducing ligand receptor 2 induces cytotoxicity and apoptosis in prostate cancer and bladder cancer cells. Urology *69*, 395–401.

Shinohara, Y., Okamoto, K., Goh, Y., Kiga, N., Tojyo, I., and Fujita, S. (2014). Inhibition of Fibrous Adhesion Formation in the Temporomandibular Joint of Tenascin-C Knockout Mice. Eur. J. Histochem. EJH *58*.

Shlyakhtina, Y., Pavet, V., and Gronemeyer, H. (2017). Dual role of DR5 in death and survival signaling leads to TRAIL resistance in cancer cells. Cell Death Dis. *8*, e3025.

Sikov, W.M., Berry, D.A., Perou, C.M., Singh, B., Cirrincione, C.T., Tolaney, S.M., Kuzma, C.S., Pluard, T.J., Somlo, G., Port, E.R., et al. (2015). Impact of the Addition of Carboplatin and/or Bevacizumab to Neoadjuvant Once-per-Week Paclitaxel Followed by Dose-Dense Doxorubicin and Cyclophosphamide on Pathologic Complete Response Rates in Stage II to III Triple-Negative Breast Cancer: CALGB 40603 (Alliance). J. Clin. Oncol. *33*, 13–21.

Silacci, M., Brack, S.S., Späth, N., Buck, A., Hillinger, S., Arni, S., Weder, W., Zardi, L., and Neri, D. (2006). Human monoclonal antibodies to domain C of tenascin-C selectively target solid tumors in vivo. Protein Eng. Des. Sel. *19*, 471–478.

Sivasankaran, B., Degen, M., Ghaffari, A., Hegi, M.E., Hamou, M.-F., Ionescu, M.-C.S., Zweifel, C., Tolnay, M., Wasner, M., Mergenthaler, S., et al. (2009). Tenascin-C Is a Novel RBPJκ-Induced Target Gene for Notch Signaling in Gliomas. Cancer Res. *69*, 458–465.

Slamon, D.J., Leyland-Jones, B., Shak, S., Fuchs, H., Paton, V., Bajamonde, A., Fleming, T., Eiermann, W., Wolter, J., Pegram, M., et al. (2001). Use of Chemotherapy plus a Monoclonal Antibody against HER2 for Metastatic Breast Cancer That Overexpresses HER2. N. Engl. J. Med. *344*, 783–792.

Sledge, G.W., Neuberg, D., Bernardo, P., Ingle, J.N., Martino, S., Rowinsky, E.K., and Wood, W.C. (2003). Phase III trial of doxorubicin, paclitaxel, and the combination of doxorubicin and paclitaxel as front-line chemotherapy for metastatic breast cancer: an intergroup trial (E1193). J. Clin. Oncol. Off. J. Am. Soc. Clin. Oncol. *21*, 588–592.

Smith, E.M., Mitsi, M., Nugent, M.A., and Symes, K. (2009). PDGF-A interactions with fibronectin reveal a critical role for heparan sulfate in directed cell migration during Xenopus gastrulation. Proc. Natl. Acad. Sci. U. S. A. *106*, 21683–21688.

Smith, N.R., Baker, D., James, N.H., Ratcliffe, K., Jenkins, M., Ashton, S.E., Sproat, G., Swann, R., Gray, N., Ryan, A., et al. (2010). Vascular Endothelial Growth Factor Receptors VEGFR-2 and VEGFR-3 Are Localized Primarily to the Vasculature in Human Primary Solid Cancers. Clin. Cancer Res. *16*, 3548–3561.

Smyth, M.J., Takeda, K., Hayakawa, Y., Peschon, J.J., van den Brink, M.R.M., and Yagita, H. (2003). Nature's TRAIL—On a Path to Cancer Immunotherapy. Immunity *18*, 1–6.

Sohn, V.Y., Arthurs, Z.M., Sebesta, J.A., and Brown, T.A. (2008). Primary tumor location impacts breast cancer survival. Am. J. Surg. *195*, 641–644.

Song, J.H., Tse, M.C.L., Bellail, A., Phuphanich, S., Khuri, F., Kneteman, N.M., and Hao, C. (2007). Lipid Rafts and Nonrafts Mediate Tumor Necrosis Factor–Related Apoptosis-Inducing Ligand–Induced Apoptotic and Nonapoptotic Signals in Non–Small Cell Lung Carcinoma Cells. Cancer Res. *67*, 6946–6955.

Soria, J.-C., Márk, Z., Zatloukal, P., Szima, B., Albert, I., Juhász, E., Pujol, J.-L., Kozielski, J., Baker, N., Smethurst, D., et al. (2011). Randomized phase II study of dulanermin in combination with paclitaxel, carboplatin, and bevacizumab in advanced non-small-cell lung cancer. J. Clin. Oncol. Off. J. Am. Soc. Clin. Oncol. *29*, 4442–4451.

Sørlie, T., Perou, C.M., Tibshirani, R., Aas, T., Geisler, S., Johnsen, H., Hastie, T., Eisen, M.B., Rijn, M. van de, Jeffrey, S.S., et al. (2001). Gene expression patterns of breast carcinomas distinguish tumor subclasses with clinical implications. Proc. Natl. Acad. Sci. *98*, 10869–10874.

Sorokin, L. (2010). The impact of the extracellular matrix on inflammation. Nat. Rev. Immunol. *10*, 712–723.

Spaeth, E.L., Dembinski, J.L., Sasser, A.K., Watson, K., Klopp, A., Hall, B., Andreeff, M., and Marini, F. (2009). Mesenchymal Stem Cell Transition to Tumor-Associated Fibroblasts Contributes to Fibrovascular Network Expansion and Tumor Progression. PLoS ONE *4*.

Spenlé, C., Saupe, F., Midwood, K., Burckel, H., Noel, G., and Orend, G. (2015). Tenascin-C: Exploitation and collateral damage in cancer management. Cell Adhes. Migr. *9*, 141–153.

Spenlé, C., Loustau, T., Murdamoothoo, D., Erne, W., Divonne, S.B. la F., Veber, R., Petti, L., Bourdely, P., Mörgelin, M., Brauchle, E.-M., et al. (2020). Tenascin-C Orchestrates an Immune-Suppressive Tumor Microenvironment in Oral Squamous Cell Carcinoma. Cancer Immunol. Res.

Spring, J., Beck, K., and Chiquet-Ehrismann, R. (1989). Two contrary functions of tenascin: Dissection of the active sites by recombinant tenascin fragments. Cell *59*, 325–334.

Sridharan, K., and Gogtay, N.J. (2016). Therapeutic nucleic acids: current clinical status. Br. J. Clin. Pharmacol. *82*, 659–672.

Srivastava, R.K., Kurzrock, R., and Shankar, S. (2010). MS-275 Sensitizes TRAIL-Resistant Breast Cancer Cells, Inhibits Angiogenesis and Metastasis, and Reverses Epithelial-Mesenchymal Transition In vivo. Mol. Cancer Ther. *9*, 3254–3266.

Staniek, J., Lorenzetti, R., Heller, B., Janowska, I., Schneider, P., Unger, S., Warnatz, K., Seidl, M., Venhoff, N., Thiel, J., et al. (2019). TRAIL-R1 and TRAIL-R2 Mediate TRAIL-Dependent Apoptosis in Activated Primary Human B Lymphocytes. Front. Immunol. *10*, 951.

Stary, G., Klein, I., Kohlhofer, S., Koszik, F., Scherzer, T., Müllauer, L., Quendler, H., Kohrgruber, N., and Stingl, G. (2009). Plasmacytoid dendritic cells express TRAIL and induce CD4+ T-cell apoptosis in HIV-1 viremic patients. Blood *114*, 3854–3863.

Stephenson, S., Care, M.A., Fan, I., Zougman, A., Westhead, D.R., Doody, G.M., and Tooze, R.M. (2019). Growth Factor–like Gene Regulation Is Separable from Survival and Maturation in Antibody-Secreting Cells. J. Immunol. Author Choice *202*, 1287–1300.

Stuckey, D.W., and Shah, K. (2013). TRAIL on trial: preclinical advances in cancer therapy. Trends Mol. Med. *19*, 685–694.

Stuelten, C.H., Busch, J.I., Tang, B., Flanders, K.C., Oshima, A., Sutton, E., Karpova, T.S., Roberts, A.B., Wakefield, L.M., and Niederhuber, J.E. (2010). Transient tumor-fibroblast interactions increase tumor cell malignancy by a TGF-Beta mediated mechanism in a mouse xenograft model of breast cancer. PloS One *5*, e9832.

Stylianopoulos, T., and Jain, R.K. (2013). Combining two strategies to improve perfusion and drug delivery in solid tumors. Proc. Natl. Acad. Sci.

SUN, T., JIANG, D., ZHANG, L., SU, Q., MAO, W., and JIANG, C. (2016). Expression profile of cathepsins indicates the potential of cathepsins B and D as prognostic factors in breast cancer patients. Oncol. Lett. *11*, 575–583.

Sun, Z., Schwenzer, A., Rupp, T., Murdamoothoo, D., Vegliante, R., Lefebvre, O., Klein, A., Hussenet, T., and Orend, G. (2018). Tenascin-C Promotes Tumor Cell Migration and Metastasis through Integrin α9β1–Mediated YAP Inhibition. Cancer Res. *78*, 950–961.

Sun, Z., Velázquez-Quesada, I., Murdamoothoo, D., Ahowesso, C., Yilmaz, A., Spenlé, C., Averous, G., Erne, W., Oberndorfer, F., Oszwald, A., et al. (2019). Tenascin-C increases lung metastasis by impacting blood vessel invasions. Matrix Biol. *83*, 26–47.

Sundquist, E., Kauppila, J.H., Veijola, J., Mroueh, R., Lehenkari, P., Laitinen, S., Risteli, J., Soini, Y., Kosma, V.-M., Sawazaki-Calone, I., et al. (2017). Tenascin-C and fibronectin expression divide early stage tongue cancer into low- and high-risk groups. Br. J. Cancer *116*, 640–648.

Tafani, M., Russo, A., Di Vito, M., Sale, P., Pellegrini, L., Schito, L., Gentileschi, S., Bracaglia, R., Marandino, F., Garaci, E., et al. (2010). Up-regulation of pro-inflammatory genes as adaptation to hypoxia in MCF-7 cells and in human mammary invasive carcinoma microenvironment. Cancer Sci. *101*, 1014–1023.

Takeda, K., Hayakawa, Y., Smyth, M.J., Kayagaki, N., Yamaguchi, N., Kakuta, S., Iwakura, Y., Yagita, H., and Okumura, K. (2001). Involvement of tumor necrosis factor-related apoptosis-inducing ligand in surveillance of tumor metastasis by liver natural killer cells. Nat. Med. *7*, 94–100.

Takiguchi, S., Korenaga, N., Inoue, K., Sugi, E., Kataoka, Y., Matsusue, K., Futagami, K., Li, Y.-J., Kukita, T., Teramoto, N., et al. (2014). Involvement of CXCL14 in osteolytic bone metastasis from lung cancer. Int. J. Oncol. *44*, 1316–1324.

Talts, J.F., Eng, H., Zhang, H.Y., Faissner, A., and Ekblom, P. (1997). Characterization of monoclonal antibodies against tenascin-C: no apparent effect on kidney development in vitro. Int. J. Dev. Biol. *41*, 39–48.

Tamada, T., Shinmi, D., Ikeda, M., Yonezawa, Y., Kataoka, S., Kuroki, R., Mori, E., and Motoki, K. (2015). TRAIL-R2 Superoligomerization Induced by Human Monoclonal Agonistic Antibody KMTR2. Sci. Rep. *5*, 17936.

Tamaoki, M., Imanaka-Yoshida, K., Yokoyama, K., Nishioka, T., Inada, H., Hiroe, M., Sakakura, T., and Yoshida, T. (2005). Tenascin-C Regulates Recruitment of Myofibroblasts during Tissue Repair after Myocardial Injury. Am. J. Pathol. *167*, 71–80.

Tanaka, K., Hiraiwa, N., Hashimoto, H., Yamazaki, Y., and Kusakabe, M. (2004). Tenascin-C regulates angiogenesis in tumor through the regulation of vascular endothelial growth factor expression. Int. J. Cancer *108*, 31–40.

Tanos, T., Rojo, L.J., Echeverria, P., and Brisken, C. (2012). ER and PR signaling nodes during mammary gland development. Breast Cancer Res. *14*, 210.

Taraseviciute, A., Vincent, B.T., Schedin, P., and Jones, P.L. (2010). Quantitative Analysis of Three-Dimensional Human Mammary Epithelial Tissue Architecture Reveals a Role for Tenascin-C in Regulating c-Met Function. Am. J. Pathol. *176*, 827–838.

Tavazoie, S.F., Alarcón, C., Oskarsson, T., Padua, D., Wang, Q., Bos, P.D., Gerald, W.L., and Massagué, J. (2008). Endogenous human microRNAs that suppress breast cancer metastasis. Nature *451*, 147–152.

Taylor, H.C., Lightner, V.A., Beyer, W.F., McCaslin, D., Briscoe, G., and Erickson, H.P. (1989). Biochemical and structural studies of tenascin/hexabrachion proteins. J. Cell. Biochem. *41*, 71–90.

Teesalu, T., Sugahara, K.N., Kotamraju, V.R., and Ruoslahti, E. (2009). C-end rule peptides mediate neuropilin-1-dependent cell, vascular, and tissue penetration. Proc. Natl. Acad. Sci. *106*, 16157–16162.

Teymournia, L., Berger, D., Kauer-Dorner, D., Poljanc, K., Seitz, W., Aiginger, H., and Kirisits, C. (2009). Comparison of PDR brachytherapy and external beam radiation therapy in the case of breast cancer. Phys. Med. Biol. *54*, 2585–2595.

Thai, L.M., Labrinidis, A., Hay, S., Liapis, V., Bouralexis, S., Welldon, K., Coventry, B.J., Findlay, D.M., and Evdokiou, A. (2006). Apo2l/Tumor Necrosis Factor–Related Apoptosis-Inducing Ligand Prevents Breast Cancer–Induced Bone Destruction in a Mouse Model. Cancer Res. *66*, 5363–5370.

Theocharis, A.D., Skandalis, S.S., Gialeli, C., and Karamanos, N.K. (2016). Extracellular matrix structure. Adv. Drug Deliv. Rev. *97*, 4–27.

Tôkés, A.-M., Paku, S., Tóth, S., Paál, E., Kulka, J., Tóth, J., and Telekes, A. (2000). Tenascin expression in primary and recurrent breast carcinomas and the effect of tenascin on breast tumor cell cultures. Pathol. Oncol. Res. *6*, 202–209.

Tolcher, A.W., Mita, M., Meropol, N.J., von Mehren, M., Patnaik, A., Padavic, K., Hill, M., Mays, T., McCoy, T., Fox, N.L., et al. (2007). Phase I pharmacokinetic and biologic correlative study of mapatumumab, a fully human monoclonal antibody with agonist activity to tumor necrosis factor-related apoptosis-inducing ligand receptor-1. J. Clin. Oncol. Off. J. Am. Soc. Clin. Oncol. *25*, 1390–1395.

Toor, S.M., Syed Khaja, A.S., El Salhat, H., Faour, I., Kanbar, J., Quadri, A.A., Albashir, M., and Elkord, E. (2017). Myeloid cells in circulation and tumor microenvironment of breast cancer patients. Cancer Immunol. Immunother. CII *66*, 753–764.

Torti, F.M., Bristow, M.M., Lum, B.L., Carter, S.K., Howes, A.E., Aston, D.A., Brown, B.W., Hannigan, J.F., Meyers, F.J., and Mitchell, E.P. (1986). Cardiotoxicity of epirubicin and doxorubicin: assessment by endomyocardial biopsy. Cancer Res. *46*, 3722–3727.

Trier, N., Hansen, P., and Houen, G. (2019). Peptides, Antibodies, Peptide Antibodies and More. Int. J. Mol. Sci. *20*.

Tsuyada, A., Chow, A., Wu, J., Somlo, G., Chu, P., Loera, S., Luu, T., Li, A.X., Wu, X., Ye, W., et al. (2012). CCL2 mediates crosstalk between cancer cells and stromal fibroblasts that regulates breast cancer stem cells. Cancer Res. *72*, 2768–2779.

Tu, M.M., Rahim, M.M.A., Sayed, C., Mahmoud, A.B., and Makrigiannis, A.P. (2017). Immunosurveillance and Immunoediting of Breast Cancer via Class I MHC Receptors. Cancer Immunol. Res. *5*, 1016–1028.

Tucker, R.P. (2018). Fibronectin. In Encyclopedia of Signaling Molecules, S. Choi, ed. (Cham: Springer International Publishing), pp. 1718–1723.

Tuthill, M.H., Montinaro, A., Zinngrebe, J., Prieske, K., Draber, P., Prieske, S., Newsom-Davis, T., von Karstedt, S., Graves, J., and Walczak, H. (2015). TRAIL-R2-specific antibodies and recombinant TRAIL can synergise to kill cancer cells. Oncogene *34*, 2138–2144.

Ursin, G., Hovanessian-Larsen, L., Parisky, Y.R., Pike, M.C., and Wu, A.H. (2005). Greatly increased occurrence of breast cancers in areas of mammographically dense tissue. Breast Cancer Res. *7*, R605–R608.

Van Audenhove, I., and Gettemans, J. (2016). Nanobodies as Versatile Tools to Understand, Diagnose, Visualize and Treat Cancer. EBioMedicine *8*, 40–48.

Vanamee, É.S., and Faustman, D.L. (2018). Structural principles of tumor necrosis factor superfamily signaling. Sci. Signal. *11*, eaao4910.

Veronesi, U., Cascinelli, N., Mariani, L., Greco, M., Saccozzi, R., Luini, A., Aguilar, M., and Marubini, E. (2002). Twenty-Year Follow-up of a Randomized Study Comparing Breast-

Conserving Surgery with Radical Mastectomy for Early Breast Cancer. N. Engl. J. Med. *347*, 1227–1232.

Vestweber, D. (2007). Adhesion and signaling molecules controlling the transmigration of leukocytes through endothelium. Immunol. Rev. *218*, 178–196.

Vonderheide, R.H., LoRusso, P.M., Khalil, M., Gartner, E.M., Khaira, D., Soulieres, D., Dorazio, P., Trosko, J.A., Rüter, J., Mariani, G.L., et al. (2010). Tremelimumab in Combination with Exemestane in Patients with Advanced Breast Cancer and Treatment-Associated Modulation of Inducible Costimulator Expression on Patient T Cells. Clin. Cancer Res. *16*, 3485–3494.

von Karstedt, S., Conti, A., Nobis, M., Montinaro, A., Hartwig, T., Lemke, J., Legler, K., Annewanter, F., Campbell, A.D., Taraborrelli, L., et al. (2015). Cancer Cell-Autonomous TRAIL-R Signaling Promotes KRAS-Driven Cancer Progression, Invasion, and Metastasis. Cancer Cell *27*, 561–573.

Vyavahare, N., Jones, P.L., Tallapragada, S., and Levy, R.J. (2000). Inhibition of Matrix Metalloproteinase Activity Attenuates Tenascin-C Production and Calcification of Implanted Purified Elastin in Rats. Am. J. Pathol. *157*, 885–893.

Wajant, H. (2019). Molecular Mode of Action of TRAIL Receptor Agonists—Common Principles and Their Translational Exploitation. Cancers *11*.

Walczak, H., Degli-Esposti, M.A., Johnson, R.S., Smolak, P.J., Waugh, J.Y., Boiani, N., Timour, M.S., Gerhart, M.J., Schooley, K.A., Smith, C.A., et al. (1997). TRAIL-R2: a novel apoptosis-mediating receptor for TRAIL. EMBO J. *16*, 5386–5397.

Walczak, H., Miller, R.E., Ariail, K., Gliniak, B., Griffith, T.S., Kubin, M., Chin, W., Jones, J., Woodward, A., Le, T., et al. (1999). Tumoricidal activity of tumor necrosis factor-related apoptosis-inducing ligand in vivo. Nat. Med. *5*, 157–163.

Walker, C., Mojares, E., and del Río Hernández, A. (2018). Role of Extracellular Matrix in Development and Cancer Progression. Int. J. Mol. Sci. *19*.

Wang, D., Liu, D., Gao, J., Liu, M., Liu, S., Jiang, M., Liu, Y., and Zheng, D. (2013). TRAIL-induced miR-146a expression suppresses CXCR4-mediated human breast cancer migration. FEBS J. *280*, 3340–3353.

Wang, H., Davis, J.S., and Wu, X. (2014). Immunoglobulin Fc domain fusion to TRAIL significantly prolongs its plasma half-life and enhances its antitumor activity. Mol. Cancer Ther. *13*, 643–650.

Wang, Q., Ji, Y., Wang, X., and Evers, B.M. (2000). Isolation and Molecular Characterization of the 5′-Upstream Region of the Human TRAIL Gene. Biochem. Biophys. Res. Commun. *276*, 466–471.

Wang, Q., Zhou, Y., Weiss, H.L., Chow, C.-W., and Evers, B.M. (2011). NFATc1 regulation of TRAIL expression in human intestinal cells. PloS One *6*, e19882.

Wang, R., Zhu, Y., Liu, X., Liao, X., He, J., and Niu, L. (2019). The Clinicopathological features and survival outcomes of patients with different metastatic sites in stage IV breast cancer. BMC Cancer *19*, 1091.

Wani, M.C., Taylor, H.L., Wall, M.E., Coggon, P., and McPhail, A.T. (1971). Plant antitumor agents. VI. The isolation and structure of taxol, a novel antileukemic and antitumor agent from Taxus brevifolia. J. Am. Chem. Soc. *93*, 2325–2327.

Wawrzyniak, D., Grabowska, M., Głodowicz, P., Kuczyński, K., Kuczyńska, B., Fedoruk-Wyszomirska, A., and Rolle, K. (2020). Down-regulation of tenascin-C inhibits breast cancer cells development by cell growth, migration, and adhesion impairment. PLOS ONE *15*, e0237889.

Weber, F., Shen, L., Fukino, K., Patocs, A., Mutter, G.L., Caldes, T., and Eng, C. (2006). Total-genome analysis of BRCA1/2-related invasive carcinomas of the breast identifies tumor stroma as potential landscaper for neoplastic initiation. Am. J. Hum. Genet. *78*, 961–972.

Weber, P., Zimmermann, D.R., Winterhalter, K.H., and Vaughan, L. (1995). Tenascin-C binds heparin by its fibronectin type III domain five. J. Biol. Chem. *270*, 4619–4623.

Wei, W., Wang, D., Shi, J., Xiang, Y., Zhang, Y., Liu, S., Liu, Y., and Zheng, D. (2010). Tumor necrosis factor (TNF)-related apoptosis-inducing ligand (TRAIL) induces chemotactic migration of monocytes via a death receptor 4-mediated RhoGTPase pathway. Mol. Immunol. *47*, 2475–2484.

Wendling, U., Walczak, H., Dörr, J., Jaboci, C., Weller, M., Krammer, P.H., and Zipp, F. (2000). Expression of TRAIL receptors in human autoreactive and foreign antigen-specific T cells. Cell Death Differ. *7*, 637–644.

Wenk, M.B., Midwood, K.S., and Schwarzbauer, J.E. (2000). Tenascin-C Suppresses Rho Activation. J. Cell Biol. *150*, 913–920.

Wijelath, E.S., Rahman, S., Namekata, M., Murray, J., Nishimura, T., Mostafavi-Pour, Z., Patel, Y., Suda, Y., Humphries, M.J., and Sobel, M. (2006). Heparin-II domain of fibronectin is a vascular endothelial growth factor-binding domain: enhancement of VEGF biological activity by a singular growth factor/matrix protein synergism. Circ. Res. *99*, 853–860.

Wiley, S.R., Schooley, K., Smolak, P.J., Din, W.S., Huang, C.-P., Nicholl, J.K., Sutherland, G.R., Smith, T.D., Rauch, C., Smith, C.A., et al. (1995). Identification and characterization of a new member of the TNF family that induces apoptosis. Immunity *3*, 673–682.

Wilson, N.S., Yang, A., Yang, B., Couto, S., Stern, H., Gogineni, A., Pitti, R., Marsters, S., Weimer, R.M., Singh, M., et al. (2012). Proapoptotic activation of death receptor 5 on tumor endothelial cells disrupts the vasculature and reduces tumor growth. Cancer Cell *22*, 80–90.

World Health Organization (2020). WHO report on cancer: setting priorities, investing wisely and providing care for all (World Health Organization).

Wu, G.S., Burns, T.F., McDonald, E.R., Meng, R.D., Kao, G., Muschel, R., Yen, T., and el-Deiry, W.S. (1999). Induction of the TRAIL receptor KILLER/DR5 in p53-dependent apoptosis but not growth arrest. Oncogene *18*, 6411–6418.

Wu, J.J., Zhang, X.D., Gillespie, S., and Hersey, P. (2005). Selection for TRAIL resistance results in melanoma cells with high proliferative potential. FEBS Lett. *579*, 1940–1944.

Wu, Y., Zhao, Y., He, X., He, Z., Wang, T., Wan, L., Chen, L., and Yan, N. (2020). Hydroxypropyl-β-cyclodextrin attenuates the epithelial-to-mesenchymal transition via endoplasmic reticulum stress in MDA-MB-231 breast cancer cells. Mol. Med. Rep. *21*, 249–257.

Xiao, C., Rui, Y., Zhou, S., Huang, Y., Wei, Y., and Wang, Z. (2020). TNF-related apoptosis-inducing ligand (TRAIL) promotes trophoblast cell invasion via miR-146a-EGFR/CXCR4 axis: A novel mechanism for preeclampsia? Placenta *93*, 8–16.

Yamakawa, M., Doh, S.J., Santosa, S.M., Montana, M., Qin, E.C., Kong, H., Han, K.-Y., Yu, C., Rosenblatt, M.I., Kazlauskas, A., et al. (2018). Potential lymphangiogenesis therapies: learning from current anti-angiogenesis therapies - A review. Med. Res. Rev. *38*, 1769–1798.

Yang, X., Merchant, M.S., Romero, M.E., Tsokos, M., Wexler, L.H., Kontny, U., Mackall, C.L., and Thiele, C.J. (2003). Induction of caspase 8 by interferon gamma renders some neuroblastoma (NB) cells sensitive to tumor necrosis factor-related apoptosis-inducing ligand (TRAIL) but reveals that a lack of membrane TR1/TR2 also contributes to TRAIL resistance in NB. Cancer Res. *63*, 1122–1129.

Yee, L.D., Mortimer, J.E., Natarajan, R., Dietze, E.C., and Seewaldt, V.L. (2020). Metabolic Health, Insulin, and Breast Cancer: Why Oncologists Should Care About Insulin. Front. Endocrinol. *11*.

Yokosaki, Y., Palmer, E.L., Prieto, A.L., Crossin, K.L., Bourdon, M.A., Pytela, R., and Sheppard, D. (1994). The integrin alpha 9 beta 1 mediates cell attachment to a non-RGD site in the third fibronectin type III repeat of tenascin. J. Biol. Chem. *269*, 26691–26696.

Yokosaki, Y., Matsuura, N., Higashiyama, S., Murakami, I., Obara, M., Yamakido, M., Shigeto, N., Chen, J., and Sheppard, D. (1998). Identification of the ligand binding site for the integrin alpha9 beta1 in the third fibronectin type III repeat of tenascin-C. J. Biol. Chem. *273*, 11423–11428.

Zang, F., Wei, X., Leng, X., Yu, M., and Sun, B. (2014). C-FLIP(L) contributes to TRAIL resistance in HER2-positive breast cancer. Biochem. Biophys. Res. Commun. *450*, 267–273.

Zapadka, K.L., Becher, F.J., Gomes dos Santos, A.L., and Jackson, S.E. (2017). Factors affecting the physical stability (aggregation) of peptide therapeutics. Interface Focus *7*, 20170030.

Zeisberg, E.M., Potenta, S., Xie, L., Zeisberg, M., and Kalluri, R. (2007). Discovery of endothelial to mesenchymal transition as a source for carcinoma-associated fibroblasts. Cancer Res. *67*, 10123–10128.

Zhang, X.R., Zhang, L.Y., Devadas, S., Li, L., Keegan, A.D., and Shi, Y.F. (2003). Reciprocal expression of TRAIL and CD95L in Th1 and Th2 cells: role of apoptosis in T helper subset differentiation. Cell Death Differ. *10*, 203–210.

Zhao, H., Wang, J., Kong, X., Li, E., Liu, Y., Du, X., Kang, Z., Tang, Y., Kuang, Y., Yang, Z., et al. (2016). CD47 Promotes Tumor Invasion and Metastasis in Non-small Cell Lung Cancer. Sci. Rep. *6*, 29719.

Zitvogel, L., Tesniere, A., and Kroemer, G. (2006). Cancer despite immunosurveillance: immunoselection and immunosubversion. Nat. Rev. Immunol. *6*, 715–727.

Zukiel, R., and Nowak, S. (2006). Suppression of human brain tumor with interference RNA specific for tenascin-C. Cancer Biol. Ther. *5*, 1002–1007.

12. Appendix

Appendix I: Tenascin-C increases lung metastasis by impacting blood vessel invasions

Appendix II: Matrix-Targeting Immunotherapy Controls Tumor Growth and Spread by Switching Macrophage Phenotype

Appendix III: Tenascin-C orchestrates an immune suppressive tumor microenvironment in oral squamous cell carcinoma

Appendix IV: Generation and characterization of dromedary Tenascin-C and Tenascin-W specific antibodies

Tenascin-C increases lung metastasis by impacting blood vessel invasions

Zhen Sun[a,b,c,d,1,2], **Inés Velázquez-Quesada**[a,b,c,d,2], **Devadarssen Murdamoothoo**[a,b,c,d], **Constance Ahowesso**[a,b,c,d], **Alev Yilmaz**[a,b,c,d], **Caroline Spenlé**[a,b,c,d], **Gerlinde Averous**[e], **William Erne**[a,b,c,d], **Felicitas Oberndorfer**[f], **Andre Oszwald**[f], **Renate Kain**[f], **Catherine Bourdon**[g], **Pierre Mangin**[g], **Claire Deligne**[h], **Kim Midwood**[h], **Chérine Abou-Faycal**[a,b,c,d], **Olivier Lefebvre**[a,b,c,d], **Annick Klein**[a,b,c,d], **Michael van der Heyden**[a,b,c,d], **Marie-Pierre Chenard**[e], **Gerhard Christofori**[i], **Carole Mathelin**[j], **Thomas Loustau**[a,b,c,d], **Thomas Hussenet**[a,b,c,d] and **Gertraud Orend**[a,b,c,d]

a - INSERM U1109 - MN3T, *The Microenvironmental Niche in Tumorigenesis and Targeted Therapy and, the Tumor Microenvironment group, France*
b - Université de Strasbourg, *Strasbourg, France*
c - LabEx Medalis, *Université de Strasbourg, France*
d - Fédération de Médecine Translationnelle de Strasbourg (FMTS), *Strasbourg, France*
e - Department of Pathology, *University Hospital Strasbourg, Strasbourg, France*
f - Department of Pathology, *Medical University of Vienna (MUW), Vienna, Austria*
g - Etablissement Français du Sang, *INSERM U949, Strasbourg, France*
h - Kennedy Institute of Rheumatology, *University of Oxford, Oxford, UK*
i - Department Medicine, *University Basel, Basel, Switzerland*
j - Department of breast diseases and surgery, *Strasbourg University Hospital, Strasbourg, France*

Correspondence to Gertraud Orend: *at: Institut d'Hématologie et d'Immunologie, Hôpital Civil, 4 rue Kirschleger, 67085 Strasbourg Cedex, France.* *gertraud.orend@inserm.fr*
https://doi.org/10.1016/j.matbio.2019.07.001

Abstract

Metastasis is a major cause of death in cancer patients. The extracellular matrix molecule tenascin-C is a known promoter of metastasis, however the underlying mechanisms are not well understood. To further analyze the impact of tenascin-C on cancer progression we generated MMTV-NeuNT mice that develop spontaneous mammary tumors, on a tenascin-C knockout background. We also developed a syngeneic orthotopic model in which tumor cells derived from a MMTV-NeuNT tumor. Tumor cells were transfected with control shRNA or with shRNA to knockdown tenascin-C expression and, were grafted into the mammary gland of immune competent, wildtype or tenascin-C knockout mice. We show that stromal-derived tenascin-C increases metastasis by reducing apoptosis and inducing the cellular plasticity of cancer cells located in pulmonary blood vessels invasions (BVI), before extravasation. We characterized BVI as organized structures of tightly packed aggregates of proliferating tumor cells with epithelial characteristics, surrounded by Fsp1+ cells, internally located platelets and, a luminal monolayer of endothelial cells. We found extracellular matrix, in particular, tenascin-C, between the stromal cells and the tumor cell cluster. In mice lacking stromal-derived tenascin-C, the organization of pulmonary BVI was significantly affected, revealing novel functions of host-derived tenascin-C in supporting the integrity of the endothelial cell coat, increasing platelet abundance, tumor cell survival, epithelial plasticity, thereby promoting overall lung metastasis. Many effects of tenascin-C observed in BVI including enhancement of cellular plasticity, survival and migration, could be explained by activation of TGF-β signaling. Finally, in several human cancers, we also observed BVI to be surrounded by an endothelial monolayer and to express tenascin-C. Expression of tenascin-C is specific to BVI and is not observed in lymphatic vascular invasions frequent in breast cancer, which lack an endothelial lining. Given

that BVI have prognostic significance for many tumor types, such as shorter cancer patient survival, increased metastasis, vessel occlusion, and organ failure, our data revealing a novel mechanism by which stromal tenascin-C promotes metastasis in human cancer, may have potential for diagnosis and therapy.

Introduction

Despite earlier diagnosis and improved treatment a high number of cancer patients die due to cancer-related complications, tumor recurrence and, most frequently, metastasis [1]. To improve patient survival a better knowledge of the mechanisms of metastasis is required. During metastasis, tumor cells disseminate from the primary tumor and invade blood or lymphatic vessels where they can be found as circulating tumor cells appearing in a variety of forms as ranging from single cells or small cell clusters up to multicellular tumor cell aggregates or tumor emboli. Tumor emboli can be classified as blood vessel invasions (BVI) or lymphatic vessel invasions (LVI), all together covered by the term lympho-vascular invasions [2–4]. The presence of vascular invasions in the primary tumor and the distant organ correlates with poorer cancer patient survival, increased metastasis, vessel occlusion and organ failure [5,6]. Therefore, targeting vascular invasions may offer novel treatment opportunities. To date, very little is known about the cellular composition of vascular invasions, nor whether there are differences in BVI in comparison to LVI.

The tumor microenvironment (TME) comprises tumor and stromal cells, soluble factors and extracellular matrix (ECM) [7]. An important ECM molecule that enhances metastasis is tenascin-C (TNC) [8,9]. As reviewed [10], TNC plays multiple roles in cancer. Recently, this has been comprehensively demonstrated in the first stochastic neuroendocrine tumor (PNET) model with abundant and no TNC, where TNC was found to enhance survival, proliferation, invasion, angiogenesis and lung metastasis [11].

By using breast cancer xenograft models, TNC was identified as a gene that mediates metastasis to the lung relevant during early steps of lung metastasis colonization; however, its relevance in immune competent breast cancer models with spontaneous tumor onset has not been confirmed [8,9,12–14]. Moreover no model existed to address the relative contribution of host and tumor cell-derived TNC on breast cancer progression in an immune competent setting.

We have chosen the MMTV-NeuNT transgenic mouse model of metastatic cancer, ectopically expressing an active ErbB2 molecule from rat under control of the MMTV enhancer, that spontaneously develops primary mammary tumors and pulmonary BVI as precursors of parenchymal metastasis [15–17]. By using our novel cancer progression models, we observed that TNC increases lung metastasis by impacting BVI at multiple levels. In patients, we observed BVI in human cancers to be similarly organized to those in the mouse models, and also express TNC. Our results may offer novel opportunities for cancer diagnosis and therapy.

Results

Tenascin-C accelerates tumor onset

We generated compound MMTV-NeuNT tumor mice deficient in *Tnc* (NeuNT-TNCKO) and compared tumorigenesis in these mice with mice expressing normal (wildtype, WT) levels of TNC (NeuNT-WT). By immunofluorescence staining of primary tumors we found TNC expressed in tumor matrix tracks (Fig. S1A) as previously shown in other cancers [18]. No TNC protein was found in TNCKO tumors (Fig. S1A, B). We compared tumor onset and observed that tumor latency was largely delayed in NeuNT-TNCKO mice (Fig. 1A). As previously described in this model all mice developed multiple tumors [16], the number of which was not affected by TNC. Mice were sacrificed 3 months after first tumor palpation and no significant difference in tumor burden, proliferation nor apoptosis between genotypes was noted (Fig. 1B, data not shown).

Tenascin-C enhances lung metastasis

We assessed lung metastasis by a stereological analysis [19] of the left and biggest lung lobe and observed no difference in the number of metastasis between NeuNT-TNCKO and NeuNT-WT mice (Fig. 1C, D). Yet, we found a larger lung surface covered by tumor cells in NeuNT-WT compared to NeuNT-TNCKO mice (Fig. 1C, E). As pulmonary BVI have been observed in Neu models [15] and were described as precursors of lung metastasis [17], we used immunohistochemistry to assess whether BVI are also common in the NeuNT model [16]. Indeed, we observed BVI in the lungs of these mice and, also in the primary tumors which had not been documented beforehand in any MMTV-Neu model (Fig. 1C, F, Fig. S1C). Surface measurement revealed that BVI are bigger in the lungs from NeuNT-WT mice than in those from NeuNT-TNCKO mice (Fig. 1F, G). As reduced proliferation and/or

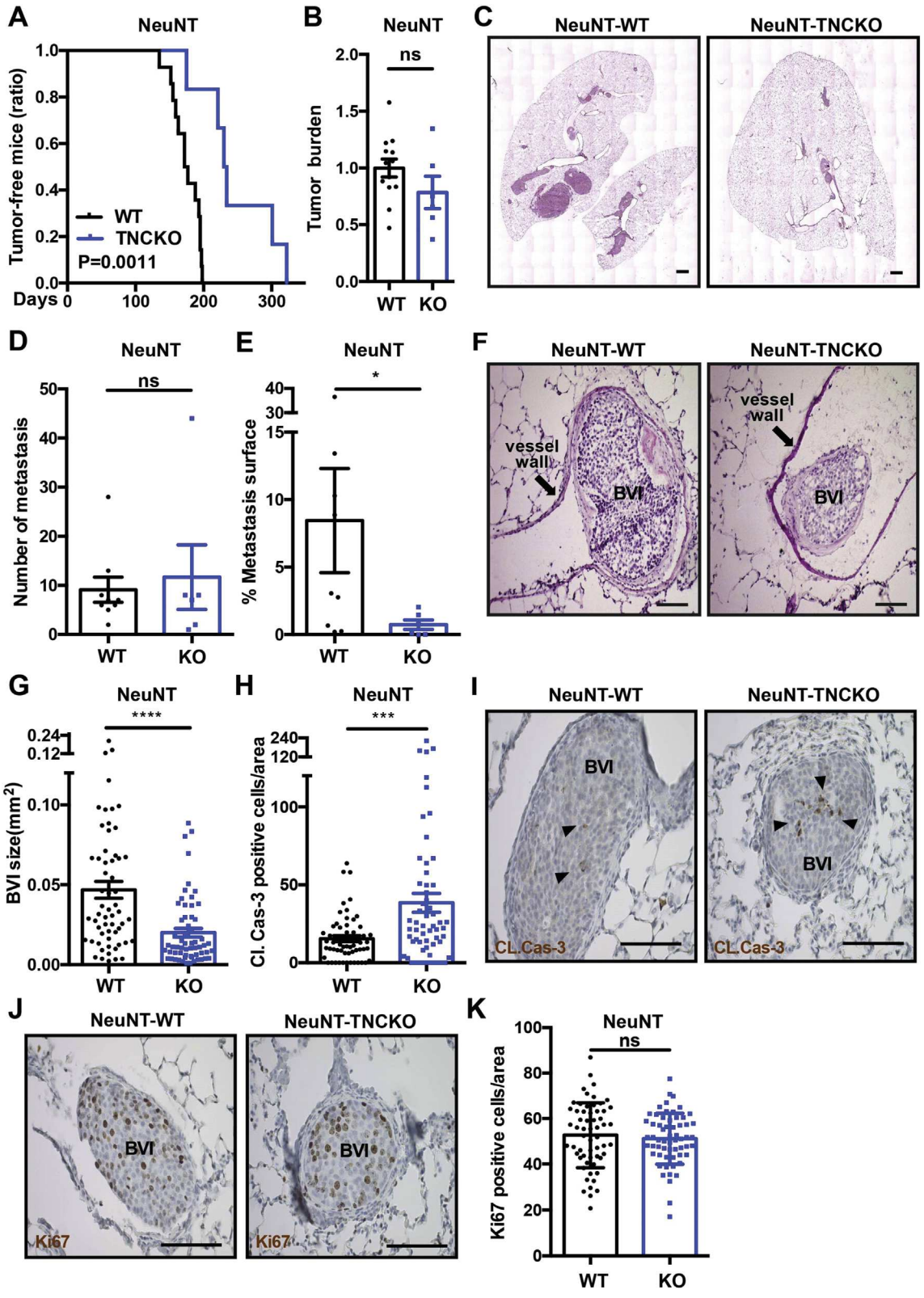
A
NeuNT
Tumor-free mice (ratio)
1.0
0.8
0.6
0.4
0.2
0.0
Days 0
100
200
300
WT
TNCKO
P=0.0011
B
NeuNT
Tumor burden
2.0
1.5
1.0
0.5
0.0
ns
WT
KO
C
NeuNT-WT
NeuNT-TNCKO
D
NeuNT
Number of metastasis
50
40
30
20
10
0
ns
WT
KO
E
NeuNT
% Metastasis surface
40
30
15
10
5
0
*
WT
KO
F
NeuNT-WT
NeuNT-TNCKO
vessel wall
BVI
vessel wall
BVI
G
NeuNT
BVI size(mm2)
0.24
0.12
0.10
0.05
0.00
****
WT
KO
H
NeuNT
Cl. Cas-3 positive cells/area
240
120
100
50
0
***
WT
KO
I
NeuNT-WT
NeuNT-TNCKO
BVI
BVI
CL.Cas-3
CL.Cas-3
J
NeuNT-WT
NeuNT-TNCKO
BVI
BVI
Ki67
Ki67
K
NeuNT
Ki67 positive cells/area
100
80
60
40
20
0
ns
WT
KO

increased apoptosis could account for a difference in BVI size, we performed staining for cleaved caspase-3 (Cl. Cas-3) and Ki67, respectively. We noticed that Cl. Cas-3+ cells are less abundant in BVI from NeuNT-WT than NeuNT-TNCKO mice, indicating that TNC promotes tumor cell survival in the BVI (Fig. 1H, I). It is remarkable that some tumor cells within the BVI proliferate, yet there is no difference in the number of Ki67+ cells between tumor mice expressing or lacking TNC (Fig. 1J, K). Similar to tumor cells in the BVI, also in the parenchymal metastasis TNC did not impact cell proliferation, but enhanced tumor cell survival (Fig. S1D-G). In summary, our data indicate that in the MMTV-NeuNT model TNC promotes cancer cell survival in pulmonary BVI as well as in parenchymal metastasis which could explain the observed larger metastatic surface in lungs from WT tumor mice.

Host-derived tenascin-C promotes growth of BVI and overall metastasis

Previous reports using a xenograft model suggested that, host-derived TNC has a minor impact on lung metastasis colonization [8,9,14]. As tumor immunity largely impacts tumor growth and metastasis, which is missing in the xenograft models, we addressed how host- versus tumor cell-derived TNC impacts cancer progression in an immune competent setting. Therefore, we established a syngeneic orthotopic grafting model by using NT193 cells that we previously had established from a MMTV-NeuNT tumor [20].

We engineered NT193 cells to downregulate *Tnc* by shRNA technology. To mitigate possible off target effects we used two different shRNA sequences (sh1TNC and sh2TNC) and, grafted the tumor cells into the mammary gland of naïve WT and TNCKO FVB mice, respectively. We confirmed *Tnc* knockdown in the cultured cells by immunoblotting (Fig. S2E). Upon immunofluorescence analysis of the arising tumors in the mammary gland we noticed that TNC levels are highest in a WT host upon engraftment of shC cells (transfected with a control shRNA sequence (shC), WT/shC or TNC-high tumors) and almost absent in KO/shTNC (or TNC-low) tumors, suggesting that the *Tnc* knockdown is stable in vivo (Fig. S2F, G). We further observed that mice with NT193 tumors develop spontaneously metastasis in the lung parenchyma as well as BVI in blood vessels of the lung. As for the MMTV-NeuNT model, with the changing levels of TNC expression we found no difference either in tumor burden (Fig. S2H) nor in lung metastasis incidence (Fig. 2A). Yet, we noticed that the lung metastasis surface is larger in TNC-high (WT/shC) than TNC-low (KO/shC) conditions. Moreover, irrespective of the cell genotype, there is a tendency towards more metastasis in WT than in TNCKO mice suggesting an involvement of host-derived TNC in promoting metastasis (Fig. 2B). Next, we determined the surface of the BVI and found that BVI derived from TNC-high (WT/shC) tumor mice are significantly bigger than from TNC-low (KO/shC) tumor mice (Fig. 2C). To address whether a difference in proliferation or survival accounts for the observed result we again stained for Ki67 and Cl. casp-3, respectively. As for the genetic MMTV-NeuNT model, in the BVI some tumor cells proliferate, yet independent of TNC (Fig. 2D, E). In contrast to proliferation, we saw that apoptosis is higher in BVI from KO tumor mice and, that in TNC-high (WT/shC) conditions apoptosis is the least (Fig. 2F, G). Altogether, these results demonstrate an important role of host-derived TNC in increasing BVI tumor cell survival and metastasis and, distinct functions of stromal and tumor cell derived TNC in metastasis.

Tenascin-C surrounds epithelial tumor cell aggregates in BVI

To understand the composition of pulmonary BVI, we analyzed tumor and lung tissue of NeuNT-WT mice. BVI were found in blood vessels of the primary tumor (Fig. S1C), and the lung, sometimes surrounded by a thick ECM layer (Fig. 3A). BVI also could completely occlude the vessel lumen and had an eventual necrotic center (Fig. 3A, S3A-C, Fig. S1C).

Fig. 1. Increased lung metastasis in the presence of TNC in MMTV-NeuNT mice **(A)** Ratio of tumor-free mice is shown for MMTV-NeuNT tumor mice with two (NeuNT-WT, $N = 13$ mice) and no (NeuNT-TNCKO, $N = 6$) TNC alleles. The absence of TNC significantly delays tumor latency (NeuNT-WT versus NeuNT-TNCKO, $p = 0.0011$; Log-rank tests). **(B)** Tumor burden of NeuNT-TNCKO tumor mice ($N = 6$) was determined and normalized to the mean tumor weight of the control group (NeuNT-WT, $N = 13$). **(C)** Representative HE images of lung metastasis from MMTV-NeuNT mice (NeuNT-WT and NeuNT-TNCKO) that had been sacrificed 3 months after tumor detection. Scale bar: 1000 μm. **(D, E)** Number of lung metastases **(D)** and of the cumulated metastatic burden (metastatic area normalized to total lung area) **(E)** in lungs of NeuNT-WT ($N = 9$) and NeuNT-TNCKO ($N = 6$) mice. **(F, G)** HE stained lung tissue was used for BVI size determination (NeuNT-WT, $N = 6$ mice, $n = 59$ BVI; NeuNT-TNCKO, $N = 6$ mice, $n = 60$ BVI). Scale bar: 100 μm. **(H–K)** measurement of apoptosis and proliferation by IHC analysis for cleaved caspase-3 (Cl. Cas-3) **(H, I)** and Ki67 **(J, K)** in BVI (NeuNT-WT, $N = 6$ mice, n = 59 BVI; NeuNT-TNCKO, $N = 6$ mice, n = 60 BVI). Dots represent number of apoptotic **(H)** and proliferative cells **(K)** in BVI per area (0.1 mm^2), respectively. Arrowhead denotes Cl. Cas-3 positive apoptotic cell **(I)**. Scale bar, 100 μm. Mean ± SEM. **(B, D, E, G, H and K)** unpaired Student t or Mann-Whitney test.

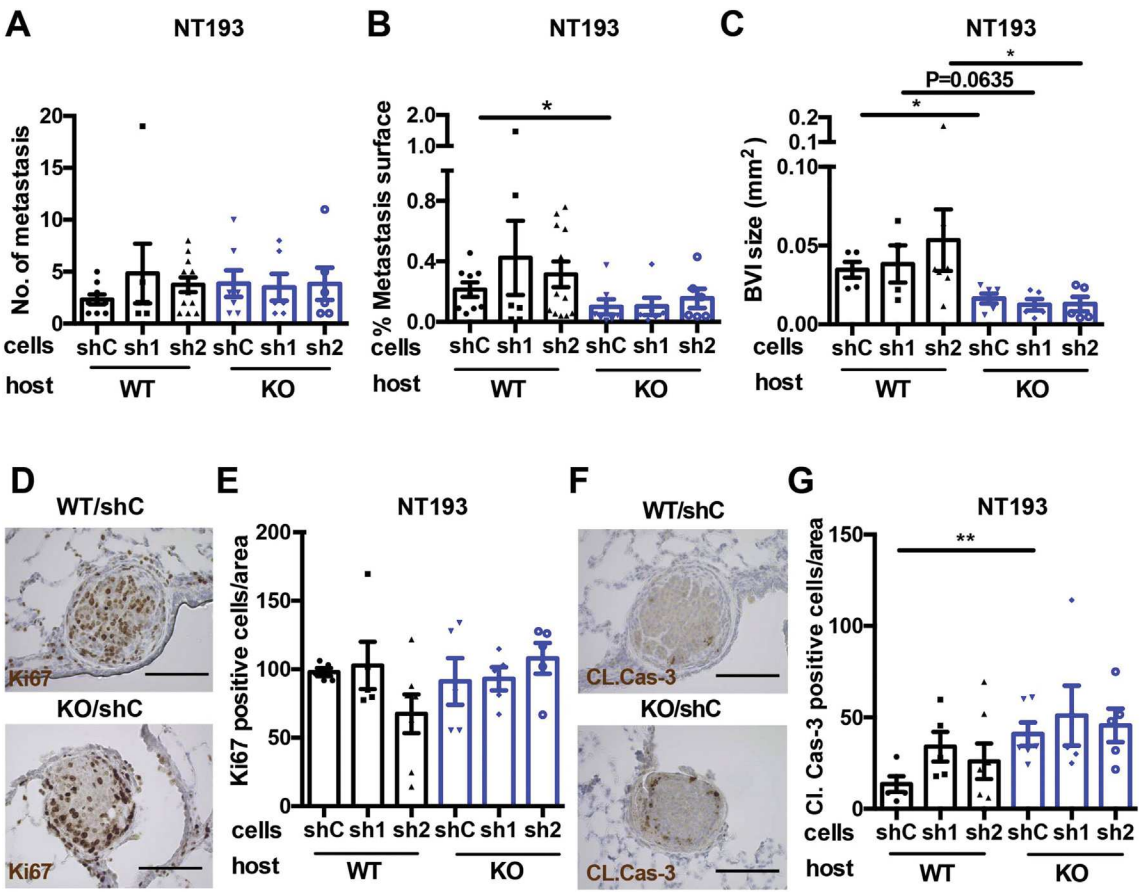

Fig. 2. Host-derived TNC promotes lung metastasis in NT193 grafted tumor mice **(A-C)** Quantification of the number of lung metastases (*N*, at least 5) **(A)**, cumulated metastatic burden (metastatic area normalized to total lung area) (*N*, at least 5) **(B)** and size of BVI **(C)** in lungs of WT and TNCKO FVB hosts after engraftment of NT193 sh control (shC), sh1TNC and sh2TNC cells (WT/shC ($N = 5$ mice); WT/sh1TNC ($N = 4$ mice); WT/sh2TNC ($N = 7$ mice); KO/shC ($N = 6$ mice); KO/sh1TNC ($N = 5$ mice); KO/sh2TNC ($N = 5$ mice). Note a bigger metastatic surface and bigger BVI in a WT host. **(D-G)** IHC analysis for Ki-67 **(D)** and cleaved caspase-3 (Cl. Cas-3) **(F)** in BVI of lungs from NT193 engrafted mice. Dots represent proliferative **(E)** and apoptotic cells in BVI **(G)** per 0.1 mm^2, respectively. Note more apoptotic cells in tumors of the KO host. Scale bar, 100 µm. Mean ± SEM, unpaired Student t or Mann-Whitney test. Statistical analysis was performed between all groups. Only statistically significant ($p < 0.05$) differences are marked.

The core of the BVI is composed of cancer cells (ErbB2+) with epithelial phenotype (CK8/18+) (Fig. 3B - D). We addressed by staining whether BVI express TNC and saw indeed abundant TNC at the periphery, yet no TNC within the tumor cell cluster that homogenously expresses ErbB2 (Fig. 3B - D). We also noticed the absence of TNC when tumor cells are extravasating from the BVI into the lung parenchyma (Fig. 3B).

Since we observed that host-derived TNC promotes BVI growth we wondered which stromal cells could be a source of TNC. Considering that Fsp1+ fibroblasts/myeloid cells were described in another breast cancer model as a source of TNC (and other molecules such as VEGFA) and, have been shown to promote tumor progression [21], we evaluated their presence in BVI. Indeed, we observed Fsp1+ cells in BVI and, an overlap of the signals for Fsp1 and TNC, suggesting that Fsp1+ cells are a likely source of TNC in BVI (Fig. 3D). A similar result was obtained in the NT193 grafting model, where the Fsp1 signal also co-localized with TNC (Fig. 3E). Of note, Fsp1+ cells are also present in BVI from NeuNT mice deficient in TNC (Fig. S3E).

Together, Fsp1-expressing cells are likely candidates to express TNC in BVI of both models. This result also demonstrates a strong similarity between the genetic and grafting model.

Tenascin-C increases abundance of platelets and integrity of the surrounding endothelial monolayer of BVI

We characterized the cellular and ECM composition of pulmonary BVI of NeuNT-WT mice, by multichannel immunofluorescence imaging of epithelial/

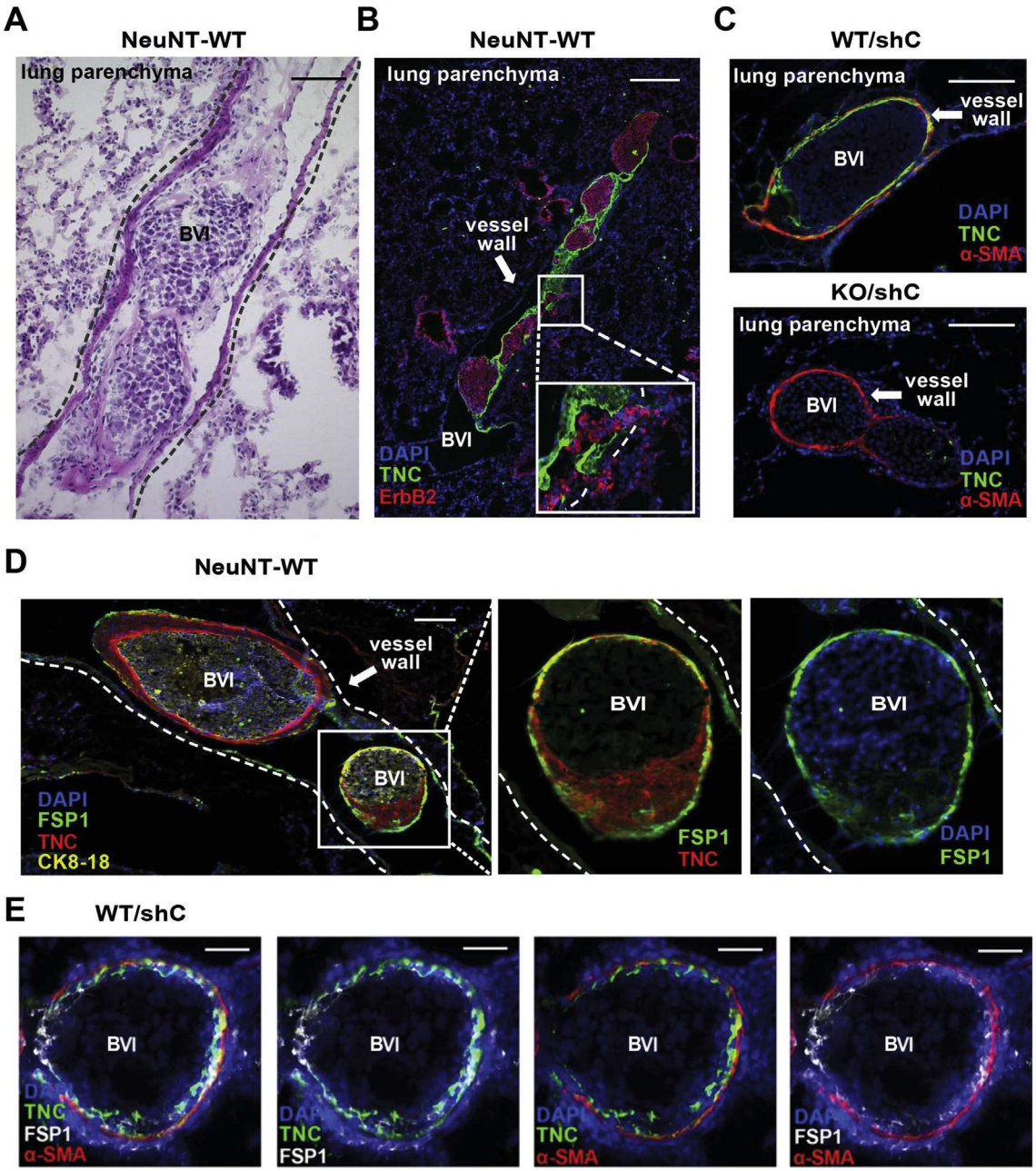

Fig. 3. TNC and Fsp1 expression in BVI **(A, B)** Representative images of BVI in NeuNT-WT lungs upon HE and IF staining for the indicated molecules. **(B)** Note that TNC (green) is expressed around tumor cells (red, ErbB2). Cell nuclei stained with DAPI. Scale bar, 100 μm **(A)**, 500 μm **(B)**. **(C)** Representative IF images for TNC (green) in BVI from WT/shC and KO/shC tumor mice. αSMA staining (red) marks the smooth muscle/pericyte layer underneath blood vessels. Note, that TNC is expressed in BVI of shC cells engrafted in a WT host, yet not in a TNCKO host indicating that TNC in BVI is of host origin. Scale bar, 100 μm. **(D, E)** Representative IF images for Fsp1+ cells and TNC in BVI from NeuNT-WT **(D)** and WT/shC lung tissue **(E)**. Note overlap of TNC with Fsp1, yet not αSMA, suggesting Fsp1+ cells as a likely source of TNC. Scale bar: 100 μm **(D)**, 50 μm **(E)**. White square represents area of higher magnification.

tumor cells (CK8/18, ErbB2), endothelial cells (CD31), platelets (CD41, RAM1), leukocytes (CD45), fibronectin (FN) and laminin (LM) in sequential lung tissue sections. We observed that in all BVI, cancer cells form a tightly packed tumor cell nest that is enveloped by a layer of Fsp1+ cells (Fig. 3D). Furthermore, a monolayer of endothelial cells, characterized by flat endothelial cell nuclei, is

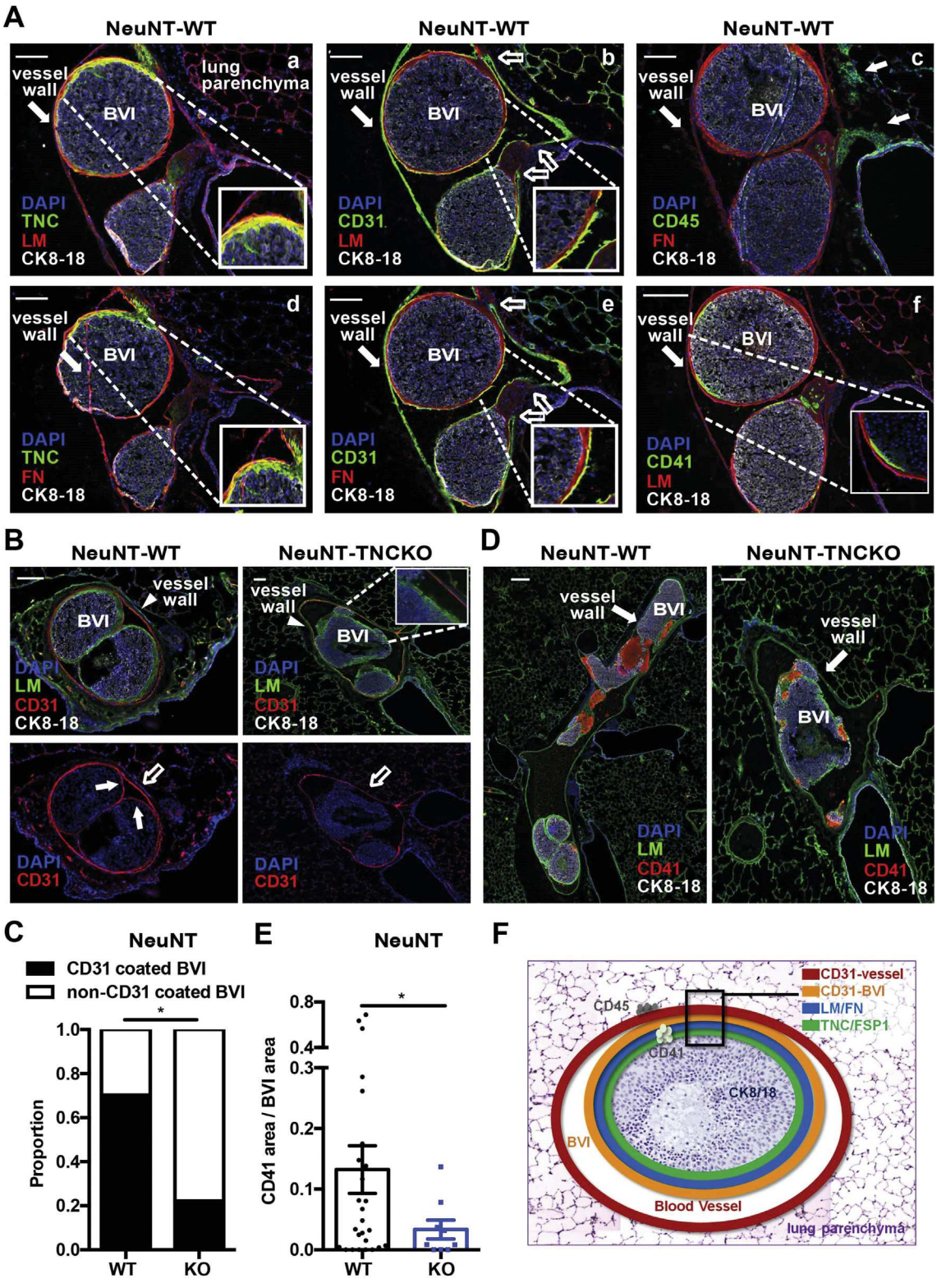

present at the luminal side of the BVI in the genetic NeuNT-WT (Fig. 4A, S4A, B) and the syngeneic NT193 TNC-high (WT/shC) model (Fig. S4C). Moreover, we found distinct layers of LM and FN between the endothelial layer and Fsp1+ cells. Neither FN, LM, TNC nor endothelial cells or

fibroblasts were found within the core of the tumor cell cluster (Fig. 4A). As plasticity is frequent in cancer and could give rise to cells with mixed tumor and stromal properties [22] we considered that the Fsp1+ cells may be of tumor cell origin. Yet, we did not see any signal overlap of Fsp1+ with CK8/18, nor ErbB2.

Furthermore, leukocytes (CD45+) were abundant, yet they were not associated with the BVI but were found outside the BVI at the basal side of the vessel wall facing the lung parenchyma (Fig. 4A, Fig. S4A). Most interestingly, the layered organization of BVI of the MMTV-NeuNT model is recapitulated in the NT193 grafting model. Again, BVI express a layer of TNC and display a core of proliferating cancer cells and, a layer of fibroblasts and endothelial cells that are separated by FN and LM (Fig. 3C, E, Fig. S4C).

We investigated the presence of platelets as they are frequently present in circulating tumor cell aggregates and can cause thromboembolism and vessel occlusion [23]. By staining for CD41 or RAM1 (recognizing Gp1b [24]), we found platelets located inside the BVI surrounded by the LM and endothelial layers. This observation suggests a role of platelets early in the evolution of the BVI (Fig. 4D, S4D-F). We also noticed an overlap of signals for CD41 and TNC which points at platelets as another potential source of TNC as was previously described in another model [25] (Fig. S4F).

Altogether, our detailed analysis revealed the organization of BVI as tightly packed cell clusters (positive for CK8/18 and ErbB2) where some tumor cells are proliferating. Moreover, the nest of tumor cells is enveloped by distinct layers of stromal cells. Whereas Fsp1+ cells, a likely source of TNC, are located adjacent around the tumor cell nest, a layer of endothelial cells is present at the luminal rim of the BVI. Interestingly, the endothelial cells are not in direct contact with TNC but are separated from TNC by other ECM, in particular LM and FN which is consistent with this ECM layer potentially protecting endothelial cells from TNC-induced apoptosis (Fig. 4F, [26,27]).

Since BVI are also present in lung vessels of NeuNT-TNCKO mice, we asked whether TNC had any impact on their organization. Staining for LM, FN and Fsp1 did not reveal gross differences between genotypes neither in the transgenic or syngeneic model, suggesting that TNC may not be required for BVI to form (Fig. 3C, 4B, D). Besides that, although we observed an endothelial monolayer around BVI in both genotypes (Fig. 4B, S4A - C) we noticed more BVI with an intact endothelial layer in NeuNT-WT as compared to NeuNT-TNCKO mice (Fig. 4B, C). Interestingly, we also observed an eventual cellular continuum between the endothelial layers of the BVI and the lung vessel wall (Fig. 4A). By quantification of CD41 we observed less platelets in pulmonary BVI from NeuNT-TNCKO than NeuNT-WT mice reminiscent of a role of TNC in promoting attachment of platelets, as previously described in a thrombosis model [24] (Fig. 4D-E).

Overall our data show that, whereas TNC is not required for the formation of pulmonary BVI, stromal TNC has multiple effects on the organization of BVI, promoting endothelial coat integrity, platelet recruitment and tumor cell survival.

Tenascin-C promotes extravasation of tumor cells from pulmonary BVI into the lung parenchyma

We investigated whether BVI are also precursors of parenchymal metastasis in the MMTV-NeuNT model as described in another MMTV-Neu model [17]. Indeed, we observed that the relative abundance of parenchymal metastasis increases over time on account of a reduced number of pulmonary BVI in the MMTV-NeuNT model (Fig. S5A). Notably, when we compared the ratio of BVI to parenchymal metastasis we found more parenchymal metastasis than BVI in lungs of NeuNT-WT compared to NeuNT-TNCKO mice (Fig. 5A). Similarly, in the NT193 grafting model we saw more parenchymal metastasis in TNC-high than TNC-low conditions (Fig. 5B). Interestingly, whereas at the site of extravasation TNC is absent, in the parenchymal metastasis TNC is expressed at the border and in matrix tracks (Fig. 3B, S5B-E).

Fig. 4. Cellular organization of BVI **(A)** Representative images of immunostainings for ECM molecules and cellular markers in BVI of lung tissue from NeuNT-WT **(A, B, D)** and NeuNT-TNCKO mice **(B, D)**. The empty arrows point at narrowing of endothelial layers reminiscent of fusion of the endothelial layers derived from the lung vasculature and the BVI. White squares in each panel delineate the field shown at higher magnification. In panel **A**(c) arrows point at CD45+ cells. In panel **A**(d) the vessel staining for FN on the left is an artefact due to disruption of the tissue. Scale bar, 100 μm. **(B)** Representative images of endothelial cells. Arrows point at the endothelial monolayer of the BVI. The empty arrow points at the blood vessel wall. Scale bar, 100 μm. **(C)** Proportion of BVI with and without a CD31 layer for each genotype (NeuNT-WT, $N = 6$ mice, $n = 27$ BVI; NeuNT-TNCKO, $N = 4$ mice, $n = 8$ BVI). Mean ± SEM, Fisher's exact test. **(D)** Representative images of platelets (CD41+) together with LM. Scale bar, 200 μm. **(E)** Platelet abundance (CD41+ area normalized to area of BVI), NeuNT-WT, $N = 6$ mice, $n = 26$ BVI; NeuNT-TNCKO, $N = 4$ mice, $n = 9$ BVI. Mean ± SEM, Mann-Whitney test. **(F)** Scheme depicting the composition of BVI. Note, that cancer cells (CK8/18+) are tightly packed inside the BVI, surrounded by Fsp1+ cells, a LM/FN layer and a luminal oriented monolayer of endothelial cells (CD31+). CD45+ leukocytes are not in direct vicinity to the BVI but are present at the basal side of the vessel wall facing the parenchyma. Also, endothelial cells are not in direct contact with TNC.

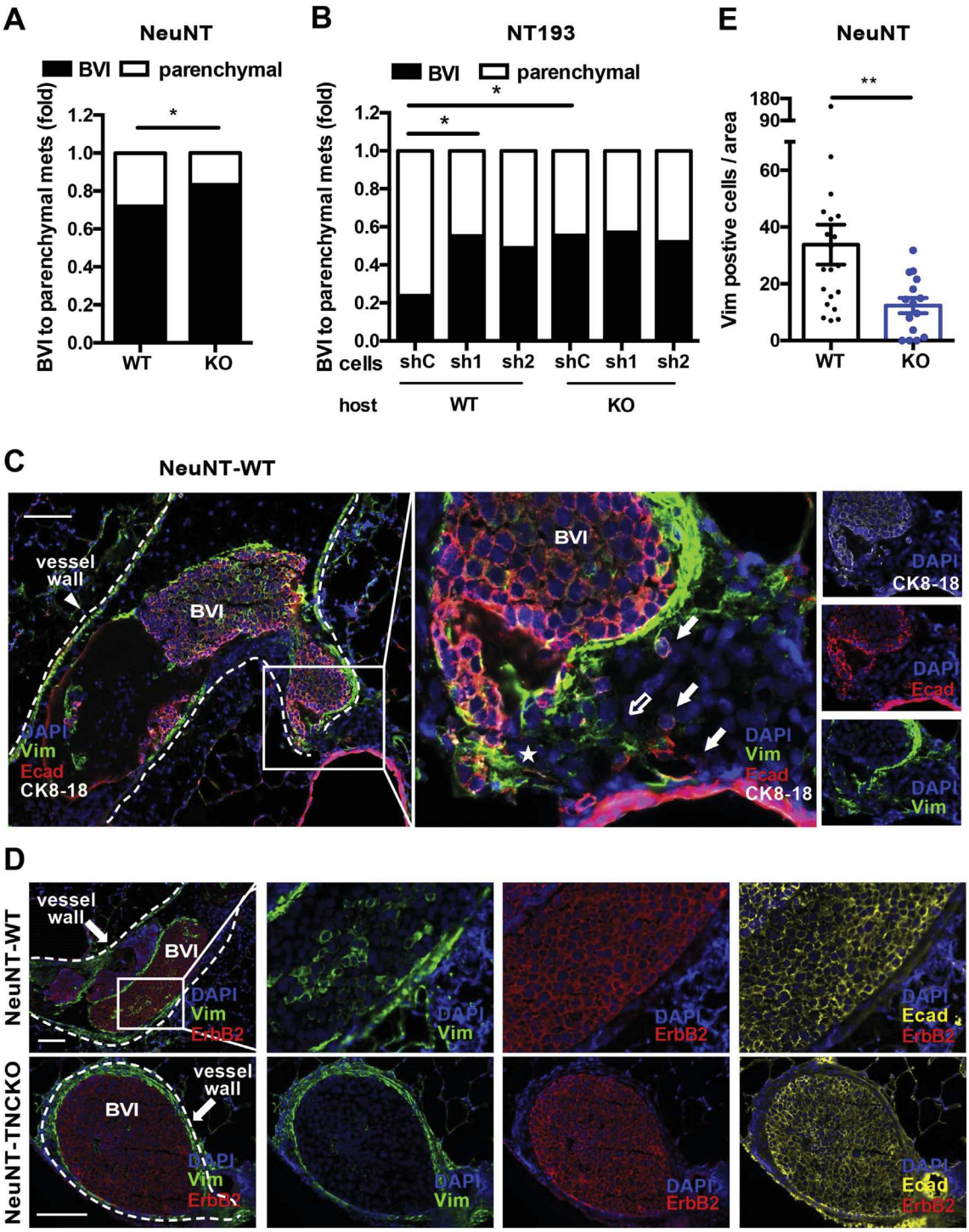

Altogether, these results suggest that TNC plays a role in progression of pulmonary BVI into parenchymal metastasis. TNC also promotes outgrowth of the parenchymal metastasis by promoting survival (Fig. S1C, D), similar as seen in a xenograft tail vein injection model [9].

Tenascin-C increases cellular plasticity in pulmonary BVI and parenchymal metastasis

As pulmonary BVI can act as precursor of parenchymal metastasis, the question arises how tumor cells enter the lung parenchyma. Epithelial-to-

mesenchymal-transition (EMT) could be a possible mechanism in the MMTV-NeuNT model as was shown to occur in the MMTV-Neu model [17]. Indeed, in some sections we observed cancer cells leaving pulmonary BVI and invading the parenchymal lung tissue (Fig. 3B, 4A, 5C). We investigated the expression of the mesenchymal transition marker vimentin and the epithelial markers CK8/18 and E-cadherin, respectively, in pulmonary BVI. While all tumor cells inside the BVI express CK8/18, E-cadherin and ErbB2, some cells also co-express vimentin (Fig. 5C, E, S5F, G). By quantification we noticed more vimentin-expressing cells inside BVI from NeuNT-WT than NeuNT-TNCKO mice (Fig. 5D, E). Similarly, we also observed vimentin+ cells inside the parenchymal metastasis of NeuNT-WT tissue indicating a mixed epithelial/mesenchymal phenotype (Fig. S5C, D). Other cells at the invading front only express vimentin but not E-cadherin, nor CK8/18 or ErbB2 (Fig. 5C). A vimentin+ and Ecad+ phenotype is reminiscent of cells undergoing a partial EMT, presumably allowing cells to invade as cell cohorts as has previously reported in another model (MMTV-PyMT, [28] (Fig. 3B, 5C). In addition, a mixed tumor cell phenotype in the parenchymal tissue suggests MET that may support tumor cell outgrowth [29].

Altogether, our results suggest that TNC promotes cellular plasticity in pulmonary BVI thereby affecting tumor cell extravasation and outgrowth of parenchymal metastasis.

Tenascin-C induces EMT in cultured tumor cells, promoting cell migration and survival through TGF-β signaling

TNC has been shown to induce an EMT-like phenotype in conjunction with TGF-β in cellular models [30,31]. Therefore, we asked whether TNC induces EMT in NT193 cells. We added purified TNC to NT193 cells grown as monolayer or as spheroid cultures and indeed observed EMT as indicated by loss of E-cadherin and gain of vimentin expression as demonstrated by immunofluorescence imaging, quantitative reverse transcription PCR (qPCR) and immunoblotting (Fig. 6A **-** **C**). Moreover, we noticed increased mRNA levels of several other EMT markers, such as *Snail*, *Slug*, *Zeb1*, *Pai-1*, *Mmp9* and *Tnc* itself upon treatment with TNC. On the contrary, mRNA levels of *E-cadherin* were found reduced (Fig. 6B).

Next, we compared cell responses to TNC with that to TGF-β and, found that similar to TNC, TGF-β induces an EMT in NT193 cells as evidenced by loss of E-cadherin and gain of vimentin expression (Fig. 6A-C, Fig. S6A, B). Notably, the TGF-β signaling inhibitor GW788388 (GW) reverts the TNC-induced mesenchymal phenotype into an epithelial one, as expression of E-cadherin is increased and that of vimentin is decreased (Fig. 6A - C, Fig. S6A, B). These results demonstrate that TNC induces EMT in NT193 cells through TGF-β signaling.

We determined downstream signaling upon TNC treatment by immunoblotting and observed that in addition to phosphorylated Smad (p-Smad2) also levels of p-Akt and p-Erk1/2 increase, suggesting an induction of both canonical and non-canonical TGF-β signaling by TNC. Moreover, all three of the TNC-induced signaling pathways are TGF-β dependent as they were blocked with GW (Fig. 6C, S6B).

As we observed platelets residing inside the pulmonary BVI and platelets are known to induce an EMT [25], we considered a potential role of platelets in EMT in our models. Indeed, in cultured cells, we found that platelets induce an EMT, since E-cadherin levels are decreased and vimentin expression is increased. Similar to TNC, also the platelet-induced EMT was blocked with GW, suggesting that a platelet-induced EMT is TGF-β signaling-dependent in NT193 cells (Fig. 6D).

Next, we asked what consequences a TNC-induced TGF-β-dependent EMT has for the cells. We used a cellular wound closure assay and observed increased migration of cells upon addition of TNC, which was comparable to the treatment with TGF-β (Fig. 6E, F). Again, this effect was blocked with GW indicating that TNC-induced EMT increases NT193 cell motility through TGF-β signaling.

Fig. 5. TNC promotes extravasation and plasticity of cancer cells in BVI **(A, B)** Proportion of BVI to parenchymal metastasis in MMTV-NeuNT mice **(A)** (NeuNT-WT, $N = 6$ mice; NeuNT-TNCKO, $N = 6$ mice), $p < 0.02$, Fisher's exact test; and in NT193 grafted mice **(B)** (WT/shC shC, $N = 5$; WT/sh1TNC, $N = 4$; WT/sh2TNC, $N = 7$; KO/shC, $N = 6$; KO/sh1TNC, $N = 5$; KO/sh2TNC, $N = 5$. Mean ± SEM). Chi-square test. Note, that combined TNC expression by the host and the tumor cells increases parenchymal metastasis. **(C, D)** Representative IF images of vimentin (green), E-cadherin (red) and CK8/18 (white) expression in BVI from NeuNT-WT mice. White squares delineate areas of higher magnification. Note, that tumor cells (CK8/18+) are invading the parenchymal lung tissue. Arrow points at single invading tumor cell with epithelial characteristics (CK8/18+ and E-cadherin+). Empty arrow points at invading vimentin+ and E-cadherin- cell. Star points at an event at the invading front. Scale bar, 100 μm. **(E)** Representative IF images of cells expressing vimentin (green), ErbB2 (red) and E-cadherin (yellow) in BVI from NeuNT-WT and NeuNT-TNCKO mice. Scale bar, 100 μm. **(E)** Quantification of tumor cells expressing both vimentin and ErbB2 normalized per BVI area (0.1 mm^2). MMTV-NeuNT (NeuNT-WT, $N = 6$ mice, $n = 20$ BVI; NeuNT-TNCKO, $N = 4$ mice, $n = 15$ BVI). Mean ± SEM, Mann-Whitney test. Statistical analysis was performed between all groups. Only statistically significant ($p < 0.05$) differences are marked.

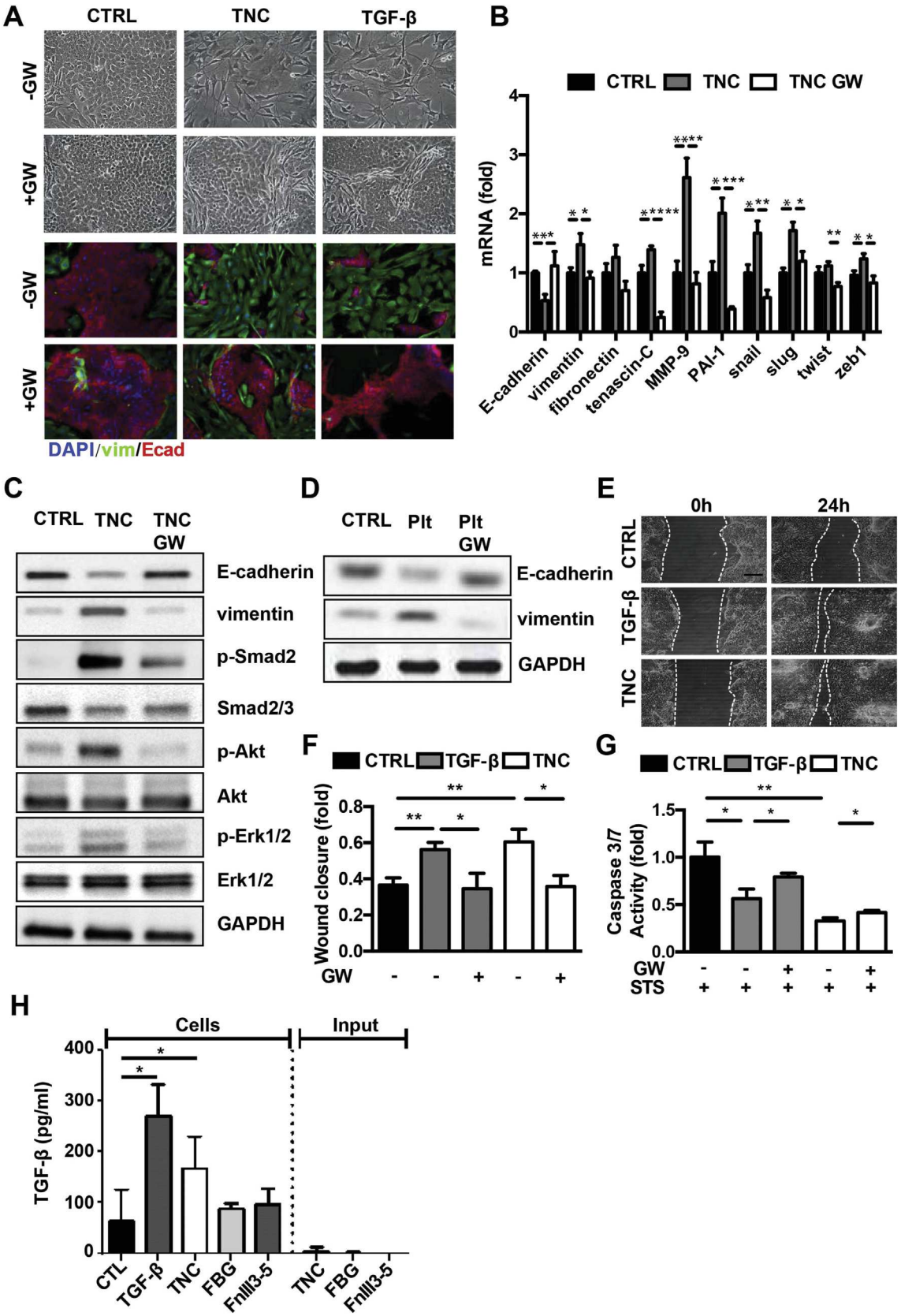
A
CTRL
TNC
TGF-β
-GW
+GW
-GW
+GW
DAPI/vim/Ecad
B
CTRL
TNC
TNC GW
mRNA (fold)
E-cadherin
vimentin
fibronectin
tenascin-C
MMP-9
PAI-1
snail
slug
twist
zeb1
C
CTRL
TNC
TNC GW
E-cadherin
vimentin
p-Smad2
Smad2/3
p-Akt
Akt
p-Erk1/2
Erk1/2
GAPDH
D
CTRL
Plt
Plt GW
E-cadherin
vimentin
GAPDH
E
0h
24h
CTRL
TGF-β
TNC
F
CTRL
TGF-β
TNC
Wound closure (fold)
GW
G
CTRL
TGF-β
TNC
Caspase 3/7 Activity (fold)
GW
STS
H
Cells
Input
TGF-β (pg/ml)
CTL
TGF-β
TNC
FBG
FnIII3-5
TNC
FBG
FnIII3-5

Since EMT provides tumor cells with survival resistance against toxic reagents [32], we next determined staurosporine-induced apoptosis by a caspase-3/7 activity assay and observed that pre-treatment of NT193 cells with TNC for 24 h reduces apoptosis. The TNC effect was similar to that of TGF-β and was reverted by GW, suggesting that a TNC-induced EMT protects against apoptosis where TGF-β signaling is important (Fig. 6G, Fig. S6D).

Next we investigated how TNC activates the TGF-β signaling pathway. Since TNC was shown to bind TGF-β [33], we investigated by ELISA whether our TNC preparations potentially contained TGF-β. Yet no TGF-β was found (Fig. 6H). We further determined whether cells potentially secrete more TGF-β upon treatment with TNC. Therefore, we added TNC to TNC-devoid NT193 sh2TNC cells (Fig. S2A) and, compared TGF-β secretion to cells that have been treated with TGF-β. Indeed, cells express more TGF-β upon treatment with TNC similar to levels detected in cells that were treated with TGF-β itself. This was not the case for the recombinant TNC domain molecule TNC-FGB (fibrinogen globe) and, TNC-FnIII3−5 (fibronectin type III repeat 3−5) that was described to bind TGF-β [33], despite 10-fold higher molarity than TNC (Fig. 6H).

Investigating the kinetics of canonical (Smad) and non-canonical (Akt, Erk1/2) TGF-β signaling [34], revealed rapid signaling activation by TNC which paralleled that of TGF-β itself and may contribute to enhanced survival by TNC. Phosphorylated Smad2 peaked around 2 h and was increased at 24 h comparable to the kinetics of p-Akt and p-Erk1/2. Levels of E-cadherin and vimentin started to drop and rise, respectively, upon addition of TNC similar to the treatment with TGF-β (Fig. S6E, F).

In conclusion, our results have shown that in NT193 cells TNC activates canonical and non-canonical TGF-β signaling with a similar kinetic as TGF-β itself, leading to increased abundance of TGF-β in the cell supernatant. How TNC increases TGF-β levels and induces TGF-β signaling remains to be determined. Importantly, our study revealed an instrumental role of TNC in inducing EMT in our cellular system and, in the pulmonary BVI.

As TGF-β signaling promoted metastasis in a MMTV-Neu model [17] induction of TGF-β signaling could explain cellular plasticity and progression of BVI into parenchymal metastasis, thus elevating total metastasis burden in MMTV-NeuNT mice. A similar mechanism as recently demonstrated for fibronectin fibrils to activate TGF-β signaling should be investigated for TNC in the future [35].

Tenascin-C is expressed in BVI from human carcinomas yet not in LVI

Vascular invasions in the primary tumor comprise an important prognostic tool and can occur in blood and lymphatic vessels [36,37]. To address whether BVI and LVI of human carcinomas express TNC, we investigated tissue from several human carcinomas with and without recorded presence of vessel invasions by sequential staining for TNC, CD31, podoplanin and platelet marker CD61 (Table S1, S3, S4). We observed BVI (tumor cell clusters inside CD31+ vessels) and LVI (tumor cell clusters inside D2−40+ vessels). In particular, we saw BVI in a total of 23 tumors comprising renal cell carcinoma (RCC), hepatocellular carcinoma (HCC) and pancreatic neuroendocrine tumors (PNET)) and, LVI in a total of 47 cases comprising pancreatic adenocarcinomas (PDAC (7 cases)) and mammary carcinomas (MaCa (40 cases)) (Fig. 7A-C, S7, Fig. S8, Table S1). Although we do not have evidence for a simultaneous existence of BVI and LVI in the same tumor this possibility cannot be ruled out. As in the MMTV-NeuNT model, we noted that BVI are surrounded by a luminal endothelial monolayer and a TNC layer. When BVI were bigger, TNC and endothelial cells were also detected inside the BVI (Fig. 7A, C, S7A, B and C). By contrast, LVI were neither covered by an endothelial cell layer nor did they express TNC (Fig. S8A, B, Table S1). Interestingly, tumor cell aggregates were present in

Fig. 6. In cultured NT193 cells TNC induces EMT promoting cell migration and survival **(A)** Phase contrast micrographs and IF images of E-cadherin (red) and vimentin (green) stained NT193 cells treated with TGF-βR1 inhibitor (GW788388) prior to addition of TNC and TGF-β for 24 h, respectively. Nuclei stained by DAPI. Scale bar, 20 μm. **(B)** Relative expression (fold change) of the indicated genes in NT193 cells upon treatment with GW788388 and TNC for 24 h ($n = 5$, five independent experiments) with normalization to GAPDH. **(C)** Detection of E-cadherin, vimentin, phosphorylated pathway markers (Smad2, Akt, and Erk1/2), respectively and expression of total markers (Smad2/3, Akt, Erk1/2) by immunoblotting with GAPDH as loading control (a representative of three independent experiments is shown). **(D)** Detection of E-cadherin and vimentin expression by immunoblotting of lysates from NT193 cells upon addition of platelets for 24 h ($n = 3$, three independent experiments). **(E, F)** Wound closure of NT193 cells, $n = 14$, five independent experiments with at least two replicates. Scale bar, 20 μm. **(G)** Assessment of staurosporine (STS) - induced apoptosis by measuring caspase-3/7 activity in NT193 cells treated as indicated, $n = 9$, three independent experiments in triplicates. **(H)** Quantification of TGF-β released by NT193 cells upon treatment with TNC, TNC-FBG and TNC-FnIII3−5 by ELISA. Note that purified TNC and recombinant TNC domain molecules are free of TGF-β. **B, F, G, H,** Mean ± SEM, unpaired Student *t*-test. Statistical analysis was performed between all groups. Only statistically significant ($p < 0.05$) differences are marked.

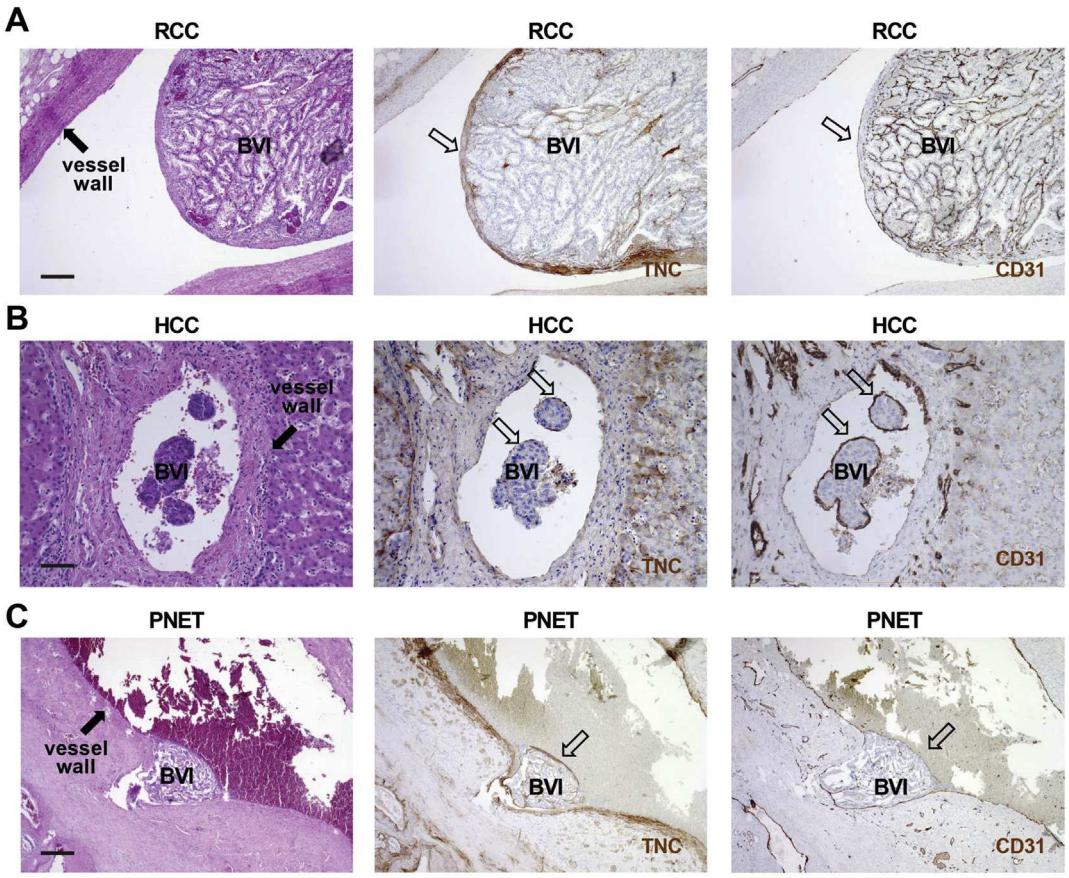

Fig. 7. BVI of human cancers are surrounded by endothelial cells and TNC Consecutive tissue sections from human RCC, HCC and PNET were stained for H&E, CD31 and TNC. Representative images are shown. Note, that BVI are surrounded by a luminal endothelial monolayer and express TNC beneath the endothelial layer (open arrows). Note, that tumor cell clusters were found to protrude into the lumen of blood vessels (filled arrows), in particular the renal veins (RCC), the portal vein and branches of the portal vein (HCC) and the stem or branches of the superior mesenteric vein (PNET). In PNET a thrombotic reaction is observed at the luminal surface of the endothelium covering the BVI (arrow). Scale bar, 50 μm.

lymphatic vessels (LVI) in MaCa independently of the subtype and appeared mostly as smaller floating cell clusters (Fig. S8B, Table S1). Upon an unbiased search in MaCa and the corresponding lung metastases we observed only LVI.

To our knowledge, these results demonstrate for the first time differences in cellular content and matrix composition between BVI and LVI. As in the murine metastatic models, in human cancers, BVI are enclosed by an endothelial monolayer and, express TNC.

Discussion

It is well established that the ECM plays an important role in tissue homeostasis enhancing pathologies including tumor malignancy and metastasis [7,38,39]. Moreover, the ECM molecule TNC which is abundantly expressed in cancer tissue enhances metastasis [9–11,40], yet by incompletely understood mechanisms. To address the roles of TNC in metastasis, we have compared NeuNT (ErbB2)-driven lung metastasis in a genetic and a novel syngeneic orthotopic breast cancer model derived thereof with high TNC to that with no or low TNC, respectively. Of note ErbB2-driven models may not well recapitulate human breast cancer metastasis where LVI are frequent, but better phenocopy cancer progression of other tumors that develop BVI in blood vessels of the lung [16,17]. Our results reveal the cellular and molecular characteristics of BVI, offering future targeting opportunities. We further elucidate multiple novel functions of host-derived TNC in progression from pulmonary BVI into parenchymal metastasis that were unknown so far.

We report that pulmonary BVI are organized as clusters of proliferating epithelial tumor cells with tight junctions. Tumor cell cohesion may contribute to synoikis, a recently identified survival mechanism with relevance for targeting [2,41]. Tumor cell nests are enveloped by a luminal endothelial cell

monolayer and Fsp1+ cells, also a likely source of TNC in this model [21]. FN and LM are expressed between the two stromal cell layers (Fig. 4). Thus targeting tumor cell cohesions in BVI, endothelial cells or TNC expression itself (e.g. by Fsp1+ cells) could represent novel strategies. This could complement already identified inhibition of ErbB2 (MMTV-NeuNT) [20] and TGF-β signaling (MMTV-Neu NDL) [17] in reducing metastasis in these models.

It is interesting to note that in the MMTV-NeuNT model TNC induces a partial EMT where TGFβ signaling may play a decisive role as we observed that TNC induces EMT in cultured tumor cells in a TGFβ dependent manner. That only some tumor cells within the BVI as well as at the rim and site of extravasation, that are not necessarily in direct contact with TNC, have gained expression of the EMT marker vimentin, is intriguing to note and suggests a paracrine effect through which TNC impacts EMT in the BVI. In vitro, TNC-induced EMT enhances migration and survival of tumor cells which may also apply in the BVI. As TGFβ signaling plays a role in promoting cancer stemness properties and survival in another model [42], future research has to clarify whether TNC also impacts cancer stemness through TGFβ signaling in this model.

Due to lack of appropriate models, until now it was difficult to assign the cellular source of TNC with a function. Grafting human tumor cells with engineered TNC levels in the tail vein of immune compromised mice previously showed that tumor cell-derived TNC is relevant in early stages of lung colonization [9] but how host TNC affects spontaneous metastasis in immune competent conditions was unknown. Now, by using our novel orthotopic immune competent transplantation model with engineered TNC levels and spontaneous metastasis and, kinetics that generate a relevant TME, we showed for the first time that host-derived TNC plays a crucial role in metastasis, before tumor cell breaching. This could be relevant for future targeting as it may not suffice to kill tumor cells, but also to target stromal cells expressing TNC.

Several concepts for the formation of BVI and their endothelialization exist, as e.g. transdifferentiation of tumor cells into endothelial cells [36], budding of tumor cells from the primary tumor [43], recruitment of bone marrow-derived endothelial progenitor cells (EPC) [44] and, endothelialization [3], where endothelial cells and TNC are active participants. In a model proposed by Sugino et al., (2002) clusters of cancer cells in the primary tumor enter the circulation through an invasion-independent pathway, form local BVI and eventually migrate until they reach the site of metastasis [43]. Notably, the size of some of the BVI in this study suggests that, if circulating BVIs existed in their model, they would be present in large vessels. Another model suggests that single cells or clusters of circulating tumor cells (CTC), with or without an ECM coating and stromal cells, proliferate in the lung vasculature forming BVI at the metastatic site. Several observations support this model. Clusters of around 50 CTC were identified in tumor-bearing mice and, represent a higher metastatic potential than single CTC [45]. Moreover, a few hours after tail vein inoculation, cancer cells found in the lumen of lung vessels were already coated with ECM and platelets. These authors suggest that BVI formation occurs when cancer cells reach pulmonary arterioles but not capillaries [3]. Here, we show that stromal cells, probably platelets or Fsp1+ cells, are a source of TNC in pulmonary BVI. The prominent location of platelets deep inside the BVI (our observation) argues for an early role of platelets in BVI formation, apparently immediately after intravasation [25]. Finally, stromal cells on pulmonary BVI can migrate from the primary tumor as proposed in another model [46].

We consider the trans-differentiation of tumor cells into endothelial cells [28] as unlikely, since endothelial cells form a contiguous monolayer and are not found inside the BVI core. Also, budding from the tumor vasculature [27] may not occur as we do not see a monolayer of αSMA+ cells underneath the endothelial layer in the BVI. Upon release into the circulation by budding, only tumor cells at the periphery of the tumor cell cluster would get in contact with platelets and therefore platelets should be placed at the rim of the BVI. Yet, this is not the case, as we see platelets inside the BVI beneath the endothelial layer. On the contrary, we consider endothelialization, where endothelial cells from the vasculature wrap around circulating tumor cells [3], a likely scenario, as we observed a mostly contiguous monolayer of endothelial cells around the BVI, in the murine model and in human cancers, occuring in the primary tumor as well as in the metastastic lung.

As in the MMTV-NeuNT model also in MMTV-NeuYD mice endothelialization of BVI is frequent, yet only when VEGFA is coexpressed (MMTV-NeuYD/VEGFA) [47]. Also, VEGFA was involved in TNC-promoted lung metastasis in the 4 T1 grafting model establishing a crosstalk of TNC with endothelial cells in metastasis [21]. As VEGFA can bind to TNC, a potential combined impact on endothelial cells is likely [11]. We showed that BVI endothelial layer integrity, tumor cell survival and overall metastasis were correlated and, promoted by TNC. Thus, it is conceivable that impacting BVI endothelialization is an important mechanism how TNC promotes metastasis. Given its role in promoting the angiogenic switch and tumor angiogenesis [11,26,27,48] future research has to determine how TNC impacts BVI endothelial cell function and endothelialization. This may involve an autocrine mechanism as previously described, where TNC

induced Wnt signaling, VEGFA and a pericellular fibronectin layer in endothelial cells [11,27]. Also a paracrine mechanism may apply where TNC induces pro-angiogenic factors in tumor cells, fibroblasts or Fsp1+ cells as previously described in other tumors [21,26]. In this scenario, TNC-induced TGFβ signaling could play a role in promoting survival of endothelial cells of the BVI.

Lympho-vascular invasions are frequently observed in routine analysis of many cancers, but incidence and relevance depends on the tumor type and subtype [49–52]. By using blood- and lymph-vessel markers recent analysis allowed to discriminate between LVI and BVI. Whereas LVI appeared smaller in size and in smaller vessels, many BVI were huge and present in bigger vessels (our results). Maybe physical properties such as local high shear stress in bigger vessels impact the size of BVI which has to be addressed in the future. So far there are only a dozen of retrospective studies that analyzed the impact of BVI versus LVI in cancer. BVI can be found inside and in the periphery of primary breast tumors, but apparently in breast cancer BVI are less frequent than LVI [5,49,53–55].

A few studies analyzed the relevance of tumor BVI versus LVI as a prognosis factor in breast cancer, but the results are controversial [5,53–55]. Disseminated lympho-vascular invasions are almost impossible to identify ante mortem [56]. Here our models could be highly relevant as both, the MMTV-NeuNT and the autochthonous grafting model that we had developed, present intra- and peritumoral BVI and, more importantly, disseminated BVI in the lung. Clinical trials of anti-angiogenic drugs failed to improve recurrence-free survival of breast cancer patients and lost approval by the FDA [57–59]. However, the presence of BVI/LVI was not considered as an inclusion factor. We believe that anti-angiogenic drugs can impair disseminated BVI, decrease metastasis and increase survival of breast cancer patients with BVI. Since BVI are frequent in many tumors and have an endothelial lining they may respond to anti-angiogeneic drugs, which has to be addressed in the future. Indeed impacting the endothelial layer of BVI may reduce metastasis, as our results from the TNCKO mice suggest, where we observed an interrupted or missing endothelial BVI monolayer and, reduced overall metastasis in the absence of TNC. Anti-angiogenic drug treatment is already applied in patients with RCC, HCC and PNET [60] thus, likely affecting BVI. Hence, TNC expression and endothelial ensheathing of BVI in tumor biopsies could be used to stratify patients that may benefit from an anti-angiogenic drug treatment targeting the BVI endothelial coat. In contrast to BVI, we have found that LVI (here observed in MaCa and PDAC) do not exhibit an endothelial layer nor TNC expression thus likely not responding well to anti-angiogenic treatment.

In summary, our study has described the composition of metastatic vascular invasions in blood vessels, BVI, and has revealed that they are different from lymphatic vessel invasions, LVI. By using a murine metastasis model with abundant or no TNC expression, we have identified host-derived TNC as an important component of BVI and that TNC increases endothelial layering and tumor cell survival, cellular plasticity and extravasation, involving TGF-β signaling. This information may present novel prognostic and therapeutic opportunities. Finally, as relevant immune competent transplantation models are scarce, our novel autochthonous model of cancer progression providing the opportunity to engineer the host as well as the tumor cells, recapitulating the TME and metastatic traits of the stochastic genetic model could be relevant for future mechanistic research and metastasis targeting.

Material and methods

Human cancer tissue

Human cancer tissue (mammary carcinoma (MaCa), MaCa lung metastasis, renal cell carcinoma (RCC), hepatocellular carcinoma (HCC), pancreatic neuroendocrine tumor (PNET)) from two sites, the Medical University of Vienna/General Hospital Vienna/Medical University Wien (MUW) and the Hôpital Universitaire de Strasbourg Hautepierre (HUS) was analyzed. In the MUW cohort 30 cases of histologically proven invasive MaCa with metastasis to the lung were investigated. In the HUS cohort, 35 breast cancer specimen were collected (November 2013 – October 2014) and selected according to clinical annotation of present vascular invasions. Patients underwent surgical treatment at the MUW, Department of Obstetrics and Gynecology and at the Department of Surgery/Division of Thoracic Surgery (MUW cohort), at the HUS for the pancreatic and hepatic tumors, and the Nouvel Hôpital Civil for the renal tumors (HUS cohort). In the MUW cohort, in 12 cases enough material was available to perform all IHC stainings (Table S3). Serial sections of 2 μm were prepared and stained with antibodies specific for TNC, Factor VIII, CD31, CD34 and podoplanin by using an automated stainer (BenchMark Ultra, Roche/Ventana). Immunohistochemical staining was carried out in accordance with the manufacturer's instructions (Ventana Medical Systems). Immunohistochemical staining for platelets (CD61) was performed using the LEICA BOND III automated Immunostainer. In the HUS cohort, 35 patients with mammary carcinoma including 29 ductal invasive carcinomas and 5 lobular invasive carcinomas were

included (Table S4). In addition, tumor tissue from 7 PDAC, 9 RCC, 9 HCC and 5 PNET was selected according to clinical annotations of present vascular invasions (HUS cohort) (Table S4). Four μm thick paraffin sections were analyzed upon staining with HE or incubation with antibodies against TNC, CD31, and podoplanin (D2−40) by using an automated stainer (BenchMark Ultra, Roche/Ventana). Immunohistochemical staining was carried out in accordance with the manufacturer's instructions (Ventana Medical Systems). Analysis of staining results was performed by two pathologists independently (FO/RK, MUW cohort of breast cancer; AO/RK MUW cohort of RCC; GA/MPC, HUS cohort of breast cancer; GA/ZS, HUS cohort of RCC, HCC, PNET) in each center. Details can be found in Table S2, S3 and S4 and results are summarized in Table S1. Ethical approval for the procedures described has been granted.

Mice

MMTV-NeuNT female mice (FVB/NCrl background) with a mutated constitutively active form of rat ErbB2 (NeuNT), expressed under control of the mouse mammary tumor virus (MMTV) regulatory region [37], were provided by Gerhard Christofori (University of Basel, Switzerland). Mice expressing NeuNT develop multifocal breast adenocarcinoma and lung metastasis; TNC +/− mice in the 129/Sv genetic background were generously donated by Reinhard Fässler [38]. Ten consecutive crosses with FVB/NCrl mice (Charles River) were done to homogenize the background. TNC +/− males were crossed with TNC +/− females to obtain TNC+/+ (WT) and TNC−/− (KO) littermates; MMTV-NeuNT mice (FVB/NCrl background) were crossed with TNC+/− mice to generate double-transgenic mice to obtain MMTV-NeuNT mice with a TNC+/+ and TNC−/− genotype. All mice were housed and handled according to the guidelines of INSERM and the ethical committee of Alsace, France (CREMEAS) (Directive 2010/63/EU on the protection of animals used for scientific purposes).

Animal experiments

Tumor size was measured every 3 or 7 days with a caliper, and tumor volume was calculated using the formula $V = (a^2{*}b)/2$, where b is the longest axis and a is the perpendicular axis to b. For the syngeneic mouse model, 10×10^6 NT193 cells were diluted in 50 μl PBS and injected orthotopically into the left fourth mammary gland. Mice were euthanized at indicated time points and mammary gland tumors and lungs were processed for histological analysis and western blot. Tissue was snap frozen in liquid nitrogen or embedded in O.C.T. (Sakura Finetek) as well as in paraffin for tissue staining.

Tissue analysis

The stereological analysis of the lung metastasis (index and number) was done as published [19]. Briefly, the left lung lobe was cut transversally into 2.0 mm thick parallel pieces, giving rise to a total of five to six pieces before paraffin embedding in parallel orientation, and cutting into 7 μm thick sections. In cases where no metastasis was found, 8 to 10 additional sections separated by 200 μm were analyzed.

HE staining

Tissue from breast tumors and lungs were prepared and fixed overnight in 4% PFA, dehydrated in 100% ethanol for 24 h, embedded in paraffin, cut in 7 μm thick sections, dewaxed and rehydrated with 100% Toluene (2 washes of 15 min) then incubated in 100%−70% alcohol solutions (10 min each) followed by a final staining with hematoxylin (Surgipath) for 5 min and washing with tap water or followed by IHC. Sections were further processed with differentiation solution (1% HCl in absolute ethanol, for 7 s), followed by washing under tap water for 10 min. Sections were then incubated in eosin (Harris) for 10 s, rinsed and dehydrated in 70% - 100% alcohol baths with rapid dips in each bath before a final wash in toluene for 15 min and embedded in Eukitt solution (Sigma).

Giemsa staining

Tissue was cut in 7 μm thick sections, dewaxed and stained with Giemsa (320310−0125, RAL) for 2 h at 37 °C, further processed in a 0.5% aqueous acetic acid solution, dehydrated and embedded with Eukitt solution.

Immunohistochemistry

Paraffin embedded tissue was rehydrated and the antigens were unmasked by boiling in 10 mM pH 6 citrate solution for 20 min. Cooled slides were washed and incubated in a peroxide solution (0.6% H2O2, 0.1% triton X-100 in PBS) to eliminate endogenous peroxidase activity. Non-specific binding sites were blocked with a blocking solution (5% normal goat serum in PBS) for 1 h at room temperature (RT) and then avidin/biotin receptors were blocked by using the avidin/biotin blocking kit as recommended by the manufacturer (Vector). Slides were incubated with the first antibody overnight at 4 °C in a humidified container. Next day, slides were washed and incubated for 45 min at room temperature with a secondary antibody (coupled to biotin). The detection of peroxidase was done using the Elite ABC system (VECTASTAIN) with DAB (Vector) as substrate. Finally, tissue

was stained with hematoxylin, dehydrated and embedded in Eukitt solution. Proliferation and apoptosis were quantified as events per area upon staining for Ki-67 and cleaved caspase-3, respectively.

Immunofluorescence staining

Tissue was air-dried and unspecific signals were reduced with blocking solution (5% normal goat or donkey serum in PBS) for 1 h at RT. Tissue sections were incubated with the primary antibody overnight at 4 °C in a humidified container. The following day the primary antibody was removed and tissue was incubated with a fluorescent secondary antibody for 1 h at RT. Slides were washed and incubated with DAPI (Sigma) to visualize the nuclei (10 min at RT). Excess of dye was removed and tissue was embedded with FluorSaveTM Reagent (Calbiochem). Fluorescent signal was analyzed with a Zeiss Axio Imager Z2 microscope. The staining procedure (fixation, blocking, antibody dilution) and image acquisition setting (microscope, magnification, light intensity, exposure time) were kept constant per experiment and genetic conditions. Quantification of immunofluorescent microscopic images was done by the ImageJ (National Institutes of Health) software using a constant threshold. The expression of TNC was scored according to the signal extent and intensity of the mosaic picture of the whole tumor. A typical fibrillar TNC staining with the MTn12 antibody in the stroma around the tumor cells was considered as positive signal (no signal was seen with the secondary antibody alone). The extent of TNC staining was scored by the percentage of the positively stained area. The stained area in each region of interest was scored as 0 for staining <5%, as 1 for 5–25%, 2 for 25–50%, 3 for 50–75%, and 4 for >75% of the stained area. The intensity of staining was scored as 0, 1, 2 and 3 representing no staining, mild (weak but detectable above control), moderate (distinct) and intense (strong) staining, respectively. The percentage of positively stained area and intensity of staining were multiplied to produce a weighted score [61].

qPCR analysis

Total RNA was prepared using TriReagent (Life Technologies) according to the manufacturer's instructions. RNA was reverse transribed (MultiScribe reverse transcriptase, Applied Biosystems) and qPCR was done on cDNA (diluted 1:5 in water) using a 7500 Real Time PCR machine (Applied Biosystems) with a SYBR green reaction mixture or Taqman reaction mixture (Applied Biosystems). Data were normalized by using a Taqman mouse *Gapdh* Endogenous Control (4333764T, Life Technology) and fold induction was calculated using the comparative Ct method (-ddCt). Primers used for qPCR are listed in Table S3.

Immunoblotting

Cell lysates were prepared in lysis buffer (25 mM Tris-HCl pH 7.6, 150 mM NaCl,1% NP-40, 1% sodium deoxycholate, 0.1% SDS) supplemented with protease inhibitor (Roche) and Phosphatase Inhibitor Cocktail (Santa Cruz). Protein concentration was determined with a Bradford Assay (BioRad). After addition of Laemmli buffer (Biorad), 20–30 μg protein lysate was separated by SDS-PAGE in precasted 4–20% gradient gels (Biorad), transferred onto nitrocellulose membranes (Biorad) using TransBlot Turbo™ Transfer System (Biorad), blocked with 5% Blocking-Grade blocker (Biorad) in 0.1% Tween 20-PBS and incubated with the primary (overnight at 4 °C) and secondary antibodies (1 h at RT) in 1.5% Blocking-Grade Blocker in 0.1%Tween 20-PBS. Protein bands were detected with the Amersham ECL Western Blotting detection reagent (GE Healthcare) or SuperSignal™ West Femto Maximum Sensitivity Substrate (ThermoFisher).

Immunofluorescence staining of cells

Cells were fixed in 4% PFA for 10 min, permeabilized in PBS-Triton 0.1% for 10 min, incubated with the primary antibody overnight at 4 °C, secondary antibody for 1 h at RT, DAPI, embedded with FluorSaveTM Reagent (Calbiochem) and analyzed with an Zeiss Axio Imager Z2 microscope.

Antibodies

The primary antibodies are shown in Table S4. Secondary antibodies were ECL horseradish peroxidase-linked (1/1000): anti-rat (NA935) and anti-rabbit (NA934V) (GE Healthcare). Secondary goat or donkey antibodies were fluorescently labeled (1/1000): anti-mouse, anti-rabbit, anti-rat, anti-guinea pig and anti-goat IgG (Jackson Laboratory).

Cell culture

NT193 cells derived from a MMTV-NeuNT primary tumor [20] were cultured in DMEM medium with 4.5 g/L glucose (GIBCO) supplemented with 10% of inactivated fetal bovine serum, penicillin (10,000 U/ml) and streptomycin (10 mg/ml). Cells were maintained at 37 °C in a humidified atmosphere of 5% CO_2.

Treatment with TGF-β and GW788388

Cells were starved in the absence of serum overnight before treatment with human recombinant TGF-β1 (100–21, PEPROTECH), recombinant TNC (purified as described [62]) or the TGF-β type I receptor inhibitor GW 788388 (Selleckchem). Cells were pretreated with the inhibitor for 45 min prior to incubation with TNC, TGF-β and platelets,

respectively. All reagents were diluted following the manufacturer's instructions.

Transduction of cells

Silencing of *Tnc* in mouse cells was done by short hairpin (sh) mediated gene expression knock down (KD). Lentiviral particles with shRNA vectors (Sigma-Aldrich) specific for *Tnc* were used. sh1, TRCN0000312137, sequence 5′-CCGGCCCG GAACTGAATATGGGATTCTCGAGAATCCCA-TATTCAGTTCCGGGTTTTTG-3′; sh2, TRCN0000312138, 5′-CCGGGCATCAACACAAC-CAGTCTAACTCGAGTTAGACTGG TTGTGTTGATGCTTTTTG-3′. Lentiviral particles encoding a non-targeting shRNA vector were used as a control (SHC202V, Sigma-Aldrich). Transduced cells were selected with normal medium supplemented with 10 μg/ml puromycin (ThermoFisher) and the selection pressure was maintained in all in vitro experiments.

Spheroid assay

NT193 cells were seeded at 5000 cells per 100 μl together with TNC (10 μg/ml) or PBS-Tween-20 (0.01%) in 96 well plates with round bottom pre-coated with 10 μg/ml of poly-HEMA (Sigma) for 24 h to allow spheroid formation and then were embedded in OCT for further immunostaining analysis.

Wound healing assay

NT193 cells (2×10^5) were grown to confluency in 24-well plates for 24 h. Confluent cell monolayers were treated 2 h with mitomycin-C (Sigma) at 2 μg/ml to inhibit proliferation before application of a scratch wound with a pipet tip. Cell debris was removed by PBS washing before addition of serum-free medium supplemented with the indicated molecules. Images of the wounding area were acquired immediately after scratching and then in the same field after 24 h. The relative wound closure was quantified by measuring the surface of the cell-free area at the time of injury and at the end point of the experiment.

Cell death assessment with caspase 3/7 activity assay

Caspase 3/7 activity assay (Promega) was performed according to the manufacturer's instructions. Briefly, 2000 cells/well were plated overnight in 96-well plates. Cells were treated as described for the indicated time period and then cell apoptosis was induced by staurosporine (1 μg/ml, Sigma) for 24 h. To measure caspase 3/7 activity, 75 μl of caspase Glo 3/7 reagent was added to each well for 1 h with constant shaking at RT. Luminescence was measured using a TriStar^2 LB942 multidetection microplate reader.

Preparation of washed platelets

Blood was drawn from the abdominal aorta of adult FVB/NCrl mice anesthetized intraperitoneally with a mixture of xylazine (20 mg/kg, Rompun, Bayer) and ketamine (100 mg/kg, Imalgene 1000, Merial). Platelets were washed using ACD-anticoagulated whole blood as previously described [63].

Enzyme-linked immunosorbent assay (ELISA)

Subconfluent NT193 sh2TNC cells (5×10^5) were grown on plastic (6 wells plates) for 24 h in full medium (10%FCS), serum starved (no serum) overnight, and incubated for 24 h in serum-free DMEM containing 0.01% Tween-20 (CTRL), TGF-β (10 ng/ml), TNC (10 μg/ml, 35 nM (MW 280 kDa)), TNC-FBG (10 μg/ml, 383 nM (MW 26.1 kDa)) and TNC-FnIII3−5 (10 μg/ml, 327 nM (MW 30.6 kDa)), respectively. All proteins were synthetized and purified as described [64]. Cells were separated from the conditioned medium by centrifugation and, secreted TGF-β was determined using ELISA (RnD Systems DY1679) following the manufacturer's recommendations.

Statistical analysis

The GraphPad Prism software (version 6) was used for graphical representations of data and statistical analyses to assess significance of observed differences. All parametric (unpaired Student *t*-test with Welch's correction in case of unequal variance) and non-parametric tests (Mann-Whitney) were performed in a two-tailed fashion. To compare the proportion of BVI and parenchymal metastases, Fisher's exact test or Chi-square test was used. Mean ± SEM. p values <0.05 were considered as statistically significant ($^*p < 0.05$; $^{**}p < 0.01$; $^{***}p < 0.001$; $^{****}p < 0.0001$).

Declaration of Competing Interest

The authors declare no competing financial interests.

Acknowledgement

We are grateful for technical support by Christiane Arnold, Fanny Steinbach, Anna Brown and the personnel of the animal facility. This work was supported by grants from Worldwide Cancer

Research/AICR (14-1070), INCa (TENPLAMET), Ligue Régional contre le Cancer CCIR Grand Est, INSERM and University Strasbourg to GO, INCa (TENPLAMET) to PM, National Natural Science Foundation of China (Grant No. 81802655) to ZS and fellowship grants from the Chinese Scholarship Council (ZS) and the Mexican scholarship program CONACYT (IVQ). KSM is supported by Arthritis Research UK.

Author contribution

ZS, IVQ and TH developed the genetic and orthotopic grafting model. ZS, IVQ, DM, AY, TH, CA, CD, WE and CS performed experiments, analyzed and interpreted the data. OL, AK, AB, MvdH and CB provided technical assistance. GA, FO, AO, MPC, CM and RK provided, analyzed and interpreted data from human cancer patients. PM supervised the platelet study. GC provided the MMTV-NeuNT mice. GC, TL, CAF and KM critically reviewed the manuscript and interpreted data. ZS, IVQ and GO conceptualized and wrote the manuscript. Grants to GO financed this study.

Appendix A. Supplementary data

Supplementary data to this article can be found online at https://doi.org/10.1016/j.matbio.2019.07.001.

Received 27 March 2019;
Received in revised form 30 May 2019;
Accepted 2 July 2019
Available online 6 July 2019

Keywords:
Blood vessel invasions;
Circulating tumor cells;
Tumor emboli;
Tenascin-C;
Cellular plasticity;
TGF-β signaling;
Lung metastasis;
Endothelialization;
Fsp1+ cells;
Endothelial cells

Current address: 1. Tongji Cancer Research Institute, Tongji Hospital, Tongji Medical College in Huazhong University of Science and Technology, Wuhan, Hubei, China. 2. Department of Gastrointestinal Surgery, Tongji Hospital, Tongji Medical College in Huazhong University of Science and Technology, Wuhan, Hubei, China.

2 Equal contribution.

Abbreviations used:
BVI, blood vessel invasions; CD31, cluster of differentiation 31; CD41, cluster of differentiation 41, integrin alpha chain 2b; Cl. Cas-3, cleaved caspase-3; CK8/18, cytokeratin 8/18; DAPI, 4′,6-diamidino-2-phenylindole; DMEM, Dulbecco's Modified Eagle's Medium; ELISA, Enzyme-linked immunosorbent assay; EPC, endothelial progenitor cells; EMT, epithelial-to-mesenchymal transition; ERK, extracellular signal-regulated kinases; ECM, extracellular matrix; FN, fibronectin; Fsp1, fibroblast-specific protein 1; GAPDH, Glyceraldehyde 3-phosphate dehydrogenase; GW788388, 4-(4-[3-(Pyridin-2-yl)-1H-pyrazol-4-yl]pyridin-2-yl)-*N*-(tetrahydro-2Hpyran-4-yl) benzamide; HCC, hepatocellular carcinoma; HE, Hematoxylin and eosin; IDC NST, invasive ductal carcinoma, no special type; KD, knock down; KO, knock out; LM, laminin; LVI, lymph vessel invasions; MaCa, mammary carcinomas; Mmp9, Matrix metallopeptidase 9; MMTV-NeuNT, mouse mammary tumor virus driven NeuNT (activated rat ErbB2 homologue) transformed; NOS, not otherwise specified; NT193, MMTV-NeuNT breast tumor derived cell line; Pai-1, plasminogen activator inhibitor-1; PBS, phosphate-buffered saline; PDAC, pancreatic ductal adenocarcinomas; PNET, pancreatic neuroendocrine tumors; PyMT, polyoma middle T antigen; RAM1, reduced Arbuscular Mycorrhization 1; RCC, renal cell carcinoma; Sh, short hairpin; Slug, snail family zinc finger 2; Snail, snail family zinc finger 1; STS, staurosporine; TGF-β, transforming growth factor β; TME, tumor microenvironment; TNBC, triple negative breast cancer; TNC, tenascin-C; VEGFA, vascular endothelial growth factor A; WT, wild type; Zeb1, zinc finger E-box-binding homeobox 1; α-SMA, alpha-smooth muscle actin.

References

[1] J.E. Talmadge, I.J. Fidler, AACR centennial series: the biology of cancer metastasis: historical perspective, Cancer Res. 70 (2010) 5649–5669, https://doi.org/10.1158/0008-5472.CAN-10-1040.

[2] S. Gkountela, F. Castro-Giner, B.M. Szczerba, M. Vetter, J. Landin, R. Scherrer, I. Krol, M.C. Scheidmann, C. Beisel, C.U. Stirnimann, C. Kurzeder, V. Heinzelmann-Schwarz, C. Rochlitz, W.P. Weber, N. Aceto, Circulating tumor cell clustering shapes dna methylation to enable metastasis seeding, Cell. 176 (2019) 98–112.e14. doi:https://doi.org/10.1016/j.cell.2018.11.046.

[3] K. Lapis, S. Paku, L.A. Liotta, Endothelialization of embolized tumor cells during metastasis formation, Clin. Exp. Metastasis. 6 (1988) 73–89.

[4] E.A. Rakha, S. Martin, A.H.S. Lee, D. Morgan, P.D.P. Pharoah, Z. Hodi, D. MacMillan, I.O. Ellis, The prognostic significance of lymphovascular invasion in invasive breast carcinoma, Cancer. 118 (2012) 3670–3680, https://doi.org/10.1002/cncr.26711.

[5] T. Fujii, R. Yajima, T. Hirakata, T. Miyamoto, T. Fujisawa, S. Tsutsumi, Y. Ynagita, M. Iijima, H. Kuwano, Impact of the prognostic value of vascular invasion, but not lymphatic

invasion, of the primary tumor in patients with breast cancer, Anticancer Res. 34 (2014) 1255–1259.
[6] I. Soerjomataram, M.W.J. Louwman, J.G. Ribot, J.A. Roukema, J.W.W. Coebergh, An overview of prognostic factors for long-term survivors of breast cancer, Breast Cancer Res. Treat. 107 (2008) 309–330, https://doi.org/10.1007/s10549-007-9556-1.
[7] M.J. Bissell, W.C. Hines, Why don't we get more cancer? A proposed role of the microenvironment in restraining cancer progression, Nat. Med. 17 (2011) 320–329, https://doi.org/10.1038/nm.2328.
[8] A.J. Minn, G.P. Gupta, P.M. Siegel, P.D. Bos, W. Shu, D.D. Giri, A. Viale, A.B. Olshen, W.L. Gerald, J. Massagué, Genes that mediate breast cancer metastasis to lung, Nature. 436 (2005) 518–524, https://doi.org/10.1038/nature03799.
[9] T. Oskarsson, S. Acharyya, X.H.-F. Zhang, S. Vanharanta, S.F. Tavazoie, P.G. Morris, R.J. Downey, K. Manova-Todorova, E. Brogi, J. Massagué, Breast cancer cells produce tenascin C as a metastatic niche component to colonize the lungs, Nat. Med. 17 (2011) 867–874, https://doi.org/10.1038/nm.2379.
[10] K.S. Midwood, M. Chiquet, R.P. Tucker, G. Orend, Tenascin-C at a glance, J. Cell Sci. 129 (2016) 4321–4327, https://doi.org/10.1242/jcs.190546.
[11] F. Saupe, A. Schwenzer, Y. Jia, I. Gasser, C. Spenlé, B. Langlois, M. Kammerer, O. Lefebvre, R. Hlushchuk, T. Rupp, M. Marko, M. van der Heyden, G. Cremel, C. Arnold, A. Klein, P. Simon-Assmann, V. Djonov, A. Neuville-Méchine, I. Esposito, J. Slotta-Huspenina, K.-P. Janssen, O. de Wever, G. Christofori, T. Hussenet, G. Orend, Tenascin-C downregulates Wnt inhibitor Dickkopf-1, promoting tumorigenesis in a neuroendocrine tumor model, Cell Reports. 5 (2013) 482–492. doi:https://doi.org/10.1016/j.celrep.2013.09.014.
[12] J. Insua-Rodríguez, M. Pein, T. Hongu, J. Meier, A. Descot, C.M. Lowy, E. De Braekeleer, H.-P. Sinn, S. Spaich, M. Sütterlin, A. Schneeweiss, T. Oskarsson, Stress signaling in breast cancer cells induces matrix components that promote chemoresistant metastasis, EMBO Mol Med. 10 (2018). doi: 10.15252/emmm.201809003.
[13] J.F. Talts, G. Wirl, M. Dictor, W.J. Muller, R. Fässler, Tenascin-C modulates tumor stroma and monocyte/macrophage recruitment but not tumor growth or metastasis in a mouse strain with spontaneous mammary cancer, J. Cell Sci. 112 (Pt 12) (1999) 1855–1864.
[14] S.F. Tavazoie, C. Alarcón, T. Oskarsson, D. Padua, Q. Wang, P.D. Bos, W.L. Gerald, J. Massagué, Endogenous human microRNAs that suppress breast cancer metastasis, Nature. 451 (2008) 147–152, https://doi.org/10.1038/nature06487.
[15] L. Bouchard, L. Lamarre, P.J. Tremblay, P. Jolicoeur, Stochastic appearance of mammary tumors in transgenic mice carrying the MMTV/c-neu oncogene, Cell. 57 (1989) 931–936.
[16] W.J. Muller, E. Sinn, P.K. Pattengale, R. Wallace, P. Leder, Single-step induction of mammary adenocarcinoma in transgenic mice bearing the activated c-neu oncogene, Cell. 54 (1988) 105–115.
[17] P.M. Siegel, W. Shu, R.D. Cardiff, W.J. Muller, J. Massagué, Transforming growth factor β signaling impairs Neu-induced mammary tumorigenesis while promoting pulmonary metastasis, Proc. Natl. Acad. Sci. 100 (2003) 8430–8435, https://doi.org/10.1073/pnas.0932636100.
[18] C. Spenlé, I. Gasser, F. Saupe, K.-P. Janssen, C. Arnold, A. Klein, M. van der Heyden, J. Mutterer, A. Neuville-Méchine, M.-P. Chenard, D. Guenot, I. Esposito, J. Slotta-Huspenina, N. Ambartsumian, P. Simon-Assmann, G. Orend, Spatial organization of the tenascin-C microenvironment in experimental and human cancer, Cell Adhes. Migr. 9 (2015) 4–13, https://doi.org/10.1080/19336918.2015.1005452.
[19] B.S. Nielsen, L.R. Lund, I.J. Christensen, M. Johnsen, P.A. Usher, L. Wulf-Andersen, T.L. Frandsen, K. Danø, H.J.G. Gundersen, A precise and efficient stereological method for determining murine lung metastasis volumes, Am. J. Pathol. 158 (2001) 1997–2003, https://doi.org/10.1016/S0002-9440(10)64671-8.
[20] A. Arpel, P. Sawma, C. Spenlé, J. Fritz, L. Meyer, N. Garnier, I. Velázquez-Quesada, T. Hussenet, S. Aci-Sèche, N. Baumlin, M. Genest, D. Brasse, P. Hubert, G. Crémel, G. Orend, P. Laquerrière, D. Bagnard, Transmembrane domain targeting peptide antagonizing ErbB2/Neu inhibits breast tumor growth and metastasis, Cell Rep. 8 (2014) 1714–1721, https://doi.org/10.1016/j.celrep.2014.07.044.
[21] J.T. O'Connell, H. Sugimoto, V.G. Cooke, B.A. MacDonald, A.I. Mehta, V.S. LeBleu, R. Dewar, R.M. Rocha, R.R. Brentani, M.B. Resnick, E.G. Neilson, M. Zeisberg, R. Kalluri, VEGF-A and Tenascin-C produced by S100A4+ stromal cells are important for metastatic colonization, Proc. Natl. Acad. Sci. 108 (2011) 16002–16007, https://doi.org/10.1073/pnas.1109493108.
[22] A. Dongre, R.A. Weinberg, New insights into the mechanisms of epithelial–mesenchymal transition and implications for cancer, Nat. Rev. Mol. Cell Biol. 20 (2019) 69, https://doi.org/10.1038/s41580-018-0080-4.
[23] C.K.S. Meikle, C.A. Kelly, P. Garg, L.M. Wuescher, R.A. Ali, R.G. Worth, Cancer and thrombosis: the platelet perspective, Frontiers in Cell and Developmental Biology. 4 (2017). doi:https://doi.org/10.3389/fcell.2016.00147.
[24] P.H. Mangin, N. Receveur, V. Wurtz, T. David, C. Gachet, F. Lanza, Identification of five novel 14-3-3 isoforms interacting with the GPIb-IX complex in platelets, J. Thromb. Haemost. 7 (2009) 1550–1555, https://doi.org/10.1111/j.1538-7836.2009.03530.x.
[25] M. Labelle, S. Begum, R.O. Hynes, Direct signaling between platelets and cancer cells induces an epithelial-mesenchymal-like transition and promotes metastasis, Cancer Cell 20 (2011) 576–590, https://doi.org/10.1016/j.ccr.2011.09.009.
[26] T. Rupp, B. Langlois, M.M. Koczorowska, A. Radwanska, Z. Sun, T. Hussenet, O. Lefebvre, D. Murdamoothoo, C. Arnold, A. Klein, M.L. Biniossek, V. Hyenne, E. Naudin, I. Velazquez-Quesada, O. Schilling, E. Van Obberghen-Schilling, G. Orend, Tenascin-C orchestrates glioblastoma angiogenesis by modulation of pro- and anti-angiogenic signaling, Cell Rep. 17 (2016) 2607–2619, https://doi.org/10.1016/j.celrep.2016.11.012.
[27] A. Radwanska, D. Grall, S. Schaub, S.B. la F. Divonne, D. Ciais, S. Rekima, T. Rupp, A. Sudaka, G. Orend, E. Van Obberghen-Schilling, Counterbalancing anti-adhesive effects of Tenascin-C through fibronectin expression in endothelial cells, Scientific Reports. 7 (2017). doi:https://doi.org/10.1038/s41598-017-13008-9.
[28] K.J. Cheung, V. Padmanaban, V. Silvestri, K. Schipper, J.D. Cohen, A.N. Fairchild, M.A. Gorin, J.E. Verdone, K.J. Pienta, J.S. Bader, A.J. Ewald, Polyclonal breast cancer metastases arise from collective dissemination of keratin 14-expressing tumor cell clusters, Proc. Natl. Acad. Sci. 113 (2016) E854–E863, https://doi.org/10.1073/pnas.1508541113.
[29] Y. Zhang, R.A. Weinberg, Epithelial-to-mesenchymal transition in cancer: complexity and opportunities, Front. Med. 12 (2018) 361–373, https://doi.org/10.1007/s11684-018-0656-6.

[30] K. Nagaharu, X. Zhang, T. Yoshida, D. Katoh, N. Hanamura, Y. Kozuka, T. Ogawa, T. Shiraishi, K. Imanaka-Yoshida, Tenascin C induces epithelial-mesenchymal transition−like change accompanied by SRC activation and focal adhesion kinase phosphorylation in human breast cancer cells, Am. J. Pathol. 178 (2011) 754−763, https://doi.org/10.1016/j.ajpath.2010.10.015.
[31] J. Xu, S. Lamouille, R. Derynck, TGF-β-induced epithelial to mesenchymal transition, Cell Res. 19 (2009) 156−172, https://doi.org/10.1038/cr.2009.5.
[32] A. Singh, J. Settleman, EMT, cancer stem cells and drug resistance: an emerging axis of evil in the war on cancer, Oncogene. 29 (2010) 4741−4751, https://doi.org/10.1038/onc.2010.215.
[33] L. De Laporte, J.J. Rice, F. Tortelli, J.A. Hubbell, Tenascin C promiscuously binds growth factors via its fifth fibronectin type III-like domain, PLoS One 8 (2013), e62076, https://doi.org/10.1371/journal.pone.0062076.
[34] C. Kolliopoulos, C.-Y. Lin, C.-H. Heldin, A. Moustakas, P. Heldin, Has2 natural antisense RNA and Hmga2 promote Has2 expression during TGFβ-induced EMT in breast cancer, Matrix Biol. 80 (2019) 29−45, https://doi.org/10.1016/j.matbio.2018.09.002.
[35] L.A. Griggs, N.T. Hassan, R.S. Malik, B.P. Griffin, B.A. Martinez, L.W. Elmore, C.A. Lemmon, Fibronectin fibrils regulate TGF-β1-induced epithelial-mesenchymal transition, Matrix Biol. 60−61 (2017) 157−175, https://doi.org/10.1016/j.matbio.2017.01.001.
[36] A. Pezzolo, F. Parodi, D. Marimpietri, L. Raffaghello, C. Cocco, A. Pistorio, M. Mosconi, C. Gambini, M. Cilli, S. Deaglio, F. Malavasi, V. Pistoia, Oct-4+/Tenascin C+ neuroblastoma cells serve as progenitors of tumor-derived endothelial cells, Cell Res. 21 (2011) 1470−1486, https://doi.org/10.1038/cr.2011.38.
[37] T. Sugino, T. Yamaguchi, G. Ogura, A. Saito, T. Hashimoto, N. Hoshi, S. Yoshida, S. Goodison, T. Suzuki, Morphological evidence for an invasion-independent metastasis pathway exists in multiple human cancers, BMC Medicine. 2 (2004). doi:https://doi.org/10.1186/1741-7015-2-9.
[38] R.V. Iozzo, M.A. Gubbiotti, Extracellular matrix: the driving force of mammalian diseases, Matrix Biol. 71−72 (2018) 1−9, https://doi.org/10.1016/j.matbio.2018.03.023.
[39] N.K. Karamanos, A.D. Theocharis, T. Neill, R.V. Iozzo, Matrix modeling and remodeling: a biological interplay regulating tissue homeostasis and diseases, Matrix Biol. 75−76 (2019) 1−11, https://doi.org/10.1016/j.matbio.2018.08.007.
[40] N. Dandachi, C. Hauser-Kronberger, E. Moré, B. Wiesener, G.W. Hacker, O. Dietze, G. Wirl, Co-expression of tenascin-C and vimentin in human breast cancer cells indicates phenotypic transdifferentiation during tumour progression: correlation with histopathological parameters, hormone receptors, and oncoproteins, J. Pathol. 193 (2001) 181−189, https://doi.org/10.1002/1096-9896(2000)9999:9999<::AID-PATH752>3.0.CO;2-V.
[41] X. Shen, R.H. Kramer, Adhesion-mediated squamous cell carcinoma survival through ligand-independent activation of epidermal growth factor receptor, Am. J. Pathol. 165 (2004) 1315−1329, https://doi.org/10.1016/S0002-9440(10)63390-1.
[42] Y. Katsuno, D.S. Meyer, Z. Zhang, K.M. Shokat, R.J. Akhurst, K. Miyazono, R. Derynck, Chronic TGF-β exposure drives stabilized EMT, tumor stemness, and cancer drug resistance with vulnerability to bitopic mTOR inhibition, Sci. Signal. 12 (2019) eaau8544. doi:https://doi.org/10.1126/scisignal.aau8544.
[43] T. Sugino, T. Kusakabe, N. Hoshi, T. Yamaguchi, T. Kawaguchi, S. Goodison, M. Sekimata, Y. Homma, T. Suzuki, An invasion-independent pathway of blood-borne metastasis, Am. J. Pathol. 160 (2002) 1973−1980.
[44] V.L.T. Ballard, A. Sharma, I. Duignan, J.M. Holm, A. Chin, R. Choi, K.A. Hajjar, S.-C. Wong, J.M. Edelberg, Vascular tenascin-C regulates cardiac endothelial phenotype and neovascularization, FASEB J. 20 (2006) 717−719, https://doi.org/10.1096/fj.05-5131fje.
[45] N. Aceto, A. Bardia, D.T. Miyamoto, M.C. Donaldson, B.S. Wittner, J.A. Spencer, M. Yu, A. Pely, A. Engstrom, H. Zhu, B.W. Brannigan, R. Kapur, S.L. Stott, T. Shioda, S. Ramaswamy, D.T. Ting, C.P. Lin, M. Toner, D.A. Haber, S. Maheswaran, Circulating tumor cell clusters are oligoclonal precursors of breast cancer metastasis, Cell. 158 (2014) 1110−1122, https://doi.org/10.1016/j.cell.2014.07.013.
[46] D.G. Duda, A.M.M.J. Duyverman, M. Kohno, M. Snuderl, E.J.A. Steller, D. Fukumura, R.K. Jain, Malignant cells facilitate lung metastasis by bringing their own soil, Proc. Natl. Acad. Sci. U. S. A. 107 (2010) 21677−21682, https://doi.org/10.1073/pnas.1016234107.
[47] R.G. Oshima, J. Lesperance, V. Munoz, L. Hebbard, B. Ranscht, N. Sharan, W.J. Muller, C.A. Hauser, R.D. Cardiff, Angiogenic acceleration of Neu induced mammary tumor progression and metastasis, Cancer Res. 64 (2004) 169−179.
[48] B. Langlois, F. Saupe, T. Rupp, C. Arnold, M. van der Heyden, G. Orend, T. Hussenet, AngioMatrix, a signature of the tumor angiogenic switch-specific matrisome, correlates with poor prognosis for glioma and colorectal cancer patients, Oncotarget 5 (2014) 10529−10545.
[49] R. Lauria, F. Perrone, C. Carlomagno, M. De Laurentiis, A. Morabito, C. Gallo, E. Varriale, G. Pettinato, L. Panico, G. Petrella, The prognostic value of lymphatic and blood vessel invasion in operable breast cancer, Cancer 76 (1995) 1772−1778.
[50] N. Knijn, U.E.M. van Exsel, M.E. de Noo, I.D. Nagtegaal, The value of intramural vascular invasion in colorectal cancer - a systematic review and meta-analysis, Histopathology. 72 (2018) 721−728, https://doi.org/10.1111/his.13404.
[51] S. Okada, S. Mizuguchi, N. Izumi, H. Komatsu, M. Toda, K. Hara, T. Okuno, T. Shibata, H. Wanibuchi, N. Nishiyama, Prognostic value of the frequency of vascular invasion in stage I non-small cell lung cancer, Gen. Thorac. Cardiovasc. Surg. 65 (2017) 32−39, https://doi.org/10.1007/s11748-016-0720-6.
[52] M.R.S. Siddiqui, C. Simillis, C. Hunter, M. Chand, J. Bhoday, A. Garant, T. Vuong, G. Artho, S. Rasheed, P. Tekkis, A.-M. Abulafi, G. Brown, A meta-analysis comparing the risk of metastases in patients with rectal cancer and MRI-detected extramural vascular invasion (mrEMVI) vs mrEMVI-negative cases, Br. J. Cancer 116 (2017) 1513−1519, https://doi.org/10.1038/bjc.2017.99.
[53] T.A. Klingen, Y. Chen, I.M. Stefansson, G. Knutsvik, K. Collett, A.L. Abrahamsen, H. Aase, H. Aas, T. Aas, E. Wik, L.A. Akslen, Tumour cell invasion into blood vessels is significantly related to breast cancer subtypes and decreased survival, J. Clin. Pathol. 70 (2017) 313−319, https://doi.org/10.1136/jclinpath-2016-203861.
[54] V.F. Marinho, K. Metze, F.S. Sanches, G.F. Rocha, H. Gobbi, Lymph vascular invasion in invasive mammary carcinomas identified by the endothelial lymphatic marker D2-40 is associated with other indicators of poor prognosis,

BMC Cancer 8 (2008) 64, https://doi.org/10.1186/1471-2407-8-64.
[55] G.G. Van den Eynden, I. Van der Auwera, S.J. Van Laere, C.G. Colpaert, P. van Dam, L.Y. Dirix, P.B. Vermeulen, E.A. Van Marck, Distinguishing blood and lymph vessel invasion in breast cancer: a prospective immunohistochemical study, Br. J. Cancer 94 (2006) 1643–1649, https://doi.org/10.1038/sj.bjc.6603152.
[56] K.E. Roberts, D. Hamele-Bena, A. Saqi, C.A. Stein, R.P. Cole, Pulmonary tumor embolism: a review of the literature, Am. J. Med. 115 (2003) 228–232.
[57] N.S. Vasudev, A.R. Reynolds, Anti-angiogenic therapy for cancer: current progress, unresolved questions and future directions, Angiogenesis 17 (2014) 471–494, https://doi.org/10.1007/s10456-014-9420-y.
[58] V. Zambonin, A. De Toma, L. Carbognin, R. Nortilli, E. Fiorio, V. Parolin, S. Pilotto, F. Cuppone, F. Pellini, D. Lombardi, G.P. Pollini, G. Tortora, E. Bria, Clinical results of randomized trials and "real-world" data exploring the impact of Bevacizumab for breast cancer: opportunities for clinical practice and perspectives for research, Expert. Opin. Biol. Ther. 17 (2017) 497–506, https://doi.org/10.1080/14712598.2017.1289171.
[59] K.C. Aalders, K. Tryfonidis, E. Senkus, F. Cardoso, Anti-angiogenic treatment in breast cancer: facts, successes, failures and future perspectives, Cancer Treat. Rev. 53 (2017) 98–110, https://doi.org/10.1016/j.ctrv.2016.12.009.
[60] M. Rajabi, S. Mousa, The role of angiogenesis in cancer treatment, Biomedicines 5 (2017) 34, https://doi.org/10.3390/biomedicines5020034.
[61] M. Shi, X. He, W. Wei, J. Wang, T. Zhang, X. Shen, Tenascin-C induces resistance to apoptosis in pancreatic cancer cell through activation of ERK/NF-κB pathway, Apoptosis. 20 (2015) 843–857, https://doi.org/10.1007/s10495-015-1106-4.
[62] W. Huang, R. Chiquet-Ehrismann, J.V. Moyano, A. Garcia-Pardo, G. Orend, Interference of tenascin-C with syndecan-4 binding to fibronectin blocks cell adhesion and stimulates tumor cell proliferation, Cancer Res. 61 (2001) 8586–8594.
[63] J.-P. Cazenave, P. Ohlmann, D. Cassel, A. Eckly, B. Hechler, C. Gachet, Preparation of Washed Platelet Suspensions From Human and Rodent Blood, in: Platelets and Megakaryocytes, Humana Press, New Jersey, 2004, pp. 013–028, https://doi.org/10.1385/1-59259-782-3:013.
[64] K. Midwood, S. Sacre, A.M. Piccinini, J. Inglis, A. Trebaul, E. Chan, S. Drexler, N. Sofat, M. Kashiwagi, G. Orend, F. Brennan, B. Foxwell, Tenascin-C is an endogenous activator of toll-like receptor 4 that is essential for maintaining inflammation in arthritic joint disease, Nat. Med. 15 (2009) 774–780, https://doi.org/10.1038/nm.1987.

Published OnlineFirst January 15, 2020; DOI: 10.1158/2326-6066.CIR-19-0276

Matrix-Targeting Immunotherapy Controls Tumor Growth and Spread by Switching Macrophage Phenotype

Claire Deligne[1], Devadarssen Murdamoothoo[2], Anís N. Gammage[1], Martha Gschwandtner[1], William Erne[2], Thomas Loustau[2], Anna M. Marzeda[1], Raphael Carapito[3], Nicodème Paul[3], Inés Velazquez-Quesada[2], Imogen Mazzier[1], Zhen Sun[2], Gertraud Orend[2], and Kim S. Midwood[1]

ABSTRACT

The interplay between cancer cells and immune cells is a key determinant of tumor survival. Here, we uncovered how tumors exploit the immunomodulatory properties of the extracellular matrix to create a microenvironment that enables their escape from immune surveillance. Using orthotopic grafting of mammary tumor cells in immunocompetent mice and autochthonous models of breast cancer, we discovered how tenascin-C, a matrix molecule absent from most healthy adult tissues but expressed at high levels and associated with poor patient prognosis in many solid cancers, controls the immune status of the tumor microenvironment. We found that, although host-derived tenascin-C promoted immunity via recruitment of proinflammatory, antitumoral macrophages, tumor-derived tenascin-C subverted host defense by polarizing tumor-associated macrophages toward a pathogenic, immune-suppressive phenotype. Therapeutic monoclonal antibodies that blocked tenascin-C activation of Toll-like receptor 4 reversed this phenotypic switch *in vitro* and reduced tumor growth and lung metastasis *in vivo*, providing enhanced benefit in combination with anti–PD-L1 over either treatment alone. Combined tenascin-C: macrophage gene-expression signatures delineated a significant survival benefit in people with breast cancer. These data revealed a new approach to targeting tumor-specific macrophage polarization that may be effective in controlling the growth and spread of breast tumors.

Introduction

The immune system can detect tumors and mount an efficient defense against them, but tumors can evolve to develop effective strategies to evade immune elimination. The importance of the interplay between tumor cells and immune cells in determining whether cancers will progress provided a landmark shift in disease philosophy, opening therapeutic avenues beyond targeting only tumor cells. The first wave of immuno-oncology therapies focuses on tumor-infiltrating lymphocytes (TIL). TILs reliably predict good prognosis and sensitivity to neoadjuvant chemotherapy treatment in many solid cancers (1) and correlate with high mutational burden (2). Therapies that reactivate TILs, via engaging their immune checkpoints, expanding mutation-specific T cells, or injecting antigen-specific T cells, have revolutionized the treatment of cancer, offering an alternative tumor killing mechanism, as well as the possibility of generating long-lasting immunity against the cancer. However, this approach does not work for all patients, nor all types of tumors, and can be associated with severe autoimmune side effects (reviewed in ref. 3).

In contrast to TILs, tumor-associated macrophages (TAM) are frequently associated with poor outcomes in patients, prompting the development of therapies directed against these cells (reviewed in refs. 4–6). Approaches include inhibition of macrophage survival, proliferation, and differentiation by targeting colony-stimulating factor receptor-1 (CSFR-1), blockade of their recruitment by targeting CCR2 (chemokine C-C motif receptor 2), modulating their polarization by targeting macrophage receptor with collagenous structure (MARCO), or their activation by engaging the costimulatory signal CD40. Macrophage-targeting therapies have been hailed as a useful complement for immune-checkpoint therapies such as anti–CTLA-4 and anti–PD-1/PD-L1 treatment, providing a multihit approach to enable parallel lymphocyte reactivation and TAM blockade, as well as synergistically widening T-cell repertoire and activity. However, the clinical efficacy of macrophage-targeting drugs has been mixed (4, 5). These results may, in part, be due to the complexity of the macrophage compartment. Although many cancers are infiltrated by immunosuppressive TAM populations, a variety of other TAM subsets, including tumoricidal macrophages that exert killing or phagocytic activity, metastasis-associated macrophages, and proangiogenic macrophages, also exist (7). It is not clear what dictates TAM heterogeneity but understanding more about the factors in the tumor microenvironment (TME) that influence macrophage phenotype may enable the development of therapies that specifically target pathogenic TAM subsets.

The tissue microenvironment is a key determinant of macrophage phenotype. Tissues comprise a selection of secreted proteins, encompassing extracellular matrix molecules, matrix-associated proteins, growth factors, chemokines and cytokines, and enzymes including proteases (8). These complex 3D networks provide essential context for cell behavior, driving site-specific gene-expression programs to enable geographically adapted cell behavior. Emerging evidence is starting to reveal factors underlying macrophage specialization in the liver, gut, and brain (9) and how macrophage transplantation from the

[1]Kennedy Institute of Rheumatology, Nuffield Department of Orthopaedics, Rheumatology and Musculoskeletal Sciences, University of Oxford, Oxford, United Kingdom. [2]University of Strasbourg, INSERM U1109, MN3T and The Tumor Microenvironment Laboratory, Fédération de Médecine Translationnelle de Strasbourg (FMTS), Strasbourg, France. [3]Laboratoire d'ImmunoRhumatologie Moléculaire, GENOMAX platform, INSERM UMR_S 1109, Faculté de Médecine, Fédération Hospitalo-Universitaire OMICARE, Fédération de Médecine Translationnelle de Strasbourg (FMTS), LabEx TRANSPLANTEX, Université de Strasbourg, Strasbourg, France.

Note: Supplementary data for this article are available at Cancer Immunology Research Online (http://cancerimmunolres.aacrjournals.org/).

Corresponding Author: Kim S. Midwood, Kennedy Institute of Rheumatology, University of Oxford, Roosevelt Drive, Headington, Oxford OX3 7FY, UK. Phone: 44-1865-612-646; E-mail: kim.midwood@kennedy.ox.ac.uk

Cancer Immunol Res 2020;8:368–82

doi: 10.1158/2326-6066.CIR-19-0276

Published OnlineFirst January 15, 2020; DOI: 10.1158/2326-6066.CIR-19-0276

peritoneum to the lungs reshapes tissue-dependent functions and characteristics (10). Macrophage responses to infection and how soluble factors, such as GM-CSF and IL4, can influence macrophage behavior are also known (11). Most solid cancers are made up of a tumor-specific extracellular matrix that has a different composition and organization to that of healthy tissue (12). However, how this altered microenvironment affects macrophage behavior is not fully understood.

Here, we examined tenascin-C, a matrix molecule absent from most healthy tissues, but whose expression in solid tumors is frequently associated with poor prognosis (13). This large multimodular molecule has been shown to modulate angiogenesis (14, 15), stem cell fitness (13), and tumor stiffness (16) during tumor growth and metastasis. Tenascin-C can also shape innate and adaptive immune responses (17), but its role in tumor immunity remains unclear. In this study, we explored the impact of tenascin-C on the immune axis in breast cancer and examined the therapeutic potential of specifically blocking its immunomodulatory action.

Materials and Methods

Mice

Wild-type FVB mice were purchased from Charles River Laboratories, and tenascin-C knockout mice on an FVB background were generated as described in ref. 18. Two- to 3-month-old females were used for the experiments. MMTV-NeuNT female mice (FVB/NCrl background) with a mutated constitutively active form of rat ErbB2 (NeuNT) expressed under the control of the mouse mammary tumor virus (MMTV) regulatory region were purchased from The Jackson Laboratory. All animal procedures were carried out in accordance with the UK Animals (Scientific Procedures) Act 1986 and with the University of Oxford (Clinical Medicine) Ethical Committee approval.

Cell lines

The mouse mammary cancer cell line NT193 was derived from an MMTV-NeuNT tumor (19) and has previously been engineered to express high or low/no tenascin-C by transduction with a lentivirus expressing shRNA against tenascin-C (TNC^-) or control shRNA (TNC^+). Lentiviral particles with shRNA vectors (Sigma-Aldrich) specific for *Tnc* were used (sh2, TRCN0000312138, 5′-CCGGGCATCAACACAACCAGTCTAACTCGAGTTAGACTGGTTGTGTTGATGCTTTTTG-3′). Lentiviral particles encoding a nontargeting shRNA vector were used as a control (SHC202V, Sigma-Aldrich; ref. 18). NT193 cells were cultured in DMEM supplemented with 10% inactivated fetal bovine serum, penicillin (10,000 U/mL), streptomycin (10 mg/mL), and puromycin (10 μg/mL; all from Sigma-Aldrich). Cells were maintained at 37°C in a humidified atmosphere of 5% CO_2 and were cultivated for a minimum of 1 week and a maximum of 1 month (roughly 4 passages) before use. Cells were periodically checked for tenascin-C and vimentin expression by Western blotting and tested to be negative for *Mycoplasma* (Thermo Fisher).

Western blotting

NT193 cells were lysed using RIPA buffer with protease inhibitor cocktail I (12801640; Fisher Scientific) at 1:1,000, and the protein concentration was determined using a BCA assay (Thermo Fisher). Five percent polyacrylamide gels were prepared, and protein (20 μg/well) was loaded in Laemmli buffer diluted 1/6 (stock solution: 2.5 mL of 0.5 M Tris-HCl pH 6.8; 1.2 g SDS; 2.5 mL β-mercaptoethanol; 5 mL glycerol; 5 mg bromophenol blue). Separated proteins were transferred to a nitrocellulose membrane using a TransBlot Turbo transfer machine (Bio-Rad). Membranes were blocked for 1 hour in blocking buffer (PBS, 0.05% Tween20, 5% BSA) and incubated overnight with primary antibodies recognizing tenascin-C (MTn-12; Sigma-Aldrich) at 1/4,000, vimentin (V5255, Sigma-Aldrich) at 1/2,000 or beta actin (937215; Enzo Life Science) at 1/1,000, and then for 1 hour with secondary antibody (anti-rat IgG A5795; Sigma-Aldrich, anti-mouse IgG P0260; DAKO) at 1/20,000 in blocking buffer. Proteins were detected with ECL Amersham reagent using Amersham Hyperfilm ECL (VWR International) and a Curix 60 film processor (AGFA).

Tumor engraftment and *in vivo* treatments

For the orthotopic grafting model, 10×10^6 NT193 TNC^+ or TNC^- cells were injected into the left fourth mammary gland of 2- to 3-month-old female FVB mice in 50 μL sterile PBS at day 0. Tumor size was measured every 3 days using calipers, and the volume of the tumor was calculated using the formula $V = (L \times H \times W)/2$. For the spontaneous model, the apparition of mammary tumors in MMTV-NeuNT mice was monitored from 4 months of age at least once a week, and the experiment started once a tumor became detectable by palpation (day 0). Clodronate liposomes and control liposomes (Liposoma) were prepared according to the manufacturer's recommendations and injected intravenously at 10 μL/g of mouse or intratumorally at 1 μL/g of mouse on days 1 and 7 after engraftment of NT193 TNC^+ or TNC^- tumor cells. The efficacy of myeloid cell depletion was tested by flow cytometry staining of blood sampled from the tail vein, 7 days after the last injection, by detection of $CD45^+CD11b^+$ cells (using anti-CD45–PE-Cy7 (30F11) and anti-CD11b–PerCP-Cy5.5 (M1/70) from BioLegend). Antibodies recognizing the fibrinogen-like globe (FBG) domain of tenascin-C (anti-FBG; Clone C3, Nascient Ltd.; ref. 20) was given as 6 intraperitoneal (i.p.) injections on days 1, 4, 7, 11, 15, and 18 at 5, 10, or 20 mg/kg in 200 μL sterile PBS. Anti–PD-L1 antibody (10F.9G2; Bio X Cell) was given as 2 i.p. injections of 150 μg in 200 μL sterile PBS on days 1 and 4 (21). Mice were sacrificed when the tumor reached 1.2 cm, and tumors and lungs were collected.

Metastasis analysis

Tissues from paraffin-embedded lung lobes were cut from 46 MMTV-NeuNT mice at 6 different depths separated by at least 500 μm from each other throughout the tissue (sagittal sections; 7 μm) and stained with hematoxylin and eosin to assess lung pathology. The number of metastasis per image were counted, from a minimum of 10 images per section, on an AxioScope.A1 (Zeiss) microscope, at 20× magnification, and their size was measured using ImageJ software.

Tenascin-C ELISA

Isolated tumor cells

Tumor tissue was cut into small pieces and digested in RPMI medium supplemented with 5% of inactivated fetal bovine serum, penicillin (10,000 U/mL), streptomycin (10 mg/mL), Liberase TM (500 μg/mL; Roche), and DNAse (100 μg/mL; Roche) for 30 minutes at 37°C under agitation. Cells were plated at 1×10^6 cells/mL in complete DMEM supplemented with 10% of inactivated fetal bovine serum, penicillin (10,000 U/mL), and streptomycin (10 mg/mL) for 5 days. Puromycin (10 μg/mL) was added to select for tumor cells. Adherent cells were collected, and cell lysates prepared in RIPA buffer supplemented with protease inhibitor cocktail I (12801640; Fisher Scientific) at 1/1,000.

Published OnlineFirst January 15, 2020; DOI: 10.1158/2326-6066.CIR-19-0276

Whole tumors

Harvested tumors were frozen in liquid nitrogen and mechanically disrupted before being lysed in RIPA buffer supplemented with protease inhibitors, as indicated above. Tenascin-C concentration in the lysates was assessed by ELISA (Tenascin-C Large FnIII-B kit, Demeditec). Two hundred nanograms of protein/well was loaded, and the optic density was measured using a FLUOstar Omega plate reader (BMG Labtech). Tenascin-C concentrations were calculated from a standard curve prepared with recombinant tenascin-C following the manufacturer's recommendations.

Flow cytometry and antibodies

Tumor tissue was cut into small pieces and digested in RPMI medium supplemented with 5% of inactivated fetal bovine serum, penicillin (10,000 U/mL), streptomycin (10 mg/mL), Liberase TM (500 μg/mL; Roche), and DNAse (100 μg/mL; Roche) for 30 minutes at 37°C under agitation. Surface and intracellular flow cytometry staining of isolated cells was performed according to standard protocols and analyzed on an LSRFortessa (BD Biosciences). Briefly, 1.10^6 cells were saturated for 15 minutes in the presence of Fc Block (TruStain FcX, 101319, BioLegend) and incubated for 25 minutes with the surface antibodies mix diluted at 1/200 in PBS 2% FCS. For intracellular staining, cells were then permeabilized and fixed for 30 minutes in the presence of a Fix/perm solution (554722, BD Biosciences) and incubated for 30 minutes with the intracellular antibodies diluted at 1/100 in the perm/wash buffer (554723, BD Biosciences). Surface antibodies: anti–Ly-6C–Brilliant Violet 785 (HK1.4), anti–Ly-6G–Brilliant Violet 650 (1A8), anti-CD206–Alexa Fluor 700 (C068C2), anti-CD11c– Alexa Fluor 594 (N418), anti-CD115–APC/Cy7 (AFS98), anti-CD45–PE-Cy7 (30F11), anti-CD11b–PerCP-Cy5.5 (M1/70), anti-F4/80–Pacific Blue (BM8), anti-CD8α–Pacific Blue (53-6.7), anti-CD3–Brilliant Violet 785 (17A2), anti-CD86–Brilliant Violet 650 (GL-1), anti-TLR4–APC (SA15-21) from BioLegend; anti-IA/IE–FITC (2G9) from BD Biosciences; and anti-CD4–PE-Texas Red (GK1.5) from Abcam. Intracellular antibodies: anti-IL17A–Alexa Fluor 700 (TC11-18H10.1) from BioLegend; anti-IRF5–PE (903430) from R&D Systems; and anti-IFNγ–Alexa Fluor 594 (XMG1.2) from BD Biosciences. Tenascin-C was detected using anti-FBG at 10 μg/mL followed by anti-human IgG-AF488 (BioLegend). Dead cells were stained using a Live/Dead yellow kit (Thermo Fisher). FlowJo software version 10 was used for data analysis. Cell populations were defined as follows: M1-like macrophages: $CD45^+CD11b^+CD11c^+F4/80^+IRF5^+$; M2-like macrophages: $CD45^+CD11b^+CD11c^+F4/80^+CD206^+$; monocytes: $CD45^+CD11b^+CD115^+Ly6C^+$; neutrophils: $CD45^+CD11b^+CD115^-Ly6C^+Ly6G^{hi}$; Th1: $CD45^+CD3^+CD4^+IFN\gamma^+$; Th17: $CD45^+CD3^+CD4^+IL17A^+$.

Immunofluorescence

Optimal cutting temperature–embedded tumor sections (7 μm-thick) were incubated with blocking solution [PBS, 5% goat serum (G9023, Sigma-Aldrich), 5% rat serum (R9759, Sigma-Aldrich), 1% FCS] for 1 hour at room temperature before incubation with primary antibody overnight at 4°C [anti–tenascin-C from Sigma-Aldrich (MTn-12)) at 10 μg/mL; anti–F4/80-PE (BM8) and anti–CD206-APC (C068C2) from BioLegend] both at 1/100. The slides were then incubated with secondary antibody for 1 hour at room temperature (anti-IgG1-AF488, BioLegend) at 1/200, counterstained with DAPI (Thermo Fisher), and embedded with Fluoromount-G (Invitrogen). The fluorescent signal was analyzed with a Zeiss Axio Imager microscope. Five random 20× fields per section were analyzed by ImageJ (NIH) to assess the infiltration of macrophages, as well as their spatial distribution between the tumor nest and the stroma (1 section per tumor, 5 tumors per group). Macrophage subsets and tenascin-C localization in the tumor were also analyzed and displayed as a line scan using FiJi software.

Gene-expression analysis in whole tumor tissue

Total RNA was prepared from harvested tumors using TriReagent (Life Technologies) with a tissue homogenizer (Omni International) according to the manufacturer's instructions. RNA integrity was assessed with an Agilent total RNA Pico Kit on a 2100 Bioanalyzer instrument (Agilent Technologies; RINs ranged from 7.6 to 8.2), and ribosomal RNA was depleted with the Low Input RiboMinus Eukaryote System v2 kit (Thermo Fisher). To prepare the sequencing library, the Ion Total RNA-sep kit v2 (Thermo Fisher) was used following the manufacturer's instructions. The libraries were loaded at a concentration of 20 pmol/L on an Ion PI Chip (Thermo Fisher) using the Ion Chef Instrument (Thermo Fisher). Sequencing was performed on an Ion Proton sequencer (Thermo Fisher) with the Ion PI Hi-Q Sequencing 200 Kit (Thermo Fisher). Transcriptomic data were processed using the RNASeqAnalysis plugin from the Torrent Suite Software 5.06, and the reads were mapped using STAR and Bowtie2 (22, 23). The total read maps are available in binary alignment map (BAM) format for raw read count extraction. Read counts were found with the htseq-count tool of the Python package HTSeq (24). Differential analyses were performed using the DESEQ2 package from the Bioconductor framework (25). Upregulated and downregulated genes were selected based on the adjusted *P*-value cutoff 10%. Data can be accessed via SRA accession number PRJNA587450.

Gene-expression analysis in TAM

Tumor-infiltrating macrophages were isolated by mechanical dissociation of the tumor tissue and enzymatic digestion with DMEM supplemented with 5 % of inactivated fetal bovine serum, penicillin (10,000 U/mL), streptomycin (10 mg/mL), Liberase TM (500 μg/mL; Roche), and DNAse (100 μg/mL; Roche) for 30 minutes at 37°C under agitation and then purified by sorting $CD11b^+F4/80^+$ cells using a BD FACSAria III. RNA isolation was performed using the RNeasy Microkit (Qiagen). The concentration and purity of the isolated RNA was determined using a NanoDrop One (Thermo Fisher). One hundred nanograms of RNA was reverse transcribed using the High-Capacity cDNA Reverse Transcription kit (Thermo Fisher). The real-time qPCR reaction was performed in 384-well plates on a Viia7 Real-Time PCR system (Thermo Fisher) using the TaqMan Universal PCR Master Mix (Thermo Fisher) and the following TaqMan primers (all Thermo Fisher) in triplicate: *ARG-1*: Mm00475988_m1, *CD86*: Mm00444540_m1, *MRC1*: Mm01329362_m1, *TNF*: Mm99999068_m1, HPRT: Mm00446968_m1. Data were analyzed using the ΔCt method and expressed as a percentage of *HPRT*.

Coculture assays

T-cell isolation

T cells were isolated from spleens of naïve female wild-type FVB mice (10–12 weeks of age) by mechanical dissociation of the tissue, purified by negative magnetic sorting (Pan T-cell isolation kit II, 130-095-130 and LS columns, 130-042-401, Miltenyi Biotec), and loaded with 10 μmol/L of CFSE (BD Biosciences) on the first day of coculture. The purity of sorted cells was systematically assessed by FACS to be >95%. Coculturing conditions are described below. Proliferation was calculated using flow cytometry (BD LSRII) and analyzed with FlowJo software (Tree Star) to assess the decreasing mean fluorescence

Published OnlineFirst January 15, 2020; DOI: 10.1158/2326-6066.CIR-19-0276

intensity (MFI) of CFSE in T cells on the last day of coculture, as CFSE intracellular content is reduced upon each cell division.

Myeloid cells

Bone marrow–derived macrophages (BMM) were isolated by flushing the bone marrow out of the femur of naïve wild-type FVB mice. BMM were then differentiated by plating 2×10^6 cells for 7 days in the presence of GM-CSF (50 ng/mL; PeproTech) and adherent/loosely adherent cells were collected using ice-cold PBS. Given that the tumor-associated macrophage population we identified in our model was $CD11b^+CD11c^+$, we chose GM-CSF–differentiated BMM that are $CD11b^+CD11c^+$ rather than M-CSF–differentiated BMM that only express CD11b. We observed comparable results in coculture systems using both cell subsets.

Tumor-infiltrating myeloid cells were isolated by mechanical dissociation of the tumor tissue from mice and enzymatic digestion, as stated above, for 30 minutes at 37°C under agitation and then purified by positive magnetic sorting of $CD11b^+$ cells (CD11b microbeads, 130-049-601 and LS columns, 130-042-40, Miltenyi Biotec). Coculturing conditions are described below.

Culture conditions

NT193 tumor cells were detached from tissue culture plates and treated with mitomycin (50 μg/mL; Sigma-Aldrich) to block their proliferation. 1×10^6 tumor cells/mL were cultured in RPMI medium supplemented with 5% of inactivated fetal bovine serum, penicillin (10,000 U/mL), streptomycin (10 mg/mL), and 10 μmol/L of β-mercaptoethanol with BMM, $CD11b^+$ tumor–infiltrating myeloid cells, or T cells using all cells at a 1:1 ratio. Tumor cells and BMM or $CD11b^+$ tumor–infiltrating myeloid cells were cultured for 5 days, and tumor cells with T cells were cultured for 10 days. Murine IL2 (50 ng/mL; PeproTech), IL7 (50 ng/mL; PeproTech), and LEAF-grade anti-CD3 (BioLegend) at 1 μg/mL were added in T-cell cocultures. The following inhibitors were used: TLR4 inhibitor (TAK242, Invivogen) was added at 5 μmol/L, EGFR inhibitor (Tyrphostin, Sigma-Aldrich) was added at 1 μmol/L, and integrin β1 and β3 inhibitor (Echistatin, Sigma-Aldrich) was added at 50 nmol/L to BMM cocultures every 5 days. In some experiments, LPS was added at 1 ng/mL (L2887, Sigma-Aldrich) on the first day of coculture. Anti-FBG antibody was added to all cocultures every 5 days of coculture at a molar ratio corresponding to 1:10, 1:1, or 5:1 to the concentration of tenascin-C produced (2 ng/mL, 260 ng/mL, or 1.3 μg/mL, respectively) by TNC^+ tumor cells over 5 days of culture.

Readouts

Culture supernatants were collected at the end of cocultures as detailed in the culture conditions. Murine IL1β, IL4, IL6, IL8, IL10, IL12, TNFα, and TGFβ (DuoSet ELISA kits, R&D Systems) and tenascin-C (Tenascin-C Large FnIII-B kit, Demeditec) were quantified by ELISA. Supernatants were diluted at 1/2 for IL1β, IL4, IL10, IL12, and TGFβ, at 1/5 for IL6, IL8, and TNFα and at 1/20 for tenascin-C. The optic density was measured using a FLUOstar Omega (BMG Labtech) plate reader, and concentrations were calculated from a standard curve using standards provided in the kit following the manufacturer's recommendations. Flow-cytometric analysis was performed on the cells extracted from cocultures or from harvested mouse organs on a BD LSRII or a LSRFortessa using the following antibodies: anti–CD206-Alexa Fluor 700 (C068C2), anti–CD45–PE-Cy7 (30F11), anti–CD11b–PerCP-Cy5.5 (M1/70), anti–F4/80-Pacific Blue (BM8) anti–CD8α- Pacific Blue (53-6.7), anti–CD3-Brilliant Violet 785 (17A2), anti–CD86- Brilliant Violet 650 (GL-1) from BioLegend; anti–iNOS-PE-eFluor 610 (61-5920-80) from Thermo Fisher; anti-IA/IE–FITC (2G9) from BD Biosciences; and anti-CD4- PE-Texas Red (GK1.5) from Abcam. Dead cells were stained using a Live/Dead yellow kit (Thermo Fisher). Flow cytometry analysis was performed using FlowJo software (Tree Star).

Human tumor RNA sequencing data analysis

Bulk RNA sequencing (RNA-seq) data of 1,045 primary tumors from The Cancer Genome Atlas (TCGA) Breast Invasive Carcinoma cohort (BRCA-US) were retrieved from the Genomic Data Commons via the TCGA biolinks package in R (version 2.9.4; ref. 26). Transcripts were quantified and normalized by the original authors (27) using the RSEM algorithm (28), and these values were multiplied by 10^6 to provide transcripts per million (TPM). TPM values were $\log2(x + 1)$ transformed prior to analysis. Pairwise correlations of *TNC* versus all other genes were performed using the Spearman rank test, and *P* values were adjusted with the Benjamini–Hochberg correction (i.e., false discovery rate, FDR). The relative abundance of tumor-infiltrating immune cells was estimated by computational deconvolution of 22 immune cell types using the CIBERSORT method and LM22 gene signature matrix (29). CIBERSORT was run with 100 permutations and with quantile normalization disabled. Unscaled data are shown. The estimated abundance of "M2 Macrophages" from CIBERSORT analysis, alongside *TNC* expression, was used to stratify tumors, in each case by selection of the upper and lower 20% of cases. Kaplan–Meier survival analysis using the log-rank test was performed on stratified tumor subsets within the TCGA biolinks package (26). The numbers of patients at risk between the time points of 0, 1,000, 2,000, and 3,000 days, respectively, for each subset were TNC-low, M2-low: 37, 14, 2, 1; TNC-high, M2-low: 39, 23, 9, 1; TNC-low, M2-high: 44, 19, 7, 4; TNC-high, M2-high: 35, 17, 7, 3.

Statistical analysis

Statistical analyses were performed with Prism software (GraphPad). The Student unpaired *t* test was used to determine the significance of differences from Gaussian data sets. For non-Gaussian data sets, the Mann–Whitney test was used to determine the significance of differences between unpaired sets of data and the Wilcoxon test for paired sets of data. *P* values <0.05 were considered statistically significant. Data are representative of at least two individual experiments, expressed as the mean ± SEM (*, $P < 0.05$; **, $P < 0.01$; ***, $P < 0.001$; ****, $P < 0.0001$).

Results

Tumor-derived tenascin-C dictates pathogenic TAM activity

Tenascin-C expression correlates with dismal prognosis in people with breast cancer (13) and is linked to earlier tumor onset and larger lung metastases in immunocompetent mouse models of this disease (13, 18). A number of potential cellular sources of this matrix molecule are found in the TME. It can be derived from stromal cells (such as cancer-associated fibroblasts; ref. 30), immune cells (31), and tumor cells themselves (32). To dissect the contribution of tenascin-C from different sources to the immune axis in breast cancer, we first grafted mammary tumor cells expressing high tenascin-C (TNC^+) or expressing low tenascin-C (TNC^-) into the mammary gland of wild-type mice. This model enables specific examination of the impact of tenascin-C expressed by the tumor cell in the context of a wild-type host response to tumor engraftment. As described previously (18), grafting TNC^+ tumor cells resulted in accelerated tumor growth compared with grafting TNC^- tumor cells (**Fig. 1A** and **B**;

Published OnlineFirst January 15, 2020; DOI: 10.1158/2326-6066.CIR-19-0276

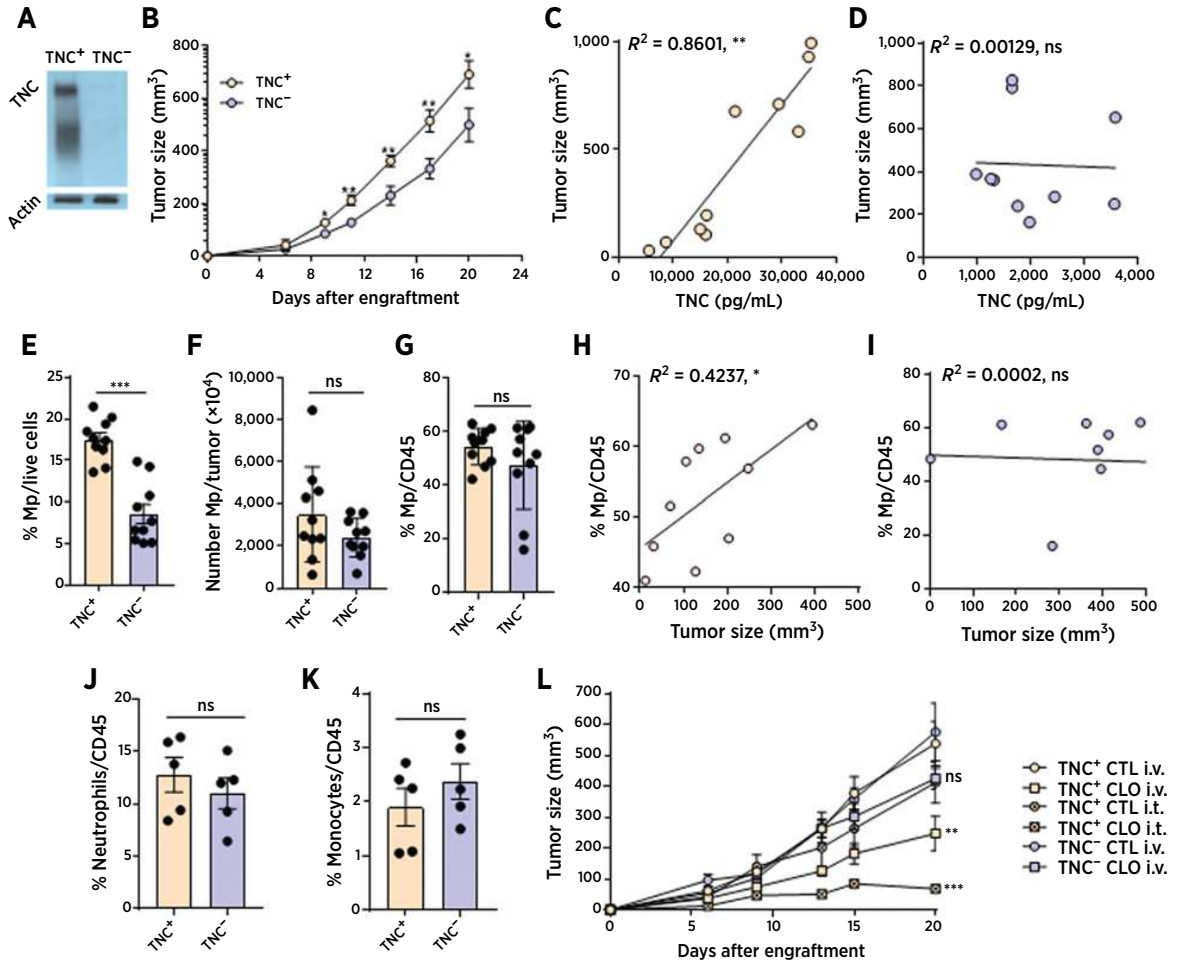

Figure 1.

Tumor-derived tenascin-C favors tumor growth in association with macrophages. **A,** Representative Western blot of tenascin-C expression in NT193 TNC$^+$ and TNC$^-$ murine mammary tumor cell lines in culture before grafting. **B,** Tumor growth of wild-type mice engrafted with TNC$^+$ (orange) or TNC$^-$ (purple) tumor cells; $n = 8$/group. Correlation between TNC$^+$ (**C**) and TNC$^-$ (**D**) tumor size 3 weeks after engraftment and the concentration of tenascin-C expressed by tumor cells extracted from corresponding tumors; $n = 10$/group. **E–G,** Number and percentage of macrophages (Mp, CD45$^+$F4/80$^+$CD11b$^+$CD11c$^+$) in TNC$^+$ and TNC$^-$ tumors 3 weeks after engraftment and their correlation with the size of TNC$^+$ (**H**) and TNC$^-$ (**I**) tumors at the time of sacrifice; $n = 10$/group. **J** and **K,** Percentage of neutrophils (CD45$^+$CD11b$^+$CD115$^-$Ly6C$^+$Ly6G^{hi}) and monocytes (CD45$^+$CD11b$^+$CD115$^+$Ly6C$^+$) in TNC$^+$ and TNC$^-$ tumors 3 weeks after engraftment. **L,** Tumor growth of TNC$^+$ and TNC$^-$ tumor–bearing mice that received an intravenous (i.v.) or intratumoral (i.t.) injection of clodronate liposomes (CLO) or control liposomes (CTL); $n = 5$–10/group. Data are representative of at least two independent experiments and are represented as the mean ± SEM. Mann–Whitney nonparametric *t* test was used to compare data sets. *, $P < 0.05$; **, $P < 0.01$; ***, $P < 0.001$. ns, not significant; TNC, tenascin-C.

Supplementary Fig. S1A and S1B), despite comparable cell proliferation *in vitro* (Supplementary Fig. S1C). We further showed that tumor size correlated with the concentration of tumor-derived tenascin-C following grafting of TNC$^+$ cells (**Fig. 1C** and **D**). Tumor size did not correlate with total levels of tenascin-C in the tumor following grafting of either TNC$^+$ or TNC$^-$ cells (Supplementary Fig. S1D–S1G). These data implied a pathogenic role for tumor cell–derived tenascin-C that is not compensated for by expression of host-derived tenascin-C in TNC$^-$ tumors. Flow-cytometric analysis of TNC$^+$ and TNC$^-$ tumors 3 weeks after engraftment revealed a high percentage of TAM in the immune infiltrate, with fewer macrophages per live cells observed in TNC$^-$ tumors compared with TNC$^+$ tumors (**Fig. 1E**). Although TNC$^+$ and TNC$^-$ tumors contained comparable numbers of macrophages per tumor volume and a similar proportion of macrophages within the CD45$^+$ compartment (**Fig. 1F** and **G**), the proportion of TAM correlated with tumor growth only in mice engrafted with TNC$^+$ tumor cells (**Fig. 1H** and **I**). This effect was specific to macrophages. The proportion of neutrophils and monocytes was not affected by tumor cell expression of tenascin-C (**Fig. 1J** and **K**) nor was tumor growth linked to the proportion of these myeloid cell subsets [neutrophils, TNC$^+$: $R^2 = 0.05773$ (ns), TNC$^-$: $R^2 = 0.07005$ (ns); monocytes, TNC$^+$: $R^2 = 0.001424$ (ns), TNC$^-$: $R^2 = 0.02704$ (ns)]. Phagocyte depletion by intravenous administration of clodronate liposomes following engraftment of TNC$^+$ or TNC$^-$ tumor cells significantly reduced the growth of TNC$^+$ tumors but had little impact on TNC$^-$ tumors. Administration of clodronate liposomes

Published OnlineFirst January 15, 2020; DOI: 10.1158/2326-6066.CIR-19-0276

intratumorally almost completely prevented the growth of TNC$^+$ tumors (**Fig. 1L**). Together, these data indicate that the levels of tumor cell–derived tenascin-C within the TME contribute to TAM pathogenicity.

Tenascin-C modulates TAM phenotype and spatial positioning

To determine whether tumor cell–derived tenascin-C fostered changes in macrophage behavior, we assessed qualitative differences in TAM phenotype following the engraftment of TNC$^+$ and TNC$^-$ tumor cells into wild-type mice. Macrophages from TNC$^+$ tumors comprised a higher proportion of CD206$^+$ macrophages than TNC$^-$ tumors, whereas the proportion of IRF5$^+$ macrophages was comparable (**Fig. 2A–C**), suggesting elevated M2-like, immune-suppressive macrophages in a tenascin-C–rich TME. Expression of M1 macrophage–associated genes, including *Tnf* and *Cd86*, was lower in macrophages sorted from TNC$^+$ tumors compared with macrophages sorted from TNC$^-$ tumors, whereas expression of M2 macrophage–associated genes, including *Mrc1* (CD206) and *Arg1*, were significantly elevated in macrophages isolated from a tenascin-C–rich TME (**Fig. 2D**). Macrophages isolated from TNC$^+$ tumors also exhibited lower CD86, MHCI, and MHCII surface expression than TNC$^-$ tumors (**Fig. 2E–G**), suggesting an immature phenotype restricted to CD206$^+$ (*Mrc1*) subset (Supplementary Fig. S2A and S2B). Coculture of BMM isolated from naïve, wild-type mice with TNC$^+$ or TNC$^-$ tumor cells recapitulated these data. Surface expression of CD206 was significantly higher on BMM in TNC$^+$ tumor cell cultures and MHCI and MHCII were significantly reduced compared with BMM cocultured with TNC$^-$ tumor cells or to BMM activated with lipopolysaccharide (LPS; Supplementary Fig. S2C–S2E). Cocultures containing either TNC$^+$ or TNC$^-$ tumor cells secreted little detectable IL1β, IL4, IL10, and IL12 but secreted more TGFβ and similar IL8 compared with LPS-activated cells. Cocultures containing TNC$^+$ tumor cells secreted higher IL6 and expressed lower iNOS than TNC$^-$ cells (**Fig. 2H**). Immunofluorescent staining of tumors revealed that F4/80$^+$ macrophages colocalized with tenascin-C in niches or tracks extending throughout the TME within both TNC$^+$ and TNC$^-$ tumors, although these tracks appeared thinner in TNC$^-$ tumors. Costaining with CD206 confirmed a higher number of CD206$^+$ TAM in TNC$^+$ tumors, whereas fewer CD206$^+$ TAM were detected in TNC$^-$ tumors (**Fig. 2I–K**; Supplementary Fig. S2F). Together, these data demonstrated that macrophage positioning in tenascin-C–rich niches in the TME occurred irrespective of tenascin-C expression by the tumor and that high tumor-derived tenascin-C was associated with phenotypic changes in TAM, favoring an immature CD206$^+$CD86^{lo}MHCI^{lo}MHCII^{lo} phenotype.

Host-derived tenascin-C contributes to an antitumoral TAM phenotype

Our results showed that tumor cell–derived tenascin-C promoted an immune-suppressive, protumoral, M2-like macrophage response. However, both stromal and immune cells within the TME can also synthesize tenascin-C. Studies showing that mice lacking tenascin-C fail to effectively recruit and polarize M1-like macrophages in response to experimental myocardial infarction or aortic constriction (33, 34) prompted us to investigate whether host-derived tenascin-C promoted antitumoral macrophage behavior. To address this, we grafted mammary tumor cells expressing high tenascin-C (TNC$^+$) into the mammary gland of wild-type mice or into the mammary gland of tenascin-C–null mice. This model enables examination of the impact of tenascin-C expressed by the host without changing the tumor cell–derived tenascin-C. Flow-cytometric analysis revealed fewer macrophages in tumors grafted into tenascin-C–null mice compared with tumors grafted into wild-type mice (**Fig. 3A**). Macrophages from tumors grafted into knockout mice comprised a higher proportion of CD206$^+$ macrophages than wild-type mice (**Fig. 3B**) and exhibited lower MHCII surface expression (**Fig. 3C**). Expression of M1 macrophage–associated genes, including *Cd86, Irf5*, and *Nos2,* was lower in tumors isolated from tenascin-C knockout mice compared with wild-type mice, whereas expression of the M2 macrophage–associated gene *Arg1* was elevated in tumors from knockout mice (Supplementary Table S1). Immunofluorescence staining revealed that F4/80$^+$ macrophages colocalized with tenascin-C tracks in tumors grafted into both wild-type and tenascin-C–null mice, whereas costaining with CD206 confirmed a higher number of CD206$^+$ TAM in tumors from tenascin-C knockout mice compared with wild-type mice (**Fig. 3D** and **E**). Together, these data indicated that host-derived tenascin-C drove an M1-like TAM response comprising a CD206^{lo}MHCII^{hi} phenotype.

Tumor-derived tenascin-C–programmed macrophages drive altered TIL responses

Our data indicated that TAM function differently within TMEs in which tumor- versus host-derived tenascin-C dominated and suggest that high tenascin-C expression by tumor cells subverted host defense responses by switching the TAM phenotype from an antitumoral phenotype toward a protumoral phenotype. To further examine the consequences of TAM reprogramming by tumor-derived tenascin-C, we assessed whether the altered phenotype and cytokine profile of macrophages following grafting of TNC$^+$ and TNC$^-$ tumor cells into wild-type mice affected macrophage effector function. We cocultured purified splenic T cells from naïve wild-type FVB mice with TNC$^+$ or TNC$^-$ tumor cells in the presence or absence of naïve wild-type BMM. T cells cultured with tumor cells alone exhibited low proliferation, which was comparable between TNC$^+$ and TNC$^-$ tumors. However, T cells cultured with TNC$^+$ tumor cells and BMM proliferated significantly less than T cells cultured with TNC$^-$ tumor cells and BMM (**Fig. 4A** and **B**). Similarly, CD11b$^+$ cells sorted from TNC$^-$ tumors were associated with significantly more T-cell proliferation than CD11b$^+$ cells isolated from TNC$^+$ tumors (**Fig. 4C**), suggesting that TNC$^+$-associated macrophages were less efficient at driving T-cell proliferation. CD11b$^+$ cells sorted from TNC$^+$ tumors drove significantly more IL17 synthesis in culture with naïve T cells than CD11b$^+$ cells isolated from TNC$^-$ tumors. IFNγ remained unchanged (**Fig. 4D** and **E**), consistent with a higher proportion of Th17 cells in TNC$^+$ tumors compared with TNC$^-$ tumors (**Fig. 4F** and **G**). Together, these results support a dual role for macrophages programmed by tumor cell–derived tenascin-C in the generation of Th17-based inflammation, accompanied by a phenotype that fails to support T-cell proliferation.

TLR4 activation by the FBG domain of tenascin-C drives the altered TAM phenotype

We next investigated the mechanism by which tumor-derived tenascin-C affects macrophage behavior. Tenascin-C is a large multimodular molecule comprising a series of different domains that each exert specific effects on cell behavior through distinct receptor binding capabilities, including integrins, epidermal growth factor receptor (EGFR), and TLR4 (17). Surface expression of MHCII (**Fig. 5A**) and IL6 synthesis (**Fig. 5B**) by wild-type BMM in coculture with TNC$^+$ tumor cells was rescued to levels exhibited by wild-type BMM cocultured with TNC$^-$ tumor cells by adding increasing doses of TAK242, a small-molecule inhibitor of TLR4 signaling. Inhibition of RGD-dependent integrin binding using echistatin or inhibition of EGFR kinase activity using tyrphostin had no effect on the BMM

Published OnlineFirst January 15, 2020; DOI: 10.1158/2326-6066.CIR-19-0276

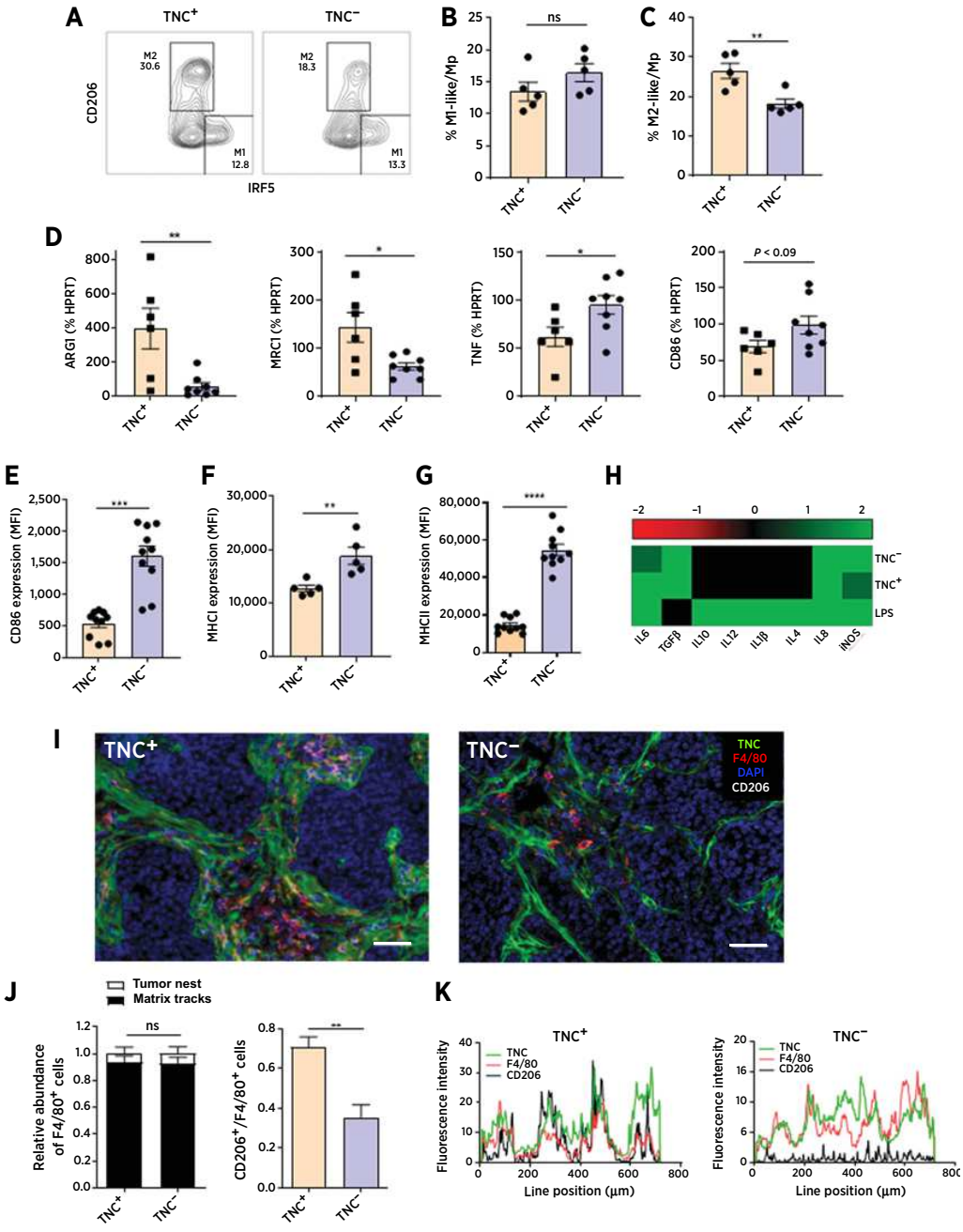

Figure 2.

Tumor-derived tenascin-C skews the phenotype of TAM. Representative plots (**A**) and percentage of M1-like (defined as IRF5$^+$; **B**) and M2-like (defined as CD206$^+$; **C**) macrophages in TNC$^+$ and TNC$^-$ tumors 3 weeks after engraftment into wild-type mice; $n = 5$/group. **D,** Gene-expression analysis of macrophages sorted from TNC$^+$ or TNC$^-$ tumors. Data are expressed relative to expression of the endogenous control gene *Hprt*; $n = 6$ (TNC$^+$) or 8 (TNC$^-$). **E–G,** Expression of CD86, MHCI, and MHCII on macrophages from TNC$^+$ or TNC$^-$ tumors; $n = 5$–10/group. **H,** Heat map representation of IL1β, IL4, IL6, IL8, IL10, IL12, TGFβ secretion, and intracellular iNOS during coculture of naïve BMM with TNC$^+$ or TNC$^-$ tumor cells for 5 days or following LPS activation. Data are expressed relative to unstimulated BMM cultured for 5 days in the absence of tumor cells; $n = 3$–6/group. **I,** Representative images of tenascin-C, F4/80, and CD206 localization in TNC$^+$ and TNC$^-$ tumors 3 weeks after engraftment into wild-type mice. **J,** Quantification of the number of F4/80$^+$ cells in tenascin-C–rich tracks or in the tumor stroma (left), and the proportion of CD206$^+$ cells in TNC$^+$ or TNC$^-$ tumors; $n = 5$/group (right). **K,** The fluorescence intensity of tenascin-C, F4/80, and CD206 in each tumor displayed in the corresponding image in Supplementary Fig. S2F (dashed line). Scale bars, 50 μm. Data are representative of at least two independent experiments and are represented as the mean ± SEM. Mann–Whitney nonparametric *t* test was used to compare data sets. *, $P < 0.05$; **, $P < 0.01$; ***, $P < 0.001$; ****, $P < 0.0001$. ns, not significant; TNC, tenascin-C.

Published OnlineFirst January 15, 2020; DOI: 10.1158/2326-6066.CIR-19-0276

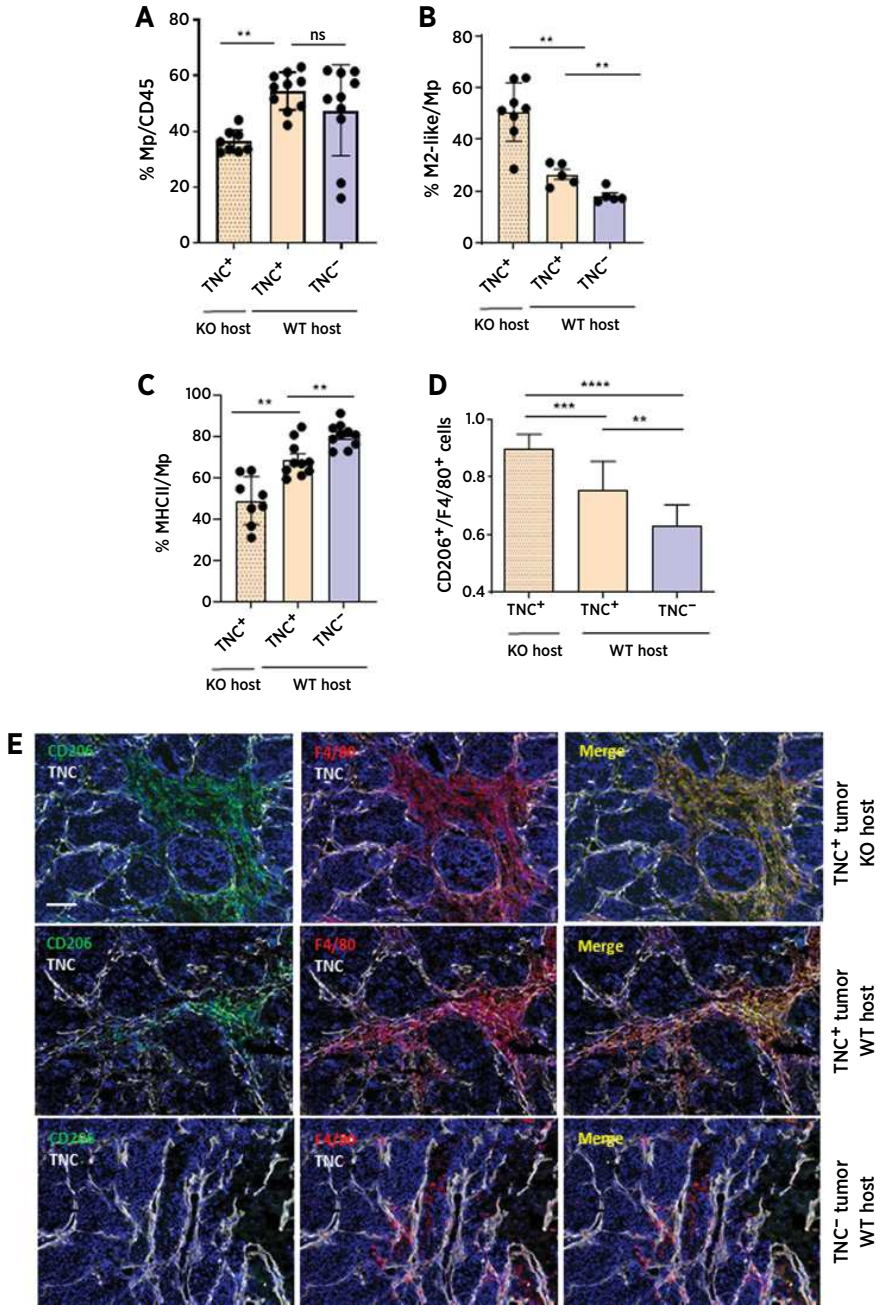

Figure 3.

Host-derived tenascin-C promotes an antitumoral macrophage phenotype. **A,** Percentage of macrophages (Mp, $CD45^+F4/80^+CD11b^+CD11c^+$) in TNC^+ and TNC^- tumors 3 weeks after engraftment into wild-type (WT) or tenascin-C–null (KO) mice. Percentage of M2-like ($CD206^+$; **B**) and $MHCII^+$ (**C**) macrophages in tumors 3 weeks after engraftment; n = 5–10/group. **D,** Quantification of the proportion of $CD206^+$ cells among $F4/80^+$ cells in tumor sections. **E,** Representative images of tenascin-C, F4/80, and CD206 localization 3 weeks after tumor engraftment; $n = 5$/group. Data are representative of at least two independent experiments and are represented as the mean ± SEM, except for the box and whiskers graphs, representing the median, and minimum to maximum values. Mann–Whitney nonparametric t test was used to compare data sets. Scale bar, 100 μm. **, $P < 0.01$; ***, $P < 0.001$; ****, $P < 0.0001$. ns, not significant; TNC, tenascin-C.

phenotype (Supplementary Fig. S3A–S3D). Addition of TAK242 also rescued the proliferation of T cells in coculture with BMM and TNC^+ tumor cells (**Fig. 5C** and **D**). Antibodies that prevent the FBG domain of tenascin-C from binding to and activating TLR4 (20) recovered expression of MHCII by BMM (**Fig. 5E**), decreased IL6 production (**Fig. 5F**), and rescued $CD8^+$ T-cell proliferation (**Fig. 5G** and **H**) in cocultures with TNC^+ tumor cells. Together, these data indicated that FBG activation of TLR4 was necessary for tumor-derived tenascin-C–mediated macrophage polarization *in vitro*.

Anti-FBG immunotherapy reduces primary tumor growth and metastasis

We next determined whether blocking FBG activation of TLR4 affected macrophage phenotype *in vivo*, and if this affected tumor growth and spread. We titrated 3 doses of anti-FBG, starting treatment 24 hours after mammary gland engraftment of TNC^+ tumor cells into wild-type mice, based on dosing from preclinical models of arthritis (20). To benchmark the effects of anti-FBG, we used anti–PD-L1 due to the reported efficacy in patients with breast cancer (35),

Published OnlineFirst January 15, 2020; DOI: 10.1158/2326-6066.CIR-19-0276

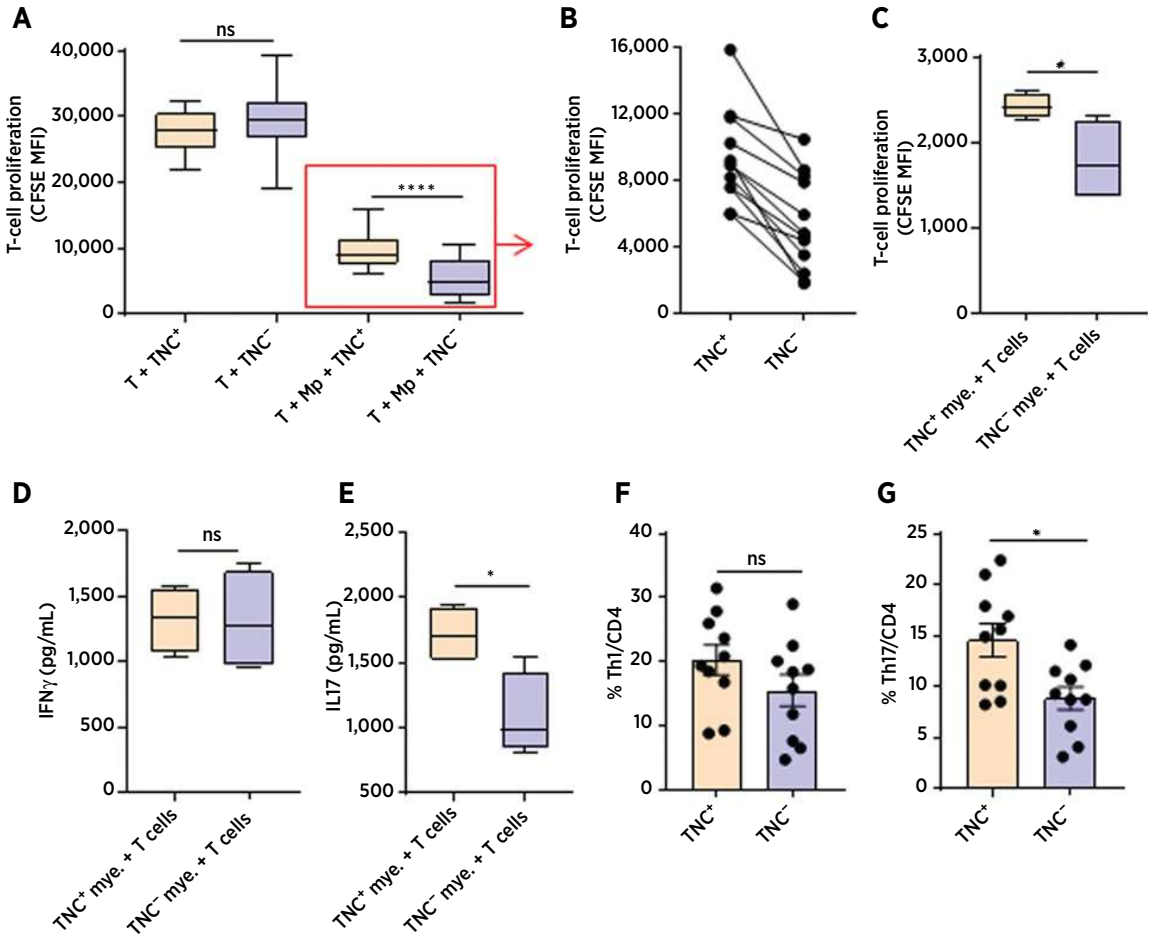

Figure 4.

Tenascin-C–conditioned macrophages fail to support T-cell proliferation and favor the polarization of Th17 cells. Naïve wild-type T cells loaded with CFSE dye were cocultured for 10 days with TNC^+ or TNC^- tumor cells in the presence (T + Mp + $TNC^{+/-}$) or absence (T + $TNC^{+/-}$) of naïve wild-type BMM; $n = 10$/group. **A,** CFSE MFI indicating T-cell proliferation under the indicated conditions. **B,** Closer assessment of the boxed data set in **A**. **C,** Proliferation of naïve T cells cultured in the presence of $CD11b^+$ myeloid cells sorted from TNC^+ (TNC^+mye) or TNC^- tumors (TNC^- mye); $n = 6$/group. Quantification of secreted IFNγ (**D**) and IL17 (**E**) from cultures of naïve T cells with $CD11b^+$ cells sorted from TNC^+ and TNC^- tumors; $n = 6$/group. Percentage of Th1 ($CD45^+CD3^+CD4^+IFN\gamma^+$; **F**) and Th17 ($CD45^+CD3^+CD4^+IL17A^+$; **G**) cells in TNC^+ and TNC^- tumors 3 weeks after engraftment; $n = 10$/group. Data are representative of at least two independent experiments and are represented as the mean ± SEM, except for the box and whisker graphs, representing the median, and minimum to maximum values. Mann–Whitney nonparametric *t* and parametric *t* tests were used to compare data sets. *, $P < 0.05$; ****, $P < 0.0001$. ns, not significant; TNC, tenascin-C.

selecting a dosage known to reduce tumor volume in both spontaneous and grafting murine models of breast cancer (21, 36). Antibody treatment was well tolerated, and mice exhibited no side effects (Supplementary Fig. S4A). Treatment with anti-FBG led to a dose-dependent reduction in the growth of primary tumors compared with isotype control–treated mice (Supplementary Fig. S4B) and had comparable efficacy to anti–PD-L1 treatment (**Fig. 6A**). Treatment with 10 mg/kg of anti-FBG did not affect the size of metastases observed in the lungs but was associated with reduced incidence of lung metastasis, with fewer metastases observed in animals that received anti-FBG compared with isotype control antibody ($P = 0.058$; Supplementary Fig. S4C). Anti-FBG treatment also significantly increased expression of TLR4 and MHCII on TAM, decreased Th17 cell abundance, and induced a trend toward a higher proportion of tumor-infiltrating $CD8^+$ T cells (**Fig. 6B–G**). Anti-FBG treatment did not influence the localization of $F4/80^+$ cells within tenascin-C–rich tracks in the TME, but these cells were less clustered within the TME. Anti-FBG treatment was also associated with fewer $CD206^+$ macrophages that were restricted to the periphery of the tumor compared with isotype control–treated tumors (**Fig. 6H**).

To assess the efficacy of anti-FBG treatment in a more heterogeneous model that better recapitulates spontaneous tumor progression, we used MMTV-NeuNT FVB mice, which develop mammary tumors and lung metastases around 6 months of age. Upon tumor detection, mice were treated with anti-FBG alone, anti–PD-L1 alone, the 2 antibodies in combination, or their respective isotype controls. Treatment with anti-FBG alone led to a reduction of tumor growth comparable to treatment with anti–PD-L1 alone (**Fig. 6I**), whereas

Published OnlineFirst January 15, 2020; DOI: 10.1158/2326-6066.CIR-19-0276

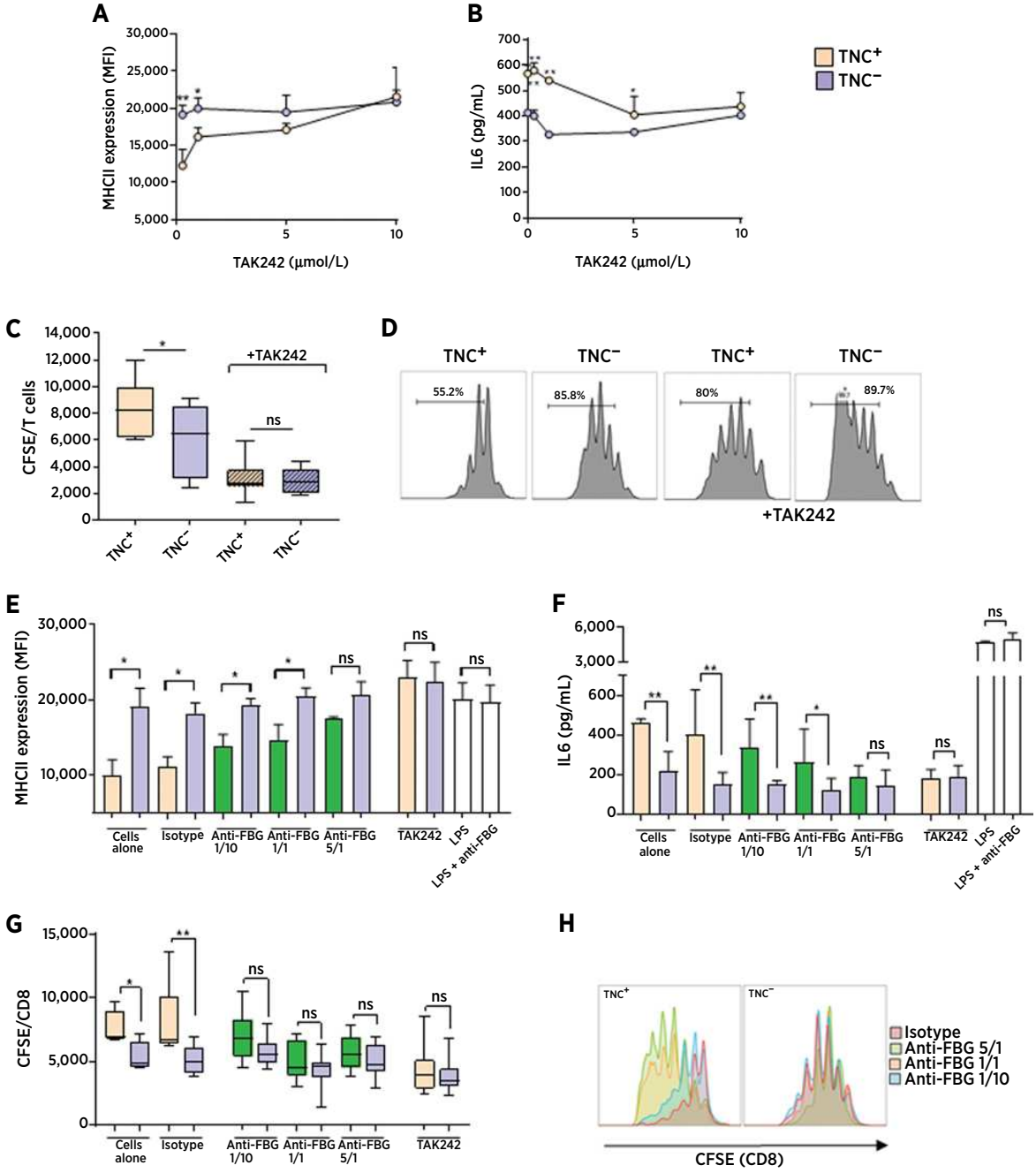

Figure 5.

Activation of TLR4 by the FBG domain of tenascin-C induces a phenotypic switch in macrophages. Expression of MHCII (**A**) and secretion of IL6 (**B**) by BMM after coculture with TNC$^+$ or TNC$^-$ tumor cells for 5 days in the presence of increasing doses of TAK242; $n = 4$/group. **C** and **D,** Proliferation (by CFSE) of naïve purified T cells cocultured with BMM and TNC$^+$ or TNC$^-$ tumor cells in the presence of TAK242; $n = 8$/group. Expression of MHCII (**E**) and secretion of IL6 (**F**) by BMM after coculture with TNC$^+$ or TNC$^-$ tumor cells for 5 days in the presence of anti-FBG at a molar ratio of 1:10, 1:1, or 5:1 to the concentration of tenascin-C produced by TNC$^+$ tumor cells over 5 days of culture (green), isotype control (5:1), or 5 μmol/L TAK242. Stimulation of BMM with LPS in the absence of tumor cells (white) was not susceptible to anti-FBG treatment; $n = 3$–6/group. **G** and **H,** Proliferation of naïve purified T cells cocultured with BMM and TNC$^+$ or TNC$^-$ tumor cells in the presence of anti-FBG; $n = 4$–8/group. Data are representative of at least two independent experiments and are represented as the mean ± SEM, except for the box and whisker graphs, representing the median, and minimum to maximum values. Mann–Whitney non-parametric *t* test was used to compare data sets. *, $P < 0.05$; **, $P < 0.01$. ns, not significant; TNC, tenascin-C.

Published OnlineFirst January 15, 2020; DOI: 10.1158/2326-6066.CIR-19-0276

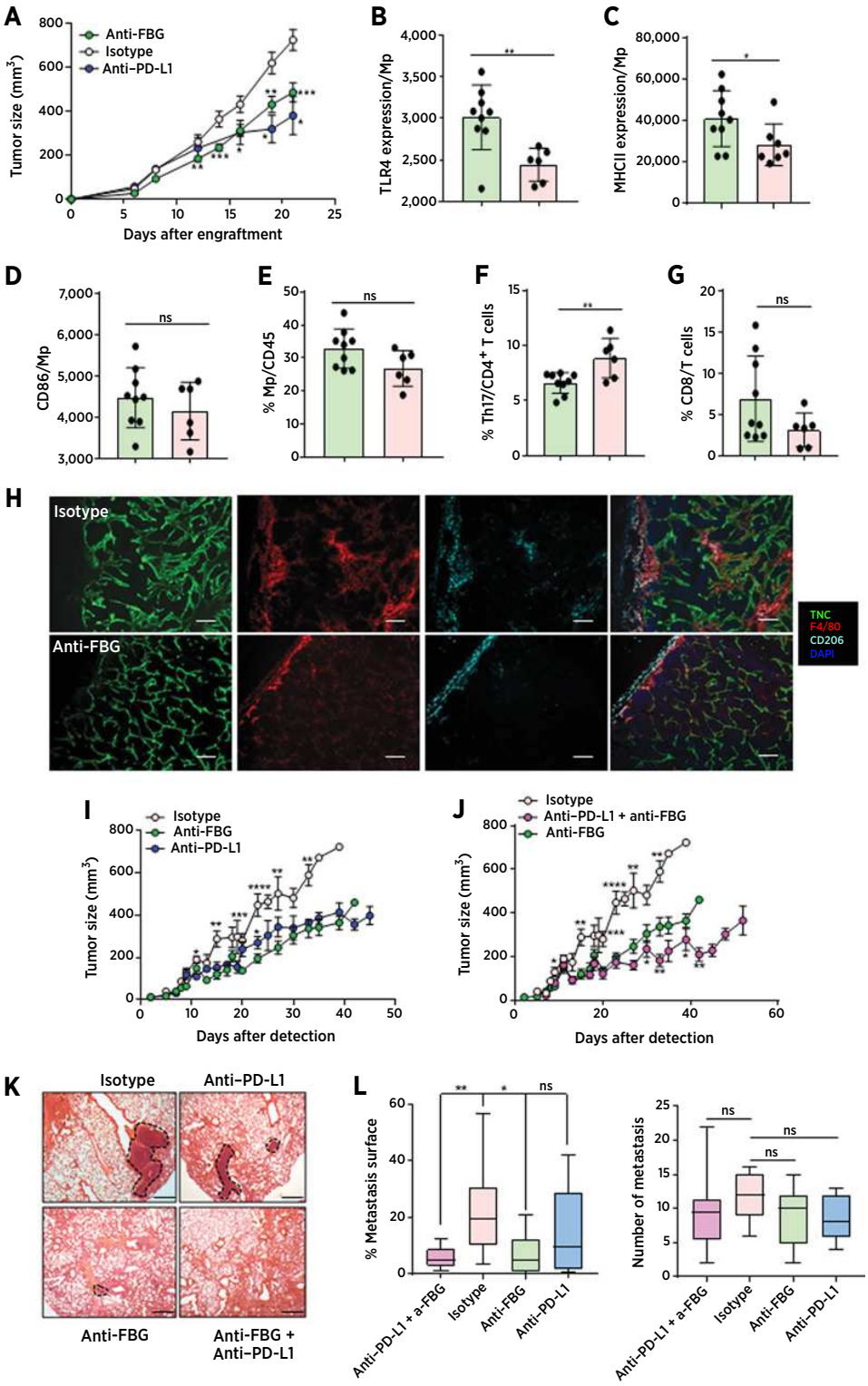

Published OnlineFirst January 15, 2020; DOI: 10.1158/2326-6066.CIR-19-0276

combination treatment led to significantly enhanced, and sustained, inhibition of tumor growth (**Fig. 6J**). Treatment with anti-FBG alone or together with anti–PD-L1 led to a significant reduction in the percentage of TAM and augmentation of the proportion of $CD8^+$ T cells compared with the isotype group and to treatment with anti–PD-L1 alone. MHCII was upregulated in the combination group alone (Supplementary Fig. S5). Finally, treatment with anti-FBG alone or together with anti–PD-L1 reduced the size of lung metastases compared with the isotype group and to treatment with anti–PD-L1 alone (**Fig. 6K** and **L**). Together, these results demonstrated that anti-FBG treatment could reduce both primary tumor growth and metastasis and that combination treatment with anti–PD-L1 results in significantly improved outcome compared with either antibody alone, with anti-FBG providing an effect on tumor spread that was not obtained by checkpoint inhibition alone.

Tenascin-C is associated with a prognostic immune signature in human breast tumors

To investigate whether the tenascin-C–dependent pathogenic TAM phenotypes we observed in the mouse were conserved in human disease, bulk RNA-seq data of 1,045 human breast tumors from TCGA were analyzed. Pairwise correlations of tenascin-C revealed significant positive associations with macrophage-related genes (*CD68* and *CSF1R*) and genes associated with the polarization of macrophages toward a protumoral M2-like phenotype (*CD163, CD204, CD206,* and *TGM2*), but not with other genes, including markers of cell proliferation (*Ki67*) or M1-like phenotype (*IRF5*; **Fig. 7A**). To gain insight into the composition of the tumoral immune compartment, CIBERSORT analysis was performed to computationally deconvolve the estimated abundances of 22 different immune cell types. The predicted immune infiltrate was predominantly composed of M2-like macrophages and a reciprocally low infiltration of proinflammatory M1-like macrophages (**Fig. 7B**), consistent with published literature (7). Stratification of tumors based upon tenascin-C expression and predicted M2-infiltration indicated that patients with combined tenascin-C–low and M2-low status were completely protected up to 10 years after diagnosis, whereas prognosis was poorer for patients whose tumors contained higher tenascin-C and M2 macrophages (**Fig. 7C**). Together, these data implied an orthologous role for tenascin-C–mediated switching of TAM phenotype that may contribute to the progression of human disease.

Discussion

High numbers of TAM correlate with poor prognosis in people with breast cancer (37). However, the factors driving TAM pathogenicity in this disease are not well understood. In this study, we showed that host-derived tenascin-C promoted antitumoral immunity in murine models of breast cancer, via recruitment of proinflammatory macrophages to the TME. In contrast, synthesis of this extracellular matrix protein by tumor cells promoted a phenotypic switch in macrophages that drove the prevalence of tumor-supportive TAM in the TME. We identified that engagement of TLR4 by the FBG domain of tumor cell–derived tenascin-C was required for tenascin-C–mediated macrophage polarization toward this phenotype *in vitro* and showed that targeting this interaction *in vivo* was sufficient to inhibit tumor growth and metastasis, conferring sustained therapeutic benefit in combination with immune-checkpoint inhibition. Finally, we observed that people with breast tumors with combined low tenascin-C expression and low M2 macrophage infiltrate exhibited improved prognoses, suggesting that tenascin-C–mediated evasion of immune elimination may also be relevant to human cancer.

As in human disease, high numbers of TAM infiltrate the TME in murine models of breast cancer, where they contribute to primary tumor growth and metastasis (7). Here, we showed that TAM pathogenicity was dependent on expression of tumor cell–derived tenascin-C within the TME and that engraftment of mammary tumor cells expressing high tenascin-C into wild-type mice favored an immature, M2-like ($CD206^{hi}MHCII^{lo}$) TAM phenotype compared with engraftment of cells expressing low tenascin-C. Grafting TNC^+ or TNC^- tumors cells into wild-type mice enabled us to specifically modulate tumor-derived tenascin-C. As a result, total tenascin-C concentrations in the TME were comparable following grafting of either type of tumor cell. However, the ratio of tumor- and host-derived tenascin-C was altered, with a shift toward more tumor cell–derived tenascin-C proving pathogenic. The proportion of infiltrating myeloid cells, and macrophage positioning within the tumor, were comparable following grafting of either TNC^+ or TNC^- tumor cells, whereas high tumor cell–derived tenascin-C promoted elevated numbers of $CD206^{hi}$ macrophages. These results contrast data showing that tenascin-C drives an M1-like macrophage phenotype in models of cardiac pathology, with more $CD206^{hi}$ macrophages observed in the hearts of tenascin-C–null mice, with higher expression of M2- and lower expression of M1-associated genes compared with wild-type mice (33, 34). This highlights a context specificity of tenascin-C modulation of macrophage behavior that is mirrored *in vitro*. Tenascin-C can induce aspects of both M1- and M2-like cell behavior, as well as fibrotic signaling, proangiogenic properties, or differentiation into foam cells, depending on the experimental setup (17). Macrophage behavior in tissues is defined by integrating multiple signals derived from the microenvironment (9), and our study highlights the importance of the cellular source of these signals.

Within the TME, tenascin-C can be produced by stromal and immune cells, and by tumor cells. To determine whether macrophages responded differently to tenascin-C from different sources, we used an alternative experimental setup in which we grafted TNC^+ tumors into wild-type or tenascin-C knockout mice, where tumor cell–derived tenascin-C expression was kept constant. We observed a higher

Figure 6.

Treatment with anti-FBG reorganizes the immune infiltrate and limits tumor growth and spread *in vivo*. **A,** Tumor growth in mice that received anti–PD-L1 (blue), anti-FBG (10 mg/kg, green), or isotype control (beige) antibodies following grafting of TNC^+ tumor cells and using treatment regimes described in Materials and Methods ($n = 14$–16/group). **B–G,** Analysis of tumor-infiltrating immune cells in mice grafted with TNC^+ tumor cells that received anti-FBG treatment at 10 mg/kg (green) or isotype control (beige); $n = 6$–9/group. **H,** Representative images of the localization of tenascin-C, F4/80, and CD206 in anti-FBG– or isotype control–treated mice 21 days following grafting of TNC^+ tumors; $n = 4$/group. Scale bar, 200 μm. **I** and **J,** Tumor growth was assessed every 3 days in MMTV-NeuNT mice that were treated with either anti-FBG (10 mg/kg, green) or anti–PD-L1 (blue), the two antibodies together (pink), or isotype control (beige); $n = 10$–12/group. **K,** Lung histology representative of metastasis incidence of each group of MMTV-NeuNT mice treated as above. The dashed line delimits the metastasis area. **L,** Quantification of number and size of lung metastasis from MMTV-NeuNT mice treated as above. Scale bar, 200 μm. Data are representative of at least two independent experiments and are represented as the mean ± SEM, except for the box and whisker graphs, representing the median, and minimum to maximum values. Mann–Whitney nonparametric *t* and parametric *t* tests were used to compare data sets. *, $P < 0.05$; **, $P < 0.01$; ***, $P < 0.001$; ****, $P < 0.0001$. ns, not significant; TNC, tenascin-C.

Published OnlineFirst January 15, 2020; DOI: 10.1158/2326-6066.CIR-19-0276

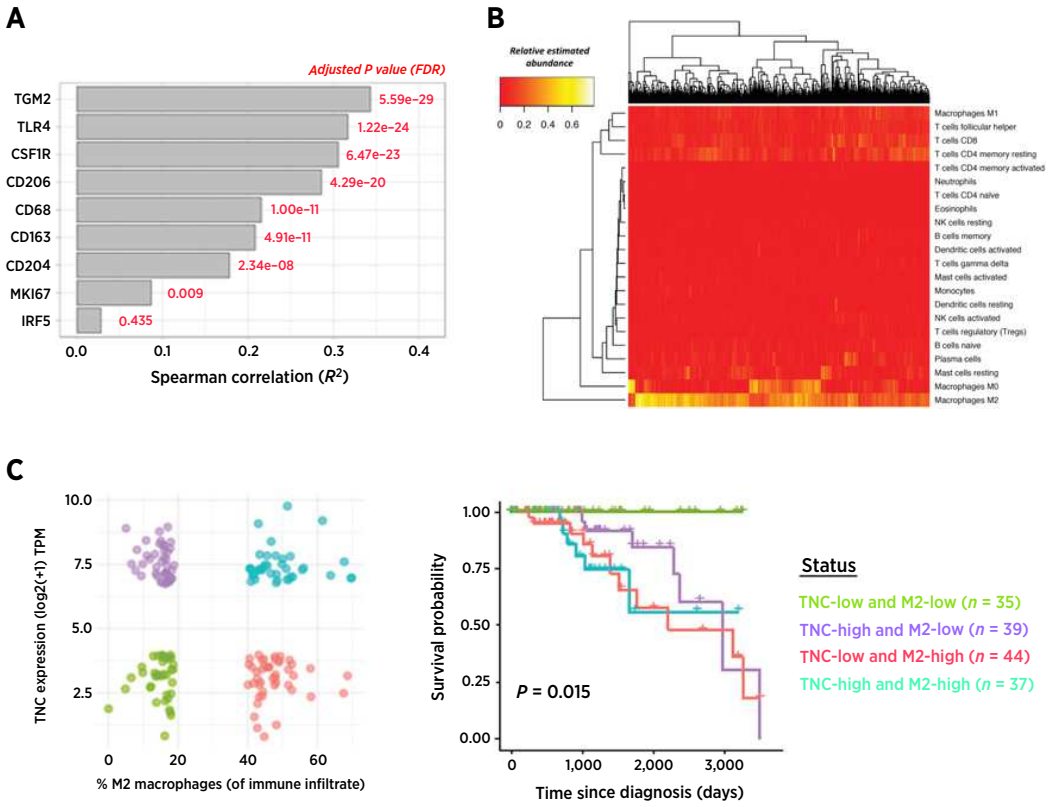

Figure 7.

Tenascin-C expression is associated with a pathogenic TAM phenotype and disease prognosis in human breast cancer. **A,** Pairwise Spearman correlations of tenascin-C with macrophage-related genes in TCGA bulk RNA-seq data set for human invasive breast carcinoma. Analysis was performed on 1,045 tumor samples from individual donors, and *P* values were adjusted with the Benjamini–Hochberg correction (FDR). **B,** Estimation of tumor-infiltrating immune cell proportions by CIBERSORT analysis, visualized by heat map and hierarchical clustering, $n = 1{,}021$. NK, natural killer. **C,** Stratification of tumors according to tenascin-C expression and estimated M2 macrophage abundance (left). Subsets in the upper or lower 20% of cases for both conditions were selected. Kaplan–Meier survival analysis of stratified tenascin-C and M2 subsets at 10 years after diagnosis (right). *P* values were calculated using the log-rank test, and *P* values < 0.05 were considered statistically significant. TNC, tenascin-C.

proportion of tumor-infiltrating macrophages in wild-type mice compared with knockout mice, consistent with the association of tenascin-C expression with macrophage infiltration in a range of other human (38–40) and murine pathology (13, 34, 41, 42), and its ability to promote macrophage migration *in vitro* (43). Also, in our model, a greater proportion of macrophages exhibited a $CD206^{hi}MHCII^{lo}$ phenotype in the absence of host-derived tenascin-C, consistent with data that indicate a role for host-derived tenascin-C in polarizing proinflammatory cell behavior (33, 34). Together, these data indicate that tenascin-C made by the host comprises part of innate defense, facilitating macrophage infiltration and organization, and favoring an aggressive M1-like phenotype, but that deposition of tenascin-C by incipient tumor cells acts locally to switch the phenotype of these macrophages to prevent elimination by the immune system.

To further investigate the mechanism by which tumor-derived tenascin-C switched TAM phenotype, we cocultured TNC^+ or TNC^- mammary tumor cells together with naïve, wild-type BMM. This model revealed that the BMM phenotype induced by tumor cell–derived tenascin-C could be reversed by inhibiting TLR4 signaling and by blocking the ability of the FBG domain of tenascin-C to bind to and activate TLR4. We also showed that treating mice with grafted TNC^+ tumors, or mice that develop spontaneous mammary tumors, with anti-FBG could effectively reduce tumor size and spread to the lungs. TAM contribute to primary tumor growth and metastasis by stimulating angiogenesis, inducing tumor cell migration, invasion, and intravasation, promoting epithelial-to-mesenchymal transition, and suppressing antitumor immunity (44–46). Although our coculture assays revealed some insight into the functional capabilities of macrophages programmed by TNC^+ tumor cells, suggesting an immune-suppressive phenotype that failed to support optimal T-cell proliferation and favored Th17 cell polarization, the precise pathogenic nature of these cells *in vivo* remains to be elucidated. Reduced Th17 cell abundance in the TME of TNC^- tumors and in anti-FBG–treated grafted tumors is consistent with data from murine models of arthritis (20). This may be of interest for further investigation given that IL17 is associated with poor prognosis in breast cancer patients (47), favors PD-L1 expression and lung metastasis, and reduces antitumor immunity in murine models of breast cancer (48). We also found here that anti-FBG therapy reduced primary tumor burden to a degree comparable to anti–PD-L1 treatment, an effect that was sustained following combination treatment, but only treatment with anti-FBG reduced

Published OnlineFirst January 15, 2020; DOI: 10.1158/2326-6066.CIR-19-0276

the size of lung metastases. These findings are consistent with data showing that high expression of tenascin-C in breast cancer is associated with marked acceleration of metastases to the lungs (13). However, whether tenascin-C–programmed TAM are directly, or solely, responsible for enhanced tumor spread within mammary tumors that comprise mixed populations of TLR4-expressing cells is not yet known, and further investigation of the impact of anti-FBG treatment on the tumor as a whole is warranted.

The prognostic value of TAM in breast cancer is not straightforward (37), and data indicate that combining phenotypic markers with TAM location may provide better diagnostic sensitivity (49). Further investigation of how matrix molecules, derived from either host or tumor, dictate macrophage distribution throughout the TME may highlight novel mechanisms underpinning these clinical observations. Our data suggest that tumor- and host-derived tenascin-C contribute differently to TAM behavior, necessitating further detailed molecular analysis of tenascin-C from different cellular sources. In tumor tissue where tenascin-C expression is low or absent, we observed a protective effect, with no deaths by 10 years, in people classified as tenascin-C–low, M2-low. Altogether, our data highlight one way in which tumor cells evade immune elimination: by synthesis of the immunomodulatory matrix molecule tenascin-C, which switches TAM phenotype.

Disclosure of Potential Conflicts of Interest

K.S. Midwood is a consultant for, reports receiving a commercial research grant from, and has ownership interest (including patents) in Nascient Ltd. No potential conflicts of interest were disclosed by the other authors.

Authors' Contributions

Conception and design: C. Deligne, R. Carapito, I. Velazquez-Quesada, Z. Sun, G. Orend, K.S. Midwood

Development of methodology: C. Deligne, D. Murdamoothoo, Z. Sun

Acquisition of data (provided animals, acquired and managed patients, provided facilities, etc.): C. Deligne, D. Murdamoothoo, M. Gschwandtner, W. Erne, T. Loustau, A.M. Marzeda, R. Carapito, I. Mazzier, Z. Sun

Analysis and interpretation of data (e.g., statistical analysis, biostatistics, computational analysis): C. Deligne, D. Murdamoothoo, A.N. Gammage, T. Loustau, N. Paul, K.S. Midwood

Writing, review, and/or revision of the manuscript: C. Deligne, D. Murdamoothoo, A.N. Gammage, M. Gschwandtner, W. Erne, T. Loustau, A.M. Marzeda, I. Velazquez-Quesada, I. Mazzier, G. Orend, K.S. Midwood

Administrative, technical, or material support (i.e., reporting or organizing data, constructing databases): C. Deligne, R. Carapito

Acknowledgments

This work was supported by grants from Worldwide Cancer Research (14-1070), the Medical Research Council, Nascient Ltd., the Kennedy Trust for Rheumatology Research, the Austrian Science Fund (FWF; J-4102), the Institut National contre le Cancer (INCa, TENPLAMET), Ligue Regional contre le Cancer Grand Est to G. Orend, fellowships to D. Murdamoothoo (Fondation ARC pour la Recherche sure le Cancer), I. Velazquez-Quesada (Conacyt Mexico), Z. Sun (Chinese Scholarship Council), and W. Erne (French Ministry of Research), a Clarendon Fund Scholarship to A.N. Gammage, and a Versus Arthritis Senior Fellowship to K.S. Midwood (20003). The authors would like to express their gratitude to the staff of the Biological Safety Unit at the Kennedy Institute of Rheumatology, in particular Elizete Araujo, Dan Andrew, and Mino Medghalchi, to Richard Corderoy at the OQF, and to the staff of the GENOMAX sequencing facility of INSERM U1109.

The costs of publication of this article were defrayed in part by the payment of page charges. This article must therefore be hereby marked *advertisement* in accordance with 18 U.S.C. Section 1734 solely to indicate this fact.

Received April 16, 2019; revised October 23, 2019; accepted January 3, 2020; published first January 15, 2020.

References

1. Denkert C, von Minckwitz G, Darb-Esfahani S, Lederer B, Heppner BI, Weber KE, et al. Tumor-infiltrating lymphocytes and prognosis in different subtypes of breast cancer: a pooled analysis of 3771 patients treated with neoadjuvant therapy. Lancet Oncol 2018;19:40–50.
2. Savas P, Salgado R, Denkert C, Sotiriou C, Darcy PK, Smyth MJ, et al. Clinical relevance of host immunity in breast cancer: from TILs to the clinic. Nat Rev Clin Oncol 2016;13:228–41.
3. O'Donnell JS, Teng MWL, Smyth MJ. Cancer immunoediting and resistance to T cell-based immunotherapy. Nat Rev Clin Oncol 2019;16:151–67.
4. Poh AR, Ernst M. Targeting macrophages in cancer: from bench to bedside. Front Oncol 2018;8:49.
5. Mantovani A, Marchesi F, Malesci A, Laghi L, Allavena P. Tumor-associated macrophages as treatment targets in oncology. Nat Rev Clin Oncol 2017;14:399–416.
6. DeNardo DG, Ruffell B. Macrophages as regulators of tumor immunity and immunotherapy. Nat Rev Immunol 2019;19:369–82.
7. Cassetta L, Pollard JW. Targeting macrophages: therapeutic approaches in cancer. Nat Rev Drug Discov 2018;17:887–904.
8. Hynes RO, Naba A. Overview of the matrisome–an inventory of extracellular matrix constituents and functions. Cold Spring Harb Perspect Biol 2012;4:a004903.
9. Amit I, Winter DR, Jung S. The role of the local environment and epigenetics in shaping macrophage identity and their effect on tissue homeostasis. Nat Immunol 2016;17:18–25.
10. Lavin Y, Winter D, Blecher-Gonen R, David E, Keren-Shaul H, Merad M, et al. Tissue-resident macrophage enhancer landscapes are shaped by the local microenvironment. Cell 2014;159:1312–26.
11. Wang N, Liang H, Zen K. Molecular mechanisms that influence the macrophage m1-m2 polarization balance. Front Immunol 2014;5:614.
12. Werb Z, Lu P. The role of stroma in tumor development. Cancer J 2015;21:250–3.
13. Oskarsson T, Acharyya S, Zhang XH-F, Vanharanta S, Tavazoie SF, Morris PG, et al. Breast cancer cells produce tenascin C as a metastatic niche component to colonize the lungs. Nat Med 2011;17:867–74.
14. Tanaka K, Hiraiwa N, Hashimoto H, Yamazaki Y, Kusakabe M. Tenascin-C regulates angiogenesis in tumor through the regulation of vascular endothelial growth factor expression. Int J Cancer 2004;108:31–40.
15. Rupp T, Langlois B, Koczorowska MM, Radwanska A, Sun Z, Hussenet T, et al. Tenascin-C orchestrates glioblastoma angiogenesis by modulation of pro- and anti-angiogenic signaling. Cell Rep 2016;17:2607–19.
16. Minn AJ, Gupta GP, Siegel PM, Bos PD, Shu W, Giri DD, et al. Genes that mediate breast cancer metastasis to lung. Nature 2005;436:518–24.
17. Marzeda AM, Midwood KS. Internal affairs: tenascin-C as a clinically relevant, endogenous driver of innate immunity. J Histochem Cytochem 2018;66:289–304.
18. Sun Z, Velázquez-Quesada I, Murdamoothoo D, Ahowesso C, Yilmaz A, Spenlé C, et al. Tenascin-C increases lung metastasis by impacting blood vessel invasions. Matrix Biol 2019;83:26–47.
19. Arpel A, Sawma P, Spenlé C, Fritz J, Meyer L, Garnier N, et al. Transmembrane domain targeting peptide antagonizing ErbB2/Neu inhibits breast tumor growth and metastasis. Cell Rep 2014;8:1714–21.
20. Aungier SR, Cartwright AJ, Schwenzer A, Marshall JL, Dyson MR, Slavny P, et al. Targeting early changes in the synovial microenvironment: a new class of immunomodulatory therapy? Ann Rheum Dis 2019;78:186–91.
21. Wu B, Sun X, Gupta HB, Yuan B, Li J, Ge F, et al. Adipose PD-L1 modulates PD-1/PD-L1 checkpoint blockade immunotherapy efficacy in breast cancer. Oncoimmunology 2018;7:e1500107.
22. Dobin A, Davis CA, Schlesinger F, Drenkow J, Zaleski C, Jha S, et al. STAR: ultrafast universal RNA-seq aligner. Bioinformatics 2013;29:15–21.

Published OnlineFirst January 15, 2020; DOI: 10.1158/2326-6066.CIR-19-0276

23. Langmead B, Salzberg SL. Fast gapped-read alignment with Bowtie 2. Nat Methods 2012;9:357–9.
24. Anders S, Pyl PT, Huber W. HTSeq–a Python framework to work with high-throughput sequencing data. Bioinformatics 2015;31:166–9.
25. Love MI, Huber W, Anders S. Moderated estimation of fold change and dispersion for RNA-seq data with DESeq2. Genome Biol 2014;15:550.
26. Colaprico A, Silva TC, Olsen C, Garofano L, Cava C, Garolini D, et al. TCGAbiolinks: an R/Bioconductor package for integrative analysis of TCGA data. Nucleic Acids Res 2016;44:e71.
27. Ciriello G, Gatza ML, Beck AH, Wilkerson MD, Rhie SK, Pastore A, et al. Comprehensive molecular portraits of invasive lobular breast cancer. Cell 2015;163:506–19.
28. Li B, Dewey CN. RSEM: accurate transcript quantification from RNA-Seq data with or without a reference genome. BMC Bioinformatics 2011;12:323.
29. Newman AM, Liu CL, Green MR, Gentles AJ, Feng W, Xu Y, et al. Robust enumeration of cell subsets from tissue expression profiles. Nat Methods 2015;12:453–7.
30. Primac I, Maquoi E, Blacher S, Heljasvaara R, Van Deun J, Smeland HY, et al. Stromal integrin alpha11 regulates PDGFR-beta signaling and promotes breast cancer progression. J Clin Invest 2019;130:4609–28.
31. Goh FG, Piccinini AM, Krausgruber T, Udalova IA, Midwood KS. Transcriptional regulation of the endogenous danger signal tenascin-C: a novel autocrine loop in inflammation. J Immunol 2010;184:2655–62.
32. Orend G, Chiquet-Ehrismann R. Tenascin-C induced signaling in cancer. Cancer Lett 2006;244:143–63.
33. Abbadi D, Laroumanie F, Bizou M, Pozzo J, Daviaud D, Delage C, et al. Local production of tenascin-C acts as a trigger for monocyte/macrophage recruitment that provokes cardiac dysfunction. Cardiovasc Res 2018;114:123–37.
34. Kimura T, Tajiri K, Sato A, Sakai S, Wang Z, Yoshida T, et al. Tenascin-C accelerates adverse ventricular remodelling after myocardial infarction by modulating macrophage polarization. Cardiovasc Res 2019;115:614–24.
35. Schmid P, Adams S, Rugo HS, Schneeweiss A, Barrios CH, Iwata H, et al. Atezolizumab and nab-paclitaxel in advanced triple-negative breast cancer. N Engl J Med 2018;379:2108–21.
36. Foote JB, Kok M, Leatherman JM, Armstrong TD, Marcinkowski BC, Ojalvo LS, et al. A STING agonist given with OX40 receptor and PD-L1 modulators primes immunity and reduces tumor growth in tolerized mice. Cancer Immunol Res 2017;5:468–79.
37. Zhao X, Qu J, Sun Y, Wang J, Liu X, Wang F, et al. Prognostic significance of tumor-associated macrophages in breast cancer: a meta-analysis of the literature. Oncotarget 2017;8:30576–86.
38. Kulla A, Liigant A, Piirsoo A, Rippin G, Asser T. Tenascin expression patterns and cells of monocyte lineage: relationship in human gliomas. Mod Pathol 2000;13:56–67.
39. Wallner K, Li C, Shah PK, Fishbein MC, Forrester JS, Kaul S, et al. Tenascin-C is expressed in macrophage-rich human coronary atherosclerotic plaque. Circulation 1999;99:1284–9.
40. Gullberg D, Velling T, Sjöberg G, Salmivirta K, Gaggero B, Tiger C-F, et al. Tenascin-C expression correlates with macrophage invasion in Duchenne muscular dystrophy and in myositis. Neuromuscul Disord 1997;7:39–54.
41. Koyama Y-I, Norose K, Kusubata M, Irie S, Kusakabe M. Differential expression of tenascin in the skin during hapten-induced dermatitis. Histochem Cell Biol 1996;106:263–73.
42. Sumioka T, Fujita N, Kitano A, Okada Y, Saika S. Impaired angiogenic response in the cornea of mice lacking tenascin C. Invest Opthalmol Vis Sci 2011;52:2462–7.
43. Wang Z, Wei Q, Han L, Cao K, Lan T, Xu Z, et al. Tenascin-c renders a proangiogenic phenotype in macrophage via annexin II. J Cell Mol Med 2018;22:429–38.
44. Aras S, Zaidi MR. TAMeless traitors: macrophages in cancer progression and metastasis. Br J Cancer 2017;117:1583–91.
45. Linde N, Casanova-Acebes M, Sosa MS, Mortha A, Rahman A, Farias E, et al. Macrophages orchestrate breast cancer early dissemination and metastasis. Nat Commun 2018;9:21.
46. Kitamura T, Doughty-Shenton D, Cassetta L, Fragkogianni S, Brownlie D, Kato Y, et al. Monocytes differentiate to immune suppressive precursors of metastasis-associated macrophages in mouse models of metastatic breast cancer. Front Immunol 2017;8:2004.
47. Chen WC, Lai YH, Chen HY, Guo HR, Su IJ, Chen HH. Interleukin-17-producing cell infiltration in the breast cancer tumour microenvironment is a poor prognostic factor. Histopathology 2013;63:225–33.
48. Ma YF, Chen C, Li D, Liu M, Lv ZW, Ji Y, et al. Targeting of interleukin (IL)-17A inhibits PDL1 expression in tumor cells and induces anticancer immunity in an estrogen receptor-negative murine model of breast cancer. Oncotarget 2017;8:7614–24.
49. Yang M, Li Z, Ren M, Li S, Zhang L, Zhang X, et al. Stromal infiltration of tumor-associated macrophages conferring poor prognosis of patients with basal-like breast carcinoma. J Cancer 2018;9:2308–16.

Published OnlineFirst January 15, 2020; DOI: 10.1158/2326-6066.CIR-19-0276

AACR American Association for Cancer Research

Cancer Immunology Research

Matrix-Targeting Immunotherapy Controls Tumor Growth and Spread by Switching Macrophage Phenotype

Claire Deligne, Devadarssen Murdamoothoo, Anís N. Gammage, et al.

Cancer Immunol Res 2020;8:368-382. Published OnlineFirst January 15, 2020.

Tenascin-C Orchestrates an Immune-Suppressive Tumor Microenvironment in Oral Squamous Cell Carcinoma

Caroline Spenlé[1], Thomas Loustau[1], Devadarssen Murdamoothoo[1], William Erne[1], Stephanie Beghelli-de la Forest Divonne[2,3], Romain Veber[4], Luciana Petti[5], Pierre Bourdely[5], Matthias Mörgelin[6], Eva-Maria Brauchle[7,8,9], Gérard Cremel[1], Vony Randrianarisoa[1], Abdouramane Camara[4], Samah Rekima[2,3], Sebastian Schaub[2,3], Kelly Nouhen[5], Thomas Imhof[10], Uwe Hansen[11], Nicodème Paul[12], Raphael Carapito[12], Nicolas Pythoud[13], Aurélie Hirschler[13], Christine Carapito[13], Hélène Dumortier[4], Christopher G. Mueller[4], Manuel Koch[10], Katja Schenke-Layland[7,8,9], Shigeyuki Kon[14], Anne Sudaka[2,3], Fabienne Anjuère[5], Ellen Van Obberghen-Schilling[2], and Gertraud Orend[1]

ABSTRACT

Inherent immune suppression represents a major challenge in the treatment of human cancer. The extracellular matrix molecule tenascin-C promotes cancer by multiple mechanisms, yet the roles of tenascin-C in tumor immunity are incompletely understood. Using a 4NQO-induced oral squamous cell carcinoma (OSCC) model with abundant and absent tenascin-C, we demonstrated that tenascin-C enforced an immune-suppressive lymphoid stroma via CCL21/CCR7 signaling, leading to increased metastatic tumors. Through TLR4, tenascin-C increased expression of CCR7 in $CD11c^+$ myeloid cells. By inducing CCL21 in lymphatic endothelial cells via integrin α9β1 and binding to CCL21, tenascin-C immobilized $CD11c^+$ cells in the stroma. Inversion of the lymph node-to-tumor CCL21 gradient, recruitment of T regulatory cells, high expression of anti-inflammatory cytokines, and matrisomal components were hallmarks of the tenascin-C–instructed lymphoid stroma. Ablation of tenascin-C or CCR7 blockade inhibited the lymphoid immune-suppressive stromal properties, reducing tumor growth, progression, and metastasis. Thus, targeting CCR7 could be relevant in human head and neck tumors, as high tenascin-C expression and an immune-suppressive stroma correlate to poor patient survival.

Introduction

Head and neck squamous cell carcinomas (HNSCC) are heterogeneous malignancies originating from the mucosal surface of the upper aerodigestive tract. The 5-year survival rate worldwide is around 50% due to disease recurrence and metastasis (1). At least two genetic subclasses of HNSCC can be distinguished, where human papillomavirus (HPV)–negative tumors, representing approximately 65% of HNSCC are caused by chronic exposure to carcinogens including tobacco and alcohol (2). The first-line treatment of HNSCC is surgery followed by radiotherapy and chemotherapy and recently immune checkpoint therapy where long-lasting effects are seen only in a fraction of patients (3, 4).

HNSCC is an immune-suppressive disease where the physiologic microenvironment changes into a protumoral state accompanied by major changes in the extracellular matrix (ECM; refs. 5–8). Tenascin-C (TNC) is one such ECM molecule that impacts the progression of several tumor types through regulation of multiple cancer hallmarks (9–11). In a nontumor context, TNC can serve as a danger-associated molecular pattern (DAMP) molecule, and trigger more severe inflammation through integrin α9β1 and TLR4 (12, 13). Although TNC is mostly absent in normal tissues, TNC is expressed in reticular fibers of lymphoid tissues where it regulates leukocyte maturation (14, 15). In cancer tissue (16–18), TNC is organized in tumor matrix tracks (TMT) that share certain features with reticular fibers and may play a role in immune cell functions in cancer tissue (10, 11, 14). Although TNC is one of the major ECM proteins upregulated in the matrix of HNSCC-associated fibroblasts (19), the precise roles of TNC in this disease have not yet been investigated.

To better understand how immune cells interact with the neoplastic stroma in HNSCC, here, we used the carcinogen 4-Nitroquinoline

[1]Université Strasbourg, INSERM U1109-MN3T, The Microenvironmental Niche in Tumorigenesis and Targeted Therapy, and The Tumor Microenvironment Laboratory, Hopital Civil, Institut d'Hématologie et d'Immunologie, Fédération de Médecine Translationnelle de Strasbourg (FMTS), Strasbourg, France. [2]Université Côte d'Azur, CNRS, INSERM, iBV, Nice, France. [3]Centre Antoine Lacassagne, Nice, France. [4]Institut de Biologie Moléculaire et Cellulaire, CNRS, UPR3572 Immunologie, Immunopathologie et Chimie Thérapeutique, Institut de Biologie Moléculaire et Cellulaire, Strasbourg, France. [5]Université Côte d'Azur, CNRS, IPMC, Valbonne-Sophia Antipolis, France. [6]Colzyx AB, Lund, Sweden. [7]Department of Women's Health, Research Institute of Women's Health, Eberhard Karls University Tübingen, Tübingen, Germany. [8]The Natural and Medical Sciences Institute (NMI) at the University of Tübingen, Reutlingen, Germany. [9]Cluster of Excellence iFIT (EXC 2180) "Image-Guided and Functionally Instructed Tumor Therapies," Eberhard Karls University Tübingen, Tübingen, Germany. [10]Institute for Dental Research and Oral, Musculoskeletal Research, Center for Biochemistry, University of Cologne, Cologne, Germany. [11]Institute for Musculoskeletal Medicine (IMM), University Hospital Muenster, Muenster, Germany. [12]INSERM U1109, GENOMAX, Strasbourg, France. [13]IPHC, Cronenbourg, France. [14]Faculty of Pharmaceutical Sciences, Hokkaido University, Sapporo, Japan.

Note: Supplementary data for this article are available at Cancer Immunology Research Online (http://cancerimmunolres.aacrjournals.org/).

C. Spenlé and T. Loustau contributed equally to this article.

Corresponding Authors: Gertraud Orend, The Tumor Microenvironment Laboratory, INSERM U1109, Strasbourg 67091, France. Phone: 3303-6885-3996; E-mail: gertraud.orend@inserm.fr; and Ellen Van Obberghen-Schilling, Université Côte d'Azur, CNRS, INSERM, iBV, Nice 06189, France. E-mail: Ellen.VAN-OBBERGHEN@unice.fr

Cancer Immunol Res 2020;XX:XX–XX

doi: 10.1158/2326-6066.CIR-20-0074

1-oxide (4NQO)–driven murine model with abundant or absent TNC. 4NQO applied in the drinking water causes DNA adduct formation thus mimicking the effects of tobacco carcinogens and induces malignant lesions mainly in the tongue and esophagus (20, 21).

We identified TNC as a molecule involved in the immunesuppressive TME in OSCC. Comparison of tumors in wild-type (WT) and TNC knockout (TNCKO) mice allowed us to demonstrate a role for TNC in OSCC progression and lymph node invasion suggesting a mechanism by which the TNC-rich tumor matrix shaped an immunesuppressive, protumoral microenvironment. These results provide relevant information for human HNSCC diagnosis and therapy.

Materials and Methods

Human tumor samples and IHC

Surgically removed tongue tumors, embedded in paraffin blocks, were retrieved from the archives of the Pathology Department of the Centre Antoine Lacassagne. Informed consent was obtained for all subjects. Patient characteristics are summarized in Supplementary Table S1. Hematoxylin and eosin staining and IHC methods were performed on serial 4-μm deparaffinized tissue microarray (TMA) sections. CD45 staining was performed on a BenchMark Ulter Automated Slide Staining system (Ventana Medical Systems, Inc., Roche Group) using monoclonal anti-CD45 (LCA; clone 2B11+PD7/26) or anti-podoplanin (D2-40) according to instructions of the manufacturer (Cell Marque). For TNC staining, intrinsic peroxidase was blocked by incubating sections with 3% hydrogen peroxide for 15 minutes. Antigen retrieval was performed in EDTA buffer pH 9.0, in a decloaking chamber (Dako, catalog number S2367). Sections were blocked in 4% goat serum for 1 hour, then incubated for 1 hour with mouse monoclonal anti-TNC (clone BC24, Sigma-Aldrich 1/1,000). After rinsing with PBS, sections were incubated with biotinylated secondary antibody (30 minutes) and biotinylated goat anti-mouse IgG (30 minutes) followed by avidin-biotin (Vector Laboratories, VECTASTAIN ABC Kit, catalog number PK-4000). Slides were incubated with 3,3′-Diaminobenzidine developing solution (Vector Lab, DAB, catalog number SK-4100) and hematoxylin before embedding into ProLong Gold antifade reagent (Invitrogen, catalog number P36930). For fluorescence staining, after permeabilization (PBS, 0.1% Triton) cells/tissue were incubated with the primary antibodies (Supplementary Table S2) overnight. Bound antibodies were detected with the appropriate Alexa-labeled secondary antibodies (Supplementary Table S2) prior to nuclear staining with DAPI (Sigma, catalog number D9542) and embedding into ProLong Gold antifade reagent (Invitrogen, catalog number P36930). Fluorescently stained sections were digitalized (40×) using a PerkinElmer Vectra Polaris imaging system and Phenochart software (Akoya Biosciences).

Quantification of human staining

Stained slides were scanned on the Hamamatsu NanoZoomer 2.0-HT Digital slide scanner (40× mode). Scans were viewed and images acquired using the NDP.view2 software. For quantification, we developed a script (based on ImageJ) optimized to be used with interactive surfaces (https://figshare.com/articles/Custom_toolbars_and_mini_applications_with_Action_Bar/3397603/3). The program and the manual are freely available at https://mycore.core-cloud.net/index.php/s/0K61LqHBrnNKShX. Randomly chosen images of noninvasive tumor areas (three per tumor, 5× magnification) were projected on an interactive digital whiteboard. A pathologist determined the regions of interest (ROI) corresponding to tumor cell nest or stroma. These ROIs where extracted after color deconvolution and thresholding to quantify CD45 staining. We then determined the ratio of area containing CD45 (holes were removed as deduced from the hematoxylin image) per image and per ROI type.

Patient survival and correlation matrix data

Public patient data (GSE27020) were analyzed by the Kaplan–Meier plotter tool (ProggeneV2 prognostic database) as described (22). The cohort was separated by the median of corresponding gene expression as "High" and "Low," respectively. Gene expression was correlated to relapse-free survival (RFS). The correlation matrix analysis by Corrplot package (R software; https///github.com/taiyun/corrplot, Taiyn and Simko) was performed on gene expression data derived from RNA chromatin immunoprecipitation (chIP) analysis from HNSCC tumors of 68 patients (23). The graphical representation was generated using the R package corrplot. The multiple testing corrections were performed using the pound method (24).

The 4NQO model and antibody treatment of tumor-bearing mice

4-NQO (Sigma-Aldrich, catalog number N8141) was administered to 8-week-old WT and TNCKO (KO; ref. 25) mice, which had been bred in house with C57BL/6J mice (Charles River) for more than 10 generations, in the drinking water at a final concentration of 100 μg/mL for 16 weeks (stock 5 mg/mL in propylene glycol). Subsequently, mice were fed with regular water for 4 weeks before sacrifice, where tongue, submandibular lymph nodes, and spleen were collected and prepared for FACS analysis, cryosectioning, mRNA, or protein extraction as described below. During tissue sampling, the general organ appearance and the number of tumors per 4 mice were determined. To assess the roles of CCL21/CCR7 signaling, mice were also subjected to the regular 4NQO protocol as described above. The last 2 weeks before sacrificing the mice, mice were given three intraperitoneal injections of IgG control antibody (200 μg, R&D Systems, catalog number MAB006) or CCR7 antibody (200 μg, R&D systems, MAB3477) as described previously (26). The injections were spaced at least 4 days apart, and the last injection took place 4 days before the sacrifice. All mice were housed and handled according to the guidelines of INSERM and the ethical committee of Alsace, France (Cremeas; Directive 2010/63/EU on the protections of animals used for scientific purposes).

Gene expression analysis

RNA from WT and TNCKO tongue tumors (3 samples per group) was isolated using the RNeasy Mini Kit (Qiagen, catalog number 74104) and RNA integrity was determined with an Agilent Bioanalyzer 2100 (Pico Kit, Agilent Technologies). Total RNA-Sequencing libraries were prepared with SMARTer Stranded Total RNA-Seq Kit v2 - Pico Input Mammalian (TaKaRa, catalog number 634411) according to the manufacturer's protocol. Libraries were pooled and sequenced (paired-end 2*75 bp) on a NextSeq500 using the NextSeq 500/550 High Output Kit v2 according to the manufacturer's instructions (Illumina, catalog number 20024907). Quality control of every sample was assessed with the NGS Core Tools FastQC and sequence reads were mapped using STAR and Bowtie2 (27, 28). The total mapped reads were finally available in BAM (Binary Alignment Map) format for raw read counts extraction. Read counts were found by the HTseq-count tool of the Python package HTSeq (29) with default parameters to generate an abundance matrix. Differential analyses were performed using the DESEQ2 (30) package of the Bioconductor framework. Upregulated and downregulated genes were selected on the basis of the P_{adj} (<0.10) and the fold change (>±0.8; Supplementary Table S3). Deregulated gene expression analysis

was performed by using the PANTHER version 11 (31) and REACTOME software (32).

Nano-LC/MS-MS analysis

Tongue tumor pieces from WT and TNCKO mice were resuspended in Laemmli buffer (10 mmol/L Tris pH 6.8, 1 mmol/L EDTA, 5% ß-mercaptoethanol, 5% SDS, 10 glycerol, 1/100 antiproteases). Proteins were extracted for 1 hour upon sonication (four times for 5 minutes). Protein concentration was determined using the RC-DC protein assay (Bio-Rad, catalog number 5000121) following the manufacturer's instructions. Forty micrograms of protein lysate for each sample were heated at 95°C for 5 minutes and stacked in an in-house prepared 5% polyacrylamide SDS-PAGE stacking gel. Gel bands were reduced and alkylated prior to overnight digestion (the ratio of enzyme/protein = 1/50) at 37°C using modified porcine trypsin (Promega, catalog number V5113). The generated peptides were extracted with 60% acetonitrile (ACN) in 0.1% formic acid (FA) followed by a second extraction with 100% ACN. Peptides were resuspended in 100 μL of water and 0.1% formic acid.

Nano-LC/MS-MS analysis was performed on a nanoAcquity UPLC device (Waters) coupled to a Q-Exactive HF-X mass spectrometer (Thermo Fisher Scientific) equipped with a Nanospray Flex ion source. Peptide separation was performed on an ACQUITY UPLC Peptide BEH C18 Column (250 mm × 75 μm with 1.7 μm diameter particles) and an ACQUITY UPLC M-Class Symmetry C18 Trap Column (20 mm × 180 μm with 5-μm diameter particles; Waters). The solvent system consisted of 0.1% FA in water (solvent A) and 0.1% FA in ACN (solvent B). Samples (800 ng) were loaded into the enrichment column over 3 minutes at 5 μL/minute with 99% of solvent A and 1% of solvent B. Peptides were eluted at 400 nL/minute with the following gradient of solvent B: from 1 to 8% over 2 minutes, from 8 to 35% over 77 minutes, and from 35 to 90% over 1 minute. Samples were injected in a randomized order. The MS capillary voltage was set to 2 kV at 250°C. The system was operated in a data-dependent acquisition mode with automatic switching between MS (mass range 375–1,500 m/z with R = 120,000 at 200 m/z, automatic gain control fixed at 3×10^6 ions, and a maximum injection time set at 60 milliseconds), and MS/MS (mass range 200–2,000 m/z with R = 15,000 at 200 m/z, automatic gain control fixed at 1×10^5, and the maximal injection time set to 60 milliseconds) modes. The twenty most abundant peptides were selected on each MS spectrum for further isolation and higher energy collision dissociation (normalized collision energy set to 27), excluding unassigned, monocharged, and superior to seven times charged ions. The dynamic exclusion time was set to 40 seconds, and "Peptide match selection" parameter of the software.

The raw data obtained for each condition were processed with MaxQuant (version 1.6.0.16; ref. 33). Peaks were assigned with the Andromeda search engine with full trypsin (Trypsin/P) specificity against an in-house generated protein sequence database containing all mouse protein entries extracted from UniProtKB-SwissProt (17 007 sequences, taxonomy identifier: 10 090, release 2019–04–09). Carbamidomethylation of cysteines was set as fixed modification, whereas oxidation of methionines and protein N-terminal acetylation were defined as variable modifications. Minimal peptide length was set to seven amino acids and up to two missed cleavage sites were allowed for trypsin digestion. Peptide mass tolerance was set to 20 ppm for the first search and 5 ppm for the main search. The maximum false discovery rate was 1% at PSM, peptide, and protein levels with the use of a target/decoy strategy.

Label-free quantification was done on unique peptides (LFQ min. ratio count of 2) with the match between runs option activated (match window of 2 minutes and alignment window of 10 minutes). Unmodified peptides and those with carbamidomethylated cysteines were used for protein quantification.

After removal of contaminants, reverse entries, proteins only identified with modified peptides and protein groups identified with less than two unique peptides, differential analyses on normalized LFQ intensities were performed using Prostar (version 1.16.6; ref. 34). A Limma *t* test was performed for the statistical analysis test calibrated with the Pounds method (35). Dysregulated proteins were selected based on the P_{adj} value (Supplementary Table S4) and further analysis were performed using the PANTHER version 11 (31) and REACTOME software (32).

Proteome profiler array

Proteins were extracted from 5 WT, 5 KO, 4 control antibody and 4 CCR7 antibody tongue tumors in lysis buffer [Triton 1× and protease inhibitors (Roche, catalog number 11697498001) diluted in 1× PBS] following the manufacturer's instructions and protein concentration of tumor samples was determined by optical density measurement (NanoDrop 2000). The expression of immunomodulatory molecules in tumor samples was measured using the Mouse XL Cytokine Array Kit (Biotechne, catalog number ARY028) according to the manufacturer's instruction. After membrane blocking, equal protein amounts from 4 or 5 pooled tumors per group were applied to the membrane overnight. Two membranes were used for each group to have an experimental duplicate. The revelation of each membrane was done by using the Cemi Reagent Mix provided in the kit and a Chemidoc Imager XRS (Bio-Rad). Quantification was done by measuring pixel density with the ImageJ software. The background signal was subtracted with the negative control spots and the positive control spots were used to normalize values of each molecule to compare membranes between each other (Supplementary Table S5).

Hematoxylin and eosin staining

The OCT-embedded tissue sections (8-μm thick) were incubated in ddH_2O before staining with hematoxylin (Surgipath, catalog number 3801560) for 30 seconds and eosin (Sigma, catalog number HT110132) for 10 seconds, spaced by 1 minute of ddH_2O washes. After the last wash, tissue sections were dehydrated 5 minutes in increasing percentage baths of ethanol (from 70% to 100%) and toluene and then covered with the Eukitt solution (Sigma, catalog number 03989).

Immunofluorescence

For immunofluorescence (IF) staining, unfixed frozen sections of 8 μm or cells fixed with 4% paraformaldehyde were incubated for 1 hour at room temperature with blocking serum (5% normal goat or donkey serum in PBS; Jackson ImmunoResearch, catalog numbers 005–000-121 and 017-000-121, respectively) and overnight directly with the primary antibodies (Supplementary Table S5). Bound antibodies were visualized with goat, rabbit, guinea pig, hamster, or rat secondary antibodies conjugated with Alexa 488, Cy3, or Cy5. DAPI (Sigma) was used to visualize nuclei. After embedding in FluorSave Reagent (Calbiochem, catalog number 345789), sections were examined using a Zeiss Axio Imager Z2 microscope. Pictures were taken with an AxioCam MRm (Zeiss) camera and Axiovision software. Control sections were processed as mentioned above with omission of the primary antibodies. The image acquisition setting (microscope, magnification, light intensity, exposure time) was kept constant per experiment and in between experimental conditions. For quantification of immune cells and positive staining area, the ImageJ software was used. CCL21, CCR7, and gp38 scoring is based on the criteria described in

Supplementary Table S6. At least two sections of 5 different tumors/mice were quantified per condition. The number of immune cells was reported in correlation to the total number of DAPI-positive cells.

Electron microscopy

Frozen and cryopreserved tissue samples were thawed and washed for 15 minutes with distilled water followed by a fixation in 2% (v/v) formaldehyde and 0.25% (v/v) glutaraldehyde in 100 mmol/L cacodylate buffer, pH 7.4, at 4°C overnight. Afterwards, tissue samples were rinsed in PBS, dehydrated in ethanol up to 70% (each step 30 minutes), and embedded in LR White embedding medium (London Resin Company, catalog number 14381-UC) using UV light for polymerization (Leica EM AFS). Ultrathin sections were cut with an ultramicrotome (Leica Ultracut UCT), collected on copper grids (Athene Grids, G202) and negatively stained with 2% uranyl acetate (Serva, catalog number 77970) for 15 minutes. Electron micrographs were taken at 60 kV with a Phillips EM-410 electron microscope using imaging plates (Ditabis).

Raman microspectroscopy

Raman images were acquired using a WITec alpha300R Raman microscope (WITec). In the upright set-up a 532 nm laser was focused through a 60× dipping objective (NA 1.0) to excite Raman scattering on tissues sections. Tissue areas within the TMTs of 150 × 200 μm were scanned using a pixel size of 1 μm and an acquisition time of 0.08 seconds per pixel. For each tumor, two to three Raman images were generated. The spectral images were then further processed and analyzed using WITec Project Five software (WITec). After cosmic ray removal and background correction, spectra of each pixel were area normalized. The tumor stroma was identified based on a specific spectral pattern, predominantly resembling collagen fibers. For each image all pixels resembling this matrix pattern were averaged. Spectral patterns of stromal matrix in WT and TNCKO were compared using univariate statistics and Principal Component Analysis (PCA). To identify CCL21 in the tumor stroma, a reference spectrum of purified mouse CCL21 (457-6C; R&D Systems) was acquired. Peaks at 757,1030, 1210, 1319, and 1,615 cm^{-1} are specific for CCL21. This spectrum was used to decompose the ECM spectra in a True Component Analysis (WITec). Here the CCL21 reference was first employed on a CCL21-positive lymph node to identify CCL21 in a physiologic condition. The CCL21 spectrum was extracted from the lymph node Raman scans and employed on the Raman data from tumor stroma. For quantification relative intensities of CCL21 in WT and TNCKO stroma was normalized to the collagenous stroma area.

TNC cloning and purification

Recombinant his-tagged human TNC was purified as described previously (36, 37) and used for incubation with cells. Murine strep-tagged TNC was used in negative EM microscopy and treatment of cells. For cloning murine TNC, a PCEP4 expression vector (Invitrogen, catalog number V04450) with TNC (NP_035737.2, aa: 174-2019) from Mus musculus was obtained from R. Chiquet-Ehrismann (FMI, Basel, Switzerland). The coding sequence was modified with a BM40 signal peptide and a N terminal double strep II tag and was confirmed by sequencing (Supplementary Table S7). To generate stable cell lines, HEK293 EBNA cells were transfected with the expression vector using Fugene HD (Promega, catalog number E2311). After 48 hours of transfection, the medium was replaced with 0.5 μg/mL containing DMEM/F12 medium with 10% FCS and the cells were grown to confluency. The protein was then purified from the supernatant by using the Streptactin matrix (IBA, Lifesciences, catalog number 2-1021-001) following the manufacturer's guidelines and was then dialyzed three times against PBS as described previously (37).

Surface plasmon resonance spectroscopy

Surface plasmon resonance binding experiments were performed on a Biacore 2000 instrument (Biacore Inc.) at 25°C. Recombinant human TNC (36) was immobilized at high surface density (around 7000 resonance units) on an activated CM5 chip (Biacore Inc., catalog number 29149604) using a standard amine-coupling procedure according to the manufacturer's instructions. Soluble molecules were added at a concentration of 10 μg/mL in 10 mmol/L sodium acetate, pH 5.0, and at a flow rate of 5 μL/minute for 20 minutes before addition of 1 mol/L ethanolamine. CCL21 (0.5, 0.87, and 2 μg in 200 μL) was added to the chip at pH 6.0 [10 mmol/L MES, pH 6.0, 150 mm sodium chloride, 0.005% (v/v) surfactant P20], or at pH 7.4 [10 mmol/L HEPES, 150 mmol/L sodium chloride, 0.005% (v/v) surfactant P20], at a flow rate of 10 μL/minute. A blank CM5 chip was used for background correction. 10 mmol/L glycine, pH 2.0, at 100 μL/minute for 1 minute was used to regenerate the chip surface between two binding experiments. A steady-state condition was used to determine the affinity of CCL21 for TNC. The Dissociation constant (K_d) was determined using the 1:1 Langmuir association model as described by the manufacturers (https://www.biacore.com/lifesciences/help/kinetic_model_1_1_binding/index.html).

Negative staining, transmission electron microscopy, and CCL21-binding assay

The interaction of TNC with CCL21 was visualized by negative staining and transmission electron microscopy as described previously (38). Briefly, TNC samples (20 nmol/L) were incubated with a 3 molar excess of CCL21 (457-6C-025 R&D Systems) for 1 hour at 37°C in Tris-buffered saline (TBS), pH 7.4. For visualization in the electron microscope, CC21 was conjugated with 5 nm colloidal gold (39). For inhibition experiments, TNC samples were preincubated with a 10 molar excess of heparin for 1 hour at 37°C. Specimens were examined in a Philips/FEI CM 100 TWIN transmission electron microscope operated at 60 kV accelerating voltage. Images were recorded with a side-mounted Olympus Veleta camera with a resolution of 2048 × 2048 pixels (2k × 2K) and the ITEM acquisitions software. Binding of CCL21 particles to TNC was determined by counting the number of gold particles along the length of the TNC monomer. Number of molecules from 500 randomly picked distinct TNC molecules were determined. As positive control, TGFβ1 was used as it binds in the 5th FNIII repeat of TNC (40). As negative controls EGF (shown not to bind to TNC; ref. 40) and BSA were used, respectively.

Cell culture

All cultured cells were checked for the absence of *Mycoplasma* (once every 2 months, PlasmoTest, Invivogen catalog number rep-pt1). Lymphatic endothelial cells (LEC) and dendritic cell (DC)–like DC2.4 were purchased from ATCC (HDMVECn, PCS-110-010, 2018) and Merck (SCC142, 2018), respectively, and reauthenticated by determination of LYVE-1 expression (LEC), CD31 (HDMVEC) and CCR7, CD80 and CD86 (DC2.4) by flow cytometry. DC2.4 cells were cultured in DMEM-glucose (Dutscher) complemented with 10% of FBS (Dutscher), 100 U/mL penicillin, 100 μg/mL streptomycin (penicillin/streptomycin, Dutscher), 40 U/mL gentamicin (Thermo Fisher Scientific) and 1× HEPES. LECs were cultured in ECGM with penicillin/streptomycin, gentamicin, and a supplemental growth factor cocktail according to Promocell (catalog number C22110). Fibroblastic reticular cells (FRC) were isolated from the lymph nodes

(popliteal, inguinal, brachial, axillary, mandibular, and cervical) of a naïve WT mouse (10 weeks old) as described previously (41). FRCs were cultured in DMEM-glucose complemented with 10% FBS, 1% penicillin/streptomycin (Sigma catalog number P4333) and gentamicin (Dutscher catalog number P06-03100). The OSCC13 cell line was established from a primary 4NQO-induced tongue tumor of a WT mouse. Cells were mechanically dissociated and cultured in DMEM-F12 with 4.5 g/L glucose, 10% FBS, 1% penicillin/streptomycin (Sigma catalog number P4333), gentamycin, and 0.4 μg/mL hydrocortisone (Sigma, catalog number H4001). Cells were cultured for 20 passages and then subcutaneously grafted in the neck of a WT mouse. After two times of grafting in WT C57Bl6-J mice, cells were cultured for 50 passages before use. Silencing of TNC in OSCC13 cells was done by short hairpin (sh)–mediated gene expression knockdown. Briefly, lentiviral particles shRNA vectors (Sigma, catalog number SHCLNV-NM_011607 MISSION shRNA Lentiviral Transduction Particles) encoding specific shRNAs for the knockdown of TNC were used (shTNC:CCGGGCATCAA-CACAACCAGTCTAACTCGAG-TTAGACTGGTTGTGTTGATGCTTTTTG). Lentiviral particles encoding a nontargeting shRNA vector were used as control (SHC202V, Sigma). Transduced cells were selected with the previously described DMEM-F12 culture medium supplemented with 10 μg/mL puromycin (Thermo Fisher Scientific, catalog number A1113802) and the selection pressure was kept in all *in vitro* experiments.

All cell lines were maintained at 37°C in a humidified atmosphere of 5% CO_2. The culture medium was refreshed every 2 to 3 days and passaged into a new dish with trypsin-EDTA (PanBiotech) upon reaching confluency. Cells were starved with DMEM-F12 medium containing 1% FBS overnight before treatment. Cells were treated for 24 hours with purified human or mouse TNC (10 μg/mL) diluted with DMEM medium complemented with 1% FBS, penicillin/streptomycin, and gentamicin. Upon TNC stimulation, the CM was collected, filtered at 0.22 μm, and stored at −80°C for future use. Cells were detached mechanically, concentrated by centrifugation, and lysed in TRIzol reagent (Invitrogen, catalog number 12044977) before storage at −80°C. Before TNC incubation, LECs were pretreated with inhibitors for TGFβRI (GW788388, 10 μmol/L, 45 minutes, Selleckchem, catalog number S2750), TLR4 (Cli95, 1 μg/mL, 6 hours, InvivoGen, catalog number tlrl-cli95), receptor tyrosine kinases (SU6668, 30 μmol/L, 60 minutes, Tocris Bioscience, catalog number 3335), integrin α9β1 [blocking antibody α9Ab, 4 μg/mL, 6 hours, provided by Shigeyuki Kon (42) and α9β1/α4β1, BOP, 1 μmol/L, 45 minutes, Tocris Bioscience, catalog number 6047].

DC2.4 activation assay

DC2.4 cells were starved with medium containing 1% FBS overnight and pretreated the day after with TLR4 (Cli95, 1 μg/mL, 6 hours) diluted in 1% FBS complemented DMEM. Cells were incubated for 24 hours with 1% FBS complemented DMEM containing lysophosphatidic acid (LPS; 1 μg/mL) or soluble TNC (10 μg/mL). Upon LPS or TNC incubation, cells were detached, lysed in TRIzol (Invitrogen) following the manufacturer's instructions, or stained with anti-CD80-FITC, anti-CD11c-PE, anti-MHCII-APC EF780, and anti-CD86-PE Cy7 from eBiosciences for FACS analysis.

Boyden chamber migration assay

Boyden chamber migration assays on DC2.4 were performed in 5-μm pore-sized polycarbonate membrane transwells (Corning Costar Co, catalog number 3421). The lower surface of the transwells were precoated with Col I (BD Biosciences, catalog number 354236), horse purified fibronectin (FN; ref. 36) and mouse purified TNC at a final concentration of 1 $\mu g/cm^2$, respectively. The bottom chambers of the transwells were filled with DMEM containing mouse or human CCL21 (100 ng/mL, 200 ng/mL, or 400 ng/mL, R&D Systems, catalog number 457-6C-025 and 366-6C-025). To assess the migration of DC2.4 toward the secretome of the LECs, CM from LECs [treated or not with TNC (10 μg/mL) for 24 hours] was placed in the bottom chamber. To block the chemotaxis of DC2.4 cells toward CCL21, cells were incubated 6 hours with CCR7 neutralizing antibodies (10 μg/mL, R&D Systems) diluted in 1% FBS complemented DMEM. DC2.4 (5×10^5) suspended in 150 μL of 1% FBS-complemented DMEM were placed into the top chamber of the transwell system. Cells were incubated for 5 hours (CCL21 in the bottom chamber) or 8 hours (CM in the bottom chamber) at 37°C in 5% CO_2. The number of migrated cells in the bottom chamber was assessed by flow cytometry after the staining of DC2.4 with anti-CD11-PE (eBiosciences).

Boyden chamber chemoretention assay

The DC2.4 chemoretention assays were done with the same set up as described in the migration protocol. After 5 hours (CCL21 conditions) or 8 hours (CM conditions) of migration, the DC2.4 cells attached to the bottom surface of the transwells were fixed in 4% PFA and stained with DAPI. Pictures were taken and analyzed by the ImageJ software. Floating cells were analyzed by flow cytometry (Supplementary Table S8).

RNA extraction and qRT-PCR

Frozen tongue tumors and cultured cells were dissolved in the TRIzol reagent (Invitrogen, catalog number 12044977) for total RNA extraction. RNA quality was confirmed by optical density measurement (OD 260 nm). cDNAs were synthesized from 1000 μg of total RNA using random primers and Moloney murine leukemia virus reverse transcriptase (MultiScribe, Applied Biosystems, catalog number 10117254). The cDNA was used for qRT-PCR in a Mx3005P Real-Time PCR System (Thermo Fisher Scientific). Reactions were carried out in duplicate for all conditions using a SYBR Green Master Mix (Thermo Fisher Scientific, catalog number 4344463) or Fast TaqMan mix (Thermo Fisher Scientific, catalog number 4444557) and expression of mouse or human *Gapdh* mRNA (Life Technologies, catalog number 433764T) was used as endogenous control in the $2^{-\Delta\Delta C_t}$ calculation. Primer sequences used for qPCR determination are listed in Supplementary Table S9.

Analysis of protein expression

Tissues or cell lysates were prepared in lysis buffer (50 mmol/L TRIS-HCl pH 7.6, 150 mmol/L NaCl, 1% NP-40, 0.5% sodium deoxycholate, and 0.1% SDS) supplemented with a phosphatase inhibitor cocktail (Santa Cruz Biotechnology, catalog number sc-45045) and protease inhibitors (Roche, catalog number 05892970001). The protein concentration of tissue samples and CM was determined by Bradford assay (Bio-Rad, catalog number 5000001) following manufacturer's instructions. Thirty micrograms of protein lysate was loaded in precasted 4% to 20% gradient gels (Bio-Rad, catalog number 4561096), together with Laemmli buffer (Bio-Rad, catalog number 1610737) and separated by SDS-PAGE. The separated proteins were then transferred onto nitrocellulose membranes (Bio-Rad, catalog number 1620113) using the TransBlot Turbo Transfer system (Bio-Rad). Nitrocellulose membranes were then blocked with 5% Blocking-Grade blocker (Bio-Rad, catalog number 1706404) in 0.1% Tween-20 PBS and incubated with the primary antibody (overnight at 4°C) and secondary antibodies (1 hour at room temperature) in 1.5% Blocking-Grade Blocker

in 0.1% Tween-20 PBS. Antibodies used are listed in Supplementary Table S2. Protein bands were detected with the Amersham ECL Western Blotting Detection Reagent (GE Healthcare, catalog number RPN2106) or SuperSignal West Femto Maximum Sensitivity Substrate (Thermo Fisher Scientific, catalog number 34095). CCL21 and IFNγ expressions were determined by using the 6-Ckine ELISA kit (Thermo Fisher Scientific, catalog number EMCCL21A) and IFNγ ELISA Kit (Thermo Fisher Scientific, catalog number BMS606), respectively, according to the manufacturer's instructions. The absorbance of each sample and standard was measured with a plate reader (MultiSkan EX, Thermo Fisher Scientific).

Flow cytometry

Tongue tumors and submandibular lymph nodes were cut into small pieces and inflated with digestion solution containing 1 mg/mL Collagenase D (Roche, catalog number 50-100-3282) and 0.2 mg/mL DNase I (Roche, catalog number 4716728001), 2% inactivated FBS in RPMI, at 37°C for 2 hours. Upon completion of digestion, 92 μL of 54 mmol/L EDTA was added and the samples were vortexed at maximal speed for 30 seconds. The resulting cell suspensions were passed through a 70-μm and 40-μm cell strainer and treated with flow cytometry buffer (PBS, 2% FBS, 1 mmol/L EDTA). After cells were counted, 2×10^6 cells per lymph node/spleen sample or 1×10^6 cells for tumor sample, were stained with Dead Viability dye-efluor 450 (Thermo Fisher Scientific, catalog number 65-0863-18) according the manufacturer's instructions. Cells were then incubated in blocking solution containing 2% FcBlock CD16/CD32 (Thermo Fisher Scientific, catalog number 14-0161-85) in flow cytometry buffer, for 15 minutes at 4°C and then stained 30 minutes at 4°C with a standard panel of immunophenotyping antibodies; solution 1: anti-CD45-FITC, anti-CD11c-PE, anti-B220-APC, anti-MHCII-APC EF780, and anti-CCR7-Percp Cy5; solution 2: anti-CD45-FITC, anti-CD3e-PE, anti-C8a-APC, anti-CD4-APC EF780, anti-Foxp3-PE Cy7, anti-CCR7-Percp Cy5, and anti-CD25-AF700; solution 3: anti-CD45-FITC, anti-Gp38-PE, anti-CD31-APC, anti-F4/80-APC EF780, anti-CCR7-Percp Cy5, and anti-CD11b-AF700 (Supplementary Table S2). Data were acquired with a Beckman Coulter Gallios flow cytometer. Adjustments and data analysis were performed by using the FlowJo software. See Supplementary Table S2 for information on the antibodies and Supplementary Tables S10–S16 for information on the gating strategy.

Statistical analysis

For all data, Gaussian distribution was tested by the d'Agostino–Pearson normality test. When data followed a Gaussian distribution, statistical differences were analyzed by unpaired *t* test (with Welch correction in case of unequal variance) or ANOVA one-way with Tukey post test. Otherwise, the Mann–Whitney test or a nonparametric ANOVA followed by Dunn post test were used to verify significance of the observed differences. All statistical analyses were performed using the GraphPad Prism software. Mean ± SEM. *P* values < 0.05 were considered as statistically significant (*, $P < 0.05$; **, $P < 0.01$; ***, $P < 0.001$).

Results

TILs were enriched in the TNC-rich stroma of OSCC

In contrast to nontumoral human tongue tissue, with weak TNC expression, TNC expression was upregulated in the tongue tumor stroma, in TMT (refs. 17, 18; **Fig. 1A**). Investigating abundance of TIL ($CD45^+$ leukocytes) revealed more TILs in the tumor stroma compared with the tumor nests (**Fig. 1B** and **C**; Supplementary Fig. S1B and S1C).

TNC enhanced OSCC onset and progression in 4NQO-induced OSCC

4NQO induced OSCC in the mucosal epithelium of mice (**Fig. 1D**; Supplementary Fig. S1D and S1E), which recapitulated human OSCC (Supplementary Fig. S1F). Whereas TNC expression was very low in tongue epithelium of nontreated mice, its expression became upregulated in the stroma of the OSCC (**Fig. 1E**).

To address whether TNC had an impact on tumorigenesis in this model we determined tumor formation in WT and TNCKO mice. TNCKO mice presented a reduced number of tumors per mouse in comparison with WT mice (**Fig. 1F**). Without TNC, tongue tumors were also significantly smaller than in WT mice (**Fig. 1G**). TNCKO mice did not develop invasive carcinomas, in contrast with WT mice (**Fig. 1H**). WT mice developed lymph node metastasis (p63 staining), which was absent in TNCKO mice (**Fig. 1I** and **J**).

TNC impacted the composition and organization of the stromal niches

Malignant tumor cells retained their epithelial (E-cadherin$^+$, CK8/18$^+$, and vimentin-negative) traits (Supplementary Fig. S2A). Tumor epithelial cell nests (p63$^+$) were separated by stromal niches (αSMA$^+$ cells), similar to human OSCC (Supplementary Fig. S2A; ref. 43). Tumors were highly vascularized (CD31 and LYVE-1) similar to human OSCC (44). No difference in vascularization, nor survival or proliferation, was seen between tumor genotypes unlike other tumors (Supplementary Fig. S2B–S2G; refs. 5, 16, 45).

Several genes (176) were differentially expressed, 120 up- and 56 downregulated in WT compared with the TNCKO tumors (Supplementary Table S2). Expression of matrisome genes (46) was largely reduced in TNCKO tumors (Supplementary Fig. S2H and S2K; Supplementary Table S3). The analysis of the matrix by Raman microspectroscopy revealed a significant difference in the PC1 score that was below (TNCKO tumors) and above zero (WT tumors; **Fig. 2A** and **B**; Supplementary Fig. S2I and S2J). TNC expression was not detected in the TNCKO tumors (**Fig. 2C**). Collagen networks differed in WT and TNCKO mice, with more parallel oriented and compactly organized collagen fibrils, in WT tumors (Supplementary Fig. S2L). TNC was expressed in TMT together with laminin (LM), fibronectin (FN), Coll IV, and Coll XII (**Fig. 2C**; Supplementary Fig. S2M and S2N).

TNC promoted leukocyte enrichment in the stroma

There was no difference in the abundance of $CD45^+$ leukocytes between the two genotypes (**Fig. 2D**). However, there were more TILs in the tumor cell nests of TNCKO tumors (**Fig. 2E** and **F**). Whereas no difference in the abundance of macrophages (F4/80$^+$, CD11b$^+$), B cells (B220$^+$), CD4 (CD3$^+$, CD4$^+$), or CD8 T lymphocytes (CD3$^+$, CD8$^+$) between tumor genotypes was seen, we observed more dendritic cells (DC; MHCII$^+$/CD11c$^+$) in TNCKO tumors (**Fig. 2G**; Supplementary Fig. S2O). CD11c$^+$ cells resided predominantly in the stroma of WT tumors, whereas more CD11c$^+$ cells infiltrated tumor cell nests in TNCKO tumors (**Fig. 2H** and **I**). In contrast to DCs, T regulatory cells (Tregs; CD4$^+$/Foxp3$^+$) were more abundant inside the tumor cell nests of WT tumors (**Fig. 2J**–**L**). Macrophages (F4/80, CD206), CD4$^+$ and CD8$^+$ T lymphocytes, and B cells (B220) were present inside the tumor cell nests and the stroma with no apparent differences between WT and TNCKO tumors (Supplementary Fig. S2R). Thus, TNC appears to orchestrate the intratumoral distribution of some leukocytes, in particular, CD11c$^+$ cells and Tregs.

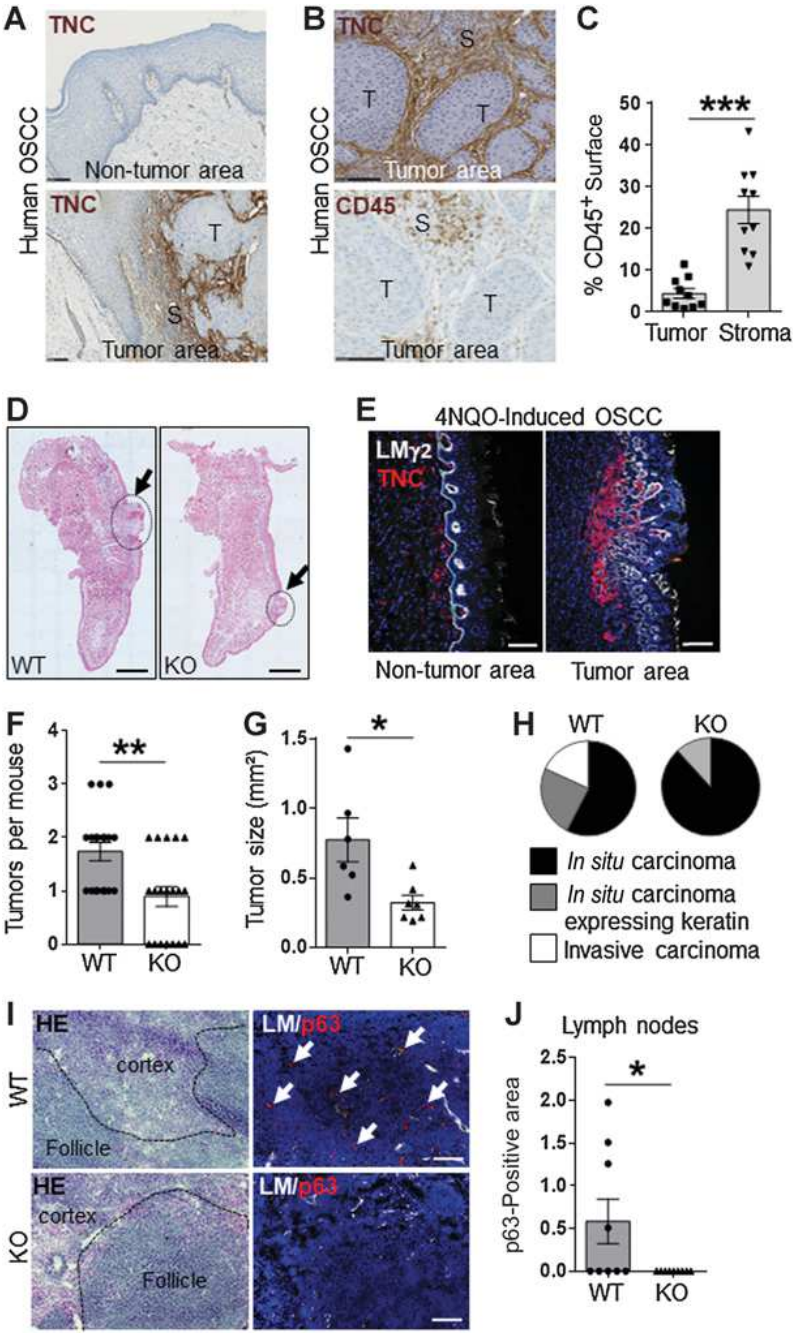

Figure 1.

TNC expression in human and murine OSCC tissue and its impact on tumorigenesis in a 4NQO-induced OSCC model. Representative (of more than 30) images of IHC staining for TNC (**A**) and CD45 (**B**) in human OSCC (tongue tumor). S, stroma; T, tumor cell nest. **C,** Differential spatial distribution of leukocytes in human OSCC. Quantification of CD45$^+$ leukocytes in the tumor epithelial nests and stroma, ($n = 10$ tumors, 3 regions per tumor). **D,** Representative composite images of hematoxylin and eosin–stained cross sections ($n = 19$) from tongues of 4NQO-treated WT and TNCKO mice. The black arrows and circles indicate the tongue tumor. **E,** Representative images ($n = 19$) of IF staining as indicated in the nontumoral and tumoral areas of a 4NQO-induced tongue lesion. Quantification of tongue tumor number (**F**) and size (**G**) in WT and TNCKO mice. $n = 19$ mice per group (**F**), $n = 6$ WT mice, $n = 7$ KO mice, and $n = 8$ to 10 images per tongue (**G**). **H,** Tongue tumor classification in WT and TNCKO mice. Lesions from WT and TNCKO mice ($n = 19$ per genotype), differentiated squamous cell carcinoma (black), *in situ* carcinoma expressing keratin (gray), or invasive carcinoma (white). **I** and **J,** Detection and quantification of mandibular lymph node metastasis in WT and TNCKO tumor mice. **I,** Representative of 20 images of lymph node tissue after hematoxylin and eosin (HE) and p63/laminin (LM/p63) staining. **J,** Quantification of p63-positive area (%) per image. Five images per lymph node, $n = 9$ mice per genotype. Mean, ± SEM, *t* test. ***, $P < 0.005$ (**C**), Mann–Whitney test; **, $P < 0.01$ (**F**); *, $P < 0.05$ (**G** and **J**). Scale bar, 50 μm (**E**), 100 μm (**A** and **I**), 200 μm (**B**), and 1,000 μm (**D**).

As CD11c$^+$ cells are antigen-presenting cells (APC) that play a role in priming T cells in the lymph nodes (47), we investigated the immune cell infiltrate of the local lymph nodes by flow cytometry. We observed more CD45$^+$ leukocytes in lymph nodes from TNCKO tumor mice (Supplementary Fig. S2P). Whereas the abundance of macrophages, B cells, and CD8 T cells was similar between genotypes, CD11c$^+$ DCs and CD4 T cells were more frequent in lymph nodes from the TNCKO mice (Supplementary Fig. S2Q). Less CD11c$^+$ cells in the lymph nodes and a reduced lymph node-to-tumor ratio of these cells in WT (251-fold) compared with TNCKO mice (878-fold) indicated that TNC may have impaired the migration of CD11c$^+$ cells toward the draining lymph nodes (**Fig. 2D**; Supplementary Fig. S3P). A higher proportion of lingual-derived DCs (high expression of MHCII and intermediate expression of CD11c; ref. 48), was observed in TNCKO lymph nodes compared with WT tumor mice indicating that DC homing to lymph nodes was reduced in WT conditions (Supplementary Fig. S2S and S2T).

TNC induced CCL21 in LECs

We observed increased CCL21 (+74%) and CCL19 (+17%) expression in WT tumors (**Fig. 3A**; Supplementary Table S4). We confirmed higher *Ccl21* mRNA and CCL21 protein expression in WT tumors (**Fig. 3B** and **C**; Supplementary Table S6). We also determined CCL21 expression in local lymph nodes and observed lower expression in lymph nodes compared with the tumors in WT mice, which could

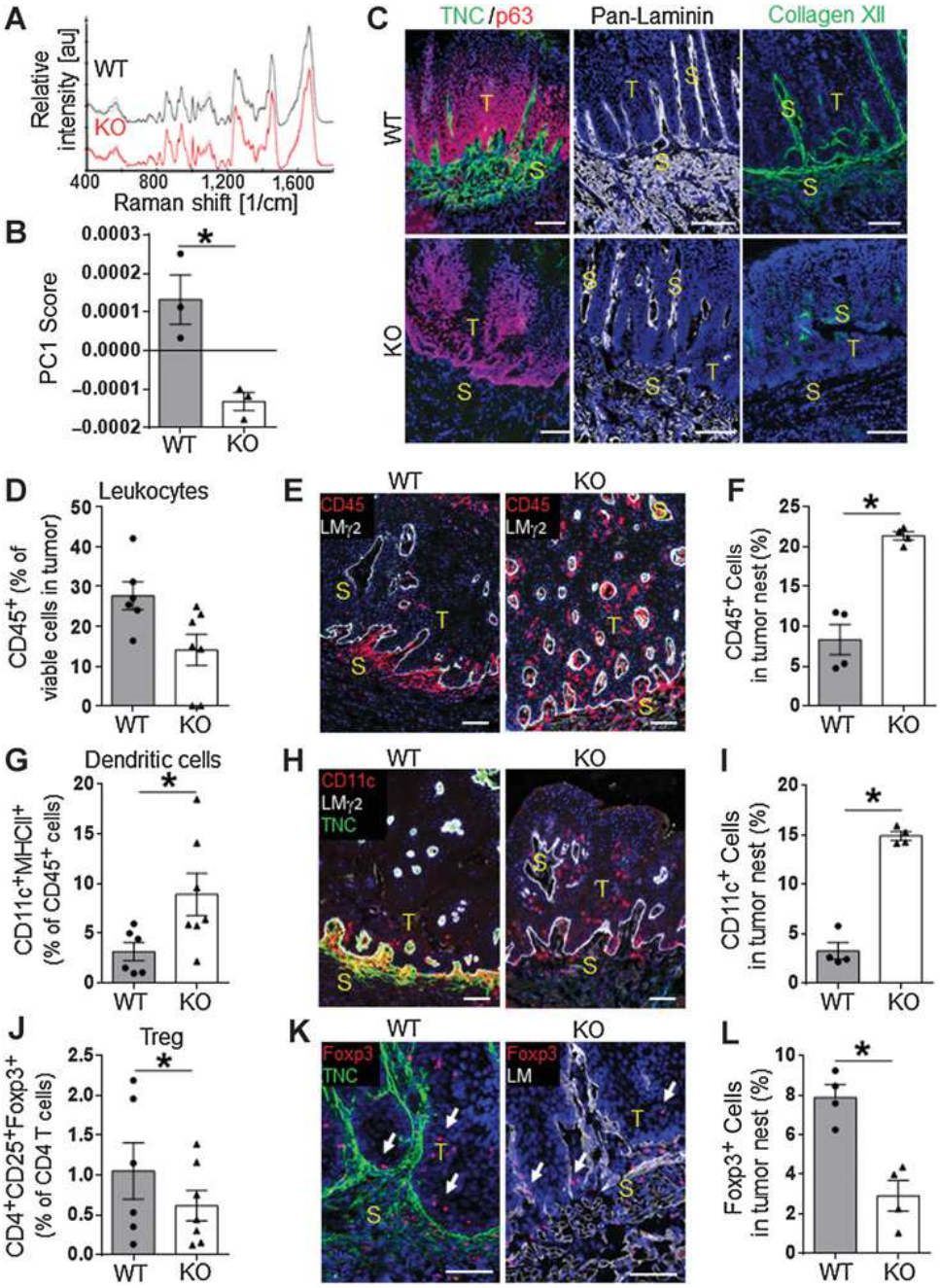

Figure 2.

TNC impacted tumor stroma organization and abundance and spatial distribution of immune cells. **A** and **B,** Raman microspectroscopic analysis of the ECM in WT and TNCKO tongue tumors. Significant differences of ECM in WT and TNCKO tumors were identified in single wave numbers 770, 820, 880, and 960 cm^{-1}, which are assigned to collagens indicating differences in collagen fiber network (**A**) and in PC1 score values (**B**). $n = 3$ per genotype. Mean ± SEM, Mann–Whitney test, *, $P = 0.018$. **C**, **E**, **H**, and **K,** Representative IF images (of at least 48) for the indicated molecules in 4NQO WT and TNCKO tumors. **D**, **G**, and **J,** Representation of the indicated cell type abundance as determined by flow cytometry. $n = 6$ WT and $n = 7$ KO mice (one tumor per mouse). **F**, **I**, and **L,** Quantification of immunostaining results to evaluate the spatial distribution of the indicated cells expressed as a ratio (percentage) of positive cells over the total of cells in the tumor nest per image. **B**, **D**, **F**, **G**, **I**, **J**, and **L,** Mean values (± SEM), 4 mice per genotype, 8 to 10 images per tumor. Mean ± SEM, Mann–Whitney test. *, $P < 0.05$; **, $P < 0.01$. Scale bar, 400 μm (**C**) and 100 μm (**E**, **H**, and **K**). S, stroma ($p63^-$); T, tumor cell nest ($p63^+$).

impact DC attraction to the lymph nodes (**Fig. 3C**). We observed no obvious difference in CCL21 and $CD11c^+$ cell abundance and localization within the lymph nodes of WT and TNCKO tumor mice (Supplementary Fig. S3A).

We used Raman microspectroscopy across the whole tumor. On the basis of specific signals of the purified CCL21 protein, we detected a similar spectrum for CCL21 in Raman images of lymph nodes and in WT and TNCKO tumors. Despite a strong background due to collagen-rich matrix, CCL21-specific peaks were identified in lymph nodes (a known source of CCL21) and stroma of WT and TNCKO tumors, whereas they were absent from the tumor cell nests and lung tissue (**Fig. 3D** and **E**; Supplementary Fig. S3B). CCL21 was significantly lower in TNCKO compared with WT tumors (**Fig. 3F–H**). LECs, typically expressing LYVE-1 and CCL21, expressed CCL21 in the OSCC, which was much less pronounced in TNCKO tumors (**Fig. 3I**). Reduced CCL21 expression was not due to less LECs in TNCKO tumors, as LECs were similarly abundant in TNCKO as in WT tumors (Supplementary Fig. S2B–S2F). Staining for CCL19, the second ligand for CCR7 revealed similar staining intensity and stromal localization in the tumors and no difference in lymph nodes of WT and TNCKO mice (Supplementary Fig. S3C and S3D).

We examined whether TNC induced CCL21 in LECs and FRCs, which reside in tumors (49) and naturally express CCL21 (50). We used human dermal LEC–expressing LYVE-1, gp38, and integrin α9β1 (Supplementary Fig. S3E) and isolated FRC (typically expressing ERTR7 and gp38; ref. 41) from lymph nodes of a naïve WT mouse

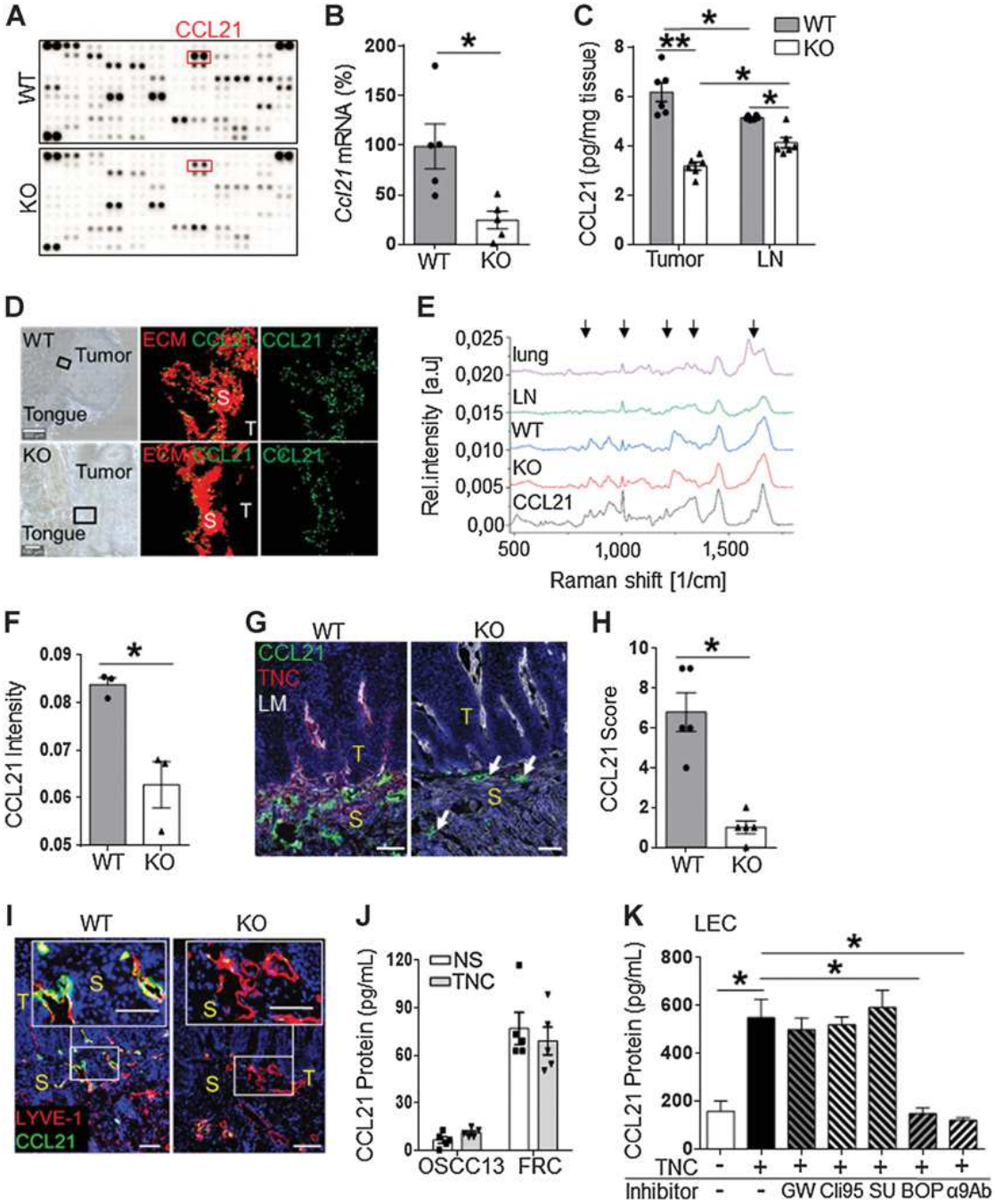

Figure 3.

TNC upregulated CCL21 in LECs. **A,** Representative picture (one of two) of the proteome profiler array of 4NQO WT and TNCKO tumors. Pixel density represents protein expression. $n = 5$ tumors pooled per condition (2 replicates). **B,** Gene expression analysis (qRTPCR) of *Ccl21* in tongue tumors of WT and TNCKO mice ($n = 5$ per genotype). **C,** Quantification of CCL21 protein by ELISA in tongue tumors and draining lymph nodes (LN) from WT and TNCKO mice. $n = 6$ per group. **D,** Raman microscopy of CCL21 in the stroma of WT and TNCKO tumors. Areas of TMTs were identified and scanned (black box). Representative of 9 Raman images of ECM (red) and CCL21 (green) for WT and TNCKO tumors. **E,** Raman spectra from lung and mandibular lymph nodes (LN) of control mice, WT and TNCKO tumors. **F,** Raman quantification of CCL21 pixel intensities in stroma of WT and TNCKO tumors. $n = 3$ tumors per genotype. **G** and **I,** Representative of 40 IF images for the indicated molecules in a WT and TNCKO tumor. **H,** Score determination of CCL21 in WT ($n = 5$) and TNCKO ($n = 5$) tumors, 8 to 10 images per tumor. ELISA for CCL21 in CM from OSCC13 and FRCs (**J**) or LECs (**K**), either nonstimulated (NS) or stimulated with TNC in the presence of the indicated inhibitors (**K**). $n = 5$ (**J**) and 3 (**K**) independent experiments. **B**, **F**, **H**, and **K,** Mean ± SEM. Mann–Whitney test, *, $P < 0.05$; Kruskal–Wallis test and Dunn posttest, *, $P < 0.05$, **, $P < 0.01$ (**C** and **J**). Scale bar, 30 μm (**D**) and 100 μm (**G** and **I**). S, stroma; T, tumor cell nest.

(Supplementary Fig. S3F). Upon exposure to TNC, there was no difference in FRCs and OSCC13 (isolated from a 4NQO-induced carcinoma, typically expressing p63 and CK8/18; ref. 51; **Fig. 3J**; Supplementary Fig. S3F and S3G). However, *Ccl21* mRNA and CCL21 protein expression largely increased in LECs upon treatment with TNC (**Fig. 3K**; Supplementary Fig. S3H).

Inhibitors for TGFβRI (GW788388), TLR4 (Cli95), and receptor tyrosine kinases (SU6668) did not alter CCL21 expression upon TNC treatment, but an antagonist for integrins α4β1/α9β1 (BOP) and an integrin α9β1 blocking antibody reduced *Ccl21* mRNA and CCL21 protein expression compared with those without induction by TNC (**Fig. 3K**; Supplementary Fig. S3H–S3J). Thus, TNC induced CCL21 in LECs via integrin α9β1.

TNC bound CCL21 and immobilized DCs

Because TNC binds several soluble factors (40), it was crucial to determine whether TNC binds to CCL21. CCL21 bound to several sites within the TNC molecule, whereas uncoated gold particles, or other gold-labeled molecules, not binding TNC (BSA and EGF; ref. 40), did not interact (**Fig. 4A** and **B**; Supplementary Fig. S4A–S4C). A major binding site for CCL21 was within the fibronectin type III repeats (FNIII), presumably in the fifth repeat, as CCL21 bound at the same site (fifth FNIII repeat) where TGFβ1 was documented to bind TNC (ref. 40; **Fig. 4B**; Supplementary Fig. S4D). Heparin blocked binding of CCL21 to the FNIII repeats (Supplementary Fig. S4E). Also, binding of CCL21 to TNC was higher at pH 6 than at pH 7 (**Fig. 4C**). The TNC/CCL21-binding strength (K_d of 5.8×10^{-8} mol/L) was lower than CCL21 binding to CCR7 but in the same range (8.4×10^{-8} mol/L; ref. 52; **Fig. 4C**).

Using migration assays, we determined whether TNC-bound CCL21 could restrain DC migration (Supplementary Fig. S4F). CCL21 attracted DCs in a concentration-dependent manner, with fewer cells migrating toward TNC compared with FN or Col I (Supplementary Fig. S4G). To determine whether DC2.4 were potentially immobilized on the TNC substratum, we measured cell retention by counting the cells tethered on the surface of the lower side of the insert (**Fig. 4D**). More DCs were

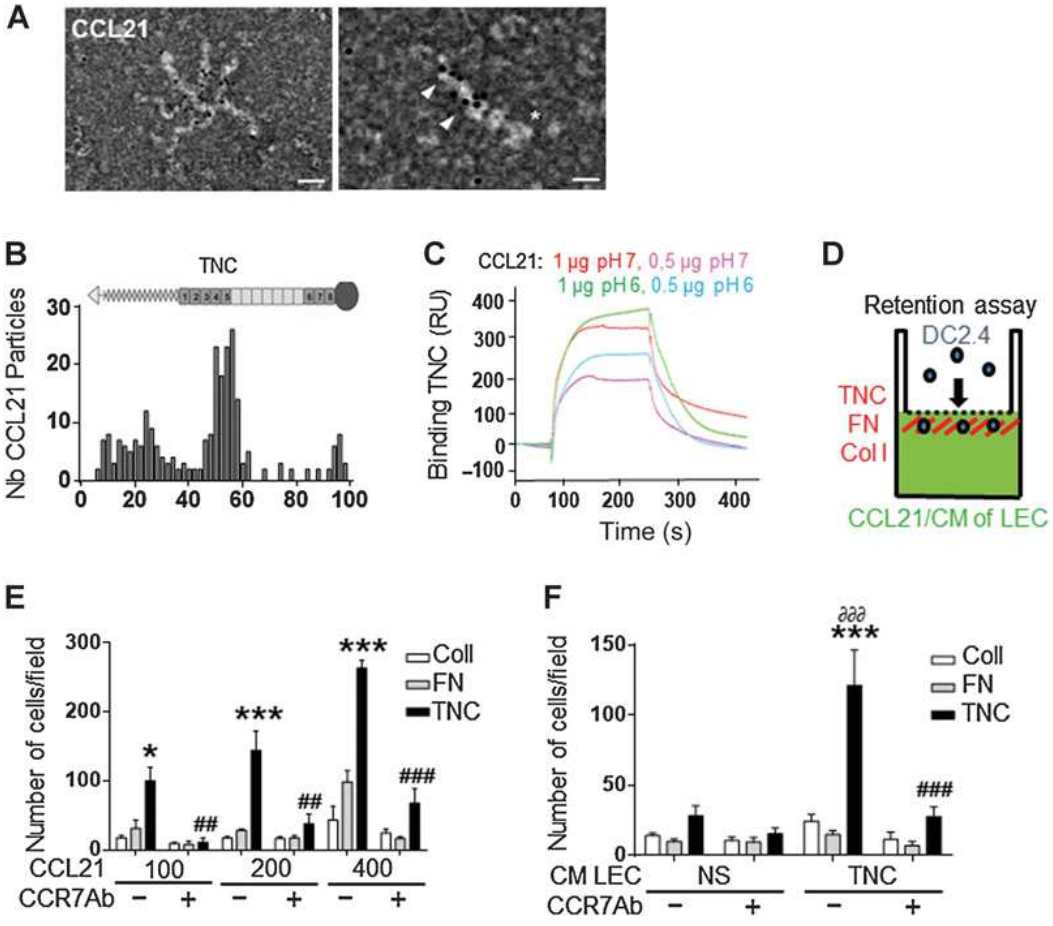

Figure 4.

TNC bound CCL21, leading to DC retention. **A** and **B,** Binding of gold-labeled CCL21 to murine TNC determined by negative staining and transmission electron microscopy. Representative of 500 micrographs (**A**), quantification of bound CCL21 particles along the length of the TNC monomer (**B**). Scale bars, 100 nm (left) and 50 nm (right). **C,** Binding of soluble CCL21 to TNC as measured by surface plasmon resonance spectrometry. K_d (1/s) = 0.0231; KD (M) = 6.78e-08; KA (1/M) = 1.47e+07. **D,** Schematic representation of the Boyden chamber transwell chemoretention assay of DC2.4 toward a gradient of CCL21 or CM of LEC upon treatment with human TNC. The bottom surface of the insert was coated with FN, Col I, or human TNC. Quantification of DC2.4 on the coated surface upon migration toward CCL21 (µg/mL, 5 hours; **E**) or CM (8 hours; **F**) and pretreatment (+) or not (-) with a CCR7 antibody (Ab). NS, nonstimulated. $n = 4$ experiments (8 wells) with 5 images per well. Mean ± SEM, Kruskal–Wallis test and Dunn posttest. *, $P < 0.05$; ***, $P < 0.005$ (relative to FN and Col I coating); ##, $P < 0.01$, ###, $P < 0.005$ (relative to CCR7 Ab condition); ∂∂∂, $P < 0.001$ (relative to NS condition).

immobilized on TNC (compared with FN or Col I), which occurred in a CCL21 dose-dependent manner and was reduced with a CCR7-blocking antibody (**Fig. 4E**). CM from TNC-treated LEC caused DC2.4 retention on TNC compared with CM from control LECs and this was abolished by blocking CCR7 (**Fig. 4F**; Supplementary Fig. S4H).

TNC shaped an immune-suppressive TME linked to increased CCR7 expression

FRC are a cellular component of reticular fibers of lymphoid tissues producing ECM and soluble factors (41). Also, cells with FRC properties (gp38$^+$, ERTR7$^+$, LYVE$^-$) populate tumors (49). We wanted to know whether TNC impacted the abundance and spatial distribution of FRC. Using gp38 as marker for FRC (with CD31-negative selection) and ERTR7 staining, there were more FRC in WT than TNCKO tumors (**Fig. 5A** and **B**; Supplementary Fig. S5A and S5B; Supplementary Table S6).

The cellular crosstalk in lymphatic tissue is regulated by CCR7 signaling (53). There was higher *Ccr7* expression and more CCR7$^+$ cells, in particular, CCR7$^+$ macrophages (CD11b$^+$/F4/80$^+$), DCs (CD11c$^+$/MHCII$^+$), and CD8$^+$ T cells in WT compared with TNCKO tumors (**Fig. 5C–F**; Supplementary Fig. S5C–S5E). CCR7$^+$CD11c$^+$ cells were less prominent in the local lymph nodes of WT tumor mice, again suggesting a potential role of TNC in impairing migration of these cells from the tumor site to the draining lymph nodes yet not within the lymph nodes (**Fig. 5G**; Supplementary Fig. S5F).

Next, we investigated whether TNC influenced the expression of CCR7. We saw higher CCR7 expression in DC2.4 upon treatment with LPS (positive control) and TNC (**Fig. 5H**; Supplementary Fig. S5G). As TNC can signal through TLR4 (13), we used Cli95 to inhibit TLR4 (54) and observed that Cli95 abolished induction of CCR7 in DC2.4 (**Fig. 5H**). Next, we asked whether TNC-induced TLR4 signaling also affected expression of the DC maturation markers CD80 and CD86. Whereas LPS increased expression of both molecules (that was blocked by Cli95), TNC did not affect their expression at the cell surface (Supplementary Fig. S5H and I). As we saw higher *Cd80* and *Cd86* in WT tumors we considered an indirect effect by the tumor cells (Supplementary Fig. S5K). Therefore, we treated DC2.4 with CM from OSCC13 shC cells, expressing TNC (and shTNC cells with undetectable TNC) and observed higher expression of *Cd80, Cd86* (and *Ccr7*), supporting a paracrine mechanism of TNC action (**Fig. 5I**; Supplementary Fig. S5J). CD80 and CD86 can be induced by IL6 and TNFα (55, 56) and we observed higher expression of both molecules in WT tumors (Supplementary Fig. S5L).

TNC also robustly increased expression of a group of genes involved in antigen processing and presentation, for example, 15 *MhcII* genes (H2), β2 microglobulin (*B2M*), transporter associated with antigen processing 1 (*Tap1*), and cathepsin S (*Ctss*), that were higher in WT than TNCKO tumors (Supplementary Fig. S5K).

Tregs (CD4$^+$/CD25$^+$/Foxp3$^+$) and CCR7$^+$ Tregs were more frequent in WT than TNCKO tumors (**Figs. 2J** and **5J**). As Tregs express anti-inflammatory cytokines, we observed higher expression of the IL10 pathway (e.g., IL10, IL1ra, IL1a/b) in WT tumors (Supplementary Fig. S5M). We observed a positive correlation between *Ccl21* expression and *Foxp3* and *Il10* expression, respectively, thus, TNC may impact Treg abundance and function through CCL21 (Supplementary Fig. S5N). In addition to *Tgfb1*, TNC upregulated molecules involved in Treg chemotaxis (e.g., *Ccl3, Ccl2, Rantes, Cxcl9, Cxcl10, P-selectin*, and *Ccl22*; **Fig. 5K**; Supplementary Fig. S5L and S5O). High expression of these genes together with a low number of CCR7$^+$ Tregs (6%) could explain that TNC increased Treg abundance, in particular, within the tumor cell nests (**Fig. 2K** and **L**).

We wondered whether TNC impacted CTL abundance and activity, as DCs and Tregs can regulate CTL responses (57). Immune-suppressive CD8$^+$ Tregs and nonprimed CCR7$^+$/CD8$^+$ T cells were more abundant in WT tumors (**Fig. 5L**; Supplementary Fig. S5E). This result suggested a potential impact of TNC on the education of CD8$^+$ T cells in the lymph nodes and their impaired activity in tumors. In support of this idea, we saw significantly less *Ifnγ, Granzyme b*, and *Perforin* expression in lymph nodes and in tumors from WT mice (**Fig. 5M**; Supplementary Fig. S5P and S5Q). Also, a majority of "positive T-cell activation"–related genes (24 of 32) were downregulated in WT tumors (Supplementary Fig. S5R). Immune checkpoint inhibitor genes [*Pdcd1* (encoding PD1), *Cd274* (encoding PDL-1), and *Ctla4*] and prostaglandin E2—related genes (*Ptges2, Ptgs2*, and *Ptger1*) were elevated in WT compared with TNCKO tumors (Supplementary Fig. S5L). Together, these data suggested an immune-suppressive TME in WT tumors.

CCR7 signaling blocklade blunted the immune-suppressive TME

To investigate whether enhanced CCR7 signaling by TNC was linked to immune suppression and tumor growth, we used a CCR7-blocking antibody. Carcinogen-exposed WT mice were treated with this (and a control) antibody. As shown in **Fig. 6A**, we observed less tumors. Investigating the numbers of leukocytes and immune subtypes, we did not see any difference between the treated groups (Supplementary Fig. S6A and S6B). Whereas the number of CCR7$^+$ leukocytes was not different in local lymph nodes and spleen, the number of CCR7$^+$ DCs (CD11c$^+$/MHCII$^+$), macrophages (CD11b$^+$/F4/80), Tregs (CD25$^+$/Foxp3$^+$), and CD8$^+$ Tregs (CD3$^+$/CD8$^+$/Foxp3$^+$) was reduced upon anti-CCR7 treatment (**Fig. 6B–E**; Supplementary Fig. S6C–S6G). These results precluded a systemic effect of the anti-CCR7 treatment such as a general depletion of CCR7$^+$ cells (or other leukocytes). After anti-CCR7 treatment, there were more CD45$^+$ and CD11c$^+$ cells in the tumor cell nests (**Fig. 6F–I**), similar to the TNCKO phenotype (**Fig. 2G–L**).

Whereas anti-CCR7 treatment did not alter CCL21 expression, the expression of many anti-inflammatory molecules was reduced, which was consistent with a lower abundance of Tregs (**Fig. 6D** and **J**; Supplementary Fig. S6F, S6H, and S6I), again similar to the TNCKO phenotype (**Figs. 2J** and **6K**). Addressing a potential impact of CCR7 blockade on the abundance of FRC, we observed less FRC (**Fig. 6K** and **L**), once more mimicking the TNCKO phenotype (**Fig. 5A** and **B**). This was reinforced by a reduced expression of several immune suppression–related genes upon anti-CCR7 treatment, including *Mrc1* (encoding CD206) and the immune checkpoint inhibitors *Pdcd1, Cd274*, and *Ctla4* (Supplementary Fig. S6J). The CCR7 antibody treatment also affected ECM-related gene expression in the tumors, notably downregulation of *Tnc* itself (Supplementary Fig. S6K).

Next we asked whether APC function and priming of CTL potentially was also enhanced. Indeed, we saw higher IFNγ, *Granzyme b*, and *Perforin* expression in the local lymph nodes and less nonprimed CD8$^+$ T cells (CCR7$^+$/CD3$^+$/CD8$^+$) inside the tumors. Higher expression of genes positively related to T-cell activation upon anti-CCR7 treatment was seen (**Fig. 6E**; Supplementary Fig. S6L–S6O). Consistently, we saw less cancer cells in the local lymph nodes of anti-CCR7–treated mice (Supplementary Fig. S6P).

An immune-suppressive TME in human OSCC correlated with poor prognosis

To address whether immune suppression through TNC/CCL21/CCR7 is potentially relevant in human OSCC, we investigated human tumors for TNC and the LEC marker podoplanin. As the murine

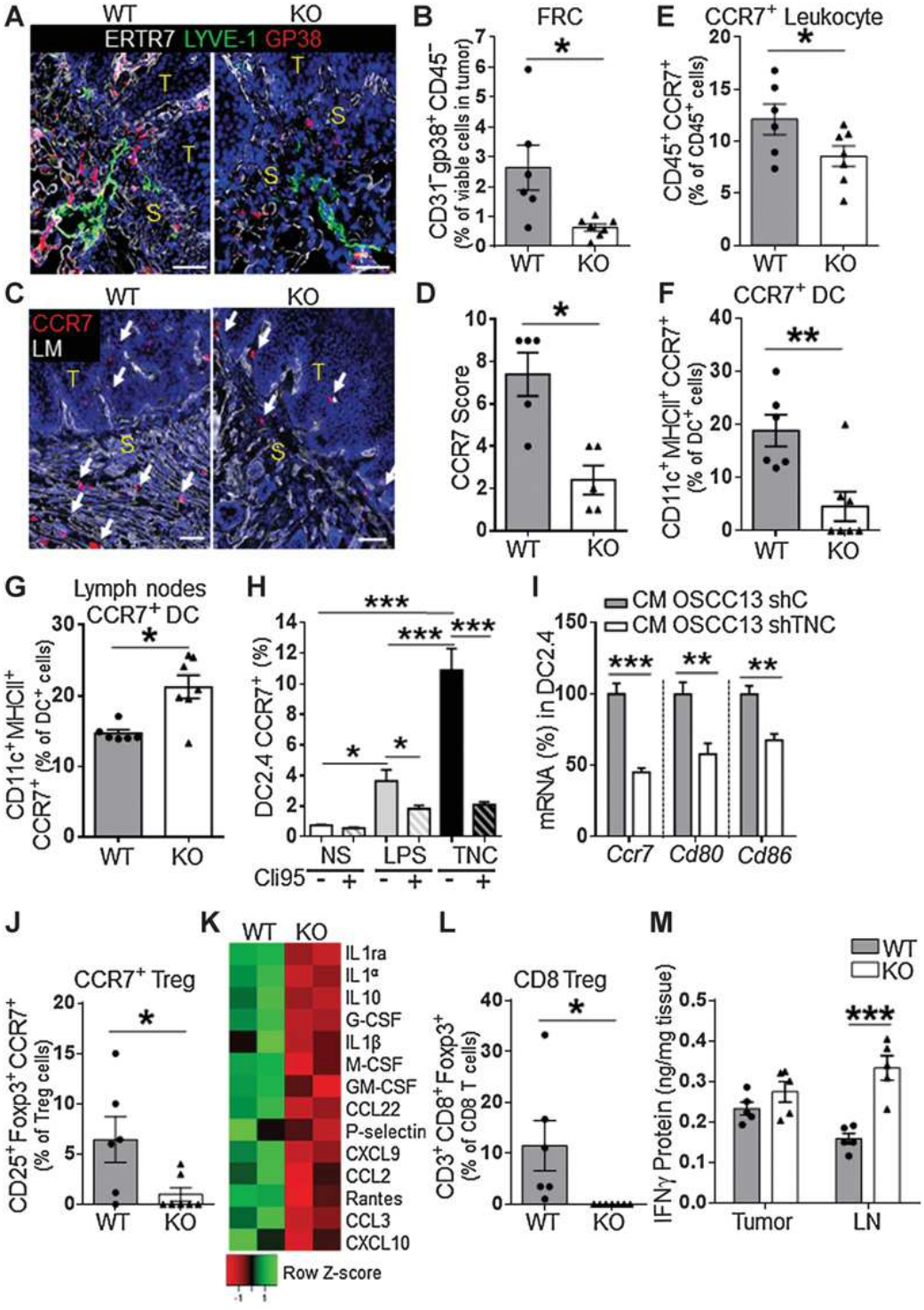

Figure 5.

Immune-suppressive and lymphoid properties of TNC-rich stroma in the murine OSCC. **A** and **C,** Representative of 20 IF images for the indicated molecules in WT and TNCKO tumors. Arrow points at signal. Quantification of cells by flow cytometry with the indicated antibodies in tumors (**B**, **E**, **F**, **J**, and **L**) and lymph nodes (**G**); WT ($n = 6$) and TNCKO ($n = 7$). **D,** Score measurement of CCR7 in tongue tumors of WT and TNCKO mice, 5 mice per genotype, 8 to 10 images per tumor. **H,** CCR7 expression analysis in DC2.4 cells by flow cytometry (% of viable cells) treated *in vitro* with the indicated conditions. NS, medium alone. Five experiments. **I,** Expression of the indicated molecules by qRTPCR upon treatment with CM as indicated. **K,** Expression of IL10 signaling pathway–related molecules (most deregulated) in pooled WT and TNCKO tumors (5 per condition) determined with a proteome profiler array in duplicate (2 membranes per condition), $P = 1.11 \times 10^{-16}$. **M,** Quantification of IFNγ protein by ELISA in the tumor and regional lymph nodes (LN) of the neck from WT and TNCKO mice. $n = 5$ per tissue and group. Mean ± SEM, Mann–Whitney test (**B**, **D**, **E**, **F**, **G**, **I**, and **J**); mean ± SEM, Kruskal–Wallis test and Dunn posttest (**H** and **M**). *, $P < 0.05$; **, $P < 0.01$; ***, $P < 0.005$. Scale bar, 100 μm (**A** and **C**). S, stroma; T, tumor cell nest.

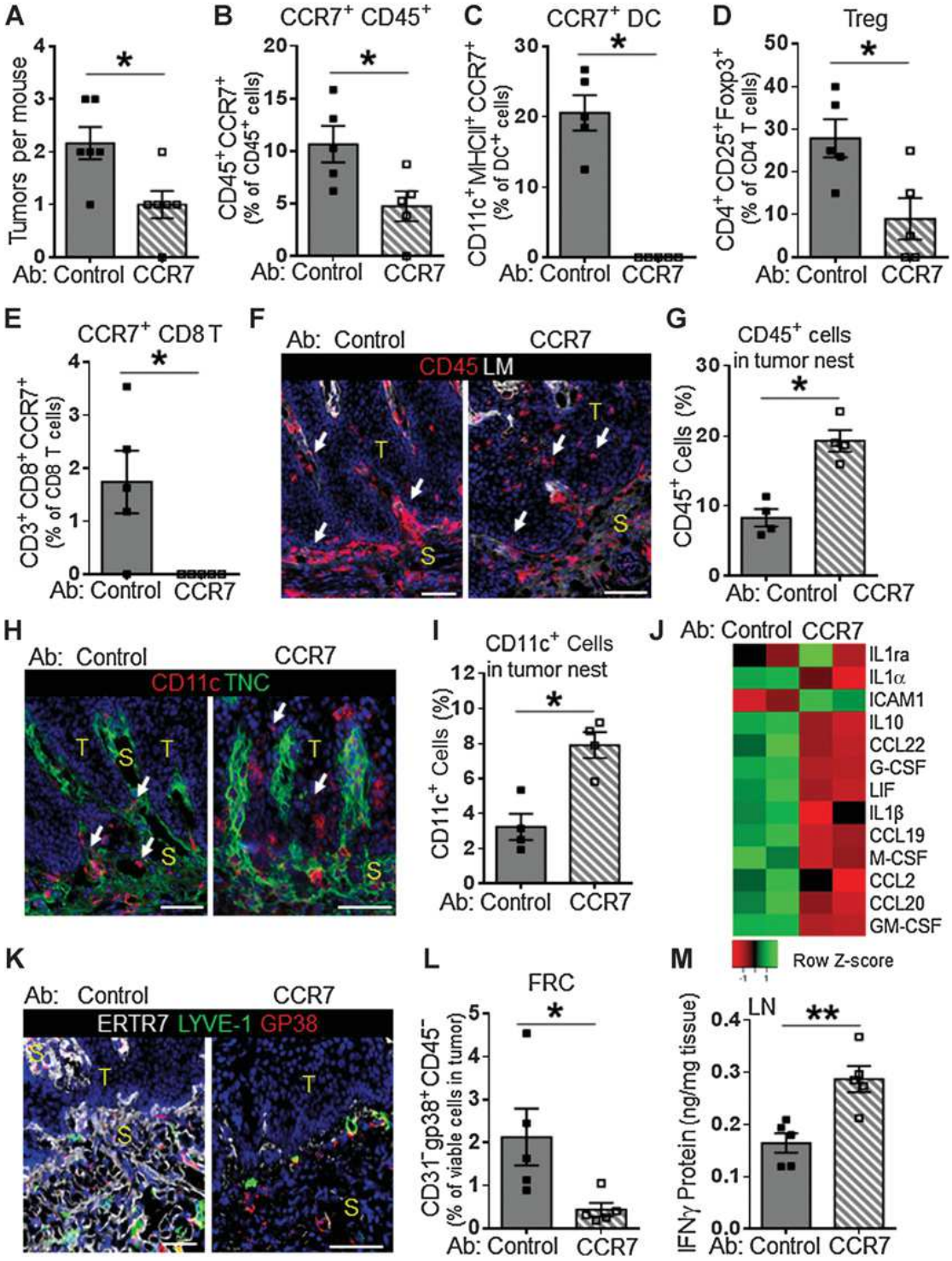

Figure 6.

CCR7 inhibition abolished the immune-suppressive phenotype mimicking TNCKO tumors. **A,** Quantification of tongue tumor number in control antibody– and CCR7 antibody–treated WT mice ($n = 5$ mice per group). **B–E** and **L,** Flow cytometry quantification of cells upon treatment of tumor-bearing WT mice with anti-CCR7 antibody ($n = 5$) or isotype control antibody ($n = 5$) as indicated. **F–I** and **K,** Spatial distribution of cells and ECM in anti-CCR7–treated tumors as determined by IF (**F**, **H**, and **K**) and quantification (**G** and **I**). **F**, **H**, and **K,** Representative images of 20 are shown of IF stainings as indicated. **G** and **I,** Quantification of the indicated cells in the tumor cell nests, mean values from 4 tumors per genotype, 8 to 10 random images per tumor. **J,** Heatmap representation of a proteome profiler array for IL10 signaling pathway–related molecules in anti-CCR7–treated tumors. $n = 5$ tumors pooled per group, experiment done in duplicate (2 membranes per group). **M,** Quantification of IFNγ protein by ELISA in the regional lymph nodes of the neck in anti-CCR7–treated mice. Mean ± SEM, Mann–Whitney test (*, $P < 0.05$; **, $P < 0.01$; **A–E**, **G**, **I**, **L**, and **M**). Scale bar, 100 μm (**F**, **H**, and **K**). Ab, antibody; S, stroma; T, tumor cell nest.

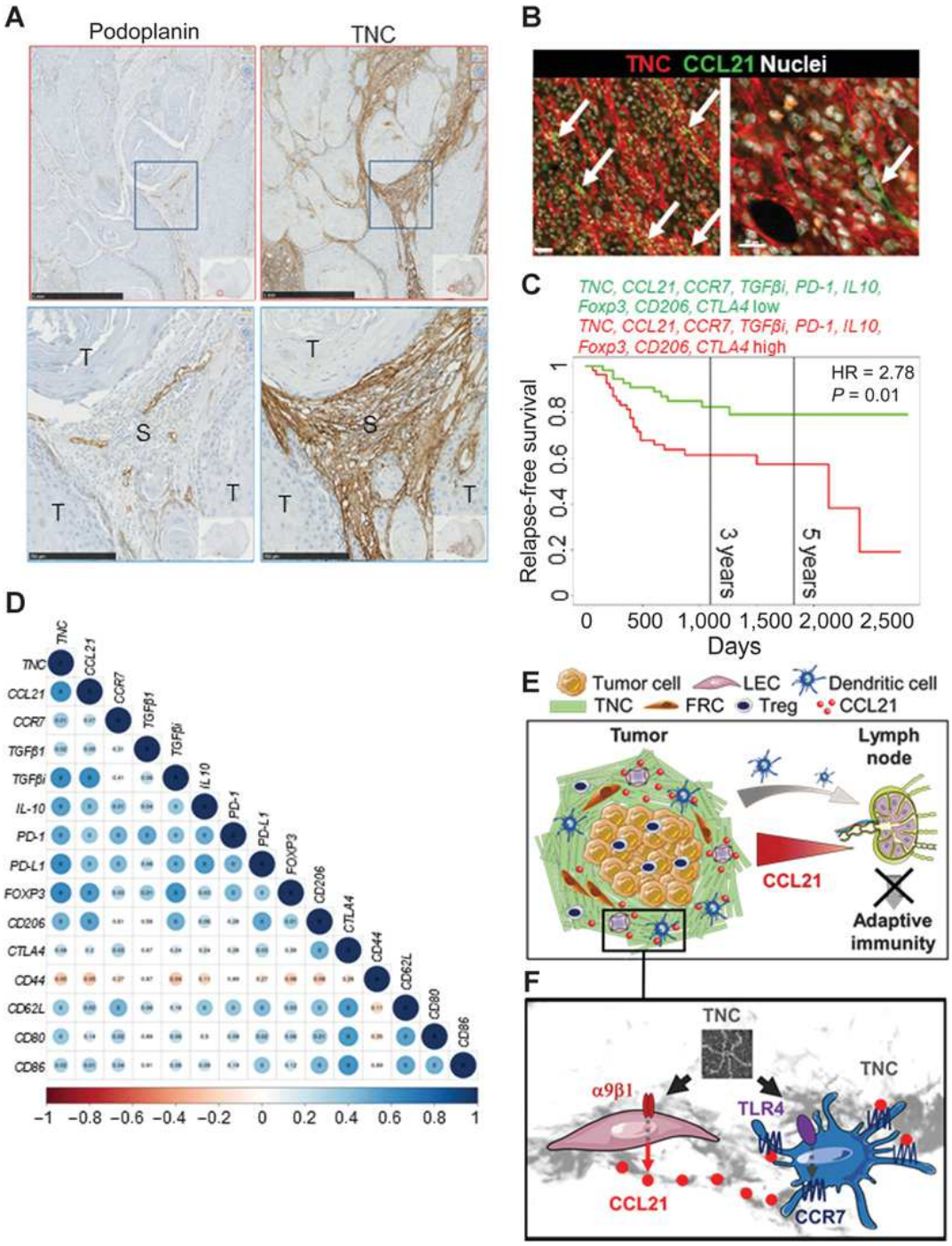

Figure 7.

TNC enforced an immune-suppressive TME in human OSCC. **A,** Representative IHC staining images for podoplanin and TNC in serial whole sections of a human tongue OSCC ($n = 102$). Scale bar, 1,000 μm (top) and 50 μm (bottom). S, stroma; T, tumor cell nest. **B,** Representative images of 40 of IF staining for CCL21 and TNC in a section of a human tongue OSCC ($n = 4$). Scale bar = 40 μm (left) and 20 μm (right). **C,** Kaplan–Meier analysis of HNSCC patient (GSE27020) survival until tumor relapse and combined expression of the indicated molecules above or below the median. HR = 2.78; $P = 0.011$; $n = 54$ per cohort. **D,** Corrplot package analysis for visualization of the correlation matrix between TNC and the indicated genes in patients with HNSCC. The values in the circles are the P_{adj} values, and the color intensities correspond to Spearman correlation values. P_{adj} values below 0.01 are annotated as 0. **E,** TNC enforced an immune-suppressive protumoral TME with lymphoid properties, thereby promoting tumor growth and progression in OSCC. TNC regulated abundance and the spatial distribution of Tregs (inside the tumor cell nest) and $CD11c^+$/DC (inside the stroma). Through binding to CCL21, TNC turned into an adhesive substratum immobilizing $CD11c^+$/DC (through CCR7 signaling), thus impairing DC migration to the regional lymph nodes, compromising adaptive immunity. **F,** In addition to increasing the abundance of FRC, a natural source of CCL21, TNC also induced expression of CCL21 in LECs (through integrin α9β1). TNC also increased CCR7 in DCs (through TLR4), thereby enforcing stromal immobilization of DCs. CCR7 blockade reduced tumor growth and progression.

model mimics the early phases of the human disease, we focused on noninvasive OSCC tissue areas. Similar to the murine tumors, LECs were embedded in TNC-rich stroma (**Fig. 7A**). We costained the tumor tissue for CCL21 and TNC and observed CCL21 expressed in TNC-rich stroma by cells with flat nuclei–forming tubes, likely representing LECs (**Fig. 7B**).

By investigating publicly available gene expression data (GSE27020), we determined expression of TNC and immune-suppressive markers. High *TNC* expression (above the median; as well as *TGFβi)* correlated with shorter time of survival until relapse-free survival (RFS), yet not with overall survival (OS) or metastasis-free survival (MFS; Supplementary Fig. S7A and S7B). Whereas high expression of *CCR7, CCL21, Foxp3, IL10, CD206, CTLA4*, and *PD-1* alone did not correlate with shorter RFS, OS, or MFS, combined high expression of all makers plus *TNC* (HR = 2.78) or *TNC* combined with *CCR7, CCL21*, and *IL10* (HR = 2.02) correlated with shorter RFS, thus supporting a potential role of TNC enforcing an immune-suppressive TME in human HNSCC that favors tumor relapse (**Fig. 7C**; Supplementary Fig. S7C–S7K). This possibility is supported by the study of RNA Affymetrix chip data from 68 patients with HNSCC (23), which shows a positive correlation between the expression of *TNC* and genes that define the immune-suppressive TME (**Fig. 7D**).

Altogether, our results showed that TNC promoted a protumorigenic TME with lymphoid properties by impacting FRC, $CD11c^+$ cells, Tregs, and CTLs involving integrin α9β1 and TRL4, as well as several chemokines and cytokines, which phenocopies human HNSCC (**Fig. 7E** and **F**).

Discussion

Fewer and smaller tongue tumors arose in absence of TNC in the 4NQO-treated mice and no invasive lesions nor lymph node invasion appeared, indicating that TNC promoted tumor progression, similar to other models (58).

TNC is expressed in TMT, also in OSCC (ref. 16 and this study). Despite similarities to reticular fibers suggesting a potential role in tumor immunity, the roles of TMT were obscure (14, 15). Here, TNC impacted the expression of collagens and several matrisomal molecules indicating that TNC may act as a master orchestrator of TMT.

TNC targets several immune subtypes, such as CTL in models of glioblastoma and prostate cancer, macrophages in breast cancer, and $CD11c^+$ cells and Tregs in OSCC as demonstrated here (58–60). Profound differences were observed between WT and TNCKO mice with respect to the immune cell infiltrate and expression of immune-suppressive molecules in tumors and local lymph nodes. The presence of TNC led to less numerous $CD11c^+/MHCII^+$ cells in the tumor nests and enhanced their retention in the stroma. Thus, in a WT tumor, $CD11c^+$ cells may be hampered in priming CTL due to poor migration of antigen-bearing DCs to draining lymph nodes, as seen elsewhere (48, 61). We observed less migratory DCs in draining lymph nodes of WT tumor mice, less nonprimed $CCR7^+$ $CD8^+$ T cells, and more poorly activated CTL in the tumors and lymph nodes of WT compared with TNCKO mice. TNC enforced infiltration of Tregs into the tumor cell nests presumably through elevated expression of Treg-attracting and maturation-promoting factors.

A role of CCL21 signaling in generating a lymphoid immunotolerogenic TME has previously been noticed; how this occurs remained unknown, with no link to matrix nor TNC provided (49). In our model, the natural source of CCL21 was LEC and FRC, and not the tumor cells (49). We identified CCL21/CCR7 signaling as a major target of TNC. Through induction of CCL21 in LEC (via α9β1 integrin) and by increasing the number of FRC, a natural source of CCL21, TNC enforced a protumoral TME and inverted the CCL21 gradient between lymph nodes and the tumor. This may have contributed to poor homing of $CD11c^+$ cells and poor activation of CTL in the lymph nodes. Inhibition of CCR7 abolished the immune-suppressive properties of the TME and subsequently reduced tumor number, tumor progression, and lymph node metastasis.

Our observations supported a dual function of TNC in tumor immunity, in which its ancient role as DAMP and as a component of reticular fibers may be exploited by tumors (10, 13, 17). CCR7 blockade phenocopied features of the TNCKO supporting a causal link between TNC and CCR7.

In human OSCC, CCL21 induction by TNC in LEC may be relevant as high expression of TNC in conjunction with CCR7, CCL21, and other immune-suppressive markers correlated with shorter RFS. Our results could improve HNSCC diagnosis and therapy such as using Raman microspectroscopy for detection of stromal CCL21. Approximately 80% of patients with combined low expression of *TNC* and the immune-suppressive markers survived longer than 5 years and may represent a group that would benefit from a less harsh treatment.

DCs were released from the TNC/CCL21 substratum upon CCR7 inhibition suggesting a potential role of CCR7 as coreceptor of β2 integrins expressed on DCs (62). Thus, targeting β2 integrins (63) could be relevant in releasing $CD11c^+$ cells from the matrix. Also targeting CCR7 may be useful because of its profound effect on abolishing the immune-suppressive properties of the TME, but not altering general immunity. CCR7 is a target in lymphomas and several metastatic cancers, but not yet in HNSCC (64). Several CCR7-targeting approaches have been developed (65–68) that could be tested in HNSCC. We have shown that targeting CCR7 appears to be safe and efficient.

TNC regulated the crosstalk of immune cells with CCL21, the positioning of TILs, especially $CD11c^+$ cells and Tregs, and, subsequently, reduced adaptive immunity, thereby facilitating escape from immunosurveillance. Blockade of CCL21/CCR7 signaling relieved the protumoral immune-suppressive properties of the TME, normalized features of the tumor bed and reduced tumorigenesis and metastasis thus, providing novel targeting opportunities.

Disclosure of Potential Conflicts of Interest

E. Van Obberghen-Schilling reports grants from Institut National du Cancer (INCa), Ligue National Contre le Cancer, and Foundation ARC during the conduct of the study. G. Orend reports grants from Institut National du Cancer (INCa) project FITMANET, Institut National du Cancer (INCa)/Ligue contre le Cancer project ECMpact, and Ligue Régionale contre le Cancer Grand Est (CCIR Est) and other from INSERM and University Strasbourg during the conduct of the study, as well as a pending patent. No potential conflicts of interest were disclosed by the other authors.

Authors' Contributions

C. Spenlé: Data curation, formal analysis, validation, investigation, visualization, methodology, writing–original draft, writing–review and editing. **T. Loustau:** Data curation, formal analysis, investigation, visualization, methodology, writing–original draft, writing–review and editing. **D. Murdamoothoo:** Investigation. **W. Erne:** Investigation. **S. Beghelli-de la Forest Divonne:** Investigation. **R. Veber:** Investigation. **L. Petti:** Investigation. **P. Bourdely:** Investigation. **M. Mörgelin:** Investigation. **E.-M. Brauchle:** Investigation. **G. Cremel:** Investigation. **V. Randrianarisoa:** Investigation. **A. Camara:** Investigation. **S. Rekima:** Investigation. **S. Schaub:** Software, investigation. **K. Nouhen:** Investigation. **T. Imhof:** Resources, investigation. **U. Hansen:** Investigation. **N. Paul:** Data curation, software. **R. Carapito:** Supervision. **N. Pythoud:** Investigation. **A. Hirschler:** Investigation. **C. Carapito:** Supervision, validation. **H. Dumortier:** Supervision, validation. **C.G. Mueller:** supervision, validation. **M. Koch:** Formal analysis, supervision, funding acquisition. **K. Schenke-Layland:** Supervision, funding acquisition, validation. **S. Kon:** Resources. **A. Sudaka:** Resources, validation,

investigation. **F. Anjuere:** conceptualization, formal analysis, supervision, funding acquisition, validation, writing–original draft. **E. Van Obberghen-Schilling:** Conceptualization, supervision, funding acquisition, validation, writing–original draft. **G. Orend:** Conceptualization, supervision, funding acquisition, validation, visualization, writing–original draft, writing–review and editing.

Acknowledgments

The authors thank O. Lefebvre, F. Steinbach, A. Klein, C. Arnold, and the animal facility for technical support; A. Molitor and A. Pichot for RNA sequencing; K. Schlattmann, C. Alampi, M. Chami, and K. Qvortrup for EM imaging assistance; N. Toussan for CD45 immunostaining; and A. Jung for access to gene expression data. This work was supported by grants from INCa, Ligue National Contre le Cancer, and the Foundation ARC (PAIR-VADS11-023, to E. Van Obberghen-Schilling and G. Orend); AAP2017.LNCC/EVO (to E. Van Obberghen-Schilling, F. Anjuere, and G. Orend); the Ligue Régionale contre le Cancer and INSERM and University Strasbourg (to G. Orend); Cancéropôle PACA and LABEX SIGNALIFE program (ANR-11-LABEX-0028-01, to E. Van Obberghen-Schilling and F. Anjuere); Deutsche Forschungsgemeinschaft (EXC 2180, INST 2388/64-1), Ministry of Science, Research and Arts of Baden Württemberg (Az.: SI-BW 01222-91, 33-729.55-3/214-8, to K. Schenke-Layland and E.-M. Brauchle); and fellowship grants from French Ministry of Research MRT (to W. Erne) and Foundation ARC (to D. Murdamoothoo).

The costs of publication of this article were defrayed in part by the payment of page charges. This article must therefore be hereby marked *advertisement* in accordance with 18 U.S.C. Section 1734 solely to indicate this fact.

Received January 25, 2020; revised April 19, 2020; accepted July 1, 2020; published first July 14, 2020.

References

1. Sacco AG, Cohen EE. Current treatment options for recurrent or metastatic head and neck squamous cell carcinoma. J Clin Oncol 2015;33:3305–13.
2. Leemans CR, Braakhuis BJM, Brakenhoff RH. The molecular biology of head and neck cancer. Nat Rev Cancer 2011;11:9–22.
3. Ferris RL. Immunology and immunotherapy of head and neck cancer. J Clin Oncol 2015;33:3293–304.
4. Seiwert TY, Burtness B, Mehra R, Weiss J, Berger R, Eder JP, et al. Safety and clinical activity of pembrolizumab for treatment of recurrent or metastatic squamous cell carcinoma of the head and neck (KEYNOTE-012): an open-label, multicentre, phase 1b trial. Lancet Oncol 2016;17:956–65.
5. Langlois B, Saupe F, Rupp T, Arnold C, van der Heyden M, Orend G, et al. AngioMatrix, a signature of the tumor angiogenic switch-specific matrisome, correlates with poor prognosis for glioma and colorectal cancer patients. Oncotarget 2014;5:10529–45.
6. Maziveyi M, Alahari SK. Cell matrix adhesions in cancer: the proteins that form the glue. Oncotarget 2017;8:48471–87.
7. Turley SJ, Cremasco V, Astarita JL. Immunological hallmarks of stromal cells in the tumour microenvironment. Nat Rev Immunol 2015;15:669–82.
8. Van Obberghen-Schilling E, Tucker RP, Saupe F, Gasser I, Cseh B, Orend G. Fibronectin and tenascin-C: accomplices in vascular morphogenesis during development and tumor growth. Int J Dev Biol 2011;55:511–25.
9. Chiquet-Ehrismann R, Orend G, Chiquet M, Tucker RP, Midwood KS. Tenascins in stem cell niches. Matrix Biol 2014;37:112–23.
10. Midwood KS, Hussenet T, Langlois B, Orend G. Advances in tenascin-C biology. Cell Mol Life Sci 2011;68:3175–99.
11. Midwood KS, Chiquet M, Tucker RP, Orend G. Tenascin-C at a glance. J Cell Sci 2016;129:4321–7.
12. Imanaka-Yoshida K, Aoki H. Tenascin-C and mechanotransduction in the development and diseases of cardiovascular system. Front Physiol 2014;5:283.
13. Midwood K, Sacre S, Piccinini AM, Inglis J, Trebaul A, Chan E, et al. Tenascin-C is an endogenous activator of Toll-like receptor 4 that is essential for maintaining inflammation in arthritic joint disease. Nat Med 2009;15:774–80.
14. Drumea-Mirancea M, Wessels JT, Müller CA, Essl M, Eble JA, Tolosa E, et al. Characterization of a conduit system containing laminin-5 in the human thymus: a potential transport system for small molecules. J Cell Sci 2006;119:1396–405.
15. Spenlé C, Saupe F, Midwood K, Burckel H, Noel G, Orend G. Tenascin-C: exploitation and collateral damage in cancer management. Cell Adh Migr 2015;9:141–53.
16. Rupp T, Langlois B, Koczorowska MM, Radwanska A, Sun Z, Hussenet T, et al. Tenascin-C orchestrates glioblastoma angiogenesis by modulation of pro- and anti-angiogenic Signaling. Cell Rep 2016;17:2607–19.
17. Spenlé C, Gasser I, Saupe F, Janssen K-P, Arnold C, Klein A, et al. Spatial organization of the tenascin-C microenvironment in experimental and human cancer. Cell Adh Migr 2015;9:4–13.
18. Sun Z, Velázquez-Quesada I, Murdamoothoo D, Ahowesso C, Yilmaz A, Spenlé C, et al. Tenascin-C increases lung metastasis by impacting blood vessel invasions. Matrix Biol 2019;83:26–47.
19. Gopal S, Veracini L, Grall D, Butori C, Schaub S, Audebert S, et al. Fibronectin-guided migration of carcinoma collectives. Nat Commun 2017;8:14105.
20. Foy JP, Tortereau A, Caulin C, Le Texier V, Lavergne E, Thomas E, et al. The dynamics of gene expression changes in a mouse model of oral tumorigenesis may help refine prevention and treatment strategies in patients with oral cancer. Oncotarget 2016;7:35932–45.
21. Wang Z, Wu VH, Allevato MM, Gilardi M, He Y, Luis Callejas-Valera J, et al. Syngeneic animal models of tobacco-associated oral cancer reveal the activity of in situ anti-CTLA-4. Nat Commun 2019;10:5546.
22. Goswami CP, Nakshatri H. PROGgeneV2: enhancements on the existing database. BMC Cancer 2014;14:970.
23. Jung AC, Job S, Ledrappier S, Macabre C, Abecassis J, de Reyniès A, et al. A poor prognosis subtype of HNSCC is consistently observed across methylome, transcriptome, and miRNome analysis. Clin Cancer Res 2013;19:4174–84.
24. Benjamini Y, Drai D, Elmer G, Kafkafi N, Golani I. Controlling the false discovery rate in behavior genetics research. Behav Brain Res 2001;125:279–84.
25. Talts JF, Wirl G, Dictor M, Muller WJ, Fässler R. Tenascin-C modulates tumor stroma and monocyte/macrophage recruitment but not tumor growth or metastasis in a mouse strain with spontaneous mammary cancer. J Cell Sci 1999;112:1855–64.
26. Somovilla-Crespo B, Alfonso-Pérez M, Cuesta-Mateos C, Carballo-de Dios C, Beltrán AE, Terrón F, et al. Anti-CCR7 therapy exerts a potent anti-tumor activity in a xenograft model of human mantle cell lymphoma. J Hematol Oncol 2013;6:89.
27. Dobin A, Davis CA, Schlesinger F, Drenkow J, Zaleski C, Jha S, et al. STAR: ultrafast universal RNA-seq aligner. Bioinformatics 2013;29:15–21.
28. Langmead B, Salzberg SL. Fast gapped-read alignment with Bowtie 2. Nat Methods 2012;9:357–9.
29. Anders S, Pyl PT, Huber W. HTSeq–a Python framework to work with high-throughput sequencing data. Bioinformatics 2015;31:166–9.
30. Love MI, Huber W, Anders S. Moderated estimation of fold change and dispersion for RNA-seq data with DESeq2. Genome Biol 2014;15:550.
31. Mi H, Huang X, Muruganujan A, Tang H, Mills C, Kang D, et al. PANTHER version 11: expanded annotation data from gene ontology and reactome pathways, and data analysis tool enhancements. Nucleic Acids Res 2017;45:D183–9.
32. Fabregat A, Sidiropoulos K, Viteri G, Forner O, Marin-Garcia P, Arnau V, et al. Reactome pathway analysis: a high-performance in-memory approach. BMC Bioinformatics 2017;18:142.
33. Tyanova S, Temu T, Cox J. The MaxQuant computational platform for mass spectrometry-based shotgun proteomics. Nat Protoc 2016;11:2301–19.
34. Wieczorek S, Combes F, Lazar C, Giai Gianetto Q, Gatto L, Dorffer A, et al. DAPAR & ProStaR: software to perform statistical analyses in quantitative discovery proteomics. Bioinformatics 2017;33:135–6.
35. Ritchie ME, Phipson B, Wu D, Hu Y, Law CW, Shi W, et al. limma powers differential expression analyses for RNA-sequencing and microarray studies. Nucleic Acids Res 2015;43:e47.
36. Huang W, Chiquet-Ehrismann R, Moyano JV, Garcia-Pardo A, Orend G. Interference of tenascin-C with syndecan-4 binding to fibronectin blocks cell adhesion and stimulates tumor cell proliferation. Cancer Res 2001;61:8586–94.
37. Giblin SP, Murdamoothoo D, Deligne C, Schwenzer A, Orend G, Midwood KS. How to detect and purify tenascin-C. Methods Cell Biol 2018;143:371–400.
38. Bober M, Enochsson C, Collin M, Mörgelin M. Collagen VI is a subepithelial adhesive target for human respiratory tract pathogens. J Innate Immun 2010;2:160–6.
39. Baschong W, Wrigley NG. Small colloidal gold conjugated to Fab fragments or to immunoglobulin G as high-resolution labels for electron microscopy: a technical overview. J Electron Microsc Tech 1990;14:313–23.

40. De Laporte L, Rice JJ, Tortelli F, Hubbell JA. Tenascin C promiscuously binds growth factors via its fifth fibronectin type III-like domain. PLoS One 2013;8: e62076.
41. Fletcher AL, Acton SE, Knoblich K. Lymph node fibroblastic reticular cells in health and disease. Nat Rev Immunol 2015;15:350–61.
42. Kanayama M, Morimoto J, Asano T, Matsui Y, Nakayama Y, Saito Y, et al. Alpha9 integrin and its ligands constitute critical joint microenvironments for development of autoimmune arthritis. J Immunol 2009;182:8015.
43. Elmusrati AA, Pilborough AE, Khurram SA, Lambert DW. Cancer-associated fibroblasts promote bone invasion in oral squamous cell carcinoma. Br J Cancer 2017;117:867–75.
44. Shivamallappa SM, Venkatraman NT, Shreedhar B, Mohanty L, Shenoy S. Role of angiogenesis in oral squamous cell carcinoma development and metastasis: an immunohistochemical study. Int J Oral Sci 2011;3:216–24.
45. Saupe F, Schwenzer A, Jia Y, Gasser I, Spenlé C, Langlois B, et al. Tenascin-C downregulates Wnt inhibitor Dickkopf-1, promoting tumorigenesis in a neuroendocrine tumor model. Cell Rep 2013;5:482–92.
46. Naba A, Clauser KR, Hoersch S, Liu H, Carr SA, Hynes RO. The matrisome: in silico definition and in vivo characterization by proteomics of normal and tumor extracellular matrices. Mol Cell Proteomics 2012;11:M111.014647.
47. Baaten B, Tinoco R, Chen A, Bradley L. Regulation of antigen-experienced T cells: lessons from the quintessential memory marker CD44. Front Immunol 2012;3:23.
48. Hervouet C, Luci C, Rol N, Rousseau D, Kissenpfennig A, Malissen B, et al. Langerhans cells prime IL-17-producing T cells and dampen genital cytotoxic responses following mucosal immunization. J Immunol 2010;184: 4842–51.
49. Shields JD, Kourtis IC, Tomei AA, Roberts JM, Swartz MA. Induction of lymphoidlike stroma and immune escape by tumors that express the chemokine CCL21. Science 2010;328:749–52.
50. Kozai M, Kubo Y, Katakai T, Kondo H, Kiyonari H, Schaeuble K, et al. Essential role of CCL21 in establishment of central self-tolerance in T cells. J Exp Med 2017;214:1925–35.
51. Frohwitter G, Buerger H, Van diest PJ, Korsching E, Kleinheinz J, Fillies T. Cytokeratin and protein expression patterns in squamous cell carcinoma of the oral cavity provide evidence for two distinct pathogenetic pathways. Oncol Lett 2016;12:107–13.
52. Lanati S, Dunn DB, Roussigné M, Emmett MS, Carriere V, Jullien D, et al. Chemotrap-1: an engineered soluble receptor that blocks chemokine-induced migration of metastatic cancer cells in vivo. Cancer Res 2010;70:8138–48.
53. Förster R, Schubel A, Breitfeld D, Kremmer E, Renner-Müller I, Wolf E, et al. CCR7 coordinates the primary immune response by establishing functional microenvironments in secondary lymphoid organs. Cell 1999;99:23–33.
54. Wang H, Mo L, Xiao X, An S, Liu X, Ba J, et al. Pplase of Dermatophagoides farinae promotes ovalbumin-induced airway allergy by modulating the functions of dendritic cells in a mouse model. Sci Rep 2017; 7:43322.
55. Trevejo JM, Marino MW, Philpott N, Josien R, Richards EC, Elkon KB, et al. TNF-α-dependent maturation of local dendritic cells is critical for activating the adaptive immune response to virus infection. Proc Natl Acad Sci U S A 2001;98: 12162–7.
56. Park SJ, Nakagawa T, Kitamura H, Atsumi T, Kamon H, Sawa S, et al. IL-6 regulates in vivo dendritic cell differentiation through STAT3 activation. J Immunol 2004;173:3844–54.
57. Osorio F, Fuentes C, López MN, Salazar-Onfray F, González FE. Role of dendritic cells in the induction of lymphocyte tolerance. Front Immunol 2015;6:535.
58. Deligne C, Murdamoothoo D, Gammage AN, Gschwandtner M, Erne W, Loustau T, et al. Matrix-targeting immunotherapy controls tumor growth and spread by switching macrophage phenotype. Cancer Immunol Res 2020;8: 368–82.
59. Huang JY, Cheng YJ, Lin YP, Lin HC, Su CC, Juliano R, et al. Extracellular matrix of glioblastoma inhibits polarization and transmigration of T cells: the role of tenascin-C in immune suppression. J Immunol 2010;185:1450–9.
60. Jachetti E, Caputo S, Mazzoleni S, Brambillasca CS, Parigi SM, Grioni M, et al. Tenascin-C protects cancer stem-like cells from immune surveillance by arresting T-cell activation. Cancer Res 2015;75:2095–108.
61. Tamoutounour S, Henri S, Lelouard H, de Bovis B, de Haar C, van der Woude CJ, et al. CD64 distinguishes macrophages from dendritic cells in the gut and reveals the Th1-inducing role of mesenteric lymph node macrophages during colitis. Eur J Immunol 2012;42:3150–66.
62. Schittenhelm L, Hilkens CM, Morrison VL. β2 integrins as regulators of dendritic cell, monocyte, and macrophage function. Front Immunol 2017;8: 1866.
63. Raab-Westphal S, Marshall JF, Goodman SL. Integrins as therapeutic targets: successes and cancers. Cancers 2017;9:110.
64. Mollica Poeta V, Massara M, Capucetti A, Bonecchi R. Chemokines and chemokine receptors: new targets for cancer immunotherapy. Front Immunol 2019;10:379.
65. Cunningham H, Kim E, August K, Vines C. Novel single chain antibodies to inhibit ccr7 mediated-entry of pediatric t-cell acute lymphoblastic leukemia into the CNS. Ann Oncol 2014;25:iv328.
66. Jakobs BD, Spannagel L, Purvanov V, Uetz-von Allmen E, Matti C, Legler DF. Engineering of nanobodies recognizing the human chemokine receptor CCR7. Int J Mol Sci 2019;20:2597.
67. Liu J, Wei Y, Luo Q, Xu F, Zhao Z, Zhang H, et al. Baicalin attenuates inflammation in mice with OVA-induced asthma by inhibiting NF-κB and suppressing CCR7/CCL19/CCL21. Int J Mol Med 2016;38:1541–8.
68. Chi BJ, Du CL, Fu YF, Zhang YN, Wang RW. Silencing of CCR7 inhibits the growth, invasion and migration of prostate cancer cells induced by VEGFC. Int J Clin Exp Pathol 2015;8:12533–40.

Biochemical and Biophysical Research Communications xxx (xxxx) xxx

Contents lists available at ScienceDirect

Biochemical and Biophysical Research Communications

journal homepage: www.elsevier.com/locate/ybbrc

Generation and characterization of dromedary Tenascin-C and Tenascin-W specific antibodies

Sayda Dhaouadi [a], Devadarssen Murdamoothoo [b], Asma Tounsi [a], William Erne [b], Rahma Benabderrazek [a], Zakaria Benlasfar [a], Lotfi Hendaoui [c], Ruth Chiquet-Ehrismann [d, 1], Samir Boubaker [e], Gertraud Orend [b], Ismaïl Hendaoui [d], Balkiss Bouhaouala-Zahar [a, f, *]

[a] Laboratoire des Venins et Molécules Thérapeutiques, Institut Pasteur Tunis, 13 Place Pasteur, BP74, 1002, Tunis- Université Tunis El Manar Tunisia, Tunisia
[b] INSERM U1109, Tumor Microenvironment Group, 1 Place de L'Hôpital, 67091, Strasbourg, France
[c] Service de Radiologie, Hôpital Mongi Slim-La Marsa-Tunisia, Tunisia
[d] Friedrich Miescher Institute for Biomedical Research, Maulbeerstrasse 66, Basel, Switzerland
[e] Service Anatomopathologie, Institut Pasteur Tunis, 13 Place Pasteur, BP74, 1002, Tunis- Université Tunis El Manar Tunisia, Tunisia
[f] Faculté de Médecine de Tunis, 15 Rue Djebel Lakhdhar, La Rabta, 1007, Tunis-Université Tunis el Manar, Tunisia

ARTICLE INFO

Article history:
Received 29 April 2020
Accepted 11 May 2020
Available online xxx

Keywords:
Tenascin-C
Tenascin-W
Biomarker
Dromedary serum
Heavy-chain IgG
Extracellular matrix
Tumor microenvironment

ABSTRACT

Tenascin-C (TNC) and tenascin-W (TNW), large hexameric glycoproteins overexpressed in the tumor microenvironment, are useful tumor biomarkers for theranostic applications. For now, polyclonal and monoclonal antibodies, as well as aptamers targeting TNC and TNW have been developed. However, the immunostaining sensitivity of antibodies is very heterogenous. The main aim of this study was to generate antibodies in dromedary that detect TNC and TNW, respectively. We show that immune sera from immunized dromedaries are able to specifically bind native TNC and TNW by ELISA and also to detect TNC and TNW in matrix tracks of mammary tumors by immunostaining. Furthermore, we demonstrate that purified IgG subtypes are able to interact specifically with TNC or TNW by ELISA and immunostaining. These camelid antibodies are a good basis to develop tools for the detection of TNC and TNW in the tumor microenvironment and could potentially have a broader application for early diagnosis of solid cancers.

1. Introduction

The tumor microenvironment (TME) plays a crucial role in tumor progression [1]. The TME is characterized by stromal cells that express extracellular matrix (ECM), growth factors, cytokines and matrix remodeling enzymes that altogether provide signaling information to stromal and cancer cells, thus regulating cell survival, proliferation, as well as invasion and metastasis [2]. Cancer biomarkers, especially within the tumor specific ECM, could represent valid targets for screening, diagnosis and monitoring of tumor progression. Tenascins (TNs) are large glycoproteins found in embryonic and adult ECM. Of the four family members, tenascin-C (TNC) and tenascin-W (TNW) have been shown to be overexpressed in the TME of solid tumors and high levels correlated with worsened prognosis for patients with breast cancer and glioblastoma [3–5]. The molecular mechanisms by which TNC and TNW promote tumor progression have been extensively investigated for TNC and to some degree also for TNW [5–8]. By using genetically engineered mice with high and low TNC expression in context of stochastic tumor onset and progression, it was clearly shown that TNC acts through multiple mechanisms thereby enhancing proliferation, invasion, angiogenesis and metastasis [7].

Several tools for detection of TNC and TNW such as polyclonal and monoclonal antibodies and aptamers have been developed over the last decades [4,9–16]. However, monoclonal antibodies (MAbs) produced in mice exhibit high immunogenicity and low penetration through solid tumors [8,17,18].

* Corresponding author. Laboratoire des Venins et Molécules Thérapeutiques; Institut Pasteur Tunis, 13 Place Pasteur, BP74, 1002, Tunis- Université Tunis El Manar Tunisia, Tunisia.
E-mail addresses: balkiss.bouhaouala@fmt.utm.tn, balkiss.bouhaouala@pasteur.tn (B. Bouhaouala-Zahar).
[1] Deceased.

https://doi.org/10.1016/j.bbrc.2020.05.077
0006-291X/

Please cite this article as: S. Dhaouadi et al., Generation and characterization of dromedary Tenascin-C and Tenascin-W specific antibodies, Biochemical and Biophysical Research Communications, https://doi.org/10.1016/j.bbrc.2020.05.077

Dromedary antibodies would be useful for multichannel immunostaining with better tissue penetration. Another potential advantage could be that dromedary antibodies may work better for staining of formalin-fixed paraffin-embedded (FFPE) tissues which remains a challenge [19,20]. Camel serum contains, in addition to conventional IgG1, an important fraction of functional antibodies called heavy chain immunoglobulins (IgG2 and IgG3) naturally devoid of both light chains and the conserved CH1 domains [21–23].

Here, we aimed to develop anti-TNC and anti-TNW single chain antibodies in dromedary. Therefore, we immunized two dromedaries with purified recombinant murine TNC and TNW or human TNC and TNW, respectively. Finally, we demonstrated that these Heavy-Chain Antibodies (HCAbs) purified from sera were specific towards the respective tenascins.

2. Materials and methods

2.1. Immunogen preparation

Recombinant protein hTNC, hTNW, mTNC and mTNW used for dromedary immunization were expressed in HEK293T cells, as C-terminal 6X His-tagged molecules. Production and purification of the tenascins were done according to the well-established protocol [10,14,24]. Briefly, supernatants were collected from cell cultures and loaded on His-Select columns (Sigma, St. Louis, MO, USA). The His-tagged tenascins were eluted with 300 mM imidazole and quantified using a Bradford assay. The purity of the proteins was checked by SDS-PAGE.

2.2. Transgenic mouse models

Two experimental mouse models have been used for *in situ* investigations of the antibodies: (i) the murine breast cancer MMTV-NeuNT model in context of wildtype levels of TNC (WT) or upon knockout of TNC (TNCKO) [25,26] and (ii) the autochthonous NT193 tumor model that was derived from the MMTV-NeuNT model. NT193 cells derived from a MMTV-NeuNT tumor of a WT mouse were engineered to express low levels of TNC with shRNA (shTNC) or maintain high levels of TNC with a control shRNA (shC). Cells were orthotopically engrafted in immune competent FVB mice with WT or TNCKO background. Tumors were extracted 11 weeks upon grafting and tissue was prepared for immunofluorescence staining (IF). TNC expression analysis by IF revealed very low TNC levels in tumors from TNCKO mice engrafted with shTNC cells (KO/shTNC) whereas tumors from shC cells engrafted in WT mice (WT/shC) showed high TNC levels [27].

2.3. Dromedary immunization protocol

Two 6 years old camels (*Camelus dromedarius*), were provided by a local veterinary at Kondar, Tunisia. Immunization was conducted according to a well-established immunization protocol approved by the Biomedical Ethics Committee of Institut Pasteur de Tunis, Tunisia (CEBM: 2015/25/I/LR11IPT08/V0) and according to the 2010/63/EU Directive for animal experiments. The dromedaries (D1, D2) were subcutaneously immunized with a mix of mTNC and mTNW (D1) and hTNC and hTNW (D2) as immunogens at increasing amounts of 200, 250, 300, 350, 400 and 400 μg for each tenascin, on days 0, 7, 14, 21, 28 and 39 or 35, respectively. The first two injections were mixed with an equal volume of complete Freud's adjuvant. Booster injections were mixed with incomplete Freund's adjuvant (Sigma Aldrich, MO, USA). Blood was withdrawn from the jugular vein before each boost. Three days after the last injection, sera were collected for further use (i.e. S1 and S2, respectively).

2.4. Solid-phase binding enzyme-linked immunosorbent assay (ELISA)

An indirect ELISA test was performed to assess the dromedary immune response. Maxisorp 96-well plates (NUNC, Rochester, NY, USA) were coated with recombinant mTNC, mTNW, hTNC and hTNW immobilized at 0.5 μg/ml per well in coating buffer (0.1 M Na_2CO_3/$NaHCO_3$, pH 9.6), and incubated overnight at 4 °C. Not-bound proteins were removed *via* five successive washes with 0.1% Tween-20/PBS and residual adsorption sites were blocked by adding 1% gelatin (wt/v), 0.05% Tween-20/PBS for 1 h at 37 °C. Diluted sera (1:8000) were added for 1 h at 37 °C. Bound dromedary IgGs were subsequently detected with a goat anti-Llama (H + L) alkaline phosphatase conjugate (Sigma, St. Louis, MO, USA) diluted at 1:5000 and incubated for 1 h at 37 °C. After washing, signal revelation was accomplished using the P-o-Phenylenediamine substrate (Sigma, St. Louis, MO, USA). As irrelevant protein, the scorpion *Androctonus Australis Hector* (AahI) toxin (0.5 μg/ml per well) was used in same plate and conditions [28]. The signal was measured at 450 nm with a plate reader (Thermo Electron Corporation Multiscan EX, MA, USA). The assay was performed in duplicates in three independent ELISA experiments.

2.5. Immunofluorescence microscopy

Immunofluorescence tests were carried-out on 7 μm thick frozen sections of the murine breast tumor tissues (NeuNT-WT, NeuNT-TNCKO and WT/NT193shC, TNCKO/NT193shTNC). First, sections were incubated with PBS for 5 min and non-specific binding sites were blocked with 5% Normal Donkey Serum (NDS)/PBS for 1 h at room temperature (RT). Subsequently, the S1-anti-mTNC/mTNW and S2-anti-hTNC/hTNW dromedary sera (1:500 to 1:5000) as well as the monoclonal rat anti-mTNC (MTn12) and the monoclonal mouse anti-mTNW (Sigma, St. Louis, MO, USA) were added (1:400 and 1:200, respectively) overnight at 4 °C. Sections were washed with NDS/PBS and then incubated with goat anti-Llama secondary antibody (Sigma, St. Louis, MO, USA) (1:1000, 90 min at RT). Alexa fluor 488 donkey anti-goat, cyanine 3 donkey anti-rat and cyanine 5 donkey anti-mouse antibodies (1:1000, 90 min, respectively) were used (Invitrogen, Carsbad, CA, USA). Cell nuclei were counterstained with 4′,6-diamidino-2-phenylindole (DAPI) for 10 min. Negative controls were performed with goat normal serum IgG instead of primary antibody. Images were acquired with an Axioplan microscope coupled with an AxioCam camera and processed using the Axiovision software version 4.6 (Carl Zeiss Vision, Aalen, Germany).

2.6. Fractionation of the serum IgGs subclasses of the camelid antibodies

The separation of the different serum immunoglobulin (IgG) subclasses was performed by successive differential adsorption of S1 and S2 on Hitrap-protein G and Hitrap-protein A-Sepharose antibody-purification columns (GE HealthCare, LifeScience, USA), as described previously [28]. Briefly, 1 ml dromedary serum (S1, S2) was loaded on the protein-G column. The IgG3 fraction was eluted with 0.15 M NaCl, 0.58% acetic acid buffer at pH 3.5 and the IgG1 fraction was subsequently eluted with 0.1 M glycine-HCl buffer at pH 2.7. The flow-through was collected and subsequently loaded on the Hitrap-protein A column to recover the IgG2 subclass. After washing and eluting with 0.15 M NaCl, 0.58% acetic acid buffer at pH 4.5, the IgG2 fraction was obtained. Collected IgG fractions were immediately neutralized with 1 M Tris-HCl, pH 9.0 and stored at −20 °C until use.

Please cite this article as: S. Dhaouadi et al., Generation and characterization of dromedary Tenascin-C and Tenascin-W specific antibodies, Biochemical and Biophysical Research Communications, https://doi.org/10.1016/j.bbrc.2020.05.077

The purity of IgG fractions was investigated by SDS-PAGE. Therefore, 5 μg of each antibody were loaded on 12% polyacrylamide gel in reducing and non-reducing conditions, followed by standard staining and destaining steps. The stained gels were scanned (Epson Perfection 4490 photo, CA, USA).

2.7. Solid-phase ELISA of the serum IgGs subclasses of the camelid antibodies

Maxisorp 96-well ELISA plates (NUNC, Rochester, NY, USA) were coated overnight at 4 °C with recombinant mTNC, mTNW, hTNC or hTNW proteins at 1 μg/ml (0.1 M Na_2CO_3/$NaHCO_3$ pH 9.6) and three negative controls were used at the same concentration (Adrenomedullin, BSA and scorpion venom *Buthus occitanus tunetanus* (BotG50)). The remaining protein binding sites were blocked with 1% gelatin (wt/v)/0.05%Tween-20/PBS. Then, IgG fractions were individually added (1 μg/ml). Subsequently, a polyclonal rabbit anti-dromedary IgG antibody was added (1:10000). The polyclonal rabbit anti-dromedary IgG complexes were revealed with a goat anti-rabbit antibody conjugated to Horse Radish Peroxydase (NA934, Amersham Biosciences, UK) (1:10000 for 1 h at 37 °C). Peroxidase substrate reaction was stopped by adding 50 μl of 2 N H_2SO_4 (Sigma, St. Louis, MO, USA). Absorbance was measured at 450 nm (Thermo Electron Corporation Multiscan EX, USA).

3. Results and discussion

3.1. Humoral responses elicited in the dromedary immunized with mTNC and mTNW

To raise immune responses against both mTNC and mTNW (S1-anti-mTNC/mTNW), the dromedary D1 was injected with increasing amounts of both recombinant mTNC and mTNW (with a total protein amount of 1900 μg each) mixed with complete or incomplete Freund's adjuvant to increase the titer of B cells expressing mTNs-specific antibodies.The immune response was monitored by ELISA to detect anti-mTNC and anti-mTNW IgGs.

Our data revealed that for both mTNC and mTNW, antigen-specific responses were elicited. As shown in Fig. 1A, mTNC and mTNW serum titer increased significantly 14 days after antigen injection (OD_{450nm} = 0.193 ± 0.016, OD_{450nm} = 0.243 ± 0.016, respectively) reaching a maximum S1 titer at day 39 (OD_{450nm} = 1.942 ± 0.074, OD_{450nm} = 1.569 ± 0.019, respectively). Comparative ELISA results revealed that the dromedary D1 developed roughly the same antibody titer towards mTNC and mTNW (not shown). These data demonstrated the successful induction of

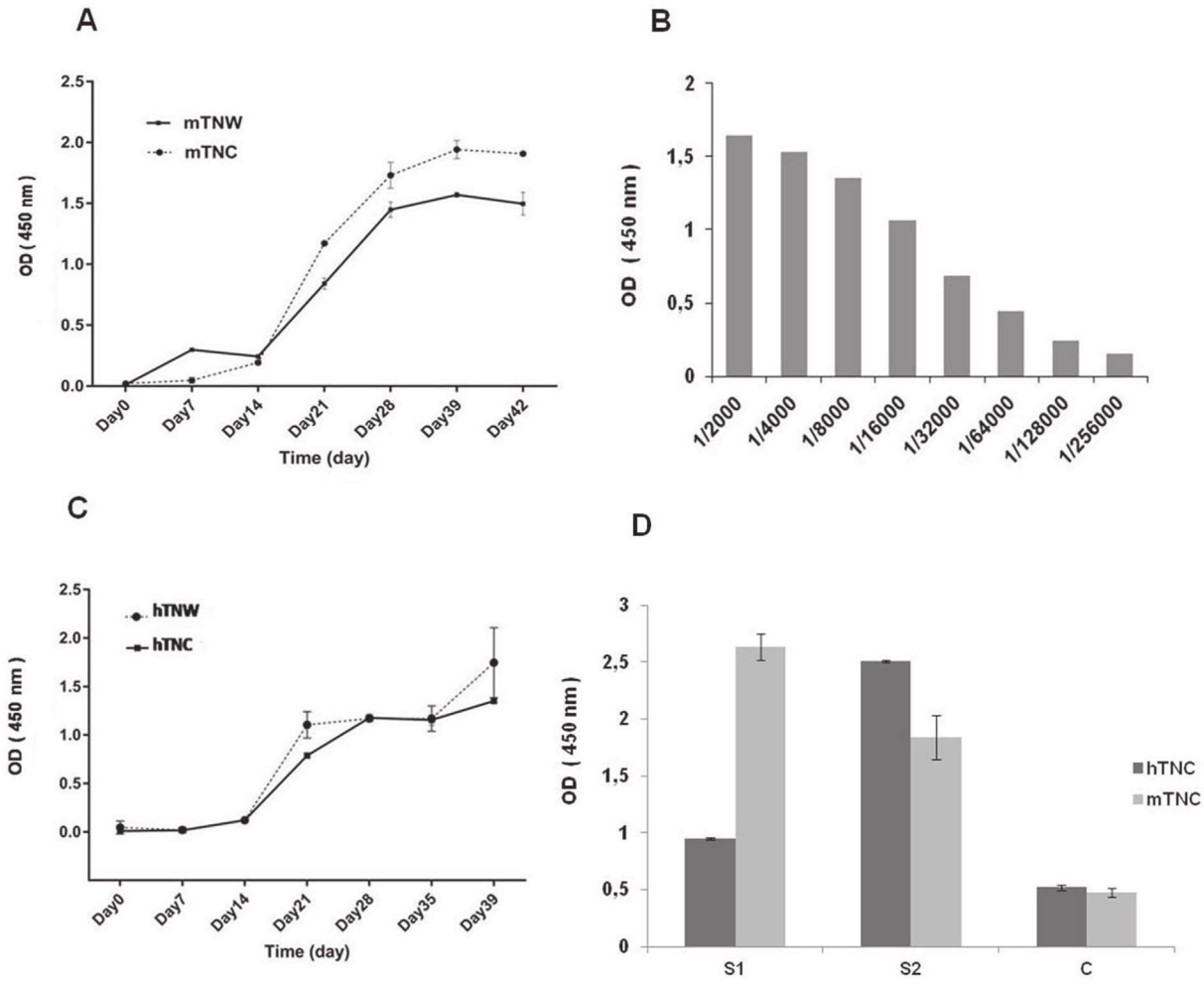

Fig. 1. TNC- and TNW-specific immune responses elicited in immunized dromedaries.

Please cite this article as: S. Dhaouadi et al., Generation and characterization of dromedary Tenascin-C and Tenascin-W specific antibodies, Biochemical and Biophysical Research Communications, https://doi.org/10.1016/j.bbrc.2020.05.077

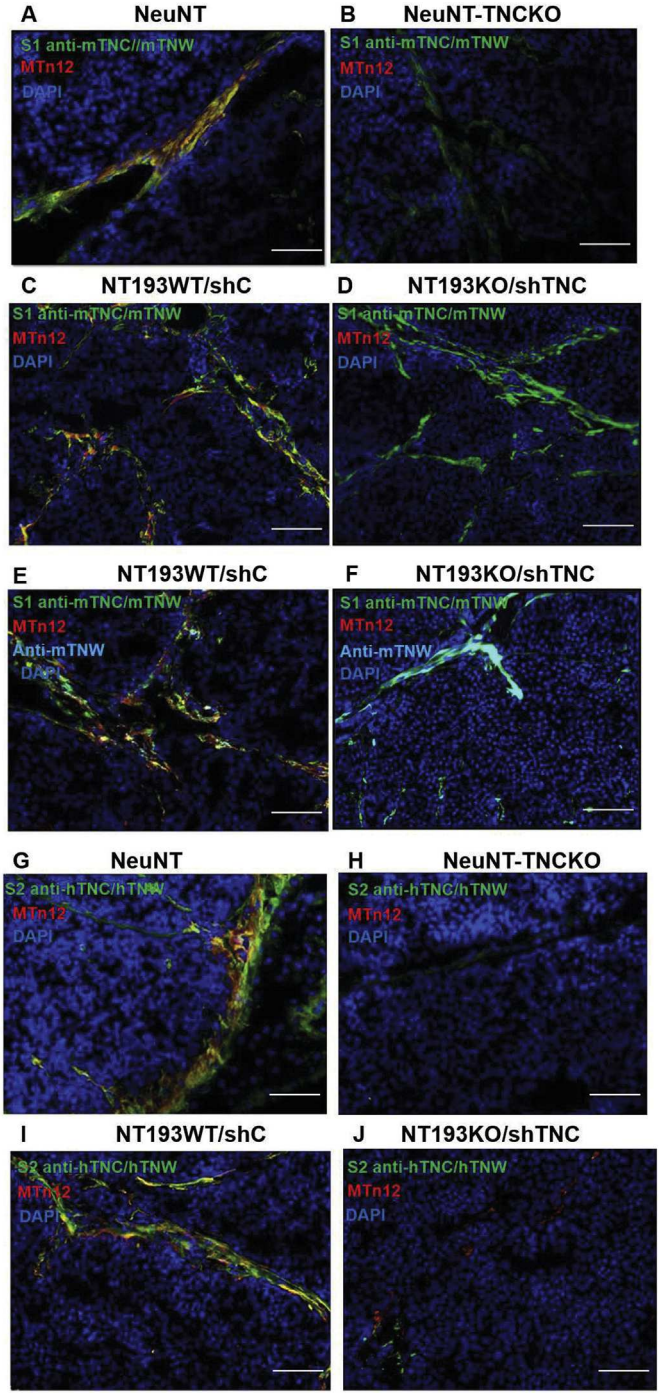

Fig. 2. In situ detection of murine TNC by the D1 and D2 dromedary sera using immunofluorescent staining.

humoral immune responses towards mTNC and mTNW. Our current results are consistent with previous studies carried out using scorpion toxin or the Ltk cell line expressing the Kv2.1 gene to elicit antigen-specific immune responses in dromedary [29,30].

3.2. Humoral responses elicited in the dromedary immunized with hTNC and hTNW

Similarly, humoral responses in dromedary were raised against hTNC and hTNW (S2-anti-hTNC/hTNW). In order to optimize the appropriate dromedary serum dilution, the reactivity of the collected serum against hTNC was tested at serial dilutions (Fig. 1B). The dromedary was injected six times with increasing amounts of both hTNC and hTNW (1900 μg in total per recombinant antigen). Blood was collected at day 39 (after the first injection) and the S2 serum was found to contain specific antibodies directed against hTNC and hTNW, respectively, as seen by ELISA (Fig. 1C). To further assess serum specificity, we used, as irrelevant protein, the AahI toxin at same concentration (negative control). The obtained result demonstrated that the D2-anti-hTNC/TNW serum did not contain antibodies against the AahI toxin (Day 0, OD_{450nm} = 0.289/ Day 35, OD_{450nm} = 0.236) and that repetitive administrations of hTNs generated potent and specific immune responses. Likewise, the dromedary anti-hTNC and hTNW antibody titer increased significantly after day 14 ($OD_{450nm} = 0.119 \pm 0.02$, $OD_{450nm} = 0.120 \pm 0.012$) and reached a maximum at day 39 (OD_{450nm} = 1.35 ± 0.05, OD_{450nm} = 1.745 ± 0.36) (Fig. 1C). Comparative investigation by ELISA revealed that the dromedary D2 developed roughly the same antibody titer towards hTNC and hTNW (not shown). These data demonstrated the successful induction of humoral immune responses towards hTNC and hTNW in dromedary, respectively.

As the human and murine TNC sequences are highly conserved [26,27], we addressed whether the polyclonal dromedary anti-hTNC immune serum (S2) recognized the murine TNC by ELISA. Indeed, the anti-hTNC serum (S2) also recognized the mTNC protein, immobilized at the same concentration of 0.5 μg/ml (Fig. 1D). However, due to limited amounts of hTNW and mTNW, cross-antigenic reactivity assessment between S1 and S2 towards mTNW and hTNW was not investigated.

3.3. Characterization of the dromedary immune serum specificity

To determine the specificity of the dromedary sera, we used IF staining of tumor tissue that is inherently rich in TNC. In particular, we used MMTV-NeuNT tumor material from WT mice where a constitutive active version of ErbB2 (from rat) induced mammary gland tumors [27]. As control, we used tumor material from TNC deficient mice (NeuNT-TNCKO) lacking the TNC protein. We also used tumor material from the NT193 autochthonous grafting model (derived from a MMTV-NeuNT tumor) with high TNC levels (WT host/shC cells) and engineered low levels of TNC (TNCKO host/shTNC cells) [26]. Immunofluorescence with MTn12 [4] confirmed that TNC is expressed in the tumor matrix tracks, as previously reported [27] (not shown). Here, we show a signal overlap with MTn12 (that binds the 6–8th fibronectin type III repeats in TNC) indicating that dromedary-anti-mTNC serum (S1) (Fig. 2A,C) as well as dromedary-anti-hTNC serum (S2) (Fig. 2G,I) recognize the murine TNC protein. Moreover, a signal was seen in tumor tissues from NeuNT-TNCKO and NT193 tumors (KO/shTNC) with largely reduced TNC expression by the dromedary-anti-mTNC serum (S1) (Fig. 2B,D) as well as by the dromedary-anti-hTNC serum (S2) (Fig. 2H). In order to validate the antigenic target recognized by the dromedary sera, we stained NT193KO/shTNC tumors with dromedary-anti-mTNC serum (S1), MTn12 and an anti-mTNW antibody. Indeed, the signal from the dromedary serum S1 overlapped with that of the anti-mTNW antibody (Fig. 2F). These results indicate that the dromedary serum S1 recognizes murine and human TNC but also recognizes murine TNW, as the dromedary was also immunized against mTNW. Here, we also showed that in addition to TNC, NT193 tumors also express TNW.

3.4. Purification of the dromedary IgGs specific to tenascins

As described previously, dromedary serum contains multiple IgG subclasses: a diverse repertoire of conventional (IgG1) and heavy-chain only antibodies (IgG2 and IgG3) which are both

Please cite this article as: S. Dhaouadi et al., Generation and characterization of dromedary Tenascin-C and Tenascin-W specific antibodies, Biochemical and Biophysical Research Communications, https://doi.org/10.1016/j.bbrc.2020.05.077

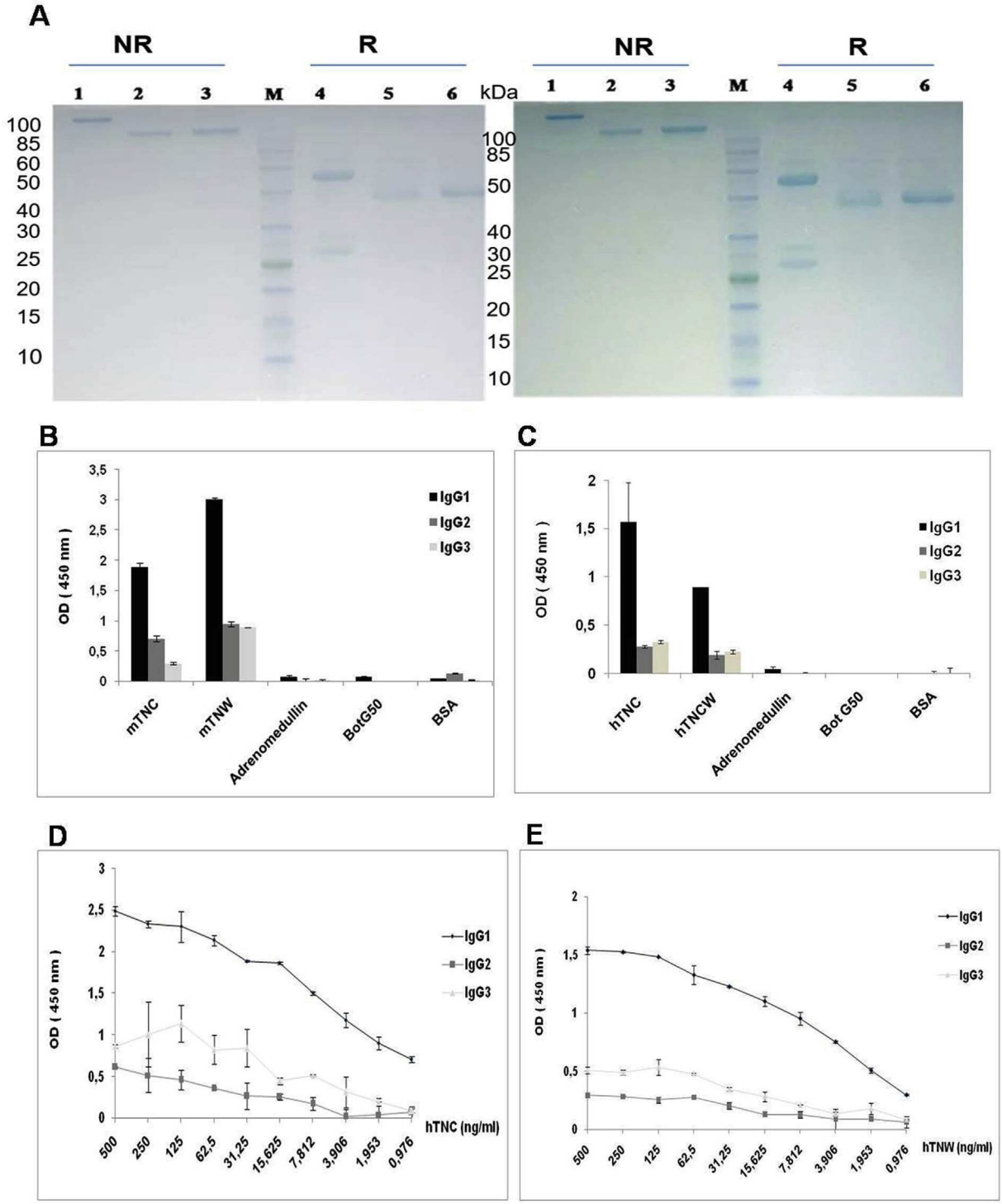

Fig. 3. SDS-PAGE of affinity-purified dromedary IgG subclasses (A) SDS-PAGE (12%) under reducing (R) and non-reducing (NR) conditions. Apparent molecular weight of IgG1 in absence (160 kDa) (lane 1) and in presence of β-mercaptoethanol (55 kDa, H-chains and 25 kDa, L-chains) (Lane 4); Homodimeric IgG2 and IgG3 of 100 kDa apparent molecular weight (lanes 2, 3) under non reducing conditions (NR), separated into two chains of 46 kDa and 50 kDa (lanes 5, 6) under reducing conditions (R). Lane M corresponds to a mass molecular marker. **(B, C)** Binding capacity and immuno-reactivity of the anti-mTNC/mTNW IgG subclasses purified from S1 (**B**) and the anti-hTNC/hTNW IgG subclasses purified from S2 (**C**). Adrenomedullin, BotG50 and BSA were used as negative controls. (**D, E**) Sensitivity of S2-derived IgG subclasses at 1 μg/ml towards recombinant hTNC **(D)** and recombinant hTNW **(E)** immobilized at serial concentrations ranging from 500 ng/ml to 0.976 ng/ml.

functional in antigen binding. In order to separate the different IgG subclasses, sera were collected at the end of the immunization protocol from the two immunized dromedaries D1 (injected with mTNC and mTW) and D2 (injected with hTNC and hTNW), respectively. These sera were subjected to differential adsorption on Hitrap Protein-G followed by adsorption on Hitrap Protein-A. According to our analysis, sera (S1 and S2) contained approximately 58% and 59% HCAbs, respectively (not shown). These HCAbs proportions are in accordance with those reported in the literature varying between 40% and 60% [28,31].

Please cite this article as: S. Dhaouadi et al., Generation and characterization of dromedary Tenascin-C and Tenascin-W specific antibodies, Biochemical and Biophysical Research Communications, https://doi.org/10.1016/j.bbrc.2020.05.077

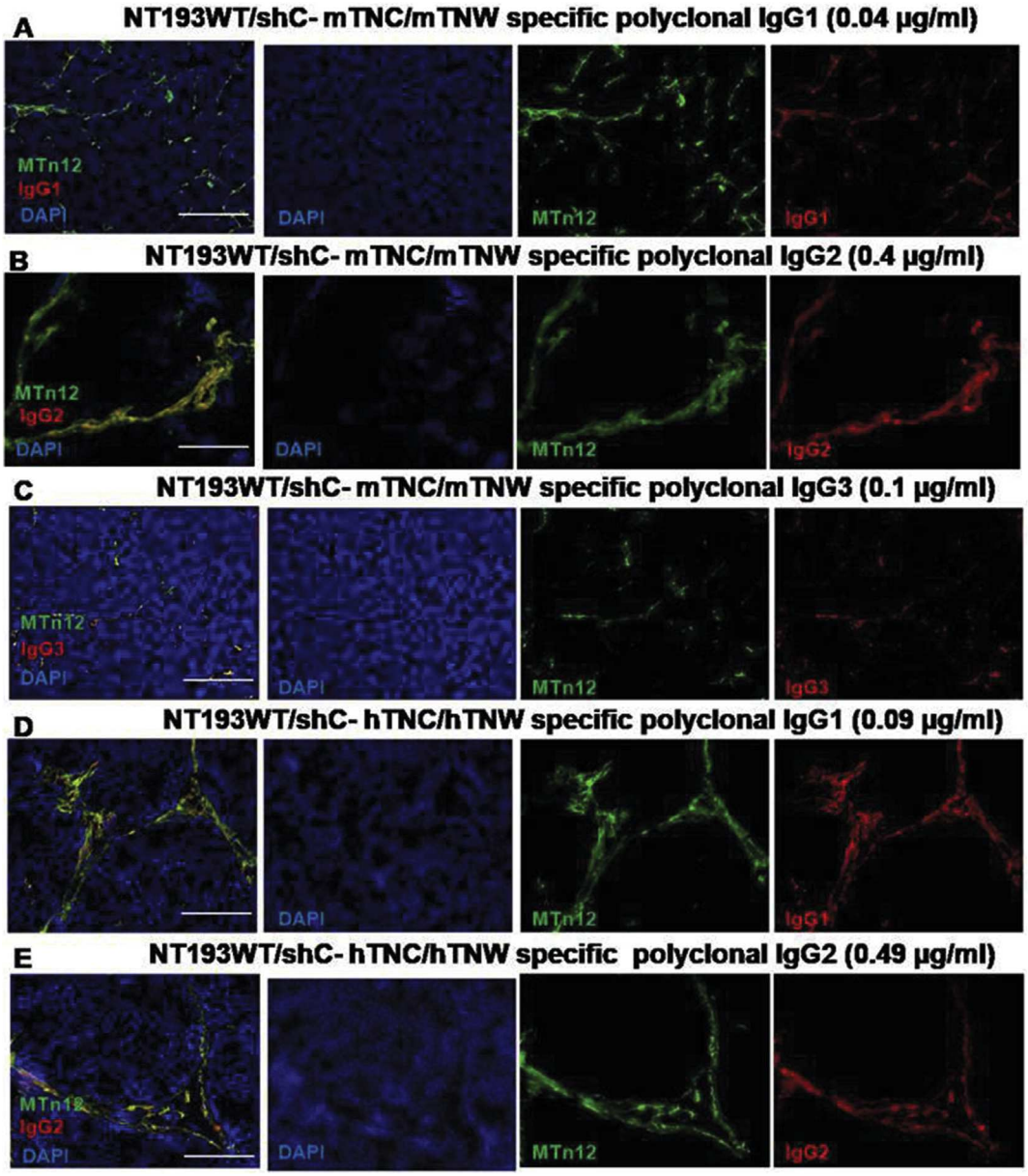

Fig. 4. Immunofluorescent staining of mTNs in murine tumors using mTN-specific D1 dromedary IgG subclasses. Mammary gland NT193WT/ shC tumors were stained with MTn12 (green) and S1-derived IgG subclasses (red). **(A)** IgG1 from S1 applied at 0.04 µg/ml, MTn12 dilution: 1:400. **(B)** IgG2 from S1 applied at 0.4 µg/ml, MTn12 dilution: 1:400. **(C)** IgG3 from S1 applied at 0.1 µg/ml, MTn12 dilution: 1:400. **(D)** IgG1 from S2 applied at 0.09 µg/ml, MTn12 dilution: 1:400. **(E)** IgG2 from S2 applied at 0.49 µg/ml, MTn12 dilution: 1:400. Scale Bar: 7 µm. (For interpretation of the references to colour in this figure legend, the reader is referred to the Web version of this article.)

The obtained IgG fractions were visualized by 12% SDS-PAGE followed by staining with Coomassie blue (Fig. 3A). Each fraction was characterized under non-reducing and reducing conditions by SDS-PAGE analysis. These experiments showed that the purified conventional IgG1 fraction (with two heavy chains and two light chains) migrated under non reducing conditions as a single protein of about 150 kDa, whereas the single chain IgG2 and IgG3 fractions migrated as a single protein species of about 100 kDa. Under reducing conditions, the purified hetero-tetrameric IgG1 fraction dissociated into the heavy chain (~55 kDa) and the light chain (~25 kDa), whereas, HCAbs fractions (IgG2 and IgG3) showed smaller single bands related to their heavy chains which lack the CH1 domain. The band of IgG2 (~50 kDa) was notably bigger than that of IgG3 (~45 kDa) because of the long hinge region characterizing this subclass of immunoglobulins (Fig. 3A).

3.5. Assessment of the dromedary IgG subclasses specificity for TNC and TNW

Two experimental approaches were performed to establish that the dromedary purified IgG subclasses recognized specifically the tenascins. First and foremost, IgG subclasses were individually assessed for their ability to bind tenascins from human and murine origins. As shown in Fig. 3B, D1 dromedary-derived immunoglobulins with specificity to mTNC and mTNW are present in all obtained IgG subtypes. Similarly, IgG subclasses purified from D2 dromedary

Please cite this article as: S. Dhaouadi et al., Generation and characterization of dromedary Tenascin-C and Tenascin-W specific antibodies, Biochemical and Biophysical Research Communications, https://doi.org/10.1016/j.bbrc.2020.05.077

serum containing immunoglobulins against hTNC and hTNW display specific binding towards these antigens (Fig. 3C). Interestingly, these IgG isotypes are able to detect low amounts of immobilized hTNC and hTNW from 50 ng to 0,7 ng by ELISA (Fig. 3D and E), which demonstrates the high specific immunoreactivities of IgG1-3 isotypes towards hTNC and hTNW. No binding to adrenomedullin, BotG50 and BSA was revealed by any of the IgG isotypes which further supports the specificity of the anti-tenascin IgG subclasses (Fig. 3B and C). Finally, we also showed by immunostaining that the D2-derived IgGs are able to detect mTNC on frozen mammary tumor tissue (Fig. 4).

Based on our results, the dromedary immune responses were mediated by both conventional antibodies and HCAbs. Interestingly, the immune response carried by IgG1 is notably more effective than those carried by HCAbs, that could be explained in part due their particular paratope conformation. However, this drawback is outstandingly compensated by the lower molecular weight of the HCAbs presumably leading to better tissue penetration. More interestingly, recognition of the tenascin antigens by HCAbs is highly specific with aptitude to interact specifically with TNC or TNW by ELISA and tissue staining thus encouraging the future investigations against the tenascins (Fig. 3D and E).

4. Conclusion

In this study, we report successful immunization of dromedaries against TNC and TNW classified as reliable tumor biomarkers for monitoring tumor progression, in two experimental murine tumor models. Our results show that TNC and TNW are able to induce high immune responses in dromedary. Purified IgG isotypes bind specifically to TNC and TNW. Moreover, we demonstrated that even non-conventional monomeric IgG subtypes (HCAbs) are able to detect native TNC and TNW in murine tumor. Such antibodies of camelid origin are useful for multichannel immunostaining and future expression analysis of tenascins in tumor sections.

Funding

This project was supported by grants from Institut Pasteur Tunis, PRF D4P1 project, Tunisia, Friedrich Miescher Institute, Basel, Swizerland (IH), INSERM and Ligue contre le Cancer CCIR Est (GO).

Declaration of competing interest

On behalf of the following co-authors, Balkiss Bouhaouala-Zahar, corresponding author from Laboratory of Venoms and Therapeutic Molecules, Institut Pasteur Tunis, 13 Place Pasteur, BP74, 1002 Tunis, Tunisia, declare No conflict of Interest.

Kinetics of anti-mTNC/mTNW (**A**) and anti-hTNC/hTNW (**C**) immune responses elicited in D1 and D2 dromedaries, respectively (1/8000) and measurement at the indicated time points upon immunization. (**B**) The titer of antibodies raised against hTNC (0.5 μg/ml) in the tested serial dilutions (1:2000 to 1:256 000). **(D)** Cross-antigenic reactivity between S1 and S2 sera in comparison to the serum taken as control collected from non immunized dromedary (i.e. S1, S2 and C, respectively) towards hTNC and mTNC (0. 5 μg/ml).

Tissues from mammary gland tumors of NeuNT **(A, G)**, NeuNT-TNCKO **(B,H)** mice and tissues from NT193WT/shC **(C,I)** and NT193KO/shTNC tumors **(D,J)** were stained with MTn12 (red) and dromedary S1 and S2 sera (green). NT193WT/shC **(E)** and NT193KO/shTNC tumors **(F)** were stained with MTn12 (red), S1 serum (green) and anti-mTNW (cyan). S1 serum from dromedary (D1) immunized also against mTNW, recognizes murine TNW which is similarly detected by anti-mTNW **(E, F). (A, B)** S1 dilution: 1:5000, MTn12 dilution: 1:400. **(C, D)** S1 dilution: 1:2000, MTn12 dilution: 1:400. **(E, F)** S1 dilution: 1:2000, MTn12 dilution:1:400, anti-mTNW antibody dilution: 1:200. **(G, H)** S2 dilution: 1:500, MTn12 dilution: 1:400. **(I, J)** S2 dilution: 1:1000, MTn12 dilution: 1:400. Scale Bar: 7 μm.

Acknowledgements

Thanks should be addressed to Dr. H. Bannour, M.Vet for his invaluable help on dromedary immunization. We are sincerely sad that we cannot share the accomplished work with RCE who had initiated this project together with BBZ.

References

[1] M.J. Bissell, W.C. Hines, Why don't we get more cancer? A proposed role of the microenvironment in restraining cancer progression, Nat. Med. 17 (2011) 320–329.
[2] M.W. Pickup, J.K. Mouw, V.M. Weaver, The extracellular matrix modulates the hallmarks of cancer, EMBO Rep. 15 (2014) 1243–1253.
[3] T. Oskarsson, S. Acharyya, X.H.-F. Zhang, S. Vanharanta, S.F. Tavazoie, P.G. Morris, R.J. Downey, K. Manova-Todorova, E. Brogi, J. Massagué, Breast cancer cells produce tenascin C as a metastatic niche component to colonize the lungs, Nat. Med. 17 (2011) 867–874.
[4] G. Orend, R. Chiquet-Ehrismann, Tenascin-C induced signaling in cancer, Canc. Lett. 244 (2006) 143–163.
[5] F. Brellier, R. Chiquet-Ehrismann, How do tenascins influence the birth and life of a malignant cell? J. Cell Mol. Med. 16 (2012) 32–40.
[6] F. Brellier, E. Martina, M. Degen, N. Heuzé-Vourc'h, A. Petit, T. Kryza, Y. Courty, L. Terracciano, C. Ruiz, R. Chiquet-Ehrismann, Tenascin-W is a better cancer biomarker than tenascin-C for most human solid tumors, BMC Clin. Pathol. 12 (2012) 1–10.
[7] K.S. Midwood, G. Orend, The role of tenascin-C in tissue injury and tumorigenesis, J. Cell Commun. Signal. 3 (2009) 287–310.
[8] K.S. Midwood, T. Hussenet, B. Langlois, G. Orend, Advances in tenascin-C biology, Cell. Mol. Life Sci. 68 (2011) 3175–3199.
[9] S. Schenk, J. Muser, G. Vollmer, R. Chiquet-Ehrismann, Tenascin-C in serum: a questionable tumor marker, Int. J. Canc. 61 (1995) 443–449.
[10] A. Scherberich, Murine tenascin-W: a novel mammalian tenascin expressed in kidney and at sites of bone and smooth muscle development, J. Cell Sci. 117 (2004) 571–581.
[11] G. Akabani, D.A. Reardon, R.E. Coleman, T.Z. Wong, S.D. Metzler, J.E. Bowsher, D.P. Barboriak, J.M. Provenzale, K.L. Greer, D. DeLong, et al., Dosimetry and radiographic analysis of 131I-labeled anti-tenascin 81C6 murine monoclonal antibody in newly diagnosed patients with malignant gliomas: a Phase II study, J. Nucl. Med. 11 (2005) 1042–1051.
[12] S.S. Brack, Tumor-targeting properties of novel antibodies specific to the large isoform of tenascin-C, Clin. Canc. Res. 12 (2006) 3200–3208.
[13] M. Silacci, Human monoclonal antibodies to domain C of tenascin-C selectively target solid tumors in vivo, Protein Eng. Des. Sel. 19 (2006) 471–478.
[14] M. Degen, F. Brellier, R. Kain, C. Ruiz, L. Terracciano, G. Orend, R. Chiquet-Ehrismann, Tenascin-W is a novel marker for activated tumor stroma in low-grade human breast cancer and influences cell behavior, Can. Res. 67 (2007) 9169–9179.
[15] D.A. Reardon, M.R. Zalutsky, D.D. Bigner, Antitenascin-C monoclonal antibody radioimmunotherapy for malignant glioma patients, Expert Rev. Anticancer Ther. 7 (2007) 675–687.
[16] H.Y. Ko, K.-J. Choi, C.H. Lee, S. Kim, A multimodal nanoparticle-based cancer imaging probe simultaneously targeting nucleolin, integrin αvβ3 and tenascin-C proteins, Biomaterials 32 (2011) 1130–1138.
[17] G. Orend, R. Chiquet-Ehrismann, Tenascin-C induced signaling in cancer, Canc. Lett. 244 (2006) 143–163.
[18] C. Herold-Mende, M.M. Mueller, M.M. Bonsanto, H.P. Schmitt, S. Kunze, H.H. Steinez, Clinical impact and functional aspects of Tenascin-C expression during glioma progression, Int.J.Cancer. 98 (2002) 362–369.
[19] E. Martina, M. Degen, C. Ruegg, A. Merlo, M.M. Lino, R. Chiquet-Ehrismann, F. Brellier, Tenascin-W is a specific marker of glioma-associated blood vessels and stimulates angiogenesis in vitro, Faseb. J. 24 (2010) 778–787.
[20] N. Brösicke, A. Faissner, Role of tenascins in the ECM of gliomas, Cell Adhes. Migrat. 9 (2015) 131–140.
[21] C. Hamers-Casterman, T. Atarhouch, S. Muyldermans, G. Robinson, C. Hammers, E.B. Songa, N. Bendahman, R. Hammers, Naturally occurring antibodies devoid of light chains, Nature 363 (1993) 446–448.
[22] F. Rahbarizadeh, M.J. Rasaee, M. Forouzandeh, A. Allameh, R. Sarrami, H. Nasiry, M. Sadeghizadeh, The production and characterization of novel heavy-chain antibodies against the tandem repeat region of MUC1 mucin, Immunol. Invest. 34 (2005) 431–452.
[23] M. Haddad, C. Soukkarieh, H.E. Khalaf, A.Q. Abbady, Purification of polyclonal IgG specific for Camelid's antibodies and their recombinant nanobodies, Open Life Sci. 11 (2016) 1–9.
[24] W. Huang, C. Chiquet-Ehrismann, J.V. Moyano, A. Garcia-Pardo, G. Orend, Interference of tenascin-C with syndecan-4 binding to fibronectin blocks cell adhesion and stimulates tumor cell proliferation, Can. Res. 61 (2001)

Please cite this article as: S. Dhaouadi et al., Generation and characterization of dromedary Tenascin-C and Tenascin-W specific antibodies, Biochemical and Biophysical Research Communications, https://doi.org/10.1016/j.bbrc.2020.05.077

8586–8594.
[25] P. Taneja, D.P. Frazier, R.D. Kendig, D. Maglic, T. Sugiyama, F. Kai, N.K. Taneja, K. Inoue, MMTV mouse models and the diagnostic values of MMTV-like sequences in human breast cancer, Expert Rev. Mol. Diagn. 9 (2009) 423–440.
[26] A. Arpel, P. Sawma, C. Spenlé, J. Fritz, L. Meyer, N. Garnier, I. Velázquez-Quesada, T. Hussenet, S. Aci-Sèche, N. Baumlin, et al., Transmembrane domain targeting peptide antagonizing ErbB2/neu inhibits breast tumor growth and metastasis, Cell Rep. 8 (2014) 1714–1721.
[27] Z. Sun, I. Velázquez-Quesada, D. Murdamoothoo, C. Ahowesso, A. Yilmaz, C. Spenlé, G. Averous, W. Erne, F. Oberndorfer, A. Oszwald, et al., Tenascin-C increases lung metastasis by impacting blood vessel invasions, Matrix Biol. 83 (2019) 26–47.
[28] I. Hmila, R. Ben Abderrazek-Ben Abdallah, D. Saerens, Z. Benlasfar, K. Conrath, M. El Ayeb, S. Muyeldermans, B. Bouhaouala-Zahar, VHH, bivalent domains and chimeric Heavy chain-only antibodies with high neutralizing efficacy for scorpion toxin AahI', Mol. Immunol. 45 (2008) 3847–3856.
[29] F. Meddeb-Mouelhi, B. Bouhaouala-Zahar, Z. Benlasfar, M. Hammadi, T. Mejri, M. Moslah, H. Karoui, T. Khorchani, M.E. Ayeb, Immunized camel sera and derived immunoglobulin subclasses neutralizing Androctonus australis hector scorpion toxins, Toxicon 42 (2003) 785–791.
[30] R. Hassiki, A.J. Labro, Z. Benlasfar, C. Vincke, M. Somia, M. El Ayeb, S. Muyldermans, D.J. Snyders, B. Bouhaouala-Zahar, Dromedary immune response and specific Kv2.1 antibody generation using a specific immunization approach, Int. J. Biol. Macromol. 93 (2016) 167–171.
[31] R. Van der Linden, B. de Geus, W. Stok, W. Bos, D. van Wassenaar, T. Verrips, L. Frenken, Induction of immune responses and molecular cloning of the heavy chain antibody repertoire of Lama glama, J. Immunol. Methods 240 (2000) 185–195.

Please cite this article as: S. Dhaouadi et al., Generation and characterization of dromedary Tenascin-C and Tenascin-W specific antibodies, Biochemical and Biophysical Research Communications, https://doi.org/10.1016/j.bbrc.2020.05.077

William ERNE

Modulation des effets de TRAIL par la matrice extracellulaire dans le cancer et développement de nouveaux peptides ciblant la Ténascine-C

Résumé

La protéine matricielle ténascine-C (TNC) est très exprimée dans les pathologies impliquant un remodelage tissulaire. Dans le cancer, la TNC favorise la croissance tumorale et les métastases, ce qui est corrélé à un mauvais pronostic. Dans cette thèse, j'ai étudié l'impact de la TNC sur la signalisation de TRAIL dans le cancer du sein et j'ai développé de nouveaux peptides visant à inhiber les fonctions de la TNC. J'ai démontré que les cellules épithéliales du cancer du sein peuvent exprimer TRAIL sans mourir, malgré leur sensibilité au traitement combiné TRAIL+MD5-1. *In vivo*, TRAIL a diminué la croissance tumorale en recrutant des cellules myéloïdes via CXCR4. J'ai montré que la TNC diminuait l'activité antitumorale de TRAIL en liant TRAIL, en induisant la signalisation de survie du TGFβ et en abaissant l'expression de TRAIL. J'ai décrit un MOtif de REgulation de la MAtrice (MAREMO) dans la TNC qui a été utilisé pour développer des peptides spécifiques ciblant les fonctions inhibitrices de la TNC lors de la chémorétention, l'interaction avec d'autres protéines matricielles et les récepteurs cellulaires, et la résistance à TRAIL. En ciblant la TNC avec des peptides MAREMO, nous pourrions rétablir le contrôle antitumoral de TRAIL. Dans l'ensemble, un nouveau mécanisme de la façon dont la TNC corrompt l'immunité antitumorale a été mis au jour et présente un potentiel pour de futures thérapies.

Résumé en anglais

The matrix protein tenascin-C (TNC) is highly expressed in pathologies implicating tissue remodeling. In cancer, TNC promotes tumor growth and metastasis, correlating with poor prognosis. In this thesis, I studied the impact of TNC on TRAIL signaling in breast cancer and I developed new peptides aiming to inhibit the functions of TNC. I demonstrated that epithelial breast cancer cells can express TRAIL without dying despite being sensitive to killing by combined TRAIL+MD5-1 treatment. *In vivo*, TRAIL reduced tumor growth through recruiting myeloid cells via CXCR4. I showed that TNC decreased TRAIL anti-tumor activity by trapping TRAIL, by inducing TGFβ survival signaling and by lowering TRAIL expression. I described a MAtrix REgulating MOtif (MAREMO) in TNC that was used to develop specific peptides targeting TNC inhibiting functions in chemoretention, interaction with other matrix proteins and cellular receptors, and TRAIL resistance. By targeting TNC with MAREMO peptides, we may restore TRAIL anti-tumoral control. Altogether, a novel mechanism of how TNC corrupts anti-tumor immunity was revealed that has potential for future therapies.

Keywords: tenascin-C, tumor microenvironment, breast cancer, apoptosis, immune response, targeting peptides